PROGRAMA DE DOCTORADO EN QUÍMICA-3154 R.D. 99/2011

APLICACIÓN DE METODOLOGÍAS ACTUALES A LA SÍNTESIS DE MOLÉCULAS DE INTERÉS FARMACOLÓGICO Y ESTRUCTURAS MOLECULARES COMPLEJAS BASADAS EN INTERACCIONES DÉBILES

Doctorando:

Pedro Juan Llabrés Campaner

Directores:

Belén Abarca González

Rafael Ballesteros Campos

Rafael Ballesteros Garrido

Valencia, septiembre 2018

Dña. Belén Abarca González, Catedrática del Departamento de Química Orgánica de la Universidad de Valencia, D. Rafael Ballesteros Campos, Catedrático del Departamento de Química Orgánica de la Universidad de Valencia y el Dr. D. Rafael Ballesteros Garrido, Investigador contratado del CSIC

CERTIFICAN:

Que **D. Pedro Juan Llabrés Campaner**, ha realizado bajo nuestra dirección la Tesis Doctoral titulada:

APLICACIÓN DE METODOLOGÍAS ACTUALES A LA SÍNTESIS DE MOLÉCULAS DE INTERÉS FARMACOLÓGICO Y ESTRUCTURAS MOLECULARES COMPLEJAS BASADAS EN INTERACCIONES DÉBILES

Y autorizan la presentación de la correspondiente memoria en la Facultad de Química para que se cumplan los trámites reglamentarios.

Y para que así conste a los efectos oportunos y a petición del interesado expiden y firman la presente autorización.

En Burjassot, a 25 de septiembre de 2018

Fdo: Belén Abarca González **Fdo: Rafael Ballesteros Campos**

Fdo: Rafael Ballesteros Garrido

Ante todo, quería expresar mi agradecimiento a mis directores de tesis, Dña. Belén Abarca González y D. Rafael Ballesteros Campos, por abrirme las puertas de su laboratorio y darme la oportunidad de aprender de ellos, además de por el apoyo constante pese a las adversidades.

Agradecer especialmente a Rafa Jr., 'mi mentor', por haberme dado la confianza que necesitaba desde el primer día y haberme dejado participar en sus fantásticas ideas. Gracias también por hacerme sentir como en casa pese a estar fuera de mi isla, aconsejarme y enseñarme sitios de la Comunitat Valenciana.

A mis padres, por pensar siempre primero en mi formación y apoyarme en todas las decisiones que he tomado. Por expresar siempre su orgullo hacia mí y simplificarme las cosas que me parecían difíciles.

A tu, per viure amb jo aquesta aventura, per ser sa meva companyera de viatge i de vida, en las buenas y en las malas, da igual si a Palma, a Madrid o a Sagunt. Se que aquesta tesis l'he fet gràcies a tu, perquè sempre has cregut en mi. T'estim.

A Lluís, por ser mi colega de carrera y de tesis, y mi familia en Valencia.

A mis familiares y amigos, por estar siempre pendientes, venir a visitarme, y alegrarse por mis éxitos.

Y por supuesto, un especial recuerdo a los profesores y compañeros doctorandos de departamento y facultad.

Es mejor arrepentirse de las cosas que has hecho,

que de las que por miedo nunca hiciste.

ÍNDICE GENERAL

RESUMEN/ABSTRACT

La presente tesis doctoral titulada "Aplicación de Metodologías Actuales a la Síntesis de Moléculas de Interés Farmacológico y Estructuras Moleculares Complejas basadas en Interacciones Débiles" está centrada en el concepto de 'Complejidad Molecular', tanto en términos de *composición*, *constitución*, *configuración* o *conformación*.

Tres han sido las entidades químicas que han supuesto la fuente de inspiración a la hora de afrontar esta tesis doctoral y que constituyen claros ejemplos de 'Complejidad Molecular': el **glicoaldehído** debido a su *complejidad estructural* (combinación de efecto electrónicos entre el grupo alcohol y el grupo aldehído; tautomería ceto-enólica…), el **diquat** debido a su *complejidad configuracional* (ejes de quiralidad que pueden llevar a cambios conformacionales con gran influencia en las aplicaciones) y el **MOF-5** debido a su *complejidad supramolecular*, (en la que los enlaces no covalentes son la base para formar esta estructura).

Por lo tanto, el conjunto del manuscrito se divide en **tres partes** bien diferenciadas, en las que puede apreciarse una perspectiva distinta del concepto de '*Complejidad Molecular*':

En la **primera parte**, se han abordado las reacciones de *Autotransferencia de Hidrógeno* o de *Préstamo de Hidrógeno*, mediante el uso de aminas aromáticas y dioles, en una catálisis de tipo heterogénea, intentando respetar la mayoría de los preceptos de la *Química Verde*. Este sistema catalítico ha permitido la transformación del etilenglicol en **glicoaldehído**, compuesto de gran complejidad molecular y difícilmente sintetizable debido a su elevada reactividad, que ha sido propuesta como molécula fundamental en el origen de la vida y clave en la ruta de homologación de los azúcares a partir del formaldehído. Gracias a esa transformación se ha podido desarrollar una metodología para alquilar aminas aromáticas con etilenglicol y obtener así β-amino alcoholes. Además, se ha extrapolado esta metodología catalítica a la creación de más complejidad molecular aplicable a la síntesis de productos de alto valor añadido en química farmacéutica, como por ejemplo indoles no sustituidos en el anillo pirrólico.

En la **segunda parte**, la investigación se ha orientado a la obtención de nuevos derivados de diquat basados en [1,2,3]triazolo[1,5-*a*]piridinas y [1,2,3]triazolo[1,5-*a*]quinolinas, las cuales han sido objeto de estudio en nuestro grupo de investigación durante muchos años. Además, se han evaluado sus propiedades estructurales, configuracionales y conformacionales, así como las físico-químicas, y su posible interacción con ADN.

Finalmente, la **tercera parte** se ha enfocado a la química de materiales, mediante la preparación de Metal-Organic Frameworks (MOFs) transparentes no conocidos hasta el momento, y que se han tratado de utilizar como contenedores de moléculas, las cuales quedan confinadas en los huecos de las redes cristalinas del material. Así, se ha podido llevar a cabo el estudio de esas moléculas en estado sólido, donde muchas veces presentan propiedades completamente diferentes a las que presentan en disolución. De esta forma, nuestros MOFs han actuado como "disolventes sólidos". Además, también se ha hecho un estudio de la relación existente entre la composición molecular de un MOF y el tamaño macroscópico de los cristales obtenidos, siendo esta una de las primeras aproximaciones a este campo.

Esta tesis es, por tanto, una tesis **multidisciplinar** dentro de la Química, ya que se ha llevado a cabo síntesis, aislamiento y caracterización de nuevas moléculas; se han utilizado numerosas técnicas y aparatos (espectroscópicas, espectrométricas, cristalográficas, de resonancia magnética nuclear…); y se ha explorado la química de materiales.

This doctoral thesis entitled "Application of Current Methodologies to the Synthesis of Molecules with Pharmacological Interest and Complex Molecular Structures based on Weak Interactions" is focused on the concept of 'Molecular Complexity', both in terms of composition, constitution, configuration or conformation.

Three were the chemical entities that have been the source of inspiration when facing this doctoral thesis and that are clear examples of 'Molecular Complexity': the **glycoaldehyde** due to its structural complexity (combination of electronic effect between the alcohol group and the aldehyde group, keto-enolic tautomerism...), the **diqua**t due to its configurational complexity (chirality axes that can lead to conformational changes with great influence in their applications) and the **MOF-5** due to its supramolecular complexity in that non-covalent bonds are the basis for forming these structures).

Therefore, the whole of the manuscript is divided into three well differentiated parts, in which a different perspective of the concept of 'Molecular Complexity' can be seen:

In the **first part**, the Borrowing Hydrogen (or Hydrogen Autotransfer) reactions, by the use of aromatic amines and diols, in heterogeneous type catalysis, trying to respect most of the precepts of Green Chemistry or Green Chemistry, have been addressed. This catalytic system has allowed the transformation of ethylene glycol into **glycoaldehyde**, great complex molecule and very difficult to synthesize due to its high reactivity, which has been proposed as a fundamental molecule at the origin of life and key in the route of homologation of sugars from formaldehyde. Thanks to this transformation, we have been able to develop a methodology to rent aromatic amines with ethylene glicol, obtaining β-amino alcohols. In addition, this catalytic methodology has been amplified to the creation of more molecular complexity applicable to the synthesis of high added value products in pharmaceutical industry, such as, for example, pyrrole-ring unsubstituted indoles.

In the **second part**, the research has focused on obtaining new diquat derivatives based on [1,2,3]triazolo[1,5-*a*]pyridines and [1,2,3]triazolo[1,5-*a*]quinolines, which have been studied in our research group for many years. In addition, their structural, configurational and conformational properties, as well as the physico-chemical properties, and their possible interaction with DNA have been evaluated.

Finally, the **third part** has focused on materials chemistry, through the preparation of transparent **Metal-Organic Frameworks** (MOFs) that have not been previously obtained, and that have been tried to be used as containers for molecules, which are confined in the pores of the crystalline framework of the material. Thus, it has been possible to carry out the study of these molecules in the solid state, where they often have properties completely different from those present in solution. In this way, our MOFs have acted as "solid solvents". In addition, a study has also been made of the relationship between the molecular composition of an MOF and the macroscopic size of the crystals obtained, this being one of the first approaches to this field.

This thesis is, therefore, a **multidisciplinary** thesis within Chemistry, since synthesis, isolation and characterization of new molecules have been carried out; numerous techniques and apparatus have been used (spectroscopic, spectrometric, crystallographic, nuclear magnetic resonance...); and the chemistry of materials has been explored.

INTRODUCCIÓN GENERAL Y OBJETIVOS

Se dice que *complejidad* es la cualidad de lo que está compuesto de diversos elementos interrelacionados.[1] Nos referimos con el término *Sistema Complejo* a una agrupación de partes interrelacionadas que presentan propiedades y comportamientos no evidentes a partir de la suma de las partes que lo componen.

Aunque la noción de complejidad se ha utilizado en muchos campos, constituye uno de los pilares fundamentales de las ciencias básicas, biológicas y, más recientemente, de las ciencias de la información.[2]

A medida que un sistema simple formado por pocos componentes presenta propiedades emergentes que no pueden deducirse por las de sus componentes básicos, decimos que hay un aumento de complejidad.

En el ámbito de la química, una molécula como el agua debería ser un sistema simple ya que solo posee dos tipos de átomos (hidrógeno y oxígeno). Sin embargo, solamente a partir de estos elementos es difícil justificar que haya una diferencia tan notable con moléculas de igual tamaño y geometría como el amoníaco, el metano, el dióxido de carbono, el sulfuro de dihidrógeno, etc. La razón de este comportamiento radica fundamentalmente en la electronegatividad del átomo de oxígeno. Además, este carácter electronegativo provoca que aparezca una propiedad emergente, la formación de enlaces de hidrógeno, que explican algunas de las propiedades maravillosas del agua como la gran diferencia entre los puntos de fusión (0ºC) y de ebullición (100ºC) o su descenso de densidad y aumento de volumen al solidificar. Este sistema de dos átomos es capaz de interaccionar con muchas otras sustancias, y por ello puede ser el disolvente, el reactivo, la base o el ácido de los sistemas biológicos.

Podemos hablar de **Complejidad Molecular** atendiendo a la estructura de una molécula, es decir, al conjunto de propiedades derivadas de su ***COMPOSICIÓN*** *(*conjunto de átomos que forman la molécula), de su ***CONSTITUCIÓN*** (conectividad entre sus átomos), de su ***CONFIGURACIÓN*** (disposición espacial no intercambiable a baja energía) y de su ***CONFORMACIÓN*** (diferentes disposiciones espaciales que puede asumir en rangos pequeños de energía).

Uno de los más destacados ejemplos de complejidad molecular lo constituye la *Palitoxina* (*Figura 1*), una toxina de estructura no proteica aislada de un coral del género *Palytoa* en 1971 por Moore y Scheuer,[3] y sintetizada por Kishi y colaboradores en 1994.[4] Con una composición $C_{129}H_{223}N_3O_{54}$, la *Palitoxina* presenta 64 centros estereogénicos definidos frente a 1.019 posibles estereoisómeros. Obviamente, en la *Figura 1* no se representan las conformaciones más estables por evidentes motivos de simplicidad.

[1] Wikipedia

[2] F. Capra, **2008**, *La trama de la* vida, Ed. Anagrama.

[3] R.E. Moore, P.J. Scheuer, *Science*, **1971**, *172 (3982)*, 495–498.

[4] a) J.K. Cha, W.J. Christ, J.M. Finan, H. Fujioka, Y. Kishi, L.L. Klein, S.S. Ko, J. Leder, W.W. McWhorter, K-P. Pfaff, M. Yonaga, D. Uemura, Y.J. Hirata, *J. Am. Chem. Soc.*, **1982**, *104*, 7369. b) R.W. Armstrong, J.M. Beau, S.H. Cheon, W.J. Christ, H. Fujioka, W.H. Ham, L.D. Hawkins, H. Jin, S.H. Kang, Y. Kishi, M.J. Martinelli, W.W. McWhorter, M. Mizuno, M. Nakata, A.E. Stutz, F.X. Talmas, M. Taniguchi, J.A. Tino, K. Ueda, J. Uenishi, J.B. White, M.Y. Yonaga, *J. Am. Chem. Soc.*, **1989**, *111*, 7530. c) Y. Kishi, *Pure Appl. Chem*., **1993**, *65*, 771. d) E.M. Suh, Y. Kishi*, J. Am. Chem. Soc.,* **1994**, *116*, 11205.

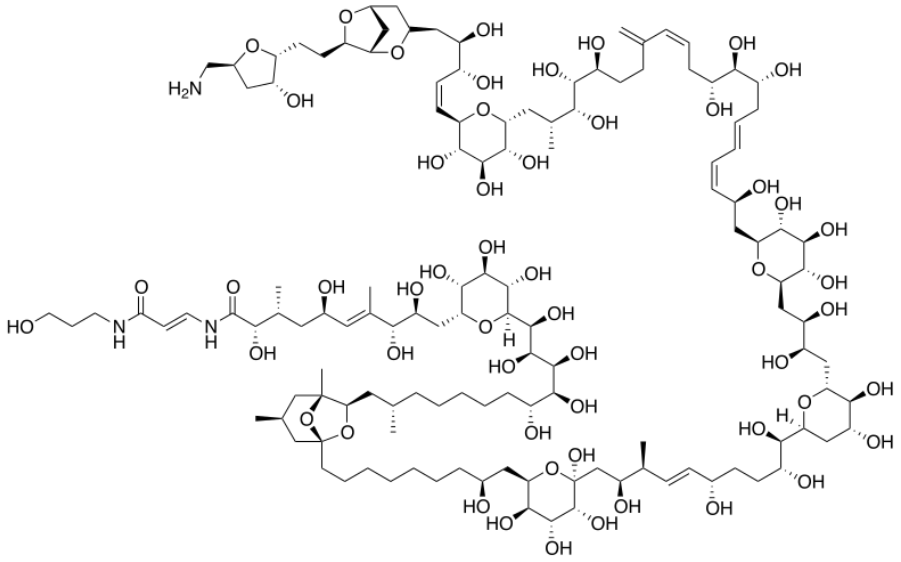

Figura 1. Estructura de la *Palitoxina*.

Si atendemos a la definición en el marco de la teoría de la Complejidad de la información (formulada por Andrei Kolmogórov) dice que "la complejidad de un objeto finito queda definida por el tamaño del programa informático (en sentido teórico) que permite reproducir ese objeto".[5] El nombre (en inglés) IUPAC de la *Palitoxina* sería el programa que codifica la estructura y en este caso sería:

2S, 3R, 5R, 6E, 8R, 9S)-10-[(2R, 3R, 4R, 5S, 6R)-6-[(1S, 2R, 3S, 4S, 5R, 11S)-11-{[(1R, 3S, 5S, 7R)-5-[(8S)-9-[(2R, 3R, 4R, 5R, 6S)-6-[(2S, 3S, 4E, 6S, 9R, 10R)-10-[(2S, 4R, 5S, 6R)-6-[(2R, 3R)-4-[(2R, 3S, 4R, 5R, 6S)-6-[(2S, 3Z, 5E, 8R, 9S, 10R, 12Z, 17S, 18R, 19R, 20R)-20-{[(2R, 3R, 4R, 5S, 6R)-6-[(1Z, 3R, 4R)-5-[(1S, 3R, 5R, 7R)-7-{2-[(2R, 3R, 5S)-5-(aminomethyl)-3-hydroxyoxolan-2-yl]ethyl}-2,6-dioxabicyclo[3.2.1]octan-3-yl]-3,4-dihydroxypent-1-en-1-yl]-3,4,5-trihydroxyoxan-2-yl] methyl } -2, 8, 9, 10, 17, 18, 19-heptahydroxy-14-methylideneheneicosa-3, 5, 12-trien-1-yl]-3, 4, 5-trihydroxyoxan-2-yl]-2, 3-dihydroxybutyl]-4, 5-dihydroxy-oxan-2-yl]-2, 6, 9, 10-tetrahydroxy-3-methyldec-4-en-1-yl]-3, 4, 5, 6-tetrahydroxyoxan-2-yl]-8-hydroxy-nonyl]-1, 3-dimethyl-6, 8-dioxabicyclo[3.2.1]octan-7-yl]methyl}-1, 2, 3, 4, 5-pentahydroxydodecyl]-3, 4, 5-trihydroxyoxan-2-yl]-2, 5, 8, 9-tetrahydroxy-N-[(1E)-2-[(3-hydroxypropyl)-C-hydroxycarbonimidoyl]eth-1-en-1-yl]-3, 7-dimethyldec-6-enimidic acid.

Este caso es sorprendente por la extremada complejidad que presenta dado el gran número de átomos que componen su fórmula molecular. No obstante, existen otras muchas moléculas que, teniendo pocos átomos, generan extremada complejidad teórica como el caso del *Bulvaleno*, una molécula $C_{10}H_{10}$ que, como consecuencia de la tautomería de valencia, puede presentar hasta 1.209.000 isómeros en rápida interconversión. En el *Bulvaleno* (*Figura 2*) todos los átomos de hidrógeno son iguales por RMN a 120ºC, apareciendo un solo singlete a 4.2 ppm.[6]

[5] M. Gell-Mann, (1995), *El quark y el jaguar*, Tusquets Editores S.A.
[6] A. Ault, *J. Chem. Educ.,* **2001**, *78*, 924.

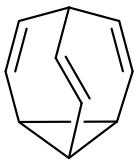

Figura 2. Estructura del *Bulvaleno* (triciclo[3.3.2.0]deca-2,7,9-trieno)

Por otro lado, la simple introducción de heteroátomos en un hidrocarburo (la funcionalización) provoca la aparición de numerosas estructuras que en algún caso son muy poco conocidas debido a la complejidad inherente a su reactividad. Así, si tratamos de describir diferentes moléculas con dos átomos de carbono y diferentes combinaciones de átomos de hidrógeno y oxígeno veremos una amplia gama de diferentes compuestos que pueden describirse (*Figura 3*).

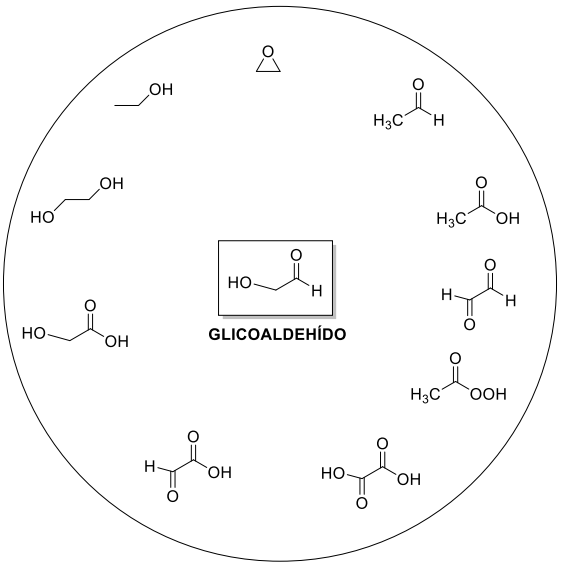

Figura 3. Diferentes estructuras que pueden obtenerse solamente con dos átomos de carbono (C) y algunos de hidrógeno (H) y oxígeno (O). Se destaca el glicoaldehído como ejemplo de gran complejidad.

Todos, salvo el ácido peracético (que se prepara *in situ* a partir de ácido acético y peróxido de hidrógeno) y el glicoaldehído (2-hidroxiacetaldehído), son comerciales. La razón de la complejidad estructural del glicoaldehído, radica en la combinación de efectos electrónicos entre grupo alcohol y el grupo aldehído (*Figura 4*). El grupo alcohol ejerce un efecto inductivo atractor sobre el carbono carbonílico, haciéndolo más reactivo. Por otra parte, la tautomería ceto-enólica existente permite que el glicoaldehído pueda presentar dos tautómeros enólicos Z y E[7] (*Figura 4, en medio*).

[7] L.M. Azofra, M.M. Quesada-Moreno, I. Alkorta, J.R. Avilés-Moreno, J. Elguero, J.J. López-González, *ChemPhysChem.*, **2015**, *16*, 2226.

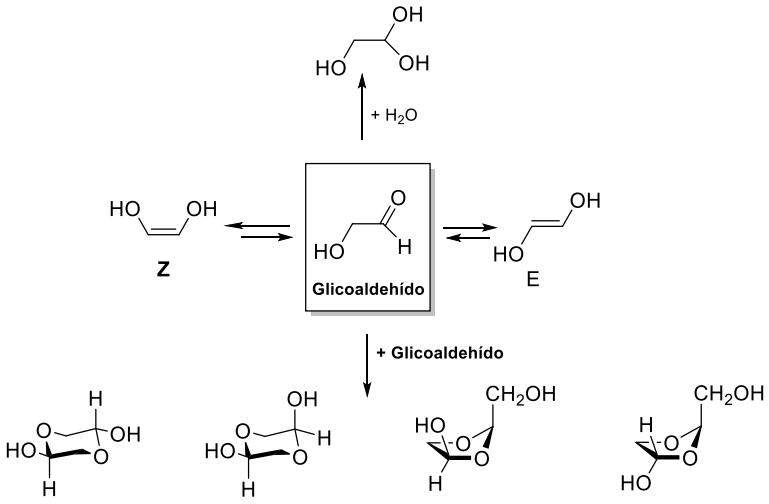

Figura 4. Estructuras posibles derivadas del glicoaldehído ($C_2H_4O_2$).

Como consecuencia de la gran reactividad del carbonilo aldehídico, en presencia de agua puede dar un hidrato (*Figura 4, arriba*), y también consigo mismo puede generar un dímero hemiacetálico ciclohexánico y/o ciclopentánico que, además, al poseer dos centros quirales derivan en dos diastereoisómeros (el *trans* y el *cis*), y cada uno de ellos con su correspondiente enantiómero (*Figura 4, abajo*). Estos dímeros pueden interconvertirse fácilmente al poseer dos carbonos anoméricos.[7,8] El glicoaldehído no es una molécula comercial, y solo lo es la mezcla de dímeros. Como muestra de la complejidad de este producto, en la *Figura 5* se describe el espectro de RNM de ^{1}H del dímero comercializado.[8]

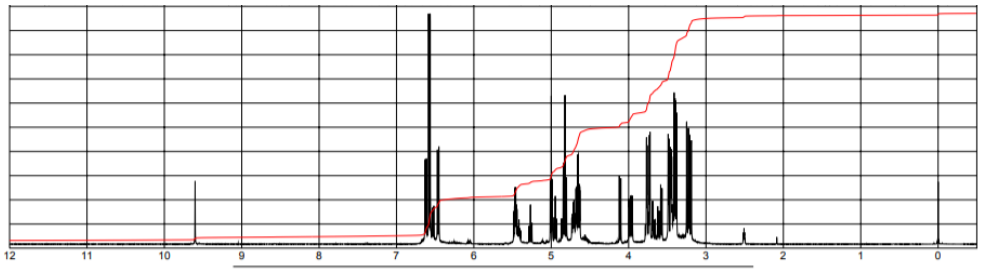

Figura 5. Espectro de RMN de ^{1}H del dímero de glicoaldehído comercializado de la mezcla dímero

Un aspecto interesante del glicoaldehído reside en que se ha propuesto como una molécula fundamental en el origen de la vida, y se ha formulado como clave en la ruta de homologación de los azucares a partir del formaldehído ("Formose reaction", *Esquema 1*), aunque el paso del formaldehído a glicoaldehído es muy cuestionado.[9]

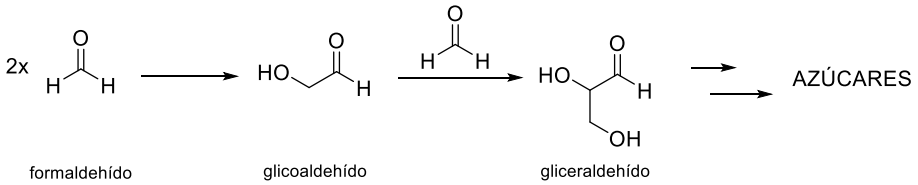

Esquema 1. Ruta sintética simplificada de la *Formose reaction*.

[8] Comercializado por Sigma-Aldrich G6805

[9] D. Ritson, J.D. Sutherland, *Nat. Chem.*, **2012**, *4*, 895.

La complejidad funcional de esta pequeña molécula ha hecho que pocas veces se pueda utilizar y que haya pocas síntesis de ella. Se ha descrito recientemente una síntesis a partir de celulosa por tratamiento con ácido wolfrámico[10] con un bajo rendimiento del 26%.

Otro ejemplo de complejidad molecular lo constituye la aparición de ejes de quiralidad en ciertas moléculas. La 2,2'-bipiridina (**BIPY**) es una sencilla molécula con enormes aplicaciones. En agosto de 2018 presentaba en el buscador Scifinder Scholar 49.160 entradas. Cuando se dialquila con 1,2-dibromoetano se obtiene un compuesto di-catiónico conocido como *Diquat* (**1**), formalmente un dibromuro de 6,7-dihidrodipirido[1,2-*a*:2',1'-*c*]pyrazine-5,8-diinio (*Figura 6*). Este compuesto **1**, preparado por primera vez por Jones y colaboradores,[11] presentó aplicaciones como herbicida, aunque actualmente no se utiliza por su elevada toxicidad.[12]

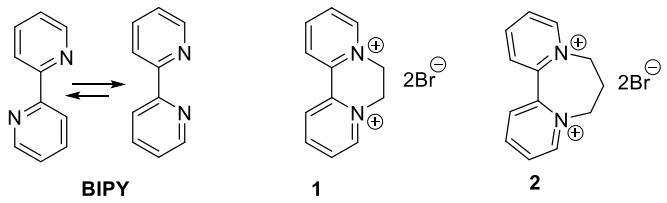

Figura 6. Estructuras de la 2,2'-bipiridina (**BIPY**), diquat (**1**) y un homólogo con un puente de tres carbonos (**2**).

Tanto el compuesto **1** como su homólogo **2**, pueden presentar atropoisomería, presentándose como un par de enantiómeros dependiendo del ángulo diedro entre los dos anillos de piridina (*Figura 7*).

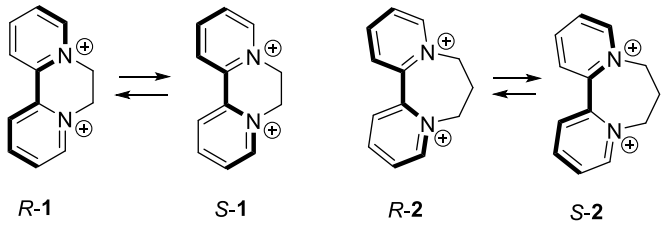

Figura 7. Enantiómeros posibles de **1** y **2**, obtenidos por cambios en el ángulo diedro de los dos anillos de piridina.

Así, las variaciones conformacionales del orden de 17-18 Kcal·mol^{-1}, aunque pequeñas, pueden llegar a constituir una barrera energética que permita la separación de estos enantiómeros. Este hecho, fue estudiado por J. Lacour y colaboradores, [13] consiguiendo su resolución usando aniones quirales como TRISPHAT o BINPHAT (*Figura 8*).

[10] G. Liang, A. Wang, L. Li, G. Xu, N. Yan, T. Zhang, *Angew. Chem. Int. Ed.*, **2017**, *56*, 3050.
[11] R.L. Jones, R.C. Brian, R.F. Homer, J. Stubbs, *Nature*, **1958**, *181*, 446.
[12] US Environmental Protection Agency (EPA). Pesticide Poisoning Handbook. (**2005**) Chapter 12. Paraquat and Diquat.
[13] a) C. Pasquini, V. Desvergnes-Breuil, J.J. Jodry, A. Dalla Cort, J. Lacour, *Tetrahedron Lett.,* **2002**, *43*, 423. b) J. Vachon, G. Bernandinelli, J. Lacour, *Chem. Eur. J.*, **2010**, *16*, 2797.

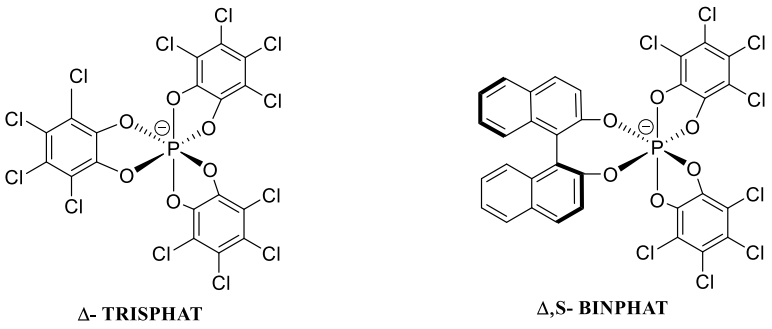

Figura 8. Estructura del TRISPHAT y el BINPHAT.

En el diquat y sus derivados, la complejidad radica en los cambios conformacionales/configuracionales presentes y también en su capacidad para interaccionar con moléculas aniónicas quirales. La combinación de aromaticidad y carácter dicatiónico ha sugerido que estos compuestos pudieran interaccionar con la hebra de ADN, no solo como polianión sino también como agentes intercalantes de forma análoga al bromuro de etidio (*Figura 9*).[14]

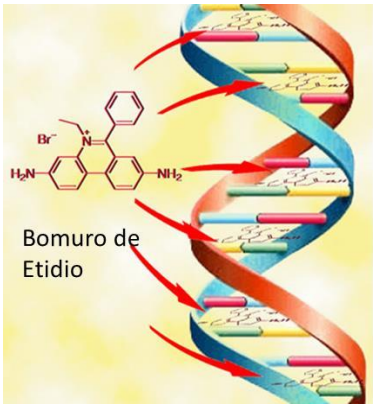

Figura 9. Estructura del bromuro de etidio, molécula capaz de intercalar en la hebra de ADN.

Esta interacción entre una biomolécula como el ADN y una molécula como el diquat **1** constituye otro ejemplo de complejidad, una **complejidad supramolecular**, en donde la formación de enlaces no covalentes es la base de la interacción de acuerdo con la definición dada por J.M. Lehn en 1995.[15]

En otro orden, los llamados *procesos de autoensamblaje* a partir de diferentes moléculas constituyen un método potente a la par que eficaz para la creación espontánea y programada de estructuras complejas y de arquitecturas de escala nanométrica.[16] En este contexto de creación de complejidad a partir de pequeñas moléculas, se puede considerar los procesos de autoensamblaje a partir de ligandos orgánicos pequeños y iones metálicos para crear supermoléculas.

Los cationes metálicos presentan esa posibilidad, ya que poseen números de coordinación variables y una preferencia geométrica dependiendo del tipo de catión (carga, tamaño,

[14] Q. Zhang, C. Wang, W. Liu, X. Zhang, S. Zhuang, *Environ. Chem. Lett.*, **2012**, *10*, 35.
[15] J.M. Lehn, *Supramolecular Chemistry, Concepts and Perspectives*, VCH, Weinheim, **1995**.
[16] a) J.M. Lehn, *Angew. Chem. Int. Ed.*, **1990,** *29*, 1304. b) J.M. Lehn, *Angew. Chem. Int. Ed.*, **1988,** *27*, 90. c) G.M. Whitesides, J.P. Mathias, C.T. Seto, *Science*, **1991**, *254*, 1312. d) D.S. Lawrence, T. Jiang, M. Levett, *Chem. Rev.*, **1995**, *35*, 2229.

estabilidad cinética y termodinámica de complejos formados, afinidad por diferentes ligandos…).

Así surgen los *Metal-Organic Frameworks* (MOF),[17] también llamados polímeros de coordinación porosos (PCP)[18] o redes de coordinación porosas (PCN).[19] Son híbridos orgánico-inorgánicos ensamblados de iones metálicos y ligandos orgánicos. Los MOF combinan las características beneficiosas respectivas de componentes inorgánicos y orgánicos, pero también a menudo exhiben propiedades únicas que exceden las expectativas de una mezcla simple de los componentes, de acuerdo con la clásica definición de sistema complejo.[20]

En los últimos años, se ha dedicado un gran esfuerzo en la síntesis de MOF como nuevos materiales con actividad catalítica y de almacenamiento de gases,[21] así como en diferentes aplicaciones en el campo de la biomedicina.[22]

Uno de los MOF más conocidos es el denominado MOF-5, preparado por Yagui y colaboradores en 2003.[23] Se obtiene fácilmente mezclando óxido de zinc y ácido tereftálico, generando un sólido reticulado de estructura cúbica (*Figura 10*).

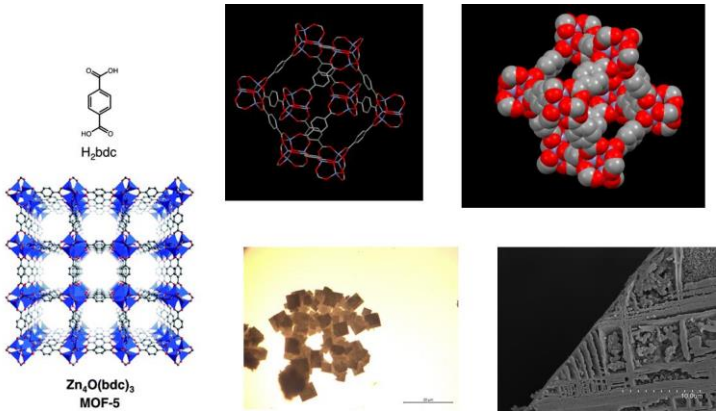

Figura 10. Estructura cúbica del MOF-5. Imágenes obtenidas mediante lupa de aumento y SEM.

Los tres ejemplos comentados hasta ahora: el **glicoaldehído**, el **diquat** y el **MOF-5**, han sido los objetivos fundamentales de esta tesis o, mejor dicho, la fuente de inspiración para la creación y/o el estudio sistemático de complejidad molecular o supramolecular.

---

[17] a) S. Lee, E. A. Kapustin, O.M. Yaghi, *Science*, **2016**, *353*, 808. b) H. Li, M. Eddaoudi, M. O'Keeffe, O.M. Yaghi, *Nature*, **1999**, *402*, 276. c) B. Moulton, M.J. Zaworotko, *Chem. Rev.*, **2001,** *101*, 1629.

[18] a) T. Kajiwara, M. Fujii, M. Tsujimoto, K. Kobayashi, M. Higuchi, K. Tanaka, S. Kitagawa, *Angew. Chem. Int. Ed.*, **2016**, *55*, 2697. b) M.L. Foo, R. Matsuda, Y. Hijikata, R. Krishna, H. Sato, S. Horike, A. Hori, J.G. Duan, Y. Sato, Y. Kubota, M. Takata, S. Kitagawa, *J. Am. Chem. Soc.*, **2016,** *138*, 3022. c) J. Reboul, S. Furukawa, N. Horike, M. Tsotsalas, K. Hirai, H. Uehara, M. Kondo, N. Louvain, O. Sakata, S. Kitagawa, *Nat. Mater.*, **2012**, *11*, 717.

[19] a) H. Kitagawa, H. Ohtsu, M. Kawano, *Angew. Chem. Int. Ed.*, **2013**, *52*, 12395. b) J.Y. Park, D.W. Feng, H.C. Zhou, *J. Am. Chem. Soc.*, **2015**, *137*, 11801. c) D.W. Feng, T.F. Liu, J. Su, M. Bosch, Z.W. Wei, W. Wan, D.Q. Yuan, Y.P. Chen, X. Wang, K.C. Wang, X.Z. Lian, Z.Y. Gu, J. Park, X.D. Zou, H.C. Zhou, *Nat. Commun.*, **2015**, *6*, 5979.

[20] a) T.R. Cook, Y.R. Zheng, P.J. Stang, *Chem. Rev.*, **2013**, *113*, 734. b) H.C. Zhou, J.R. Long, O.M. Yaghi, *Chem. Rev.*, **2012**, *112*, 673.

[21] a) S.M.J. Rogge, A. Bavykina, J. Hajek, H. Garcia, A.I. Olivos-Suarez, A. Sepúlveda-Escribano, A. Vimont, G. Clet, P. Bazin, F. Kapteijn, M. Daturi, E.V. Ramos-Fernandez, F.X. Llabres i Xamena, V. Van Speybroeck, J. Gascon, *Chem. Soc. Rev.*, **2017**, *46*, 3134. b) L. Zhu, X.Q Liu, H.L. Jiang, L.B. Sun, *Chem. Rev.*, **2017**, *117*, 8129. c) J. Gascon, A. Corma, F. Kapteijn, F.X. Llabres i Xamena, *ACS Catal.*, **2014**, *4*, 361. d) A. Corma, H. Garcia, F.X. Llabres i Xamena, *Chem. Rev.*, **2010**, *110*, 4606.

[22] P. Horcajada, R. Gref, T. Baati, P.K. Allan, G. Maurin, P. Couvreur, G. Férey, R.E. Morris, C. Serre, *Chem. Rev.*, **2012**, *112*, 1232.

[23] L.N. Rosi, J. Eckert, M. Eddaoudi, D.T. Vodak, J. Kim, M. O'Keefe, O.M. Yaghi, *Science*, **2003**, *300*, 1127.

Para ello, nos hemos basado en la idea de la utilización de diferentes metodologías sintéticas que nos permitiesen generar moléculas diversas que pudieran tener interesantes aplicaciones a partir de cada uno de los ejemplos comentados.

En la *primera parte* de esta tesis, se han abordado las **'REACCIONES DE AUTOTRANSFERENCIA DE HIDRÓGENO DE AMINAS AROMÁTICAS Y DIOLES CON CATÁLISIS HETEREOGÉNEA'**.

En el año 2006, en un artículo de Carey y colaboradores[24] mostraron un estudio de las reacciones utilizadas en la preparación de moléculas candidatas a fármacos (hits) basado en los departamentos de Process Chemistry R&D de Glaxo Smith Kline, Astra Zeneca y Pfizer. En este trabajo sobre 128 hits y 1.039 transformaciones se observó que un 19% (196 reacciones) correspondieron a alquilaciones de heteroátomos, un 11% a formación de enlaces C-C y 5% a la formación de heterociclos aromáticos, entre otros muchos tipos de reacciones estudiadas. Del 19% de alquilaciones de heteroátomos, un 57% corresponde a la formación de enlaces C-N y, de estas, un 36% corresponde a las alquilaciones con haluros de alquilo y un 20% a la alquilación reductiva. Ambos tipos de reacciones suelen además estar implicadas en la formación de heterociclos. Así pues, se constata la importancia de las alquilaciones de aminas en el campo de la Química Médica.

Los métodos de alquilación de aminas son variados.[25] En términos generales, las alquilaciones con haluros de alquilo son problemáticas debido a su toxicidad, especialmente a escala industrial, y también a que presentan productos de polialquilaciones (*Figura 11a*). Otros métodos más eficaces consisten en la preparación de amidas y posterior reducción, o bien la preparación de iminas y reducción, pero estos requieren procesos reductivos con hidruros o hidrógeno que necesitan especiales condiciones de seguridad además de producir residuos.

Las nuevas metodologías basadas en reacciones como la *Autotransferencia de Hidrógeno con catálisis heterogénea* entran en este campo ofreciendo alternativas sostenibles, verdes y además a precios competitivos ya que emplean como agente alquilante alcoholes (*Figura 11b*).

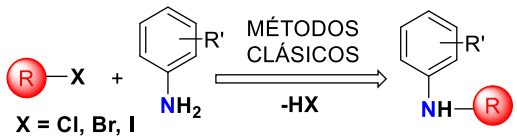

a) Ruta tradicional usando reacciones con haluros de alquilo

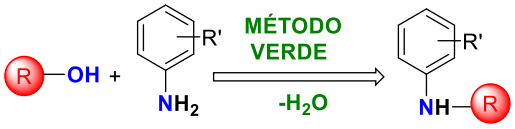

b) Ruta verde usando reacciones de autotransferencia de hidrógeno

Figura 11. a) Ruta tradicional de alquilación de aminas. **b)** Ruta alternativa más verde basada en las reacciones de Autotransferencia de Hidrógeno.

[24] J.S. Carey, D. Laffan, C. Thomson, M.T. Williams, *Org. Biomol. Chem.*, **2006**, *4*, 2337.
[25] M.B. Smitth, J. March, *March's Advanced Organic Chemistry*, Wiley-Interscience, New York, **2001**, 4.

Las reacciones de Autotransferencia de Hidrógeno (**H**ydrogen **A**utotransfer)(**HA**),[26] también denominadas de Préstamo de Hidrógeno (**B**orrowing **H**ydrogen)(**BH**)[27] son un tipo de reacciones de transferencia de hidrógeno en las cuales un sustrato, que puede considerarse no activado (alcohol, amina o alcano), se activa por deshidrogenación mediada por un catalizador, dando lugar a un sustrato más reactivo (aldehído o cetona, imina o alqueno), el cual reacciona y forma un producto que se hidrogena regenerando a su vez al catalizador (*Esquema 2*).

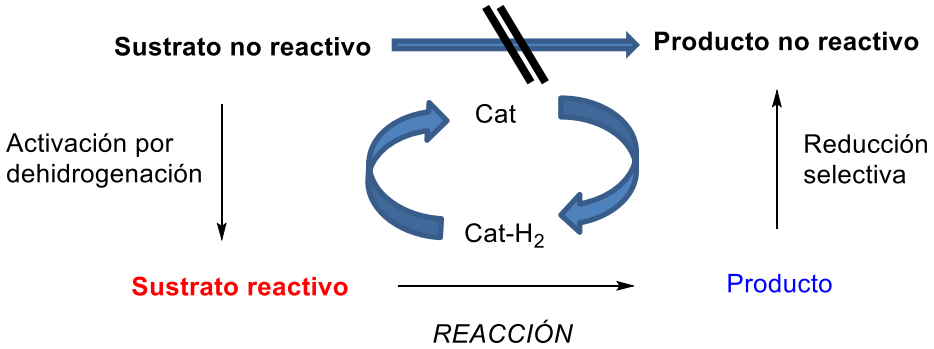

Esquema 2. Esquema genérico de las reacciones de Autotransferencia de Hidrógeno.

En este tipo de reacciones no hay reducción ni oxidación neta, solo hay un paso intermedio en el que el catalizador capta temporalmente hidrógeno del sustrato para dar lugar al sustrato activado, que es capaz de reaccionar y formar un producto que finalmente se hidrogena de nuevo. Se entiende que es un préstamo o una autotransferencia de hidrógeno, en cuanto que el catalizador solo lo capta temporalmente del sustrato y luego lo devuelve al producto. Cabe destacar que en función del tipo de catalizador elegido la reacción procederá mediante un intermedio de monohidruro o dihidruro metálico.

La mayor parte de las reacciones HA/BH se han estudiado con catálisis homogénea usando complejos de metales como el Rutenio, Iridio, Paladio y son mucho menores los estudios con catálisis heterogénea donde estos metales se encuentran soportados en sólidos inertes (carbono, alúmina, TiO_2 etc.).[28]

Aunque los procesos llevados a cabo con catálisis homogénea son mucho más eficaces, presentan el gran inconveniente del elevado coste económico del catalizador que termina perdiéndose en el transcurso de la purificación. Por el contrario, la catálisis heterogénea, permite la recuperación del catalizador por filtración y su reutilización, por lo que desde un punto de vista industrial y medioambiental tiene enormes ventajas.[28]

Las reacciones HA/BH son de una gran eficiencia atómica, ya que son capaces de conseguir la activación de sustratos sin utilizar gran número de reactivos ni hidrógeno molecular, por lo que están englobadas en el campo de la Química Verde.[29] Además, por norma general el subproducto de estas es una molécula de agua.

Aunque las reacciones de Autotransferencia de Hidrógeno pueden clasificarse en función del sustrato que se activa, en nuestro caso nos interesa centrarnos solo en la **activación de alcoholes** y más concretamente de **etilenglicol** o **glicoles**.

---

[26] G. Guillena, D.J. Ramon, M. Yus, *Chem. Rev.*, **2010**, *110*, 1611.
[27] M. Hamid, P.A. Slatford, J.M.J. Williams, *Adv. Synth. Catal.*, **2007**, *349*, 1555.
[28] a) A. Corma, J. Navas, M.J. Sabater, *Chem. Rev.*, **2018**, *118(4)*, 1410-1459. b) Q. Yan, Q. Wang, Z. Yu, *Chem. Soc. Rev.*, **2015**, *44*, 2305-2329. c) K. Shimizu, *Catal. Sci. Technol.*, **2015**, *5*, 1412.
[29] P.T. Anastas, J.C. Warner, *Green Chemistry: Theory and Practice*, Oxford University Press, New York, **1998**, p.30.

Los alcoholes se activan a aldehídos o cetonas, los cuales, por el mecanismo comentado anteriormente reaccionan con aminas para dar lugar a reacciones de *N*-alquilación.[27, 29, 30] Estas son las reacciones de Autotransferencia de Hidrógeno más estudiadas y en ellas hemos centrado nuestra atención.[28]

Cuando se utiliza etilenglicol (1,2-etanodiol), el primer proceso que se puede formar es su oxidación a **glicoaldehído**. Este proceso no debería ser fácil y, si se formase este aldehído (que como ya hemos indicado anteriormente no es comercial), debería ser muy reactivo por lo que fácilmente se incorporaría al ciclo correspondiente (*Esquema 3*).

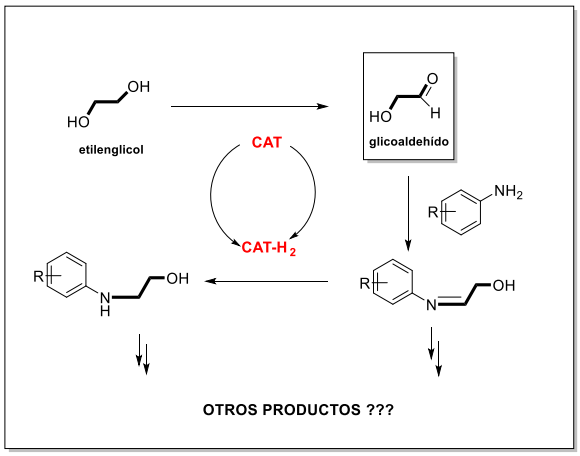

Esquema 3. Reacción de Autotransferencia de Hidrógeno utilizando etilenglicol, del cual se puede obtener glicoaldehído, que rápidamente debería reaccionar con un nucleófilo, en este caso una anilina. El ciclo se completaría con la hidrogenación de la imina formada para obtener un β-amino alcohol.

Naturalmente, cualquiera de los productos intermedios podría seguir reaccionando por otros caminos iniciando una *Reacción Domino*[31] que pararía cuando se alcanzasen productos termodinámicamente estables.

Así, teniendo en cuenta estos antecedentes, los **objetivos** de esta primera parte han sido:

- *Conseguir un sistema catalítico heterogéneo que pueda transformar el etilenglicol en glicoaldehído.*

- *Utilizar estas condiciones con una metodología de Autotransferencia de Hidrógeno (o Préstamo de Hidrógeno) para alquilar aminas aromáticas y obtener β-amino alcoholes.*

- *Utilizar esta metodología para explorar sus posibilidades en la creación de complejidad molecular aplicable a la síntesis de productos de alto valor añadido.*

[30] a) D.M. Roundhill, *Chem. Rev.*, **1992**, *92*, 1. b) S. Narayanan, K. Deshpande, *Appl. Catal. Gen.*, **2000**, *199*, 1. c) T.D. Nixon, M.K. Whittlesey, J.M.J. Williams, *Dalton Trans.*, **2009**, 753. d) A.J.A. Watson, J.A.G. Williams, *Science*, **2010**, *329*, 635.
[31] L.F. Tietze, *Chem. Rev.,* **1996**, *96*, 115.

La *segunda parte* de esta tesis se basa en la '**SÍNTESIS DE NUEVOS DIQUATS BASADOS EN [1,2,3]TRIAZOLO[1,5-*a*]PIRIDINAS Y [1,2,3]TRIAZOLO[1,5-*a*]QUINOLINAS Y SU INTERACCIÓN CON ADN'**.

Partiendo de la complejidad molecular del diquat y sus derivados, basada en los equilibrios conformacionales que generan ejes quirales, estos pueden presentarse como enantiómeros. Los derivados de diquat más estudiados se basan en 2,2'-bipiridinas (**BIPY**) más o menos funcionalizadas en función de los objetivos de los diferentes equipos de investigación.

En nuestro caso, nuestro grupo de investigación ha estudiado exhaustivamente la química de las [1,2,3]triazolo[1,5-*a*]piridinas y benzoanálogos,[32] como la [1,2,3]triazolo[1,5-*a*]quinolina.

Existen algunas triazolopiridinas como la 3-(2-piridil)-[1,2,3]triazolo[1,5-*a*]piridinas[33] y triazoloquinolinas como la 3-(2-piridil)-[1,2,3]triazolo[1,5-*a*]quinolina[34] que presentan una analogía estructural con las 2,2'-bipiridinas y, en consecuencia, son susceptibles de formar diquats por reacción de alquilación con 1,2-dibromoetano o 1,3-dibromopropano (*Figura 12*).

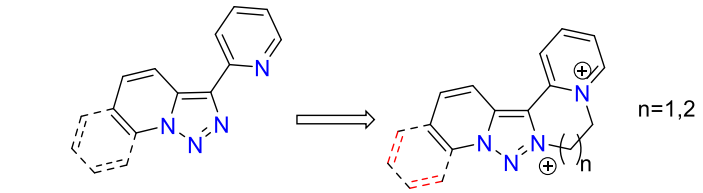

Figura 12. Propuesta de obtención de derivados de diquats a partir de 3-(2-piridil)-[1,2,3]triazolo[1,5-*a*]piridina o 3-(2-piridil)-[1,2,3]triazolo[1,5-*a*]quinolina.

Al no ser sistemas simétricos como los basados en la 2,2'-bipiridina, estos sistemas serían mucho más complejos desde el punto de vista electrónico, de conformación y de configuración, además de romper con la simetría C2 presente en los sistemas originales, cosa que facilitaría un estudio profundo de sus espectros de RMN.

Así pues, los **objetivos** generales de esta segunda parte consistirían en:

- *La preparación de estos nuevos derivados de diquat basados en triazolopiridinas y triazoloquinolinas, su estudio estructural, configuracional y conformacional.*

- *Estudiar las propiedades fisicoquímicas de estos derivados en relación con los diquats conocidos.*

- *Estudiar la interacción con ADN mediante técnicas espectroscópicas (UV-Vis, fluorescencia) para establecer la posibilidad de que estas moléculas pudieran tener actividad antineoplásica.*

[32] B. Abarca, R. Ballesteros-Garrido, *1,2,3-Triazoles Fused to Aromatic Rings from Chemistry of 1,2,3-triazoles.* Editors: Dehaen W, Bakulev V, Springuer A. Switzerland. **2015**, 325-378.
[33] a) P.L. Bataglia, M. Carcelli, F. Ferraro, L. Mavilla, C. Pilizzi, G.L. Pilizzi, *Chem. Soc. Dalton Trans.*, **1994,** 2651. b) B. Abarca, R. Ballesteros, M. Elmasnaouy, *Tetrahedron,* **1998,** *54,* 15287.
[34] R. Ballesteros-Garrido, F. Blanco, R. Ballesteros, F.R. Leroux, B. Abarca, F. Colobert, I. Alkorta, J. Elguero, *Eur. J. Org. Chem.*, **2009**, *33*, 5765.

La *tercera y última parte* de esta tesis, que lleva por título '**PREPARACIÓN DE METAL-ORGANIC FRAMEWORKS (MOF) Y ESTUDIO DE SUS APLICACIONES'**, se basa en la utilización de sólidos reticulados conocidos como MOF (Metal-Organic Frameworks) para la creación de complejidad por interacción de estos materiales con diferentes moléculas. La encapsulación de moléculas de interés fisicoquímico o farmacológico, el estudio de su velocidad de difusión y las aplicaciones que pudieran derivarse son algunos de los aspectos que se abordarán.

La idea fundamental de esta parte trata de utilizar MOF como contenedores de moléculas, de forma que las moléculas contenidas en los huecos de las redes cristalinas puedan estudiarse en estado sólido donde muchas veces presentan propiedades completamente diferentes a moléculas en disolución. Es decir, que los MOF puedan actuar como *disolventes sólidos*.

Recientemente, Ballesteros-Garrido y colaboradores[35] han publicado sobre estas ideas utilizando MOF-5 para contener en su interior **PDA** (perylene-3,4,9,10-tetracarboxylic dianhydride) (*Figura 13*). Esta molécula no es fluorescente en disolución, sin embargo, mostró una intensa fluorescencia una vez se ha introducido en el MOF-5 (PDA@MOF-5).

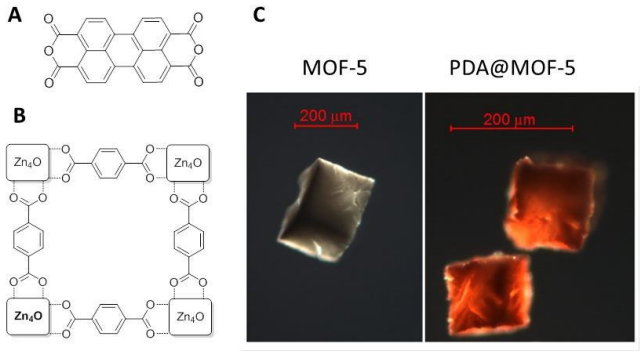

Figura 13. a) Estructura del PDA, **b)** Representación de la celda unidad del MOF-5, **c)** Imágenes de microscopio óptico del MOF-5 (izquierda) y PDA@MOF-5 (derecha).

En disolución, las interacciones π-staking (agregación) entre moléculas de PDA, desactivan la fluorescencia de la propia molécula. Sin embargo, cuando el PDA, se encuentra dentro del MOF-5 ya no es posible formar las interacciones π-staking y es entonces cuando puede observarse la fluorescencia (*Figura 14*).

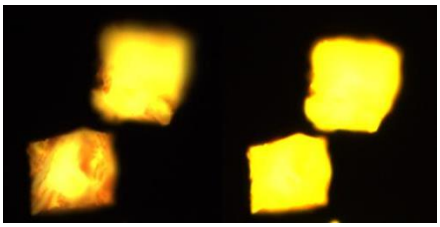

Figura 14. Imágenes de microscopio óptico de PDA@MOF-5 seco.

Estos resultados nos han llevado a plantear la posibilidad de cambiar los habituales ligandos del MOF-5 (ácido tereftálico) por otros ligandos que no presenten aromaticidad y, en consecuencia, que sean transparentes en el rango de los 250 nm, para poder así estudiar desde el punto de vista de las propiedades fisicoquímicas el encapsulamiento de moléculas como el pireno, antraceno, etc.

[35] R. Ballesteros-Garrido, A.P. da Costa, P. Atienzar, M. Alvaro, C. Baleizao, H. Garcia, *RSC Adv,* **2016,** *6*, 35191.

Además, la encapsulación de moléculas de interés biológico o farmacológico es de gran interés debido a que la posterior liberación de estas moléculas puede llevarse a cabo de forma lenta y controlada. Así, el estudio cinético de esta difusión permitiría la utilización de los MOF como dosificadores (*Figura 15*).

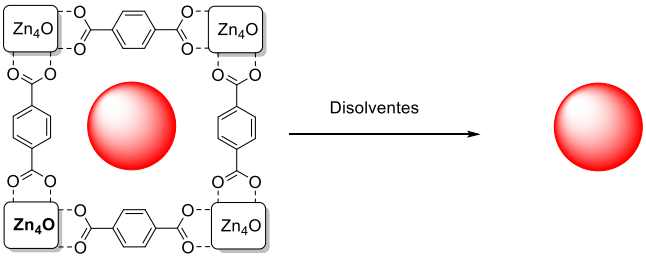

Figura 15. Encapsulación y posterior liberación controlada de moléculas en el interior de la estructura del MOF.

También es de gran interés el estudio de la relación entre los componentes atómicos y moleculares de un MOF y su posterior aspecto a escala macroscópica (geometría, color, tamaño…). Mientras que los dos primeros aspectos han sido estudiados, el control del tamaño de cristal obtenido no es un campo muy investigado. Obtener cristales de gran tamaño (a partir del milímetro de arista) permitiría su manejo individual (mono-cristal) y abriría un campo de aplicaciones.

Así, los **objetivos** de esta tercera parte se podrían formular como:

- *Síntesis de MOF análogos al MOF-5 con ligandos transparentes al UV. Encapsulación de derivados aromáticos policíclicos y estudio de sus propiedades fisicoquímicas.*

- *Estudio de la relación entre la síntesis de MOF-5 y tamaño de cristales. ¿Puede controlarse el tamaño de los MOF?*

PARTE I: REACCIONES DE AUTOTRANSFERENCIA DE HIDRÓGENO O PRÉSTAMO DE HIDRÓGENO (AH/BH) DE AMINAS AROMÁTICAS Y DIOLES CON CATÁLISIS HETEREOGÉNEA

Capítulo 1

Introducción y objetivos

Introducción

La Química, como ciencia que transforma la materia, ha sido la responsable de la preparación de centenares de miles o millones de moléculas que han permitido a la sociedad avanzar hasta alcanzar los límites que hoy en día disponemos en energía, alimentación o en salud. El químico, como arquitecto de la materia, en palabras de E. Coronado, "es capaz de diseñar y crear moléculas cada vez más complejas, moléculas que presentan propiedades físicas, químicas y biológicas que pueden ser de gran interés".[36] Hoy en día, la optimización de condiciones para llevar a cabo reacciones químicas conocidas permitiendo que preserven el medio ambiente y el desarrollo sostenible, constituyen el objeto de una rama de la química denominada "*Química Verde*" o "*Green Chemistry*".

Los principios básicos de esta disciplina que formularon en 1988 Anastas y Warner[29] pueden condensarse en doce puntos:

1. PREVENCIÓN. Es preferible evitar la formación de residuos a tener que realizar su tratamiento cuando ya se han formado.
2. ECONOMÍA ATÓMICA. Los diseños de rutas sintéticas deben permitir la máxima incorporación en el producto final de los materiales utilizados como reactivos.
3. SÍNTESIS MENOS TÓXICAS. Se deben diseñar las rutas sintéticas de manera que se generen sustancias que tengan baja o ninguna toxicidad para la salud humana y el medio ambiente.
4. DISEÑO DE PRODUCTOS QUÍMICOS SEGUROS. Los nuevos compuestos sintetizados deben preservar la eficacia y reducir la toxicidad.
5. EMPLEO DE DISOLVENTES SEGUROS. El uso de sustancias auxiliares en la reacción (disolventes, absorbentes, etc.) debe ser mínimo e inocuo. Deben evitarse disolventes halogenados.
6. DISMINUCIÓN DEL CONSUMO DE ENERGÍA. Los requerimientos energéticos deben considerarse por su impacto económico y en el ambiente, y deben ser minimizados, priorizando metodologías a temperatura y presión ambiente.
7. EMPLEO DE MATERIAS PRIMAS PROVENIENTES DE RECURSOS RENOVABLES.
8. REDUCCIÓN DE LOS PRODUCTOS DERIVADOS. Evitar pasos intermedios innecesarios en las rutas sintéticas.
9. USO DE PROCESOS DE CATÁLISIS. Dar preferencia a reactivos catalíticos (homogéneos, heterogéneos, etc.) frente a los estequiométricos.
10. DISEÑO PARA LA DEGRADACIÓN. Diseñar los productos químicos para que, al final de su función útil, éstos no persistan en el medio ambiente y se degraden a productos inocuos.
11. ANÁLISIS DE CONTAMINANTES EN TIEMPO REAL. Desarrollar metodologías analíticas que permitan la monitorización y el control en tiempo real de las reacciones químicas.
12. MINIMIZACIÓN DE RIESGOS DE ACCIDENTES QUÍMICOS. Se deben elegir las sustancias a modo de minimizar su potencial riesgo de accidente.

[36] E. Coronado, *Anales de la Real Sociedad Español de Química*, **2011**, *1*, 21-27.

Entre todas las directrices, el uso de reacciones catalíticas para la obtención de compuestos es sin duda una de las más investigadas, siendo un campo de estudio en sí mismo, con el diseño de novedosos catalizadores que permiten realizar reacciones hasta entonces muy difíciles.

Existen un gran número de estructuras moleculares de gran interés para la industria farmacéutica debido a su potencial como precursoras de agentes terapéuticos que, debido a las condiciones de sus metodologías sintéticas, no son suficientemente exploradas, o lo son llevando a cabo síntesis no respetuosas con la 'química verde'. Por ello, la exploración de nuevas rutas sintéticas basadas en procesos catalíticos para la obtención barata, eficiente y 'verde' de estas estructuras tiene un gran potencial hoy en día.

Un ejemplo de estructuras moleculares de interés farmacológico son los β-amino alcoholes aromáticos. Estas estructuras, de apariencia simple, poseen un esqueleto particular que les permite ser precursores de gran número de moléculas con demostradas propiedades terapéuticas, como las morfolinas, pirazinas, carbenos *N*-heterocíclicos, *N*-arilaminoacidos, indoles…entre otras muchas moléculas que ya se comercializan como fármacos (*Figura I.1*).

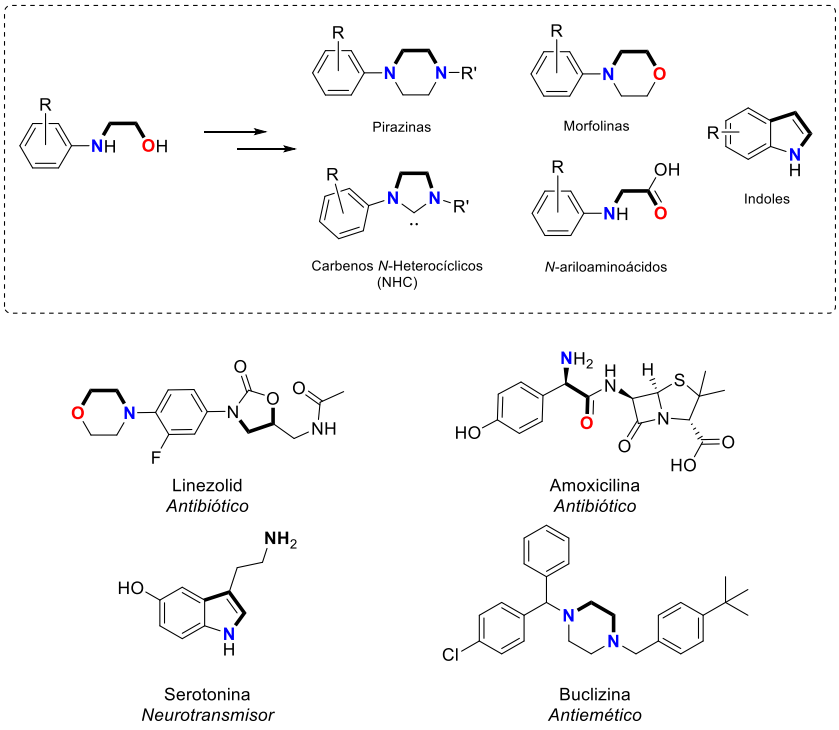

Figura I.1. Estructuras de interés farmacológico y fármacos comercializados que presentan el esqueleto de β-amino alcoholes en su estructura.

La obtención clásica de β-amino alcoholes aromáticos conlleva el uso de agentes halogenados (2-cloroetanol o 2-bromoetanol), apertura térmica de epóxidos, etc (*Esquema I.1*). Todas ellas de poco interés para la industria farmacéutica.

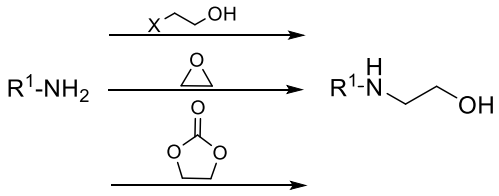

Esquema I.1. Metodologías clásicas de obtención de β-amino alcoholes

Conseguir una síntesis de β-amino alcoholes aromáticos que cumpla con la mayoría de los preceptos de la 'química verde' sería sin duda provechoso para la industria farmacéutica, que dispondría fácilmente de un precursor de varias estructuras muy útiles en química médica.

En esta línea, se evaluó la capacidad de las reacciones de Autotransferencia de Hidrógeno para llevar a cabo la alquilación. Las reacciones de Autotransferencia de Hidrógeno,[26,27,28] como se ha expuesto en la introducción general, son reacciones catalíticas que comienzan con la reducción de, por ejemplo, un alcohol (también amina o alcano) mediante un catalizador con capacidad de captar hidrógeno, generando así un aldehído o cetona (o imina o alqueno). En presencia de, por ejemplo, una amina, puede darse lugar a una imina, perdiéndose una molécula de agua. El catalizador hidrogenado puede transferir los hidrógenos a esa imina, generando finalmente una amina alquilada (*Esquema I.2*).

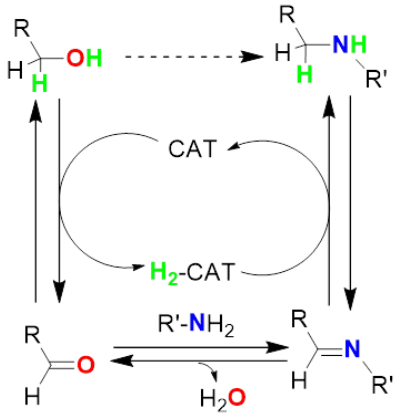

Esquema I.2. Mecanismo general de las reacciones de Autotransferencia de Hidrógeno entre alcoholes y aminas.

Como se ve, es un proceso que cumple con varios preceptos de la 'Química Verde' (ver página 33) en cuanto a que no genera más residuos que una molécula de agua (1), cuenta con una gran economía atómica (2), no genera sustancias químicas peligrosas (3), se evita el uso de sustancias halogenadas (5), no existen productos intermedios (8) y es un proceso catalítico (9).

En el año 2012, en el marco de la Tesis Doctoral de la Dra. Rosa Adam, se comenzó a explorar en nuestro grupo el uso de las reacciones de Autotransferencia de Hidrógeno para hidrogenar y alquilar quinolinas, obteniendo 1,2,3,4-tetrahidroquinolinas y 1,2,3,4-tetrahidroquinolinas alquiladas (*Esquema I.3*).[37]

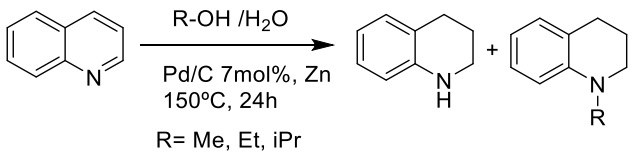

Esquema I.3. Propuesta de aplicación de la Autotransferencia de Hidrógeno a la hidrogenación y posterior alquilación de quinolinas.

El uso de etilenglicol al final del artículo abrió la puerta a la obtención de indoles derivados de 1,2,3,4-tetrahidroquinolina. Nunca llegó a detectarse el producto β-amino alcohólico, ya que

[37] B. Abarca, R. Adam, R. Ballesteros, *Org. Biomol. Chem.*, **2012**, *10*, 1826.

se producía una ciclación intramolecular con el anillo aromático, resultando en el indol derivado de la tetrahidroquinolina, un producto final de mucho interés (*Esquema I.4*).

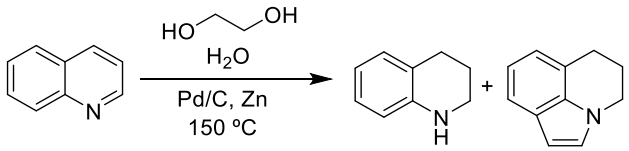

Esquema I.4. Alquilación de quinolina con etilenglicol y obtención de indoles.

Cabe destacar que para que esta reacción tuviera luga, el etilenglicol tuvo que transformarse en glicoaldehído, y este reaccionar rápidamente con la 1,2,3,4-tetrahidroquinolina. Como se comentó en la introducción general, la obtención de glicoaldehído es muy difícil, y con este método logramos controlar su obtención, y además su reactividad.

A raíz de este trabajo se comenzó a explorar la posibilidad de obtener β-amino alcoholes a partir de aminas y etilenglicol en nuestro grupo, eligiendo aminas que no pudieran derivar en otros productos una vez formado el amino alcohol, como en el caso de la quinolina.

Para ello, se optó por retirar la tensión asociada al anillo de 1,2,3,4-tetrahidroquinolina y trabajar con anilinas, desfavoreciendo así la ciclación intramolecular. Los antecedentes bibliográficos de obtención de β-amino alcoholes a partir de anilinas y etilenglicol en una reacción catalítica de Autotransferencia de Hidrógeno consistían en catálisis heterogénea en las cuales no se partía de etilenglicol puro sino de su carbonato cíclico preparado por reacción con carbonato de dietilo y el propio etilenglicol.[38] Además, se usaban condiciones de presión y temperatura elevadas o catalizadores no comerciales difíciles de sintetizar.

En el trabajo de nuestro grupo[37] se usó zinc metal reproduciendo las condiciones de Sasson y colaboradores,[39] pero en el transcurso de la investigación se demostró por Difracción de Rayos X en polvo que el Zn se transformaba en óxido de zinc (ZnO) y que este nuevo catalizador podía seguir utilizándose. Por ello, concluimos que era mucho más interesante utilizar directamente óxido de zinc como co-catalizador ya que este cambio hacía la reacción mucho más sostenible y medio ambientalmente más aceptable.

Así, la propuesta de metodología sintética consistió en la reacción de una anilina disuelta en un medio etilenglicol:agua (donde el etilenglicol actúa a la vez de disolvente y de reactivo), utilizando un catalizador barato y comercial como el Pd/C (captador de hidrógeno), con la ayuda de ZnO como activante del proceso, a presión atmosférica y atmósfera no inerte, a la temperatura y tiempo de reacción necesarios para obtener buenas conversiones y selectividades (*Esquema I.5*).

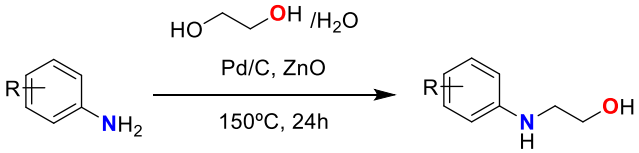

Esquema I.5. Obtención de β-amino alcoholes aromáticos a partir de anilinas y etilenglicol, mediante una reacción de Autotransferencia de Hidrógeno. Condiciones finales optimizadas.

[38] A.B. Shivarkar, S.P. Gupte, R.V. Chaudhari, *Ind. Eng. Chem. Res.*, **2008**, *47(8)*, 2484.
[39] S. Mukhopadhyay, G. Rothenberg, H. Wiener, Y. Sasson, *New J. Chem.*, **2000**, *24*, 305.

Posteriormente, se evaluó el uso de otros dioles para la obtención de β-, γ- o ε-amino alcoholes, aplicando las mismas condiciones de reacción, con el objetivo de evaluar aún más el alcance y los límites de esta metodología sintética (*Esquema I.6*).

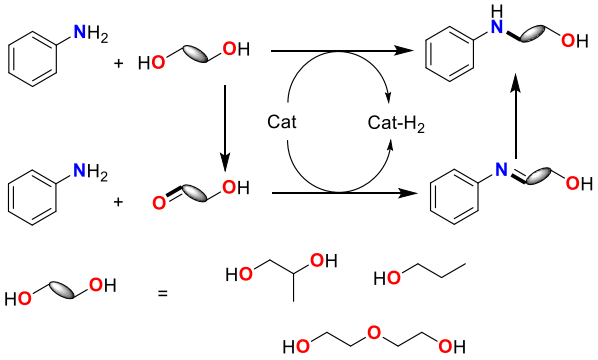

Esquema I.6. Reacciones de Autotransferencia de Hidrógeno con diferentes dioles para la obtención de β-, γ- y ε-amino alcoholes.

Finalmente, y a raíz de la completa caracterización de todos los productos secundarios obtenidos en las reacciones anteriores, se propuso orientar selectivamente esta metodología hacia la formación de indoles, moléculas mucho más relevantes en la industria farmacéutica. Para ello nos basamos en las reacciones de 'Heterogeneous Acceptorless Dehydrogenative Condensation' (HADC) o 'Condensación Deshidrogenativa sin Aceptores Heterogéneos', descritas por Kempe y colaboradores en 2017[40] (*Esquema I.7*).

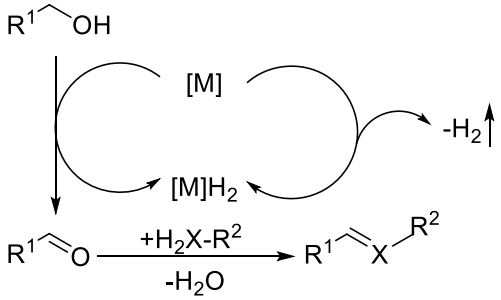

Esquema I.7. Ruta genérica de una Condensación Deshidrogenativa sin Aceptores Heterogéneos.

La idea era desfavorecer el proceso de la Autotransferencia de Hidrógeno, evitando la re-hidrogenación del intermedio imínico, promoviendo así la tautomerización de la cadena alifática hacia el derivado aldehído, buscando la ciclación intramolecular para la posterior formación de un derivado indólico (*Esquema I.8*).

[40] T. HIlle, T. Irrgang, R. Kempe, *Angew. Chem. Int. Ed.* **2017**, *56,* 371.

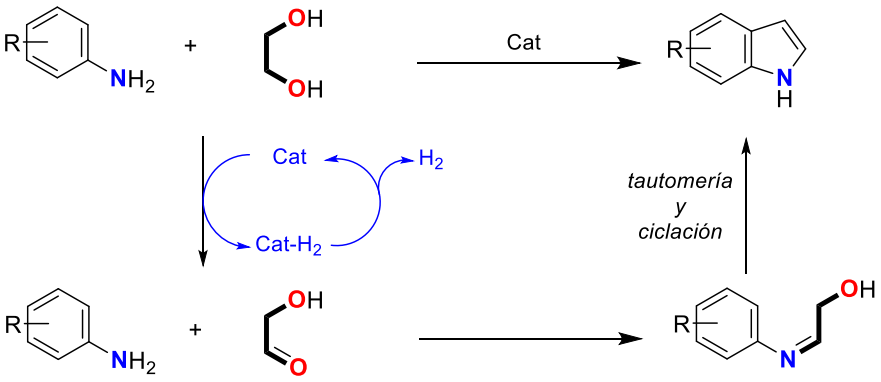

Esquema I.8. Propuesta de obtención de indoles mediante un proceso HADC con aminas aromáticas y etilenglicol.

Resultados similares con bajísimos rendimientos se habían propuesto por Watanabe y colaboradores[41] usando catálisis homogénea de rutenio y sin proponer un mecanismo claro. Shim y colaboradores[42] utilizaron etanolamina y catálisis homogénea con Rutenio y cloruro de estaño, mientras que Jianjun y colaboradores[43] lo consiguieron también usando catálisis heterogénea con plata.

Objetivos

Teniendo en cuenta lo expuesto anteriormente y siguiendo la línea de investigación sobre las reacciones de Autotransferencia de Hidrógeno para la obtención de amino alcoholes y derivados, los objetivos propuestos en esta primera parte de la tesis doctoral son:

- Elaborar y optimizar una metodología catalítica novedosa que permita la obtención de β-amino alcoholes aromáticos partiendo de moléculas sencillas como son las anilinas, utilizando disolventes no halogenados, catalizadores baratos y condiciones de reacción que no requieran atmósfera inerte.
- Evaluar tanto el alcance como los límites de esta metodología: uso de diferentes anilinas, dioles y catalizadores.
- Controlar la selectividad de esta metodología para derivarla a la obtención de indoles.
- Estudiar el proceso tautomérico de esta metodología.

[41] Y. Tsuji, K.T. Huh, Y. Watanabe, *J. Org. Chem.*, **1987**, *52(9)*, 1673.
[42] C.S. Cho, J.H. Kim, T.J. Kim, S.C. Shim, *Tetrahedron*, **2001**, *57(16)*, 3321.
[43] S. Yanyun, X. Junde, M. Maoqian, L. Jianjun, *J. Chem. Pharm. Res.*, **2013**, *5(12)*, 279.

Capítulo 2

Antecedentes bibliográficos de las Reacciones de Autotransferencia de Hidrógeno con dioles

Las reacciones de Autotransferencia de Hidrógeno son una buena herramienta sintética para, por ejemplo, la aminación de alcoholes, la alquilación de aminas o amoníaco, la formación de heterociclos de nitrógeno aromáticos o no aromáticos, la formación de enlaces C-C, C-N, C-O o C-S, la β-funcionalización de alcoholes o la activación de alquenos.[28,44,45,46]

Una búsqueda en el buscador SciFinder Scholar da una idea del estado de este tipo de reacciones: los resultados escribiendo "Hydrogen Autotransfer" mostraron 77 publicaciones desde 2006, y los resultados escribiendo "Borrowing Hydrogen" mostraron 187 publicaciones desde 2003. Un total de 264 publicaciones en los últimos 15 años muestran la importancia de esta metodología sintética en el ámbito de la catálisis reciente.

Siendo más rigurosos, y centrándonos en la utilización de dioles en lugar de alcoholes, la búsqueda dio como resultado 12 publicaciones conteniendo "Hydrogen Autotransfer" y "Diols" desde 2011, y 36 publicaciones conteniendo "Borrowing Hydrogen" y "Diols" desde 2004.

Por tanto, el uso de dioles en procesos de Autotransferencia de Hidrógeno o Préstamo de Hidrógeno no es nuevo, y se han utilizado en diversas investigaciones.

Algunos trabajos que hoy en día se incluyen en reacciones de HA/BH no fueron en su día así clasificados a pesar de la importancia que presentaban. Watanabe y colaboradores[41] en 1986 plantearon un exhaustivo estudio de la utilización de glicoles y anilinas obteniendo indoles, quinolinas y pirazinas. (*Esquema I.9*)

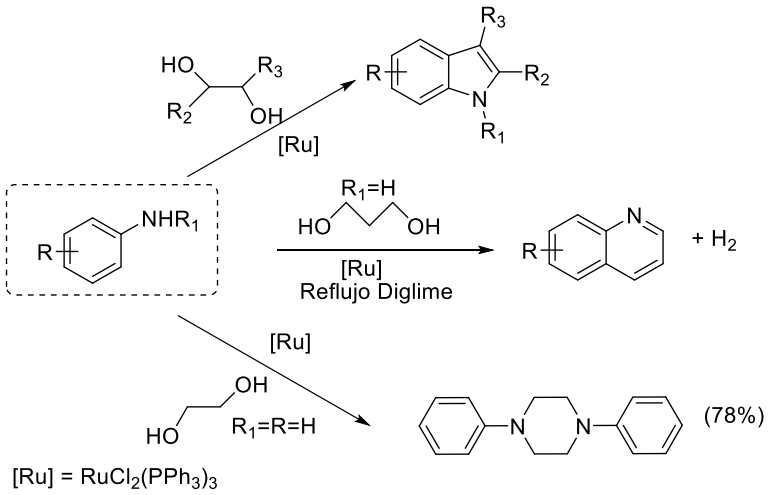

Esquema I.9. Obtención de indoles, quinolinas y pirazinas mediante reacción de anilina con glicoles en una catálisis homogénea con Ru mediante Autotransferencia de Hidrógeno.[41]

Los autores utilizan un complejo de Ru(II) y trifenilfosfina a altas temperaturas (180-200ºC) en autoclaves, utilizando como disolvente en unos casos *diglyme* y en otros los propios glicoles o las anilinas. Aunque se pueden considerar (a tenor de los resultados) excelentes métodos sintéticos para estos heterocíclicos, los rendimientos oscilan entre medios y bajos y dependen mucho de las condiciones de reacción. Mecanísticamente postulan la presencia de aril amino alcoholes pero no los detectan, y cuando los preparan aparte, no obtienen los resultados esperados.

[44] M.H.S.A. Hamid, P.A. Slatford, J.M.J. Williams, *Adv. Synth. Catal.*, **2007**, *349*, 1555.
[45] K. Shimizu, *Catal. Sci. Technol.*, **2015**, *5*, 1412.
[46] A. Corma, J. Navas, M.J. Sabater, *Chem. Rev.*, **2018**, *118*, 1410.

Esta reacción se extrapoló posteriormente a *N*,*N*-dialquilureas obteniéndose 2,3-dihidroimidazol-2-onas con rendimientos medios en condiciones duras de temperatura (180ºC) y presión (THF como disolvente en autoclaves).[47] (*Esquema I.10*)

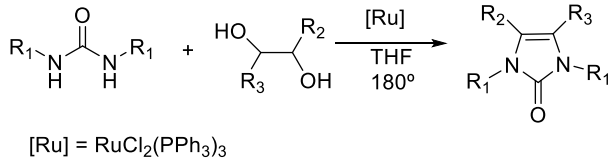

Esquema I.10. Obtención imidazolonas mediante reacción de ureas con glicoles en una catálisis homogénea con Ru mediante Autotransferencia de Hidrógeno.[47]

De forma análoga a Watanabe, en 1990 Doh y colaboradores[48] obtuvieron piperazinas derivadas de la reacción de anilina y etilenglicol, en un proceso de Autotransferencia de Hidrógeno catalizada de manera homogénea por $RuCl_2(PPh_3)_3$ en dioxano a alta temperatura (*Esquema I.11*).

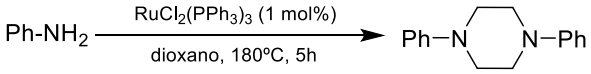

Esquema I.11. Obtención de piperazinas mediante reacción de anilina con etilenglicol en una catálisis homogénea con Ru mediante Autotransferencia de Hidrógeno (Doh *et al*).[48]

Autores como Yamaguchi en 2004,[49] Williams en 2005,[50] Seayad en 2015,[51] Yu en 2011[52] o Ishii en 2009,[53] han descrito reacciones de *N*-alquilación con dioles seguida de ciclación intramolecular generando así aminas cíclicas usando condiciones de catálisis heterogéneas con complejos de iridio, rutenio, etc (*Esquemas I.12-16*).

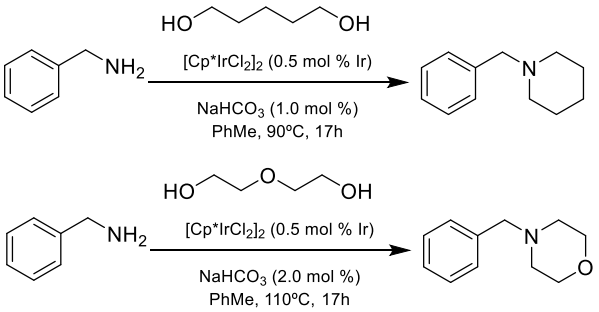

Esquema I.12. Alquilación de aminas con dioles y posterior ciclación intramolecular en una catálisis homogénea con Ir mediante AH (Yamaguchi *et al*).[49]

Williams y colaboradores[50] proponen claramente un mecanismo de "Borrowing Hydrogen" donde la primera etapa es la oxidación del diol para dar lugar al hidroxialdehído que condensa rápidamente con la amina para generar la imina correspondiente. El metal que ha producido la oxidación se encuentra ahora preparado para hidrogenar la imina. Un nuevo ciclo da lugar a un

[47] T. Kondo, S. Kotachi, Y. Watanabe, *Chem. Commun.*, **1992**, 1318.
[48] K.T. Huh, S.C. Shim, C.H. Doh, *Bull. Korean Chem. Soc.*, **1990**, *11 (1)*, 45
[49] K. Fujita, T. Fujii, R. Yamaguchi, *Org. Lett.*, **2004**, *6*, 3525.
[50] G. Cami-Kobeci, P.A. Slatford, M.K. Whittlesey, J.M.J. Williams, *Bioorg. Med. Chem. Lett.*, **2005**, *15*, 535.
[51] S.P. Shan, X. Xiaoke, B. Gnanaprakasam, T.T. Dang, B. Ramalingam, H.V. Huynh, A.M. Seayad, *RSC Adv.*, **2015**, *5*, 4434.
[52] L. Wang, W. He, K. Wu, S. He, C. Sun, Z. Yu, *Tetrahedron Lett.*, **2011**, *52*, 7103.
[53] K. Koda, T. Matsu-ura, Y. Obora, Y. Ishii, *Chem. Lett.*, **2009**, *38*, 838.

aminoaldehido que espontáneamente cicla y se hidrogena obteniéndose las pirrolidinas correspondientes.

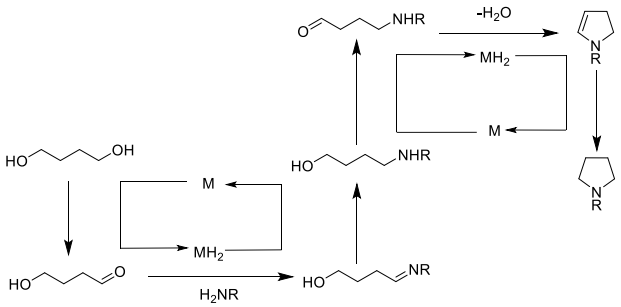

Esquema I.13. Alquilación de aminas con 1,4-butanodiol y posterior ciclación intramolecular en una catálisis con un metal de transición mediante HA/BH (Williams *et al*).[50]

En 2015, Seayad y colaboradores[51] mejoran estos resultados usando un complejo de rutenio mucho más elaborado.

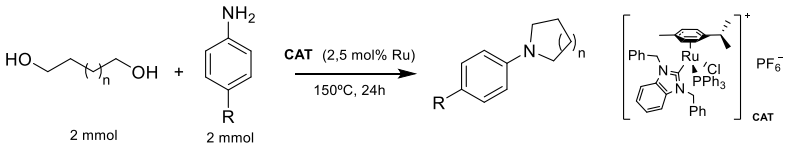

Esquema I.14. Alquilación de anilinas sustituidas con dioles y posterior ciclación intramolecular en una catálisis homogénea con Ru mediante AH (Seayad *et al*).[51]

De forma análoga a los trabajos de Williams[50] y Yamaguchi[49], Yu y colaboradores[52] obtuvieron diaminas a partir de dioles y aminas secundarias, pero usando catálisis heterogénea de Pt/Sn soportados en alúmina.

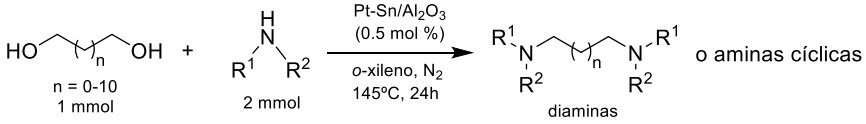

Esquema I.15. Alquilación de aminas con dioles para obtener diaminas o aminas cíclicas por ciclación intramolecular en una catálisis hetereogénea con Pt mediante AH (Yu *et al*).[52]

Ishii y colaboradores[53] obtuvieron derivados benzocondensados de quinolinas e indoles a partir de 1-aminonaftaleno y 1,3-propanodiol o etilenglicol usando catalizadores de iridio en condiciones básicas.

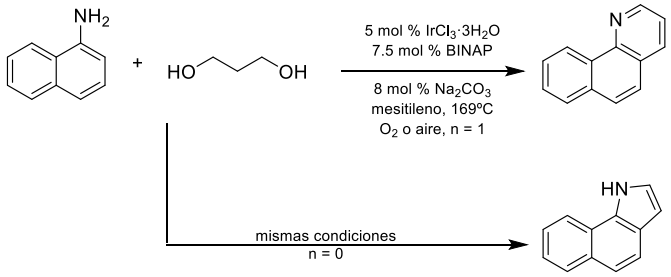

Esquema I.16. Alquilación de 1-naftilamina con 1,2 o 1,3-propanodiol y posterior ciclación intramolecular en una catálisis homogénea con Ir mediante AH (Ishii *et al*).[53]

La formación de indoles a partir de anilinas y dioles o glicoles, ha sido explorada de forma irregular y desde Watanabe ha habido algunos progresos poco sistematizados como puede verse en el caso de Ishii y colaboradores. (*Esquema 1.16).* En el año 2001 Cho y colaboradores[42] publicaron un artículo informando de la obtención de indoles con anilinas y cloruros de etanolamonio usando catálisis homogénea de Rutenio (*Esquema I.17*).

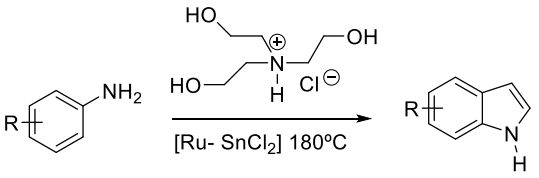

Esquema I.17. Obtención de indol a partir de aminoalcoholes terciarios con catálisis de rutenio y estaño (Cho *et al*).[42]

Posteriormente, en el año 2010 se comunicó una síntesis de 3-metilindol en fase vapor a partir de anilina y glicerina con catálisis heterogénea usando Cu depositado en sílice y alúmina a 340-350ºC, con bajo rendimiento.[54] Con catálisis de Ag-Cd soportada en sílice y etilenglicol a 240ºC en reactor a presión, se obtuvieron también el indol como producto principal.[43] (*Esquema 1.18).*

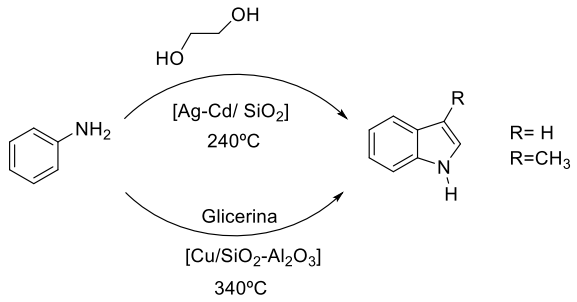

Esquema I.18. Obtención de indoles a partir de anilinas con catálisis hetereogenea de Cu y Ag-Cd (Shi *et al*[54] y Jianjun *et al*[43]).

Dentro de los trabajos con etilenglicol destaca los publicados por R.V. Chaudhari[38] que plantea una ruta eficiente de β-amino alcoholes a partir de anilinas, etilenglicol y dietilcarbonato en presencia de Na-Y zeolitas. Básicamente transforma el etilenglicol en el carbonato de etileno por reacción de transesterificación y este es el reactivo. Es un trabajo exhaustivo, pero se obtienen mezclas y los rendimientos de los aminoalcoholes no son buenos (*Esquema I.19*).

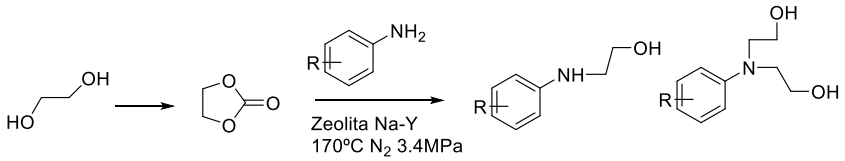

Esquema I.19. Obtención de β-aminoalcoholes a partir de etilenglicol y anilinas con catálisis heterogénea de Zeolitas Na-Y (Chaudhari *et al*[38]).

Es este trabajo el primero que plantea y aísla como intermedios los β-amino alcoholes que Williams[50] en el 2005 había formulado como intermedios. Fabris y colaboradores[55] también han estudiado esta reacción en metanol a 180ºC en presencia de zeolitas obteniendo

[54] W. Sun, D.Y. Liu, H.Y. Zhu, L. Shi, *Catal. Commun.*, **2010**, *12(2)*, 147.
[55] M. Selva, A. Perosa, M. Fabris, *Green Chem.*, **2008**, *10*, 1068.

metilaciones de la anilina usando dimetilcarbonato y β-amino alcoholes usando carbonato de etileno.

El uso de etilenglicol en reacciones HA/BH se llevó a cabo por Adam y colaboradores[37] que estudiaron la alquilación y reducción de quinolinas con alcoholes/agua (o metanol, etanol isopropanol) con catálisis de Pd/C y Zn metal en autoclaves a 150ºC. En estas condiciones el zinc se transforma en óxido de zinc (demostrado por Difracción de Rayos X de Polvo) y este, sigue actuando como catalizador (*Esquema I.20*).

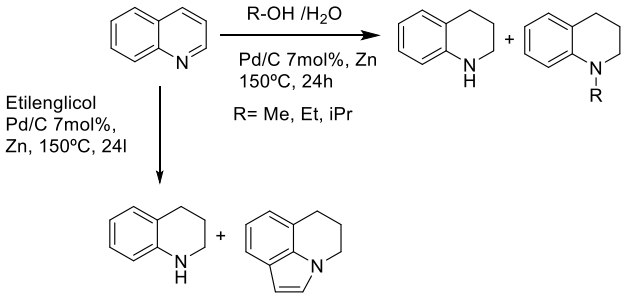

Esquema I.20. Obtención de tetrahidroquinolinas *N*-sustituidas a partir de quinolinas por reacciones HA/BH con alcoholes y obtención de indoles con etilenglicol (Adam *et al*[37]).

Corma y colaboradores[56] utilizando un catalizador bifuncional de Pd/MgO prepararon piperazinas por reacción de etilenglicol con 1,2 diamino compuestos con buenos rendimientos a 160ºC en acetonitrilo (*Esquema I.21*).

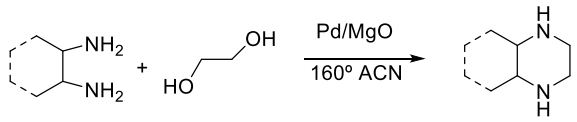

Esquema I.21. Obtención de piperazinas a partir de 1,2- diaminas y etilenglicol (Corma *et al*[56]).

Un aspecto interesante de este trabajo radica en que cuando se usan 1,2-diaminas quirales, se obtienen por lo general piperazinas quirales, no modificándose los centros estereogénicos.

Más recientemente, Beller y colaboradores utilizaron 1,2-dioles para la obtención de γ-butirolactonas mediante Autotransferencia de Hidrógeno seguida de una reacción de Knoevenagel con ciclación intramolecular en 2015,[57] y para la obtención de oxazolidin-2-onas en 2016,[58] siempre en presencia de derivados de Ru y con catálisis homogénea (*Esquemas I.22-23*).

[56] A. Corma, T. Rodenas, M.J. Sabater, *Chem. Eur. J.*, **2010**, *16(1)*, 254.
[57] M. Pena-Lopez, H. Neumann, M. Beller, *Chem. Commun.*, **2015**, *51*, 13082.
[58] M. Pena-Lopez, H. Neumann, M. Beller, *Angew. Chem. Int. Ed.*, **2016**, *55*, 7826.

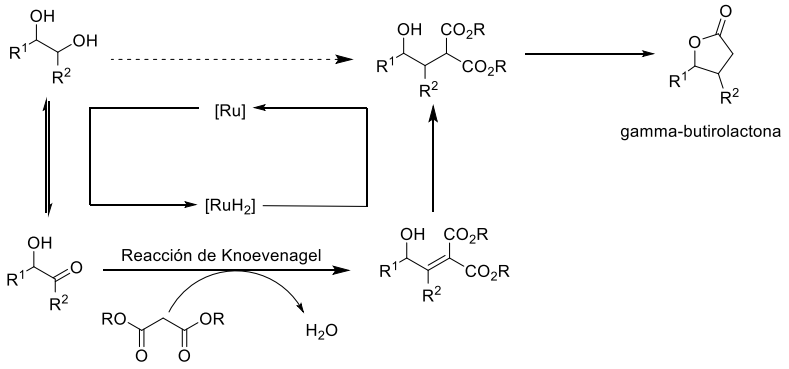

Esquema I.22. Obtención de γ-butirolactonas mediante reacción Autotransferencia de Hidrógeno de un 1,2-diol, seguida de una reacción de Knoevenagel con ciclación intramolecular (Beller *et al*).[57]

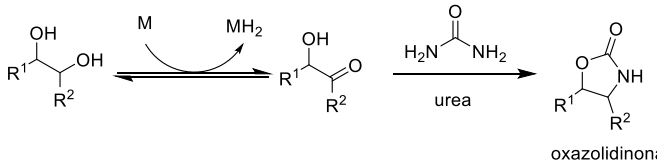

Esquema I.23. Obtención de oxazolidin-2-onas mediante reacción Autotransferencia de Hidrógeno de un 1,2-diol y urea (Beller *et al*).[58]

En 2013, Ohta y colaboradores[59] abordaron también la síntesis de β-amino alcoholes a partir de dioles, mediante la reacción de 1-fenil-1,2-etanodiol, con catálisis homogénea enantioselectiva con Ru (*Esquema I.24*).

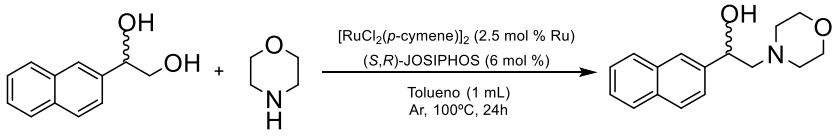

Esquema I.24. Obtención de β-amino alcohol mediante la reacción de un 1,2-diol con morfolina en una reacción Autotransferencia de Hidrógeno catalizada por Ru.[59]

Se puede concluir que el uso de dioles en reacciones de Autotransferencia de Hidrógeno se ha centrado en gran medida en la funcionalización inicial de aminas, para seguir con una reacción posterior que diera lugar a piperazinas, aminas cíclicas, butirolactonas u oxazolidinas, pero casi nunca la reacción se ha detenido en el amino alcohol como tal. La Autotransferencia de Hidrógeno se ha utilizado como etapa previa.

[59] A.E. Putra, Y. Oe, T. Ohta, *Eur. J. Org. Chem.*, **2013**, 6146.

Capítulo 3

Tetrahedron, 2017, 73, 5552-5561

Tetrahedron 73 (2017) 5552–5561

Contents lists available at ScienceDirect

Tetrahedron

journal homepage: www.elsevier.com/locate/tet

β-Amino alcohols from anilines and ethylene glycol through heterogeneous Borrowing Hydrogen reaction

Pedro J. Llabres-Campaner, Rafael Ballesteros-Garrido*, Rafael Ballesteros, Belén Abarca

Departament de Química Orgànica, Universitat de València, Av. Vicent Andrés Estellés s/n, 46100, Burjassot, Valencia, Spain

ABSTRACT

Borrowing Hydrogen (BH), also called Hydrogen Autotransfer (HA), reaction with neat ethylene glycol represents a key step in the preparation of b-amino alcohols. However, due to the stability of ethylene glycol, mono-activation has rarely been achieved. Herein, a combination of Pd/C and ZnO is reported as heterogeneous catalyst for this BH/HA reaction. This system results in an extremely air and moisture stable, and economic catalyst able to mono-functionalize ethylene glycol in water, without further activation of the diol. In this work, different diols and aromatic amines have been explored affording a new approach towards amino alcohols. This study reveals how the combination of two solid species can afford interesting catalytic properties in heterogeneous phase. ZnO activates ethylene glycol while Pd/C is the responsible of the BH/HA cycle. This catalytic system has also been found useful to dehydrogenate indoles affording indolines that undergo in situ BH/HA cycle prior to re-aromatization, representing a tandem heterogeneous process.

Introduction

The development of green processes in organic synthesis represents a major goal nowadays.[1] From atom economy[2] to the use of environmentally friend reagents, many different strategies can be employed for the development of green reactions. Borrowing Hydrogen (BH) reactions[3,4] (also called Hydrogen Autotransfer (HA) reactions[5]) (*Figure 1, top*) represent a unique opportunity for the creation of molecular complexity with extremely high atom economy and, in many cases, under green principles. Important results concerning the preparation of secondary unsymmetrical amines, starting from primary amines and alcohols, are reported. Recently, Michlik and Kempe[6] employed this methodology for the preparation of pyrroles coupling two BH/HA processes with amino alcohols. The preparation of β-amino alcohols (vicinal or 1,2-amino alcohols) by means of BH/HA reactions under heterogeneous catalysis is a major goal due to the relevance of these compounds.[7,8] In addition, efficient preparation of β-amino alcohols derived from anilines is a key step in the preparation of important compounds like pyrroles.[6] Retrosynthetic analysis indicates that under controlled BH/HA conditions aniline and ethylene glycol may lead towards β-amino alcohols (*Figure 1, bottom*).

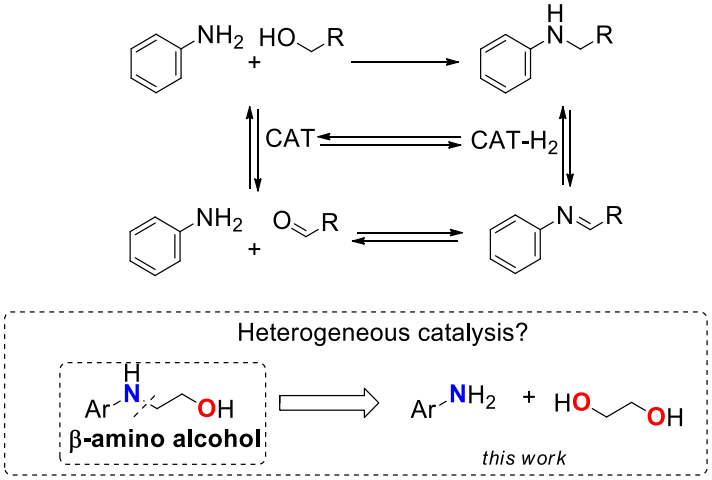

Figure 1. BH/HA strategy for the preparation of unsymmetrical amines (up) and retro synthetic approach to β-amino alcohols with ethylene glycol (down).

However, in the literature, Kempe has reported this reaction in 32% yield with transition metal complex as catalyst starting from anilines and in presence of an excess of ethylene glycol.[6a] Börner also reported on monoaminations with an homogeneous Iridium pincer catalyst in excellent yields.[6b] Another important reaction reported by Williams with a secondary amine (phenyl benzyl amine) yielded 70% under homogeneous Ru catalysis.[9] Watanabe also reported on the formation of indoles and cyclic compounds under similar conditions, the formation of cyclic compounds was also reported by Beller.[10] Those examples are by far the most efficient ones with ethylene glycol and any other alternative found in the literature requires 300ºC or transformation of ethylene glycol into a better reagent with diethyl carbonate.[11,12] Even more, diols are also used to generate typically cyclic compounds like pyrrolidines that came from functionalization of both alcohols.[9] In view of this, single functionalization of ethylene glycol is challenging and relevant. Herein, we report our recent advances on the use of BH/HA reactions to obtain β-amino alcohols, based on a heterogeneous catalysis. The catalytic system is formed by Pd/C and ZnO, and different aryl amines have been reacted with ethylene glycol, in order to test the scope of this heterogeneous catalysis, less common in BH/HA processes.[13]

The challenge in the use of ethylene glycol as reagent relies on its stability compared to benzylic alcohols that are normally used in BH/HA reactions. It is important to enhance that diols are rarely used because they trend to react twice, yielding dimers or cyclic compounds.[10] The choice of the catalyst represents the key of the process, because an extremely powerful catalyst may be able to di-oxidize the glycol or the final β-amino alcohol, leading to different products as Milstein reported.[14] Thus, preparing β-amino alcohols using ethylene glycol as reagent remains a challenge.

Results and Discussion

Recently, in our group, we developed a tandem process of hydrogenation and BH/HA in alcohol/water mixtures at high temperature with metallic Zn as reducing agent and under Pd/C catalysis.[15] Understanding that Pd/C could undergo BH/HA cycle, we firstly investigated these conditions. However, the presence of Zn(0) as electron donor represented non-green conditions, so we thought about ZnO as an activating agent for the glycol. Zinc oxide is an amphoteric material that can activate alcohols.[16-22] Indeed, under our previous studies, Zn(0) was transformed in situ into ZnO. There are a few reports in the literature indicating that ZnO nanoparticles can act as catalyst[23] it is almost stable over the catalysis, cheap and can be recovered with de Pd/C after reaction, being a greener reagent compared to metal Zn.

The first screening of conditions was performed at 200ºC and 64h, observing complete degradation of the starting aniline **1** and no traces of β-amino alcohol. Either with Zn or ZnO, 24 or 64 hours were extremely hard conditions and induced complete transformation of the product without any selectivity (*Table 1, entries 1 to 3*). Surprisingly, when we reduced the temperature to 150ºC, excellent conversion and selectivity was observed, and the corresponding β-amino alcohol **2a** was isolated in 88% yield (*Table 1, entry 4 and Figure S1*).

Evaluating the kinetics of the reaction, 24 h was found to be efficient for high conversions and selectivity (*Table 1, entries 4 to 8*). Moreover, no degradation of the product was observed at longer times. Reaction was clear yielding to product **2a** with small traces of dimeric compounds (*Table S2*). The 1:1 solvents ratio was also optimal, as long as any modification induced lower conversion (*Table 1, entries 8 to 10*).

In this reaction, ethylene glycol is employed also as solvent, however, the absence of water afforded no conversion (*Table 1, entry 9*). Any other modifications of these conditions afforded lower conversions. When comparing Pd/C with common commercial heterogeneous BH/HA catalysts Pt/Al_2O_3 or Ru/Al_2O_3[13] (*Table 1, entries 17 and 18*), moderate conversions and selectivities were observed under the same conditions. As long as catalyst support may have significant influence, more specific Pt/C and Ru/C were also evaluated. However, the overall conversion and selectivity were smaller (See SI for complete details).

The stability of the catalytic system was evaluated by means of PXRD before and after the reaction observing no significant changes (*Figure S2*). Reuses without any cleaning of the catalyst, just removing by decantation the liquid phase and adding amine and solvents again, afforded 70% of conversion up to three rounds. ICP analysis indicated no significant Pd or Zn leaching after the reaction. However, small modification on the ZnO particle size was detected that may explain this decrease in combination of the inevitable loss of catalyst during the decantation (see the SI for more details). Hot filtration test confirmed a complete heterogeneous process (*Scheme S3*).

Table 1. Screening conditions for the preparation of β-amino alcohol **2a** by Heterogeneous BH/HA Reaction

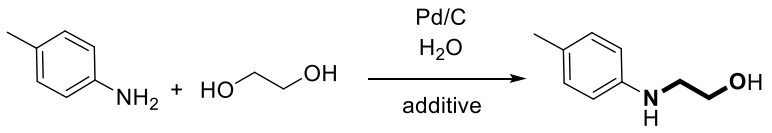

1 **2a**

Entry	1	T	Time	EG	Water	Catalyst	Additive	Conversion[a]	Selectivity
1	1 mmol	200ºC	64h	6 mL	6 mL	Pd/C 7%	Zn 3eq.	99%	0%
2	1 mmol	200ºC	64h	6 mL	6 mL	Pd/C 7%	ZnO 3eq.	99%	0%
3	1 mmol	200ºC	24h	6 mL	6 mL	Pd/C 7%	ZnO 3eq.	99%	0%
4	**1 mmol**	**150ºC**	**24h**	**6 mL**	**6 ml**	**Pd/C 7%**	**ZnO 3eq.**	**92%**	**98% (88%)[b]**
5	1 mmol	150ºC	0,5h	6 ml	6 ml	Pd/C 7%	ZnO 3eq.	0%	0%
6	1 mmol	150ºC	6h	6 ml	6 ml	Pd/C 7%	ZnO 3eq.	67%	71%
7	1 mmol	150ºC	12h	6 ml	6 ml	Pd/C 7%	ZnO 3eq.	90%	82%
8	1 mmol	150ºC	64h	6 mL	6 ml	Pd/C 7%	ZnO 3eq.	99%	90%
9	1 mmol	150ºC	24h	12 mL	0 mL	Pd/C 7%	ZnO 3eq.	0%	0%
10	1 mmol	150ºC	64h	0,25 ml	6 ml	Pd/C 7%	ZnO 3eq.	<5%	99%
11	1 mmol	150ºC	24h	6 ml	6 ml	Pd/C 7%	no ZnO	<5%	99%
12	1 mmol	150ºC	24h	6 ml	6 ml	Pd/C 7%	ZnO 1eq.	50%	99%
13	1 mmol	150ºC	24h	6 ml	6 ml	Pd/C 7%	ZnO 2eq.	56%	80%
14	2 mmol	150ºC	24h	6 ml	6 ml	Pd/C 7%	ZnO 4eq.	99%	66%
15	1 mmol	150ºC	24h	6 ml	6 ml	Pd/C 3%	ZnO 3eq.	50%	75%
16	1mmol	150ºC	24h	6 ml	6 ml	Pt/Al_2O_3 7%	ZnO 3eq.	47%	80%
17	1 mmol	150ºC	24h	6 ml	6 ml	Ru/Al_2O_3 7%	ZnO 3eq.	21%	71%
18	1mmol	150ºC	24h	6 ml	6 ml	Pt/C 7%	ZnO 3eq.	81%	37%
19	1 mmol	150ºC	24h	6 ml	6 ml	Ru/C 7%	ZnO 3eq.	71%	65%

a. Conversion obtained by ^{1}H-NMR. Selectivity measured towards **2a**. b. Isolated yield after purification.

Once optimized the reaction conditions for the preparation of β-amino alcohol **2a**, the scope of the reaction was studied (*Figure 2*). In view of the major challenge that represents diols in BH/HA processes different aromatic amines were selected as reagents in order to avoid any side reactions on the initial amine as Williams reported with some amino alcohols.[10] In general, all reagents afforded moderated to good conversion and selectivity.

First, different mono-methyl anilines were submitted to the conditions, affording compounds **2a**-**2i**. Conversion decreased with steric hindrance at the ortho position, but in all cases β-amino alcohols were isolated in moderate yields. Compound **2j**, derived from aniline, was also obtained in 65%. When the substituents were strong electron withdrawing groups, no conversion was observed (**2k**, **2l** and **2m**). However, moderate withdrawing groups like fluorine

allowed the isolation of the desired amino alcohols **2n**, **2o** and **2p** (34%, 32% and 23% isolated yields). Trifluoromethyl and trifluoromethoxyl groups were also employed and afforded alcohols **2q**, **2r** and **2s** in moderate yields. Amino alcohols **2t**, **2u**, **2v** and **2w** contain methoxyl groups. In almost all cases, side products traces (*indoles **3** and/or dimers **4** and **5**, Table S2*) could be isolated. These compounds are known to appear when ethylene glycol and anilines are heated and are the main responsible of yield dicrease.[10]

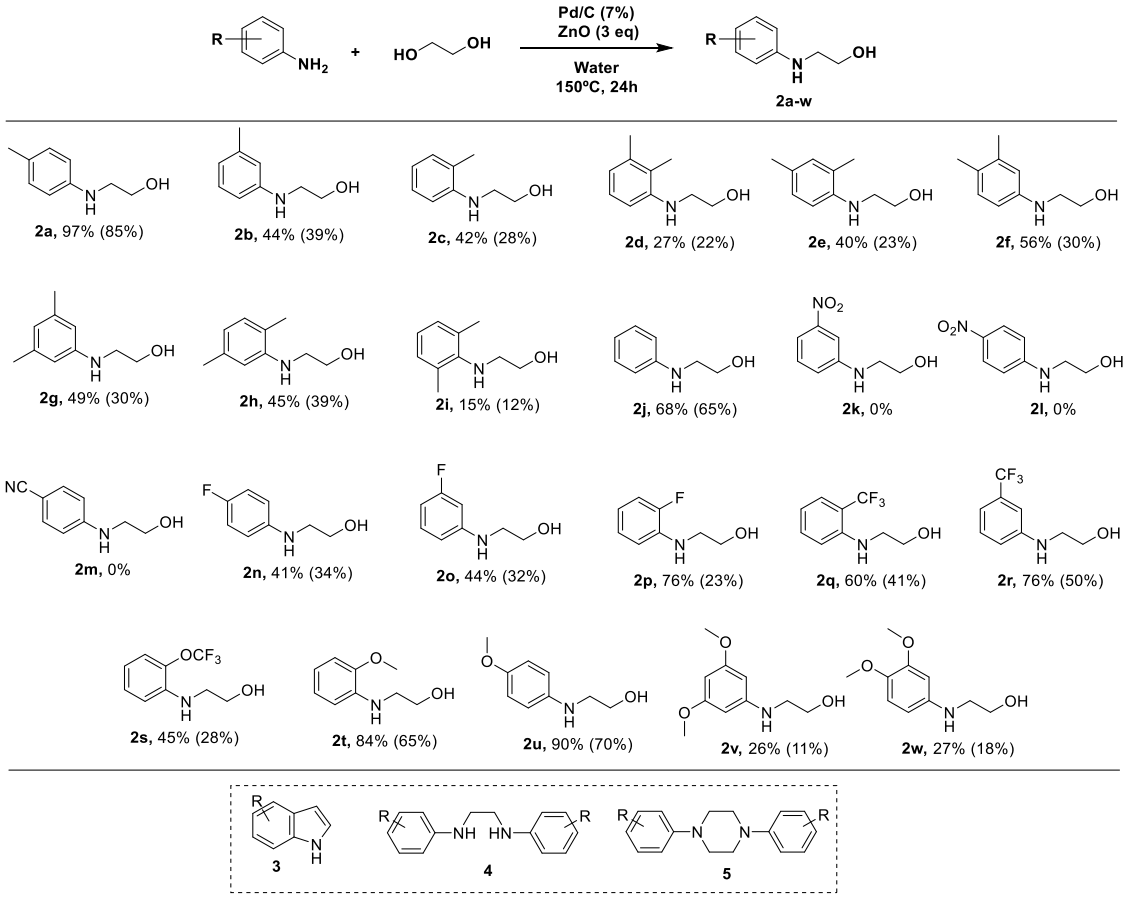

Figure 2. Scope of the catalysis reaction using different aryl amines. Structure of side compounds (**3**-**5**). ^{1}H-NMR and isolated yields (brackets) are shown.

We also wanted to explore to possibility of inducing strain in the amine by using 1,2,3,4-tetrahydroquinoline (**6**) as long as in our previous work we determine that this compound generates indole in a more efficient way.[15] When the reaction was performed with **6** the amount of indole increased (*Figure 3*) yielding to compounds **7a** in 45% yield and **7b** in 45%. With a methoxide derivative **8** similar behavior was observed, yielding **9a** in 18% and **9b** in 16% (isolated yields).

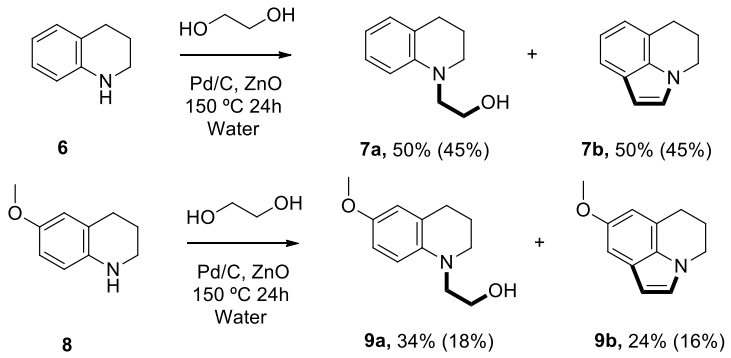

Figure 3. Heterogeneous BH/HA reactions with tetrahydroquinolines **6** and **8**. Yields obtained by ^{1}H-NMR and isolated yields.

In view of these results, a rational mechanism could be proposed for this reaction. The formation of amino alcohols follows a typical BH/HA pathway, being Pd/C the responsible for the hydrogenation/dehydrogenation process. In addition, as it has been shown in Table 1, ZnO is required to activate alcohol. Many examples reported in the literature with diols under homogeneous[4,24] or heterogeneous[13] catalysis afford the double functionalization.[25] This avoids the formation of amino alcohols yielding to diamines, either inter- or intramolecular as it is the case when Pd/MgO is used as catalyst with ethylene glycol as reported by Corma.[26] Kempe and Williams methodologies[6,9] are the unique successful conditions for this challenging mono activation of ethylene glycol. These methodologies employed an excess of ethylene glycol (significantly smaller than in our conditions, 3 eq[6] or 5 eq[9]) and solvents. However, by using our systems, even having a large excess of glycol (it is indeed co-solvent with water), we are able to obtain the amino alcohols without anhydrous conditions.

In *Figure 4*, the rational mechanism is represented. Normal BH/HA pathway is employed for the formation of amino alcohol. Ethylene glycol is transformed into the corresponding mono-aldehyde by means of Pd/C in presence of ZnO as activating agent (conversion decreases when smaller amount of ZnO are employed, *Table 1 entries 12 and 13*). The relatively long reaction times required (24h) and also the absence of 2-hydroxyacetaldehyde in the crude may indicate that this first process is the rate limiting one. This hypothesis may be supported by the fact that this step must be mediated by both heterogeneous catalysts, while all the subsequent steps require just Pd/C. In addition, ZnO may be partially soluble under our conditions.[27] The interaction between both catalyst may be facilitated thanks to this solubility combined with the excess (300%) of ZnO. Then, the amine generates the corresponding imine that is reduced yielding to the β-amino alcohol closing BH/HA cycle. However, with ethylene glycol, a tautomeric equilibrium of this imine can yield to a different compound that may undergo indole formation or dimers. Williams[9] and Bruneau[24] reported on a similar tautomeric feature with amino alcohols under BH/HA reactions in homogeneous phase. When imine is generated, the tautomeric pathway implicates a migration of the double bond. This migration is also well known in the literature and employed in the Voigth reaction for the preparation of β-amino ketones.[28] This takes place through the aliphatic chain yielding to an enol that is formally a hidden indole. In order to capture intermediates, 1,2-diamino benzene was employed to give alcohol **10**[29a] in excellent yield by means of condensation, suggesting once again that the imine is an intermediate, even if it has not been detected in any example.

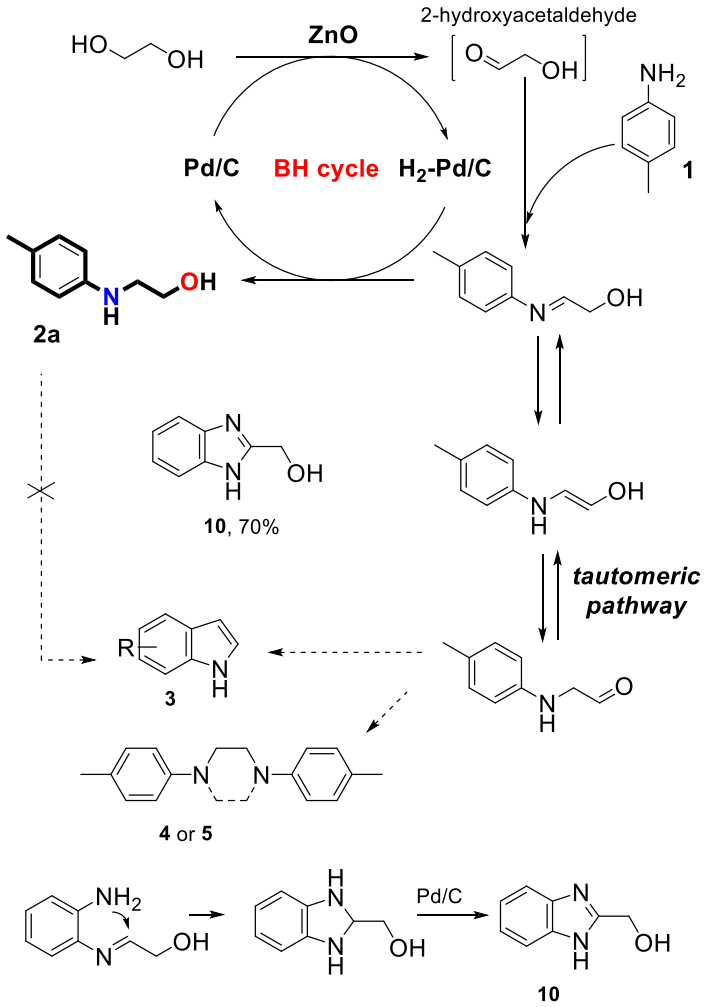

Figure 4. Rational mechanism and key intermediates

Indole formation has been found more efficient using **6** compared to anilines that require activation of the aromatic ring (*Figure 5*). Rigidity in **6** induces an intermediate with the adequate geometry leading to a more efficient indole formation. In anilines, free rotation may difficult the achieving of this intermediate and is responsible of smaller yields. Even if the formation of the indole reduces the yield of the amino alcohol, a straight synthesis of indoles also represents a major advancement in catalysis. However, the formation of indole cannot be produced by over reaction of the corresponding β-amino alcohol. When compound **7a** was submitted to the reaction conditions, no conversion was observed (*Scheme S4*).

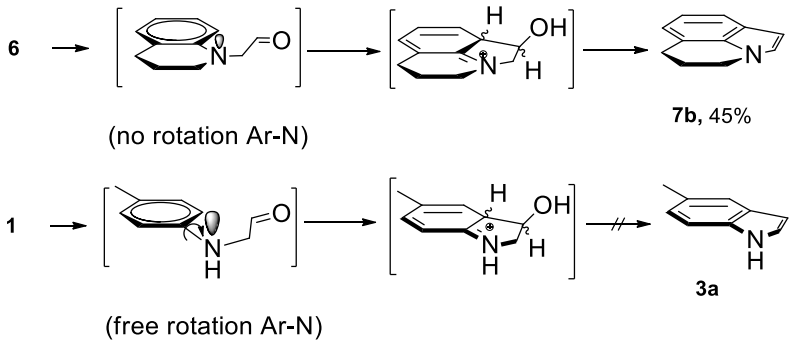

Figure 5. Structural differences in indole formation between 1,2,3,4-tetrahydroquinoline (**6**) and *p*-toluidine (**1**) intermediates.

In order to verify this mechanism some tests were performed (See the SI for more details). To add evidences of imine tautomerism, deuteration essays in **6** reactions were carried out. The D/H ratios agree with this double bond migration (*Scheme S1*). Alcohol **7a** was also oxidized under Swern conditions yielding to an aldehyde that evolved spontaneously to **7b** proving that this aldehyde is extremely reactive under our reaction conditions (*Scheme S2*). However, imine intermediates were not isolated, compared with Corma results.[26] This is also in agreement with the inability of the catalyst to dehydrogenate β-amino alcohols (*Scheme S4*). Diols and anilines can be transformed into indoles with homogenous catalysis, but normally diols have methyl substituents.[29b,29c]

Finally, tandem reactions were tested. In view of the difficulty that requires activation of ethylene glycol, we considered that under these conditions we may be able to hydrogenate indoles (*Figure 6*). Under heterogeneous conditions, this kind of reaction is proposed without this hydrogenation step.[30] However, Williams and Beller[31] reported on the pre-formation of indolines as a part of a more functional BH/HA cycle and end up by re-aromatization towards and alkylated indole.

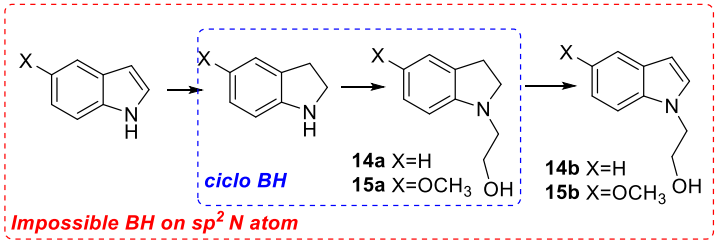

Starting Reagent	Conversion	Combined selectivity
Indole (**11**) (X=H)	72%	65% (**14a**+**14b**)
Indoline (**12**) (X=H)	>95%	75% (**14a**+**14b**)
5-Methoxy indole (**13**) ($X=OCH_3$)	52%	>95%(**15a**+**15b**)

Figure 6. Tandem functional BH/HA cycles.

To check this, we performed reactions with indole (**11**), indoline (**12**) and 5-methoxy indole (**13**). In all cases amino alcohols were isolated, proving that our catalyst was able to hydrogenate the five-member ring generating an amine that could undergo BH/HA cycle. The combined selectivity of **14a-b** or **15a-b** proves that Pd/C, ZnO combination is a powerful catalyst that is not only able to activate ethylene glycol but also dehydrogenate/hydrogenate indoles.

Conclusion

The combination of Pd/C and ZnO has been proved to be an adequate heterogeneous catalyst for the single-alcohol activation of ethylene glycol in presence of aromatic amines under BH/HA cycles in water/ethylene glycol mixture. We have prepared a large family of β-amino alcohols by a new protocol. In addition, major secondary products of this reaction are indoles, and even their low yield, it represents also a major input on a straight synthesis of these heterocycles. The present methodology reveals to be useful as long as it is air and moisture stable. Furthermore, we have proved that Pd/C, ZnO is also able to hydrogenate indoles to indolines inducing tandem BH/HA reactions all of them driven by a heterogeneous catalyst. All

these reactions are possible by a mono-activation of ethylene glycol that takes place thanks to the combination of Pd/C and ZnO and an excess of glycol. This is the unique heterogeneous approach towards β-amino alcohols with high atom efficiency (due to the BH/HA process), and without derivatization of glycol. The complementarity between BH/HA common economical catalyst (Pd/C) with and alcohol activation agents (ZnO) represents a different approach towards extremely stable poly alcohols. Further studies are undergoing with the aim reducing the amount of ethylene glycol as well as the use of different diols.

Experimental Methods

General procedure: 1 mmol of amine, 0.07 mmol of Pd/C, 3 mmol of ZnO, 6 mL of distilled water and 6 mL of ethylene glycol were mixed manually inside a 20 mL Teflon flask. Then it was sealed into a steel autoclave and introduced in a preheated oven at 150ºC for 24h. The reaction mixture was cooled to room temperature, 25 mL of distilled water were added and the crude was filtered through a 0.2 μm Teflon filter. The reaction mixture was extracted with ethyl acetate 3x15 ml and organic layers were combined, dried with Na_2SO_4, filtered and concentrated affording the reaction crude that was cheeked by NMR. Crude reaction was purified by chromatotron (1 mm, silica, from hexane to hexane/AcOEt 1:3) affording pure β-amino alcohols. Similar conditions were employed with tetrahydroquinolines **6** and **8**. Tandem reactions were performed under the same conditions employing indoles or indoline instead of aniline. For all isolated compounds in this work that are new: name, structure, isolated yield, physical aspect and characterization by ^{1}H-NMR, ^{13}C-NMR, HRMS and IR are shown. For those products that are already described in the literature: name, structure, isolated yield, physical aspect, and characterization by ^{1}H-NMR and ^{13}C-NMR are shown. An isolated yield defined as "traces" is referred to an amount of isolated product between 1 and 5 mg, considering this range of values not enough to give a representative yield.

2-(4-Methylphenylamino)ethanol (**2a**)32 Isolated yield: 130 mg (88%). Oil. 1H NMR (300 MHz, CDCl3) δ: 7.01 (d, J=8.6 Hz, 2H), 6.60 (d, J=8.5 Hz, 2H), 3.82 (t, J= 5.2 Hz, 2H), 3.28 (t, J= 5.2 Hz, 2H), 2.85 (bs, 1H), 2.25 (s, 3H). 13C NMR (75 MHz, CDCl3) δ: 145.8(1C, C), 129.9 (2C, CH), 127.5 (1C, C), 113.7 (2C, CH), 61.4 (1C, CH2), 46.8 (1C, CH2), 20.5 (1C, CH3).

2-(3-Methylphenylamino)ethanol (**2b**)[33] Isolated yield: 60 mg (39%). Oil. ^{1}H NMR (300 MHz, $CDCl_3$) δ: 7.00 (dd, J=11.0; 5.1 Hz, 1H), 6.44 (m, 3H), 3.71 (t, J=5.2 Hz, 2H), 3.19 (t, J=5.2 Hz, 2H), 2.82 (s, 1H), 2.20 (s, 3H). ^{13}C NMR (75 MHz, $CDCl_3$) δ: 148.4 (1C, C), 139.5 (1C, C), 129.6(1C, CH), 119.4 (1C, CH), 114.4 (1C, CH), 110.9 (1C, CH), 61.7 (1C, CH_2), 46.7 (1C, CH_2), 22.0 (1C, CH_3).

2-(2-Methylphenylamino)ethanol (**2c**)[34] Isolated yield: 44 mg (28%). Oil. ^{1}H NMR (300 MHz, $CDCl_3$) δ: 7.12 (m, 2H), 6.69 (m, 2H), 3.87 (t, J= 5.1 Hz, 2H), 3.35 (t, J= 5.1 Hz, 2H), 2.18 (s, 3H). ^{13}C NMR (75 MHz, $CDCl_3$) δ: 146.1 (1C, C), 130.4 (1C, CH), 127.2(1C, CH), 122.7 (1C, C), 117.6(1C, CH), 110.2 (1C, CH), 61.3 (1C, CH_2), 46.1 (1C, CH_2), 17.6 (1C, CH_3).

2-(2,3-Dimethylphenylamino)ethanol (**2d**) Isolated yield: 30 mg (22%). Oil. ^{1}H NMR (300 MHz, $CDCl_3$) δ: 7.04 (t, J = 7.8 Hz, 1H), 6.64 (d, J = 7.5 Hz, 1H), 6.56 (d, J = 8.1 Hz, 1H), 3.87 (t, J = 5.2, 2H), 3.34 (t, J = 5.2, 2H), 2.30 (s, 3H), 2.09 (s, 3H). ^{13}C NMR (75 MHz, $CDCl_3$) δ: 146.1 (1C, C), 136.9 (1C, C), 126.3(1C, CH), 121.2 (1C, C), 120.0 (1C, CH), 108.6 (1C, CH), 61.4 (1C, CH_2), 46.5 (1C, CH_2), 20.8 (1C, CH_2), 12.7 (1C, CH_3). HRMS for $C_{10}H_{15}NO$ [M+H$^+$]: calculated: 166.1220; found: 166.1219. IR (ATR): 3409, 2943, 2878, 1589, 1506, 1476, 1458, 1317, 1283, 1141, 1060, 765, 713.

2-(2,4-Dimethylphenylamino)ethanol (**2e**) Isolated yield: 30 mg (23%). Oil. ^{1}H NMR (300 MHz, $CDCl_3$) δ 6.94 (d, J = 8.1 Hz, 1H), 6.91 (s, 1H), 6.58 (d, J = 8.0 Hz, 1H), 3.86 (t, J = 5.2, 2H), 3.33 (t,

J = 5.2, 2H), 2.24 (s, 3H), 2.15 (s, 3H). ^{13}C NMR (75 MHz, $CDCl_3$) δ: 143.8 (1C, C), 131.3 (1C, CH), 127.5 (1C, CH), 127.0 (1C, C), 123.0 (1C, C), 110.6 (1C, CH), 61.4 (1C, CH_2), 46.5 (1C, CH_2), 20.7 (1C, CH_3), 17.6 (1C, CH_3). HRMS for $C_{10}H_{15}NO$ [M+H$^+$]: calculated: 166.1226; found: 166.1217. IR (ATR): 3403, 2918, 1618, 1514, 1457, 1378, 1314, 1269, 1219, 1144, 1061, 875, 804, 772, 607.

2-(3,4-Dimethylphenylamino)ethanol (**2f**) Isolated yield: 43 mg (30%). Oil. ^{1}H NMR (300 MHz, $CDCl_3$) δ: 6.96 (d, J=8.0 Hz, 1H), 6.50 (d, J=2.4 Hz, 1H), 6.44 (dd, J=8.0; 2.5, 1H), 3.81 (t, J=5.4 Hz, 2H), 3.28 (t, J=5.3 Hz, 2H), 2.72 (s, 1H), 2.21 (s, 3H), 2.17 (s, 3H). ^{13}C NMR (75 MHz, $CDCl_3$) δ: 146.3 (1C, C), 137.5 (1C, C), 130.5 (1C, CH), 126.2 (1C, C), 115.4 (1C, CH), 110.9 (1C, CH), 61.4 (1C, CH_2), 46.7 (1C, CH_2), 20.1 (1C, CH_3), 18.8 (1C, CH_3). HRMS for $C_{10}H_{15}NO$ [M+H$^+$]: calculated: 166.1226; found: 166.1225. IR (ATR): 3354, 2917, 2861, 1616, 1507, 1448, 1319, 1262, 1217, 1059, 1021, 852, 803, 703.

2-(3,5-Dimethylphenylamino)ethanol (**2g**) Isolated yield: 41 mg (30%). Oil. ^{1}H NMR (300 MHz, $CDCl_3$) δ: 6.43 (s, 1H), 6.31 (s, 2H), 3.80 (t, J=5.2 Hz, 2H), 3.28 (t, J=5.2 Hz, 2H), 2.27 (s, 6H). ^{13}C NMR (75 MHz, $CDCl_3$) δ: 148.3 (1C, C), 139.1 (2C, C), 120.1 (1C, CH), 111.4 (2C, CH), 61.4 (1C, CH_2), 46.3 (1C, CH_2), 21.6 (2C, CH_3). HRMS for $C_{10}H_{15}NO$ [M+H$^+$]: calculated: 166.1226; found: 166.1219. IR (ATR): 3381, 2927, 2842, 1601, 1574, 1504, 1456, 1373, 1346, 1329, 1302, 1241, 1212, 1194, 1131, 1095, 1058, 1011, 938, 872, 831, 800, 743, 718.

2-(2,5-Dimethylphenylamino)ethanol (**2h**) Isolated yield: 53 mg (39%). Oil. ^{1}H NMR (300 MHz, $CDCl_3$) δ: 6.87 (d, J=7.4 Hz, 1H), 6.44 (d, J=7.5 Hz, 1H), 6.40 (s, 1H), 3.78 (t, J=5.3 Hz, 2H), 3.26 (t, J=5.3 Hz, 2H). ^{13}C NMR (75 MHz, $CDCl_3$) δ: 146.2 (1C, C), 137.6 (1C, C), 130.5 (1C, CH), 120.1 (1C, C), 118.6(1C, CH), 111.5 (1C, CH), 61.7 (1C, CH_2), 46.3 (1C, CH_2), 21.9 (1C, CH_3), 17.4 (1C, CH_3). HRMS for $C_{10}H_{15}NO$ [M+H$^+$]: calculated: 166.1226; found: 166.1220. IR (ATR): 3405, 3014, 2919, 1614, 1581, 1519, 1456, 1422, 1376, 1297, 1272, 1206, 1167, 1139, 1058, 1000, 877, 842, 793.

2-(2,6-Dimethylphenylamino)ethanol (**2i**)[34] Isolated yield: 20 mg (12%). Oil. ^{1}H NMR (300 MHz, $CDCl_3$) δ: 7.01 (d, J= 7.4 Hz, 2H), 6.86 (dd, J= 7.9; 7.0 Hz, 1H), 3.80 (t, J= 5.0 Hz, 2H), 3.15 (t, J= 5.0 Hz, 2H), 2.73 (bs, 1H), 2.33 (s, 6H). ^{13}C NMR (75 MHz, $CDCl_3$) δ: 145.1 (1C, C), 130.2 (1C, C), 129.1 (2C, CH), 122.8 (1C, CH), 62.3 (1C, CH_2), 50.6 (1C, CH_2), 18.5 (2C, CH_3).

2-Phenylaminoethanol (**2j**)[35] Isolated yield: 89 mg (65%). Oil. ^{1}H NMR (300 MHz, $CDCl_3$) δ: 7.14-7.06 (m, 2H), 6.69-6.62 (m, 1H), 6.60 (dd, J= 8.6; 1.0 Hz, 2H), 3.71 (t, J= 5.3 Hz, 2H), 3.19 (t, J= 5.3 Hz, 2H). ^{13}C NMR (75 MHz, $CDCl_3$) δ: 148.2 (1C, C), 129.4 (2C, CH), 118.0 (1C, CH), 113.4 (2C, CH), 61.3 (1C, CH_2), 46.2 (1C, CH_2).

2-(4-Fluorophenylamino)ethanol (**2n**)36 Isolated yield: 52 mg (34%). Oil. 1H NMR (300 MHz, CDCl3) δ: 6.90-6.85 (m, 2H), 6.60-6.55 (m, 2H), 3.82 (m, 2H), 3.24 (t, J= 5.3 Hz, 2H). 13C NMR (75 MHz, CDCl3) δ: 164.0 (1C, C), 160.1 (1C, C), 114.6 (1C, C), 114.4 (1C, C), 115.8 (1C, C), 115.4 (1C, C), 61.4 (1C, CH2), 46.2 (1C, CH2).

2-(3-Fluorophenylamino)ethanol (**2o**) Isolated yield: 50 mg (32%). Oil. ^{1}H NMR (300 MHz, $CDCl_3$) δ: 7.03 (td, J=8.1; 6.7 Hz, 1C), 6.34 (m, 2H), 6.26 (dt, J=11.5; 2.3 Hz, 1C), 3.76 (t, J=5.2 Hz, 2H), 3.21 (t, J=5.2 Hz, 2H). ^{13}C NMR (75 MHz, $CDCl_3$) δ: 162.5 (1C, C), 149.8 (1C, C), 130.4 (1C, CH), 109.1(1C, CH), 104.4 (1C, CH), 99.9 (1C, CH), 61.1 (1C, CH_2), 45.94 (1C, CH_2). HRMS for $C_8H_{10}FNO$ [M+H$^+$]: calculated: 156.0819; found: 156.0807. IR (ATR): 3351, 2929, 1617, 1588, 1510, 1495, 1459, 1334, 1286, 1175, 1149, 1054, 997, 963, 828, 756, 681.

2-(2-Fluorophenylamino)ethanol (**2p**) Isolated yield: 35 mg (23%). Oil. ^{1}H NMR (300 MHz, $CDCl_3$) δ: 7.00 (m, 2H), 6.76 (td, J=8.4; 1.5 Hz, 1H), 6.66 (m, 1H), 3.86 (t, J=5.2 Hz, 2H), 3.35 (t,

J=5.2 Hz, 2H). ^{13}C NMR (75 MHz, $CDCl_3$) δ: 153.6 (1C, C), 150.4 (1C, C), 124.8 (1C, CH), 117.6 (1C, CH), 114.9 (1C, CH), 112.9 (1C, CH), 61.4 (1C, CH_2), 46.0 (1H, CH_2). HRMS for $C_8H_{11}FNO$ [M+H$^+$]: calculated: 156.0825; found: 156.0811. IR (ATR): 3402, 1620, 1514, 1544, 1336, 1297, 1252, 1188, 1061, 1033, 741.

2-(2-Trifluoromethylphenylamino)ethanol (**2q**) Isolated yield: 84 mg (41%). Oil. ^{1}H NMR (300 MHz, $CDCl_3$) δ: 7.87 (ddd, J= 7.9; 1.6; 0.6 Hz, 1H), 7.26 (m, 1H), 6.64 (m, 2H), 2.11 (t, J= 4.6 Hz, 2H), 3.92 (t, J= 4.6 Hz, 2H). ^{13}C NMR (75 MHz, $CDCl_3$) δ: 168.5 (1C, C), 150.7 (1C, C), 134.5 (1C, CH), 131.6 (1C, CH), 116.9 (1C, CH), 116.4 (1C, CH), 110.5 (1C, C), 66.2 (1C, CH_2), 61.6 (1C, CH_2). HRMS for $C_9H_{10}F_3NO$ [M-2H$^+$]: calculated: 204.0631; found: 204.0625. IR (ATR): 3473, 3368, 1682, 1614, 1587, 1561, 1487, 1455, 1291, 1240, 1161, 1131, 1065, 751, 702, 665.

2-(3-Trifluoromethylphenylamino)ethanol (**2r**)[37] Isolated yield: 101 mg (50%). Oil. ^{1}H NMR (300 MHz, $CDCl_3$) δ: 7.10 (t, J= 7.9 Hz, 1H), 6.82-6.77 (m, 1H), 6.67 (s, 1H), 6.61 (dd, J= 8.2; 2.3 Hz, 1H), 3.67 (t, J= 5.2 Hz, 2H), 3.15 (t, J= 5.2 Hz, 2H). ^{13}C NMR (75 MHz, $CDCl_3$) δ: 148.5 (1C, CF_3), 129.8 (1C, CH), 126.2 (1C, C), 122.6 (1C, C), 116.3 (1C, CH), 114.3 (1C, CH), 109.3 (1C, CH), 61.1 (1C, CH_2), 45.8 (1C, CH_2).

2-(2-Trifluoromethoxyphenylamino)ethanol (**2s**) Isolated yield: 59 mg (28%). Oil. ^{1}H NMR (300 MHz, $CDCl_3$) δ: 7.07 (m, 2H), 6.70 (dd, J= 8.5; 1.5 Hz, 1H), 6.62 (m, 1H), 3.78 (t, J= 5.2 Hz, 2H), 3.28 (t, J= 5.2 Hz, 2H). ^{13}C NMR (75 MHz, $CDCl_3$) δ: 140.9 (1C, C), 134.9 (1C, C), 128.1 (1C, CH), 121.4 (1C, CH), 117.4 (1C, CH), 112.8 (1C, CH), 61.5 (1C, CH_2), 46.0 (1C, CH_2). HRMS for $C_9H_{10}F_3NO_2$ [M+H$^+$]: calculated: 222.0736; found: 222.0729. IR (ATR): 3420, 2930, 2360, 1614, 1515, 1457, 1330, 1246, 1215, 1166, 1042, 923, 745, 669, 630, 604.

2-(2-Methoxyphenylamino)ethanol (**2t**)[38] Isolated yield: 108 mg (65%). Oil. ^{1}H NMR (300 MHz, $CDCl_3$) δ: 6.88 (td, J= 7.6; 1.6 Hz, 1H), 6.79 (dd, J= 7.9; 1.5 Hz, 1H), 6.72 (dd, J= 7.5; 1.6 Hz, 1H), 6.66 (dd, J= 7.8; 1.5 Hz, 1H), 3.75 (s, 3H), 3.74 (t, J= 5.3 Hz, 2H), 3.32 (t, J= 5.3 Hz, 2H). ^{13}C NMR (75 MHz, $CDCl_3$) δ: 147.3 (1C, C), 138.1 (1C, C), 121.3 (1C, CH), 117.1 (1C, CH), 110.4 (1C, CH), 109.7 (1C, CH), 61.4 (1C, CH_3), 55.5 (1C, CH_2), 46.0 (1C, CH_2).

2-(4-Methoxyphenylamino)ethanol (**2u**)[35] Isolated yield: 115 mg (70%). Oil. ^{1}H NMR (300 MHz, $CDCl_3$) δ: 6.76 (d, J= 9.2 Hz, 2H), 6.58 (d, J= 8.8 Hz, 2H), 3.74 (t, J= 5.2 Hz, 2H), 3.73 (s, 3H), 3.25 (t, J= 5.2 Hz, 2H). ^{13}C NMR (75 MHz, $CDCl_3$) δ: 152.8 (1C, C), 142.5 (1C, C), 115.1 (2C, CH), 114.9 (1C, CH), 61.3 (1C, CH_3), 55.8 (1C, CH_2), 47.1 (1C, CH_2).

2-(3,5-Dimethoxylphenylamino)ethanol (**2v**) Isolated yield: 22 mg (11%). Oil. ^{1}H NMR (300 MHz, $CDCl_3$) δ: 5.92 (t, J=2.1 Hz, 1H), 5.87 (s, 1H), 5.86 (s, 1H), 3.82 (t, J=5.2 Hz, 2H), 3.75 (s, 6H), 3.27 (t, J=5.3 Hz, 2H). ^{13}C NMR (75 MHz, $CDCl_3$) δ: 161.9 (2C, C), 149.9 (1C, C), 92.5 (2C, CH), 90.6 (1C, CH), 61.3 (1C, CH_3), 55.3 (2C, CH_2), 46.5 (1C, CH_2). HRMS for $C_{10}H_{15}NO_3$ [M+H$^+$]: calculated: 198.1125; found: 198.1113. IR (ATR): 3384, 2938, 2839, 1613, 1507, 1456, 1235, 1203, 1176, 1151, 1127, 1059, 808.

2-(3,4-Dimethoxylphenylamino)ethanol (**2w**) Isolated yield: 35 mg (18%). Oil. ^{1}H NMR (300 MHz, $CDCl_3$) δ: 6.74 (d, J= 8.5 Hz, 1H), 6.30 (d, J= 2.6 Hz, 1H), 6.20 (dd, J= 8.5; 2.6 Hz, 1H), 3.84-3.81 (m, 5H), 3.80 (s, 3H), 3.26 (t, J= 5.2 Hz, 2H). ^{13}C NMR (75 MHz, $CDCl_3$) δ: 150.1 (1C, C), 142.9 (1C, C), 142.2 (1C, C), 113.3 (1C, CH), 104.4 (1C, CH), 99.8 (1C, CH), 61.4 (1C, CH_2), 56.8 (1C, CH_3), 55.9 (1C, CH_3), 47.3 (1C, CH_2). HRMS for $C_{10}H_{15}NO_3$ [M+H$^+$]: calculated: 198.1125; found: 198.1125. IR (ATR): 3383, 2940, 2832, 1616, 1515, 1463, 1232, 1210, 1168, 1139, 1024, 797, 611.

5-Methylindole (**3a**)[39] Isolated yield: traces. Oil. ^{1}H NMR (300 MHz, $CDCl_3$) δ: 7.44 (m, 2H), 7.26 (d, J= 8.5 Hz, 1H), 7.12 (d, J= 3.0 Hz, 1H), 6.44 (d, J= 3.0 Hz, 1H), 2.39 (s, 3H). ^{13}C NMR (75 MHz, $CDCl_3$) δ: 148.0 (1C, C), 138.6 (1C, C), 134.0 (1C, C), 130.2 (1C, CH), 121.2 (2C, CH), 119.4 (1C, CH), 94.8 (1C, CH), 20.9 (1C, CH_3).

6-Methylindole (**3b**) and 4-Methylindole (**3b'**)[40] Isolated yield: 23 mg (17%, mixture). Oil. ^{1}H NMR (300 MHz, $CDCl_3$) δ: 8.15 (bs, 1H), 8.01 (bs, 1H), 7.54 (d, J= 8.1 Hz, 1H'), 7.16 (m, 5H), 6.97 (d, J= 8.3 Hz, 1H'), 6.93 (d, J= 7.2 Hz, 1H), 6.58 (s, 1H), 6.51 (s, 1H'), 2.58 (s, 3H), 2.48 (s, 3H'). ^{13}C NMR (75 MHz, $CDCl_3$) δ: 136.4 (1C', C), 135.6 (1C, C), 131.9 (1C, C), 130.4 (1C', C), 127.9(1C', C), 125.7 (1C, C), 123.6 (1C, CH), 122.2 (1C, CH), 121.7 (1C', CH), 120.4 (1C', CH), 120.0 (1C, CH), 111.1 (1C, CH), 108.7 (1C, CH), 102.5 (1C', CH), 101.2 (1C, CH), 21.8 (1C, CH_3), 18.9 (1C', CH_3).

7-Methylindole (**3c**)[41] Isolated yield: 27 mg (20%). Oil. ^{1}H NMR (300 MHz, $CDCl_3$) δ: 8.07 (bs, 1H), 7.51 (d, J= 7.5 Hz, 1H), 7.22 (s, 1H), 7.09-6.97 (m, 2H), 6.57 (s, 1H), 2.52 (s, 3H). ^{13}C NMR (75 MHz, $CDCl_3$) δ: 131.2 (1C, C), 123.9 (2C, CH and C), 122.63 (2C, CH), 120.2 (1C, CH), 118.6 (1C, CH), 103.3 (1C, CH), 16.8 (1C, CH_3).

6,7-Dimethylindole (**3d**)[42] Isolated yield: traces. Oil. ^{1}H NMR (300 MHz, $CDCl_3$) δ: 7.40 (d, J=8.0 Hz, 1H), 7.16 (m, 1H), 6.96 (d, J=8.1, 1H), 6.51 (dd, J=3.2; 2.1, 1H), 2.41 (s, 6H). ^{13}C NMR (75 MHz, $CDCl_3$) δ: 129.4 (2C, C), 123.5 (1C, CH), 122.80 (1C, CH), 117.85 (1C, CH), 103.2 (1C, CH), 19.4 (1C, CH_3), 13.3 (1C, CH_3).

5,7-Dimethylindole (**3e**)43 Isolated yield: traces. Oil. 1H NMR (300 MHz, CDCl3) δ: 7.29 (bs, 1H), 7.18 (m, 1H), 6.84 (bs, 1H), 6.48 (dd, J=3.1; 2.1, 1H), 2.47 (s, 3H), 2.42 (s, 3H). 13C NMR (75 MHz, CDCl3) δ: 133.3(1C, C), 131.3 (1C, C), 127.4 (1C, C), 124.42 (1C, CH), 124.0 (1C, CH), 119.9 (1C, C), 102.8 (1C, CH), 21.5 (1C, CH3), 16.8 (1C, CH3).

5,6-Dimethylindole (**3f**)[44] and 4,5-Dimethylindole (**3f'**)[45] Isolated yield: traces (mixture). Oil. ^{1}H NMR (300 MHz, $CDCl_3$) δ: 8.05 (bs, 1H), 7.96 (bs, 1H'), 7.40 (s, 1H'), 7.16 (m, 3H), 7.10 (t, J= 2.8 Hz, 1H'), 7.01 (d, J= 8.2 Hz, 1H), 6.54 (ddd, J= 3.1; 2.1; 0.9 Hz, 1H), 6.44 (ddd, J= 3.0; 2.0; 0.9 Hz, 1H'), 2.47 (s, 3H), 2.37 (s, 3H), 2.36 (s, 3H'), 2.35 (s, 3H'). ^{13}C NMR (75 MHz, $CDCl_3$) δ: 134.4 (2C, C), 128.6 (2C, C), 127.7 (2C, C), 126.6 (2C, C), 124.8 (1C, CH), 123.8 (1C, CH), 123.4 (1C', CH), 120.8 (1C', CH), 111.5 (1C', CH), 108.2 (1C, CH), 102.0 (1C', CH), 101.1 (1C, CH), 20.6 (1C', CH_3), 19.6 (1C', CH_3), 19.4 (1C, CH_3), 15.6 (1C, CH_3).

4,6-Dimethylindole(**3g**)[46] Isolated yield: 38 mg (32%). Oil. ^{1}H NMR (300 MHz, $CDCl_3$) δ: 8.01 (bs, 1H), 7.13 (m, 1H), 7.04 (s, 1H), 6.78 (s, 1H), 6.52 (ddd, J= 3.1; 2.1; 0.9 Hz, 1H), 2.54 (s, 3H), 2.44 (s, 3H). ^{13}C NMR (75 MHz, $CDCl_3$) δ: 136.1 (1C, C), 132.0 (1C, C), 129.9 (1C, C), 125.7 (1C, C), 122.9 (1C, CH), 122.0 (1C, CH), 108.6 (1C, CH), 101.1 (1C, CH), 21.8 (1C, CH_3), 18.8 (1C, CH_3).

4,7-Dimethylindole (**3h**)[42] Isolated yield: traces. Oil. ^{1}H NMR (300 MHz, $CDCl_3$) δ: 7.22 (m, 1H), 6.93 (d, J=7.2 Hz, 1H), 6.86 (d, J=7.1 Hz, 1H), 6.60 (m, 1H), 2.56 (s, 3H), 2.48 (s, 3H). ^{13}C NMR (75 MHz, $CDCl_3$) δ: 135.1 (1C, C), 127.9 (1C, C), 127.4 (1C, C), 123.3 (1C, CH), 122.6 (1C, CH), 120.1 (1C, CH), 117.7 (1C, C), 101.79 (1C, CH), 18.7 (1C, CH_3), 16.6 (1C, CH_3).

4,6-Dimethoxyindole (**3v**)[47] Isolated yield: traces. Oil. ^{1}H NMR (300 MHz, $CDCl_3$) δ: 8.03 (bs, 1H), 6.99 (dd, J=3.2; 2.3 Hz, 1H), 6.57 (ddd, J= 3.1; 2.2; 0.8 Hz, 1H), 6.50 (dd, J= 1.8; 0.8 Hz, 1H), 6.24 (d, J= 1.9 Hz, 1H), 3.93 (s, 3H), 3.84 (s, 3H). ^{13}C NMR (75 MHz, $CDCl_3$) δ: 157.7 (1C, C), 153.8 (1C, C), 137.3 (1C, C), 121.3 (1C, CH), 113.2 (1C, C), 99.9 (1C, CH), 91.8 (1C, CH), 86.9 (1C, CH), 55.8 (1C, CH_3), 55.5 (1C, CH_3).

5,6-Dimethoxyindole (**3w**)[48] Isolated yield: 36 mg (20%). Oil. ^{1}H NMR (300 MHz, $CDCl_3$) δ: 8.06 (bs, 1H), 7.10 (s, 1H), 7.08 (dd, J= 3.1; 2.4 Hz, 1H), 6.89 (s, 1H), 6.45 (ddd, J= 3.0; 2.1; 0.9 Hz, 1H), 3.92 (s, 3H), 3.90 (s, 3H). ^{13}C NMR (75 MHz, $CDCl_3$) δ: 147.2 (1C, C), 145.3 (1C, C), 130.3 (1C, C), 122.8 (1C, CH), 120.7 (1C, C), 102.4 (2C, CH), 94.6 (1C, CH), 56.4 (1C, CH_3), 56.3 (1C, CH_3).

N,*N*'-Bis(4-methylphenyl)-1,2-ethanediamine (**4a**) Isolated yield: traces. Oil. ^{1}H NMR (300 MHz, $CDCl_3$) δ: 7.01 (d, J= 8.0 Hz, 4H), 6.64 (d, J= 8.4 Hz, 4H), 3.39 (s, 4H), 2.25 (s, 6H). ^{13}C NMR (75 MHz, $CDCl_3$) δ: 145.1 (2C, C), 130.0 (4C, CH), 128.0 (2C, C), 114.0 (4C, CH), 44.2 (2C, CH_2), 20.5 (2C, CH_3). HRMS for $C_{16}H_{20}N_2$ [M+H$^+$]: calculated: 241.1699; found: 241.1688. IR (ATR): 2918, 2858, 1616, 1517, 1464, 1317, 1296, 1256, 1182, 1127, 806.

N,*N*'-Bis(2-methylphenyl)-1,2-ethanediamine (**4c**)[49] Isolated yield: 13 mg (24%). Oil. ^{1}H NMR (300 MHz, $CDCl_3$) δ: 7.15 (t, J=7.6 Hz, 2H), 7.08 (d, J=7.2 Hz, 2H), 6.70 (m, 4H), 3.50 (s, 4H), 2.13 (s, 6H). ^{13}C NMR (75 MHz, $CDCl_3$) δ: 130.4 (2C, CH), 127.3 (2C, CH), 122.7 (4C, C), 117.8 (2C, CH), 110.2 (2C, CH), 43.4 (2C, CH_2), 17.7 (2C, CH_3)

N,*N*'-Bis(2,4-dimethylphenyl)-1,2-ethanediamine (**4e**)[49] Isolated yield: traces. Oil. ^{1}H NMR (300 MHz, $CDCl_3$) δ: 6.87 (d, J=8.1 Hz, 2H), 6.83 (s, 2H), 6.53 (d, J=8.0 Hz, 2H), 3.38 (s, 4H), 2.16 (s, 6H), 2.03 (s, 6H). ^{13}C NMR (75 MHz, $CDCl_3$) δ: 143.7 (2C, C), 131.3 (2C, CH), 127.5 (2C, CH), 126.9 (2C, C), 110.5 (2C, CH), 43.7 (2C, CH_2), 20.5 (2C, CH_3), 17.6 (2C, CH_3).

N,*N*'-Bis(3,5-dimethylphenyl)-1,2-ethanediamine (**4g**) Isolated yield: traces. Oil. ^{1}H NMR (300 MHz, $CDCl_3$) δ: 6.40 (s, 2H), 6.29 (s, 4H), 3.36 (s, 4H), 2.24 (s, 12H). ^{13}C NMR (75 MHz, $CDCl_3$) δ: 148.1 (2C, C), 138.2 (4C, C), 120.1 (2C, CH), 111.3 (4C, CH), 43.7 (2C, CH_2), 21.6 (4C, CH_3). HRMS for $C_{18}H_{24}N_2$ [M+H$^+$]: calculated: 269.2012; found: 269.2016. IR (ATR): 2916, 2358, 2342, 1652, 1601, 1558, 1540, 1520, 1506, 1489, 1472, 1456, 1338, 1186, 819, 772.

N,*N*'-Bis(3-fluorophenyl)-1,2-ethanediamine (**4o**) Isolated yield: traces. Oil. ^{1}H NMR (300 MHz, $CDCl_3$) δ: 7.14-7.09 (m, 2H), 6.48-6.28 (m, 6H), 3.39 (s, 4H). ^{13}C NMR (75 MHz, $CDCl_3$) δ: 164.2 (d, J = 243.4 Hz, 2C, C), 149.0 (d, J = 10.6 Hz, 2C, C), 130.6 (d, J = 10.2 Hz, 2C, CH), 109.2 (d, J = 2.5 Hz, 2C, CH), 104.8 (d, J = 21.5 Hz, 2C, CH), 100.1 (d, J = 25.3 Hz, 2C, CH), 43.3 (2C, CH_2). HRMS for $C_{14}H_{14}F_2N_2$ [M+H$^+$]: calculated: 249.1198; found: 249.1202. IR (ATR): 1616, 1589, 1507, 1496, 1175, 1150, 830, 757, 682.

N,*N*'-Bis(2-trifluoromethoxyphenyl)-1,2-ethanediamine (**4s**) Isolated yield: traces. Oil. ^{1}H NMR (300 MHz, $CDCl_3$) δ: 7.19-7.12 (m, 4H), 6.77 (dd, J=8.5; 1.5 Hz, 2H), 6.73-6.66 (m, 2H), 3.46 (s, 4H). ^{13}C NMR (75 MHz, $CDCl_3$) δ: 140.4 (2C, C), 136.6 (2C, C), 127.9 (2C, CH), 122.7 (2C, C), 121.3 (2C, CH), 117.1 (2C, CH), 112.1 (2C, CH), 42.7 (2C, CH_2). HRMS for $C_{16}H_{14}F_6N_2O_2$ [M+H$^+$]: calculated: 381.1032; found: 381.1012. IR: 3454, 2928, 1612, 1558, 1514, 1472, 1328, 1248, 1217, 1166, 1043, 920, 772, 746, 674, 630, 606.

1,4-Bis(4-methylphenyl)-piperazine (**5a**) Isolated yield: traces. Oil. ^{1}H NMR (300 MHz, $CDCl_3$) δ: 7.11 (d, J= 8.6 Hz, 4H), 6.91 (d, J= 8.5 Hz, 4H), 3.30 (s, 8H), 2.29 (s, 6H). ^{13}C NMR (75 MHz, $CDCl_3$) δ: 149.3 (2C, C), 129.8 (6C, C and CH), 116.9 (4C, CH), 50.2 (4C, CH_2), 20.6 (2C, CH_3). HRMS for $C_{18}H_{22}N_2$ [M+H$^+$]: calculated: 267.1856; found: 267.1844. IR (ATR): 2953, 2919, 2855, 2820, 2360, 2343, 1743, 1615, 1515, 1489, 1452, 1384, 1317, 1293, 1265, 1229, 1211, 1180, 1150, 1041, 939, 823, 813, 771.

1,4-Bis(3-methylphenyl)-piperazine (**5b**) Isolated yield: traces. Oil. ^{1}H NMR (300 MHz, $CDCl_3$) δ: 7.19 (t, J= 7.9 Hz, 2H), 6.81 (m, 4H), 6.73 (d, J=7.3 Hz, 2H), 3.33 (s, 8H), 2.35 (s, 6H). ^{13}C NMR (75 MHz, $CDCl_3$) δ: 151.5 (2C, C), 139.0 (2C, C), 129.2 (2C, CH), 121.1 (2C, CH), 117.35 (2C, CH),

113.6 (2C, CH), 49.7 (4C, CH_2), 21.9 (2C, CH_3). HRMS for $C_{18}H_{22}N_2$ [M+H$^+$]: calculated: 267.1856; found: 267.1844. IR (ATR): 2826, 1604, 1583, 1494, 1448, 1242, 995, 955, 690, 609.

1,4-Bis(2-methylphenyl)-piperazine (**5c**) Isolated yield: traces. Oil. ^{1}H NMR (300 MHz, $CDCl_3$) δ: 7.20 (m, 4H), 7.11, (d, J=7.90 Hz, 2H), 7.01 (t, J=7.2 Hz, 2H), 3.08 (s, 8H), 2.37 (s, 6H). ^{13}C NMR (75 MHz, $CDCl_3$) δ: 151.8 (2C, C), 132.8 (2C, C), 131.3 (2C, CH), 126.7 (2C, CH), 123.3 (2C, CH), 119.3 (2C, CH), 52.4 (4C, CH_2), 18.1 (2C, CH_3). HRMS for $C_{18}H_{22}N_2$ [M+H$^+$]: calculated: 267.1856; found: 267.1854. IR (ATR): 2946, 2823, 1596, 1490, 1442, 1372, 1253, 1222, 1142, 1112, 1039, 945, 767, 722.

1,4-Bis(2,3-dimethylphenyl)-piperazine (**5d**) Isolated yield: traces. Oil. ^{1}H NMR (300 MHz, $CDCl_3$) δ: 7.11 (t, J=7.7 Hz, 2H), 7.00 (d, J=7.6 Hz, 2H), 6.92 (d, J=7.4 Hz, 2H), 3.05 (s, 8H), 2.29 (s, 6H), 2.28 (s, 6H). ^{13}C NMR (75 MHz, $CDCl_3$) δ: 151.9 (2C, C), 138.1 (2C, C), 131.5 (2C, C), 125.9 (2C, CH), 125.1(2C, CH), 116.9 (2C, CH), 52.9 (2C, CH_2), 20.8 (2C, CH_3), 14.2 (2C, CH_3). HRMS for $C_{20}H_{26}N_2$ [M+H$^+$]: calculated: 295.2169; found: 295.2163. IR (ATR): 2949, 2814, 2744, 1580, 1507, 1475, 1449, 1373, 1315, 1272, 1233, 1219, 1140, 1085, 1028, 994, 944, 775, 717.

1,4-Bis(2,4-dimethylphenyl)-piperazine (**5e**) Isolated yield: traces. Oil. ^{1}H NMR (300 MHz, $CDCl_3$) δ 7.03 (m, 6H), 3.04 (s, 8H), 2.33 (s, 6H), 2.30 (s, 6H). ^{13}C NMR (75 MHz, $CDCl_3$) δ 149.4 (2C, C), 132.8 (4C, C), 127.2 (2C, CH), 119.2 (2C, CH), 52.7 (4C, CH_2), 20.8 (2C, CH_3), 17.9 (2C, CH_3). HRMS for $C_{20}H_{26}N_2$ [M+H$^+$]: calculated: 295.2169; found: 295.2175. IR (ATR): 2943, 2813, 2359, 2343, 1504, 1447, 1370, 1353, 1311, 1293, 1257, 1234, 1220, 1163, 1143, 1125, 1044, 961, 947, 913, 888, 812, 755, 720, 668.

1,4-Bis(3,4-dimethylphenyl)-piperazine (**5f**) Isolated yield: 23 mg (20%). Oil. ^{1}H NMR (300 MHz, $CDCl_3$) δ: 7.06 (d, J= 8.2 Hz, 2H), 6.82 (d, J=2.4 Hz, 2H), 6.75 (dd, J=8.2, 2.6 Hz, 2H), 3.29 (s, 8H), 2.26 (s, 6H), 2.20 (s, 6H). ^{13}C NMR (75 MHz, $CDCl_3$) δ: 149.8 (2C, C), 137.3 (2C, C), 130.4 (2C, CH), 128.5 (2C, C), 118.5 (2C, CH), 114.2 (2C, CH), 50.3 (4C, CH_2), 20.4 (2C, CH_3), 18.9 (2C, CH_3). HRMS for $C_{20}H_{26}N_2$ [M+H$^+$]: calculated: 295.2169; found: 295.2170. IR (ATR): 2963, 2919, 2822, 1616, 1504, 1447, 1336, 1235, 1178, 1156, 1127, 1023, 1000, 961, 872, 850, 807, 703.

1,4-Bis(3,5-dimethylphenyl)-piperazine (**5g**) Isolated yield: 33 mg (27%). Oil. ^{1}H NMR (300 MHz, $CDCl_3$) δ: 6.64 (s, 4H), 6.58, (s, 2H), 3.33 (s, 8H), 2.32 (s, 6H). ^{13}C NMR (75 MHz, $CDCl_3$) δ: 151.5 (2C, C), 138.4 (2C, CH), 122.5 (4C, C), 114.5 (4C, CH), 49.9 (8C, CH_2), 21.8 (4C, CH_3). HRMS for $C_{20}H_{26}N_2$ [M+H$^+$]: calculated: 295.2169; found: 295.2168. IR (ATR): 2978, 2830, 2802, 1596, 1451, 1438, 1384, 1343, 1257, 1198, 1153, 1011, 827, 696, 685.

1,4-Bis(2,5-dimethylphenyl)-piperazine (**5h**) Isolated yield: 25 mg (20%). Oil. ^{1}H NMR (300 MHz, $CDCl_3$) δ: 7.09 (d, J=7.5 Hz, 2H), 6.92 (s, 2H), 6.83 (d, J=7.5 Hz, 2H), 3.07 (s, 8H), 2.33 (s, 6H), 2.32 (s, 6H). ^{13}C NMR (75 MHz, $CDCl_3$) δ: 151.7 (2C, C), 136.2 (2C, C), 131.1 (2C CH), 129.5 (2C, C), 123.9 (2C, CH), 120.1 (2C, CH), 52.4 (4C, CH_2), 21.4 (2C, CH_3), 17.7 (2C, CH_3). HRMS for $C_{20}H_{26}N_2$ [M+H$^+$]: calculated: 295.2159, found: 295.2167. IR: 2946, 2920, 2812, 1504, 1448, 1370, 1238, 1219, 1145, 1126, 992, 804, 772.

1,4-Bis(2,3-dimethoxyphenyl)-piperazine (**5w**) Isolated yield: traces. Oil. ^{1}H NMR (300 MHz, $CDCl_3$) δ: 6.82 (d, J= 8.7 Hz, 2H), 6.66 (bs, 2H), 6.53 (dd, J= 8.6; 2.6 Hz, 2H), 3.89 (s, 6H), 3.85 (s, 6H), 3.28 (s, 8H). ^{13}C NMR (75 MHz, $CDCl_3$) δ: 149.7 (4C, C), 112.2 (2C, CH), 108.5 (4C, C), 103.4 (2C, CH), 56.4 (2C, CH_3), 56.0 (2C, CH_3), 51.3 (4C, CH_2). HRMS for $C_{20}H_{26}N_2O_4$ [M+H$^+$]: calculated: 359.1965; found: 359.1963. IR (ATR): 2943, 2836, 2803.

N-(2-Hydroxyethyl)-1,2,3,4-tetrahydroquinoline (**7a**)[49] Isolated yield: 79 mg (45%). Oil. ^{1}H NMR (300 MHz, $CDCl_3$) δ: 7.26-6.36 (m, 4H), 3.70-3.10 (m, 6H), 2.75 (t, J= 6 Hz, 2H), 1.91 (m, 2H). ^{13}C

NMR (75 MHz, $CDCl_3$) δ: 146.0 (1C, C), 129.5 (1C, CH), 127.2 (1C, CH), 123.02 (1C, C), 116.6(1C, CH), 111.5 (1C, CH), 60.1 (1C, CH_2), 54.3 (1C, CH_2), 50.5 (1C, CH_2), 28.2 (1C, CH_2), 23.03 (1C, CH_2).

5,6-Dihydro-4*H*-pyrrolo-[3,2,1-*ij*]-quinoline (**7b**)[50] Isolated yield: 70 mg (45%). Oil. ^{1}H NMR (300 MHz, $CDCl_3$) δ: 7.37 (dd, J= 7.9; 0.8 Hz, 1H), 7.00 (d, J= 3.0 Hz, 1H), 6.94 (dd, J= 7.9; 7.1 Hz, 1H), 6.84 (dd, J= 7.1; 0.9 Hz, 1H), 6.37 (d, J= 3.0 Hz, 1H), 4.09 (t, J= 5.7 Hz, 2H), 2.93 (t, J= 6.1 Hz, 2H), 2.17 (m, 2H). ^{13}C NMR (75 MHz, $CDCl_3$) δ: 134.3 (1C, CH), 126.1 (1C, CH), 126.0 (1C, C), 122.0 (1C, C), 119.8 (1C, CH), 118.7 (1C, CH), 118.3(1C, CH), 100.5 (1C, CH), 44.3 (1C, CH_2), 24.9 (1C, CH_2), 23.1 (1C, CH_2).

3,4-Dihydro-6-methoxy-1(2*H*)-quinolinethanol (**9a**) Isolated yield: 39 mg (18%). Oil. ^{1}H NMR (300 MHz, $CDCl_3$) δ: 6.66 (m, 2H), 6.59 (m, 1H), 3.79 (t, J= 5.7 Hz, 2H), 3.73 (s, 3H), 3.37 (t, J= 5.7 Hz, 2H), 3.25-3.20 (m, 2H), 2.77 (t, J= 6.5 Hz, 2H), 2.01-1.89 (m, 2H). ^{13}C NMR (75 MHz, $CDCl_3$) δ: 151.7 (1C, C), 140.7 (1C, C), 125.0 (1C, C), 115.3 (1C, CH), 113.7 (1C, CH), 112.7 (1C, CH), 59.9 (1C, CH_3), 55.9 (1C, CH_2), 55.5 (1C, CH_2), 50.3 (1C, CH_2), 28.3 (1C, CH_2), 22.2 (1C, CH_2). HRMS for $C_{12}H_{17}NO_2$ [M+H$^+$]: calculated: 208.1332; found: 208.1326. IR (ATR): 3355, 2929, 1502, 1464, 1429, 1334, 1296, 1265, 1238, 1201, 1151, 1036, 1004, 922, 879, 843, 796, 721, 670, 631.

5,6-Dihydro-8-methoxy-4*H*-pyrrolo[3,2,1-*ij*]quinoline (**9b**) Isolated yield: 30 mg (16%). Oil. ^{1}H NMR (300 MHz, $CDCl_3$) δ: 7.05 (d, J= 2.9 Hz, 1H), 6.91 (d, J= 2.2 Hz, 1H), 6.62 (dd, J= 1.5; 0.6 Hz, 1H), 6.36 (d, J= 2.9 Hz, 1H), 4.13 (t, J= 5.7 Hz, 2H), 3.84 (s, 3H), 2.96 (dd, J= 8.9; 3.4 Hz, 2H), 2.28-2.17 (m, 2H). ^{13}C NMR (75 MHz, CDCl3) δ: 154.84 (1C, C), 126.34 (1C, CH), 125.8 (1C, C), 122.7 (2C, C), 109.4 (1C, CH), 100.1 (1C, CH), 99.9 (1C, CH), 56.2 (1C, CH_3), 44.2 (1C, CH_2), 25.0 (1C, CH_2), 23.2 (1C, CH_2). HRMS for $C_{12}H_{13}NO$ [M+H$^+$]: calculated: 188.1070; found: 188.1066. IR (ATR): 2938, 1618, 1601, 1495, 1436, 1394, 1342, 1298, 1261, 1234, 1218, 1140, 1047, 1031, 830, 799, 716.

1*H*-Benzimidazole-2-methanol (**10**)[28,51] Isolated yield: 103 mg (70%). Yellow powder, m.p.= 169.5-170.5 ºC. ^{1}H NMR (300 MHz, CD_3OD) δ: 7.60-7.48 (m, 2H), 7.27-7.15 (m, 2H), 4.85 (s, 2H). ^{13}C NMR (75 MHz, CD_3OD) δ: 157.6 (1C, C), 139.9 (2C, C), 122.6 (2C, CH), 117.6 (2C, CH), 58.7 (1C, CH_2).

2,3-Dihydro-1*H*-indole-1-ethanol (**14a**) & 2-Indol-1-yl-ethanol (**14b**)[52] Isolated yield: 43 mg (26%, mixture). Oil. ^{1}H NMR (300 MHz, $CDCl_3$) δ: 7.67-7.63 (m, 1H-b), 7.38 (dd, J= 8.2; 0.8 Hz, 1H-b), 7.26-7.19 (m, 1H-a), 7.16 (d, J= 3.2 Hz, 1H-a), 7.15-7.06 (m, 3H-a,b), 6.72 (td, J=7.5; 0.9 Hz, 1H-a), 6.57 (d, J= 7.8 Hz, 1H-a, 6.53 (dd, J= 3.1; 0.8 Hz, 1H-a), 4.27 (t, J= 5.3 Hz, 2H-b), 3.93 (t, J= 5.3 Hz, 2H-b), 3.80 (t, J= 5.4 Hz, 2H-a), 3.39 (t, J= 8.3 Hz, 2H-a), 3.23 (t, J= 5.3 Hz, 2H-a), 3.00 (t, J= 8.3 Hz, 2H-a). ^{13}C NMR (75 MHz, $CDCl_3$) δ: 152.8 (1C, C), 136.2 (1C, C), 130.2 (1C, C), 128.8 (1C, C), 128.5 (1C, CH-a), 127.5 (1C, CH-a,b), 124.7 (1C, CH-a,b), 121.8 (1C, CH-a), 121.2 (1C, CH-b), 119.7 (1C, CH-a,b), 118.6 (1C, CH-a), 109.4 (1C, CH-b), 107.6 (1C, CH-a), 101.6 (1C, CH-b), 62.0 (1C, CH_2-b), 60.3 (1C, CH_2-a), 54.0 (1C, CH_2-a), 52.8 (1C, CH_2-a), 48.9 (1C, CH_2-b), 28.8 (1C, CH_2-a).

2-(5-Methoxyindolin-1-yl)ethanol (**15a**) Isolated yield: 22 mg (11%). Oil. ^{1}H NMR (300 MHz, $CDCl_3$) δ: 6.78-6.75 (m, 1H), 6.66 (dd, J= 8.5; 2.6 Hz, 1H), 6.53 (d, J=8.5 Hz, 1H), 3.81 (t, J= 5.4 Hz, 2H), 3.75 (s, 3H), 3.35 (t, J= 8.1 Hz, 2H), 3.18 (t, J= 5.4 Hz, 2H), 2.97 (t, J= 8.1 Hz, 2H), 2.24 (bs, 1H). ^{13}C NMR (75 MHz, $CDCl_3$) δ: 153.8 (1C, C), 132.0 (2C, C), 112.1(2C, CH), 108.5 (1C, CH), 60.2 (1C, CH_2), 56.2 (1C, CH_2), 54.8 (1C, CH_3), 54.1 (1C, CH_2), 29.1 (1C, CH_2). HRMS for $C_{11}H_{15}NO_2$ [M+H$^+$]: calculated: 194.1176; found: 194.1171. IR (ATR): 3361, 2934, 2830, 1620, 1594, 1576, 1488, 1449, 1435, 1397, 1360, 1236, 1190, 1150, 1051, 1030, 939, 864, 833, 798, 753, 724.

2-(5-Methoxy-1H-indol-1-yl)ethanol (**15b**) Isolated yield: 20 mg (10%). Oil. ^{1}H NMR (300 MHz, $CDCl_3$) δ: 7.25 (d, J= 8.9 Hz, 1H), 7.12 (d, J= 3.1 Hz, 1H), 7.10 (d, J= 2.4 Hz, 1H), 6.88 (dd, J= 8.9; 2.5 Hz, 1H), 6.44 (dd, J= 3.1; 0.8 Hz, 1H), 4.23 (t, J= 5.3 Hz, 2H), 3.91 (t, J= 5.3 Hz, 2H), 3.85 (s, 3H). ^{13}C NMR (75 MHz, $CDCl_3$) δ: 154.3 (1C, C), 131.6 (1C, C), 129.2 (1C, C), 129.0 (1C, CH), 112.2 (1C, CH), 110.2 (1C, CH), 102.8(1C, CH), 101.3 (1C, CH), 62.2 (1C, CH_2), 56.0 (1C, CH_2), 49.0 (1C, CH_3). HRMS for $C_{11}H_{13}NO_2$ [M+H$^+$]: calculated: 192.1019; found: 192.1013. IR (ATR): 3409, 2940, 2831, 1621, 1487, 1449, 1237, 1190, 1150, 1063, 1030, 799, 721.

Associated Content

Supporting Information
Additional information, complete table of *Figure 2*, additional mechanistic experiments, ^{1}H- and ^{13}C-NMR spectra of all compounds (PDF).

Author Information
Corresponding Author:
*E-mail: rafael.ballesteros-garrido@uv.es

Notes
The authors declare no competing financial interest.

Acknowledgements
R. B-G is much indebted to the Postdoctoral fellow 2013 of the "Ministerio de Economía y Competitividad" (Spain, FPDI-2013-17464). This work was financially supported by the "Ministerio de Ciencia e Innovación" (Spain) (Project CONSOLIDER-INGENIO SUPRAMED CSD 2010-00065 and from University of Valencia (Spain) (UV-INV-AE 15-332846)). Acknowledgments to the "Central Services for Experimental Research" (SCSIE) of University of Valencia and NANBIOSIS platform. We gratefully acknowledge the suggestions and advice from the referee in order to improve the quality of this contribution.

References

1) C.J. Li, B.M. Trost, *PNAS*, **2008**, *105*, 13197.

2) B.M. Trost, *Angew. Chem. Int. Ed.*, **1995**, *34*, 259.

3) A.J.A. Watson, J.M.J. Williams, *Science*, **2010**, *329*, 635.

4) M.H.S.A. Hamid, P.A. Slatford, J.M.J. Williams, *Adv. Synth. Catal.*, **2007**, *349*, 1555.

5) G. Guillena, D.J. Ramon, M. Yus, *Chem. Rev.*, **2010**, *110*, 1611.

6) a) S. Michlik, R. Kempe, *Nat. Chem.*, **2013**, *5*, 140. b) N. Andrushko, V. Andrushko, P. Roose, K. Moonen, A. Börner, *ChemCatChem*, **2010**, *2*, 640.

7) S.C. Bergmeier, *Tetrahedron*, **2000**, *56*, 2561.

8) D.A. Ager, I. Prakash, D.R. Schaad, *Chem. Rev.*, **1996**, *96*, 835.

9) M.H.M.S. Hamid, C.L. Allen, G.W. Lamb, A.C. Maxwell, H.C. Maytum, A.J.A. Watson, J.M.J. Williams, *J. Am. Chem. Soc.*, **2009**, *131*, 1766.

10) a) Y. Tsuji, K.T. Huh, Y.J. Watanabe, *Org. Chem.*, **1987**, *52*, 1673. b) S. Bähn, A. Tillack, S. Imm, K. Mevius, D. Michalik, D. Hollmann, L. Neubert, M. Beller, *ChemSuSChem*, **2009**, *2*, 551.

11) M. Selva, A. Perosa, M. Fabris, *Green Chem.*, **2008**, *10*, 1068.

12) A.B. Shivarkar, S.P. Gupte, R.V. Chaudhari, *SYNLETT*, **2006**, *9*, 1374.

13) K.I. Shimizu, *Catal. Sci. Technol.*, **2015**, *5*, 1412.

14) B. Gnanaprakasam, E. Balaraman, Y. Ben-David, D. Milstein, *Angew. Chem. Int. Ed.*, **2011**, *50*, 12240.

15) B. Abarca, R. Adam, R. Ballesteros, *Org. Biomol. Chem.*, **2012**, *10*, 1826.

16) S.J. Kolboe, *Catal.*, **1972**, *27*, 379.

17) H.D. Müller, F. Steinbach, *Nature*, **1970**, *225*, 728.

18) J.M. Vohs, A. Barteau, *Surf. Sci.*, **1989**, *221*, 590.

19) M.I. Nokkosmäski, E.T. Kuoppala, B.A. Leppämäki, A.O.I. Krausse, *J. Anal. Appl. Pyrol.*, **2000**, *55*, 119.

20) T. Nakajima, K. Tanabe, T. Yamaguchi, I. Matsuzaki, S. Mishima, *Appl. Catal.*, **1989**, *52*, 237.

21) A. Kolodziejczak-Radzimska, T. Jesionowski, *Materials*, **2014**, *7*, 2833.

22) S.D. Lacroix, A. Pennycook, S. Liu, T.T. Eisenhart, A.C. Marr, *Catal. Sci. Technol.*, **2012**, *2*, 288.

23) a) A. Hassanpour, R.H. Khanmiri, J. Abolhasani, *Synthetic Commun.*, **2015**, *45*, 727. b) L. Dinparast, H. Valizadech, *Monatsh. Chem.*, **2015**, *146*, 313.

24) a) A. Labed, F. Jiang, I. Labed, A. Lator, M. Peters, M. Achard, A. Kabouche, Z. Kabouche, G.V.M. Sharma, C. Bruneau, *Chem. Cat. Chem.*, **2015**, *7*, 1090. b) Q. Yang, Q. Wang, Z. Yu, *Chem. Soc. Rev.*, **2015**, *44*, 2305.

25) J.A. Marsella, *J. Organomet. Chem.*, **1991**, *407*, 97.

26) A. Corma, T. Ródenas, M.J. Sabater*, Chem. Eur. J.*, **2010**, *16*, 254.

27) ZnO has been reported to be soluble in hot ethylene glycol this is in agreement with our ICP results see SI 3.1: J. Wang, Y. Chen, W. Shen, Z. Zhu, Y. Xu, Y. Fang, *Catal Comun.*, **2017**, *89*, 52.

28. a) K.J. Voight, *Prakt. Chem.*, **1886**, *34*, 1. b) Z. Wang, Comprehensive Organic Name Reactions and Reagents "Voight reaction", 2010, 2888.

29 a) L. Lorentz-Petersen, L. Nordstrom, R. Madsen, *Eur. J. Org. Chem.*, **2012**, *34*, 6752. b) J. Xing, X. Jia, *Adv. Mat. Res.*, **2011**, 668. c) M. Tursky, L.L.R. Lorentz-Petersen, L.B. Olsen, R. Madsen, *Org. Biomol. Chem.*, **2010**, *8*, 5576. This methodology has also been explored by d) M. Zhang, F. Xie, X.T. Wang, F. Yan, T. Wang, M. Chen, Y. Ding, *RSC Adv.*, **2013**, *3*, 6022.

30) S.M.A.H. Siddiki, K. Kon, K.I. Shimizu, *Green Chem.*, **2015**, *17*, 173.

31) S. Baehn, S. Imm, K. Mevius, L. Neubert, A. Tillack, J.M.J. Williams, M. Beller, *Chem. Eur. J.*, **2010**, *16*, 3590.

32) A. Shafir, P. Lichtor, S. Buchwald, *J. Am. Chem. Soc.*, **2007**, *129*, 3490.

33) H. Yin, M. Jin, W. Chen, C. Chen, L. Zheng, P. Wei, S. Ha, *Tetrahedron Lett.*, **2012**, *53*, 1265.

34) B.A. Bhanu Prasad, S.R. Gilbertson, *Org. Lett.*, **2009**, *11*, 3710.

35) M. Yang, F. Liu, *J. Org. Chem.*, **2007**, *72*, 8969.

36) P. Haldar, J. Ray, *Org. Lett.*, **2005**, *7*, 4341.

37) M. Shi, Y. Chen, *J. Fluorine Chem.*, **2003**, *122*, 219.

38) Y. Yin, K. Zhen, N. Eid, S. Howard, J. Jeong, F. Yi, J. Guo, C. Min Park, M. Bibian, W. Wu, P. Hernandez, H. Park, Y. Wu, J. Luo, P. LoGrasso, Y. Feng, *J. Med. Chem.*, **2015**, *58*, 1846.

39) P. Thansandote, D. Hulcoop, M. Langer, M. Lautens, *J. Org. Chem.*, **2009**, *74*, 1673.

40) a) **3b**: I. Taydakov, T. Dutova, E. Sidorenko, S.S. Krasnoselsky, *Chem. Heterocycl. Comp.*, **2011**, *47*, 425. b) **3b'** A. Dobbs, *J. Org. Chem.*, **2001**, *66*, 638.

41) C. Hartung, A. Fecher, B. Chapell, V. Snieckus, *Org. Lett.*, **2003**, *5*, 1899.

42) C.S. Cho, H.K. Lim, S.C. Shim, T.J. Kim, H.J. Choi, *Chem. Commun.*, **1998**, 995.

43) J. Ezquerra, C. Pedregal, C. Lamas, J. Barluenga, M. Pérez, M.A. García-Martín, J.M. González, *J. Org. Chem.*, **1996**, *61*, 5804.

44) K.L. Brown, T. Chanda, S. Zou, E.J. Valente, *Nucleos. Nucleot. Nucl.*, **2005**, *24*, 1147.

45) N. Thies, C. Hrib, E. Haak, *Chem. Eur. J.*, **2012**, *18*, 6302.

46) O. Onajole, M. Pieroni, S. Tipparaju, S. Lun, J. Stec, G. Chen, H. Gunosewoyo, H. Guo, N. Ammerman, W. Bishai, A. Kozikowski, *J. Med. Chem.*, **2013**, *56*, 4093.

47) G. Bratulescu, *Tetrahedron Lett.*, **2008**, *49*, 984.

48) L. De Luca, S. De Grazia, S. Ferro, R. Gitto, F. Christ, Z. Debyser, A. Chimirri, *Eur. J. Med. Chem.*, **2011**, *46*, 756.

49) T. Matsumura, M. Nakada, *Tetrahedron Lett.*, **2014**, *55*, 1412.

50) S. Zhuangzhi, Z. Chun, L. Si, P. Delin, D. Shengtao, C. Yuxin, J. Ning, *Angew. Chem. Int. Ed.*, **2009**, *48*, 4572.

51) M. Voigt, M. Smuda, C. Pfahler, M. Glomb, *J. Agric. Food Chem.*, **2010**, *58*, 5685.

52) J.A. Schiffner, T.H. Wöste, M. Oestreich, *Eur. Joc. Chem.*, **2010**, *1*, 174.

SUPPORTING INFORMATION

β-Amino Alcohols from Anilines and Ethylene Glycol through Heterogeneous Borrowing Hydrogen Reaction

Pedro J. Llabres-Campaner, Rafael Ballesteros-Garrido, Rafael Ballesteros and Belén Abarca.*

Departament de Química Orgànica, Universitat de València, Av. Vicent Andrés Estellés s/n, 46100 Burjassot, Valencia, Spain.

E-mail: rafael.ballesteros-garrido@uv.es

Contents

S1. Experimental procedure

S1.1. Materials and Measurements

Starting materials, if commercially available, were purchased and used as such. ^{1}H and (^{1}H decoupled) ^{13}C nuclear magnetic resonance (NMR) spectra were recorded at 300 and 75 MHz. Pd/C and ZnO were obtained commercially from Sigma Aldrich: Pd/C (Palladium on activated charcoal) 10% Pd basis; ZnO acs reagent >99%. Chemical shifts are reported in δ units, parts per million (ppm), and were measured relative to the signals for residual chloroform. Coupling constants (J) are given in Hz. COSY and HSQC experiments were performed for all compounds. IR spectra were recorded using FT-IR ATR. HRMS were recorded using TOF electrospray ionization (ESI-positive). The solvents used were of spectroscopic or equivalent grade. Water was twice distilled and passed through a Millipore apparatus. Teflon flasks were cleaned with 1M HCl water solution twice after each reaction and with water. ICP-MS were performed under Helium mode; Germanium and Rhodium were used as internal standards.

S1.2. General Procedure

1 mmol of amine (indole, 1,2,3,4-tetrahydroquinoline or indoline), 0.07 mmol of Pd/C, 3 mmol of ZnO, 6 mL of distillated water and 6 mL of ethylene glycol were mixed manually inside a 20 ml Teflon flask. Then it was sealed into a steel autoclave and introduced in a preheated oven at 150 ºC for 24h. The reaction mixture was cooled to room temperature, 25 mL of distilled water were added and the crude was filtered through a 0.2 µm Teflon filter. The reaction mixture was extracted with ethyl acetate 3x15ml and organic layers were combined, dried with Na_2SO_4, filtered and concentrated affording the reaction crude that was cheeked by NMR. Crude reaction was purified by chromatotron (1 mm, silica, from hexane to hexane/AcOEt 1:3) affording pure β–amino alcohols.

S2. Screening reactions

The initial screening conditions (*Table S1, entries 1-4*) showed that at 200ºC, during 24h or 64h, using either Zn or ZnO, the initial product was transformed completely, but without any selectivity by 2a, as it can be seen also in the first three spectra of *Figure S1*. However, a reduction of the temperature in 50ºC allowed selectivity to the β-amino alcohol 2a, without a reduction of conversion (residual signals are ethyl acetate), all spectra in *Figure S1* correspond to the crude NMR after work up to measure conversions.

Table S1. Screening condition for the preparation of β-amino alcohol **2a** by Heterogeneous BH reaction.

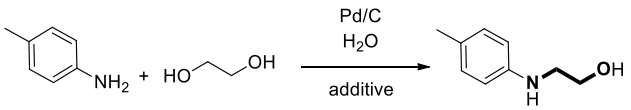

1 **2a**

Entry	*p*-toluidine (1)	T (ºC)	time	EG	water	Catalyst	Additive	Conv.[a]	Selec.
1	**1 mmol**	**200 ºC**	**64 h**	**6 mL**	**6 mL**	**Pd/C 7 %**	**Zn 3 eq.**	**99%**	**0**
2	**1 mmol**	**200 ºC**	**64 h**	**6 mL**	**6 mL**	**Pd/C 7 %**	**ZnO 3 eq.**	**99%**	**0**
3	**1 mmol**	**200 ºC**	**24 h**	**6 mL**	**6 mL**	**Pd/C 7 %**	**ZnO 3 eq.**	**99%**	**0**
4	**1 mmol**	**150 ºC**	**24 h**	**6 mL**	**6 ml**	**Pd/C 7 %**	**ZnO 3 eq.**	**92%**	**98% (88%)[b]**

a. Conversion based on *p*-toluidine by ^{1}H-NMR, selectivity measured towards **2a**. b. isolated yield.

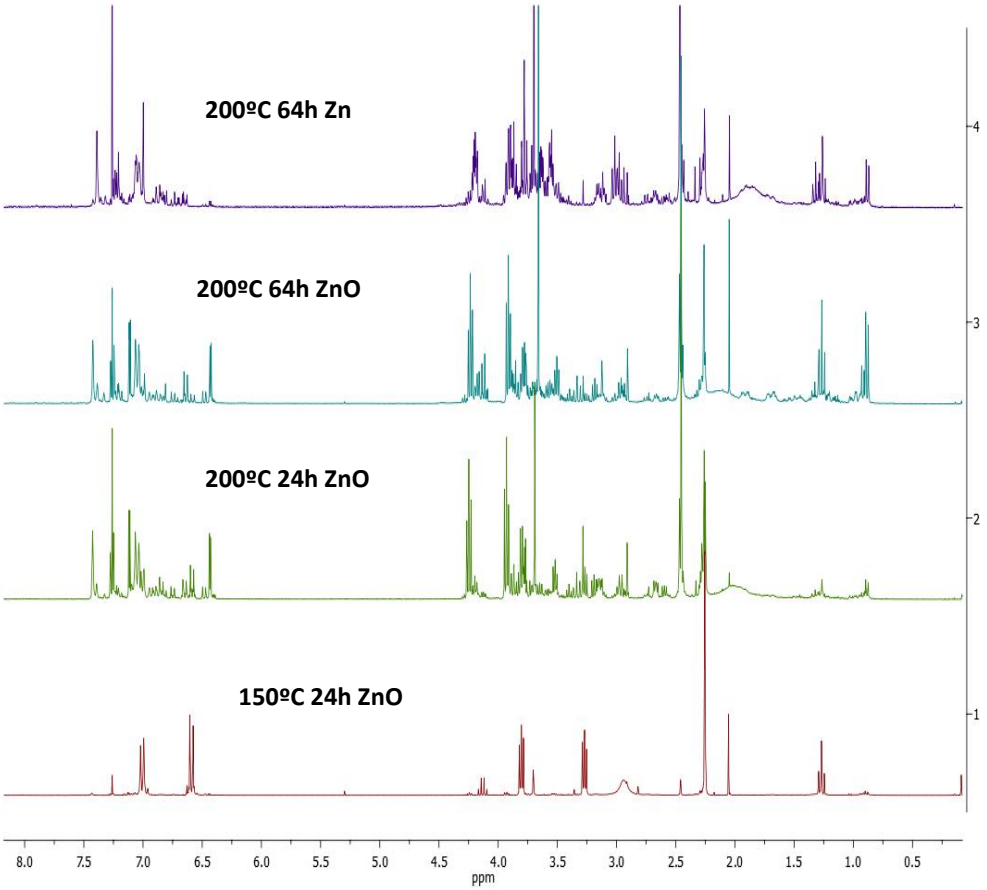

Analyzing the scope of the reaction, all side products, indoles and dimers (piperazine and ethylenediamine derivatives), were isolated and characterized when obtained amount was enough. In almost every case the amount of side product was low, according to the low selectivity. All the isolated compounds of each reaction are shown in *Table S2*.

Table S2. Isolated compounds in each reaction starting from different aryl amines.

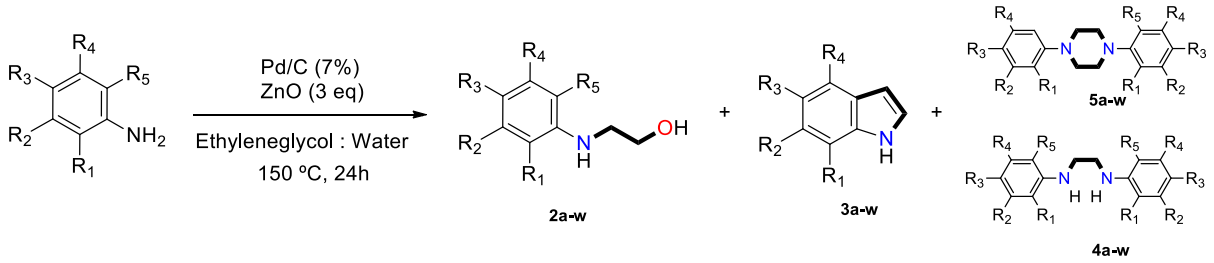

Entry	R_1	R_2	R_3	R_4	R_5	Conversion	Selectivity		2[a]	3[a]	4[a]	5[a]
A	H	H	Me	H	H	99%	98%	a	88%	traces	traces	traces
B	H	Me	H	H	H	63%	70%	b	39%	17%	traces	-
C	Me	H	H	H	H	58%	73%	c	28%	20%	traces	24%
D	Me	Me	H	H	H	47%	57%	d	22%	traces	traces	-
E	Me	H	Me	H	H	63%	64%	e	23%	traces	traces	traces
F	H	Me	Me	H	H	80%	70%	f	30%	traces	20%	-
G	H	Me	H	Me	H	75%	65%	g	30%	32%	27%	traces
H	Me	H	H	Me	H	75%	60%	h	39%	traces	20%	-
I	Me	H	H	H	Me	15%	99%	i	12%	-	-	-
J	H	H	H	H	H	79%	86%	j	65%	-	-	-
K	H	NO_2	H	H	H	< 5%	-	k	-	-	-	-
L	H	H	NO_2	H	H	< 5%	-	l	-	-	-	-
M	H	H	CN	H	H	< 5%	-	m	-	-	-	-
N	H	H	F	H	H	90%	46%	n	34%	-	-	-
O	H	F	H	H	H	51%	86%	o	32%	-	-	traces
P	F	H	H	H	H	>95%	80%	p	23%	-	traces	-
Q	CF_3	H	H	H	H	>95%	64%	q	41%	-	-	-
R	H	CF_3	H	H	H	>95%	80%	r	50%	-	-	-
S	OCF_3	H	H	H	H	>95%	45%	s	28%	-	-	traces
T	OMe	H	H	H	H	>95%	85%	t	65%	-	-	-
U	H	H	OMe	H	H	>95%	95%	u	70%	-	-	-
V	H	OMe	H	OMe	H	62%	42%	v	11%	10%	-	-
W	H	OMe	OMe	H	H	75%	36%	w	18%	20%	-	-

a: the percentage shown corresponds to the isolated yield of each compound. Traces correspond to quantities smaller than 5 mg that were isolated by chromatotron.

S3. Mechanistic Analysis

S3.1. Catalyst raw reutilization

Catalyst reutilization studies were carried out: reaction crude liquid phase was removed from the teflon flask by decantation, and new amine, ethylene glycol and water were introduced with the former catalyst. The reaction was heated again for 24 h. After three rounds, the conversion of the reaction still reaches around 70% with high selectivity (>90%).

ICP analyses were performed on the reactions crude by decantation and filtration through a PTFE 0.45 μm filter. The initial values pre reaction were <30 μg/L for Pd and 510 ± 2mg/L for Zn. After the reaction, same treatment was performed and the values obtained were <30 mg/L for Pd and 0.521 ± 0.007 mg/L. This clearly indicates that there is no Pd leach, and there is loose of the smaller particles of ZnO upon the reaction cycle (because of the filtration). Indeed, this value when calculated with reaction volume (12 mL) corresponds to 6 mg of Zn (from the overall/all size 250 mg that are employed). Further studies are ongoing to evaluate this behavior.

S3.2. Deuteration essay

Deuteration essays were taken place in order to study the double bond migration when the imine is formed. For that, compound 6 was put under the same conditions, but using D_2O as solvent (*Scheme S1*). As expected, β-amino alcohol 7a and indole 7b were formed. In the case of amino alcohol, the percentage of deuteration was identical at positions α and β to the nitrogen, while in the indole the amount of deuterium was higher at α position to the nitrogen. This indicates that, starting from the imine, there is a migration of the double bound, and equilibrium between enol and aldehyde forms is established. If the enol intermediate is hydrogenated, β-amino alcohol is obtained and the BH cycle is closed. However, the aldehyde intermediate can react with the aromatic ring by Electrophilic Aromatic Substitution (EAS), forming the corresponding indole. In this case, the BH cycle is not completed.

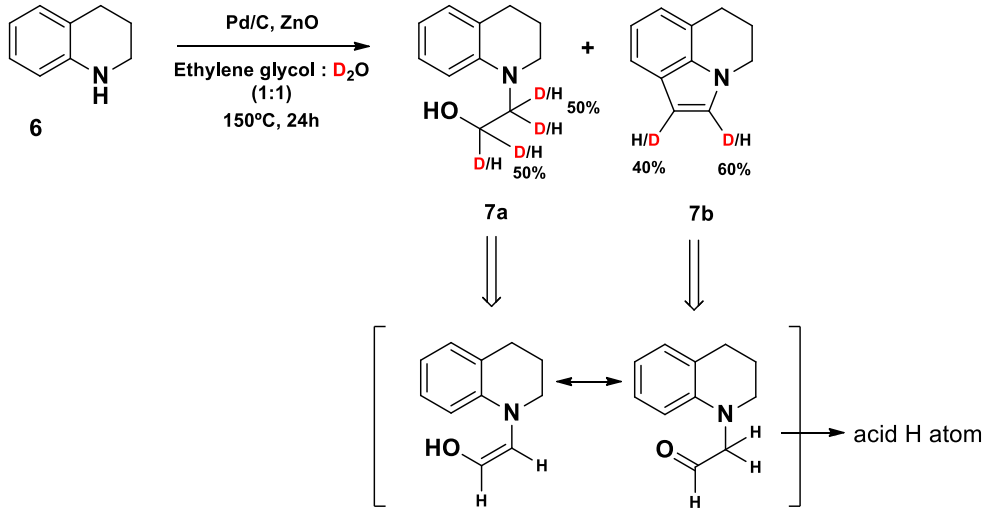

Scheme S1. Deuteration essay with **6**, using D_2O.

S3.3. Swern reaction

When Swern reaction was applied to alcohol 7a (*Scheme S2*), the aldehyde was not detected, because of the generation of indole 7b in situ. This proves that the generation of the indole goes through an aldehyde intermediate.

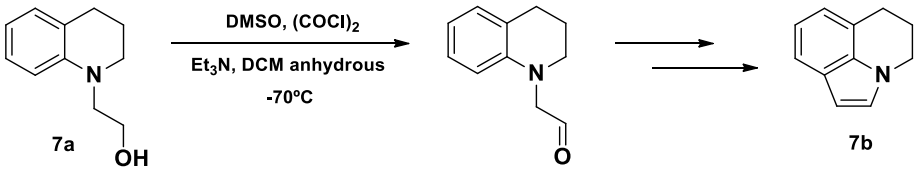

Scheme S2. Swern reaction applied to **7a**.

S3.4. Hot filtration test

In order to verify the heterogeneity of our method, hot filtration test was carried out (*Scheme S3*). After 3h of reaction, the Pd/C and the ZnO were removed by filtration, and the crude was introduced again on the autoclave and left to react for 21h. As expected, the conversion did not evolve without Pd/C and ZnO. It demonstrates that the catalysis is heterogeneous.

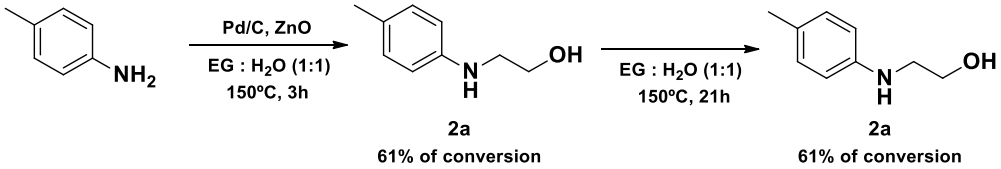

Scheme S3. Hot filtration test based on the formation of **2a**.

S3.5. Stability of β-amino alcohol

In order to verify the stability of β–amino alcohol, a test was carried out using compound 7a as reagent (*Scheme S4*). After 24h of reaction, the Pd/C and the ZnO were removed by filtration, and the crude was analyzed showing that β-amino alcohol 7a remained unaltered. Compound 7a was selected because of the large amount of indole 7b obtained with 6. As it has been proved in *Scheme S2*, if the aldehyde is generated indol must be observed. However, under our reaction conditions compounds 7a remains unaltered being indicative for: 1) Pd/C, ZnO is not activating compound 7a into a BH cycle, and 2) Compound 7a is not yielding to 7b in our reaction conditions.

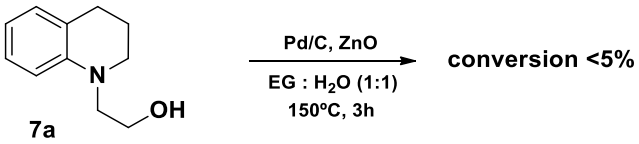

Scheme S4. Stability test applied to compound **7a**.

S3.6. X-Ray Powder Diffraction Analysis

In order to evaluate the stability of the Pd/C, ZnO system under our conditions, X-Ray Powder Diffraction of it before and after the reaction was carried out (*Figure S2*). As it can be seen, there was no change in the bands of both spectra, which verifies the stability of thesystem.

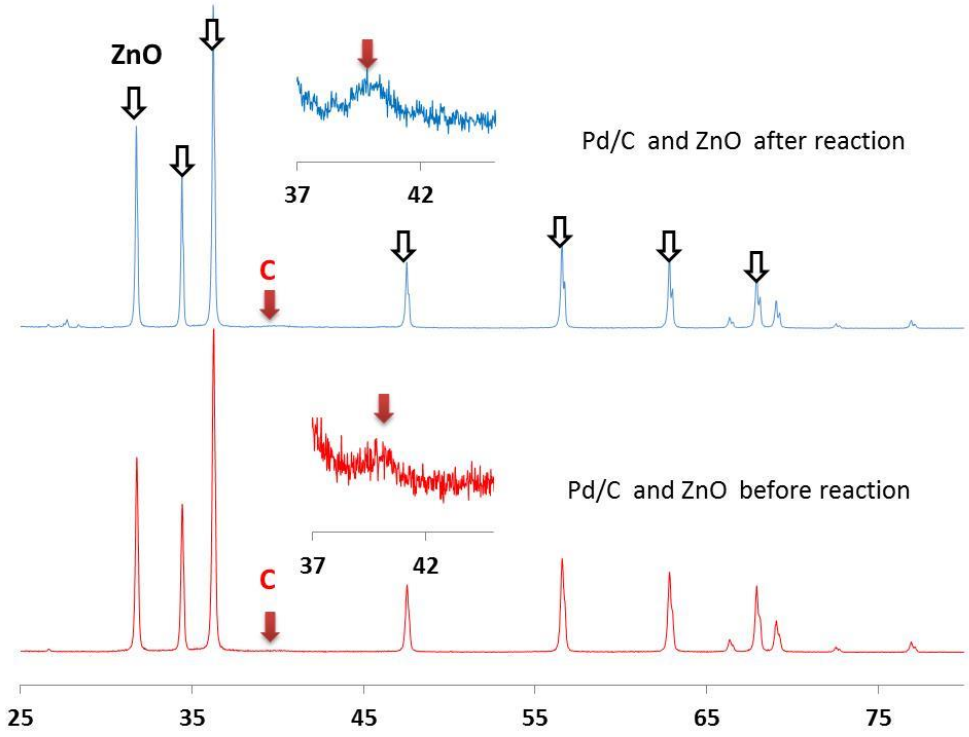

Figure S2. XRPD of Pd/C, ZnO system before and after the reaction.

SUPPORTING INFORMATION (II) – NMR SPECTRA

β-Amino Alcohols from Anilines and Ethylene Glycol through Heterogeneous Borrowing Hydrogen Reaction

Pedro J. Llabres-Campaner, Rafael Ballesteros-Garrido, Rafael Ballesteros and Belén Abarca.*

Departament de Química Orgànica, Universitat de València, Av. Vicent Andrés Estellés s/n, 46100 Burjassot, Valencia, Spain.

E-mail: rafael.ballesteros-garrido@uv.es

^{1}HNMR, ^{13}CNMR, H-COSY and edited HSQC of new compounds are shown.

2-((4-methylphenyl)amino)ethanol (2a)

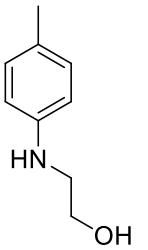

^{1}H NMR Spectrum
(300 MHz, $CDCl_3$)

^{13}C NMR Spectrum
(75 MHz, $CDCl_3$)

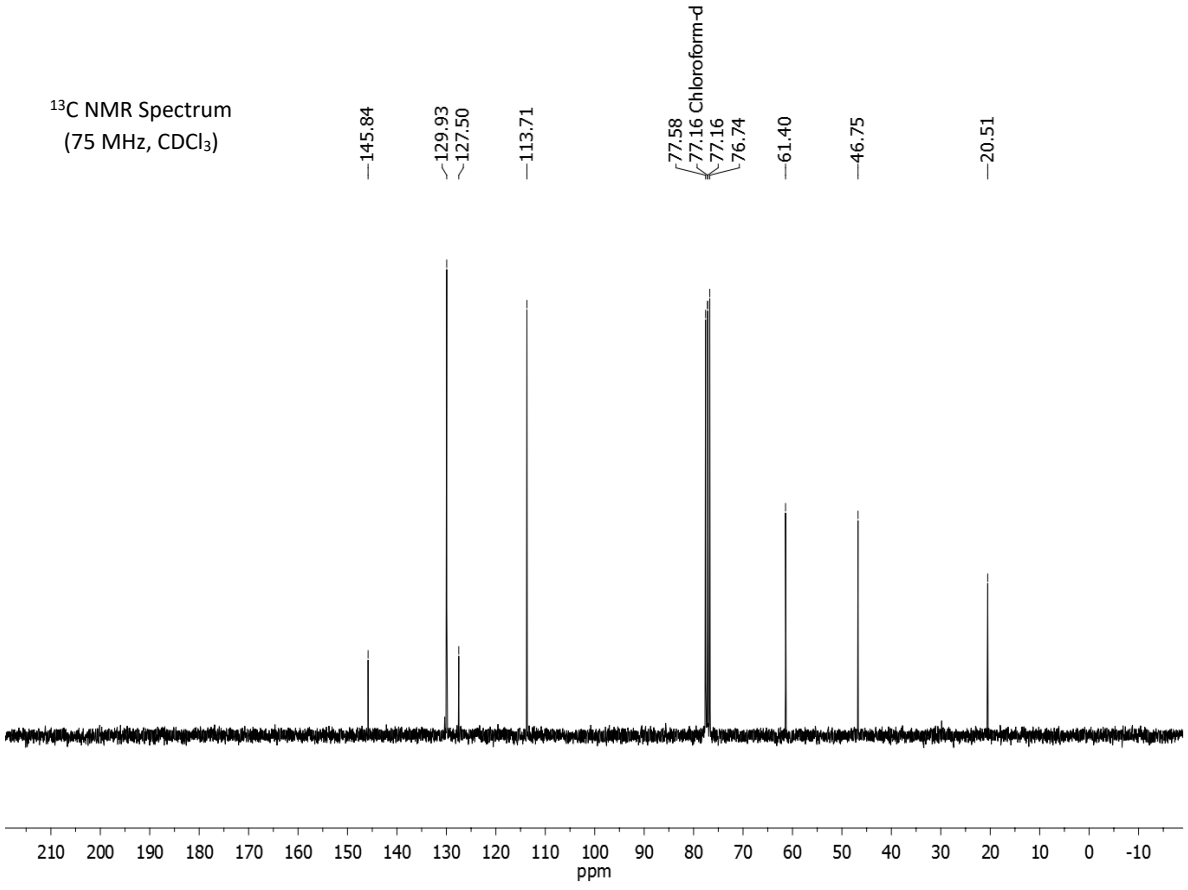

COSY Spectrum
($CDCl_3$)

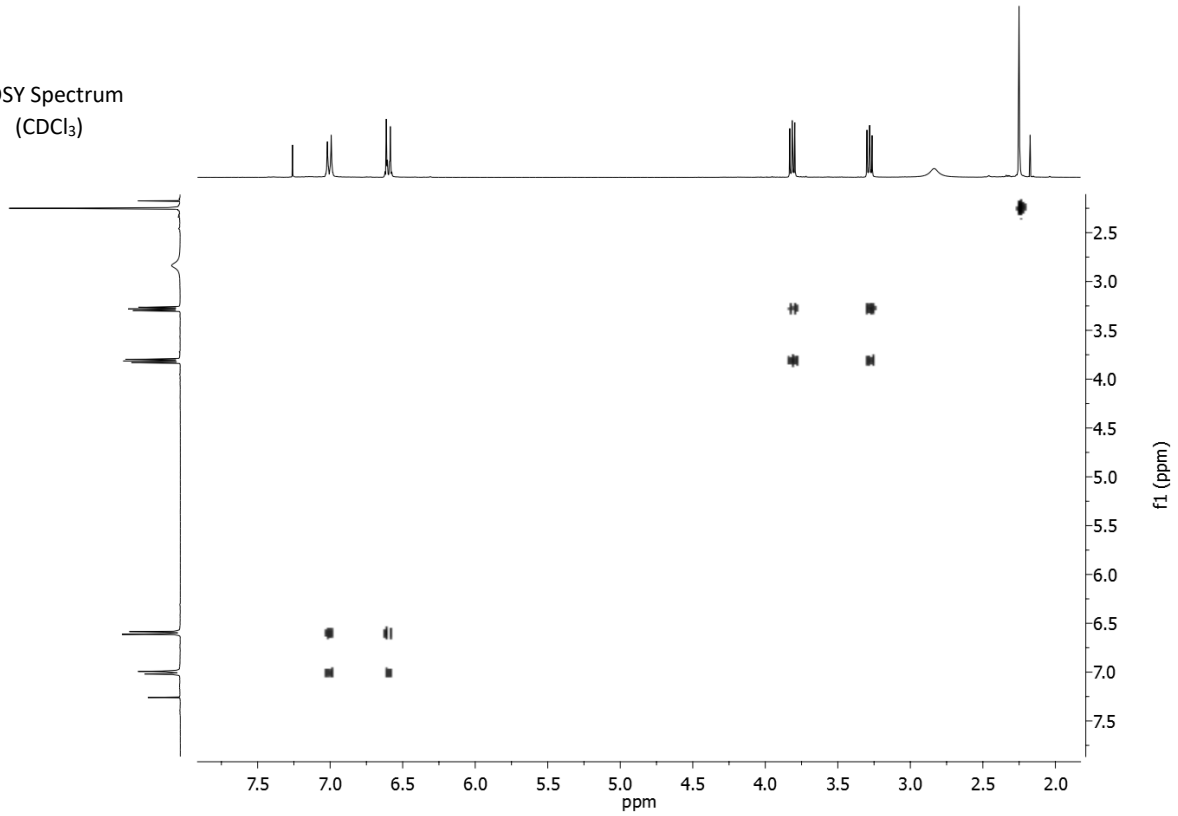

ed-HSQC Spectrum
($CDCl_3$)

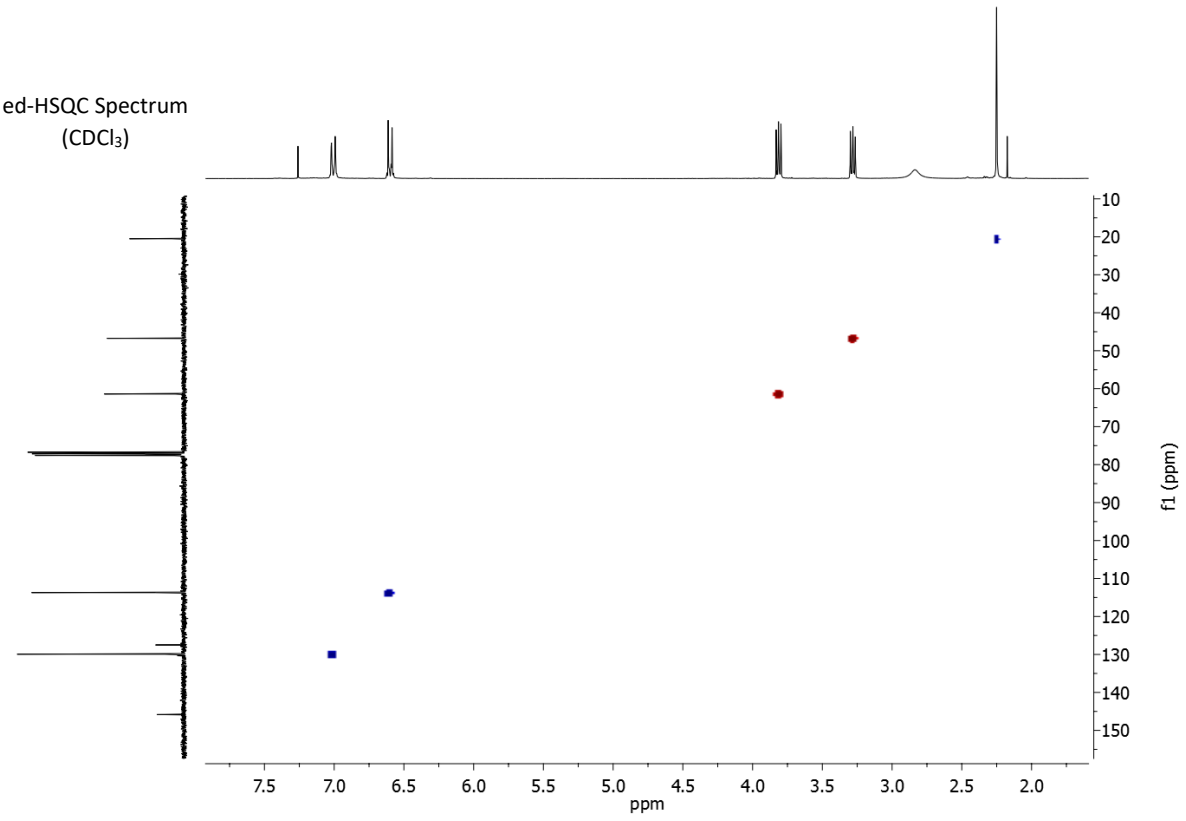

2-((3-methylphenyl)amino)ethanol (2b)

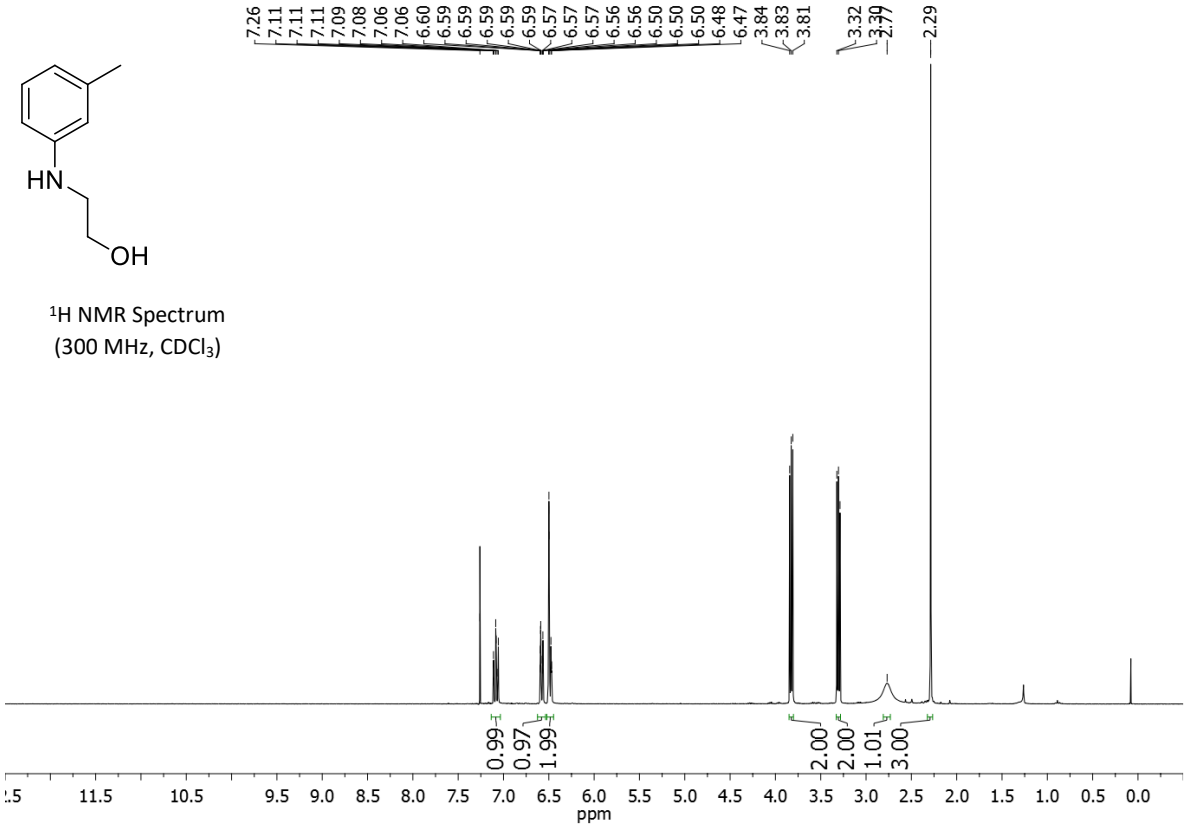

^{1}H NMR Spectrum
(300 MHz, $CDCl_3$)

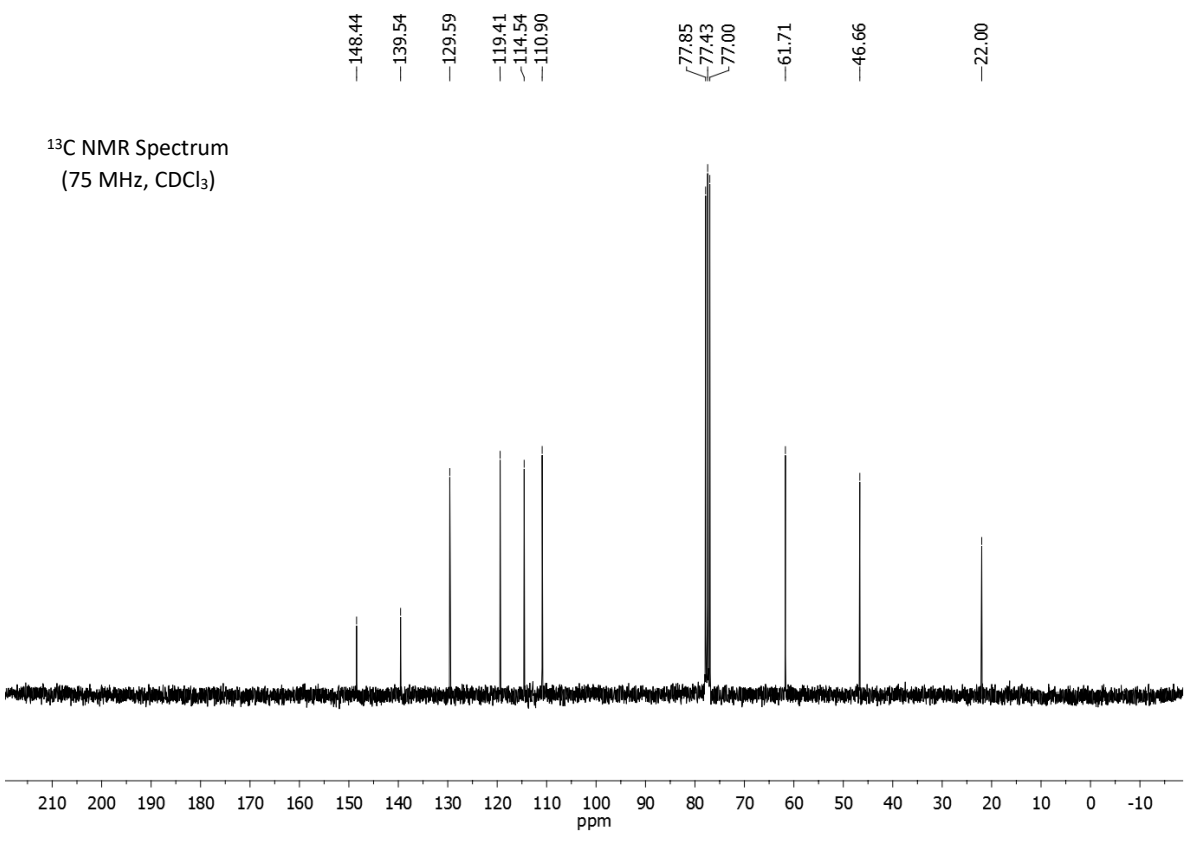

^{13}C NMR Spectrum
(75 MHz, $CDCl_3$)

COSY Spectrum ($CDCl_3$)

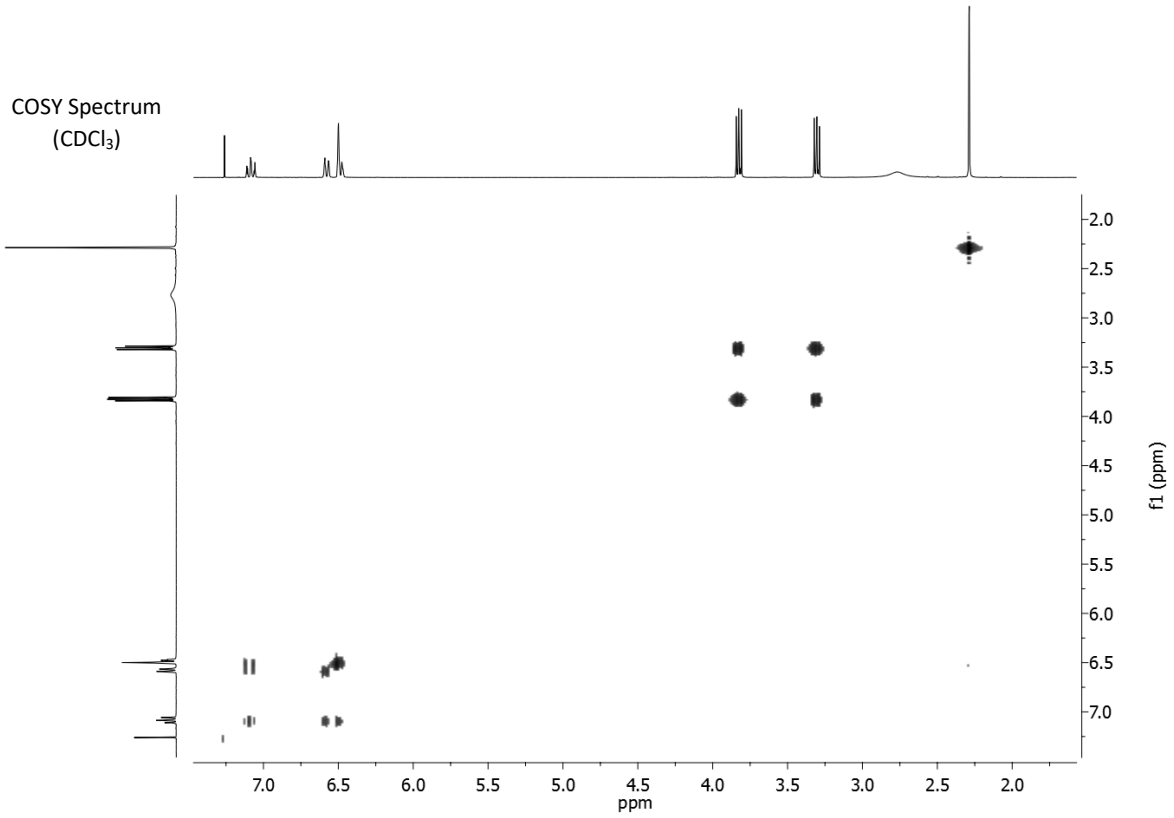

ed-HSQC Spectrum ($CDCl_3$)

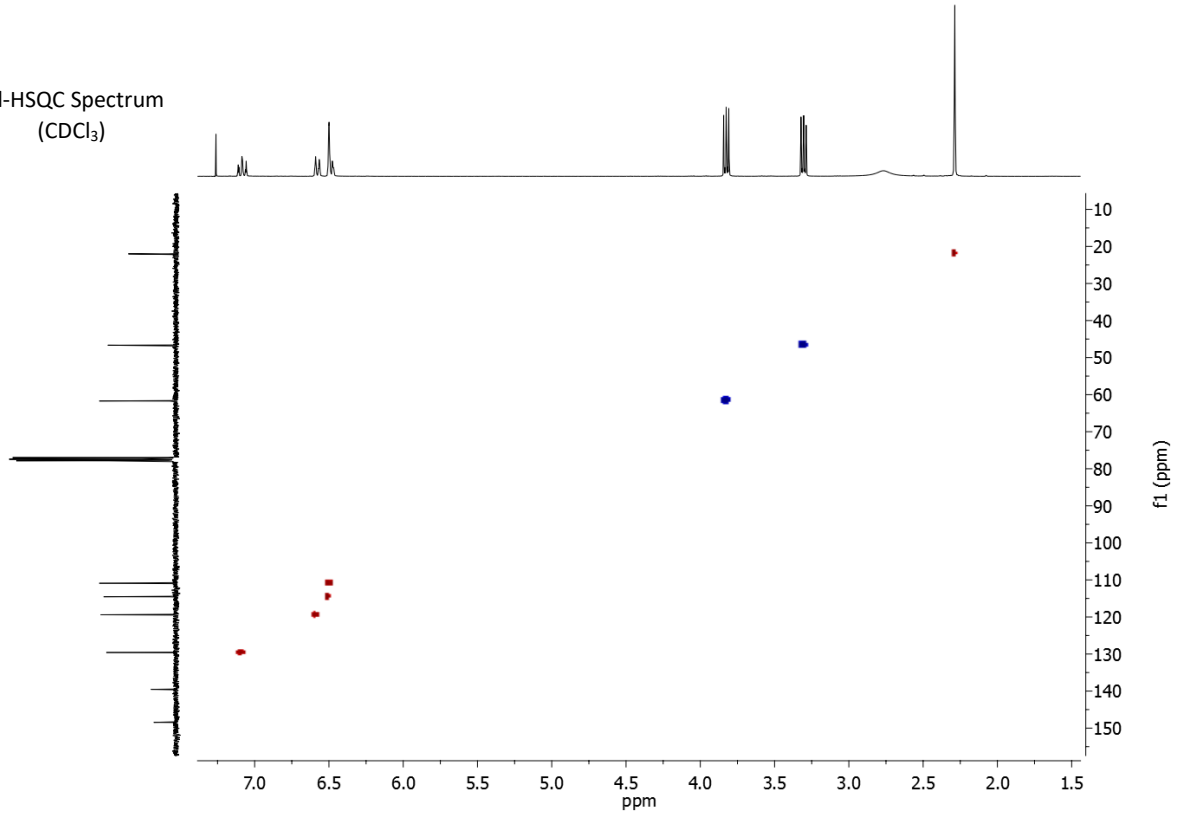

2-((2-methylphenyl)amino)ethanol (2c)

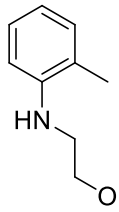

^{1}H NMR Spectrum
(300 MHz, $CDCl_3$)

^{13}C NMR Spectrum
(75 MHz, $CDCl_3$)

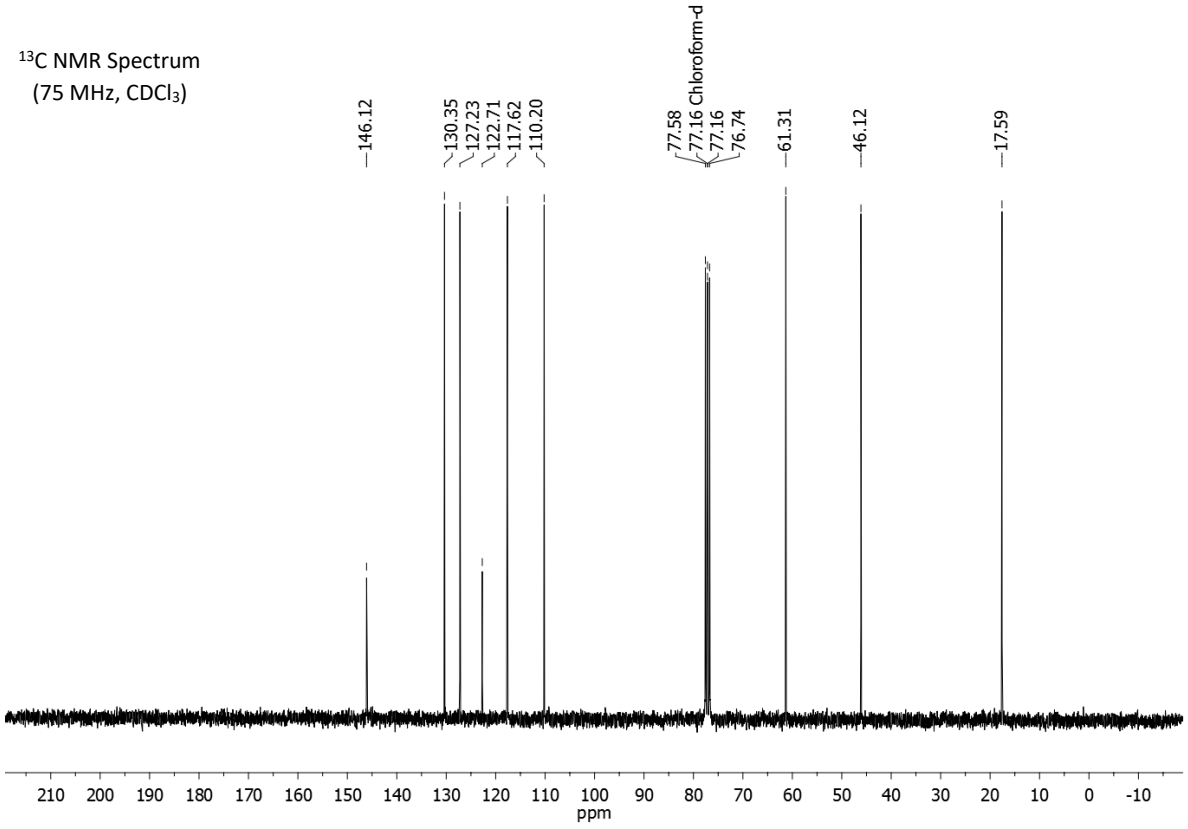

COSY Spectrum
($CDCl_3$)

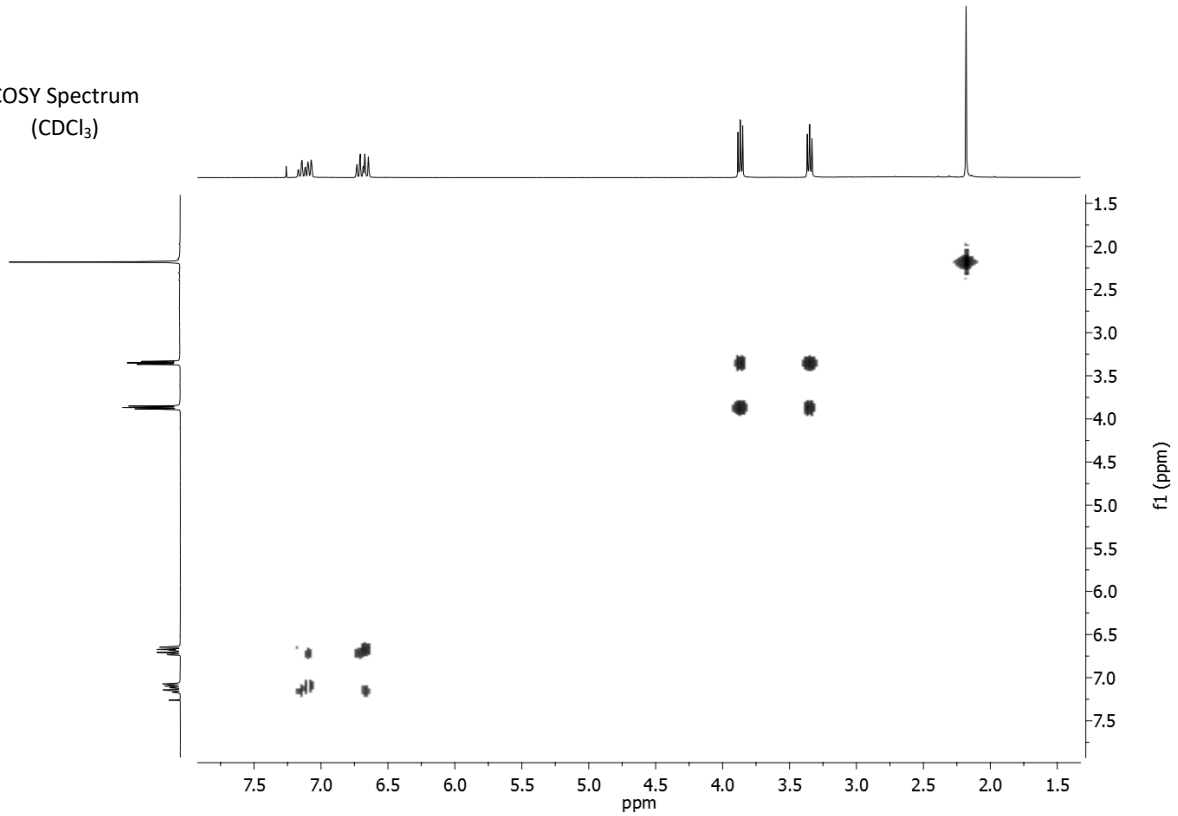

ed-HSQC Spectrum
($CDCl_3$)

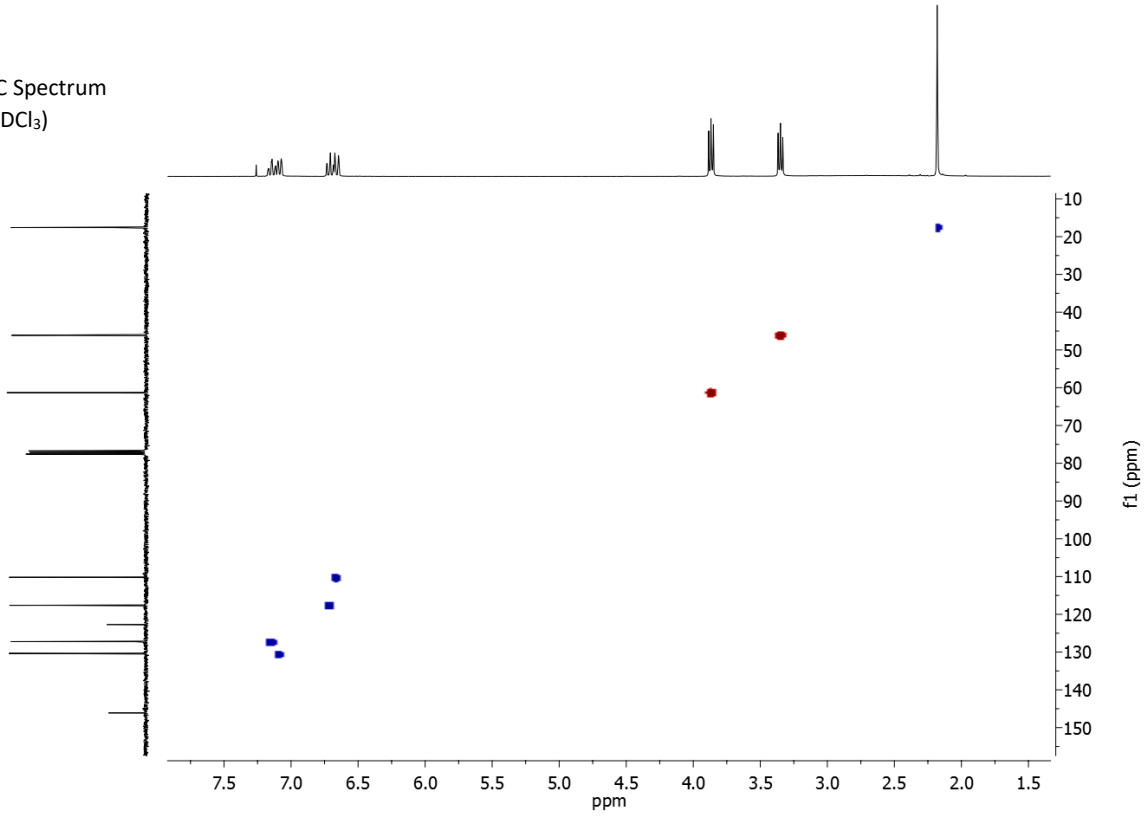

2-((2,3-dimethylphenyl)amino)ethanol (2d)

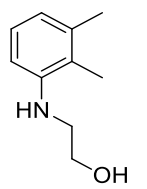

^{1}H NMR Spectrum
(300 MHz, $CDCl_3$)

^{13}C NMR Spectrum
(75 MHz, $CDCl_3$)

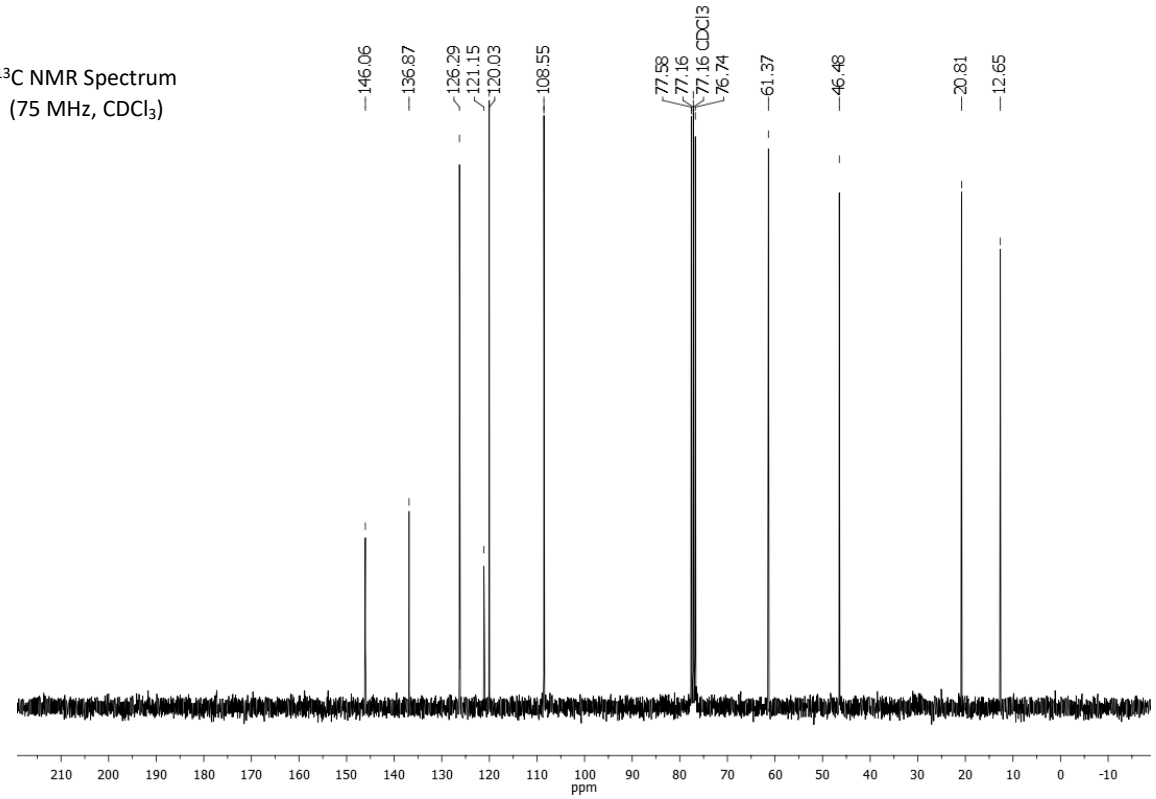

COSY Spectrum ($CDCl_3$)

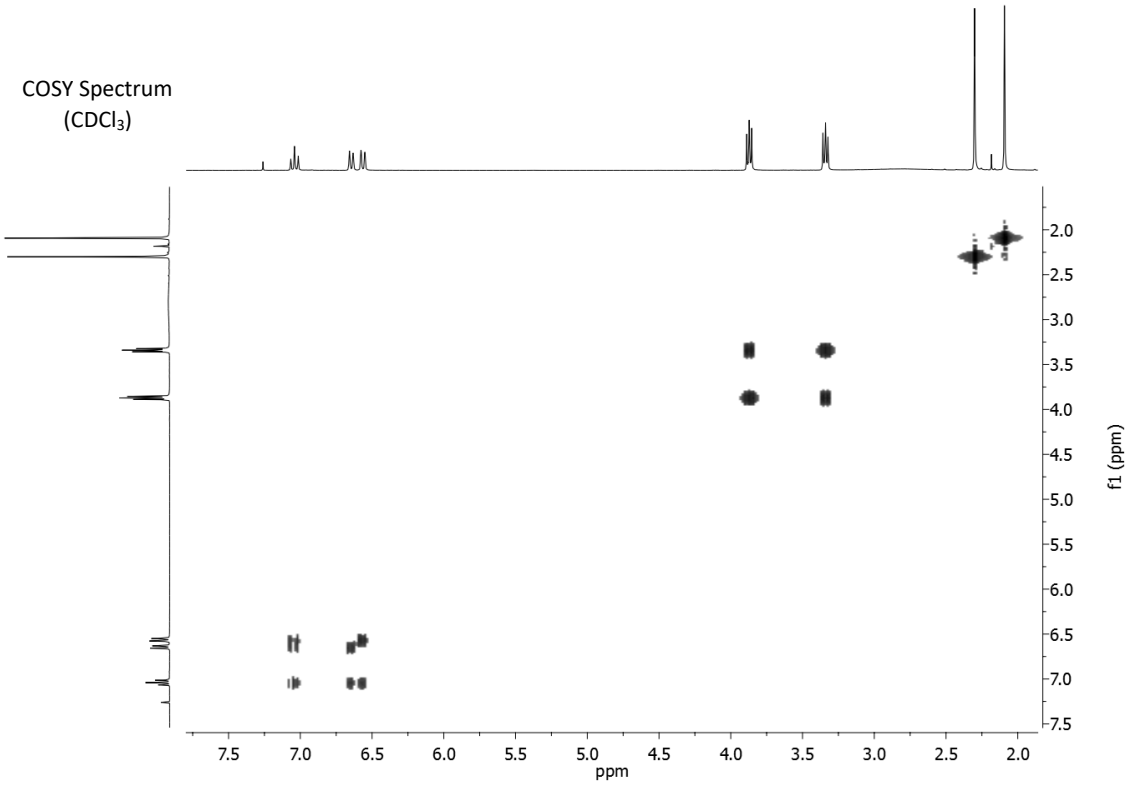

ed-HSQC Spectrum ($CDCl_3$)

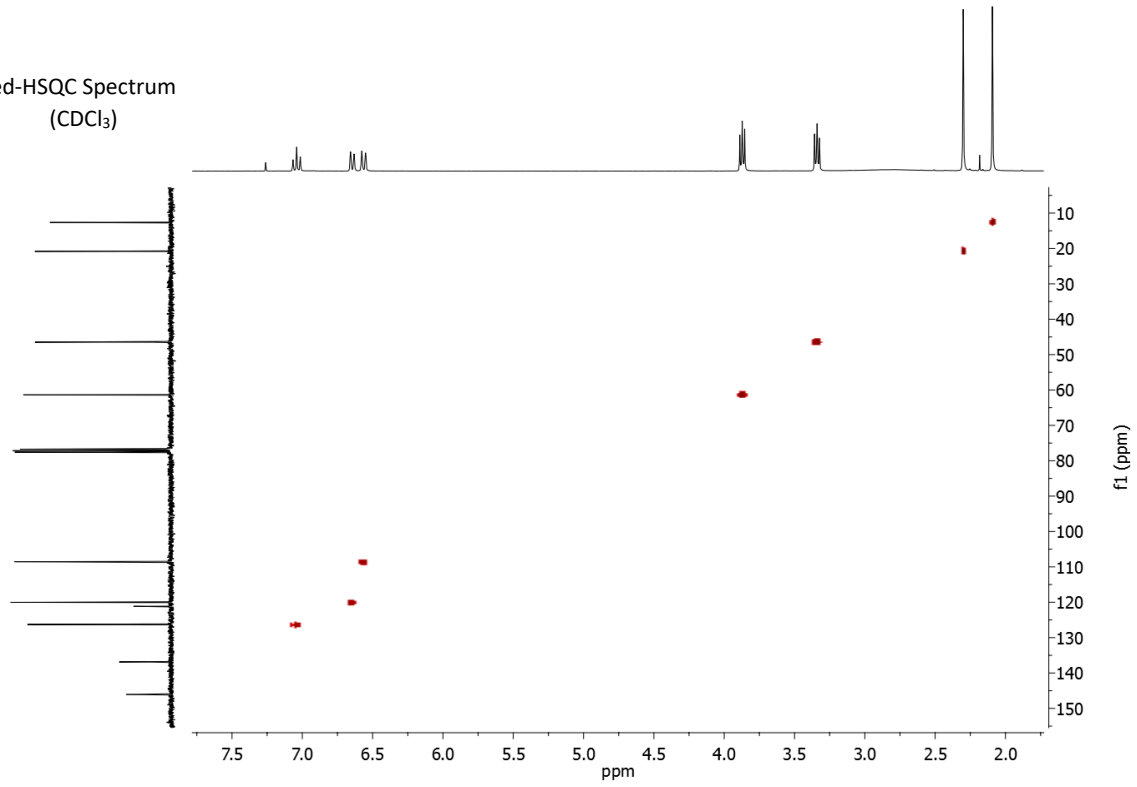

2-((2,4-dimethylphenyl)amino)ethanol (2e)

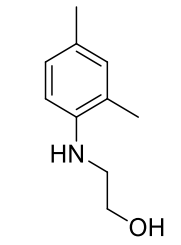

^{1}H NMR Spectrum
(300 MHz, $CDCl_3$)

^{13}C NMR Spectrum
(75 MHz, $CDCl_3$)

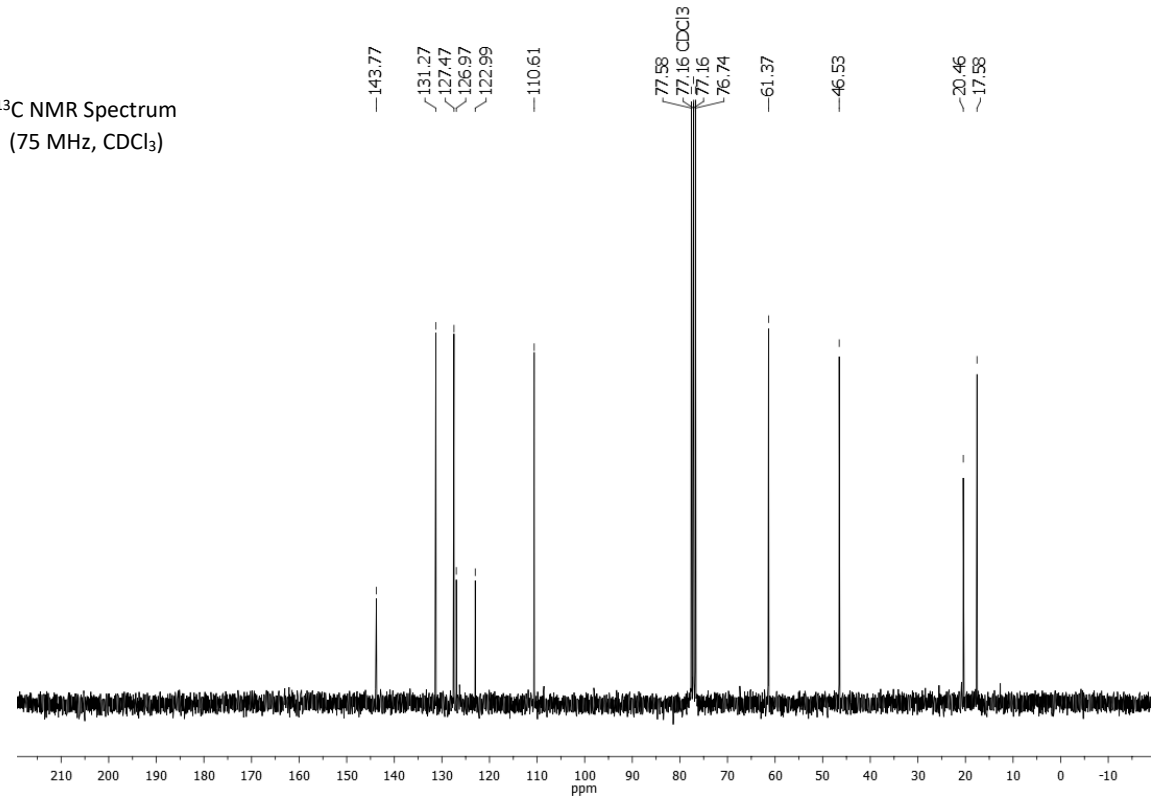

COSY Spectrum
($CDCl_3$)

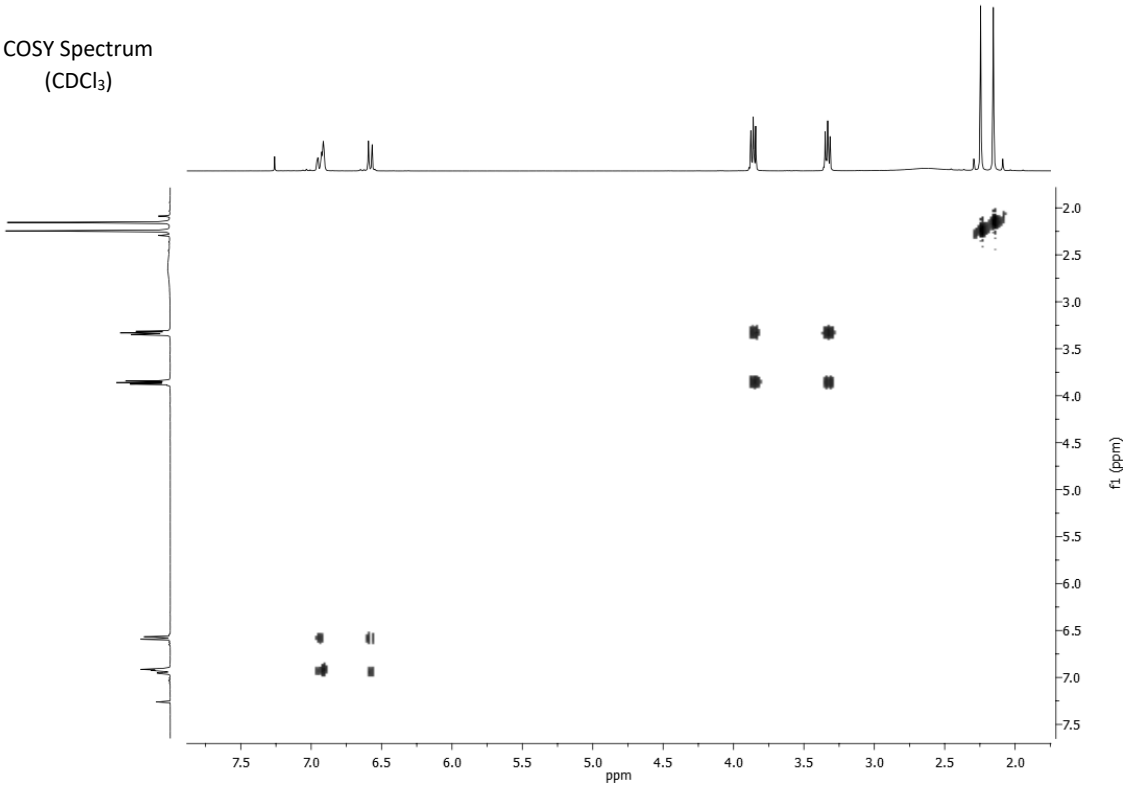

ed-HSQC Spectrum
($CDCl_3$)

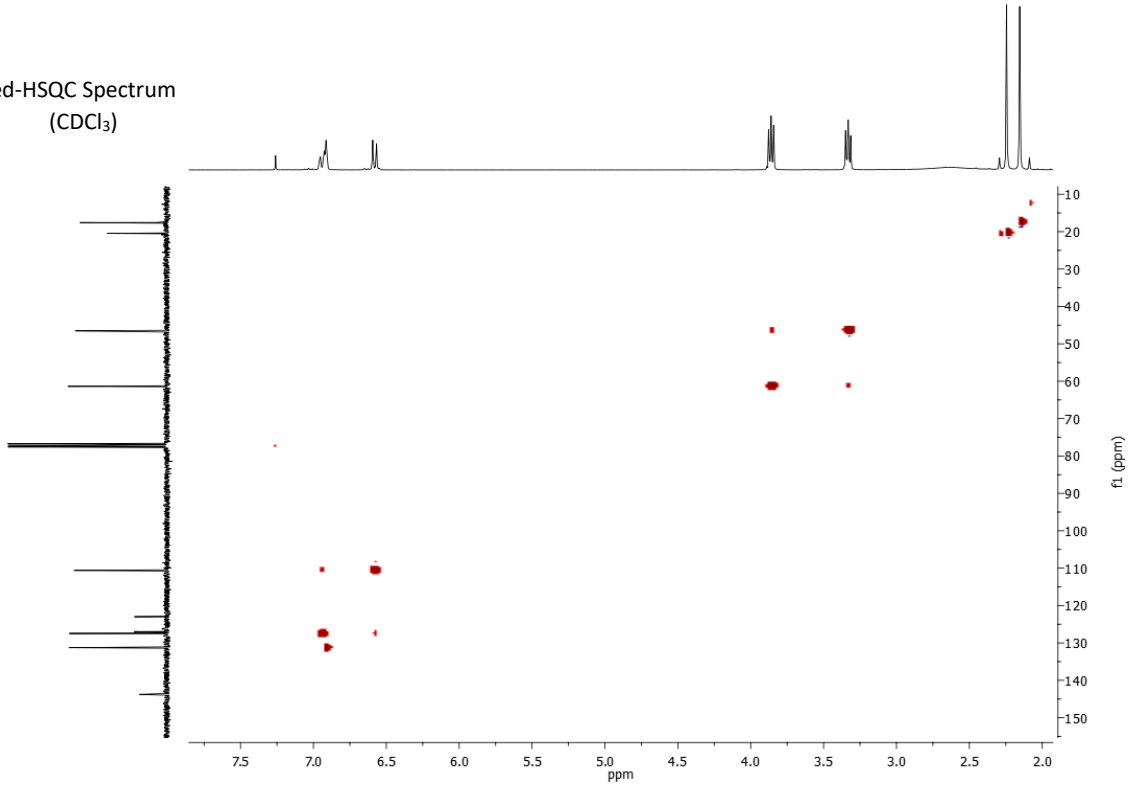

2-((3,4-dimethylphenyl)amino)ethanol (2f)

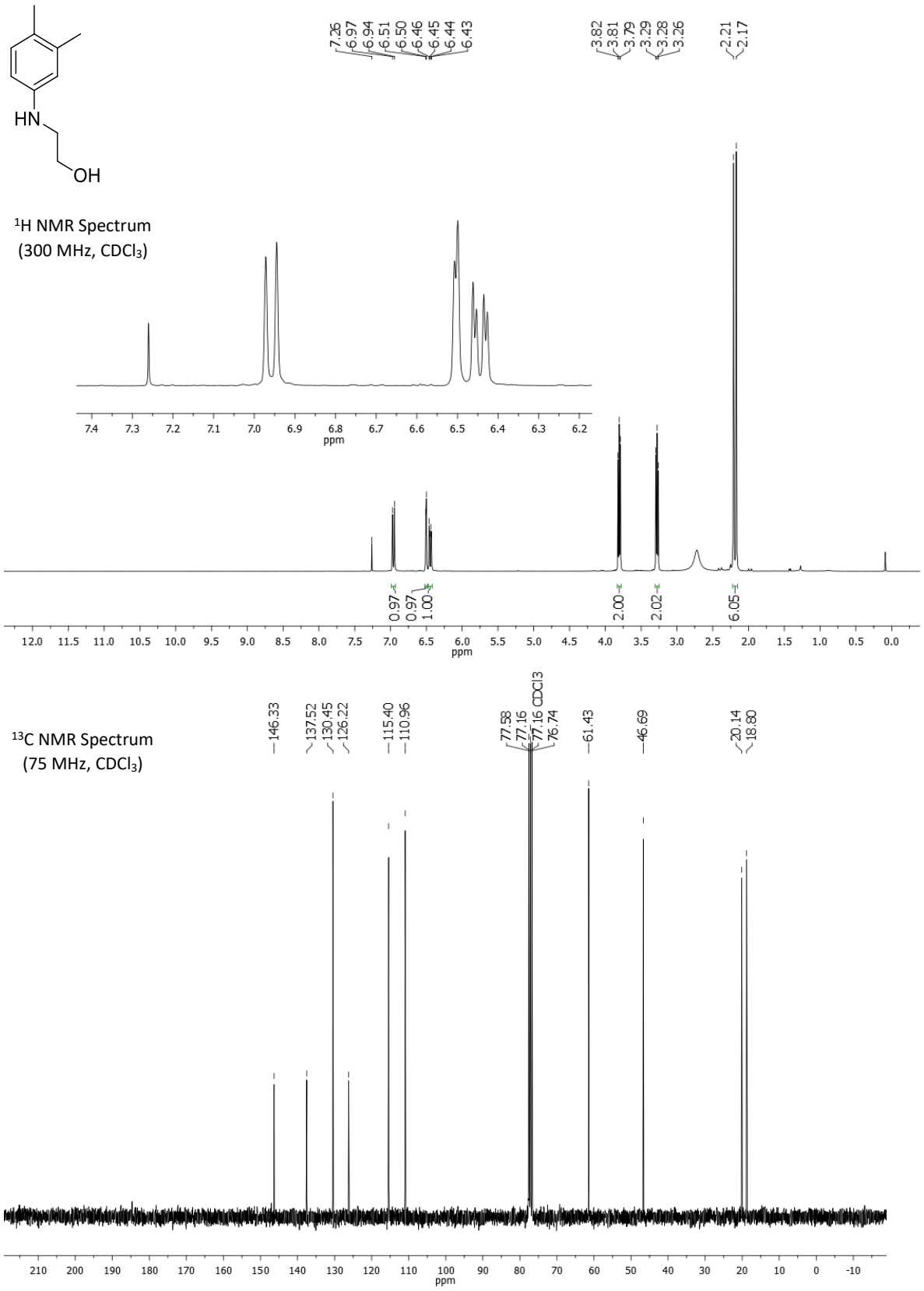

^{1}H NMR Spectrum
(300 MHz, $CDCl_3$)

^{13}C NMR Spectrum
(75 MHz, $CDCl_3$)

COSY Spectrum ($CDCl_3$)

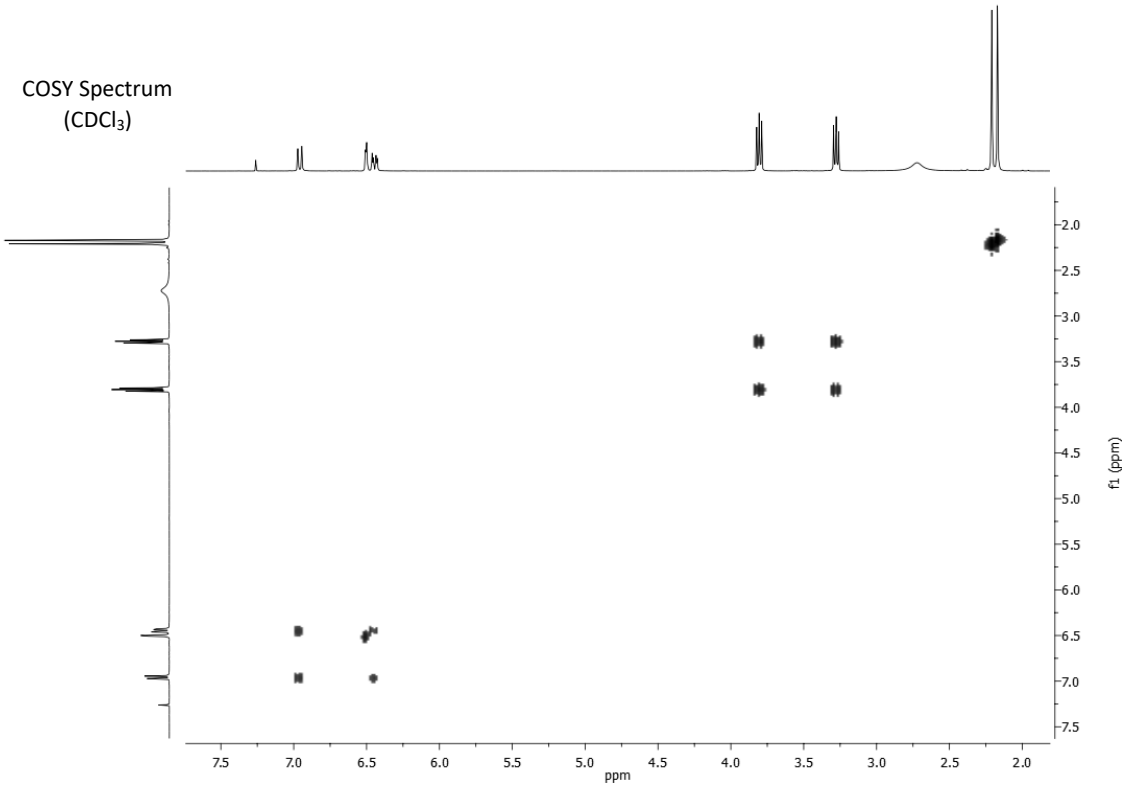

ed-HSQC Spectrum ($CDCl_3$)

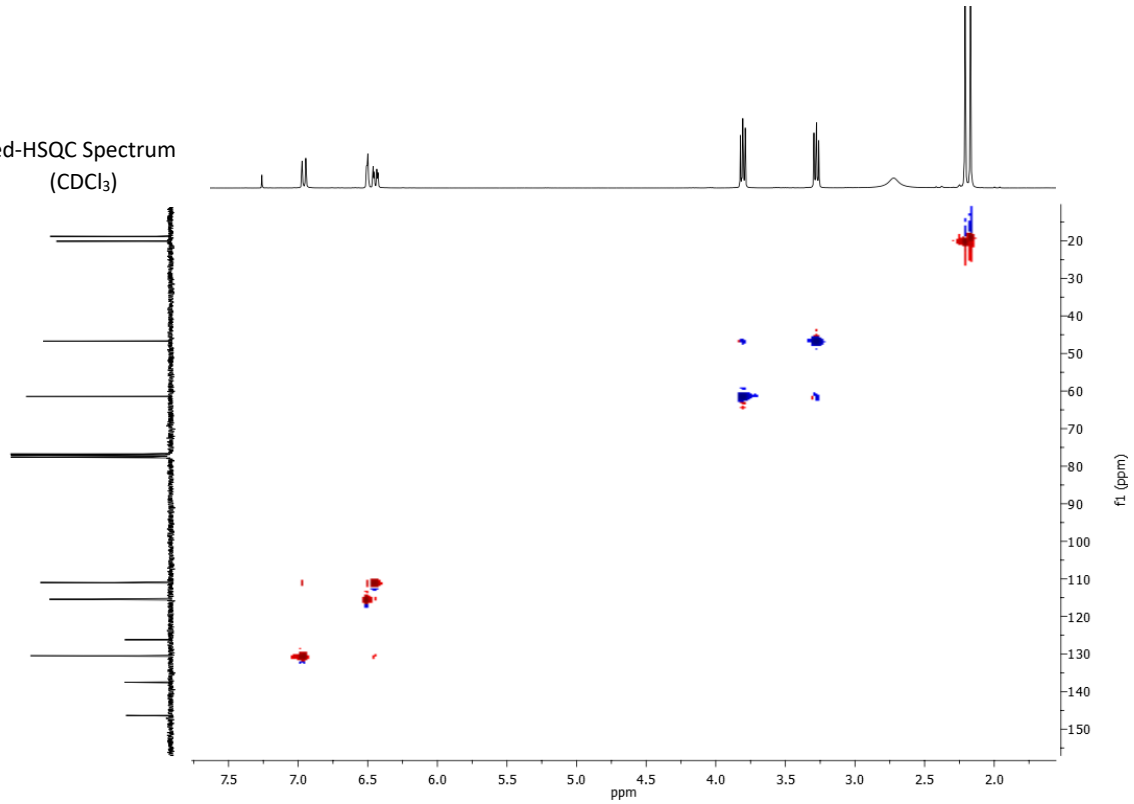

2-((3,5-dimethylphenyl)amino)ethanol (2g)

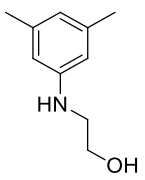

^{1}H NMR Spectrum
(300 MHz, $CDCl_3$)

^{13}C NMR Spectrum
(75 MHz, $CDCl_3$)

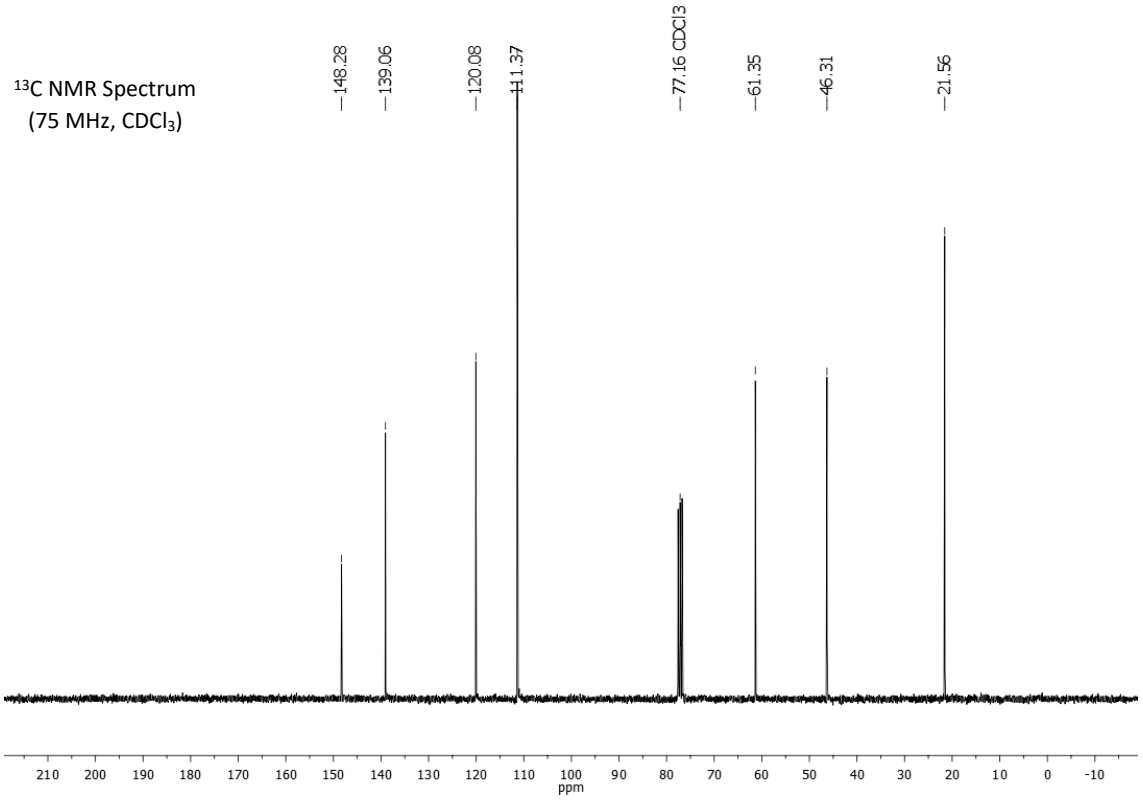

COSY Spectrum ($CDCl_3$)

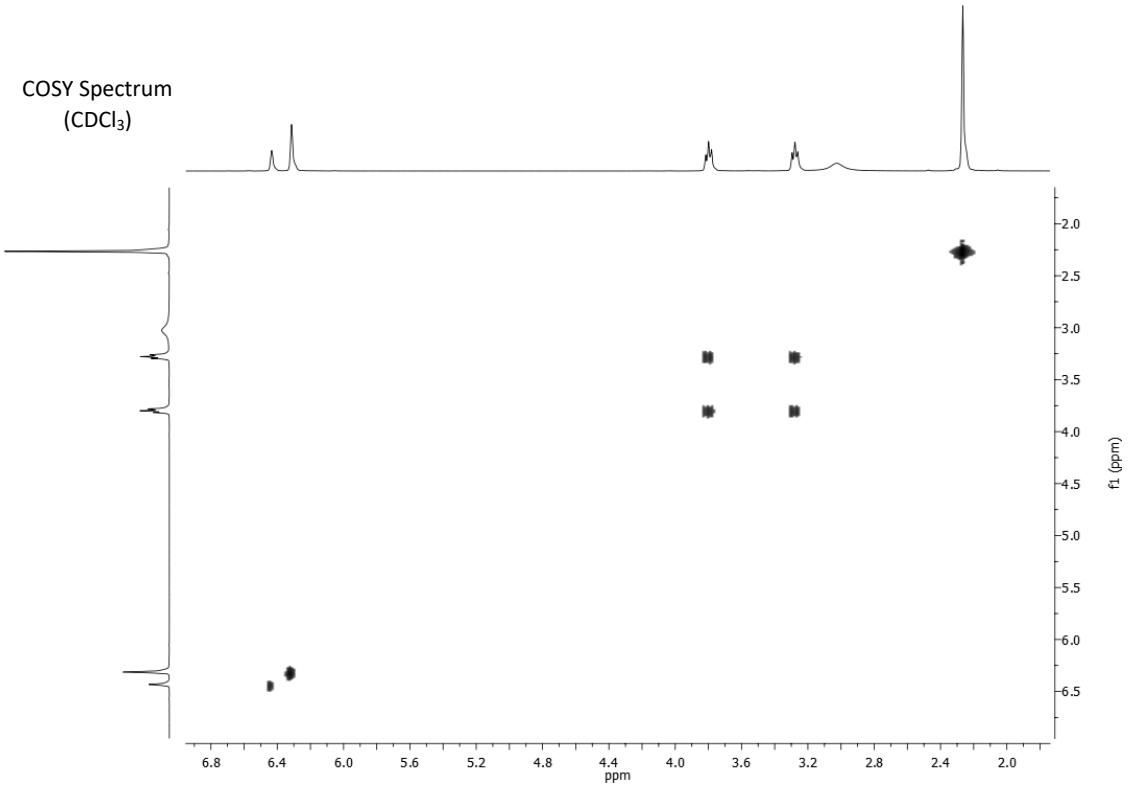

ed-HSQC Spectrum ($CDCl_3$)

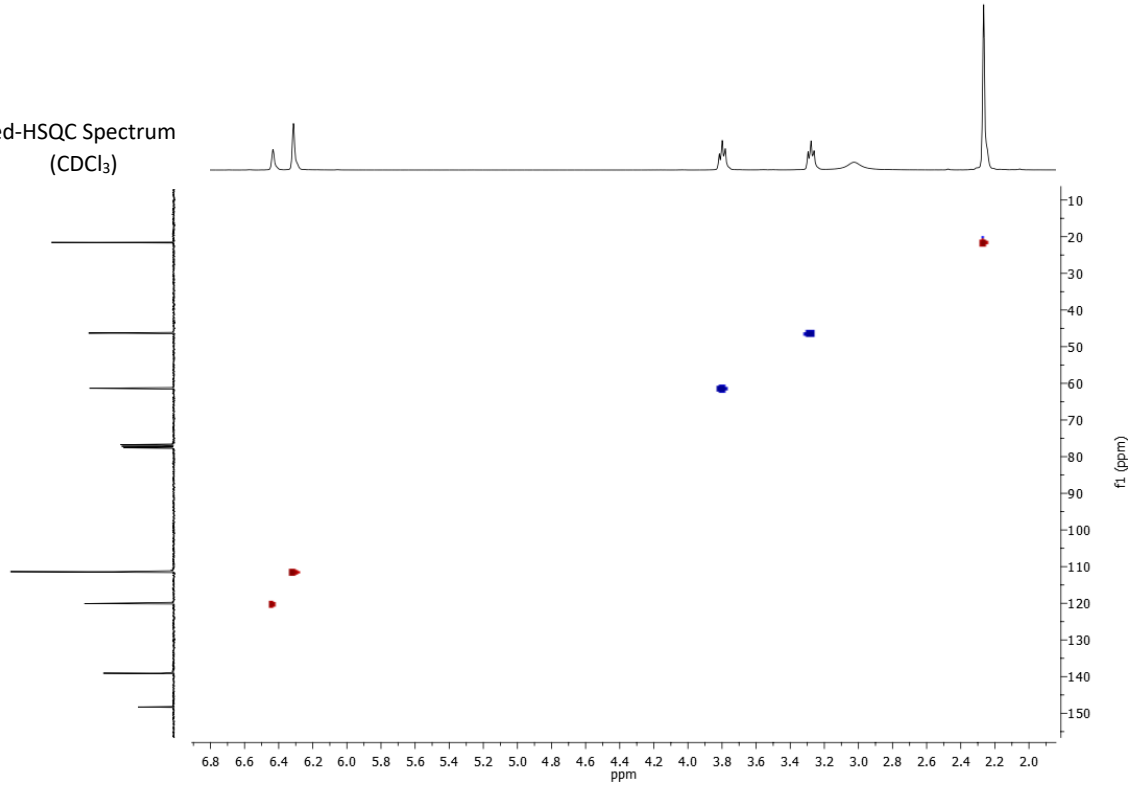

2-((2,5-dimethylphenyl)amino)ethanol (2h)

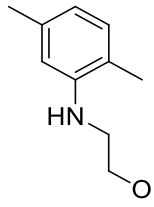

^{1}H NMR Spectrum
(300 MHz, $CDCl_3$)

^{13}C NMR Spectrum
(75 MHz, $CDCl_3$)

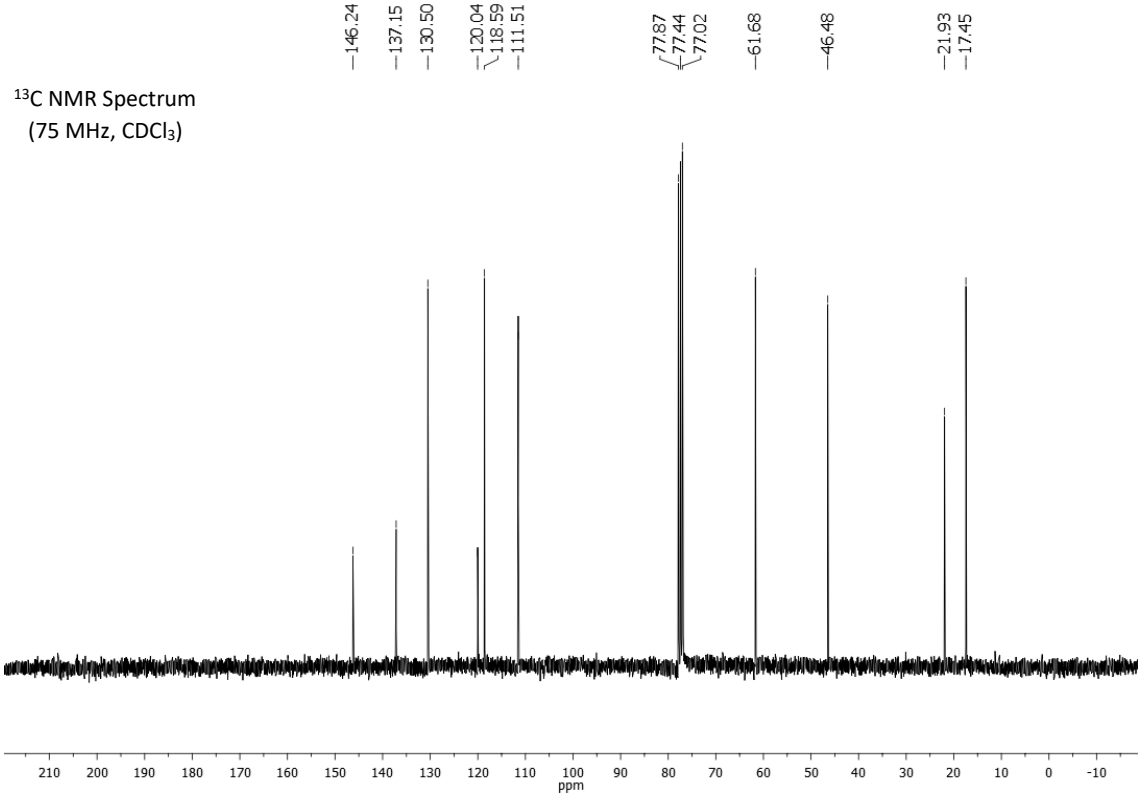

COSY Spectrum ($CDCl_3$)

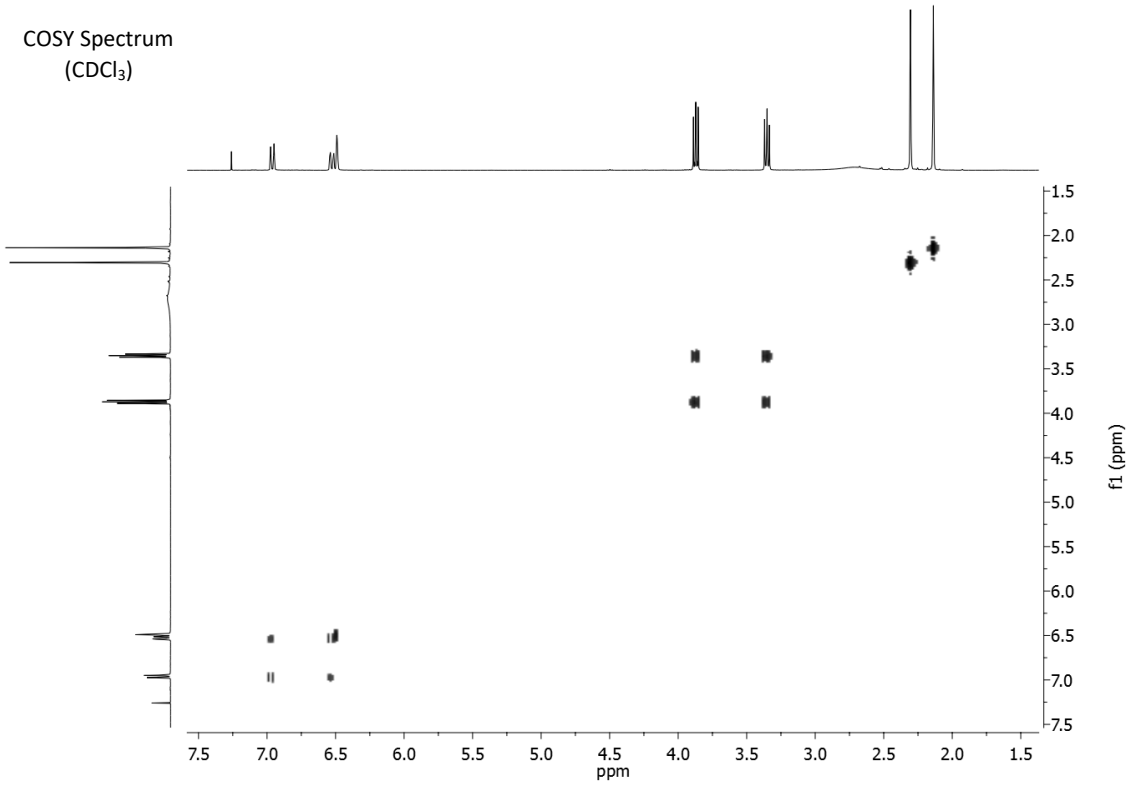

ed-HSQC Spectrum ($CDCl_3$)

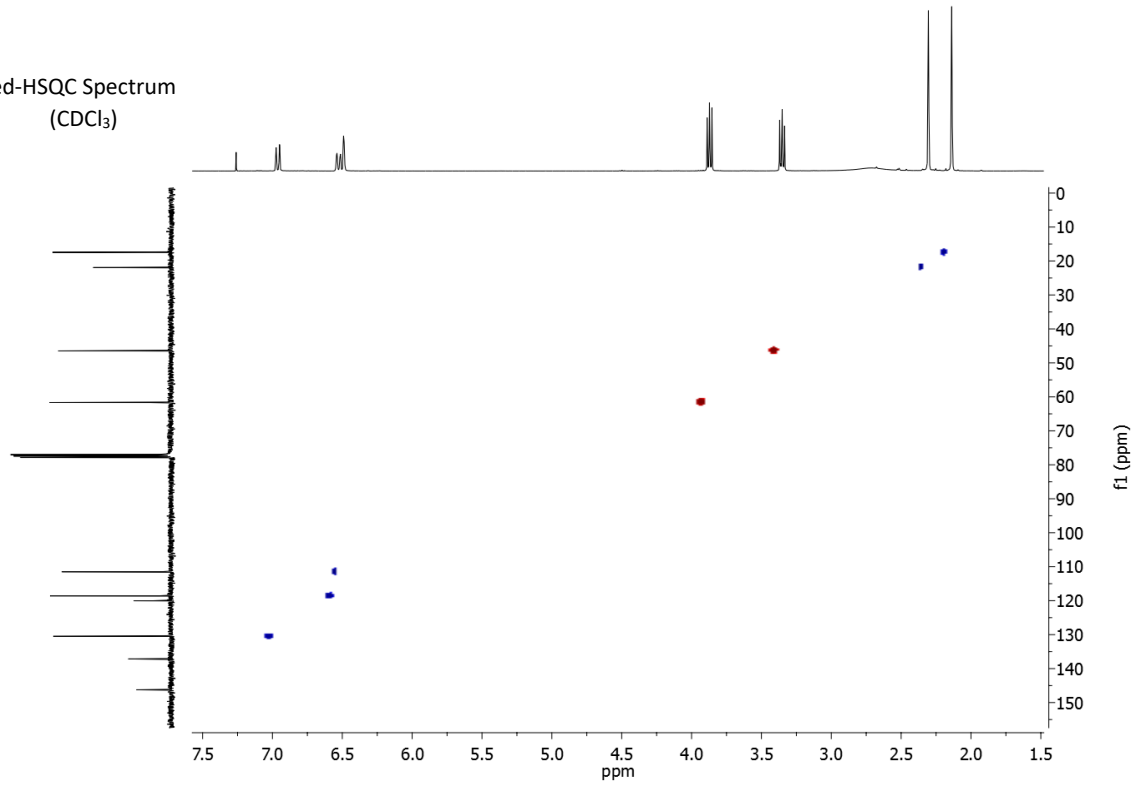

2-((2,6-dimethylphenyl)amino)ethanol (2i)

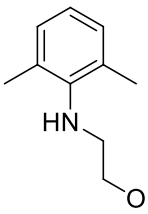

^{1}H NMR Spectrum
(300 MHz, $CDCl_3$)

^{13}C NMR Spectrum
(75 MHz, $CDCl_3$)

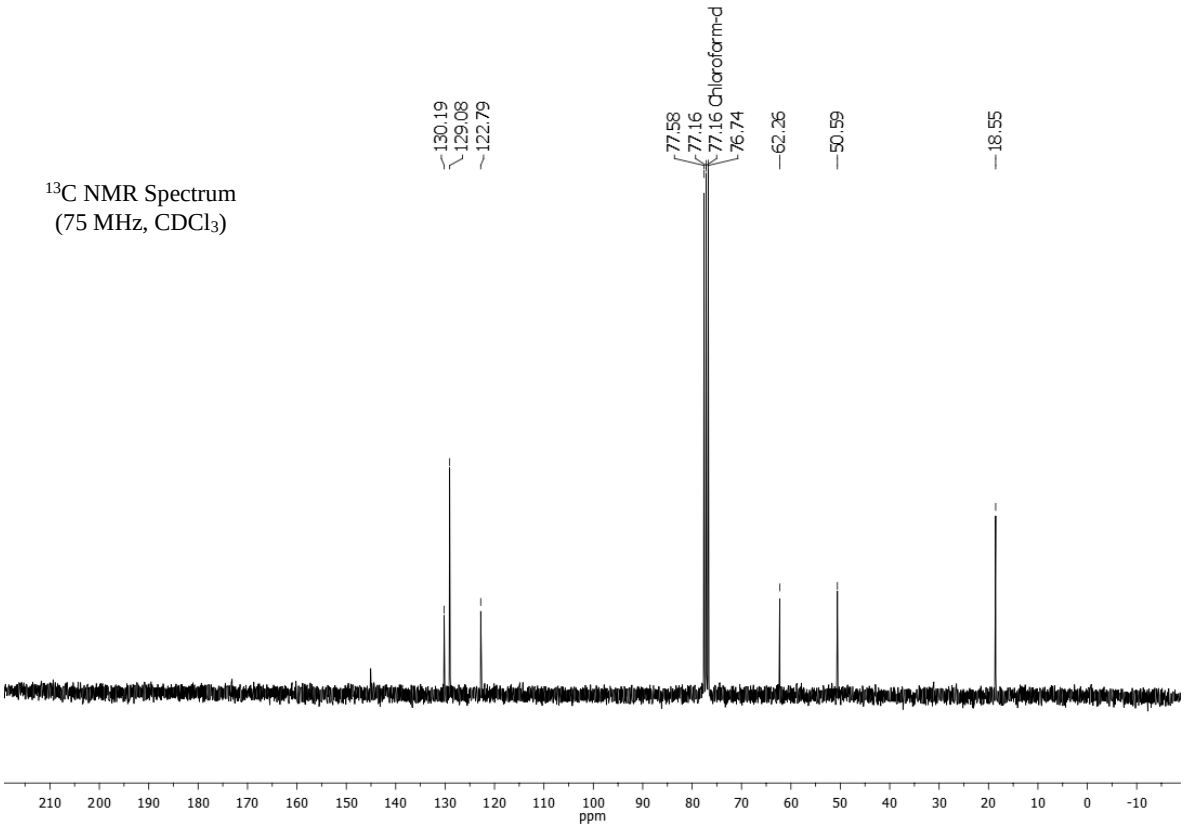

COSY Spectrum ($CDCl_3$)

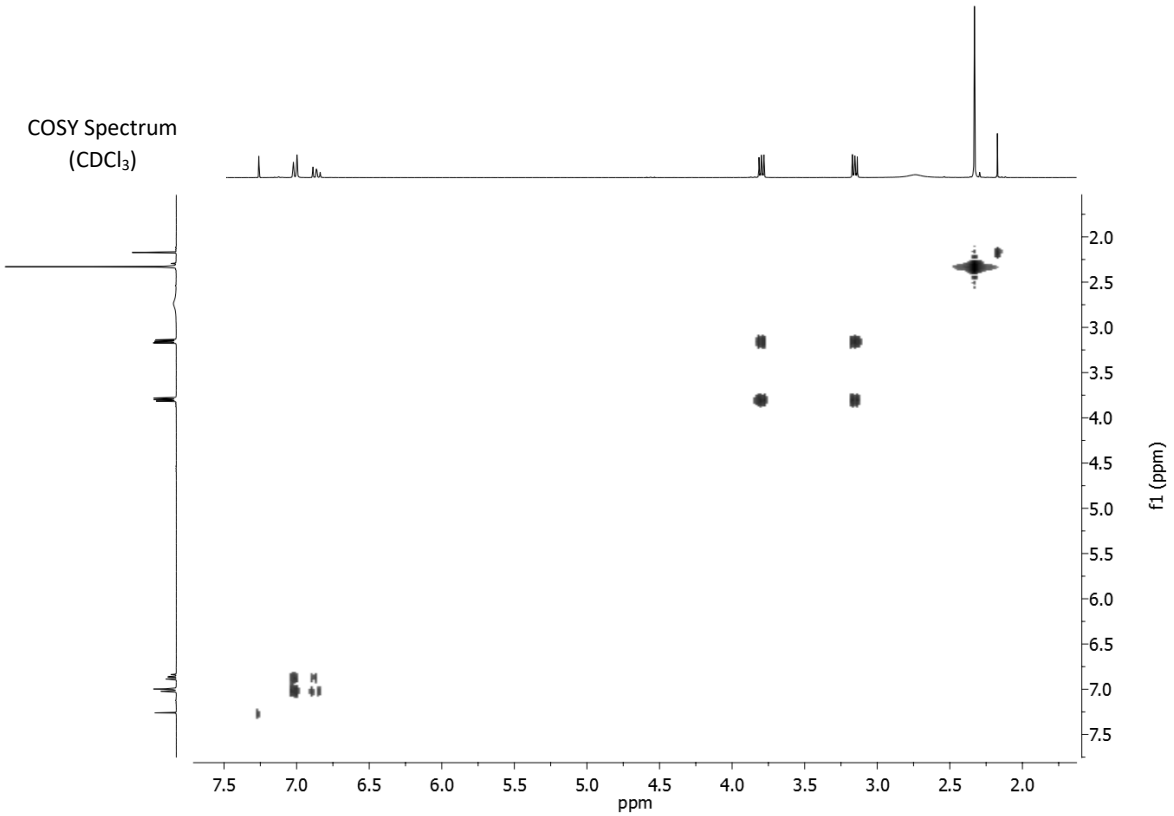

ed-HSQC Spectrum ($CDCl_3$)

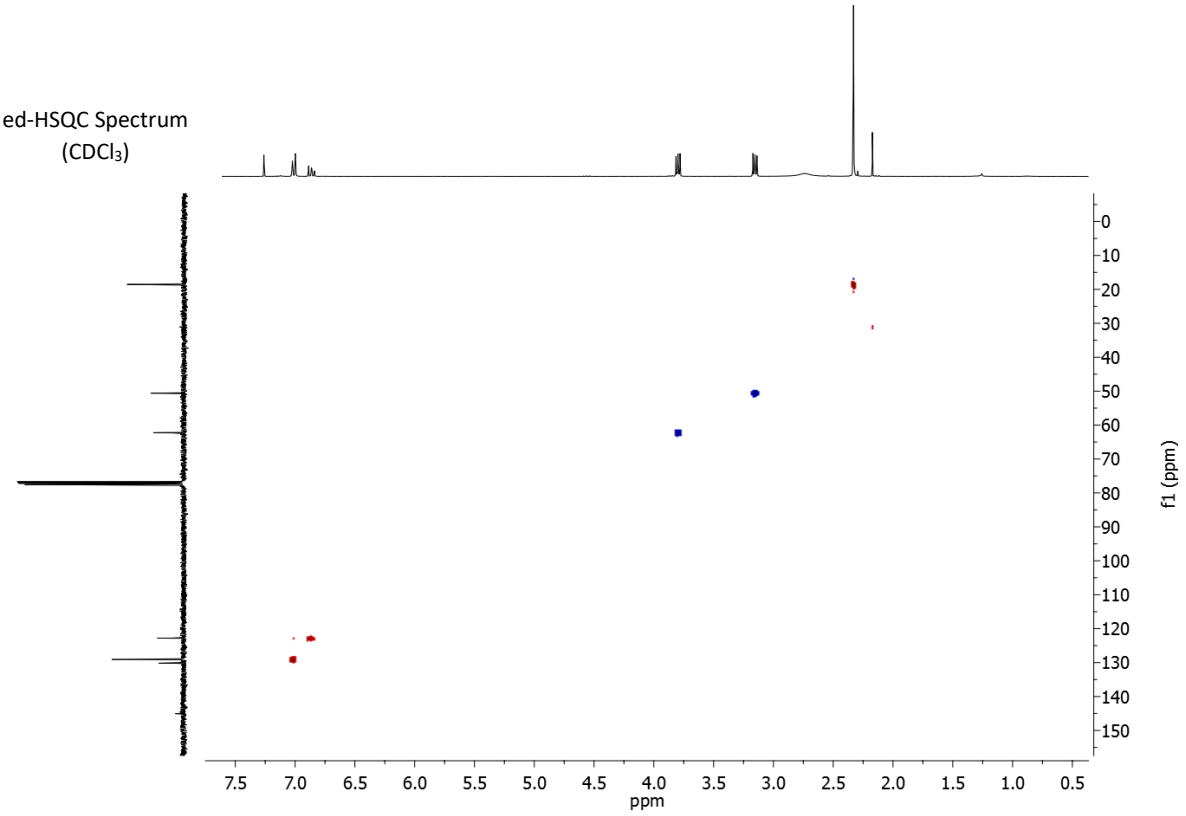

2-phenylaminoethanol (2j)

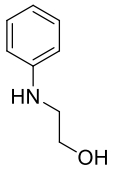

^{1}H NMR Spectrum
(300 MHz, $CDCl_3$)

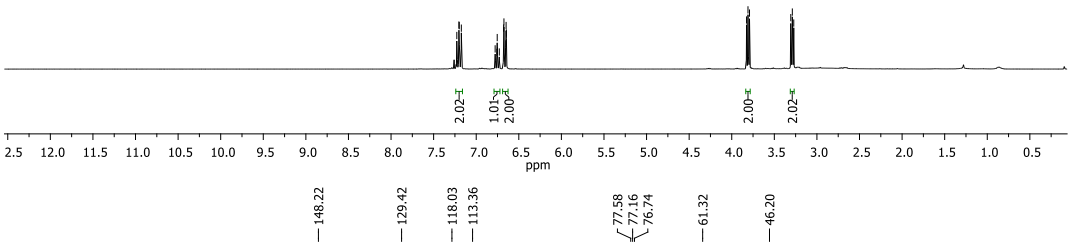

^{13}C NMR Spectrum
(75 MHz, $CDCl_3$)

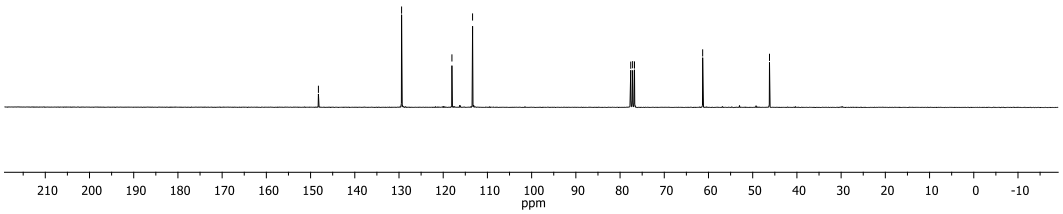

2-((4-fluorophenyl)amino)etanol (2n)

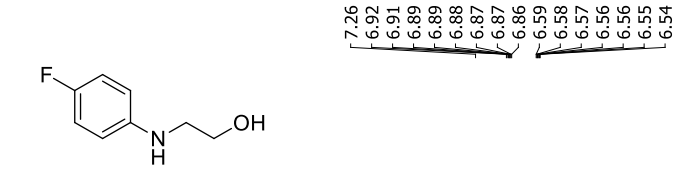

^{1}H NMR Spectrum
(300 MHz, $CDCl_3$)

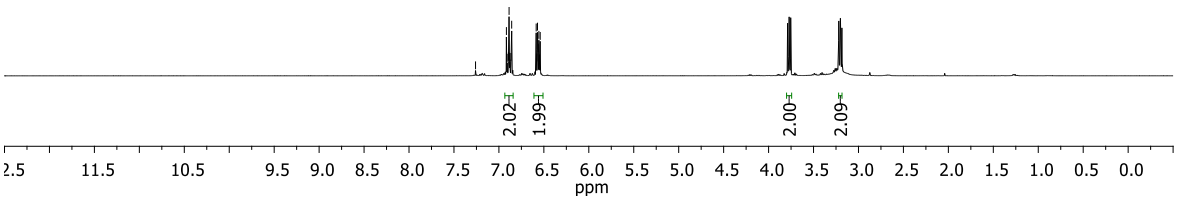

2-((3-fluorophenyl)amino)ethanol (2o)

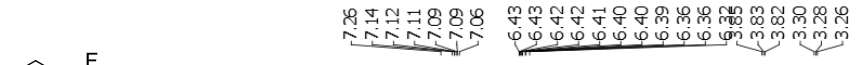

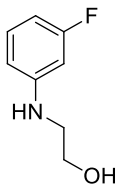

^{1}H NMR Spectrum
(300 MHz, $CDCl_3$)

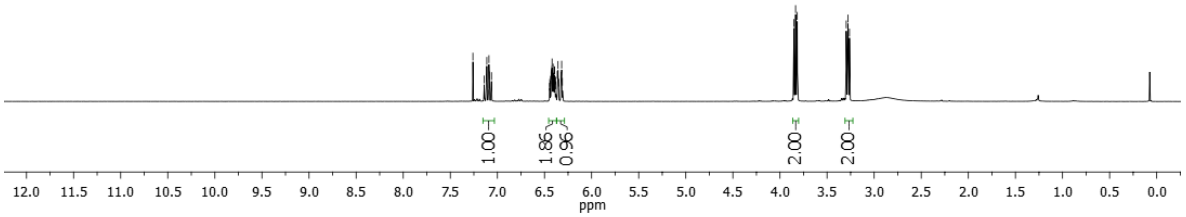

^{13}C NMR Spectrum
(75 MHz, $CDCl_3$)

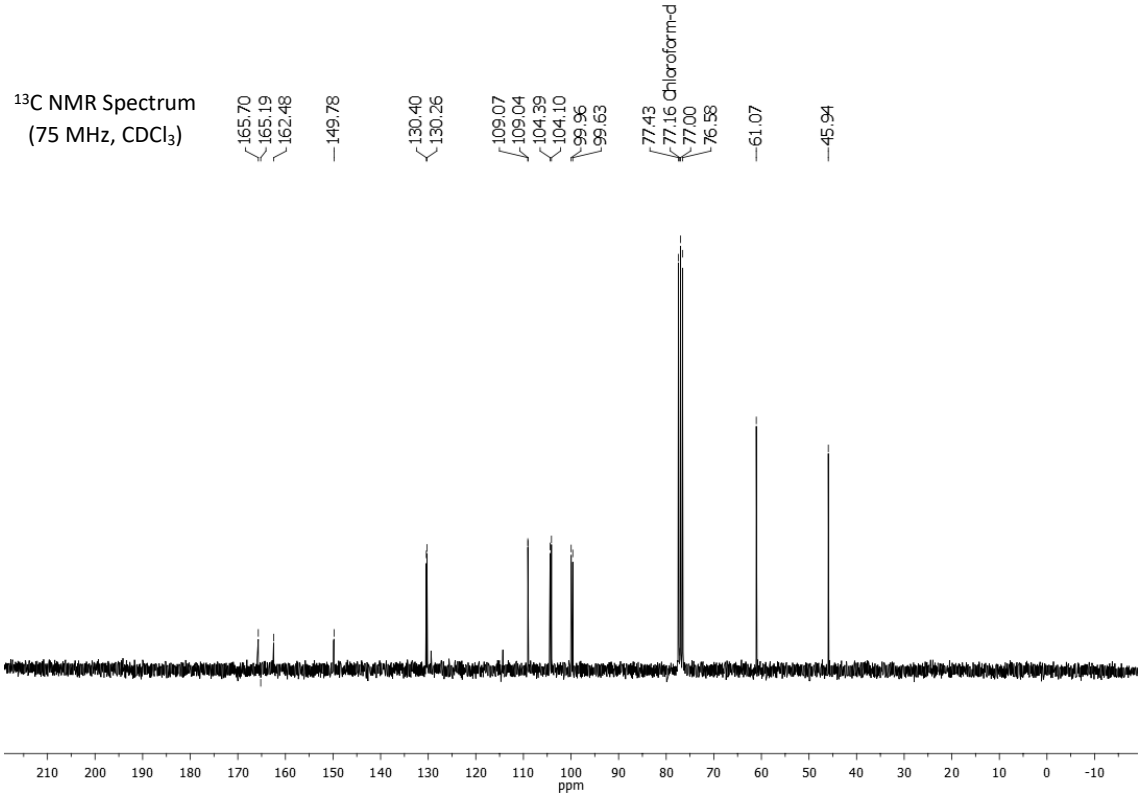

COSY Spectrum ($CDCl_3$)

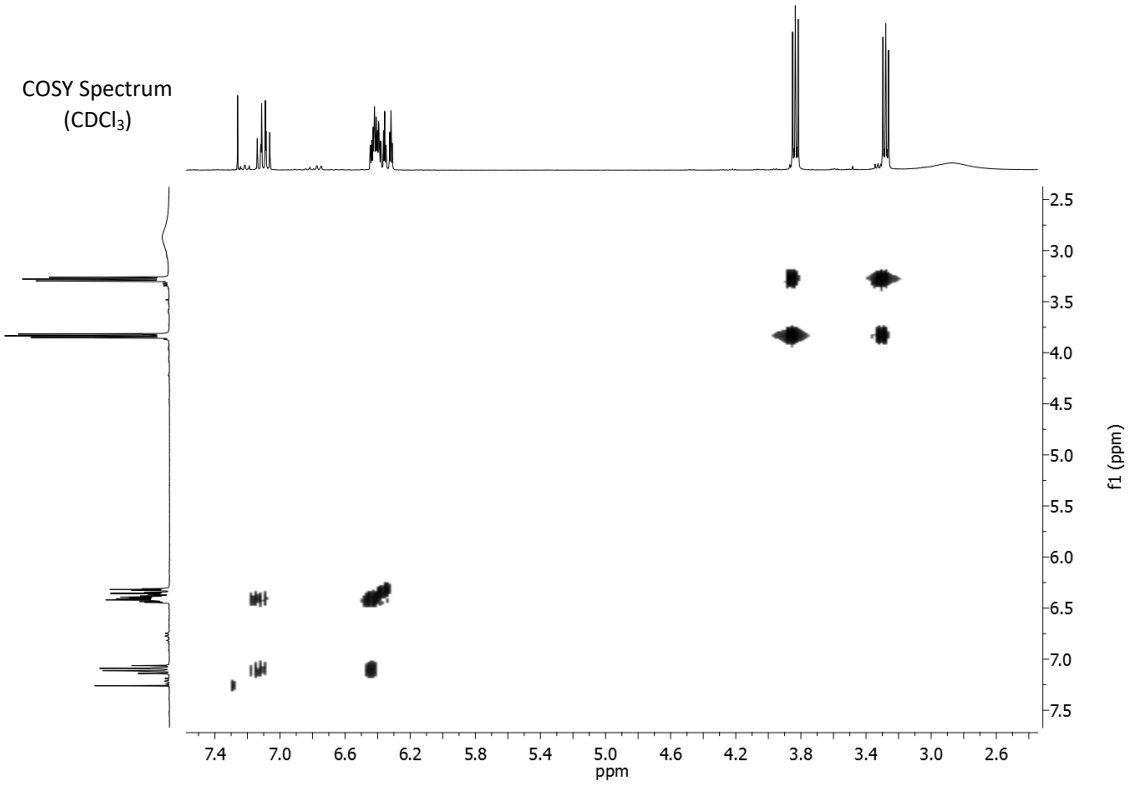

ed-HSQC Spectrum ($CDCl_3$)

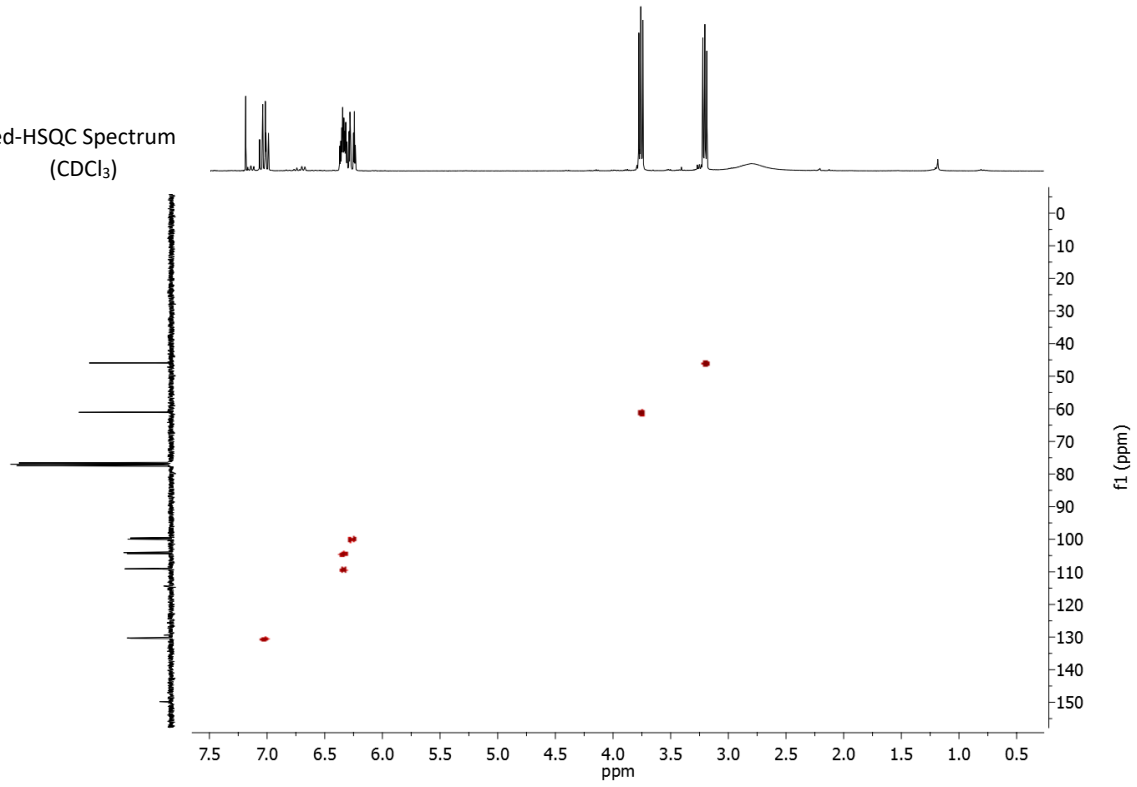

2-((2-fluorophenyl)amino)ethanol (2p)

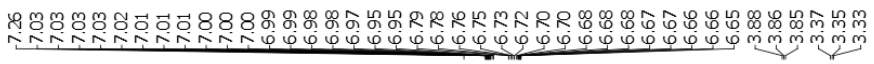

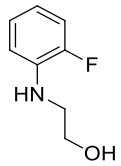

^{1}H NMR Spectrum
(300 MHz, $CDCl_3$)

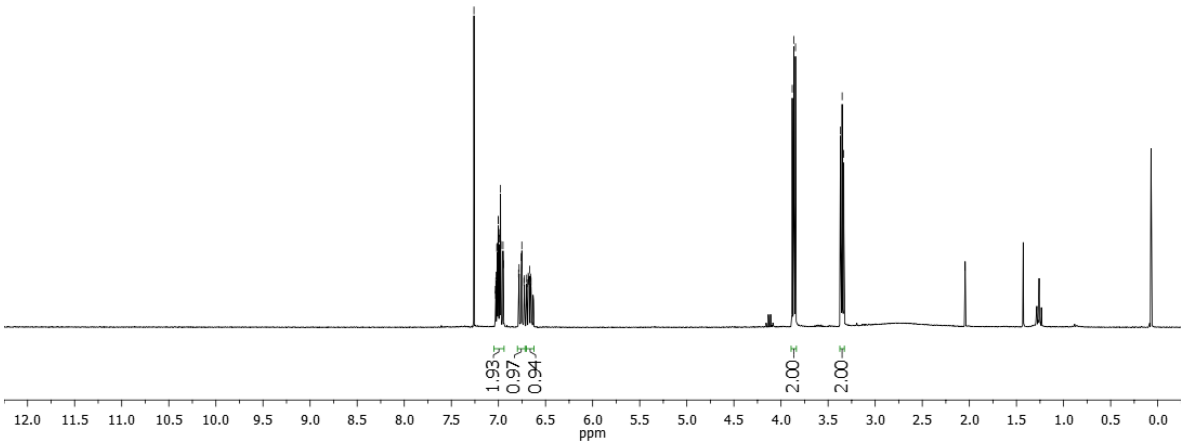

^{13}C NMR Spectrum
(75 MHz, $CDCl_3$)

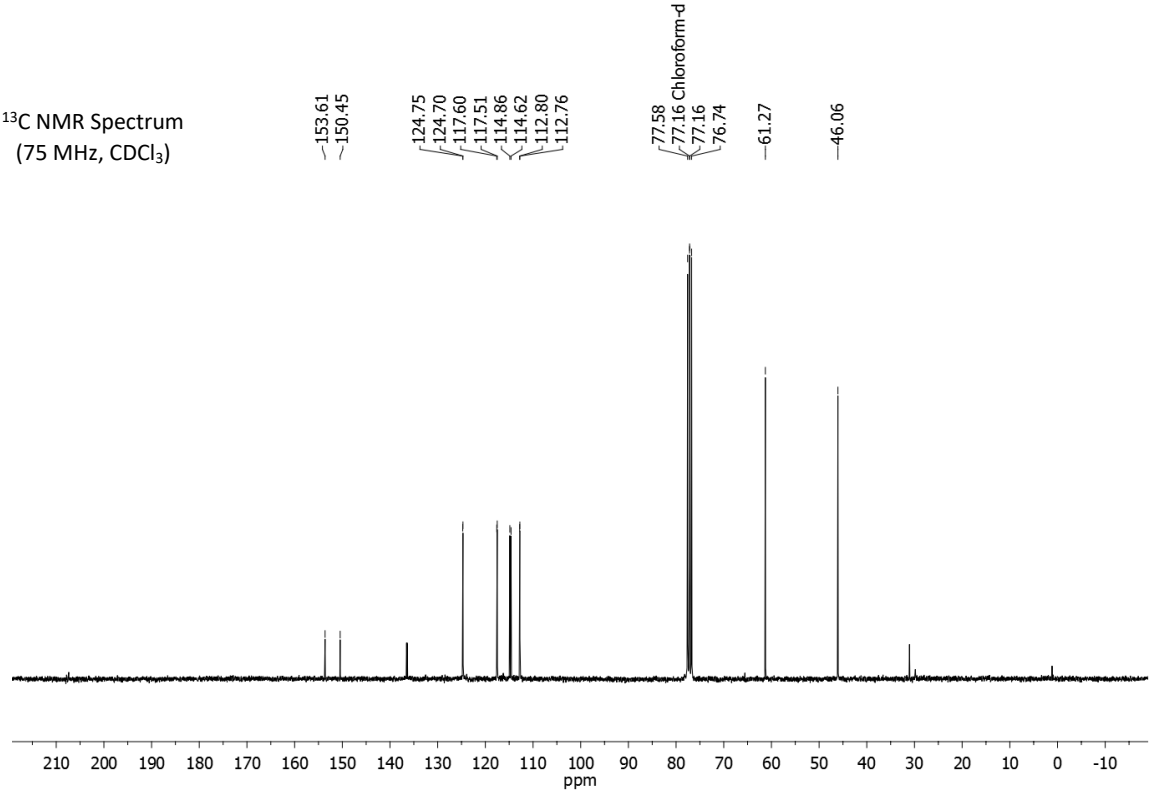

COSY Spectrum ($CDCl_3$)

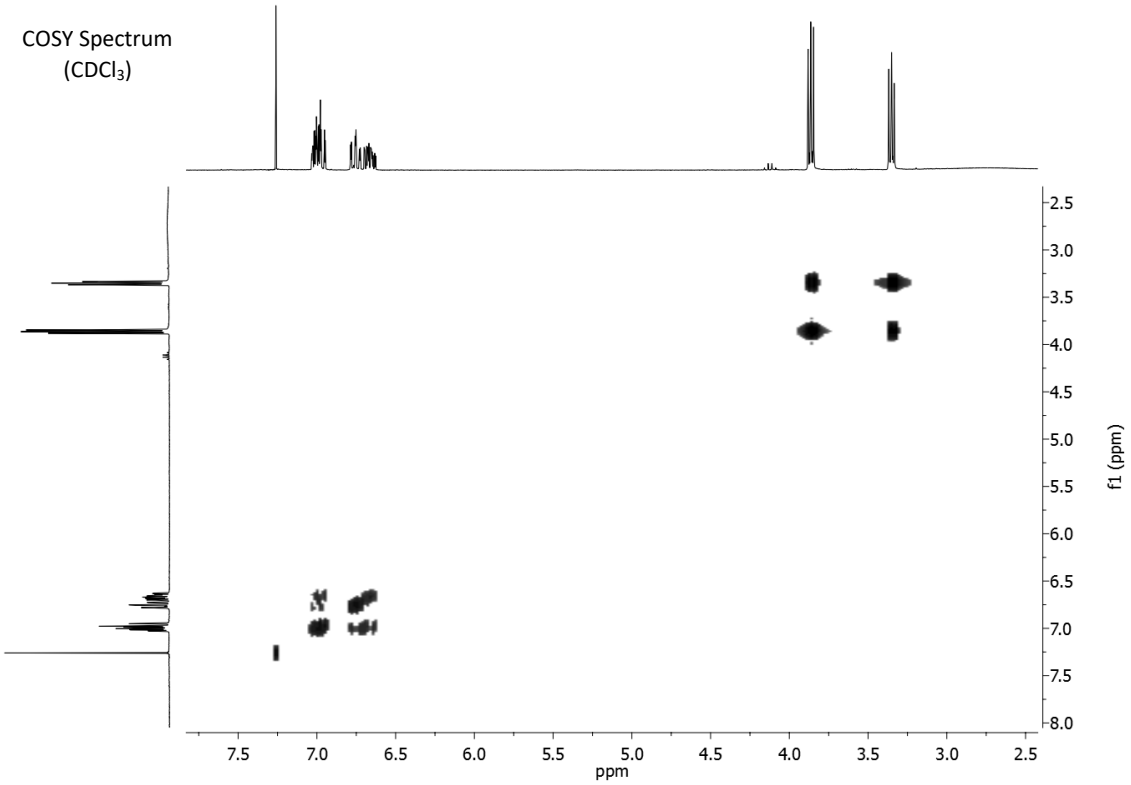

ed-HSQC Spectrum ($CDCl_3$)

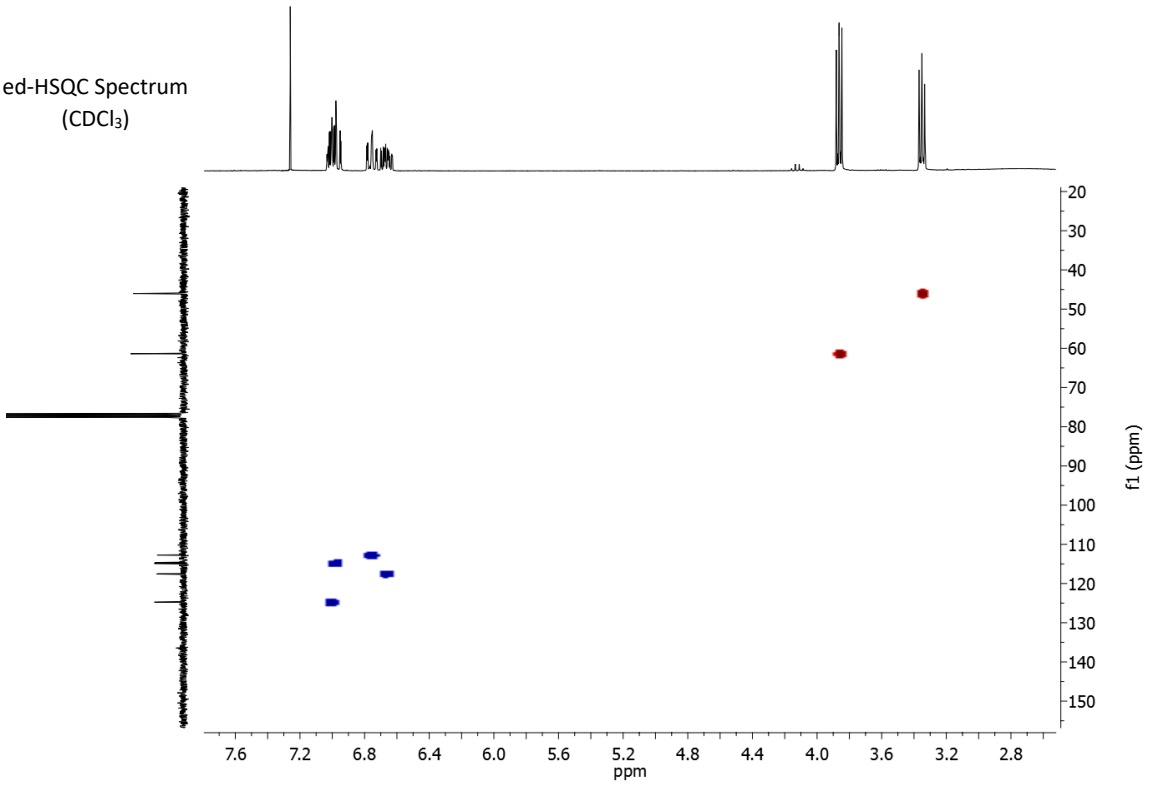

2-((2-trifluoromethylphenyl)amino)ethanol (2q)

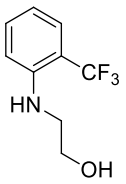

^{1}H NMR Spectrum
(300 MHz, $CDCl_3$)

^{13}C NMR Spectrum
(75 MHz, $CDCl_3$)

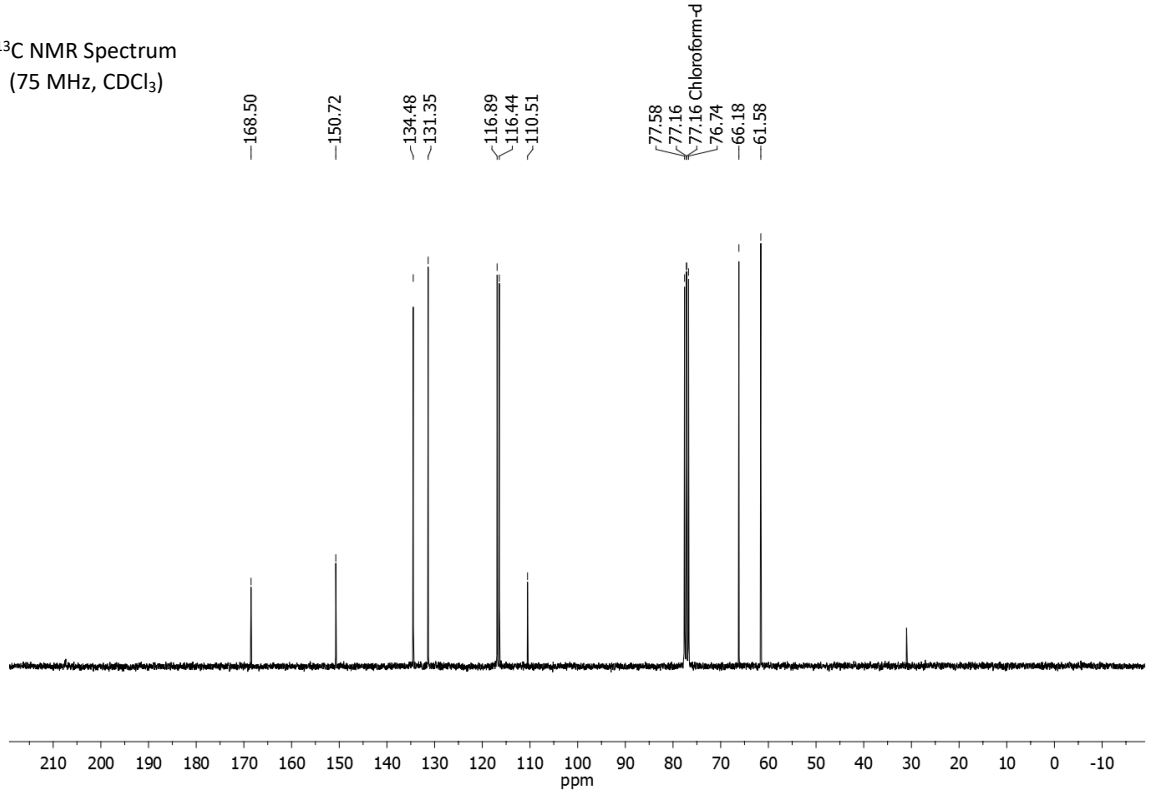

COSY Spectrum ($CDCl_3$)

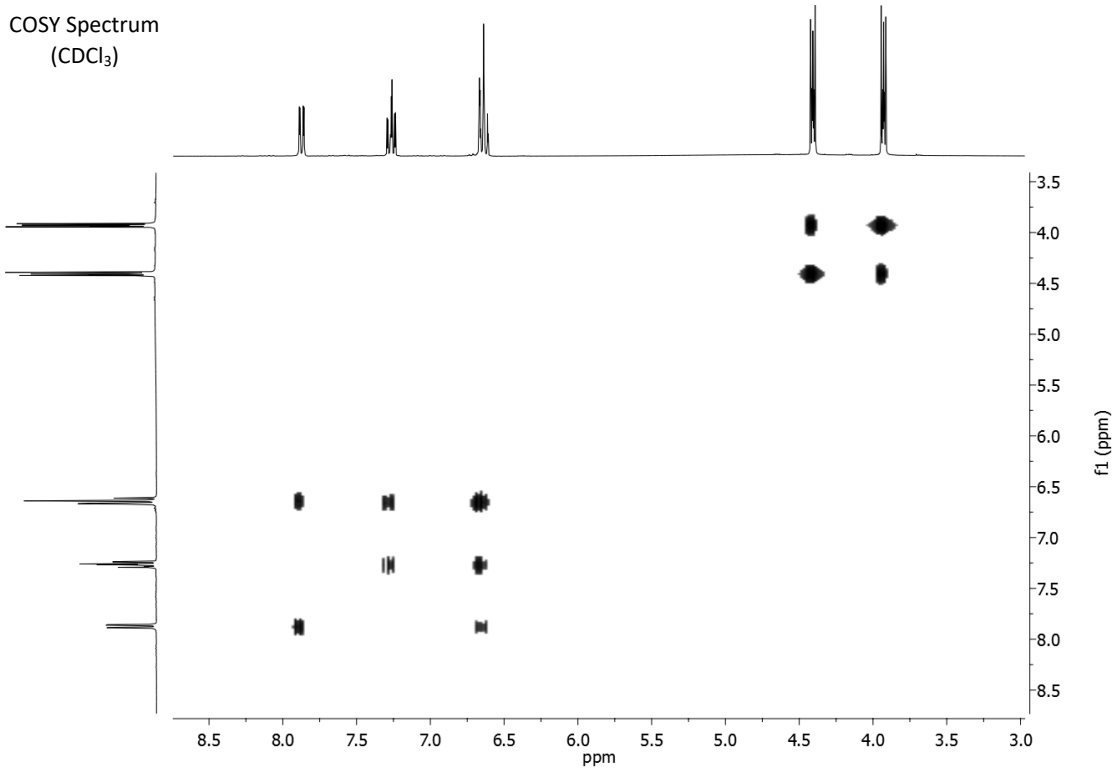

ed-HSQC Spectrum ($CDCl_3$)

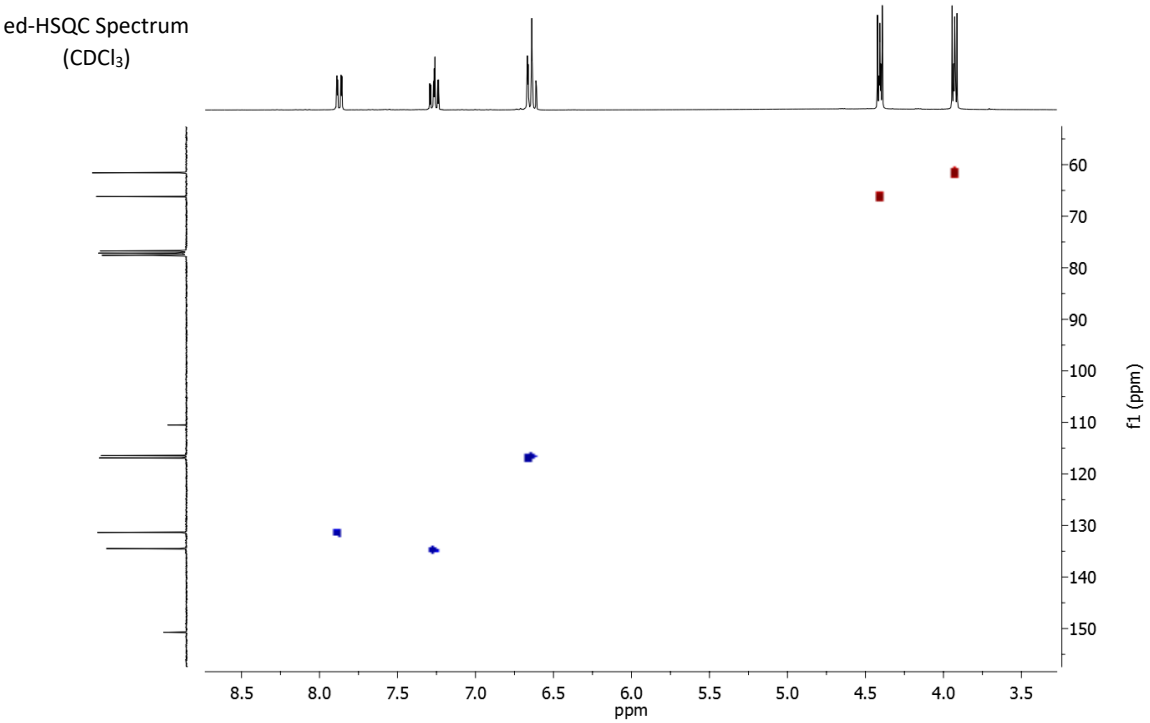

2-((3-trifluoromethylphenyl)amino)ethanol (2r)

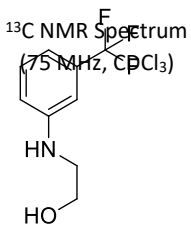

^{13}C NMR Spectrum
(75 MHz, $CDCl_3$)

^{1}H NMR Spectrum
(300 MHz, $CDCl_3$)

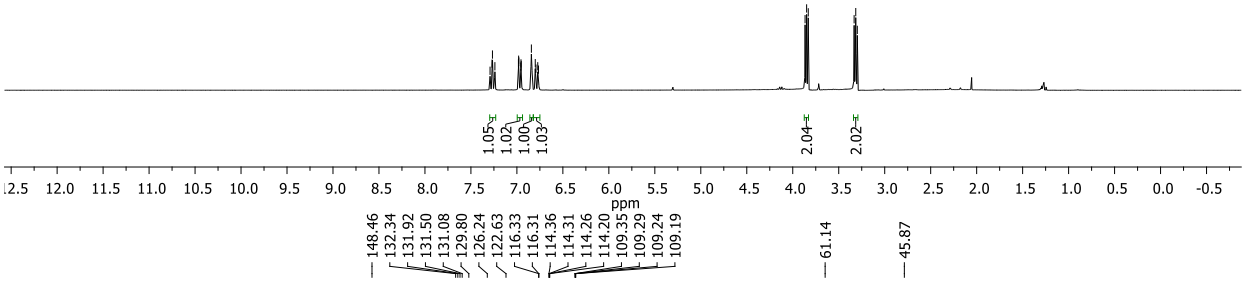

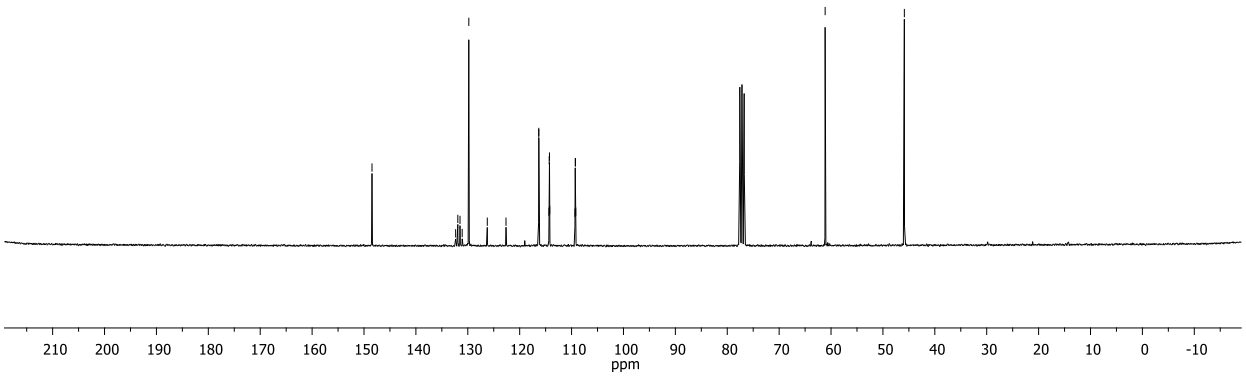

COSY Spectrum ($CDCl_3$)

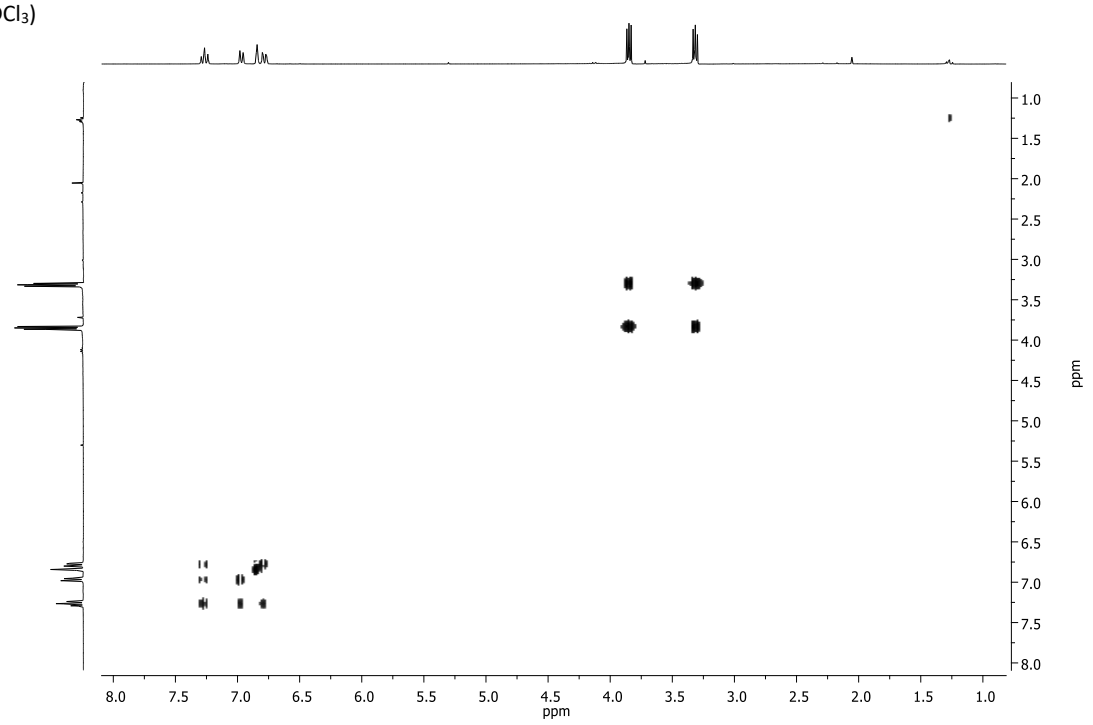

ed-HSQC Spectrum ($CDCl_3$)

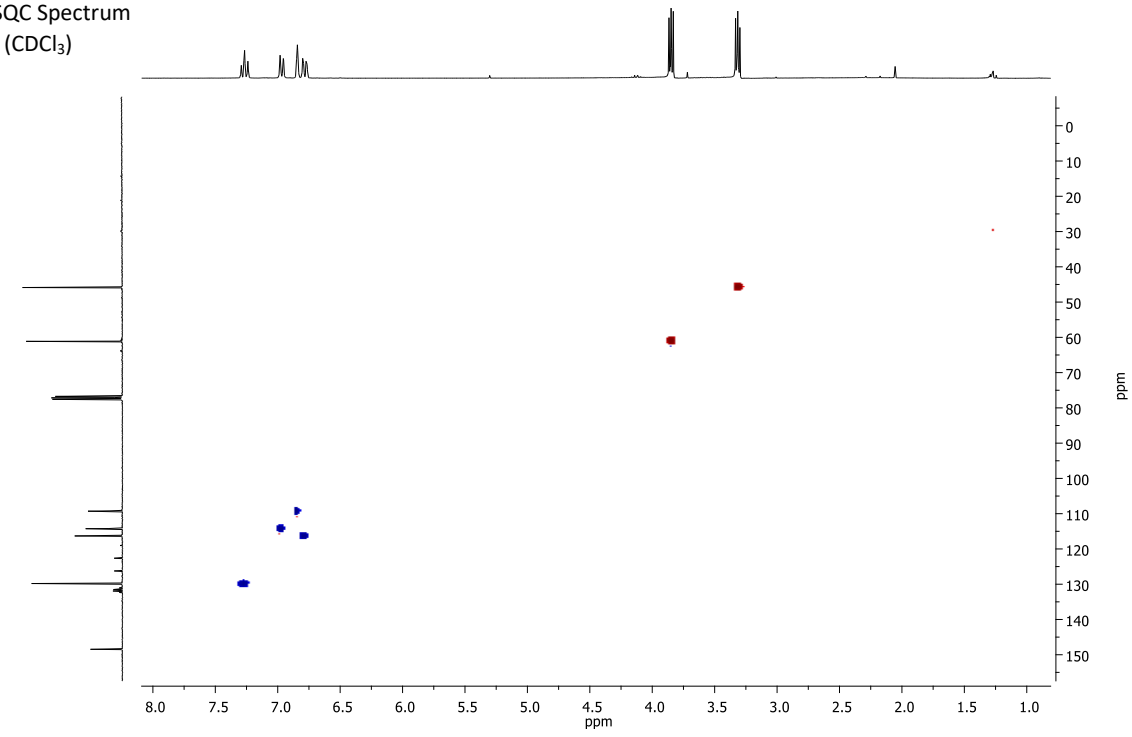

2-((2-trifluoromethoxyphenyl)amino)ethanol (2s)

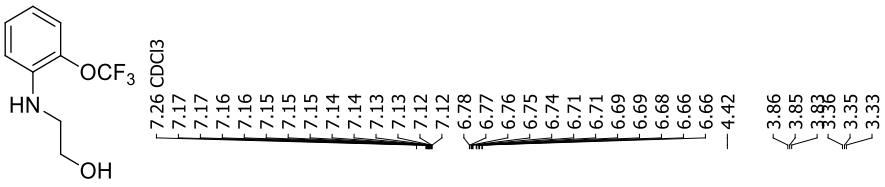

^{1}H NMR Spectrum
(300 MHz, $CDCl_3$)

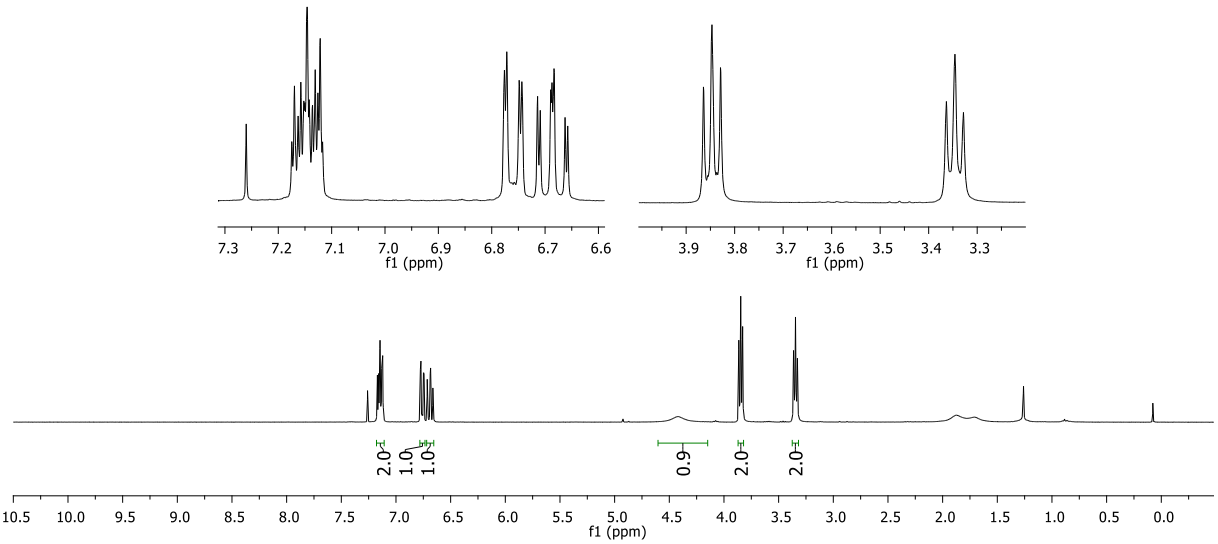

^{13}C NMR Spectrum
(75 MHz, $CDCl_3$)

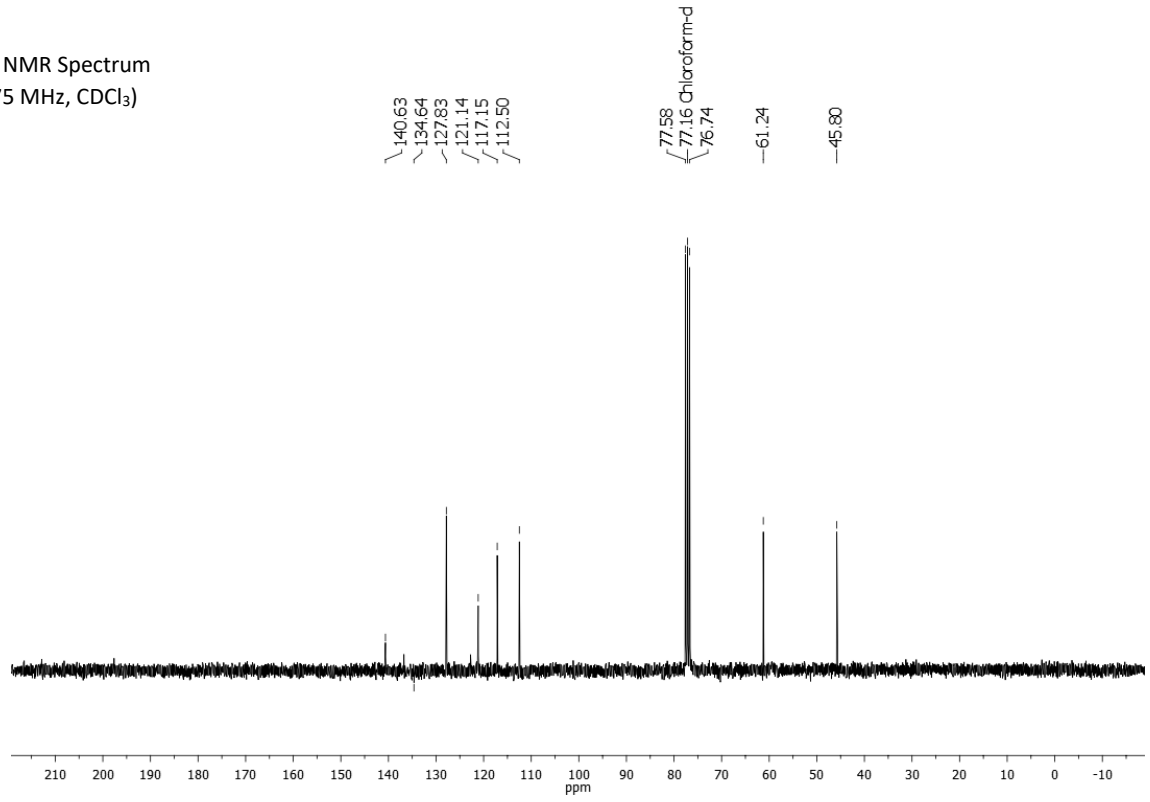

COSY Spectrum ($CDCl_3$)

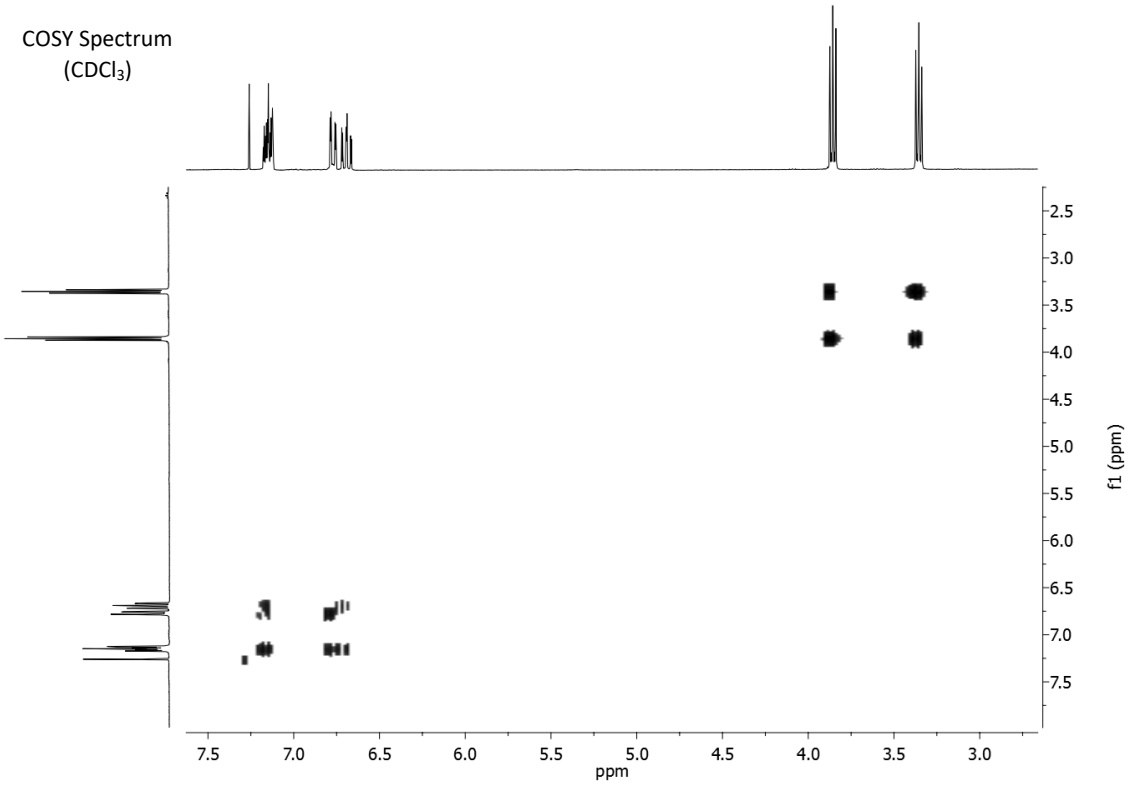

ed-HSQC Spectrum ($CDCl_3$)

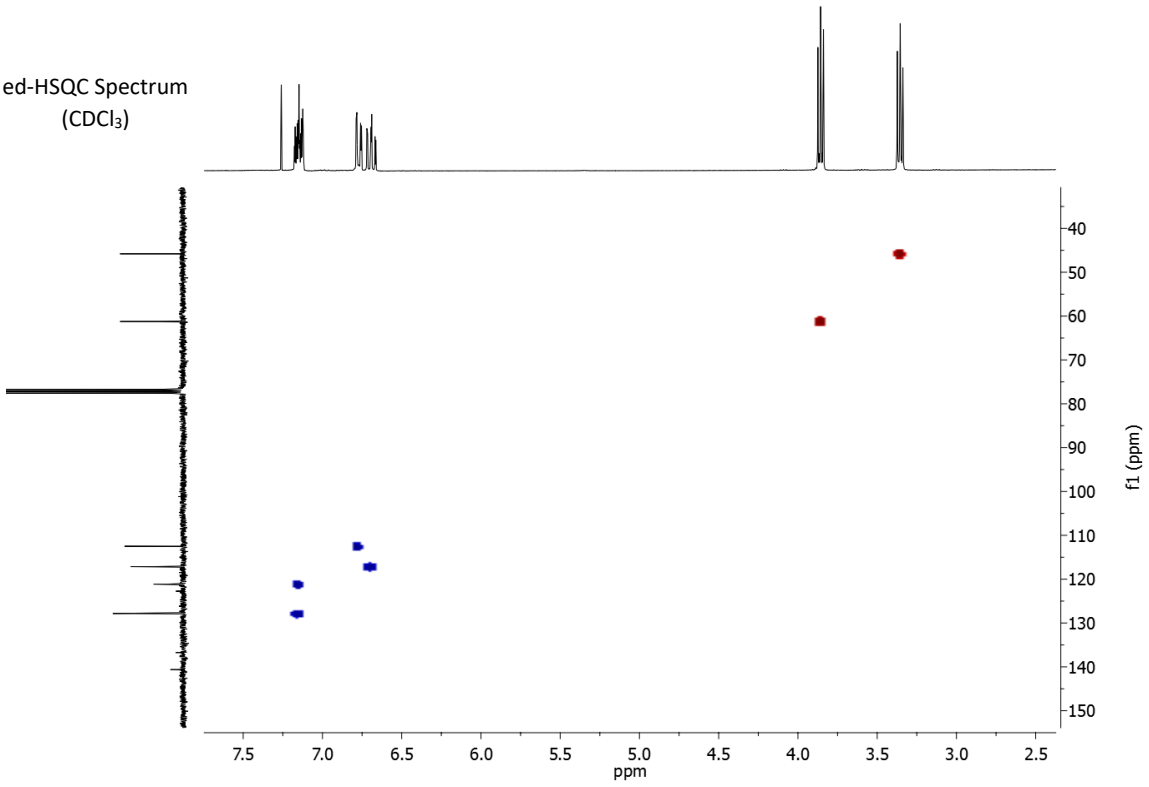

2-((2-methoxyphenyl)amino)ethanol (2t)

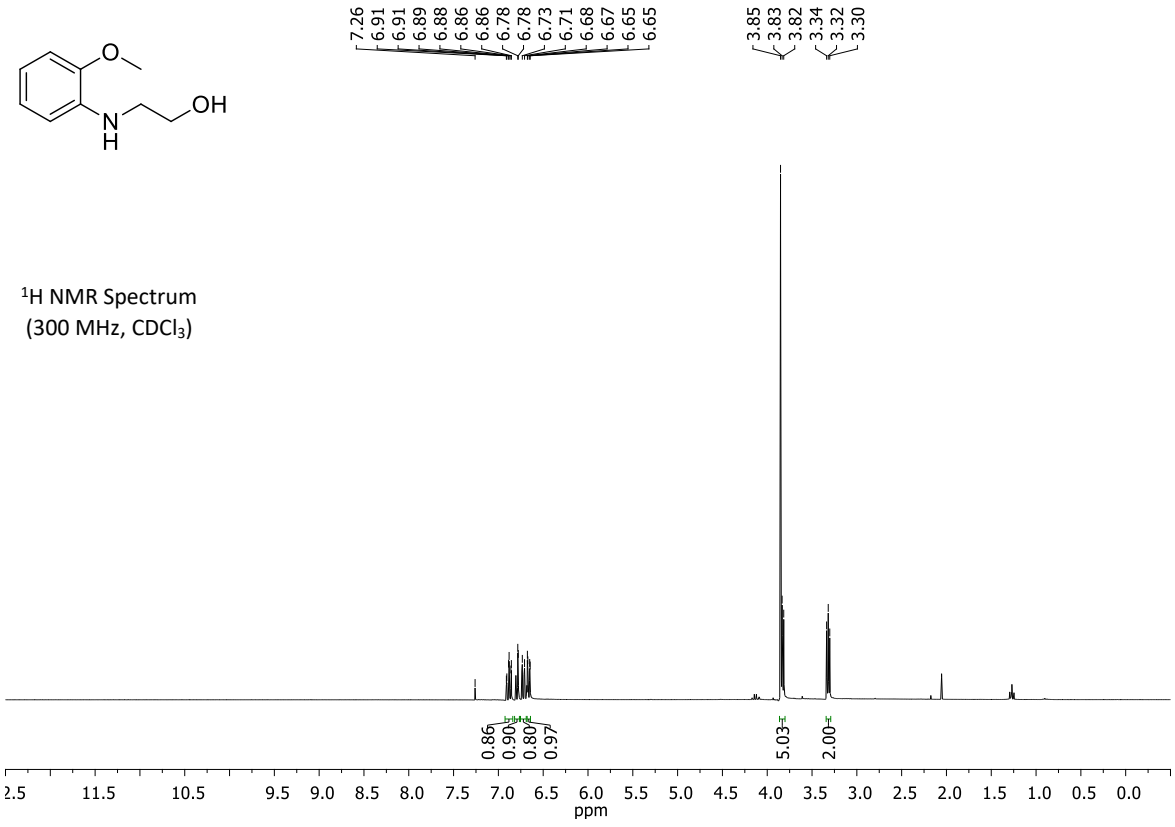

^{1}H NMR Spectrum
(300 MHz, $CDCl_3$)

2-((3,5-dimethoxylphenyl)amino)ethanol (2v)

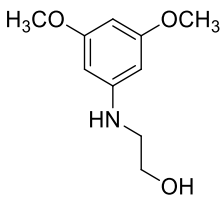

^{1}H NMR Spectrum
(300 MHz, $CDCl_3$)

^{13}C NMR Spectrum
(75 MHz, $CDCl_3$)

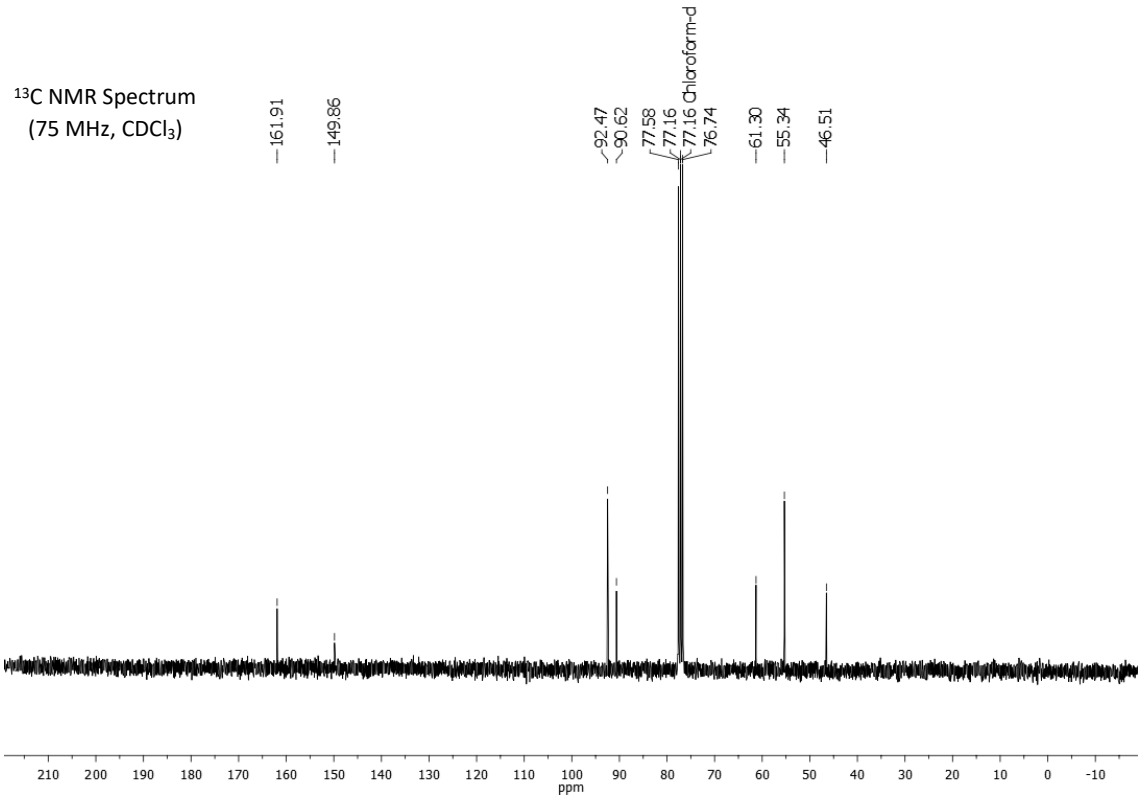

COSY Spectrum
($CDCl_3$)

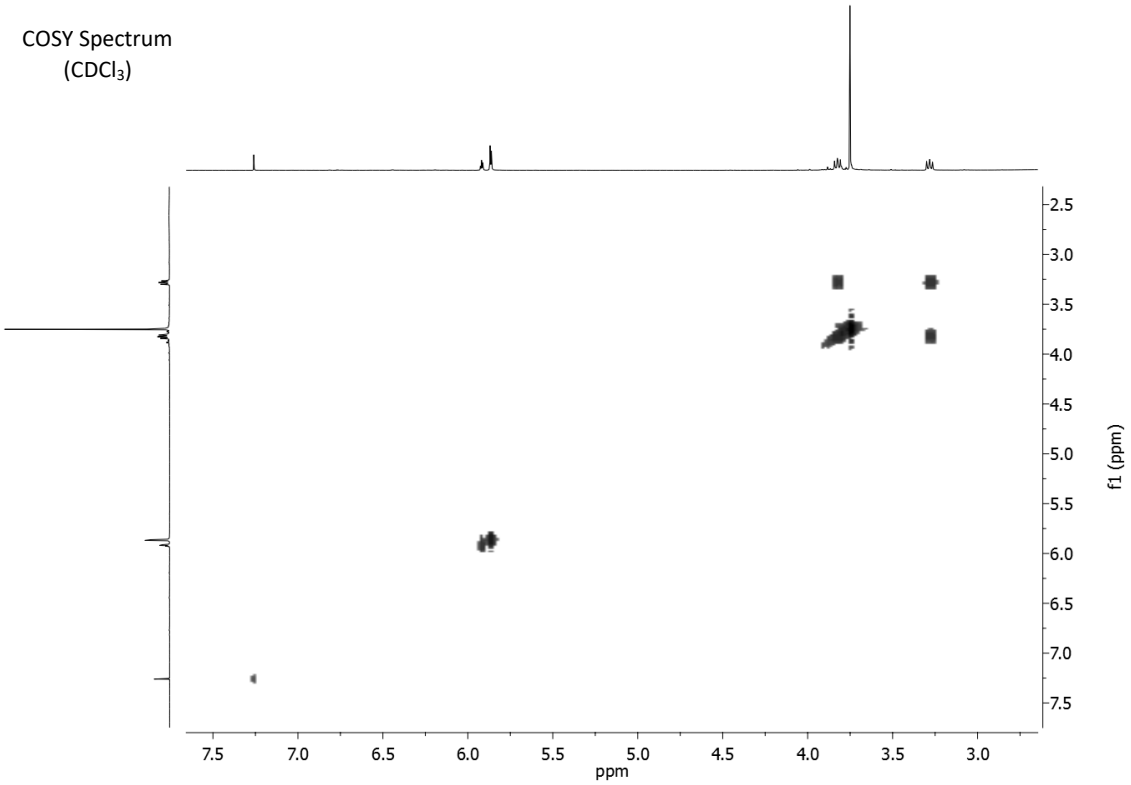

ed-HSQC Spectrum
($CDCl_3$)

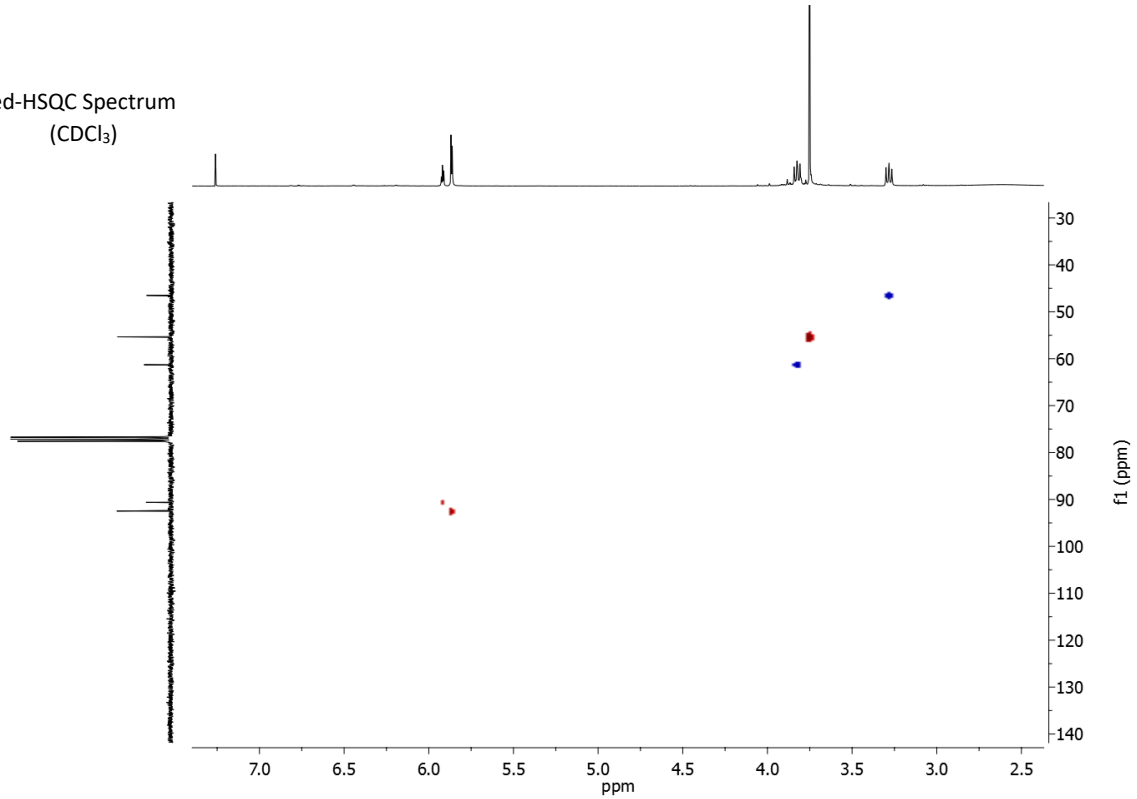

2-((3,4-dimethoxylphenyl)amino)ethanol (2w)

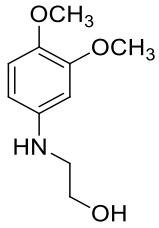

^{1}H NMR Spectrum
(300 MHz, $CDCl_3$)

^{13}C NMR Spectrum
(75 MHz, $CDCl_3$)

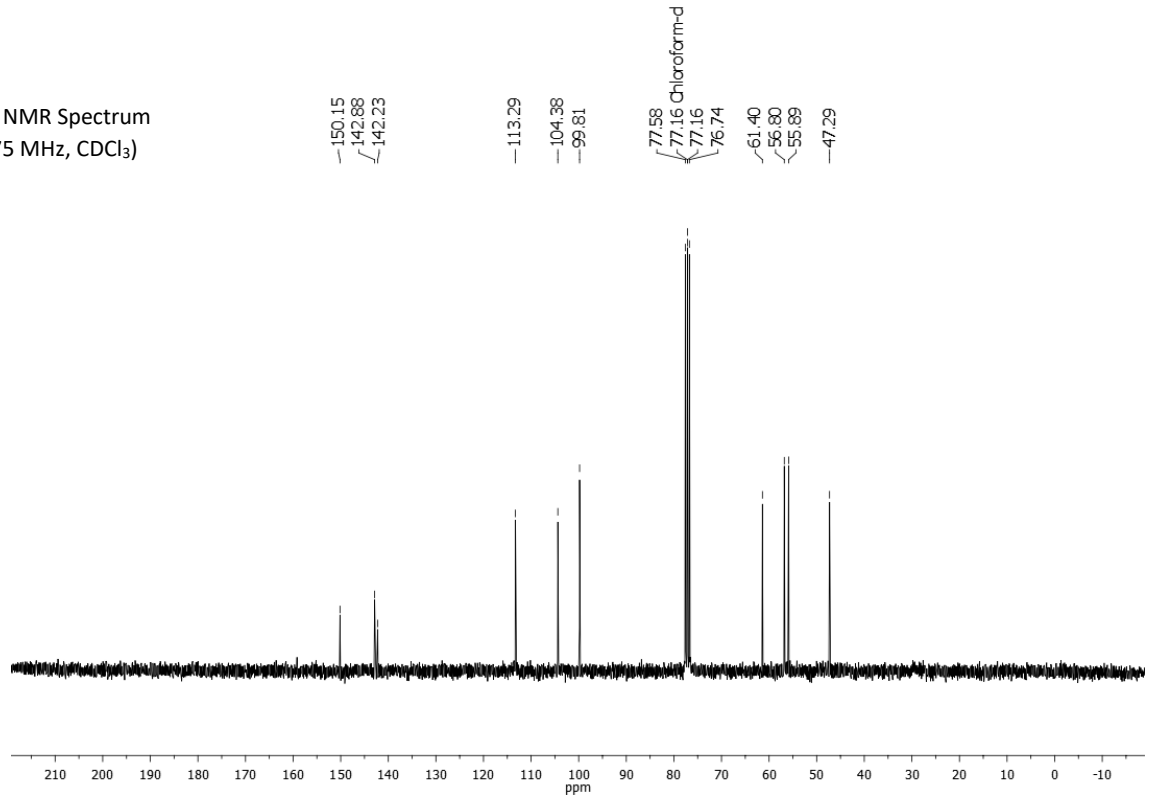

COSY Spectrum
($CDCl_3$)

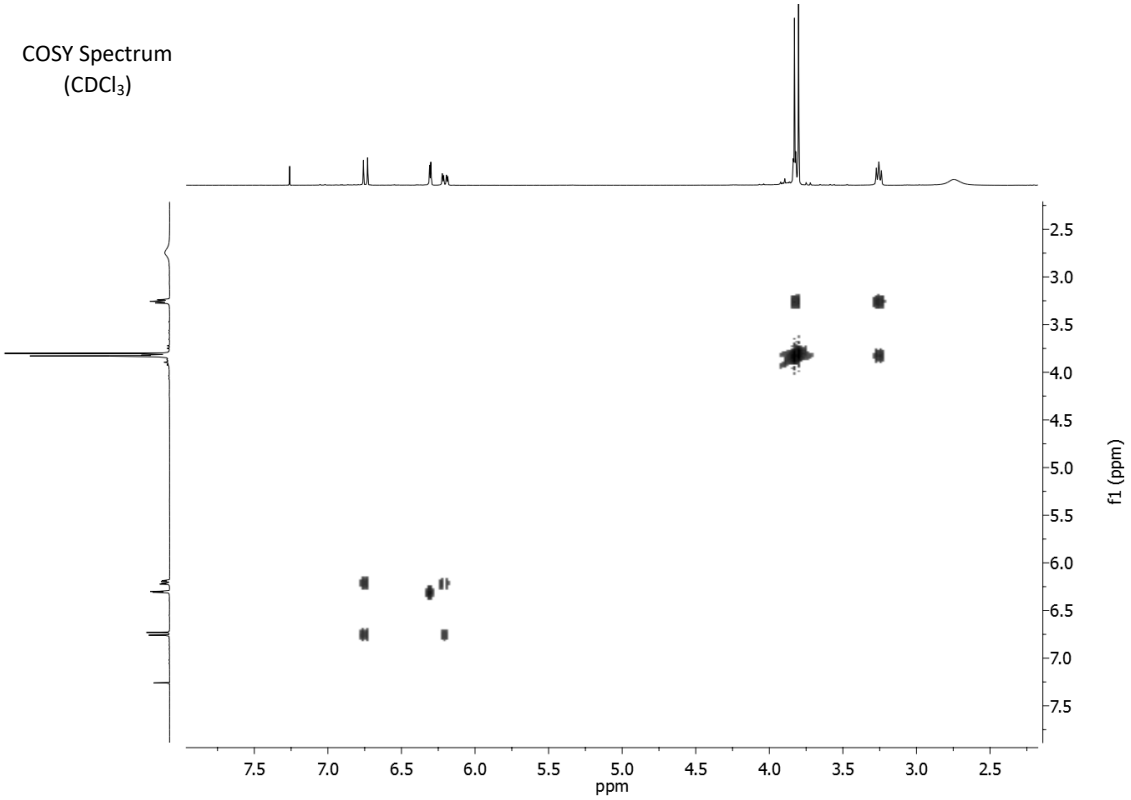

ed-HSQC Spectrum
($CDCl_3$)

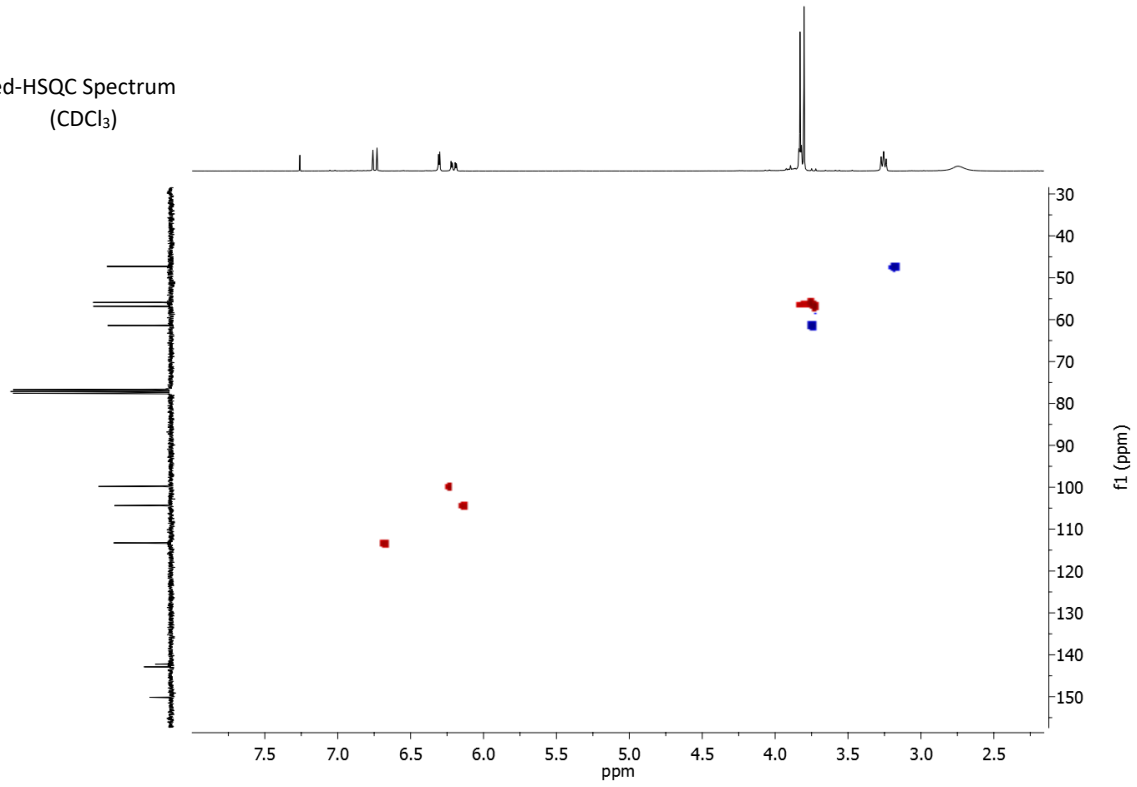

5-methylindole (3a)

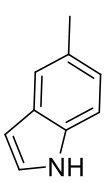

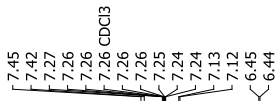

^{1}H NMR Spectrum
(300 MHz, $CDCl_3$)

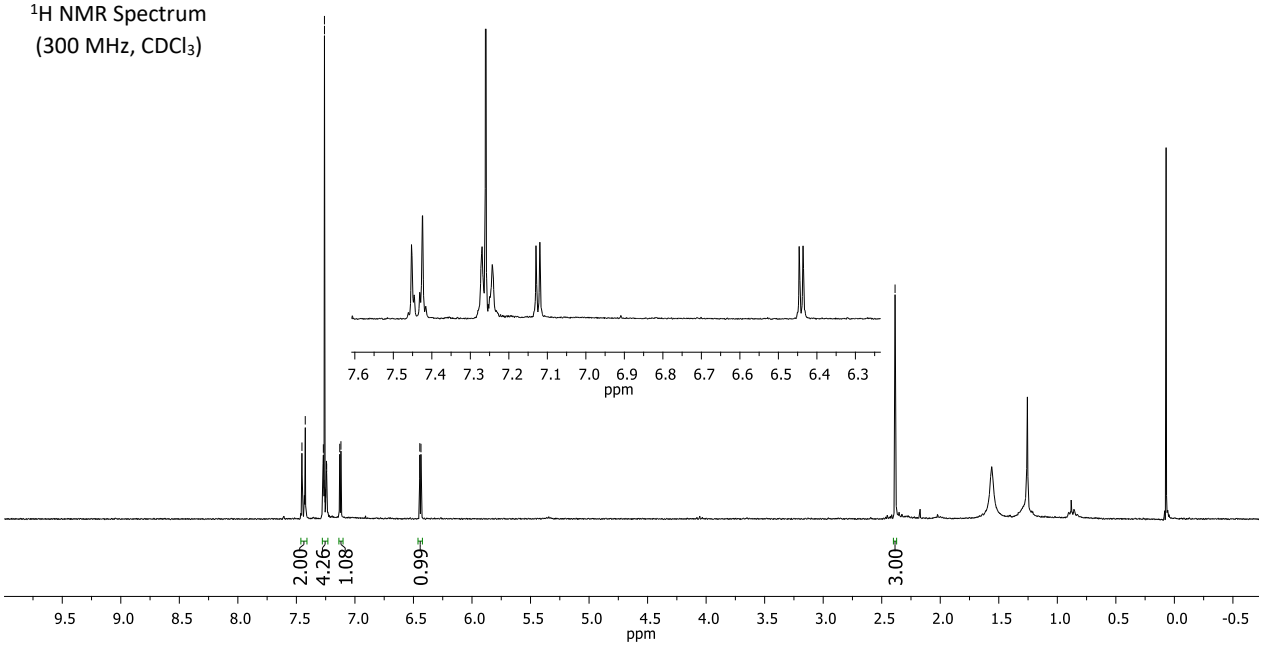

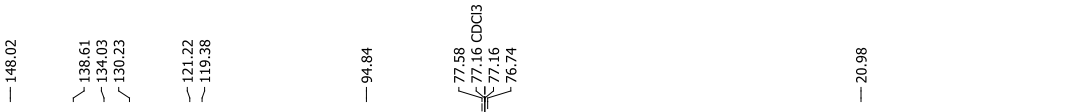

^{13}C NMR Spectrum
(75 MHz, $CDCl_3$)

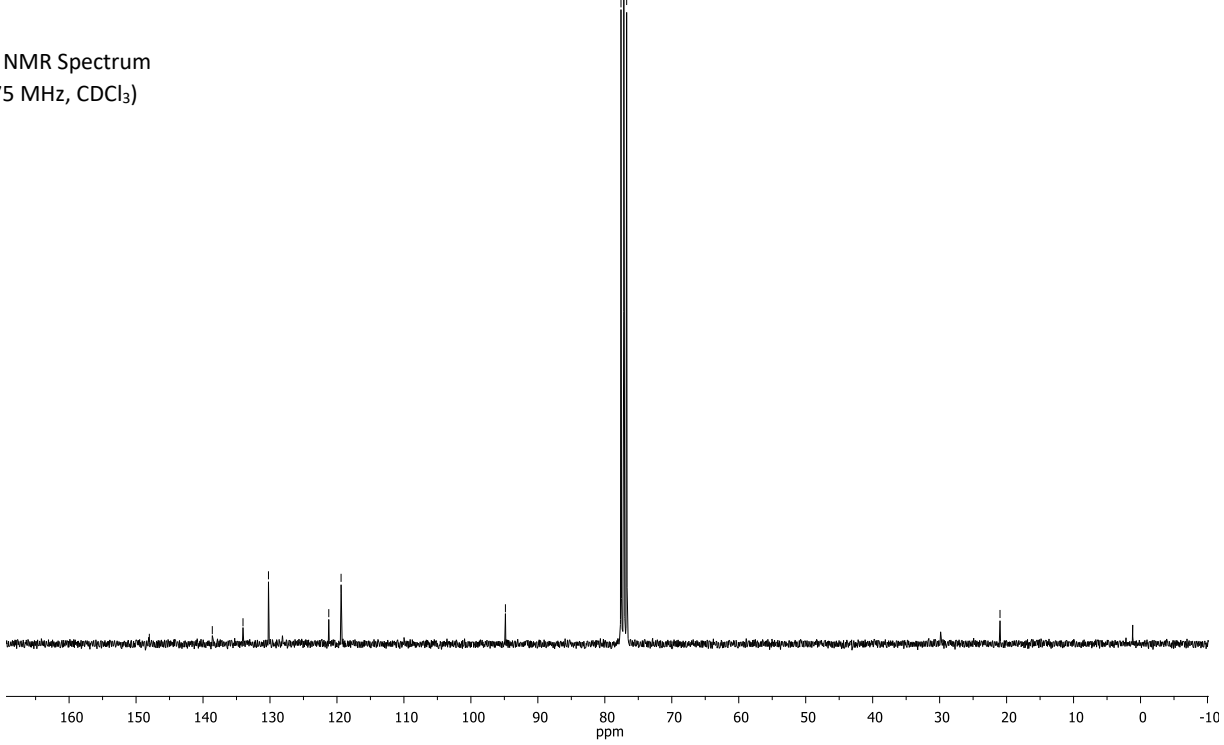

COSY Spectrum ($CDCl_3$)

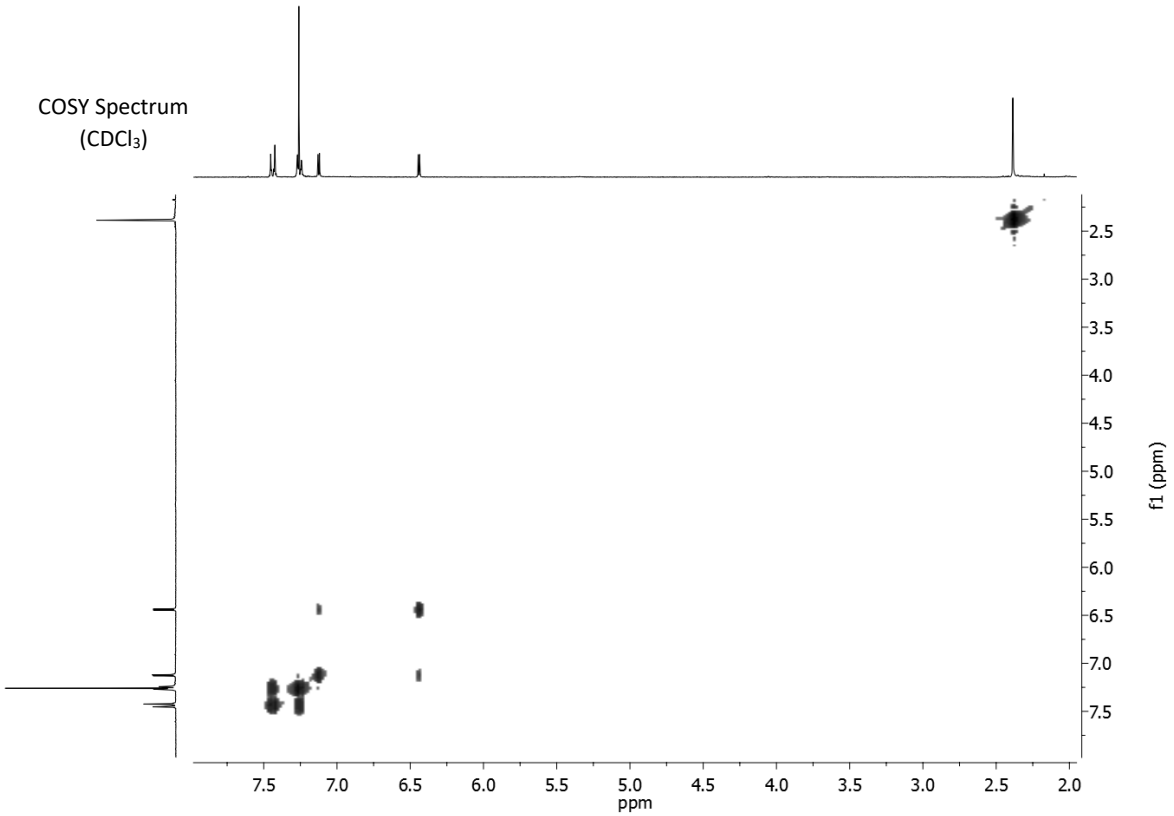

ed-HSQC Spectrum ($CDCl_3$)

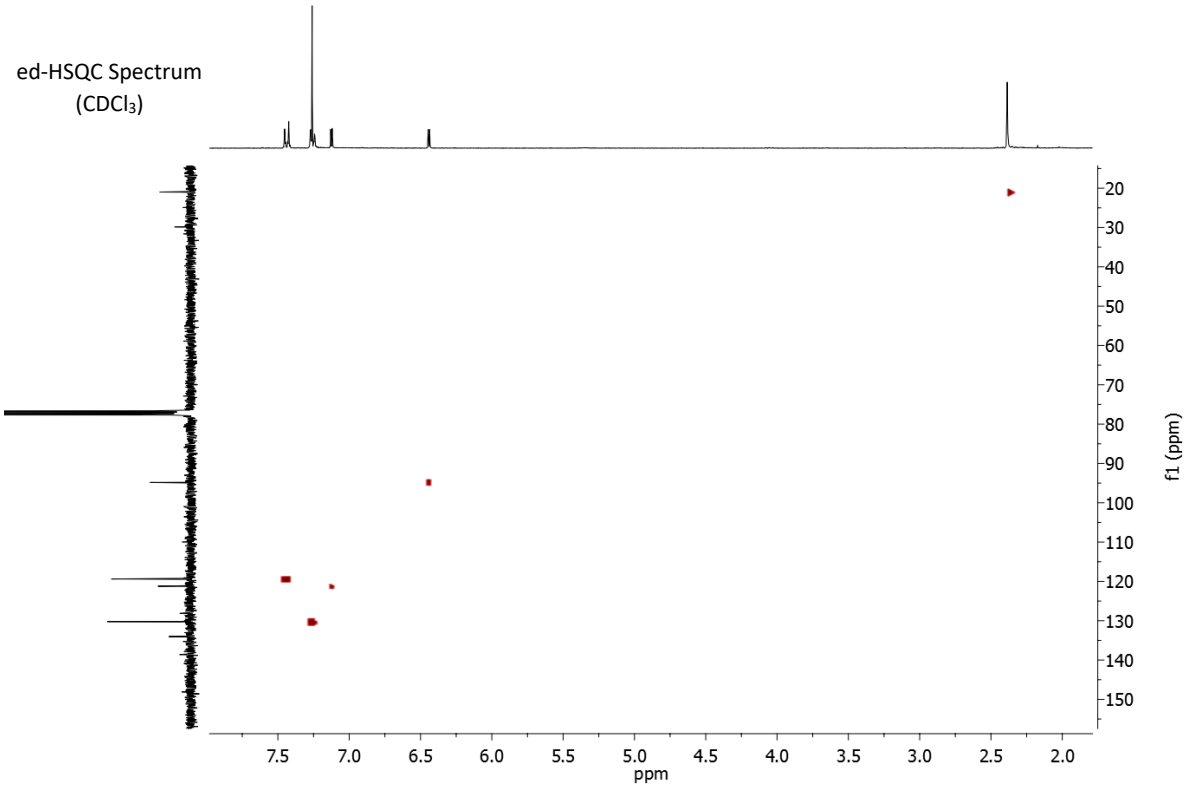

6-methylindole (3b) and 4-methylindole (3b')

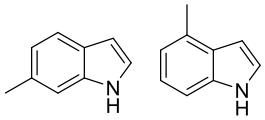

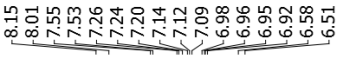

^{1}H NMR Spectrum
(300 MHz, $CDCl_3$)

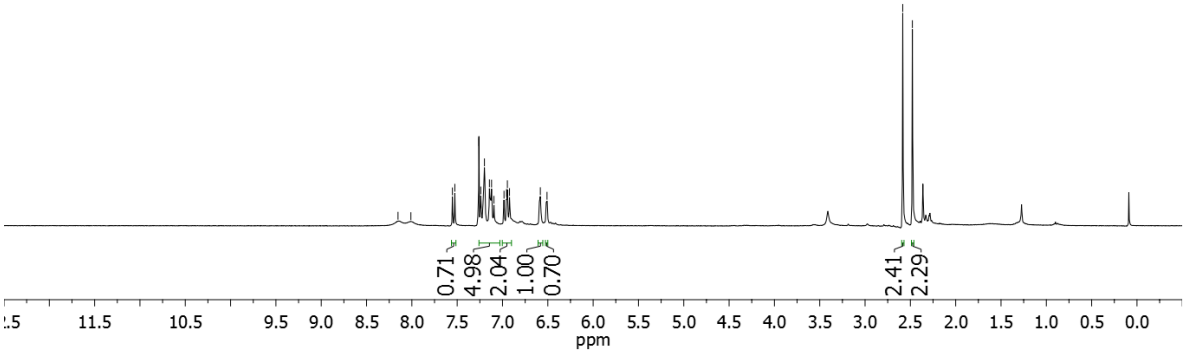

^{13}C NMR Spectrum
(75 MHz, $CDCl_3$)

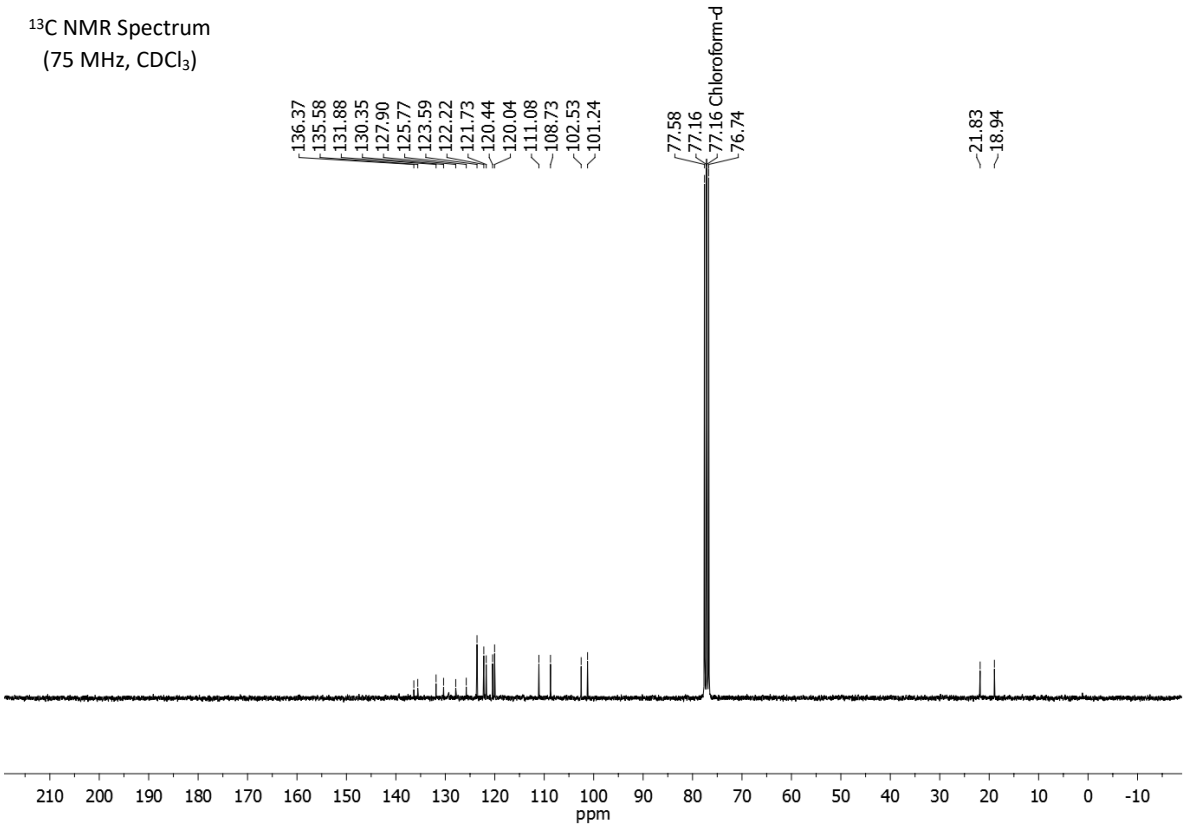

COSY Spectrum ($CDCl_3$)

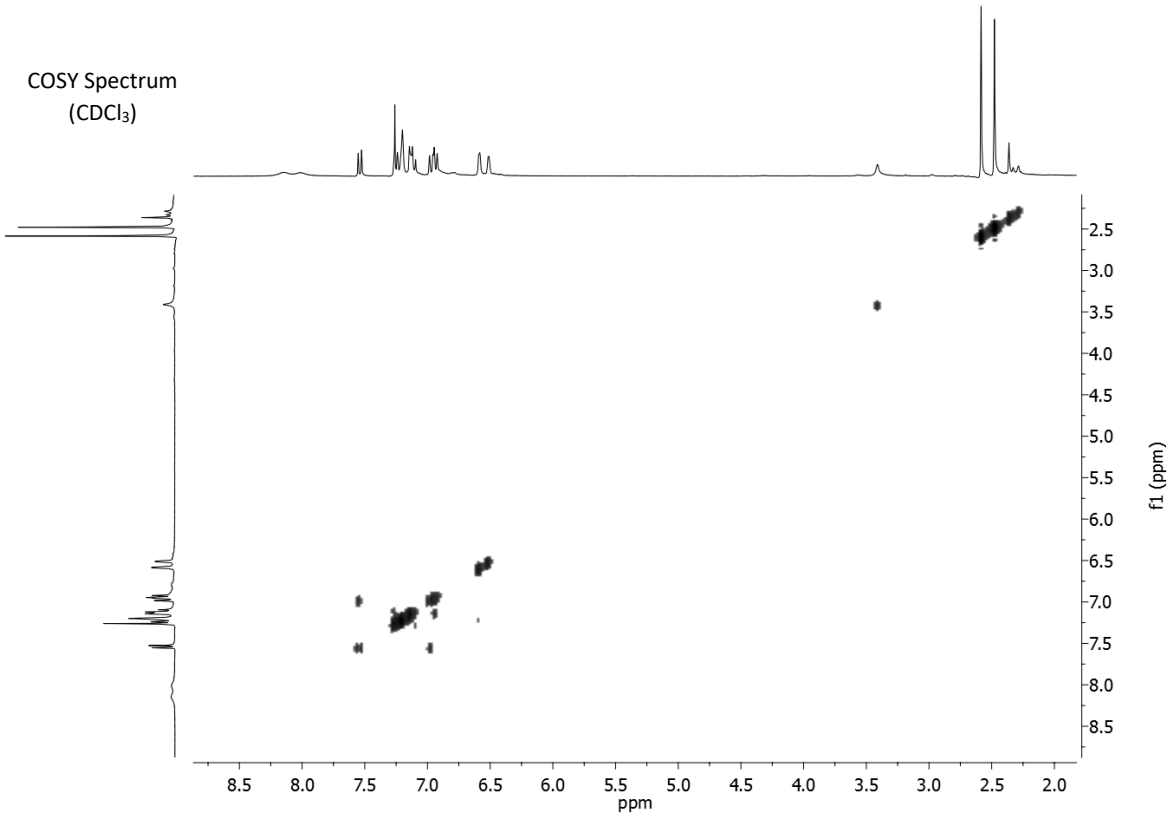

ed-HSQC Spectrum ($CDCl_3$)

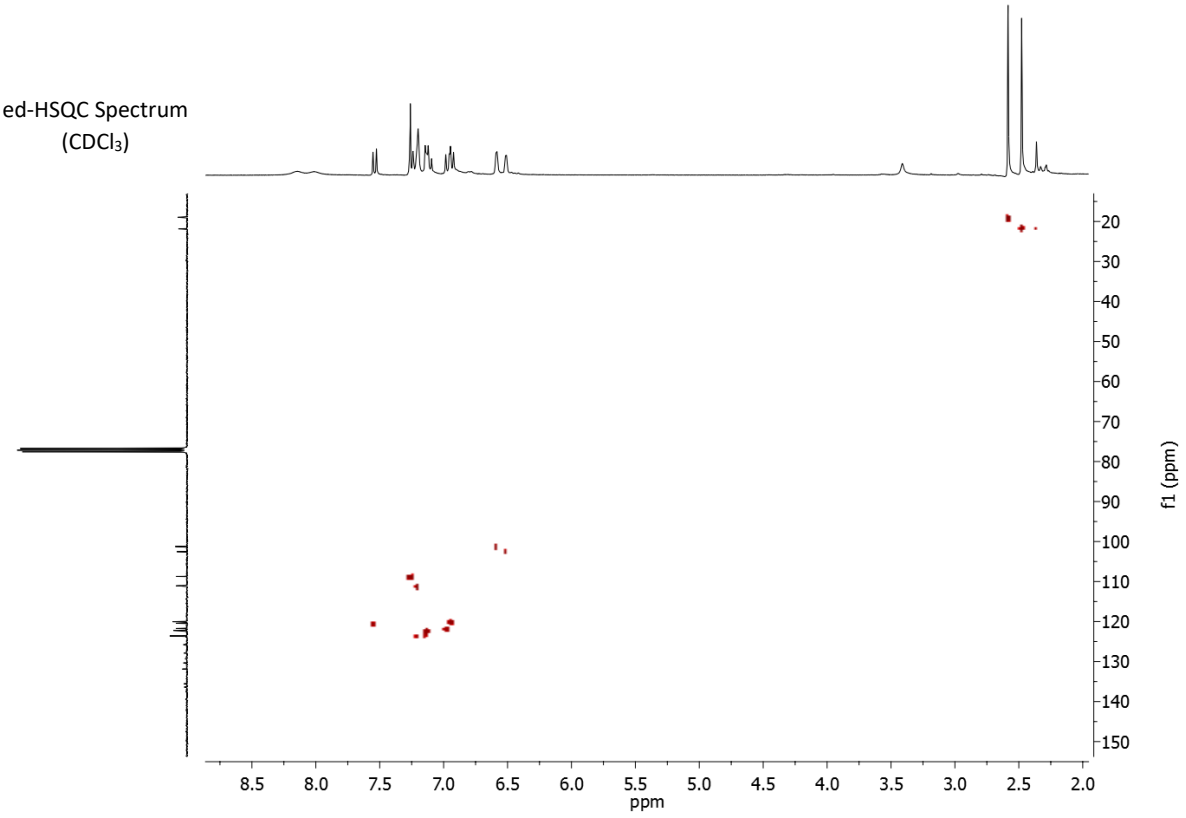

7-methylindole (3c)

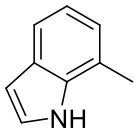

^{1}H NMR Spectrum
(300 MHz, $CDCl_3$)

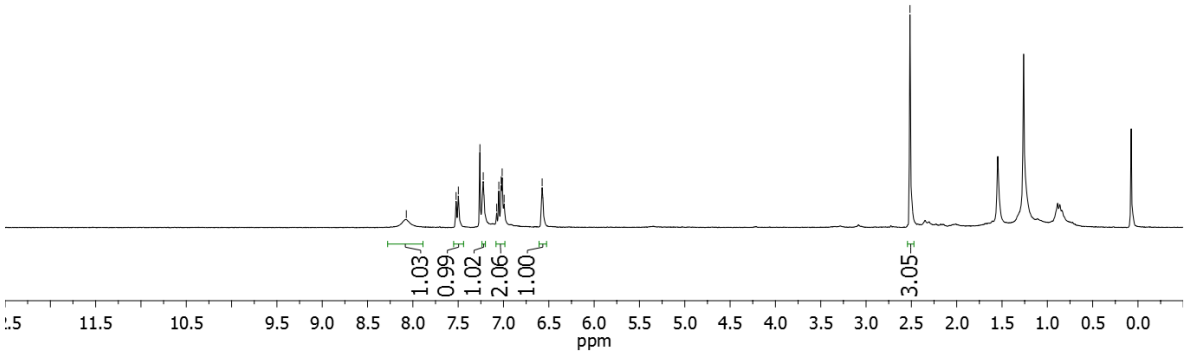

^{13}C NMR Spectrum
(75 MHz, $CDCl_3$)

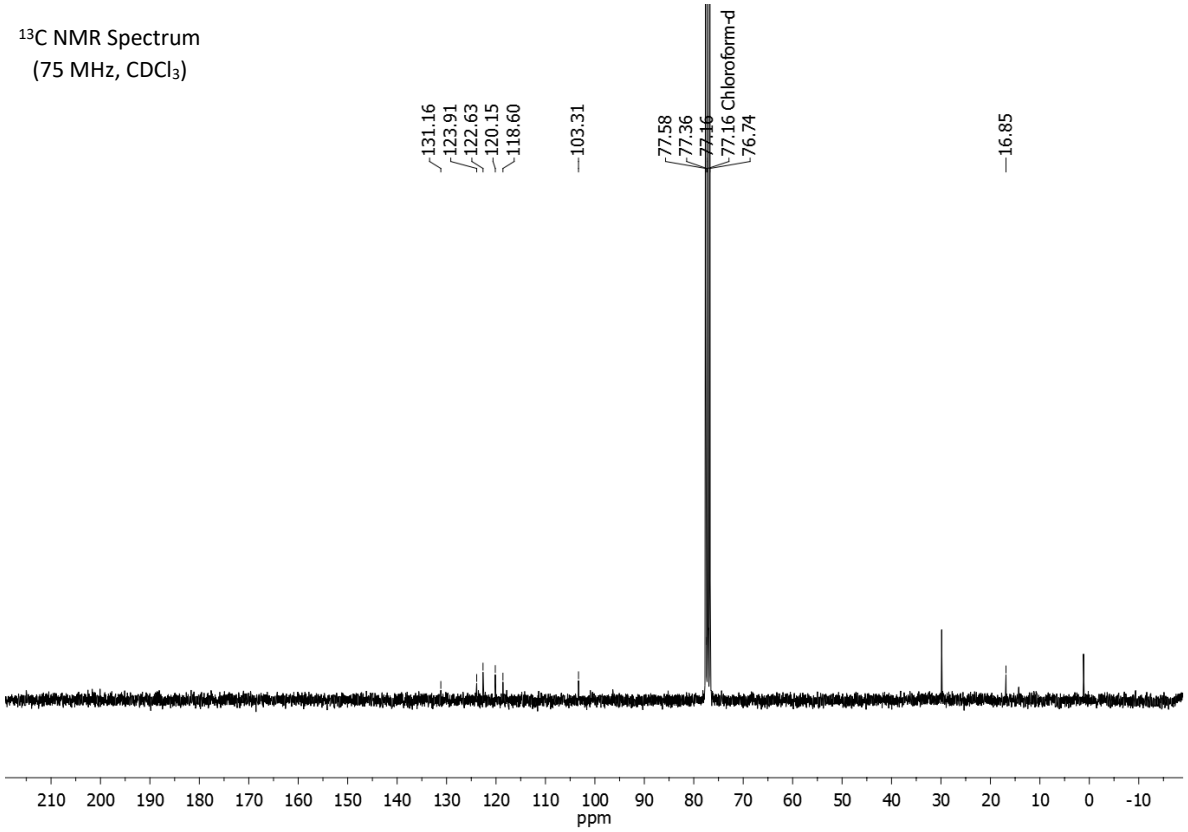

6,7-dimethylindole (3d)

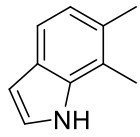

^{1}H NMR Spectrum
(300 MHz, $CDCl_3$)

^{13}C NMR Spectrum
(75 MHz, $CDCl_3$)

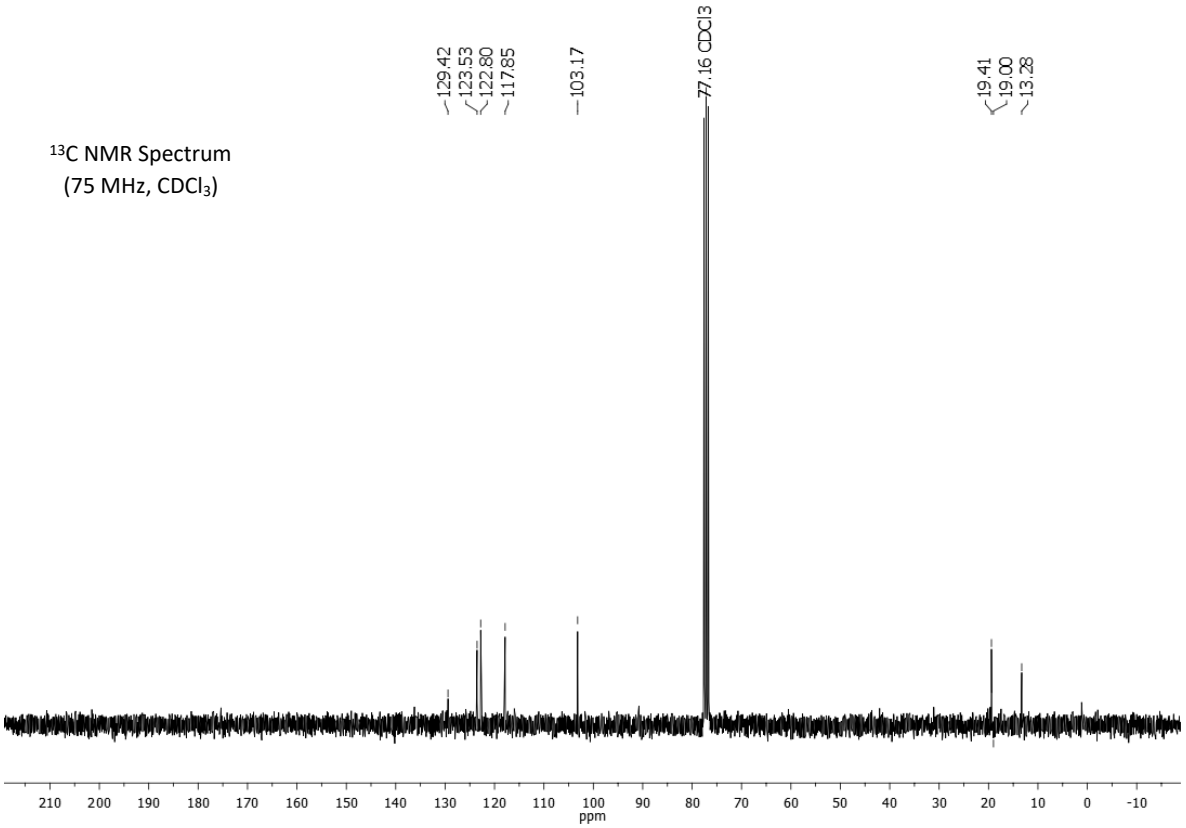

COSY Spectrum
($CDCl_3$)

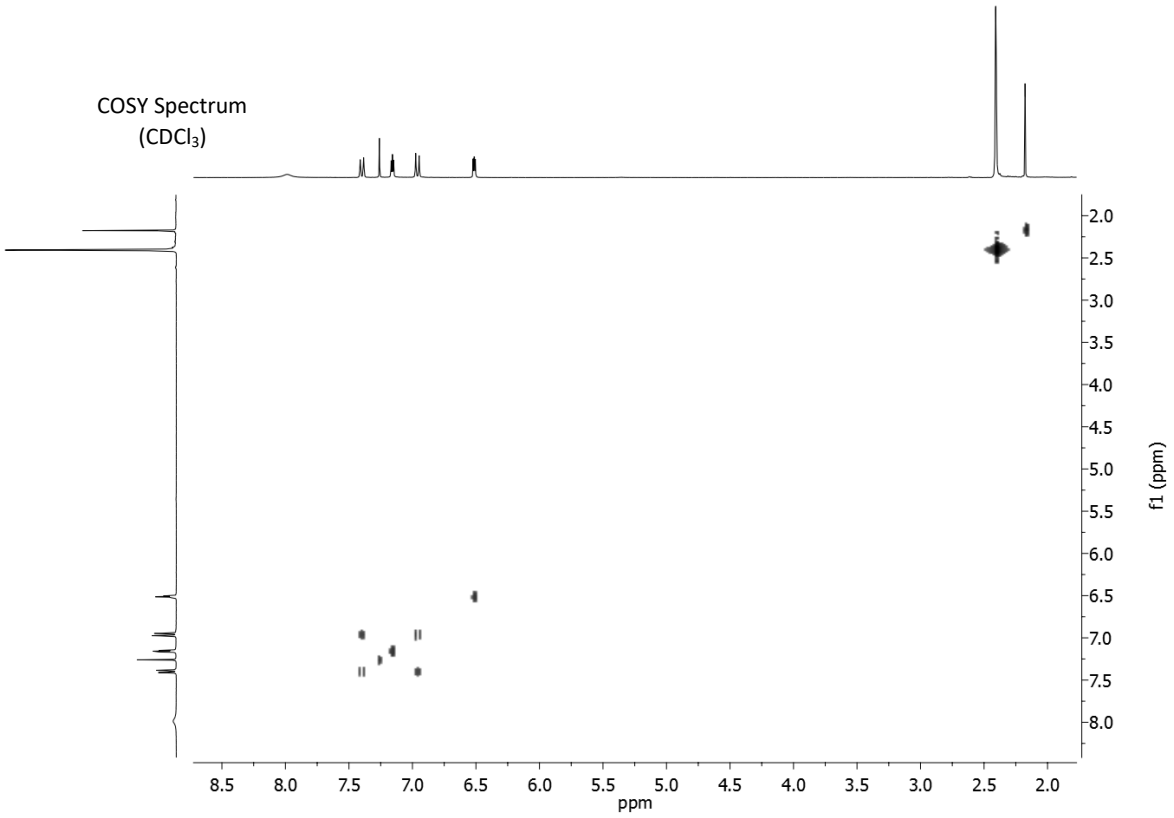

ed-HSQC Spectrum
($CDCl_3$)

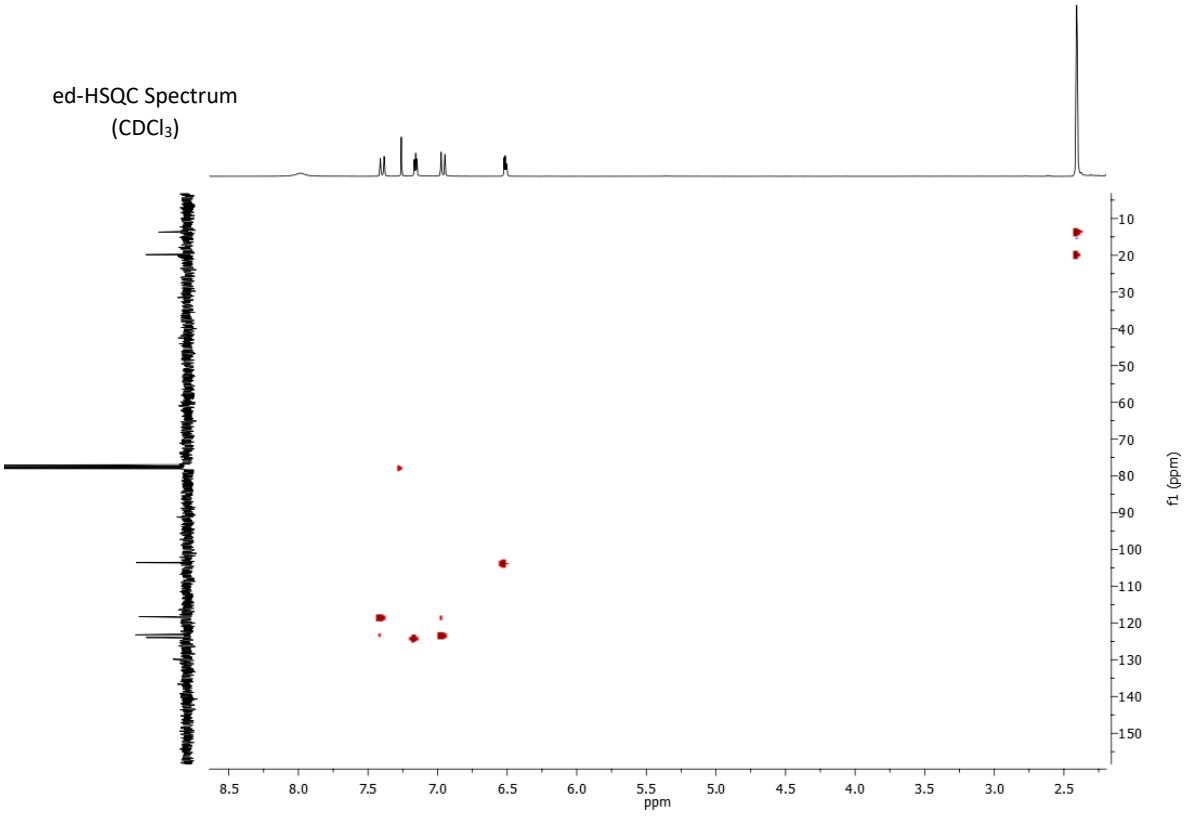

5,7-dimethylindole (3e)

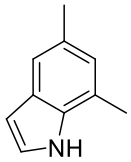

^{1}H NMR Spectrum
(300 MHz, $CDCl_3$)

^{13}C NMR Spectrum
(75 MHz, $CDCl_3$)

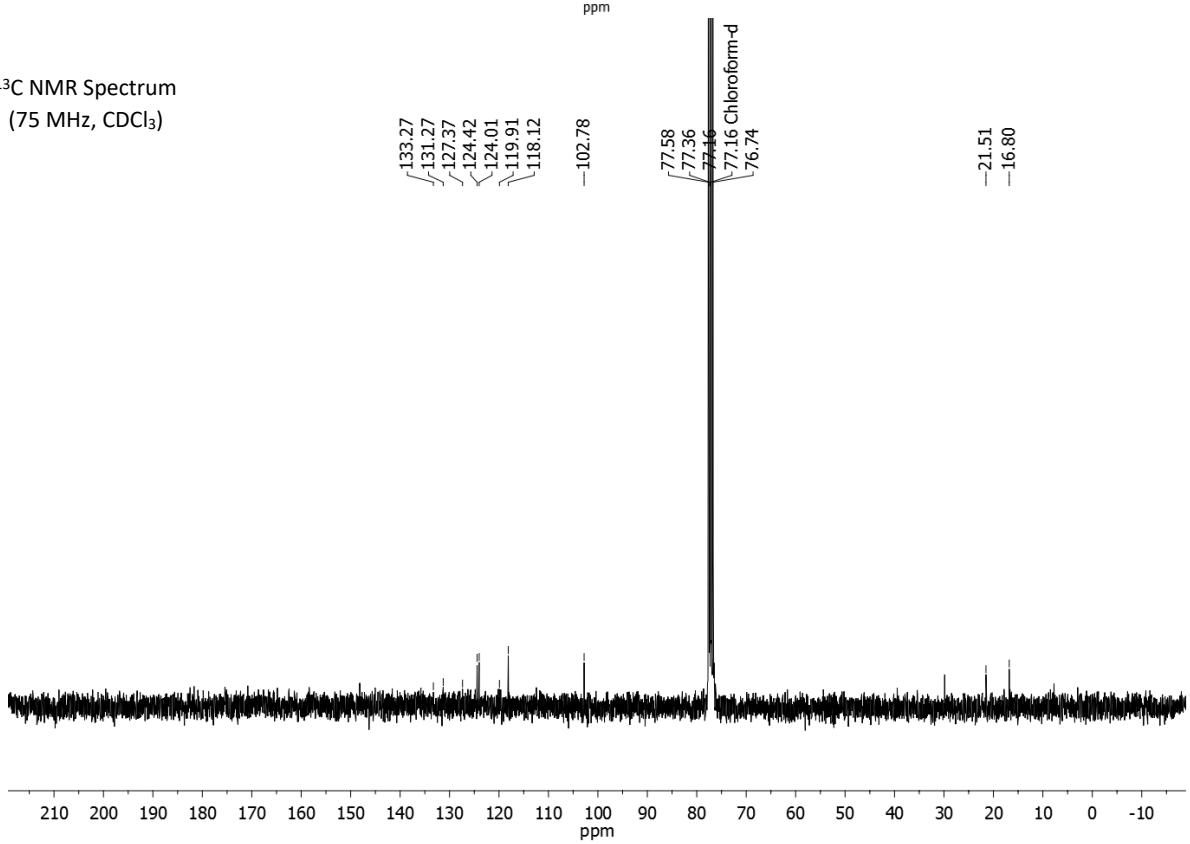

COSY Spectrum ($CDCl_3$)

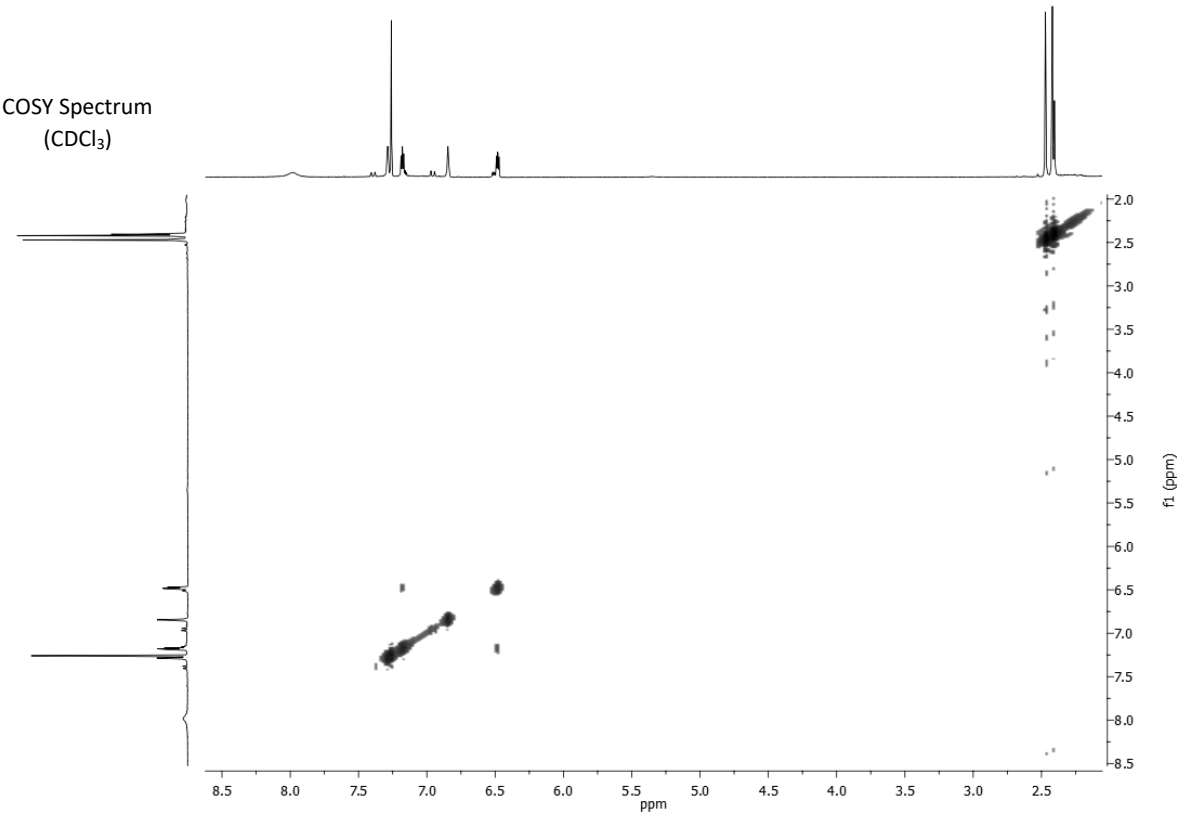

ed-HSQC Spectrum ($CDCl_3$)

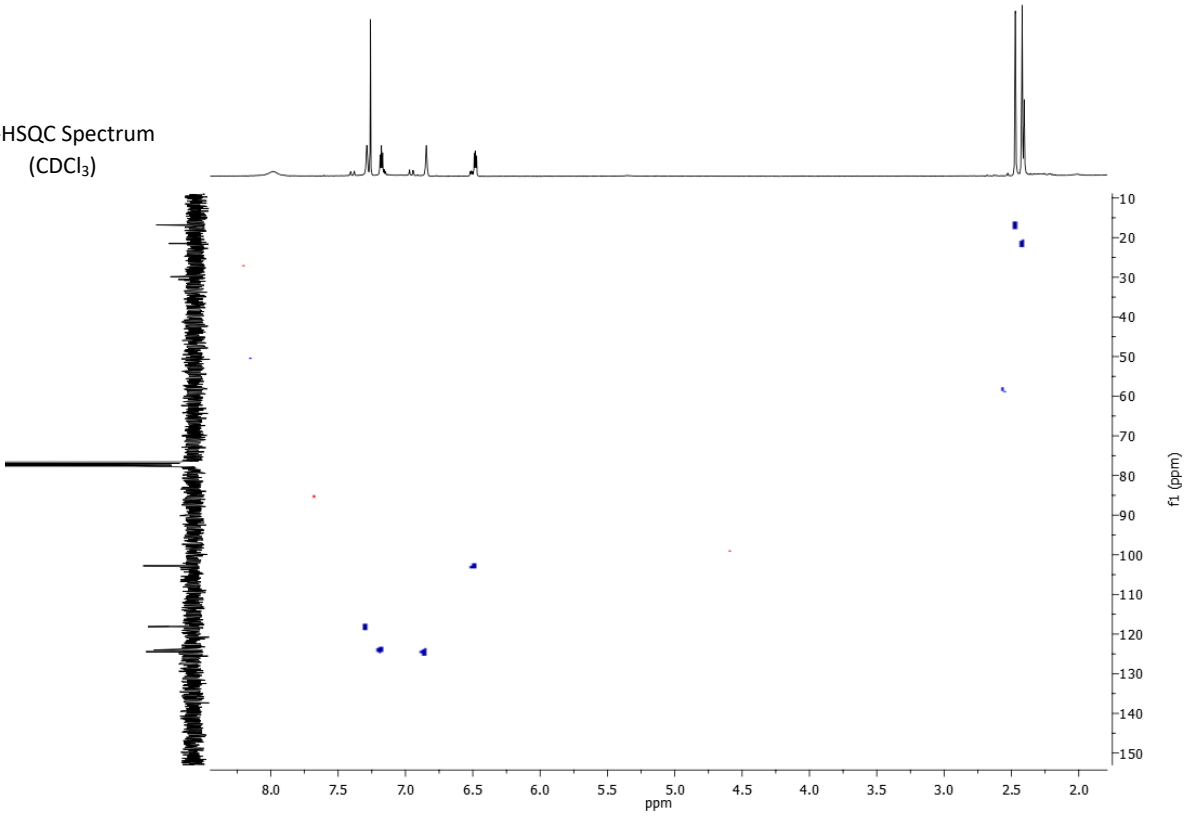

5,6-dimethylindole (3f) and 4,5-dimethylindole (3f')

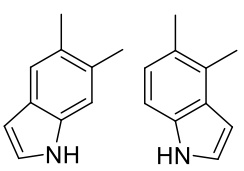

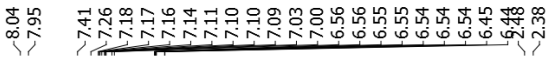

^{1}H NMR Spectrum
(300 MHz, $CDCl_3$)

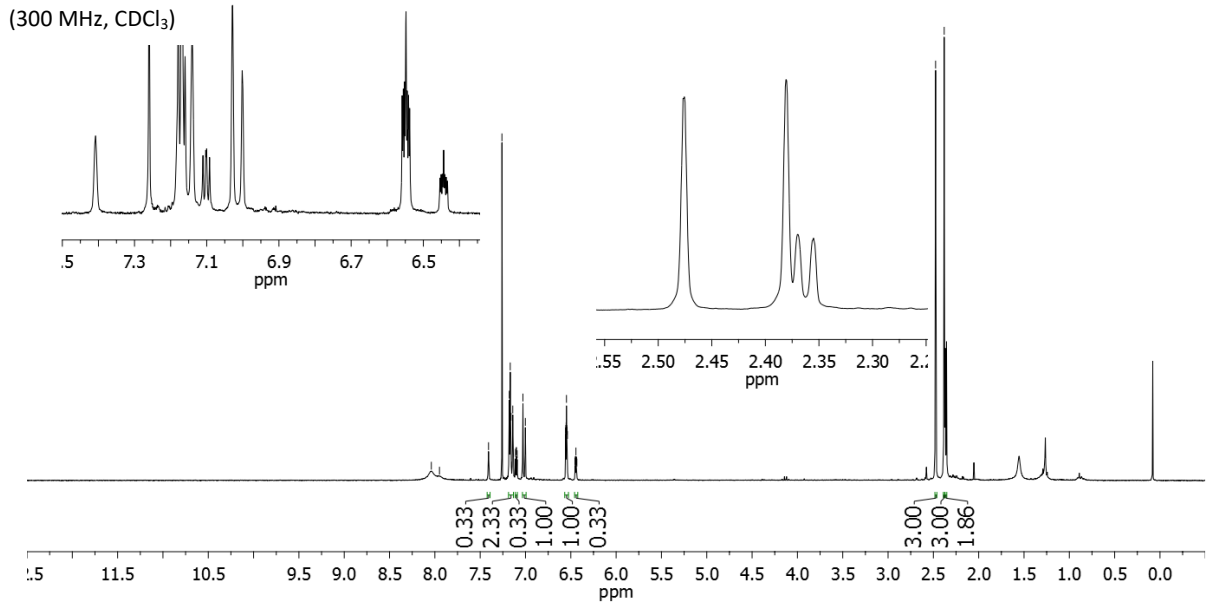

^{13}C NMR Spectrum
(75 MHz, $CDCl_3$)

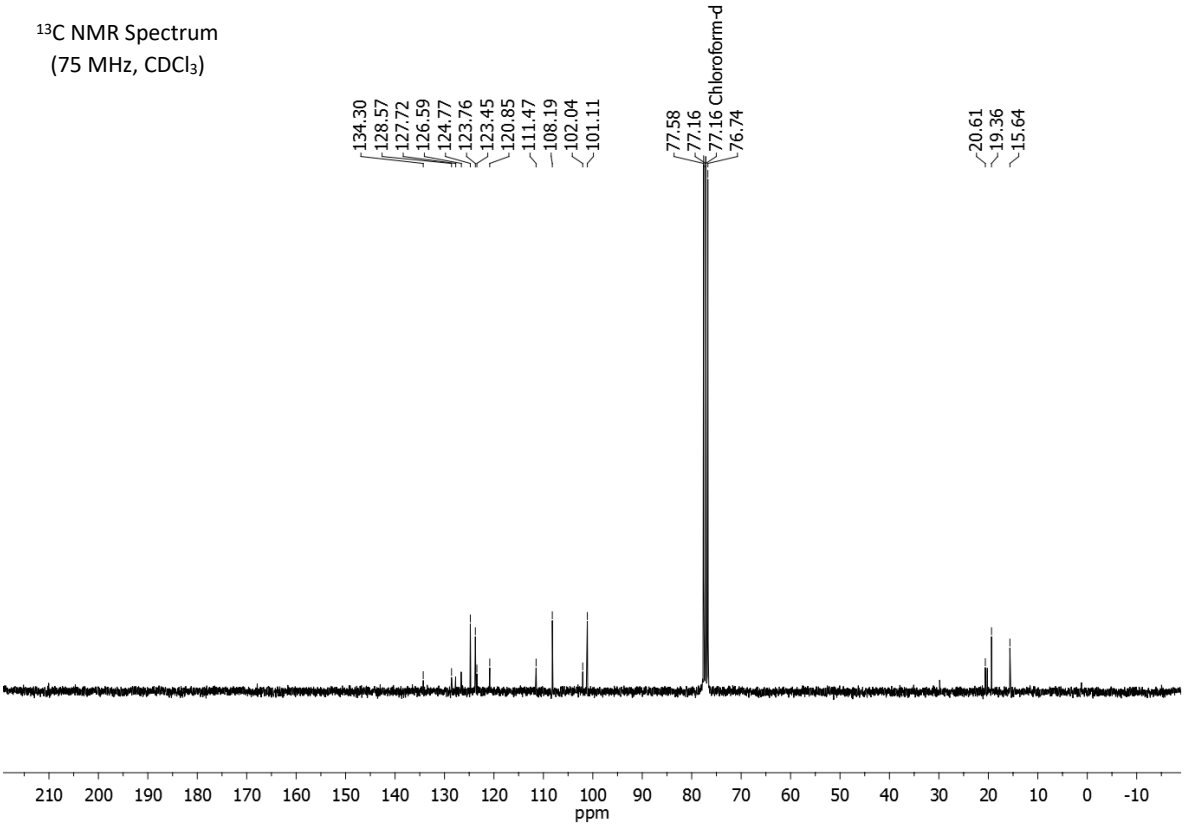

COSY Spectrum
($CDCl_3$)

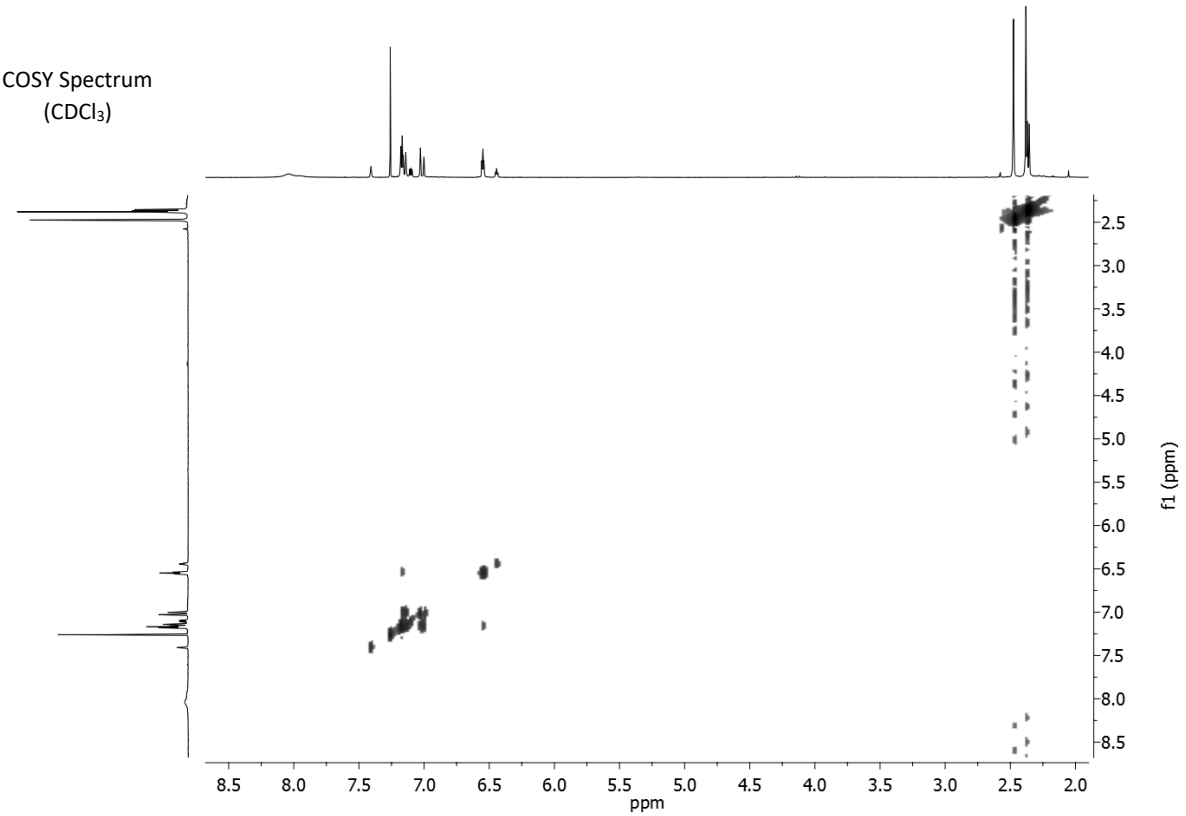

ed-HSQC Spectrum
($CDCl_3$)

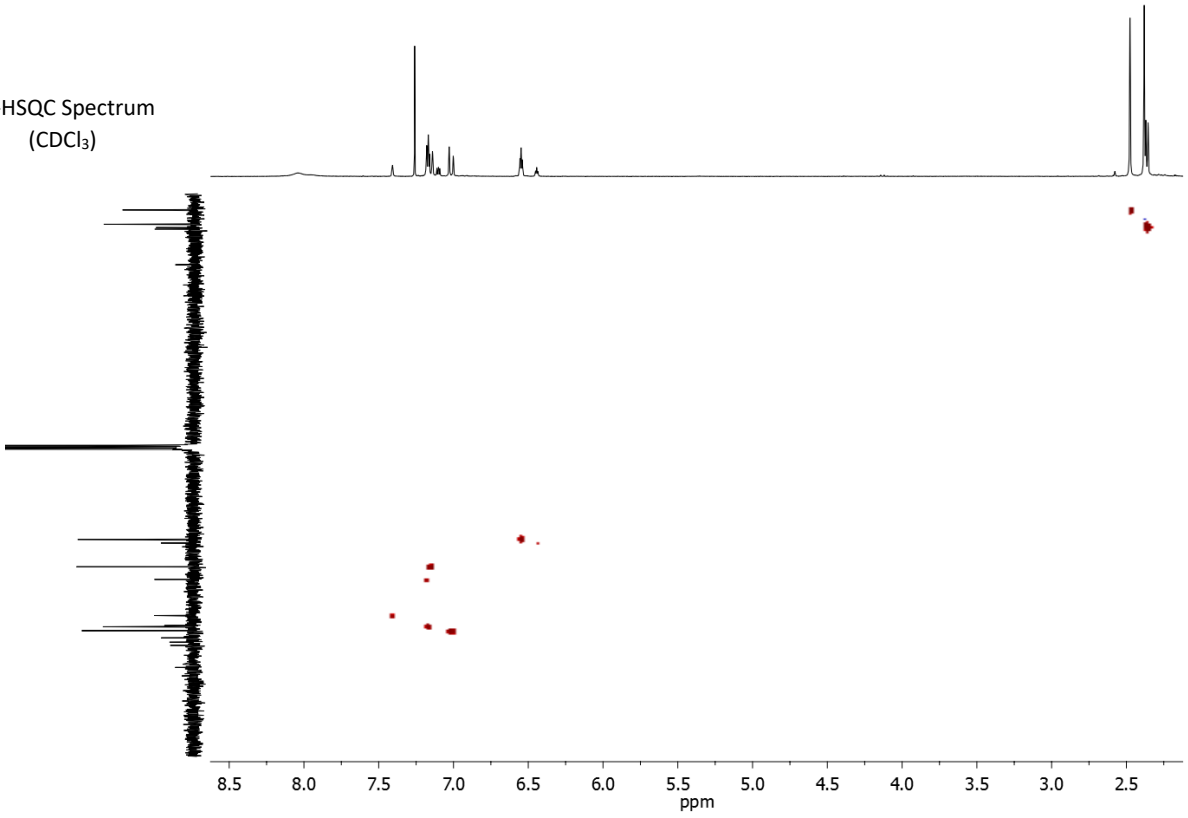

4,6-dimethylindole (3g)

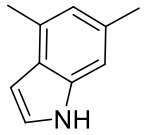

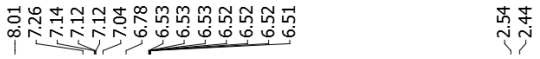

^{1}H NMR Spectrum
(300 MHz, $CDCl_3$)

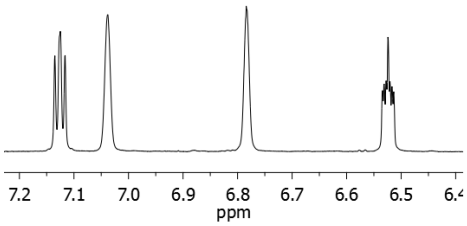

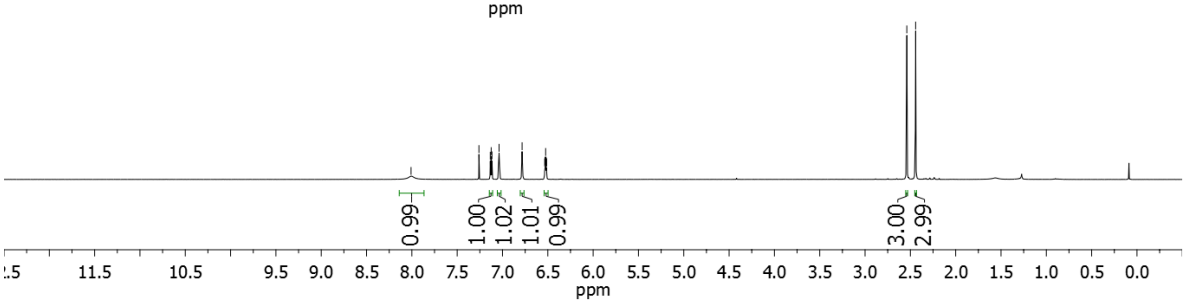

^{13}C NMR Spectrum
(75 MHz, $CDCl_3$)

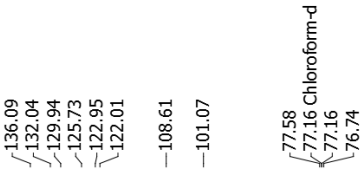

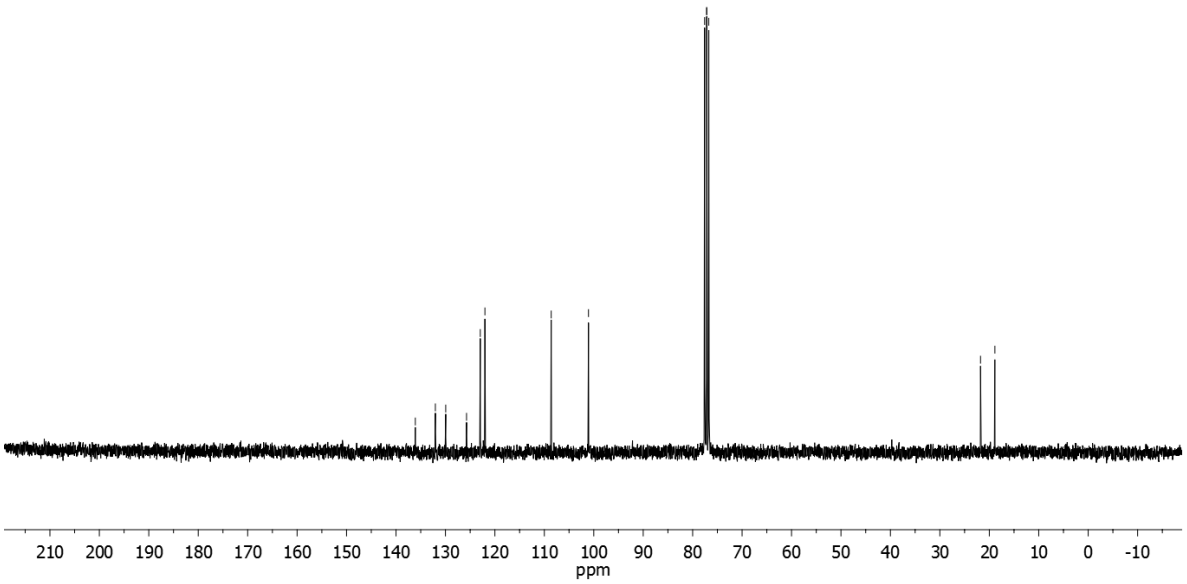

COSY Spectrum
($CDCl_3$)

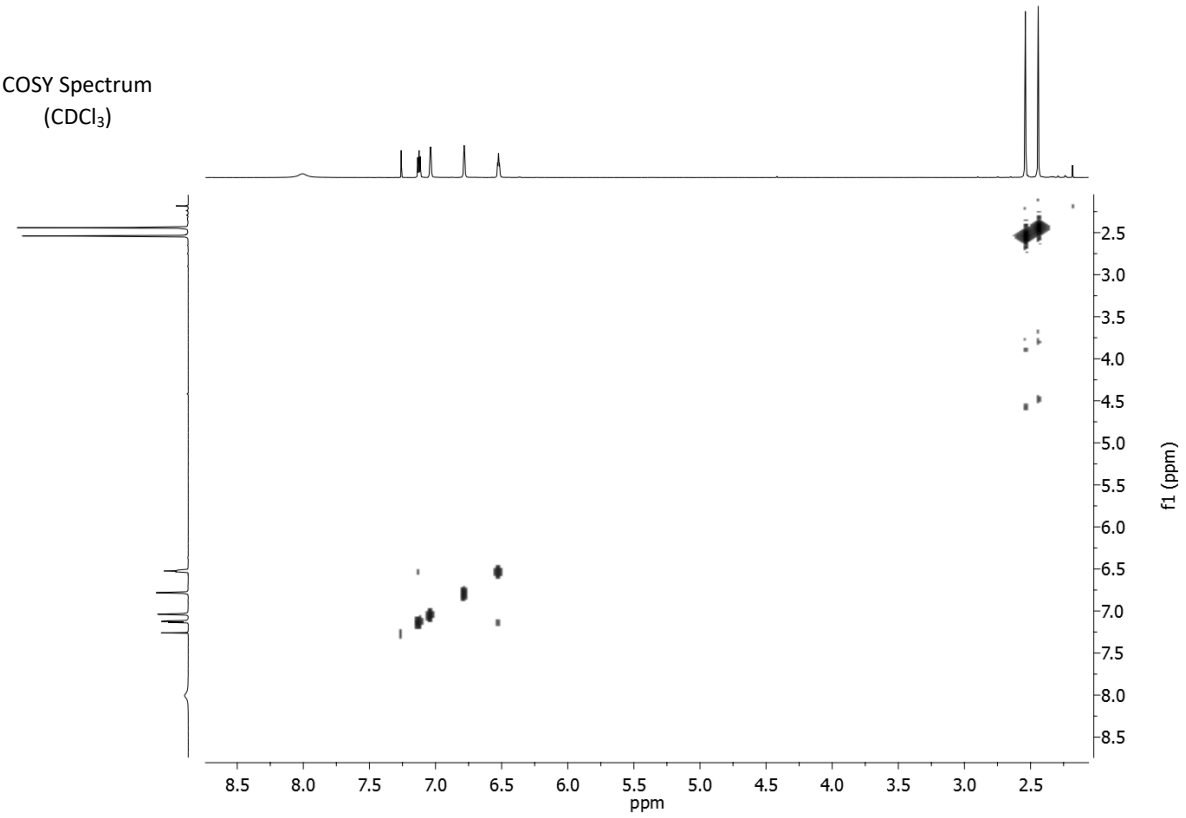

ed-HSQC Spectrum
($CDCl_3$)

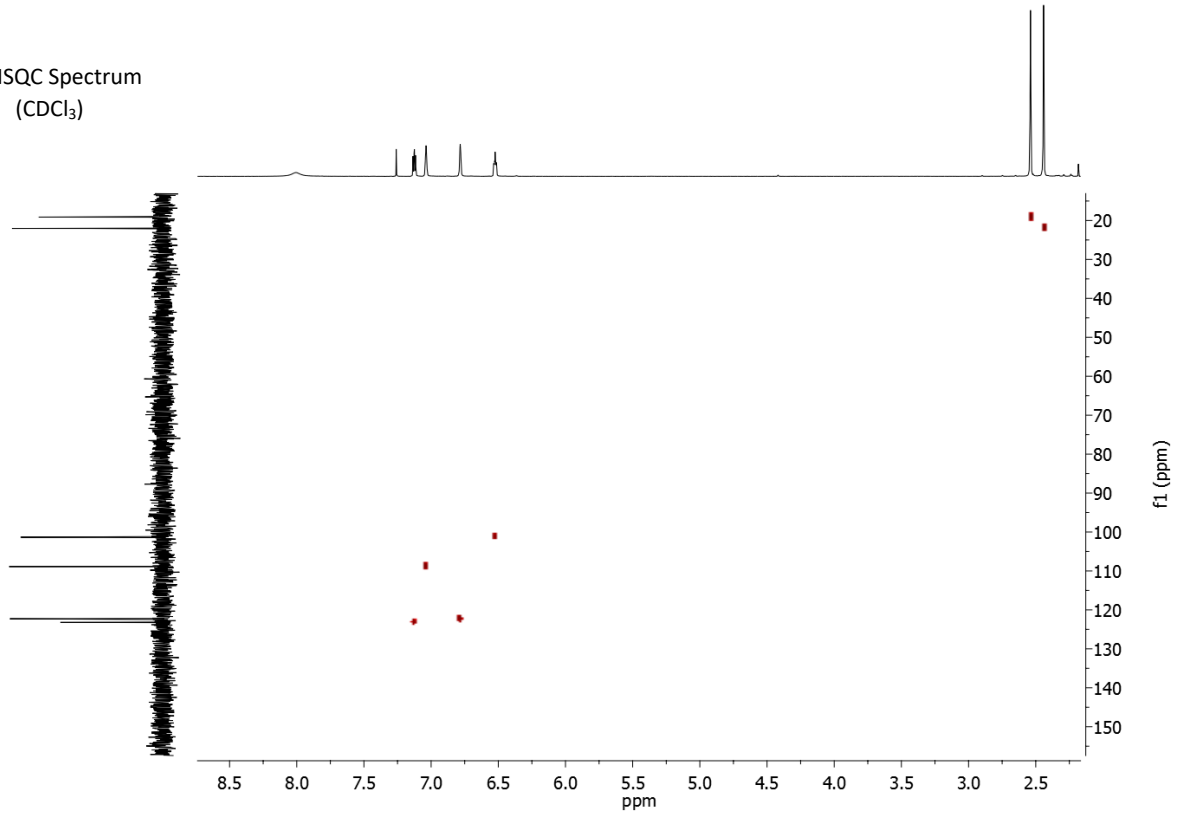

4,7-dimethylindole (3h)

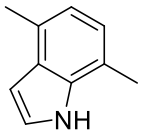

^{1}H NMR Spectrum
(300 MHz, $CDCl_3$)

^{13}C NMR Spectrum
(75 MHz, $CDCl_3$)

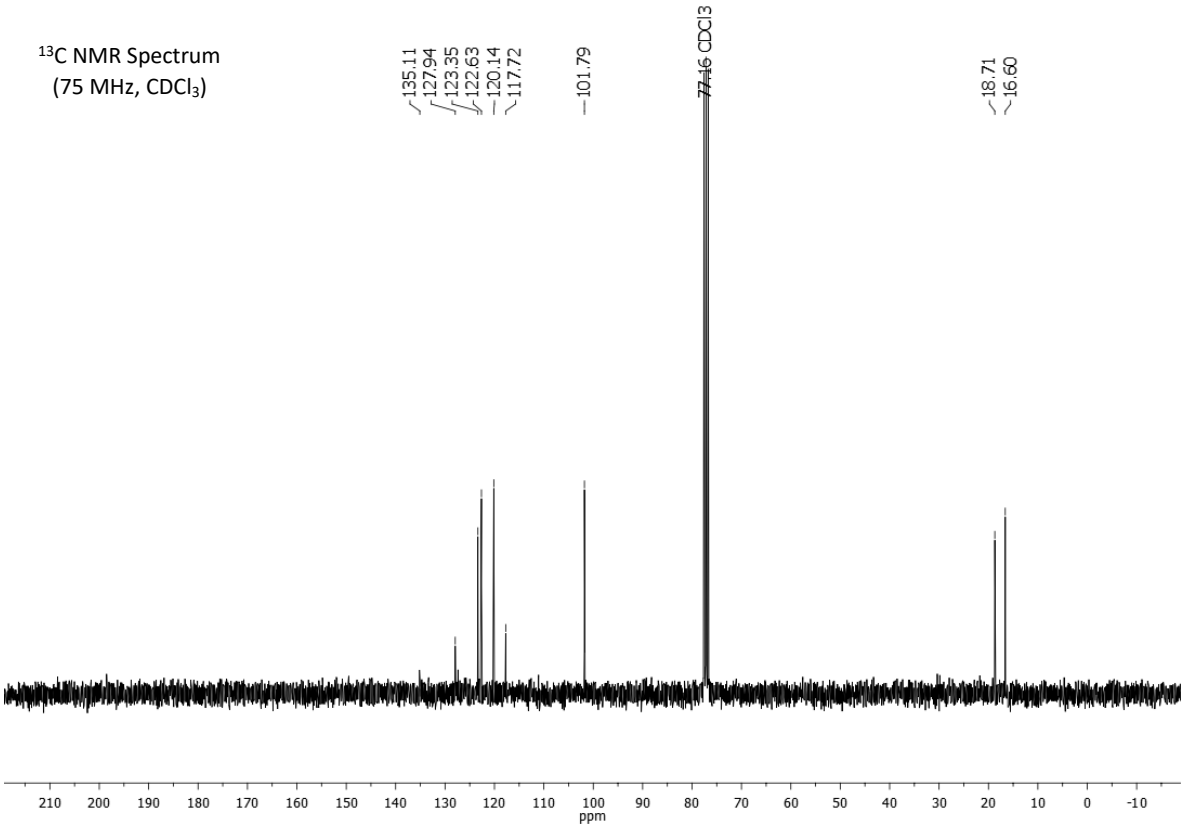

COSY Spectrum ($CDCl_3$)

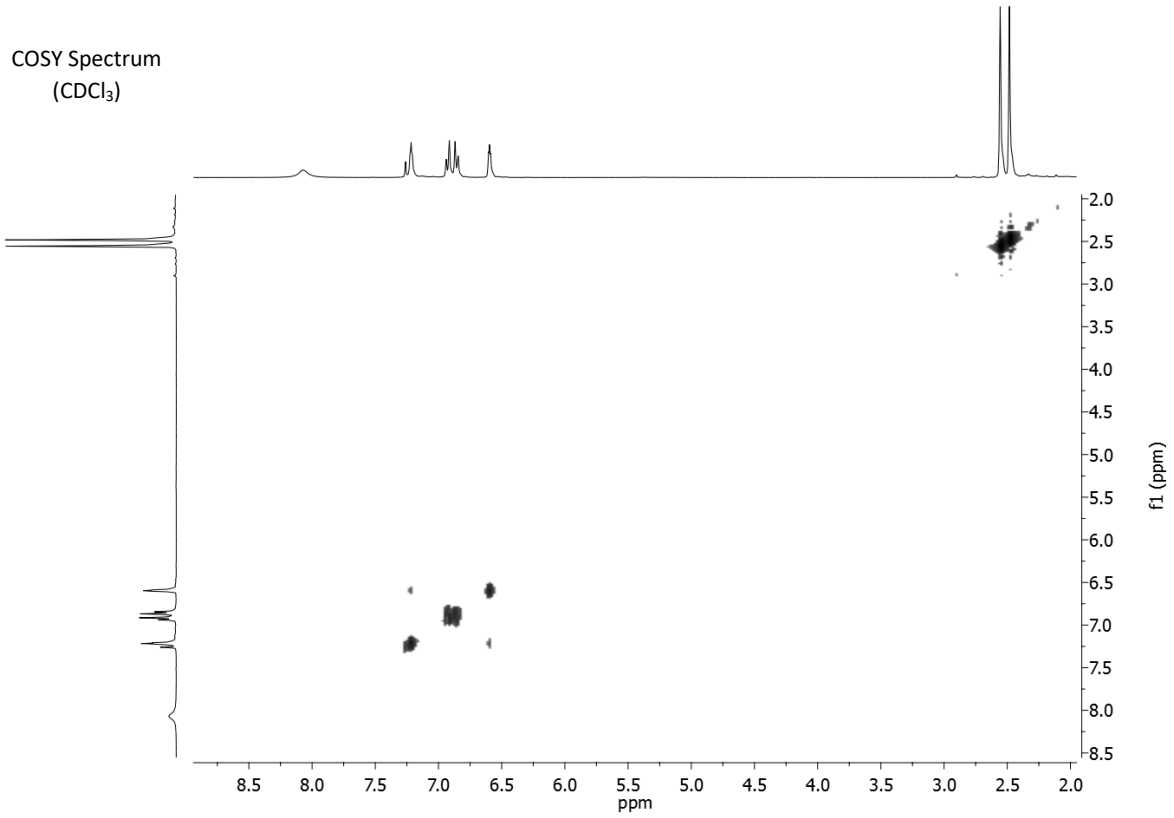

ed-HSQC Spectrum ($CDCl_3$)

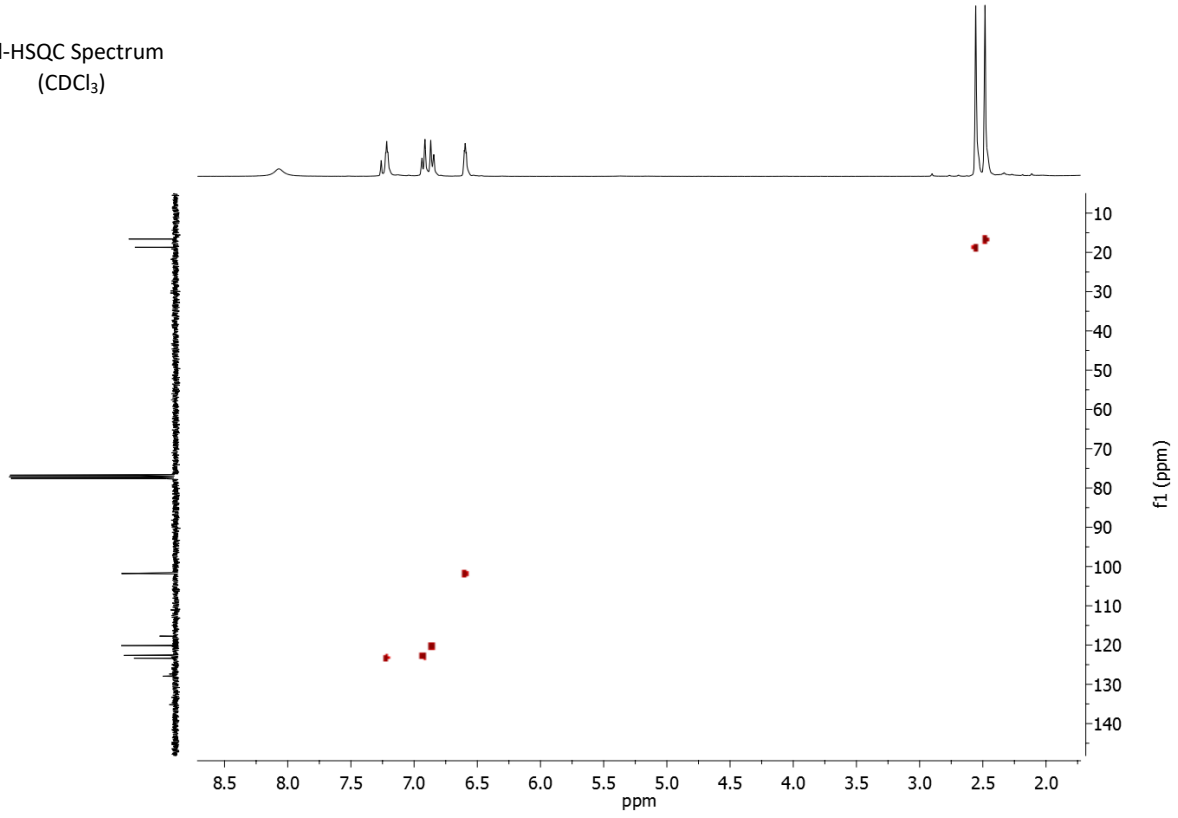

4,6-dimethoxyindole (3v)

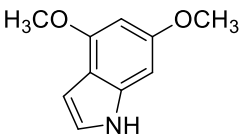

^{1}H NMR Spectrum
(300 MHz, $CDCl_3$)

^{13}C NMR Spectrum
(75 MHz, $CDCl_3$)

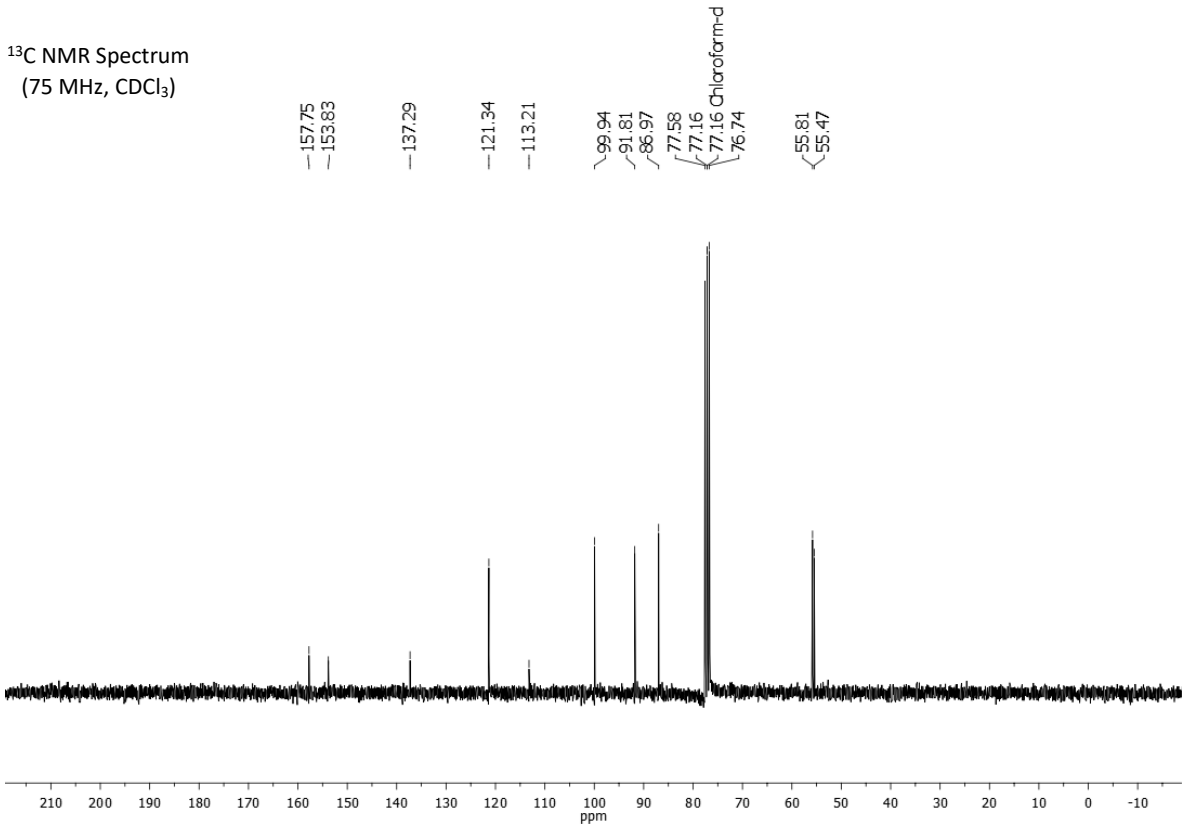

COSY Spectrum
($CDCl_3$)

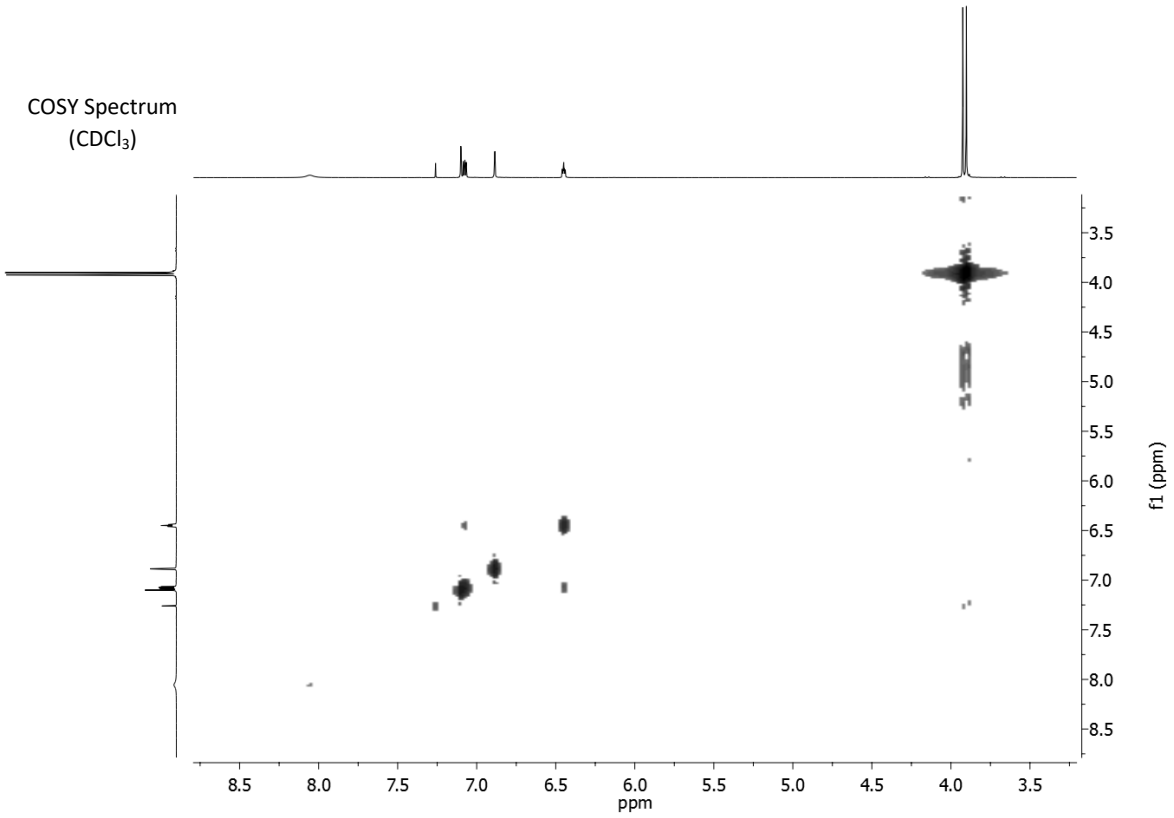

ed-HSQC Spectrum
($CDCl_3$)

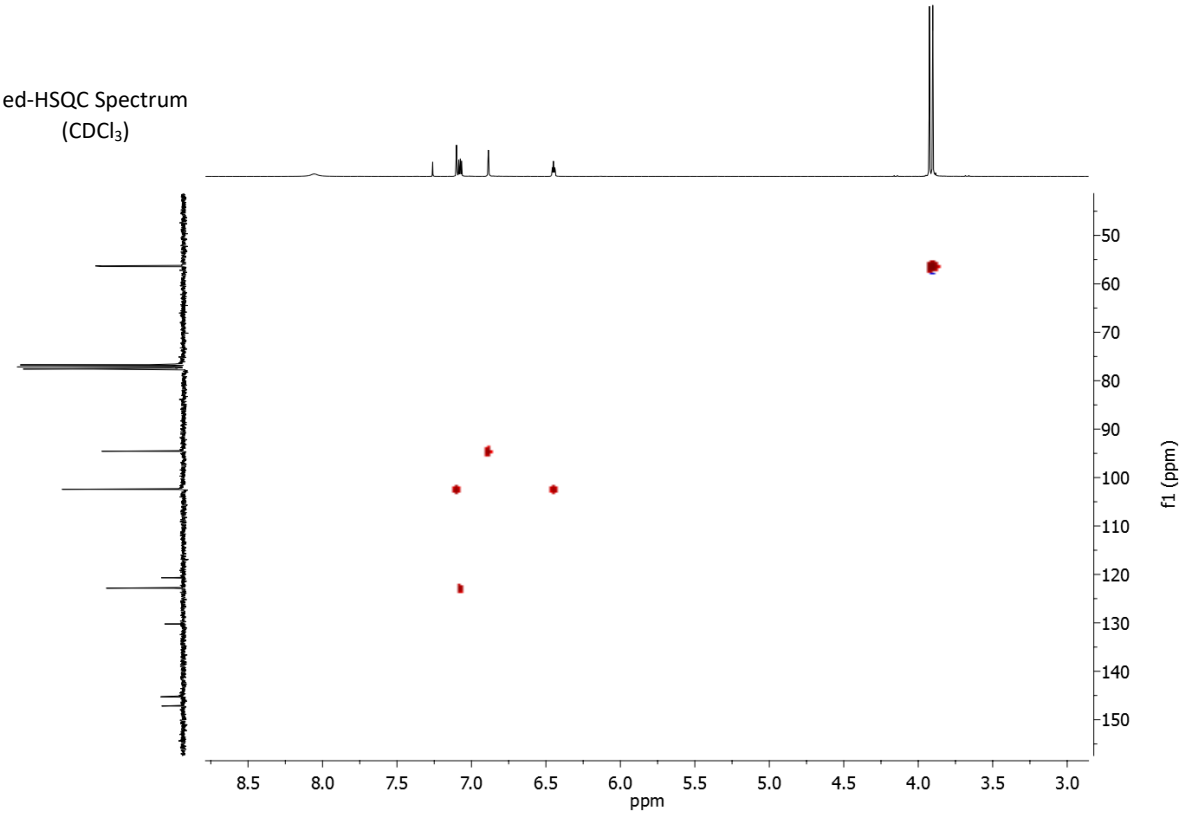

5,6-dimethoxyindole (3w)

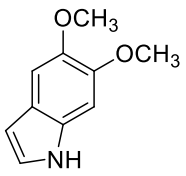

^{1}H NMR Spectrum
(300 MHz, $CDCl_3$)

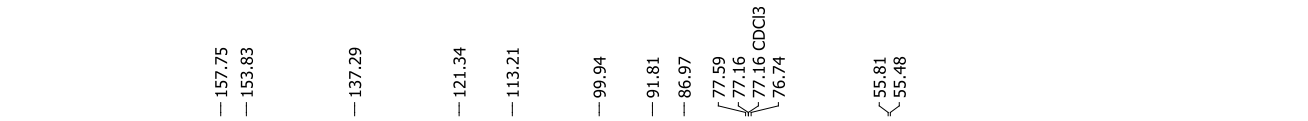

^{13}C NMR Spectrum
(75 MHz, $CDCl_3$)

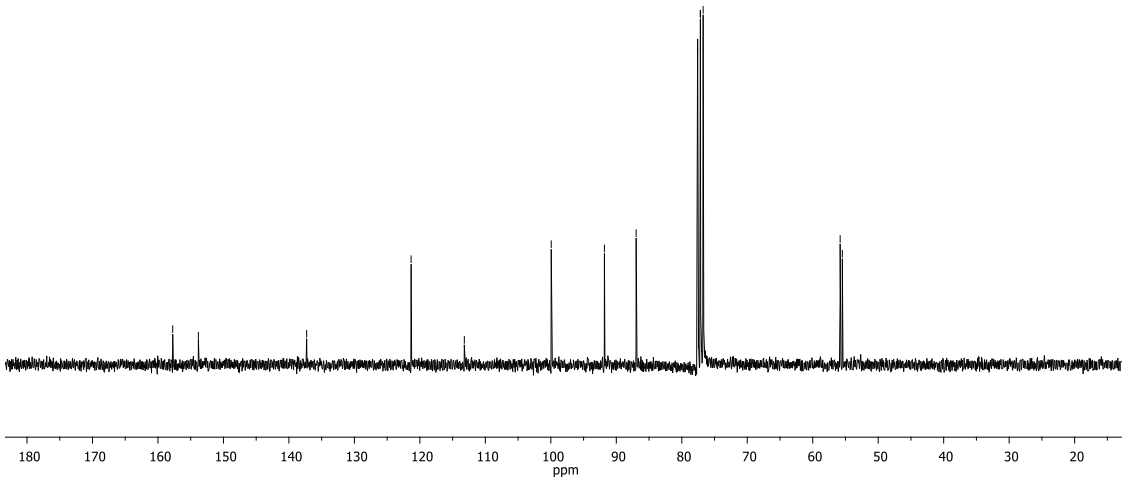

COSY Spectrum
($CDCl_3$)

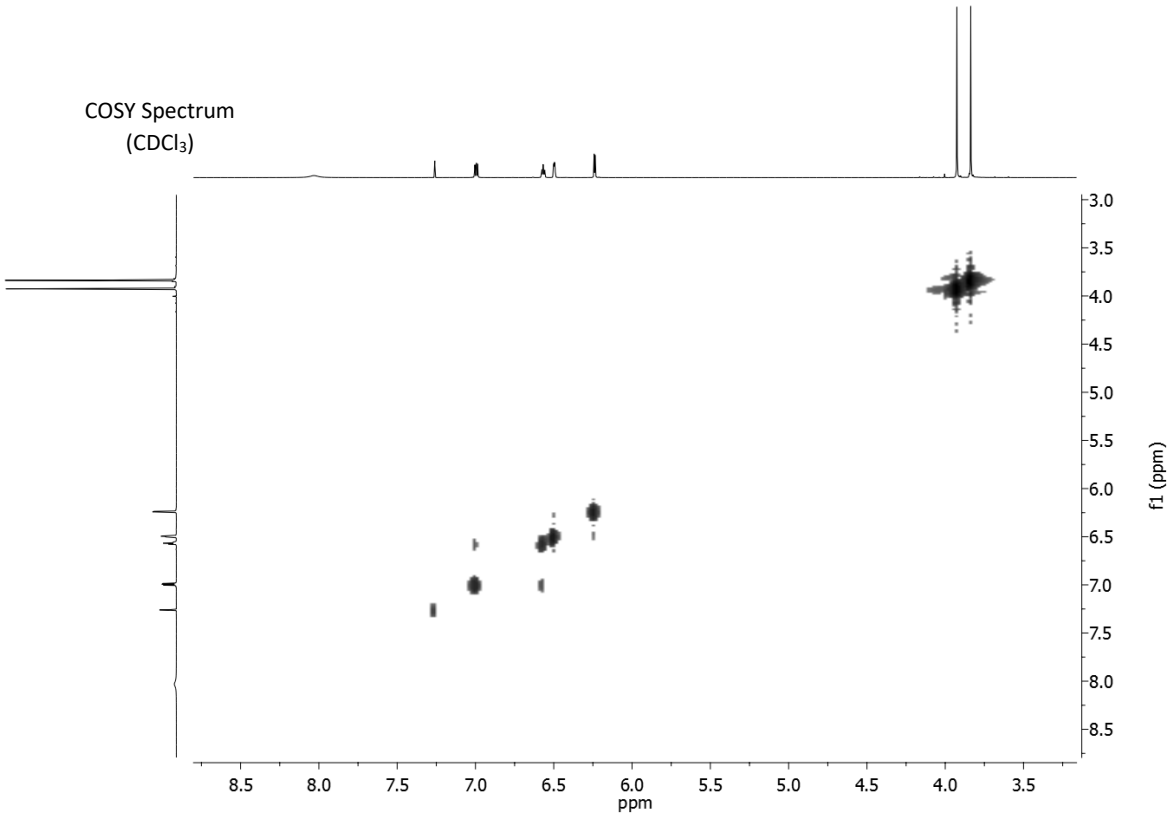

ed-HSQC Spectrum
($CDCl_3$)

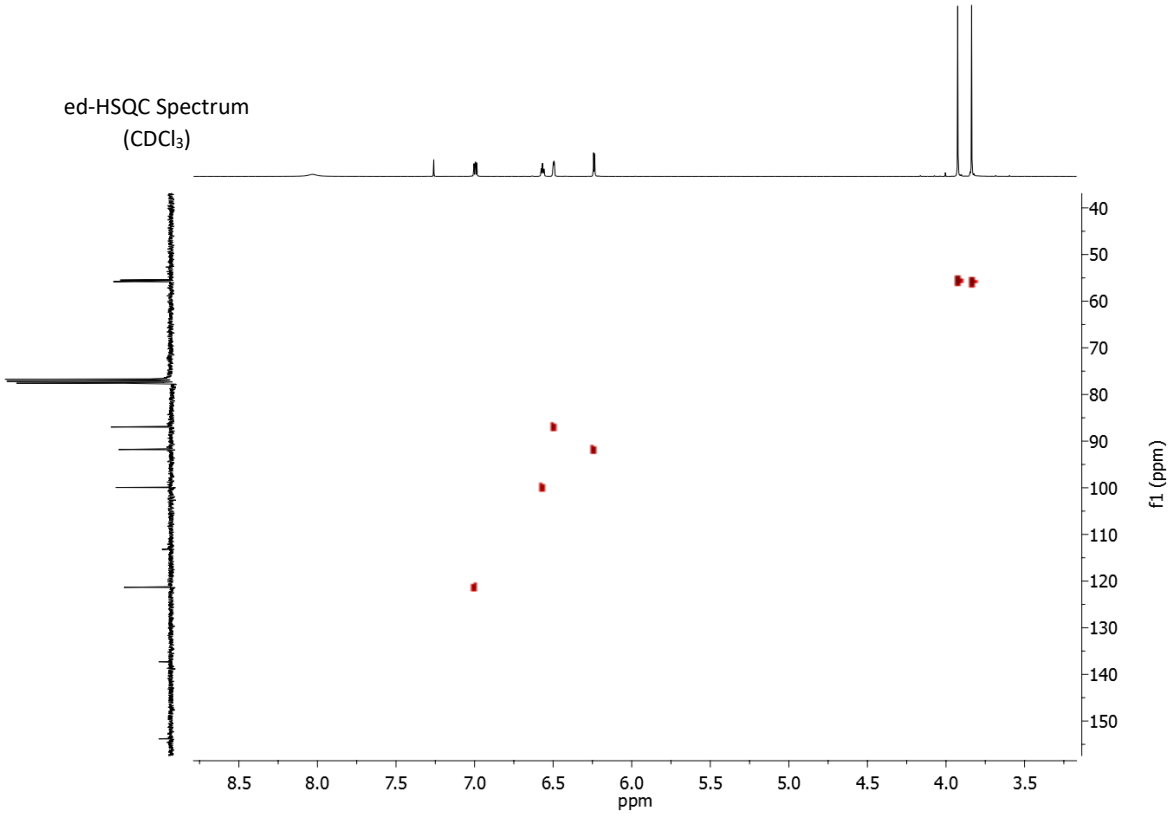

N,N'-bis(4-methylphenyl)-1,2-ethanediamine (4a)

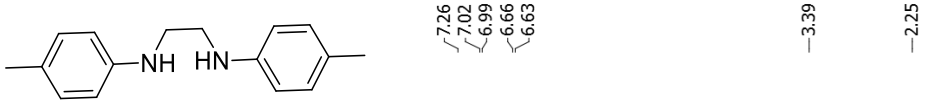

^{1}H NMR Spectrum
(300 MHz, $CDCl_3$)

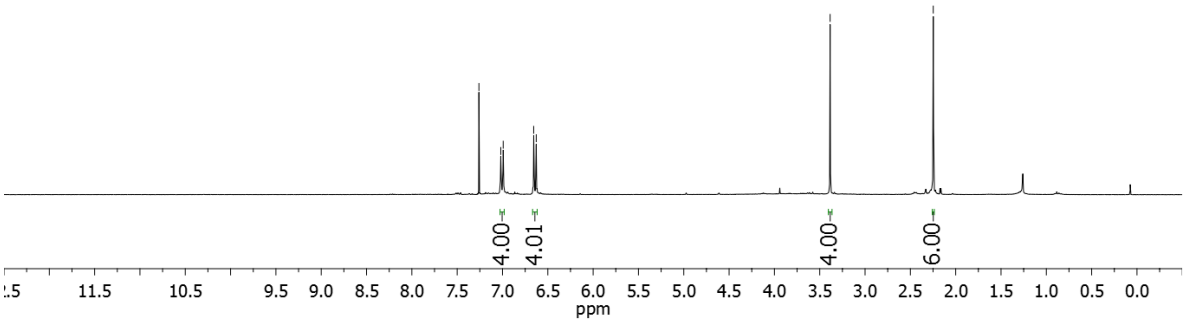

^{13}C NMR Spectrum
(75 MHz, $CDCl_3$)

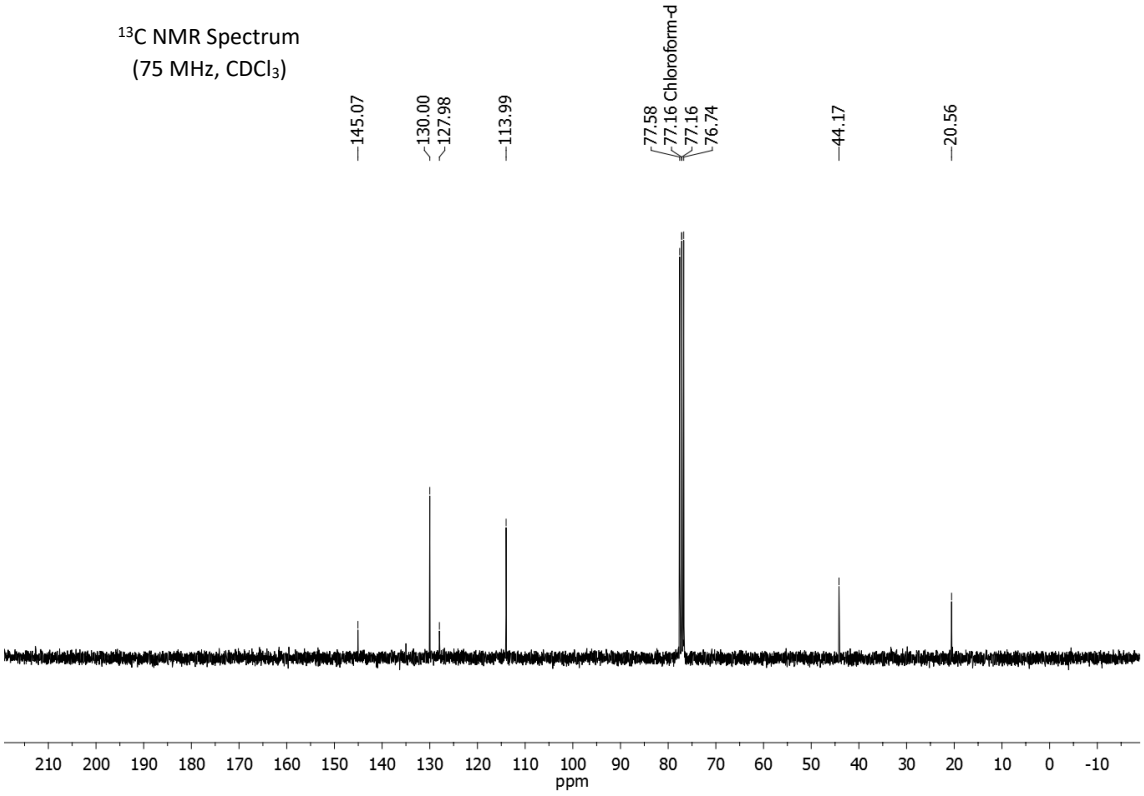

COSY Spectrum ($CDCl_3$)

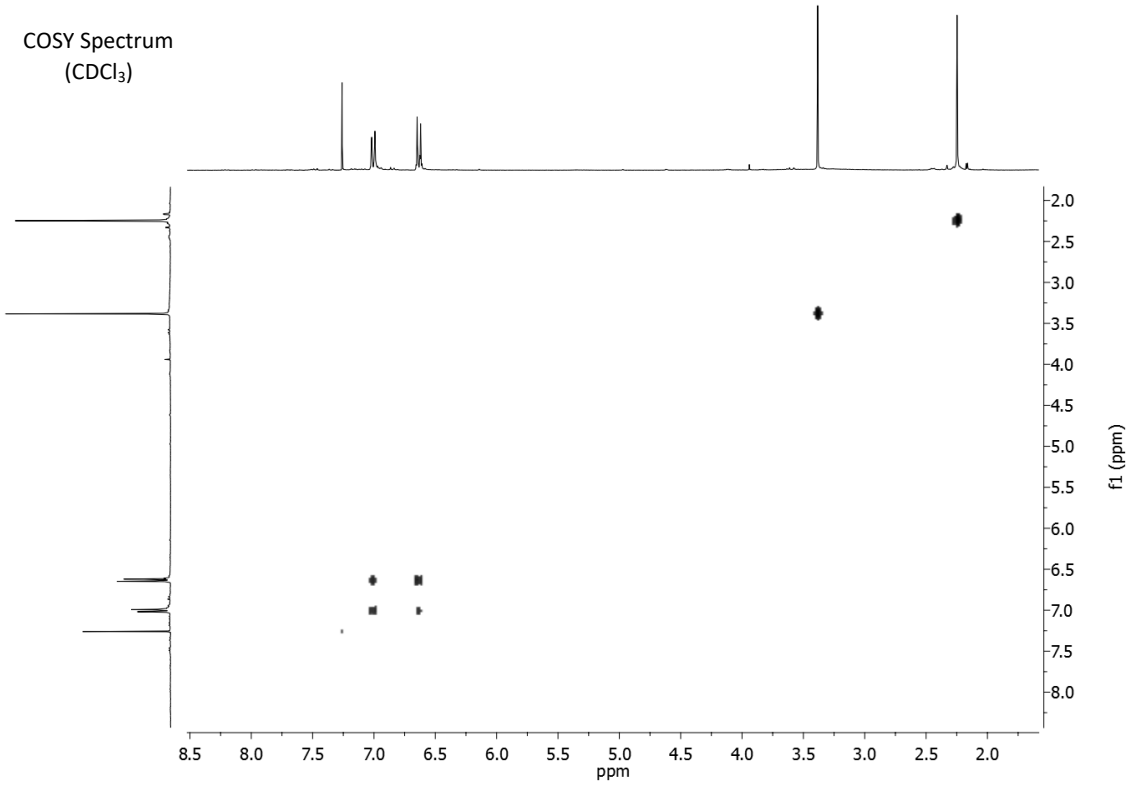

ed-HSQC Spectrum ($CDCl_3$)

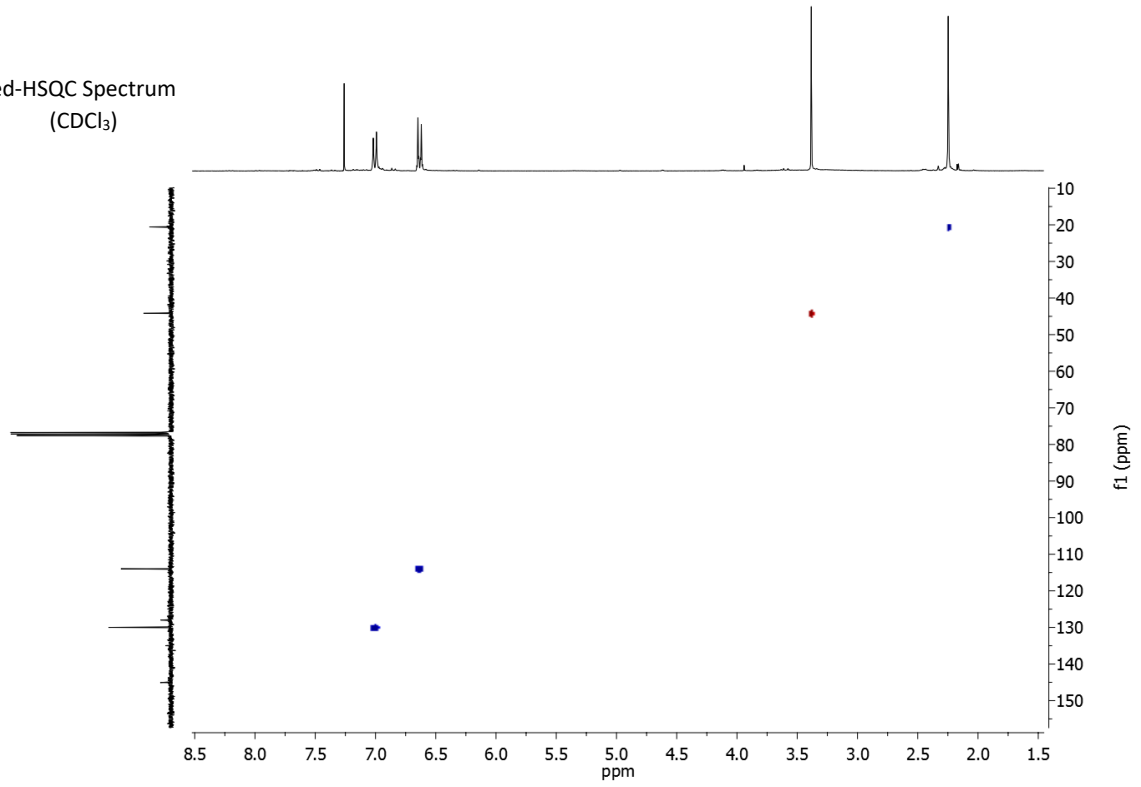

N,N'-bis(2-methylphenyl)-1,2-ethanediamine (4c)

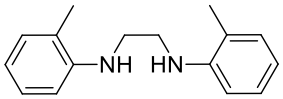

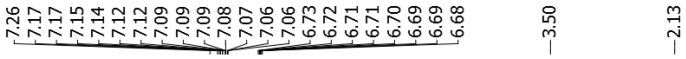

^{1}H NMR Spectrum
(300 MHz, $CDCl_3$)

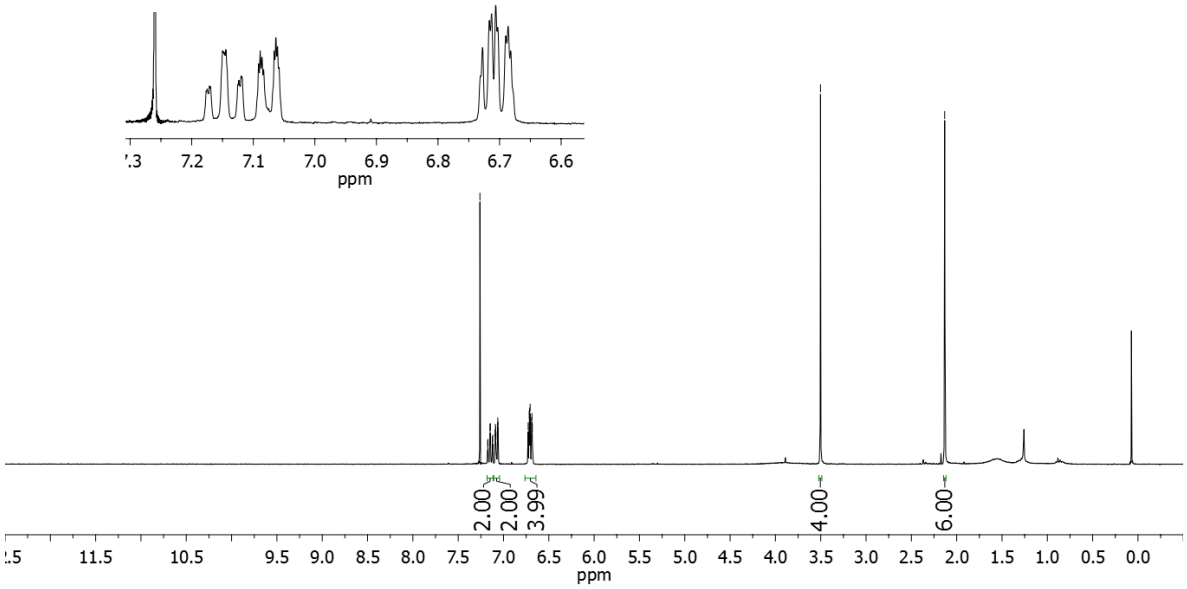

^{13}C NMR Spectrum
(75 MHz, $CDCl_3$)

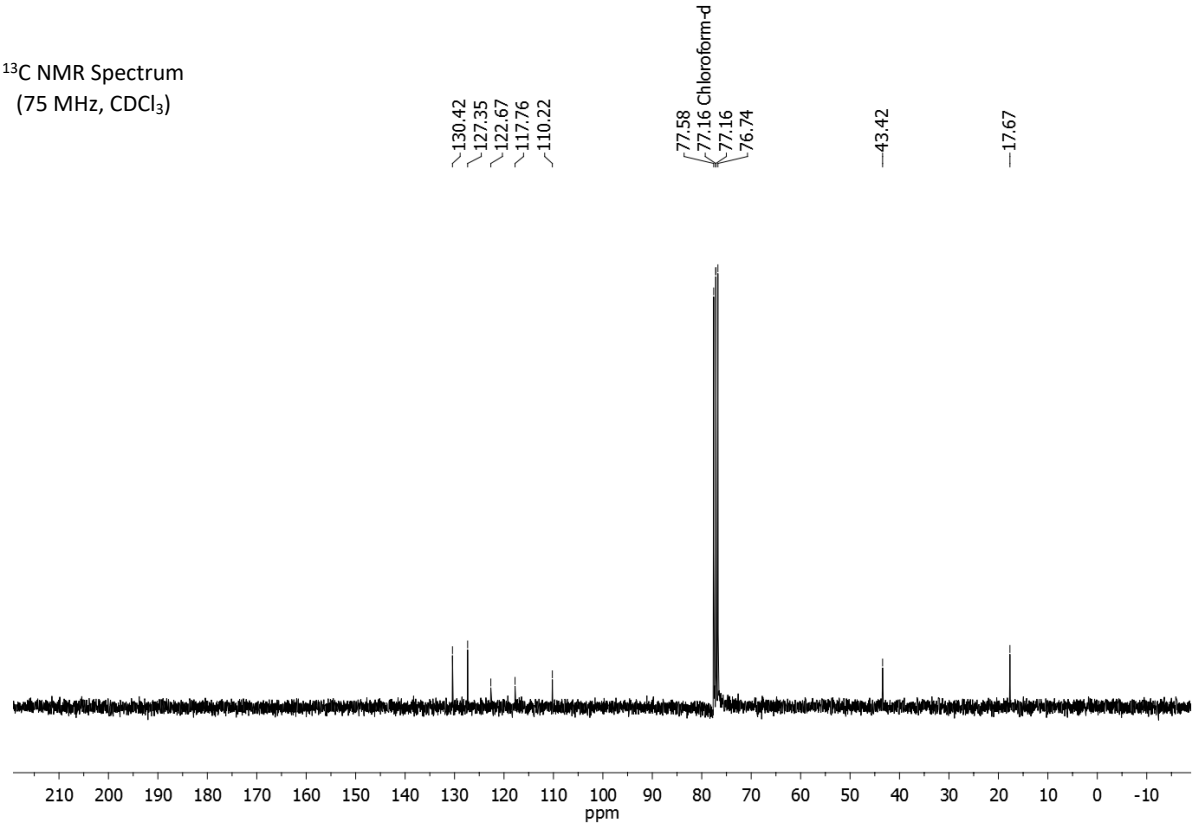

COSY Spectrum
($CDCl_3$)

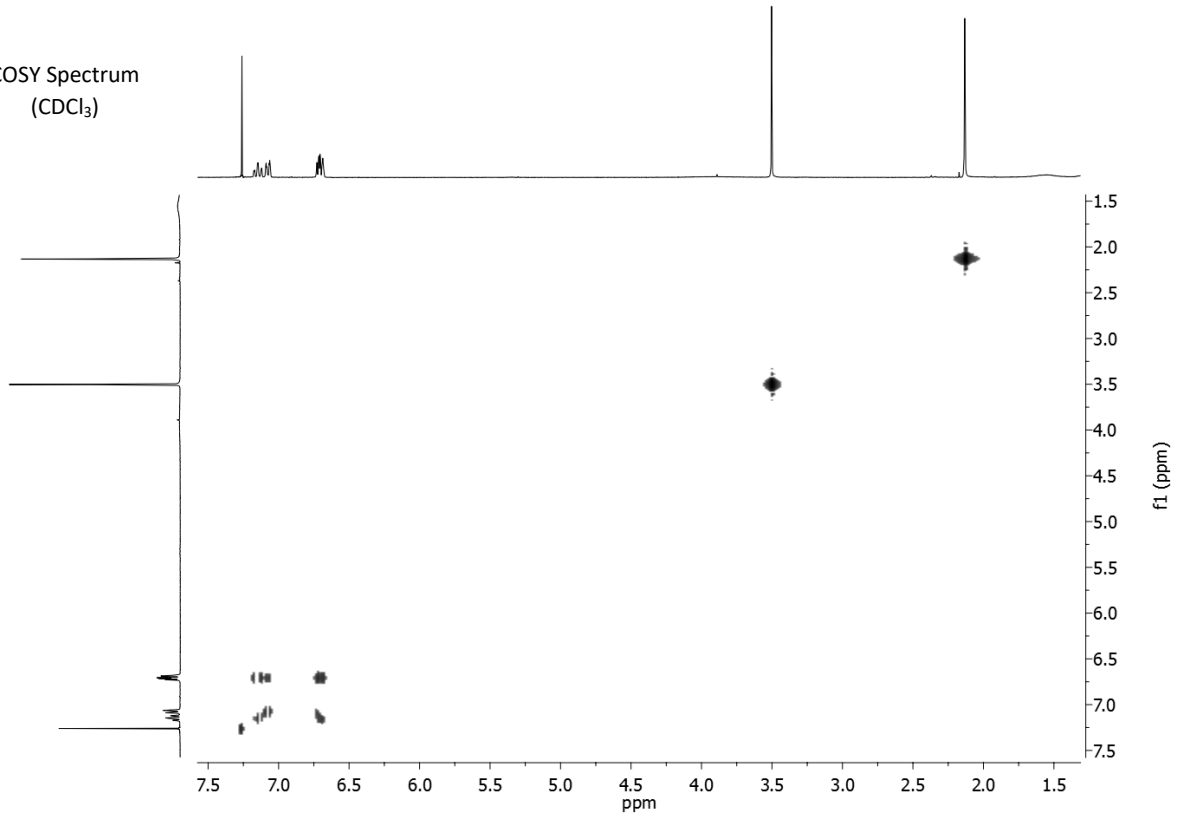

ed-HSQC Spectrum
($CDCl_3$)

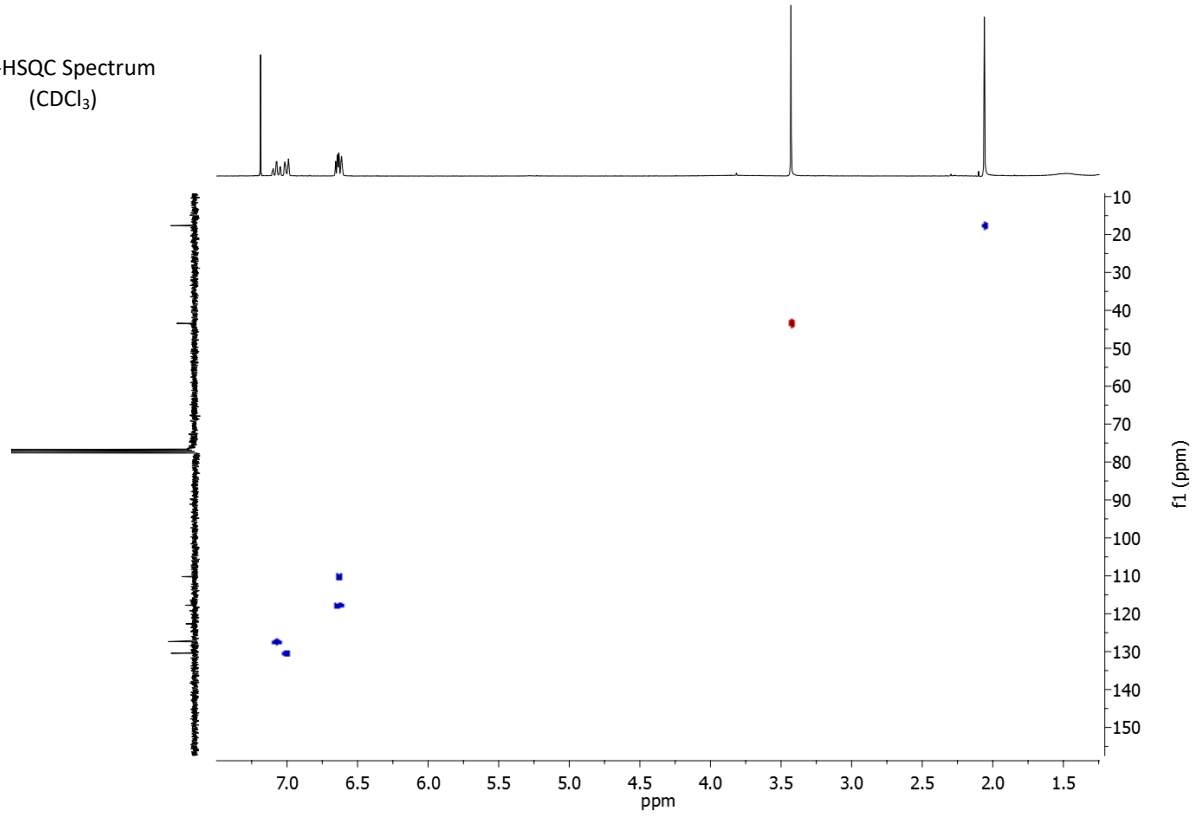

N,N'-bis(2,4-dimethylphenyl)-1,2-ethanediamine (4e)

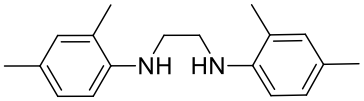

^{1}H NMR Spectrum
(300 MHz, $CDCl_3$)

^{13}C NMR Spectrum
(75 MHz, $CDCl_3$)

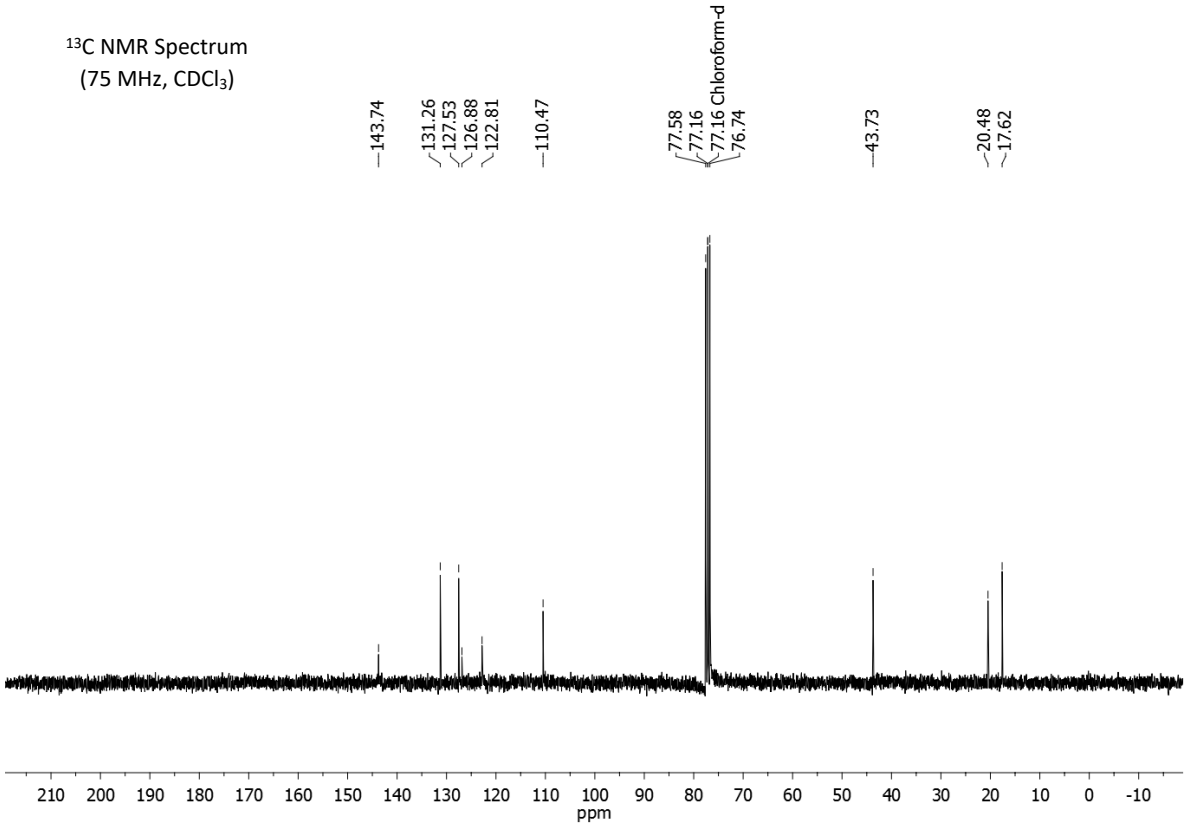

COSY Spectrum
($CDCl_3$)

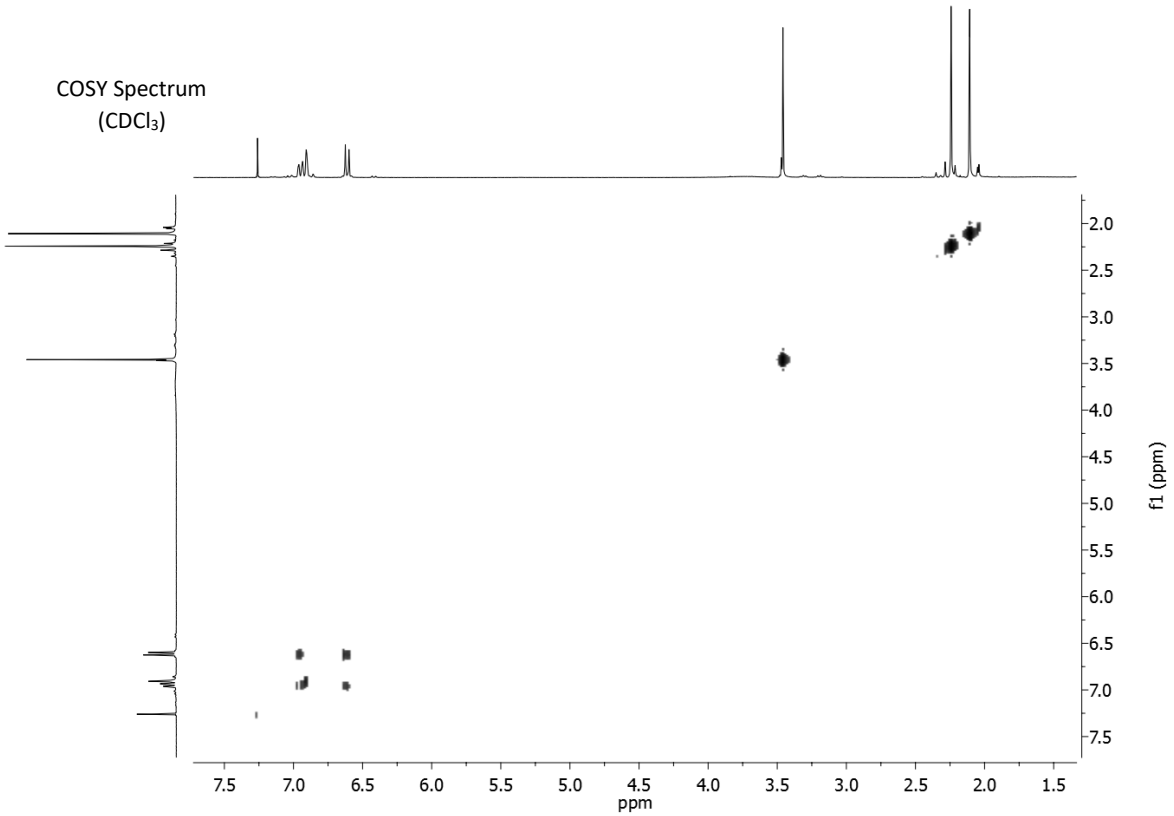

ed-HSQC Spectrum
($CDCl_3$)

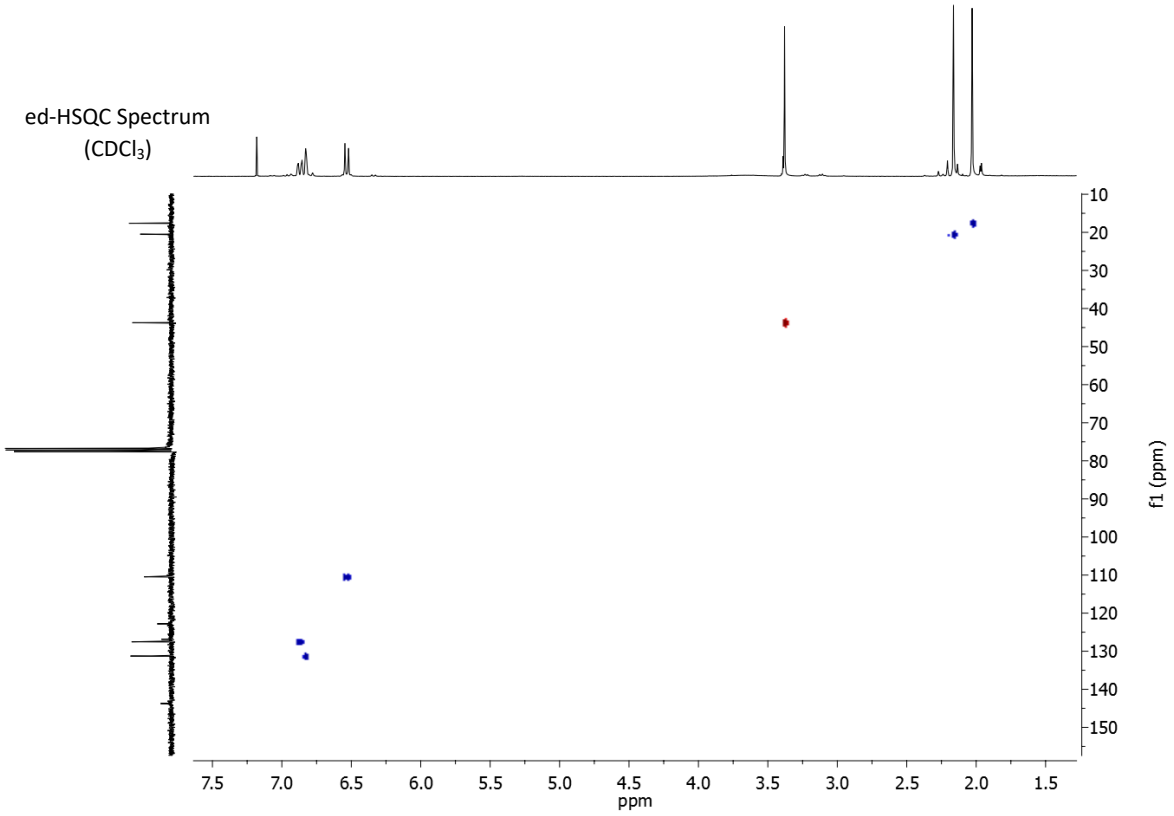

N,N'-bis(3,5-dimethylphenyl)-1,2-ethanediamine (4g)

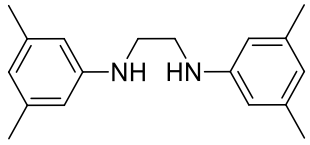

^{1}H NMR Spectrum
(300 MHz, $CDCl_3$)

^{13}C NMR Spectrum
(75 MHz, $CDCl_3$)

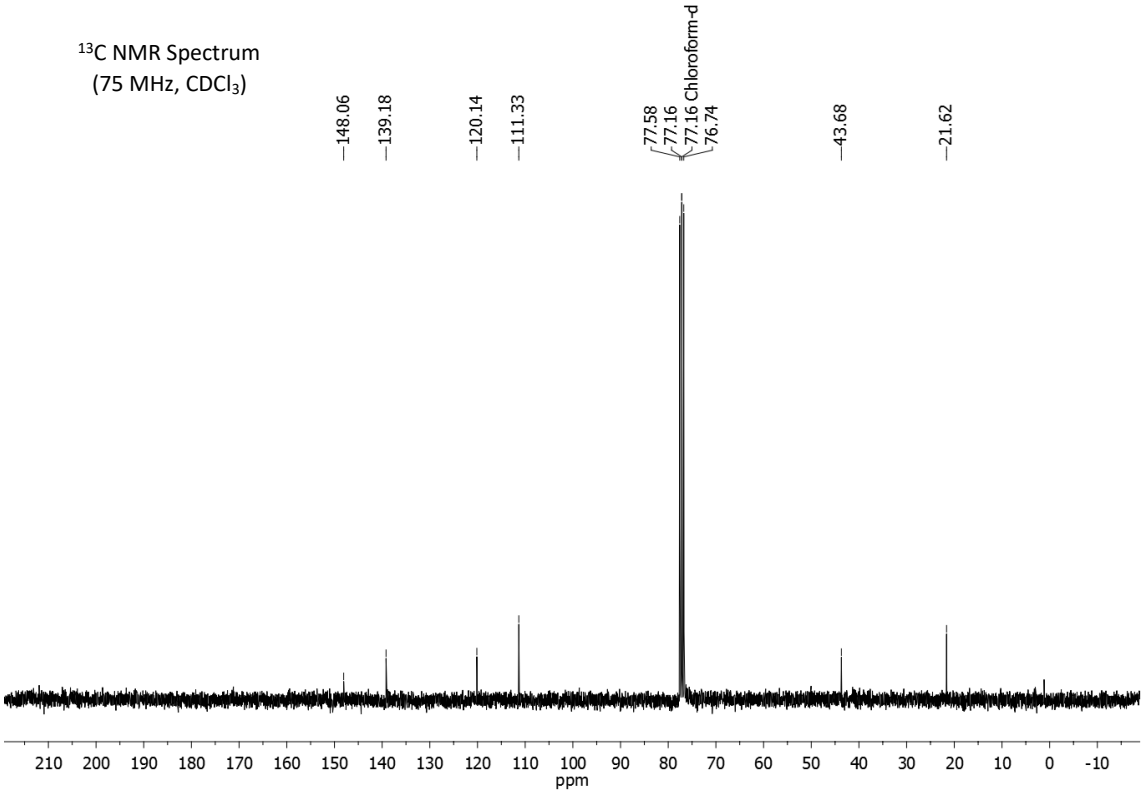

COSY Spectrum
($CDCl_3$)

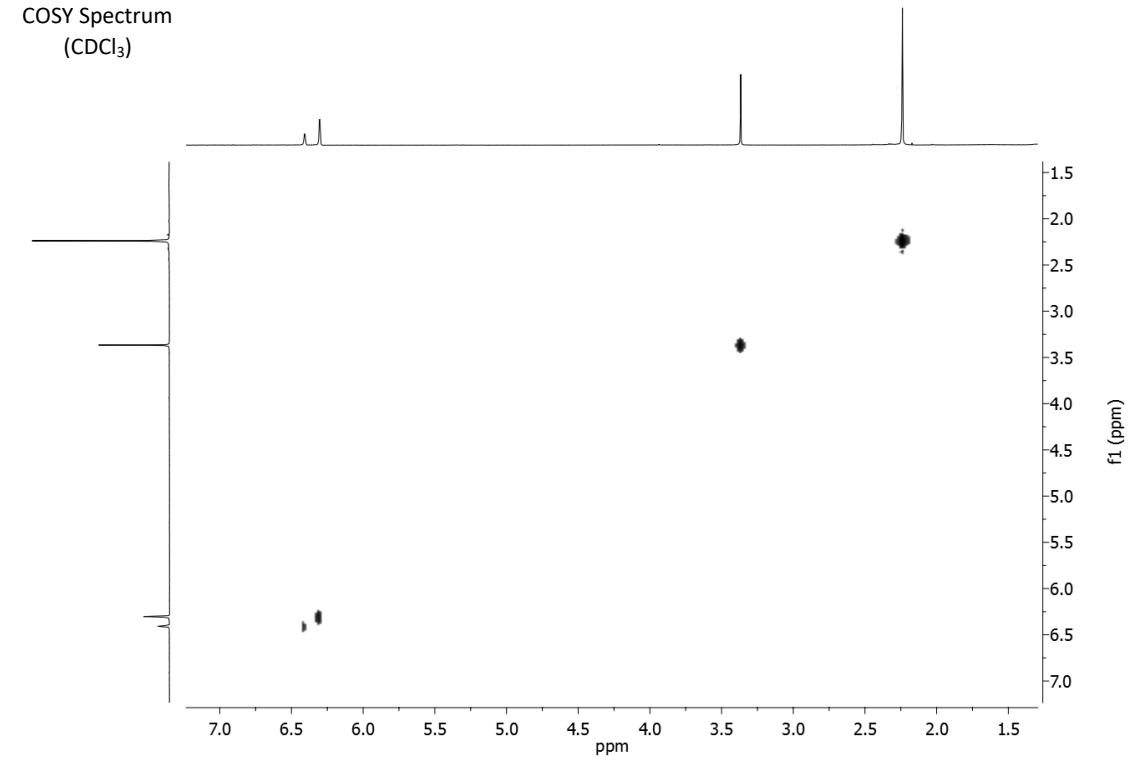

ed-HSQC Spectrum
($CDCl_3$)

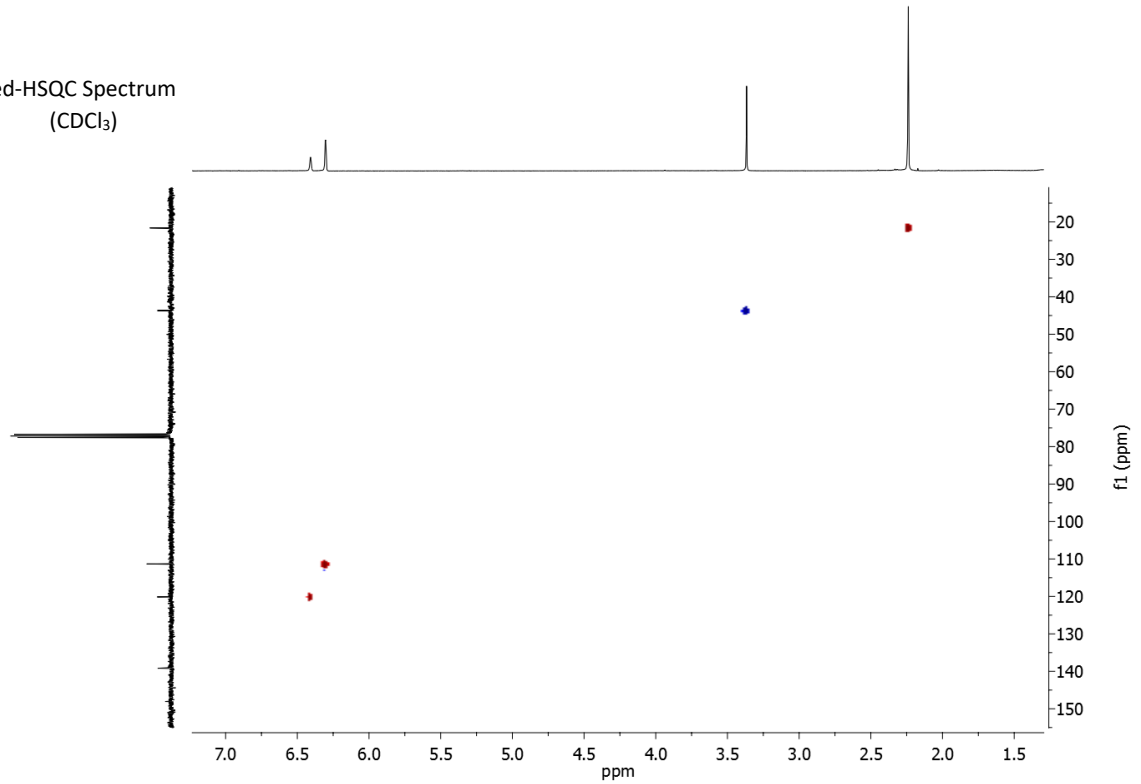

N,N'-bis(3-fluorophenyl)-1,2-ethanediamine (4o)

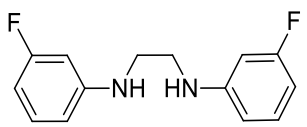

^{1}H NMR Spectrum
(300 MHz, $CDCl_3$)

^{13}C NMR Spectrum
(75 MHz, $CDCl_3$)

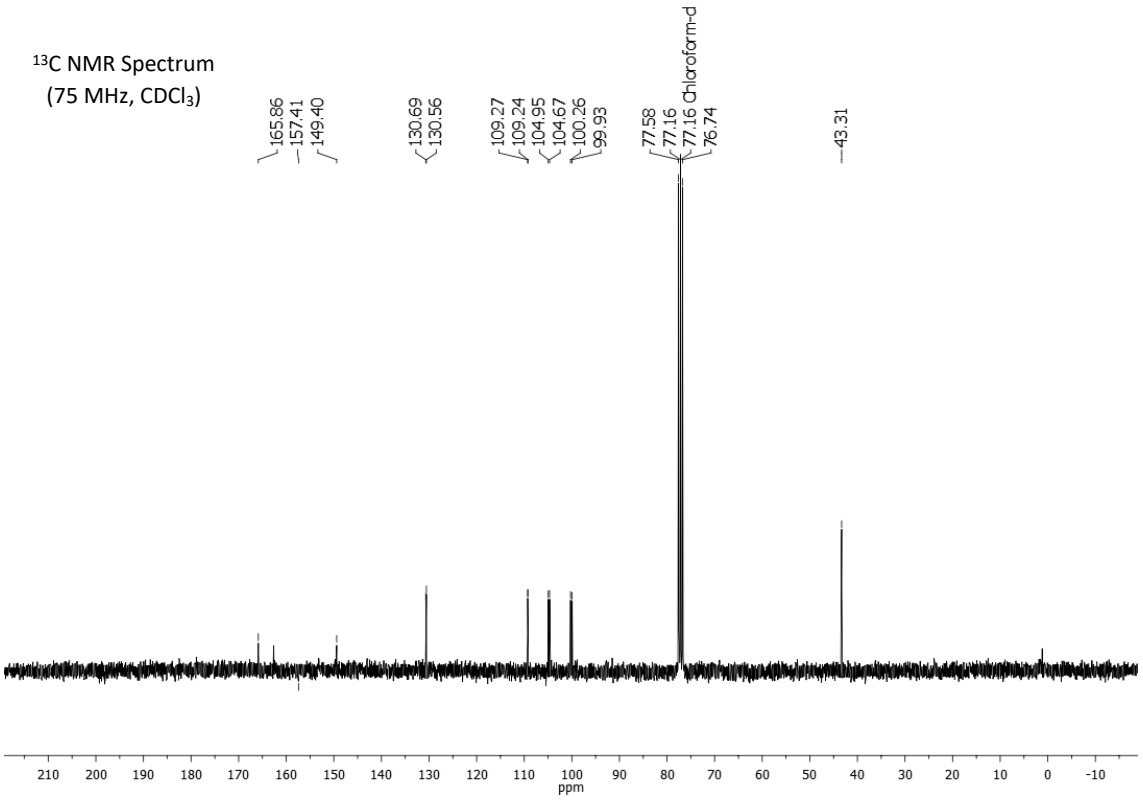

COSY Spectrum
($CDCl_3$)

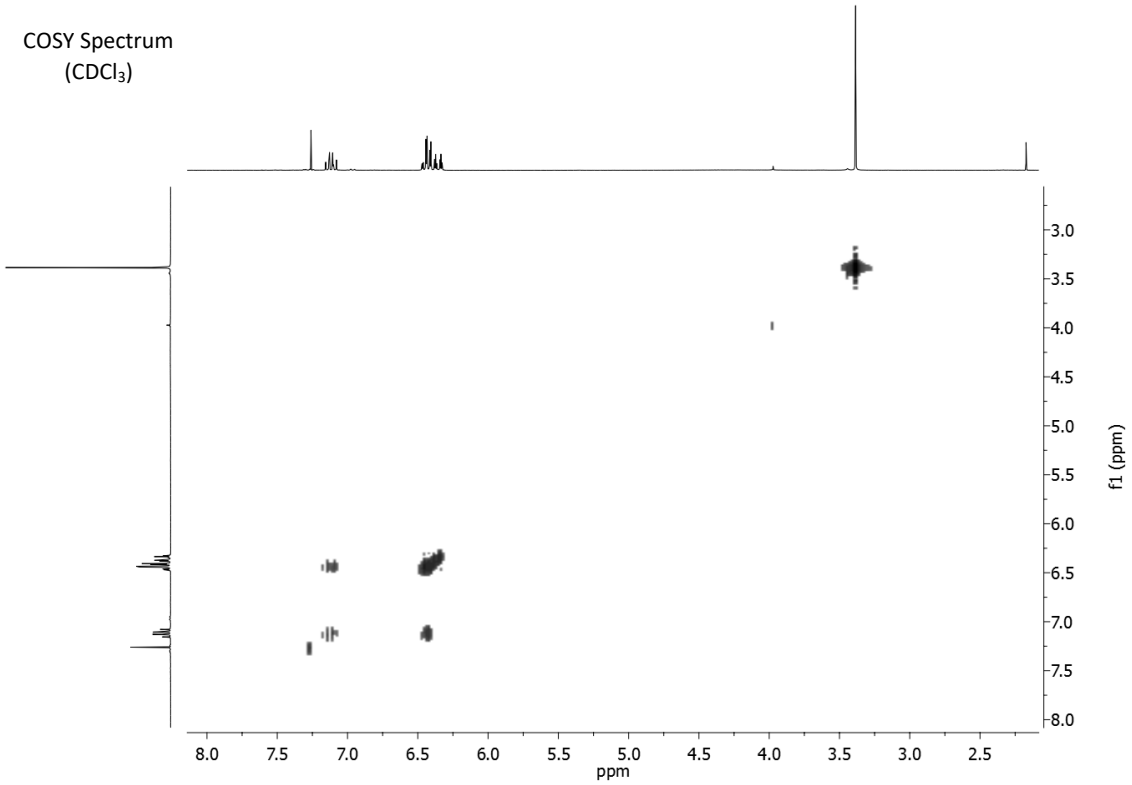

ed-HSQC Spectrum
($CDCl_3$)

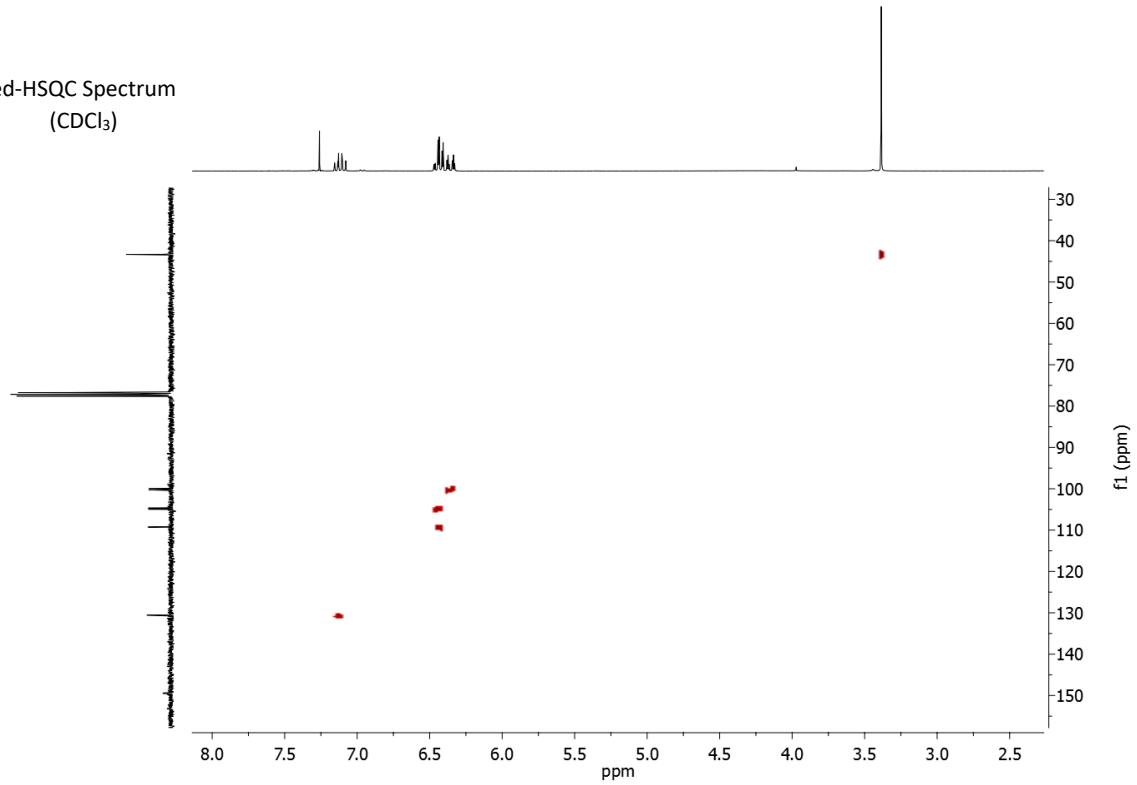

N,N'-bis(2-trifluoromethoxyphenyl)-1,2-ethanediamine (4s)

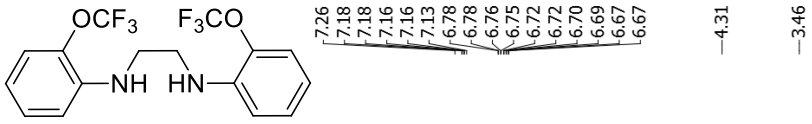

^{1}H NMR Spectrum
(300 MHz, $CDCl_3$)

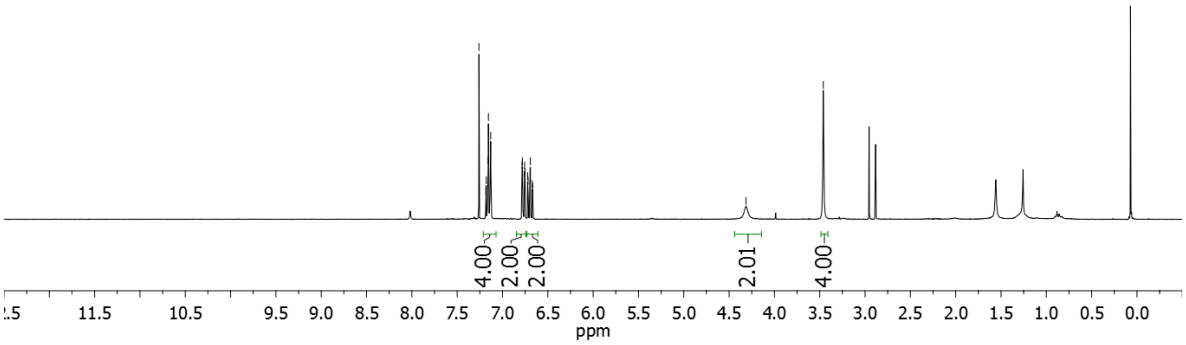

^{13}C NMR Spectrum
(75 MHz, $CDCl_3$)

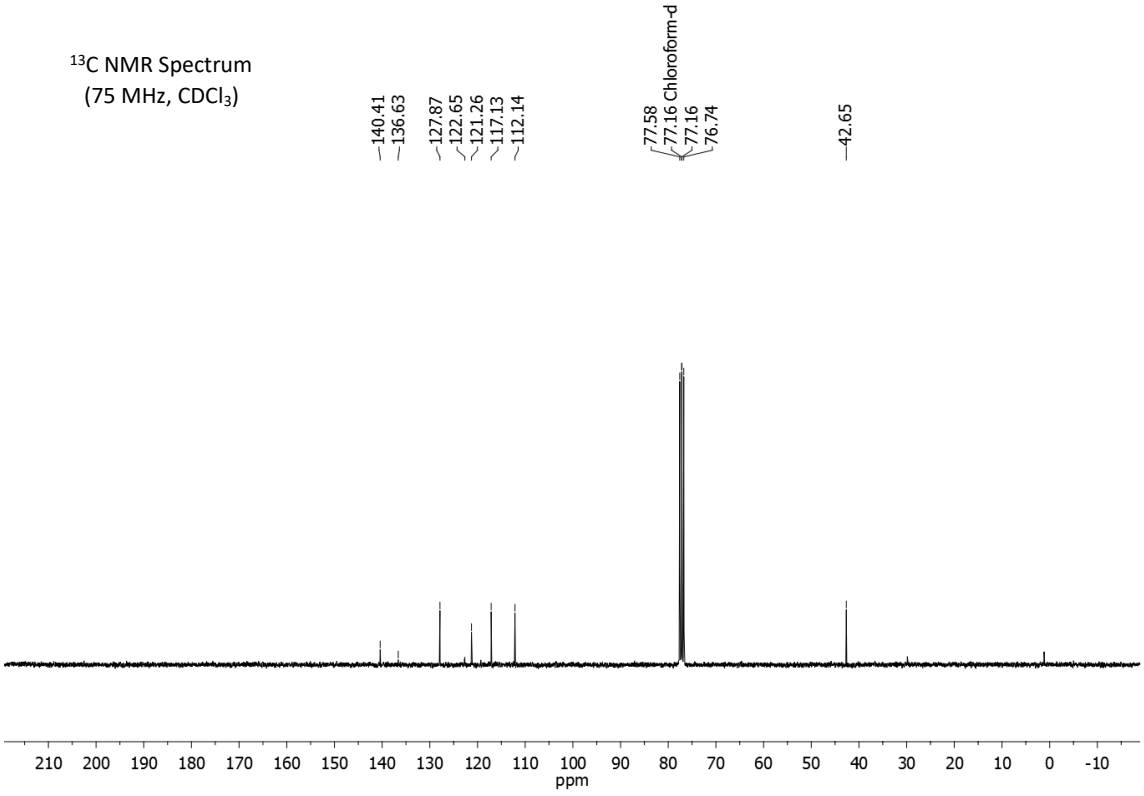

COSY Spectrum ($CDCl_3$)

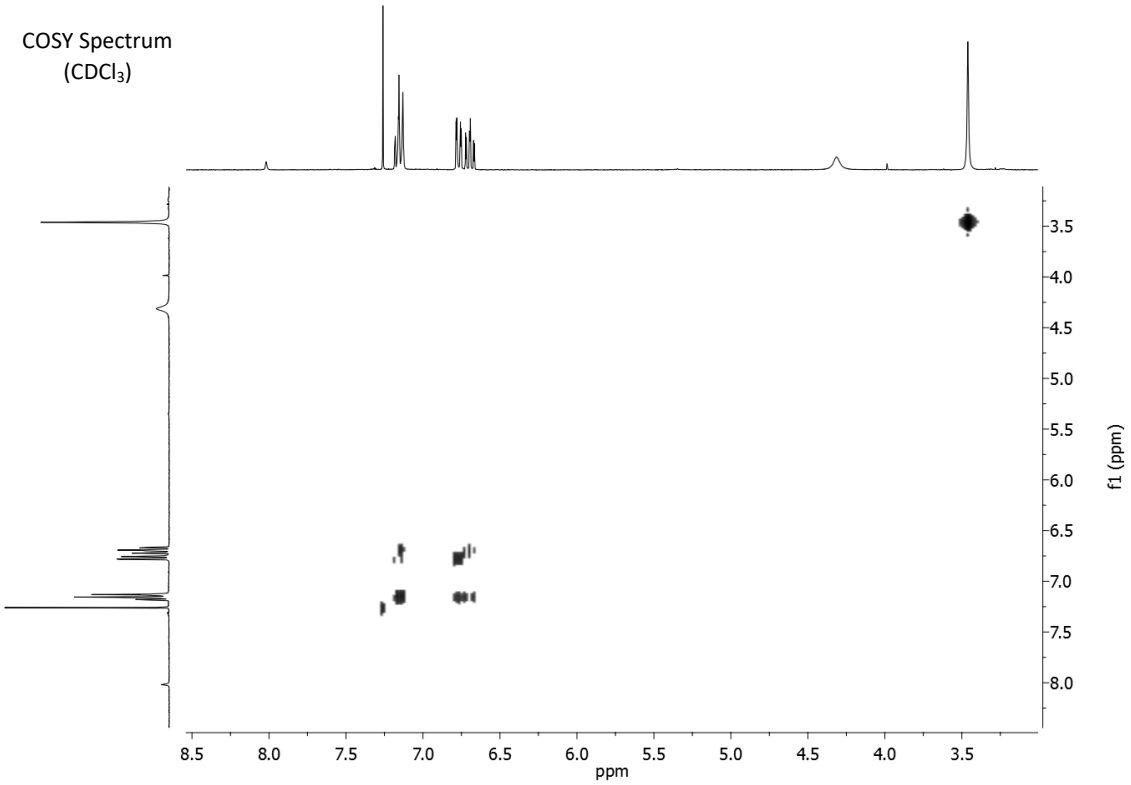

ed-HSQC Spectrum ($CDCl_3$)

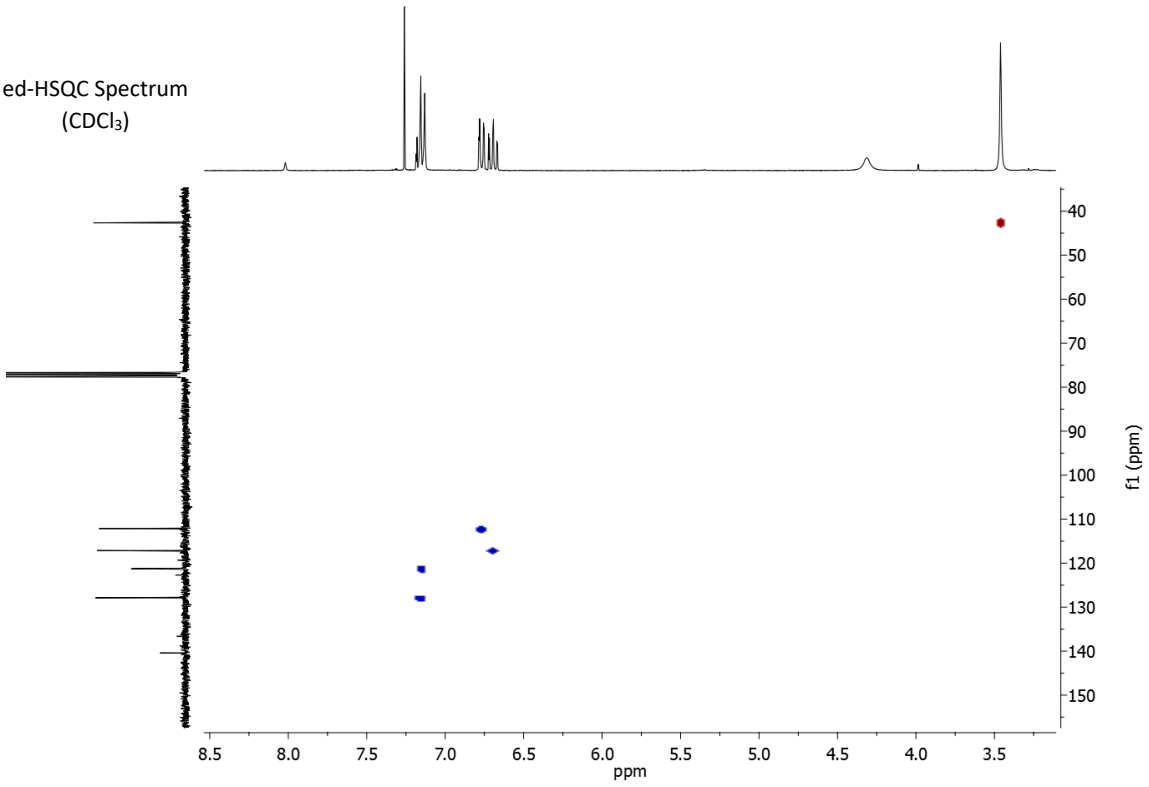

1,4-bis(4-methylphenyl)-piperazine (5a)

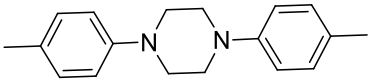

^{1}H NMR Spectrum
(300 MHz, $CDCl_3$)

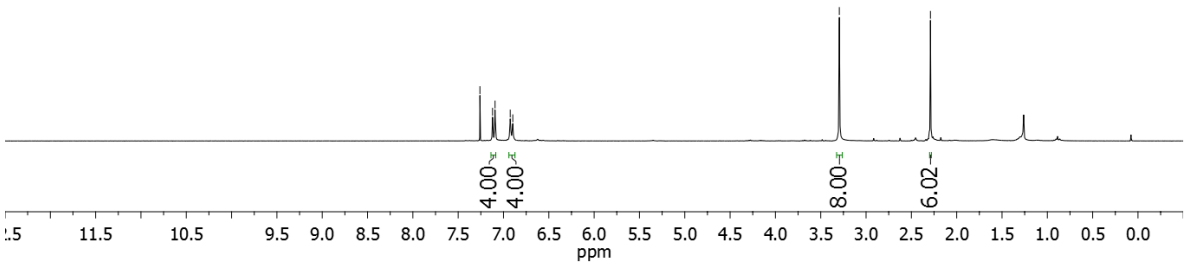

^{13}C NMR Spectrum
(75 MHz, $CDCl_3$)

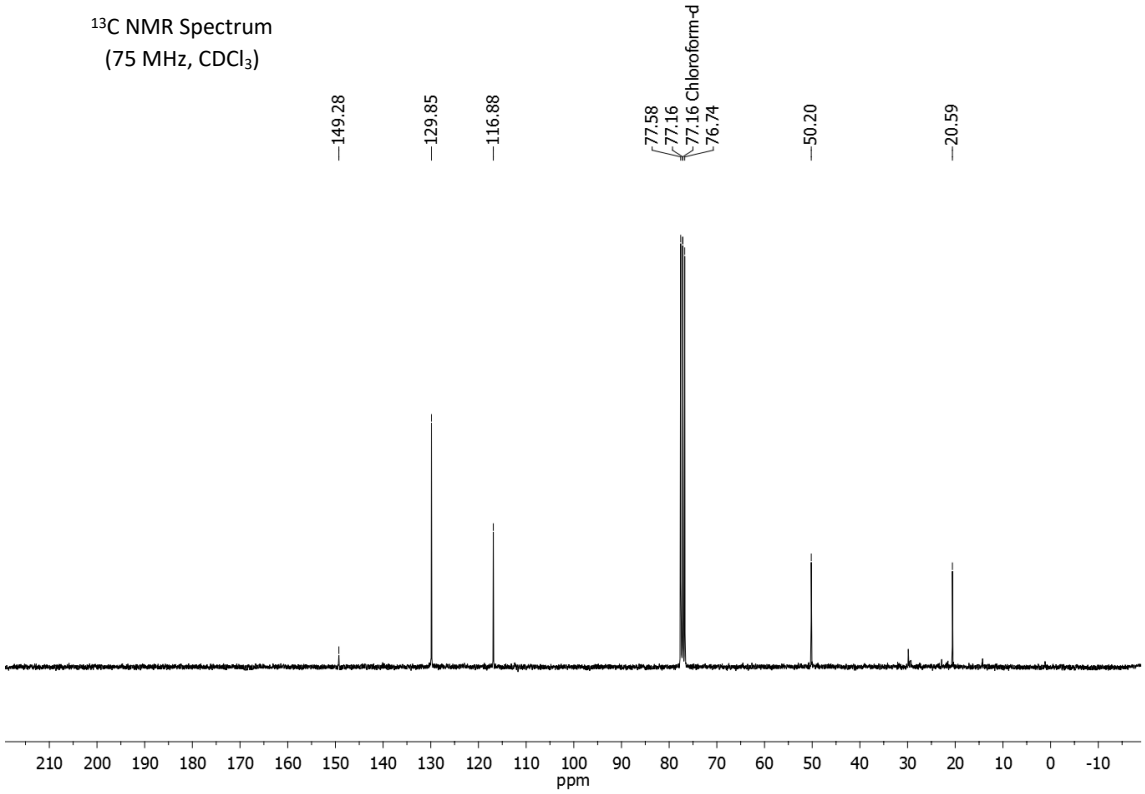

COSY Spectrum
($CDCl_3$)

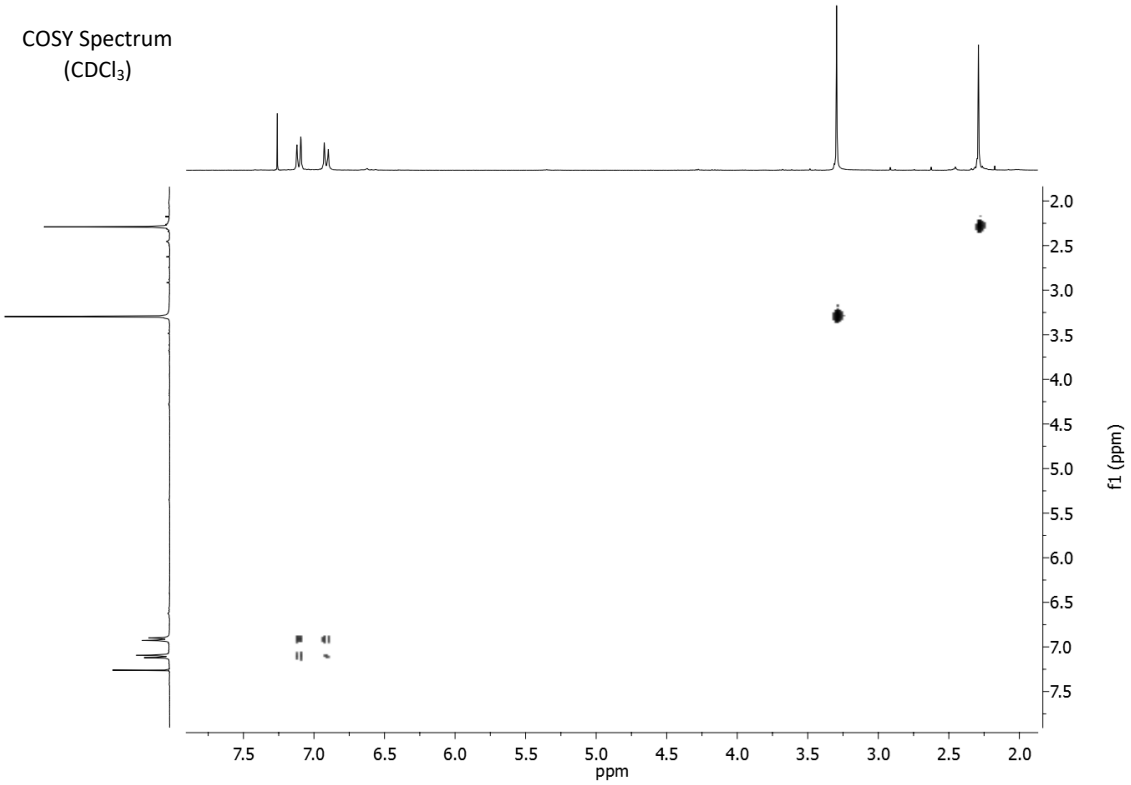

ed-HSQC Spectrum
($CDCl_3$)

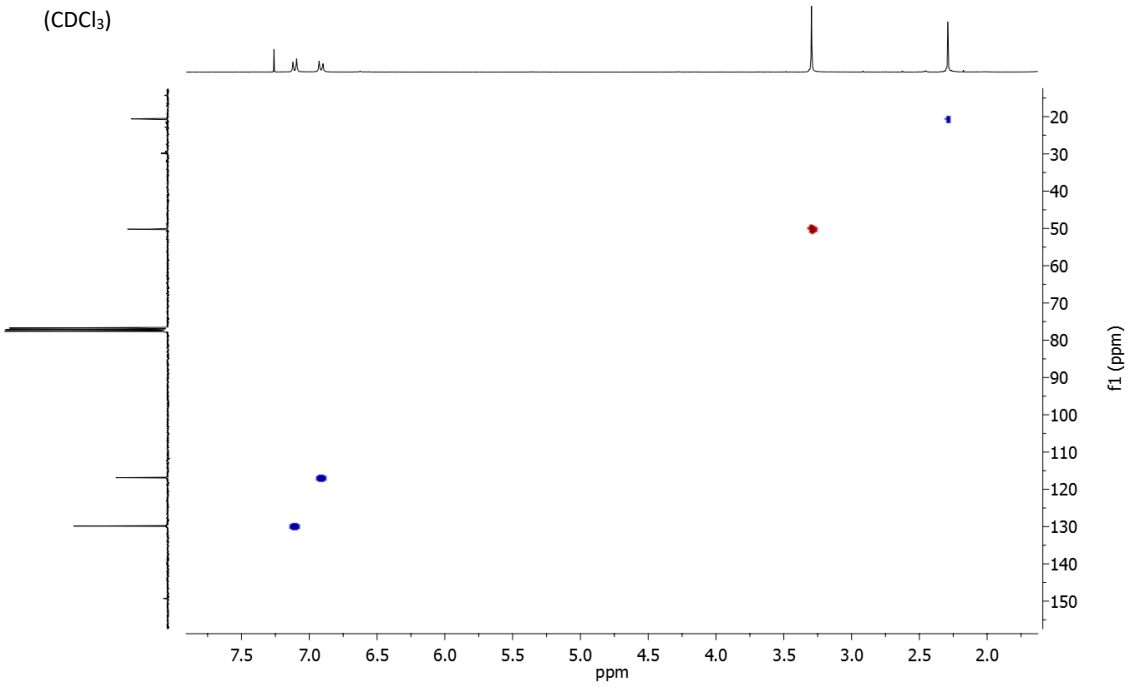

1,4-bis(3-methylphenyl)-piperazine (5b)

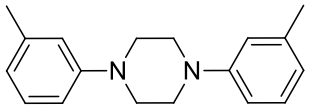

^{1}H NMR Spectrum
(300 MHz, $CDCl_3$)

^{13}C NMR Spectrum
(75 MHz, $CDCl_3$)

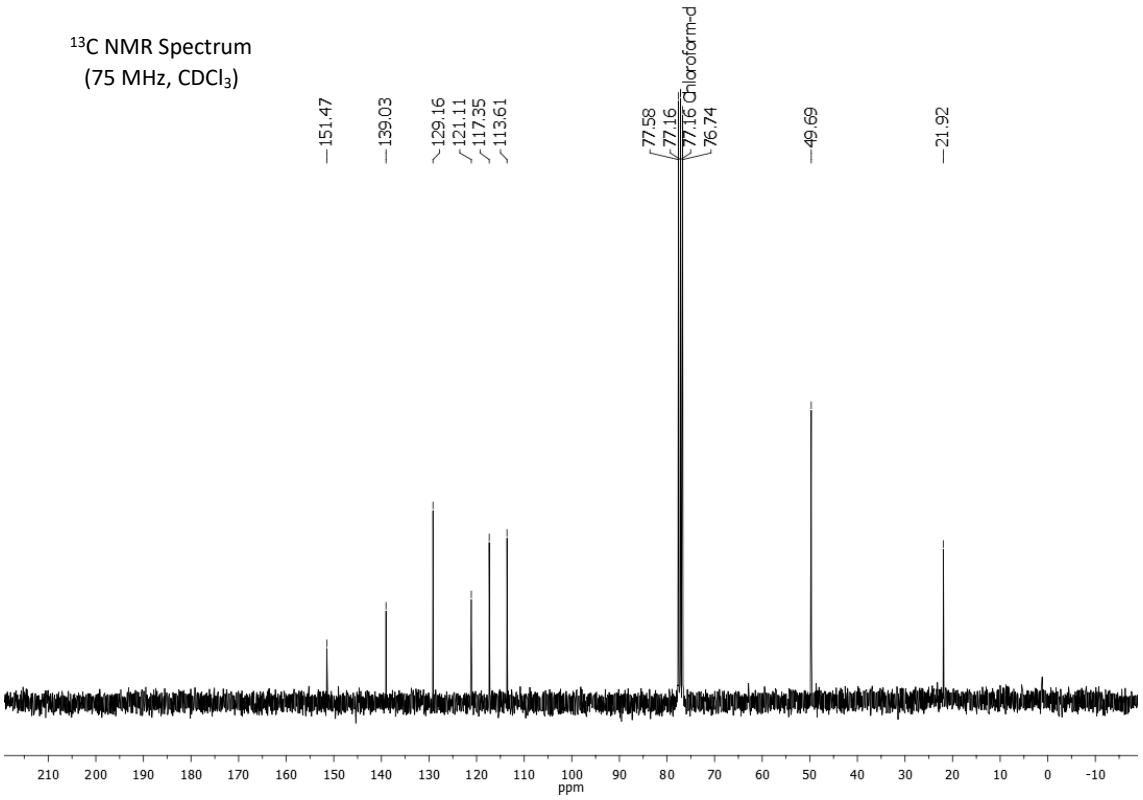

COSY Spectrum ($CDCl_3$)

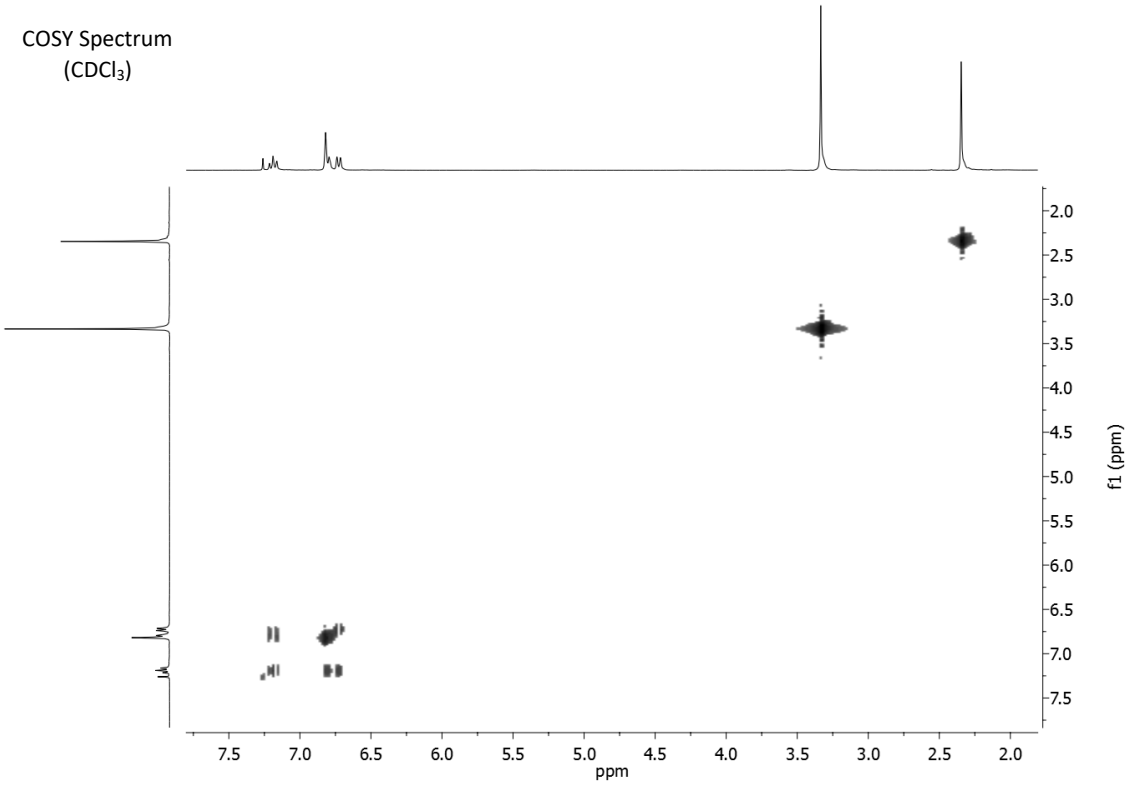

ed-HSQC Spectrum ($CDCl_3$)

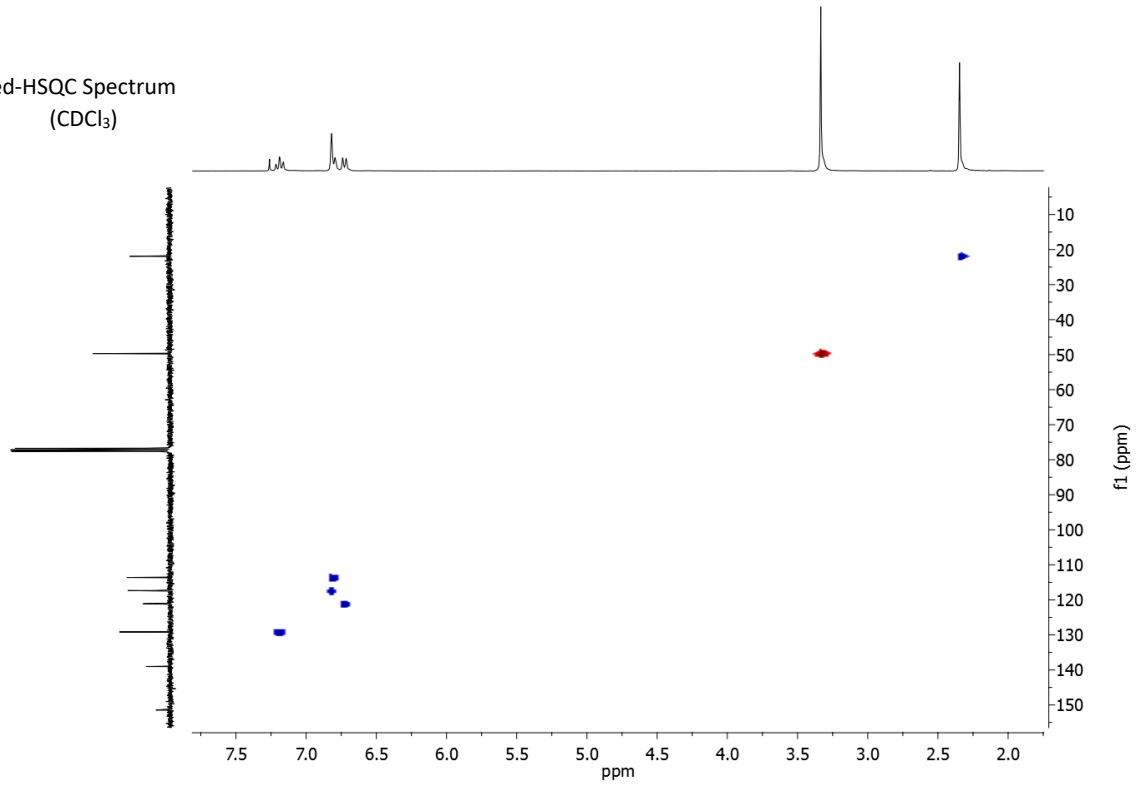

1,4-bis(2-methylphenyl)-piperazine (5c)

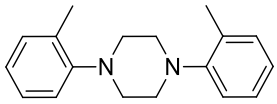

^{1}H NMR Spectrum
(300 MHz, $CDCl_3$)

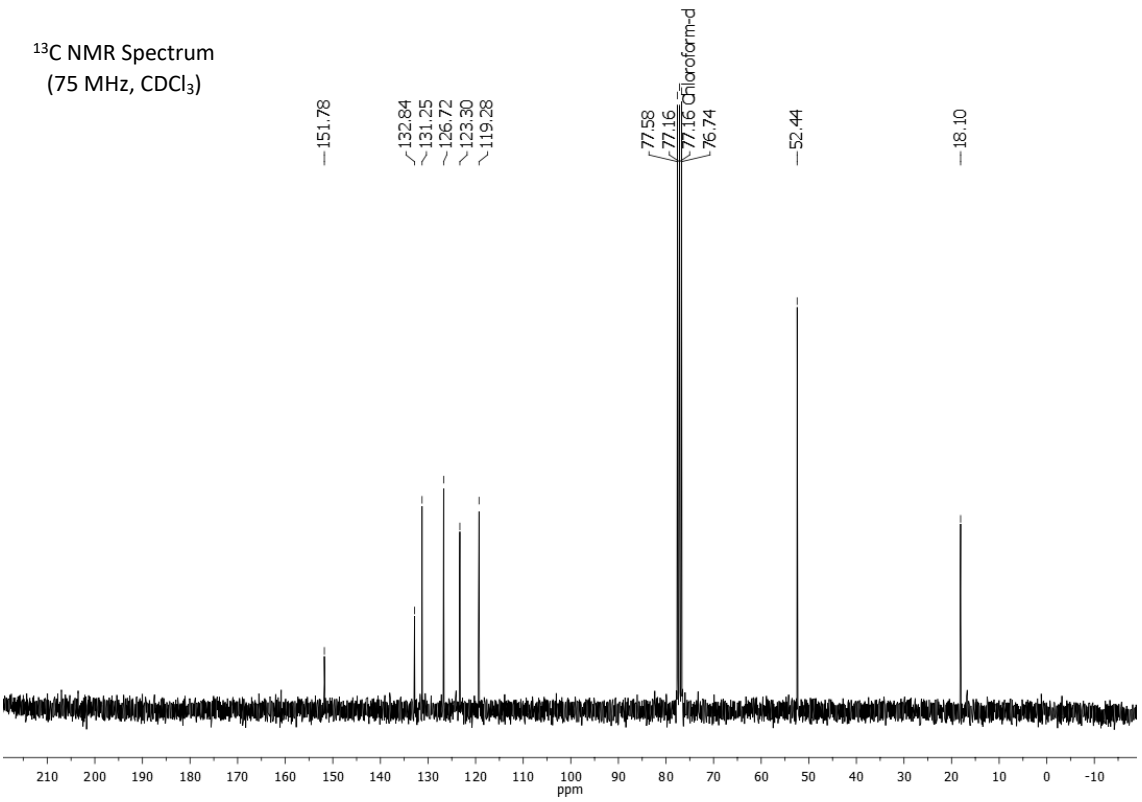

^{13}C NMR Spectrum
(75 MHz, $CDCl_3$)

COSY Spectrum ($CDCl_3$)

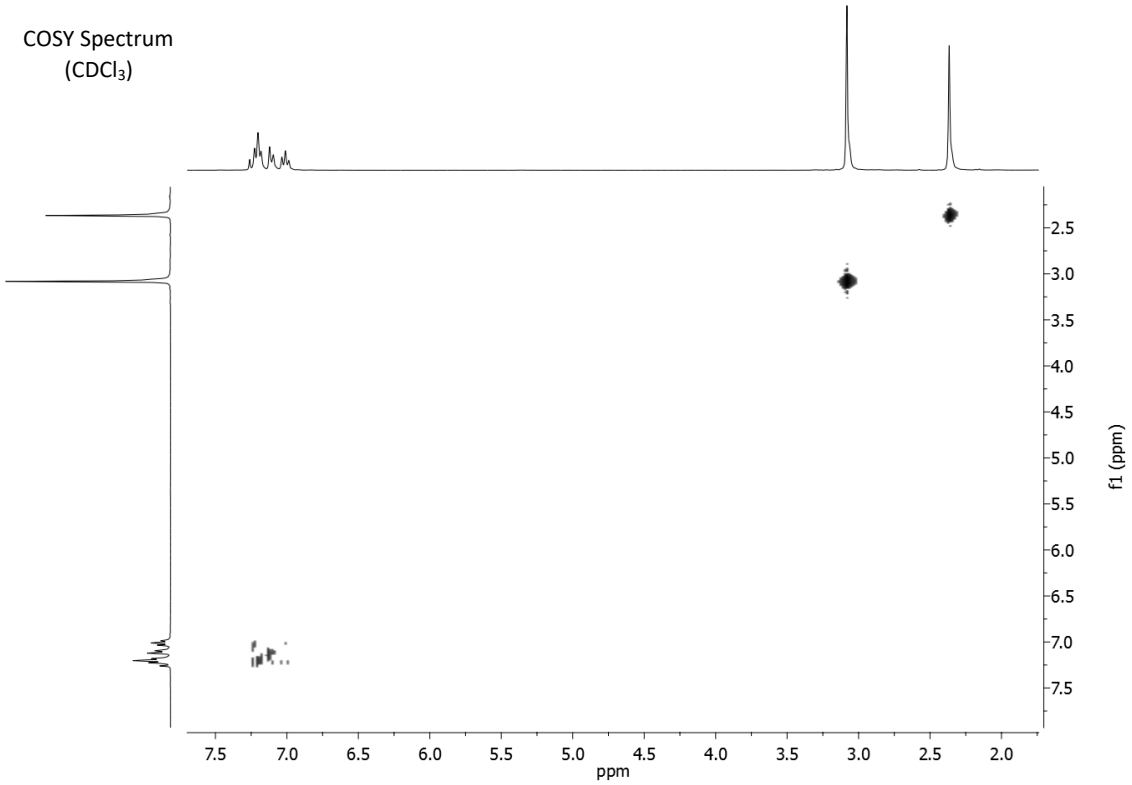

ed-HSQC Spectrum ($CDCl_3$)

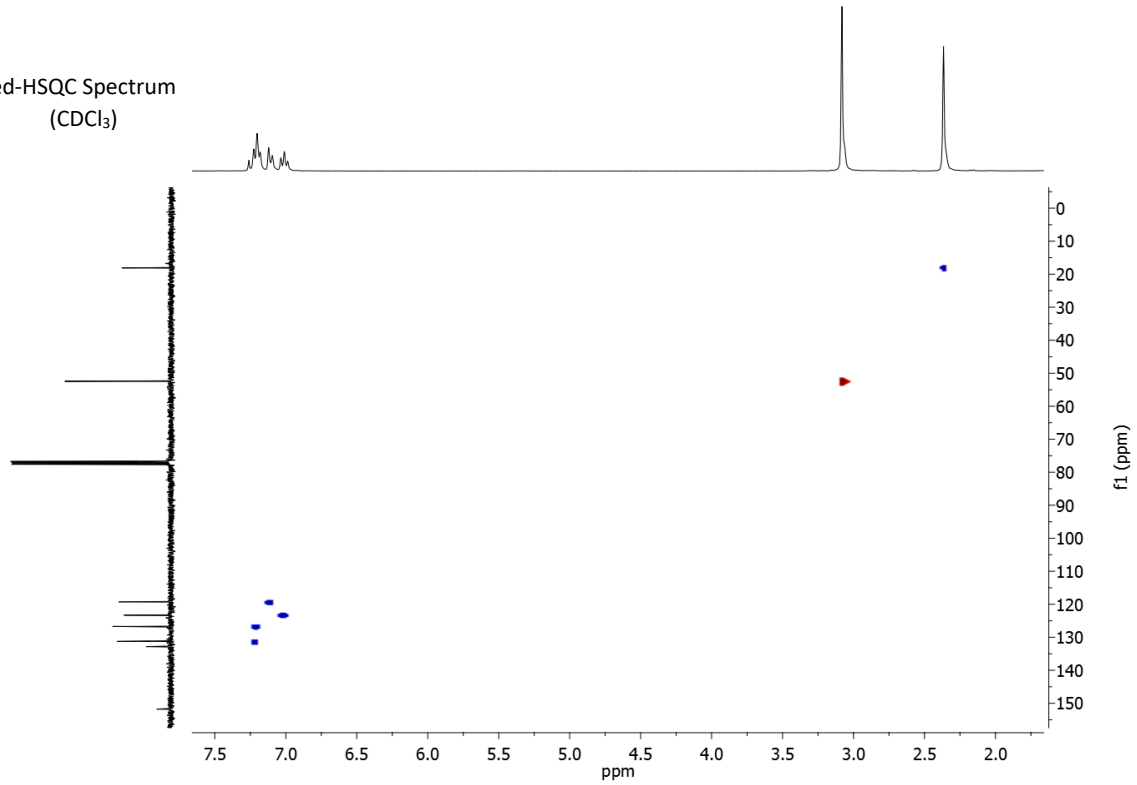

1,4-bis(2,3-dimethylphenyl)-piperazine (5d)

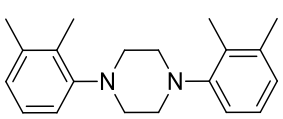

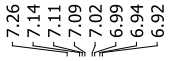

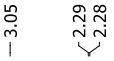

^{1}H NMR Spectrum
(300 MHz, $CDCl_3$)

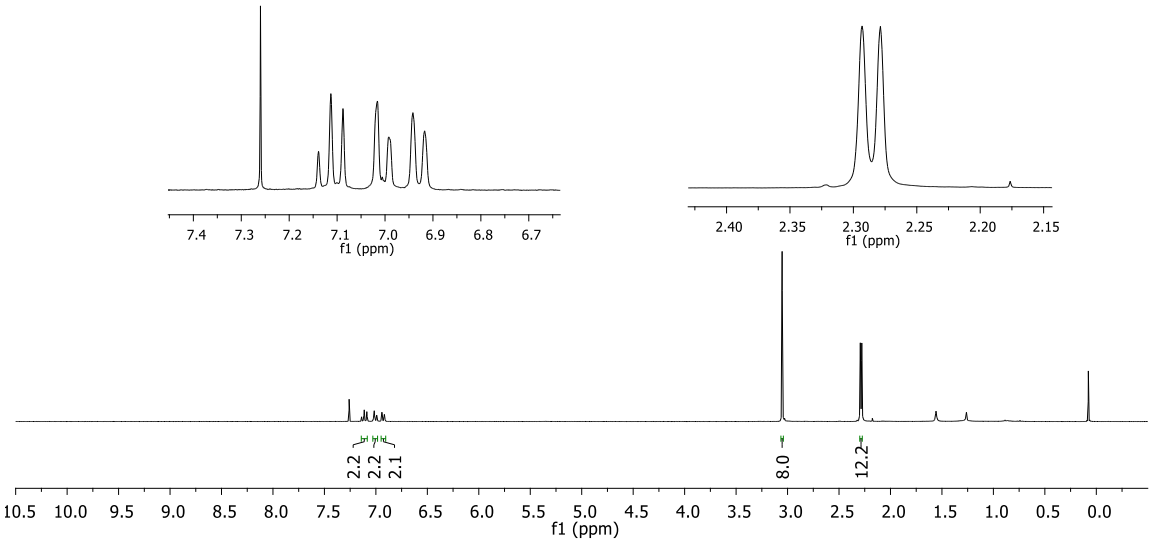

^{13}C NMR Spectrum
(75 MHz, $CDCl_3$)

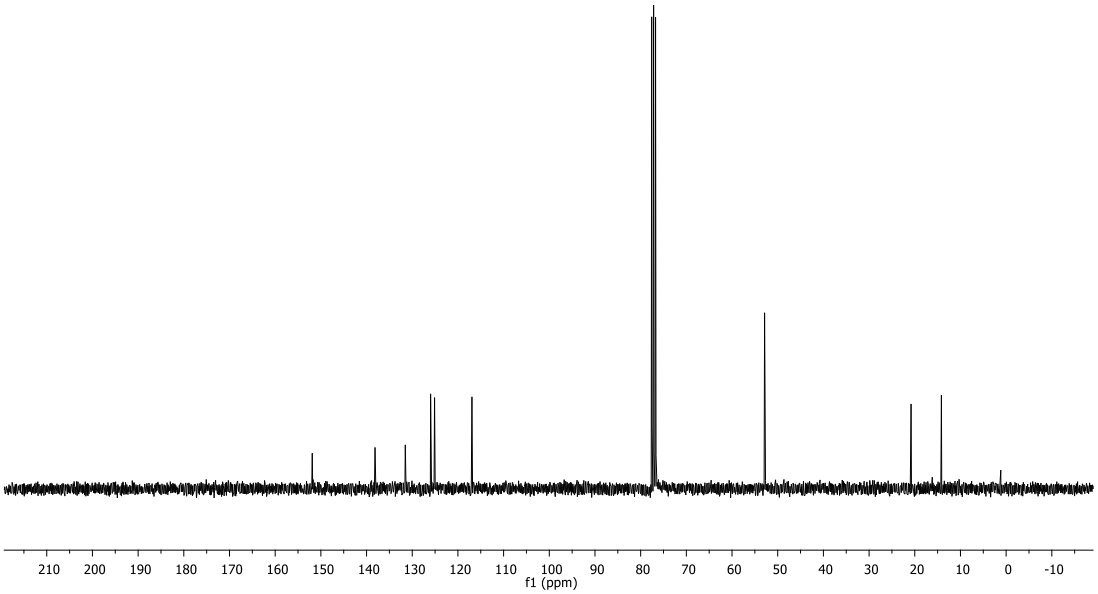

COSY Spectrum
($CDCl_3$)

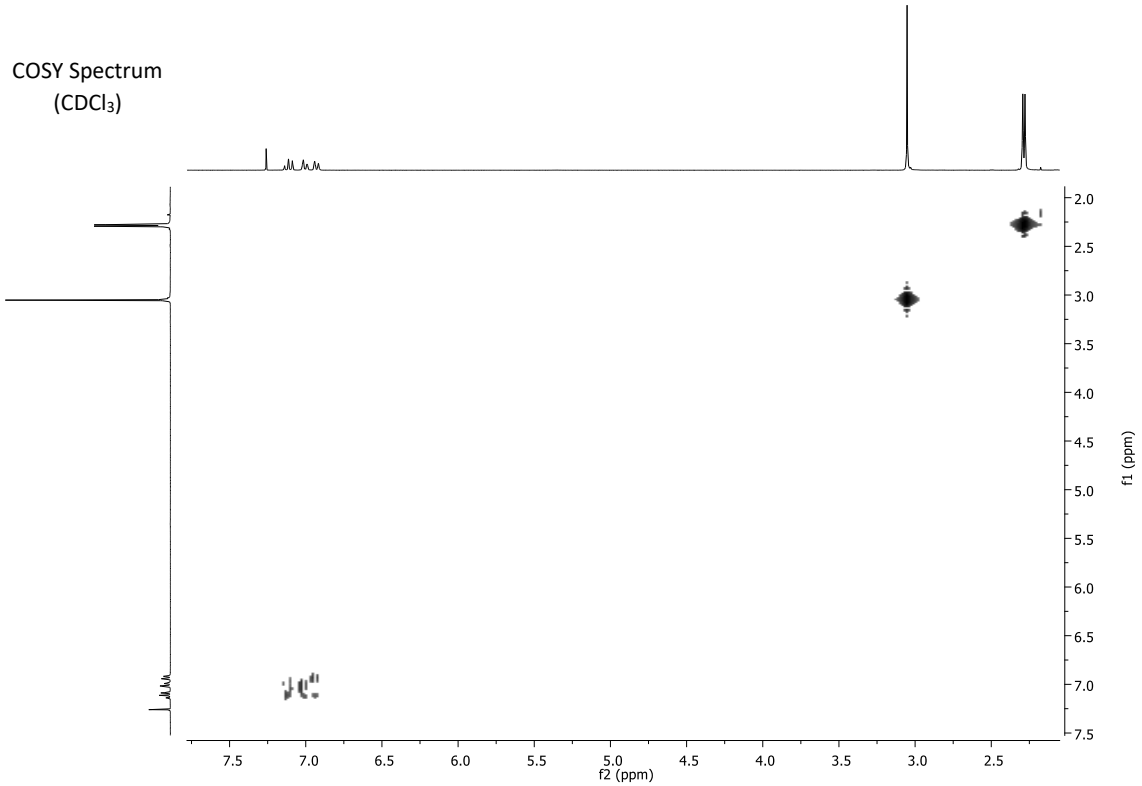

ed-HSQC Spectrum
($CDCl_3$)

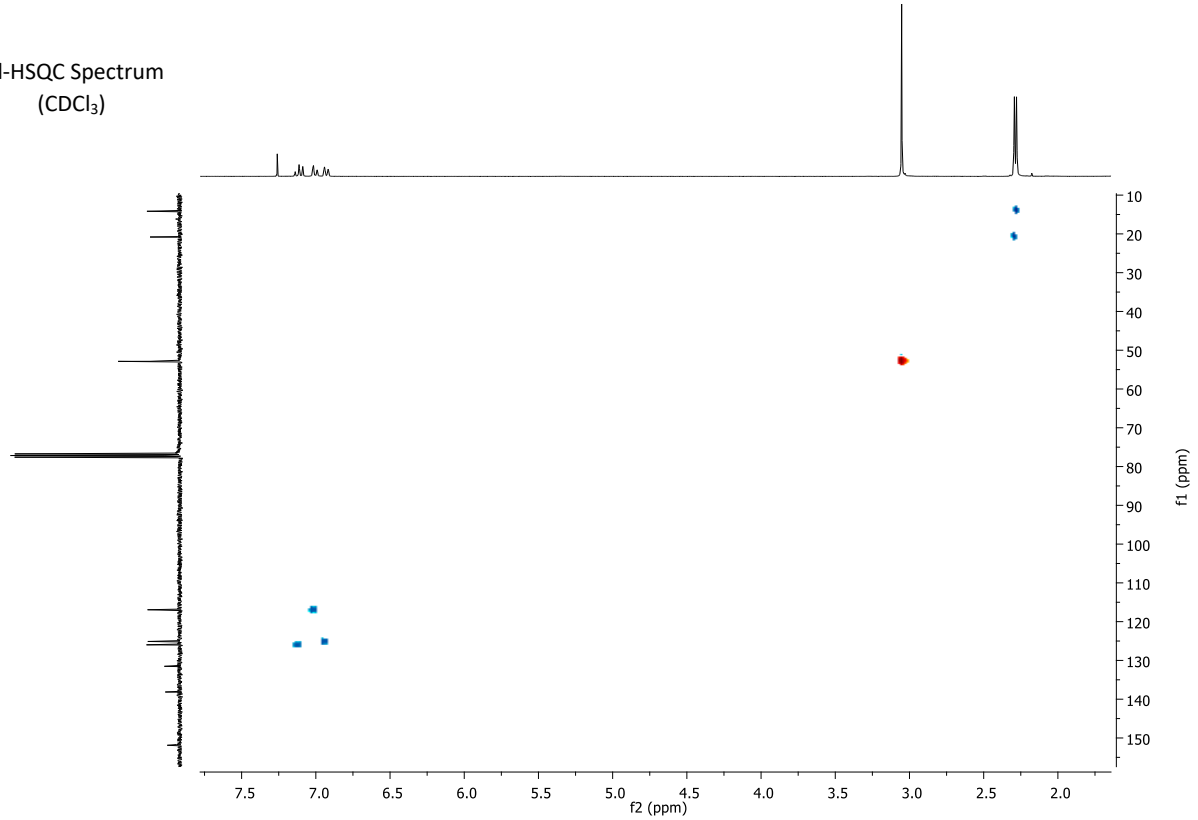

1,4-bis(2,4-dimethylphenyl)-piperazine (5e)

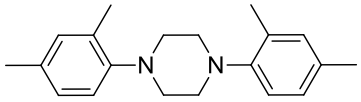

^{1}H NMR Spectrum
(300 MHz, $CDCl_3$)

^{13}C NMR Spectrum
(75 MHz, $CDCl_3$)

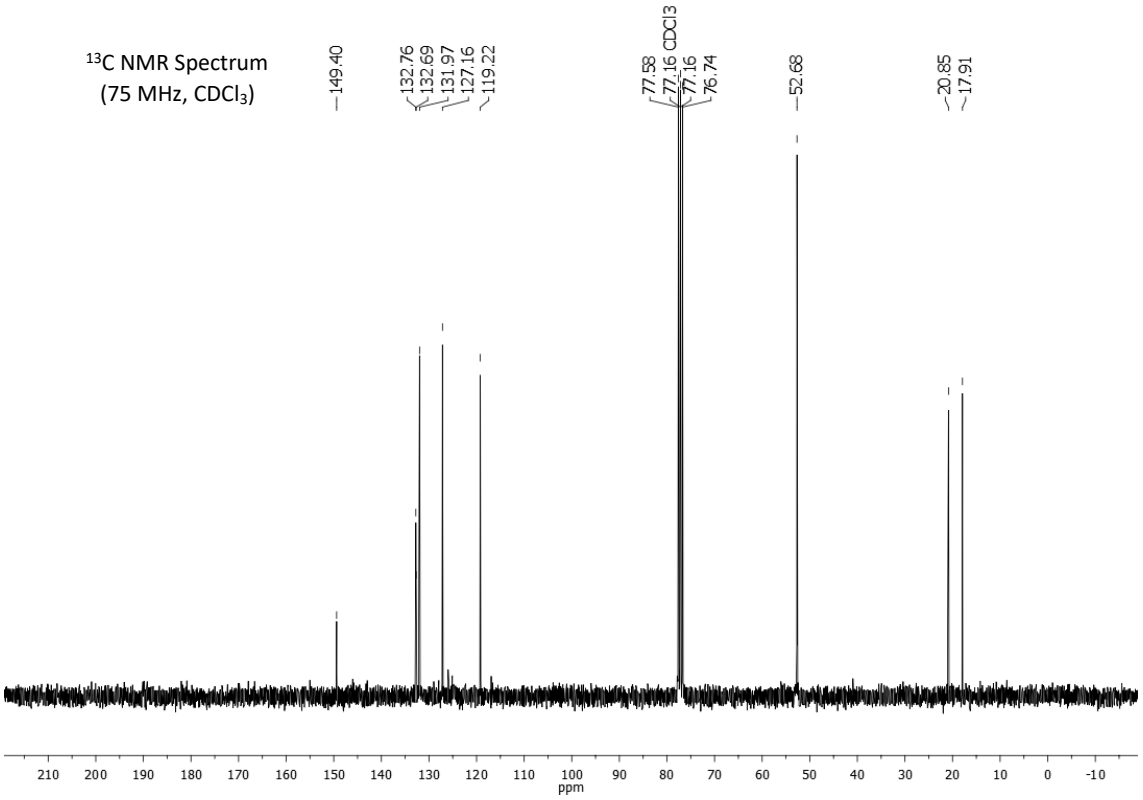

COSY Spectrum ($CDCl_3$)

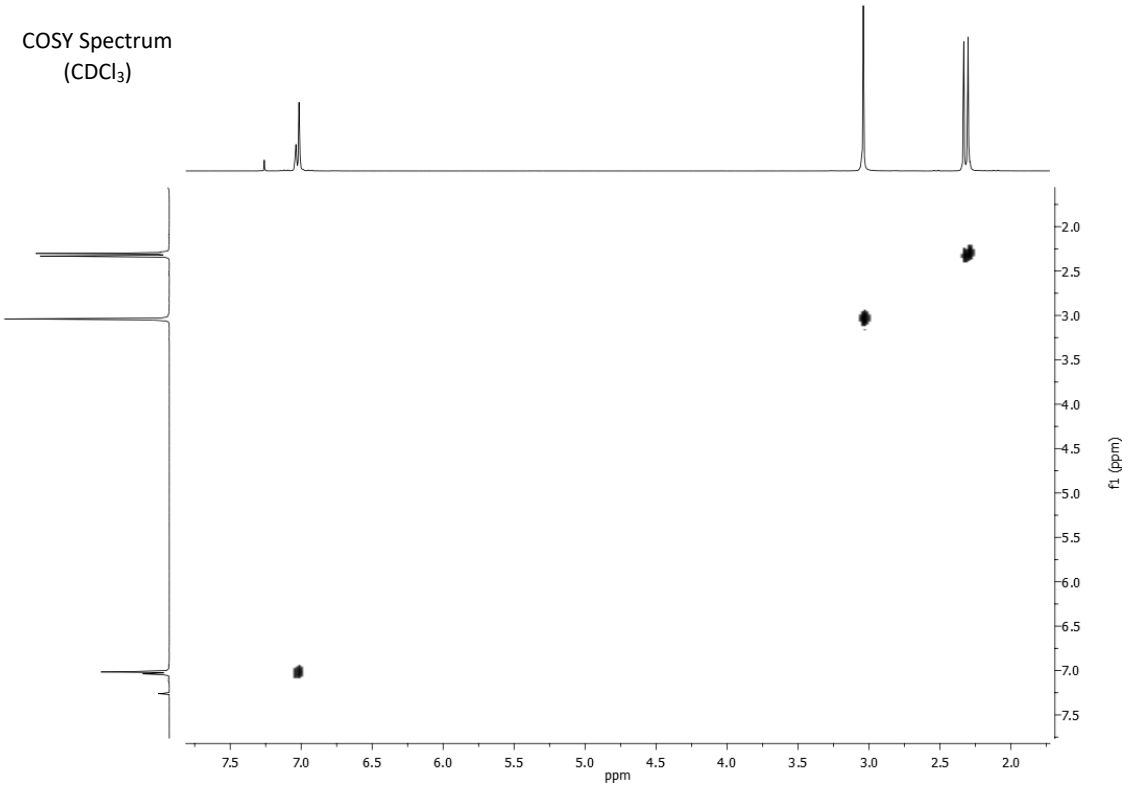

ed-HSQC Spectrum ($CDCl_3$)

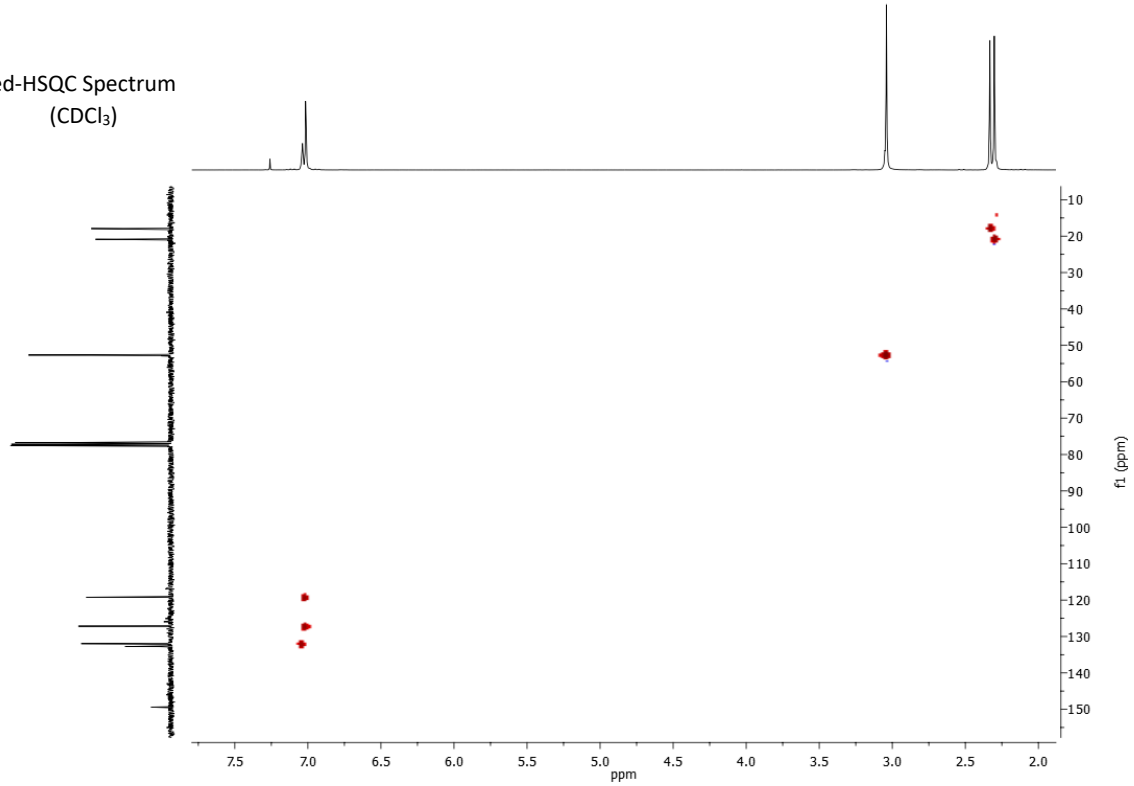

1,4-bis(3,4-dimethylphenyl)-piperazine (5f)

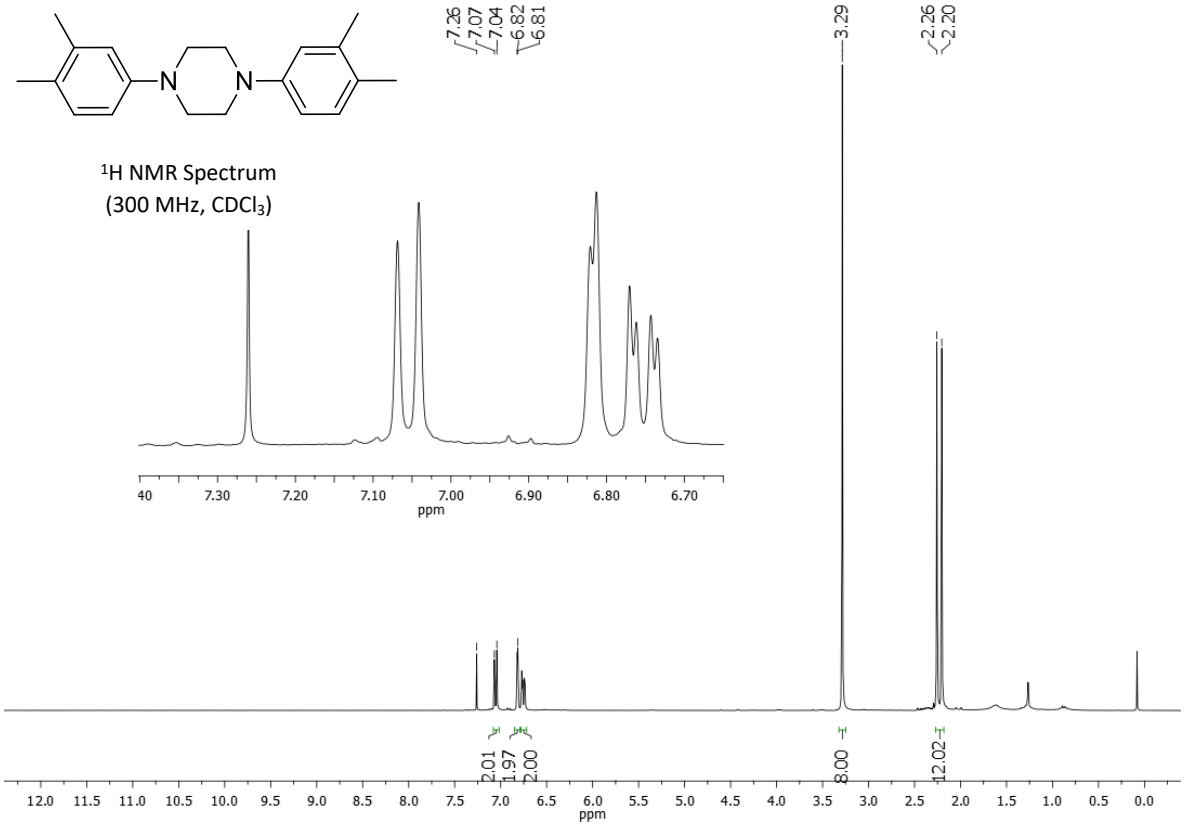

^{1}H NMR Spectrum
(300 MHz, $CDCl_3$)

^{13}C NMR Spectrum
(75 MHz, $CDCl_3$)

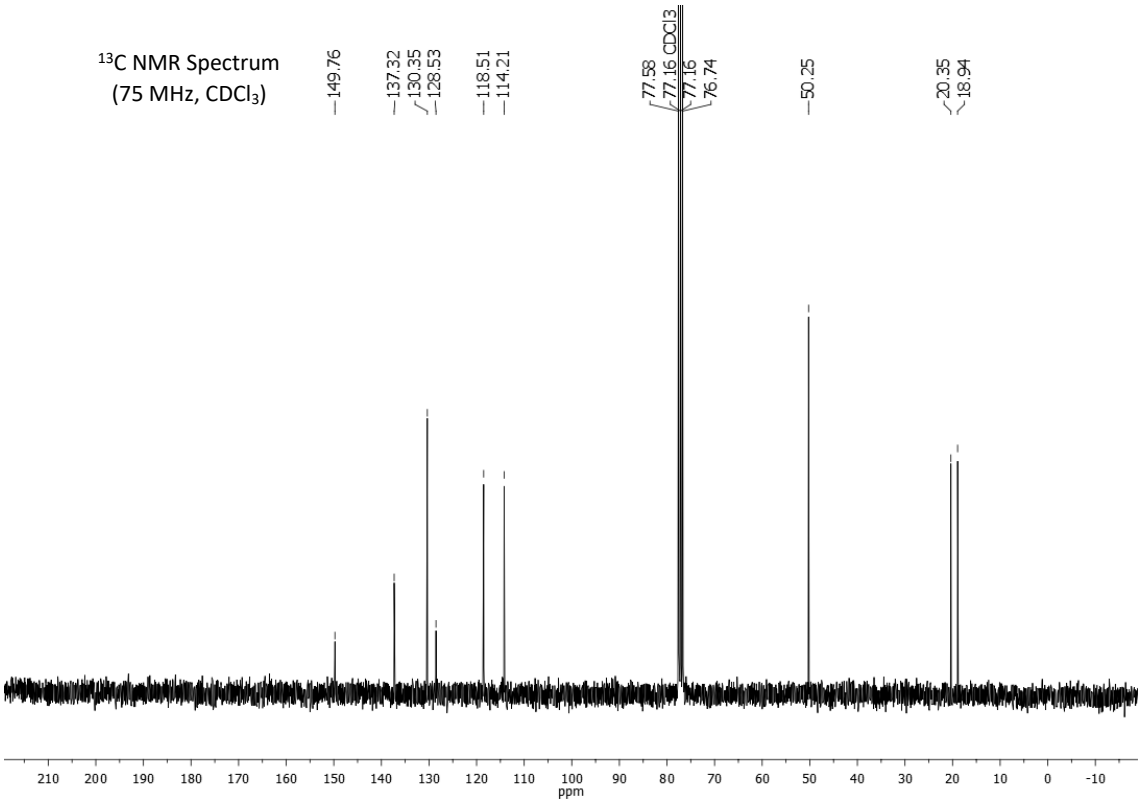

COSY Spectrum ($CDCl_3$)

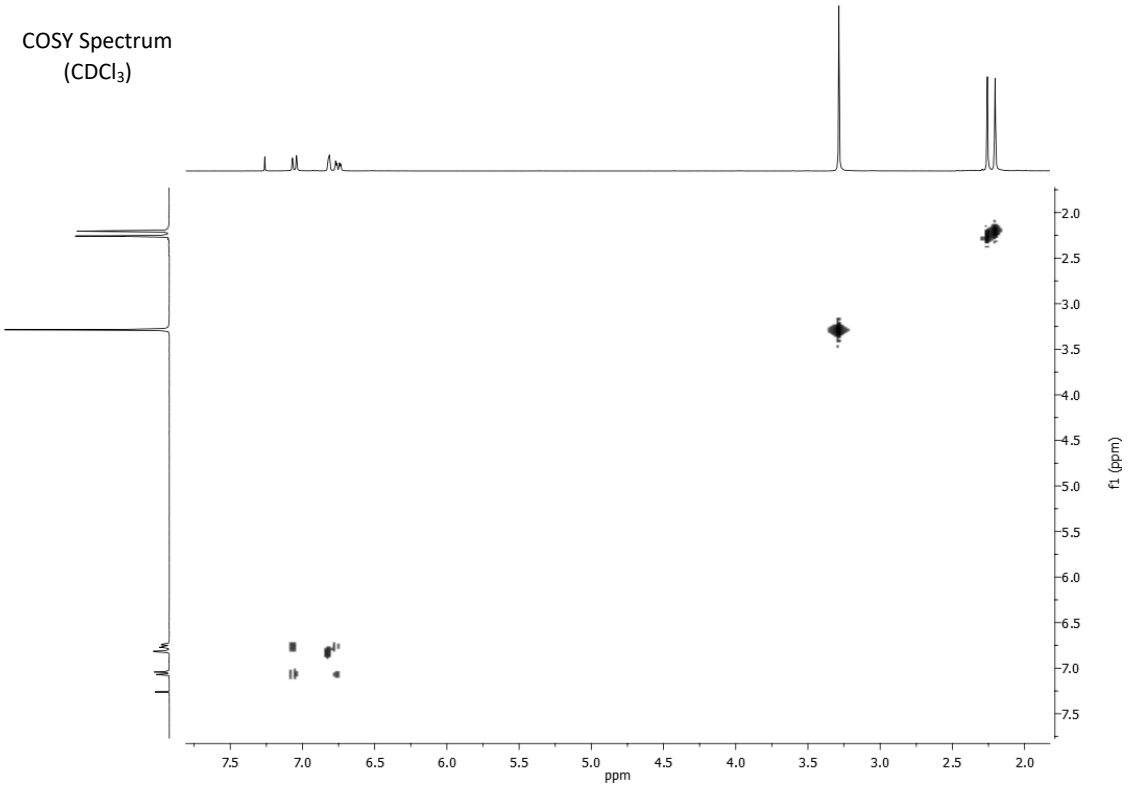

ed-HSQC Spectrum ($CDCl_3$)

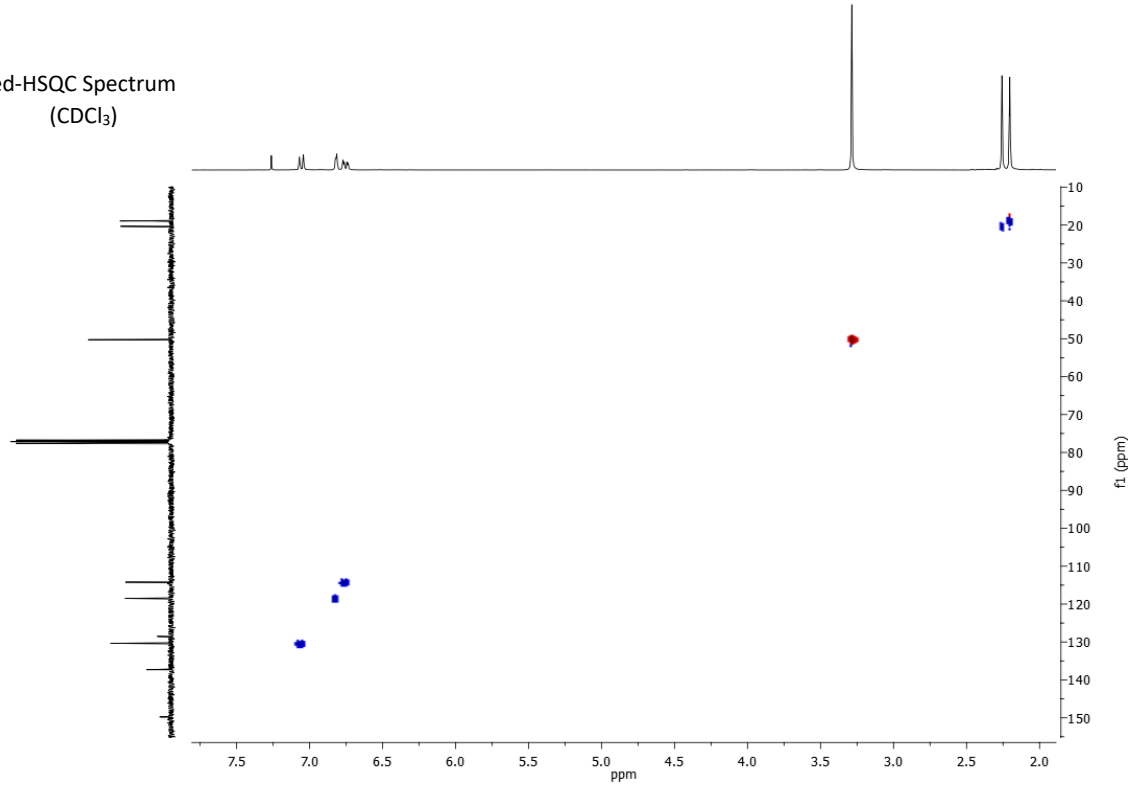

1,4-bis(3,5-dimethylphenyl)-piperazine (5g)

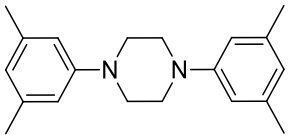

^{1}H NMR Spectrum
(300 MHz, $CDCl_3$)

^{13}C NMR Spectrum
(75 MHz, $CDCl_3$)

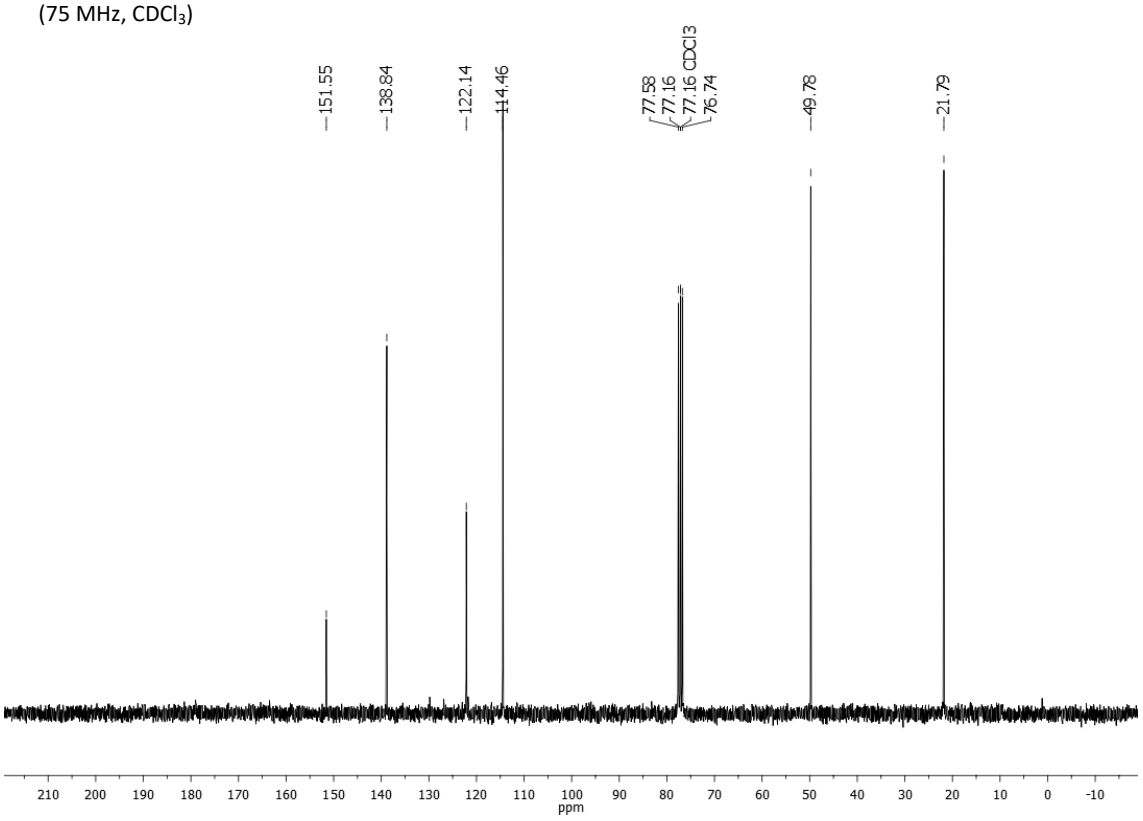

COSY Spectrum
($CDCl_3$)

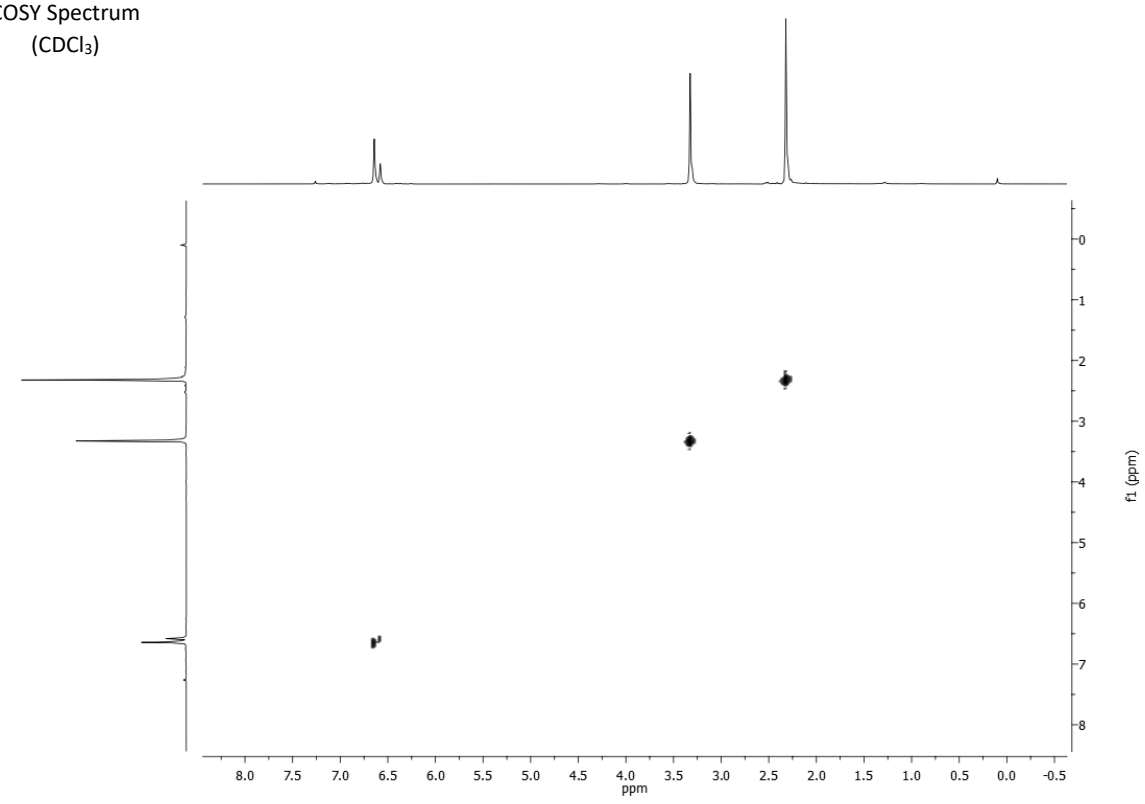

ed-HSQC Spectrum
($CDCl_3$)

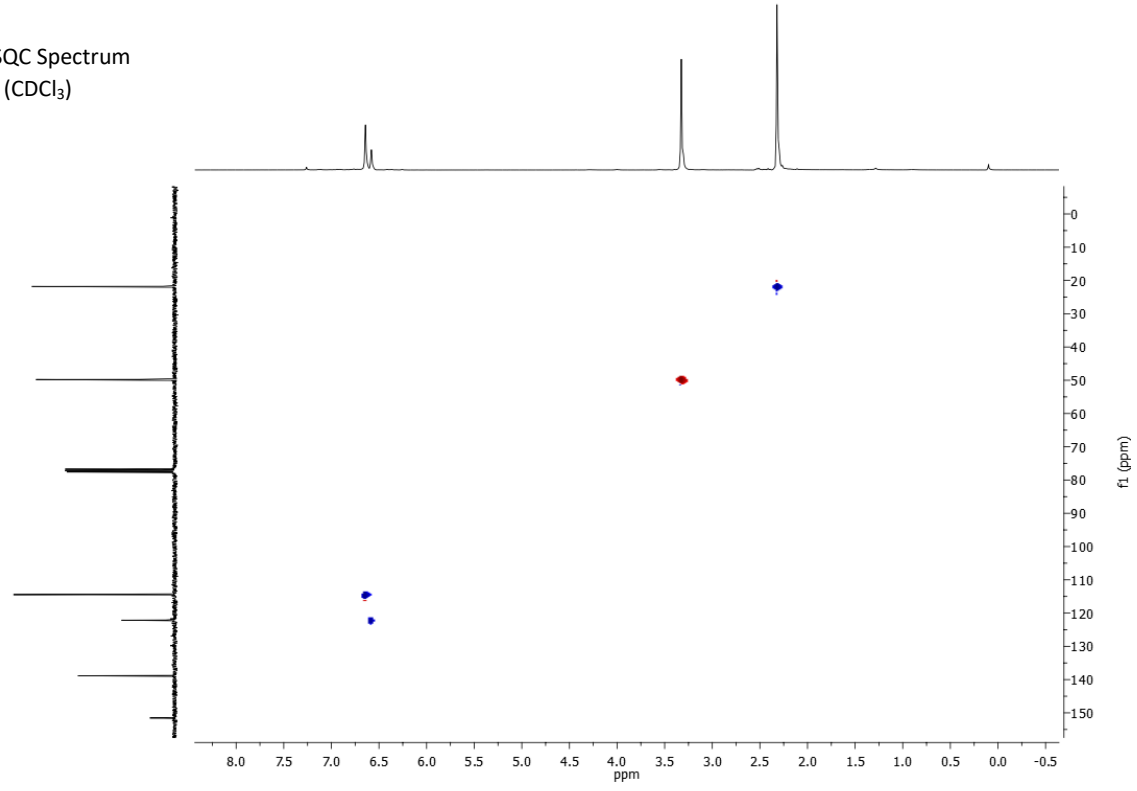

1,4-bis(2,5-dimethylphenyl)-piperazine (5h)

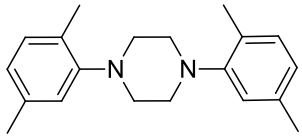

^{1}H NMR Spectrum
(300 MHz, $CDCl_3$)

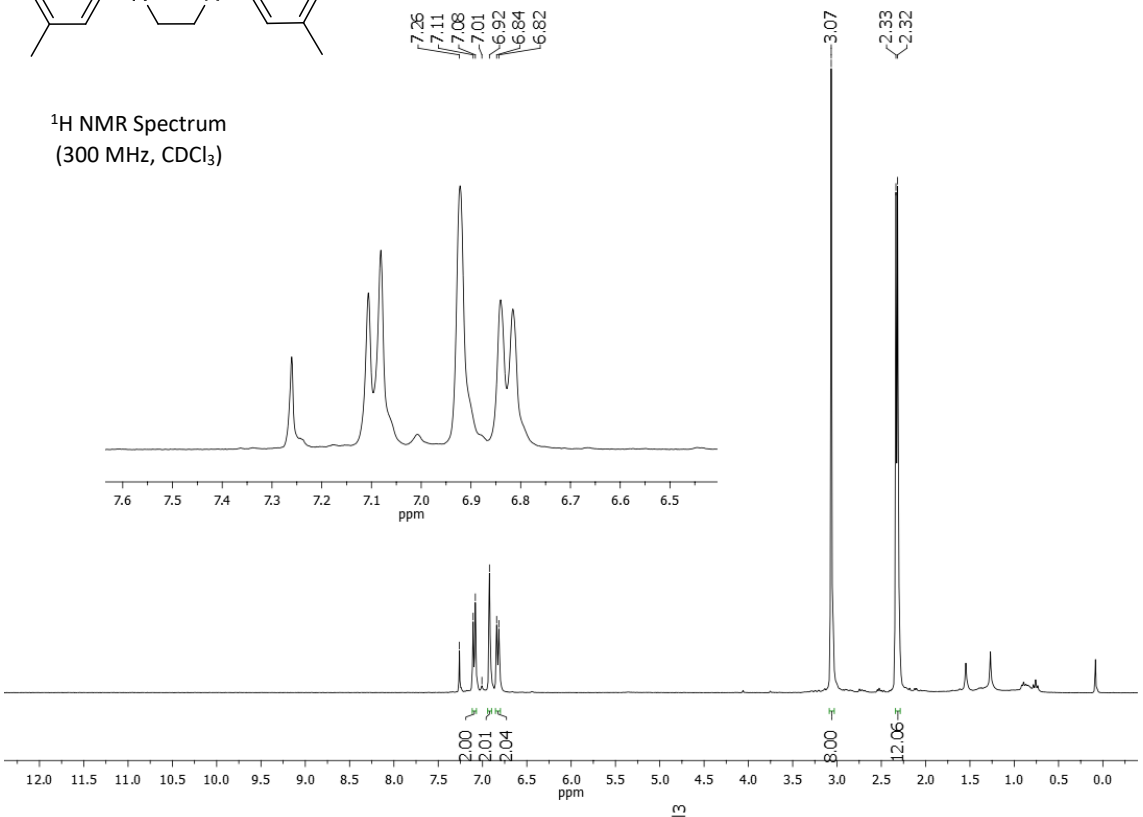

^{13}C NMR Spectrum
(75 MHz, $CDCl_3$)

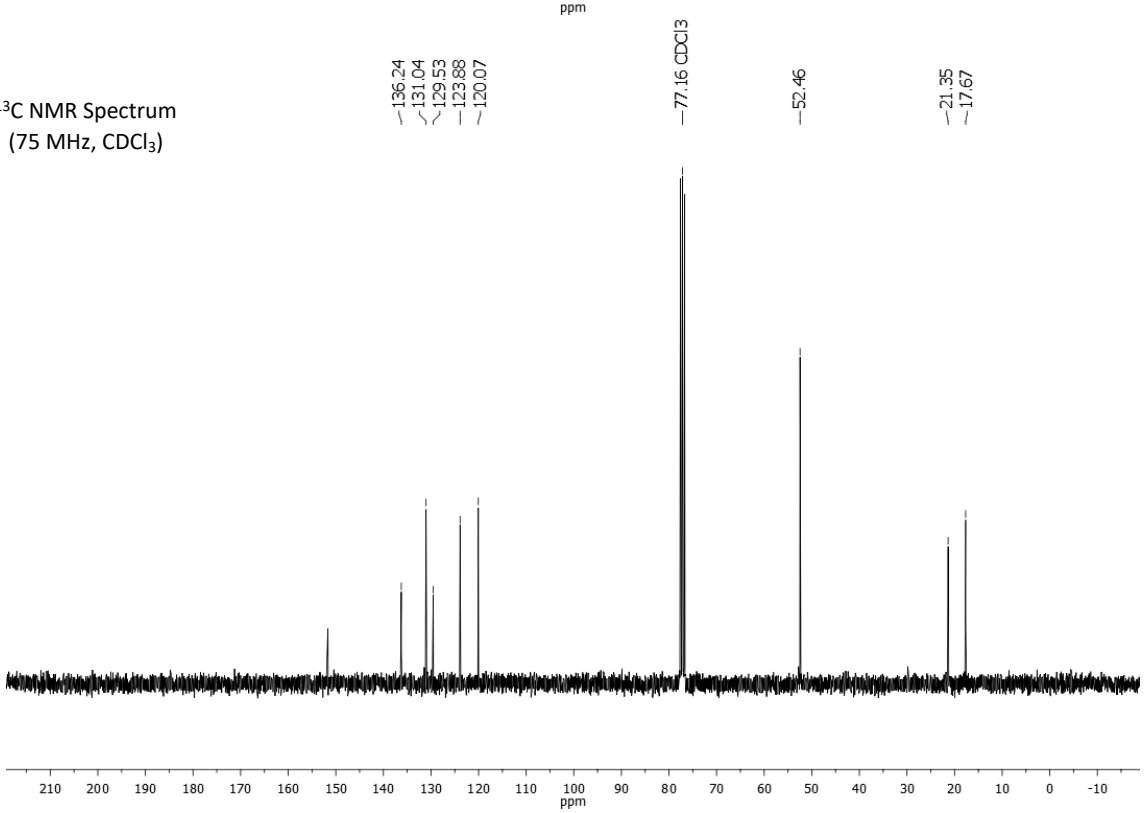

COSY Spectrum
($CDCl_3$)

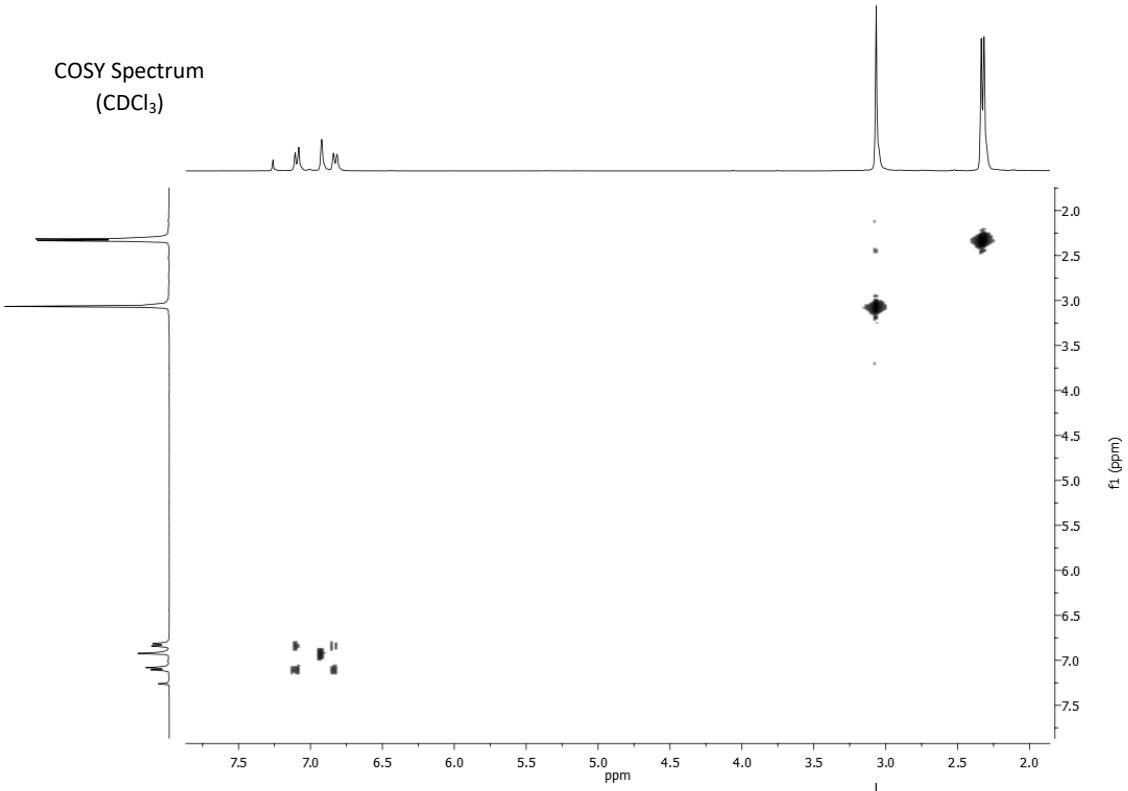

ed-HSQC Spectrum
($CDCl_3$)

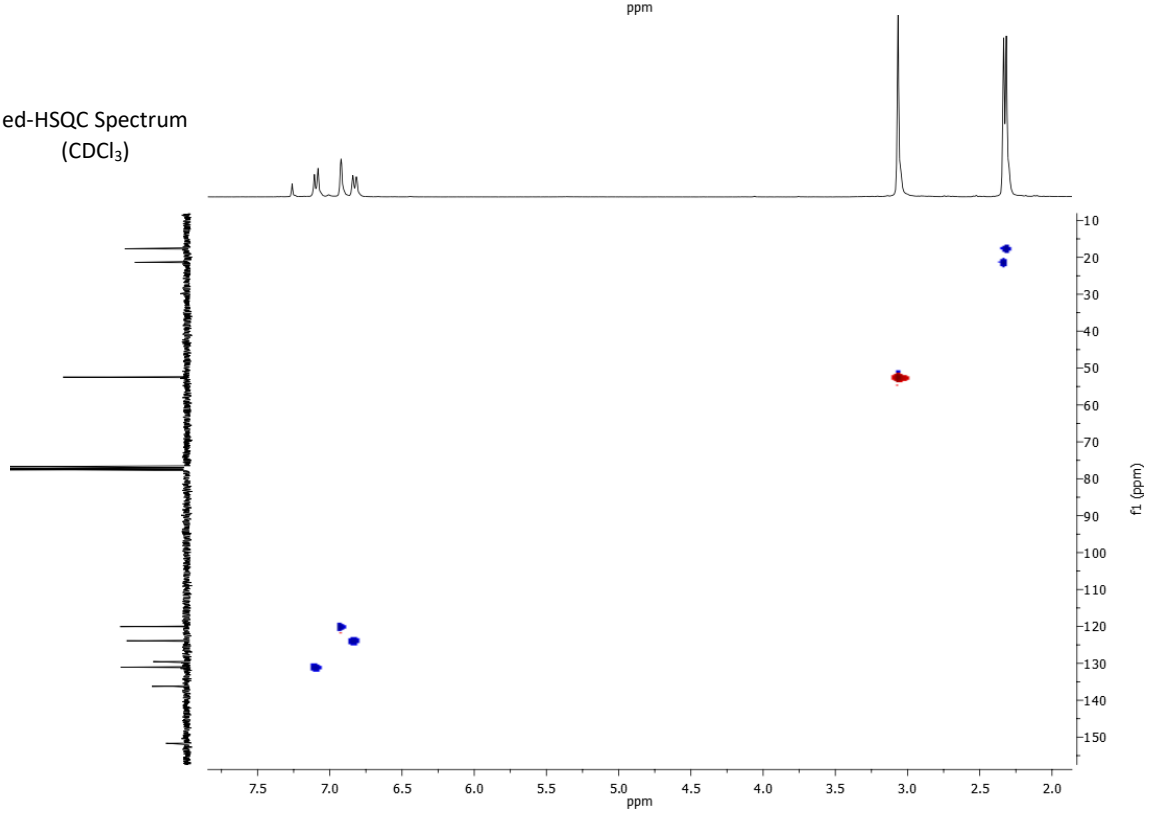

1,4-bis(2,3-dimethoxyphenyl)-piperazine (5w)

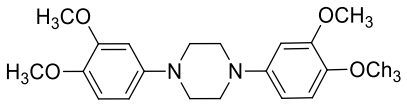

^{1}H NMR Spectrum
(300 MHz, $CDCl_3$)

^{13}C NMR Spectrum
(75 MHz, $CDCl_3$)

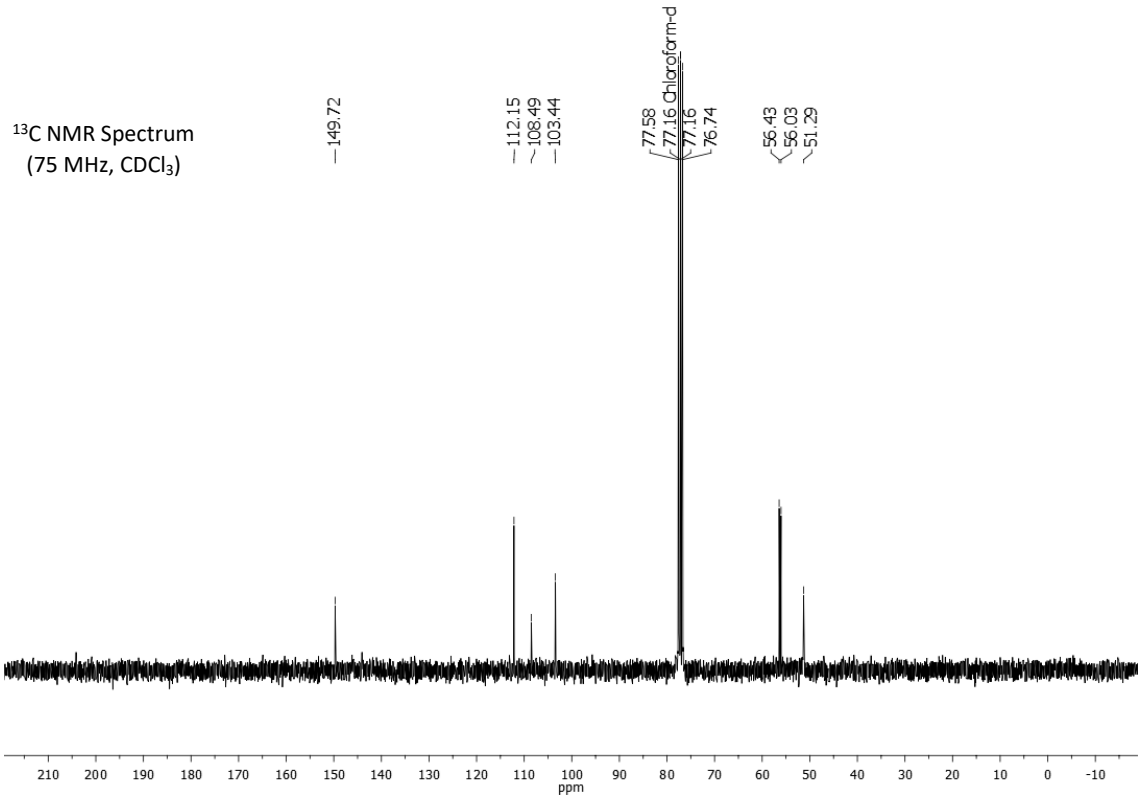

COSY Spectrum
($CDCl_3$)

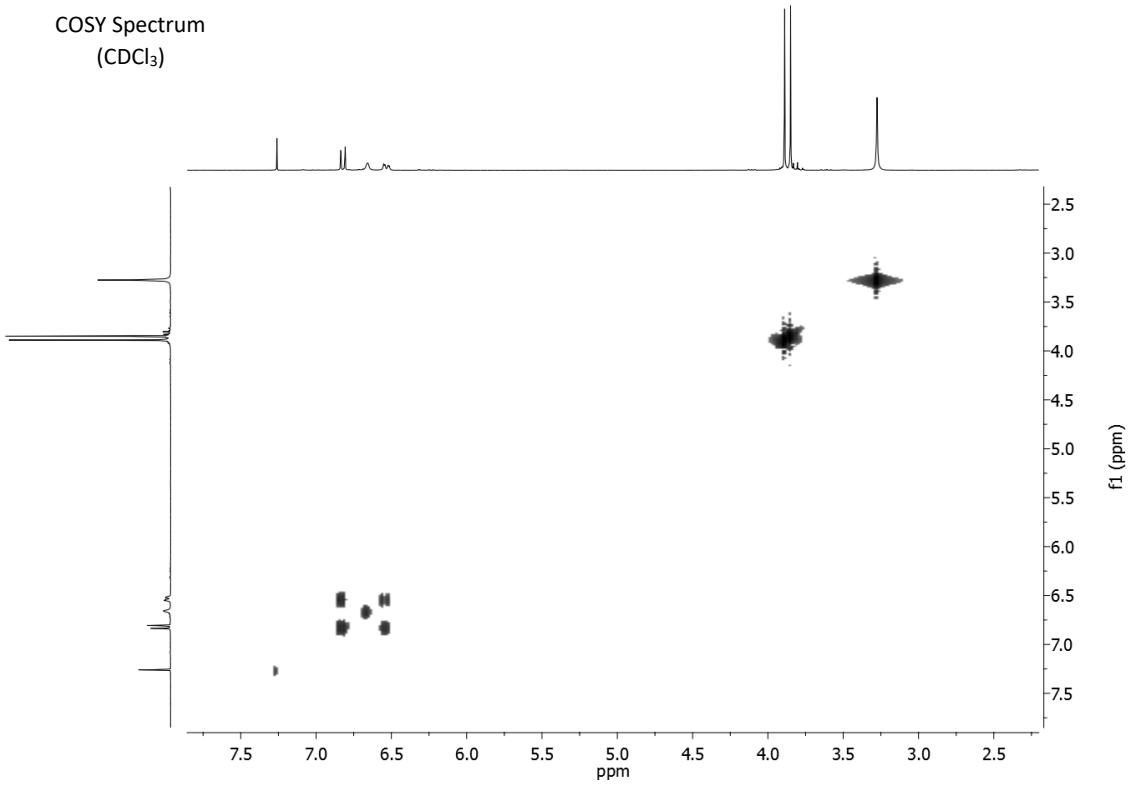

ed-HSQC Spectrum
($CDCl_3$)

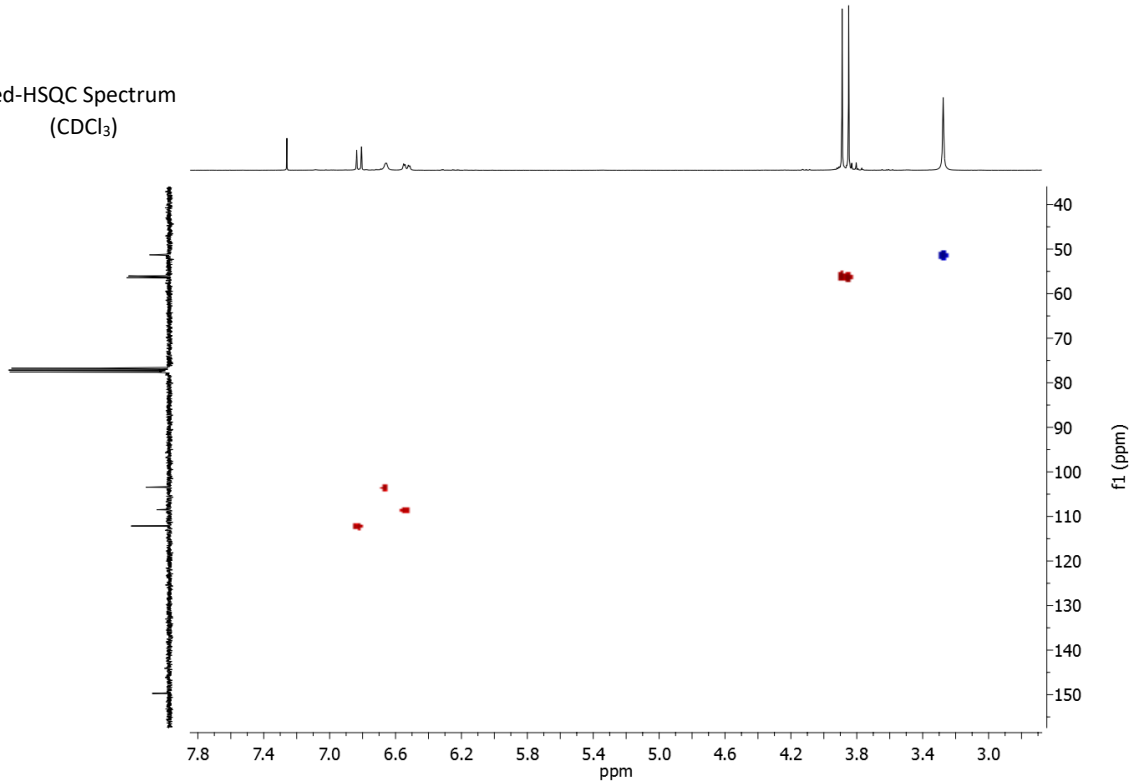

N-(2-hydroxyethyl)-1,2,3,4-tetrahydroquinoline (7a)

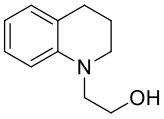

^{1}H NMR Spectrum
(300 MHz, $CDCl_3$)

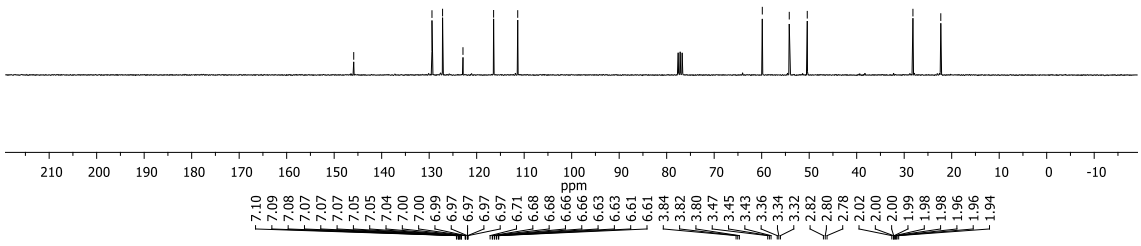

^{13}C NMR Spectrum
(75 MHz, $CDCl_3$)

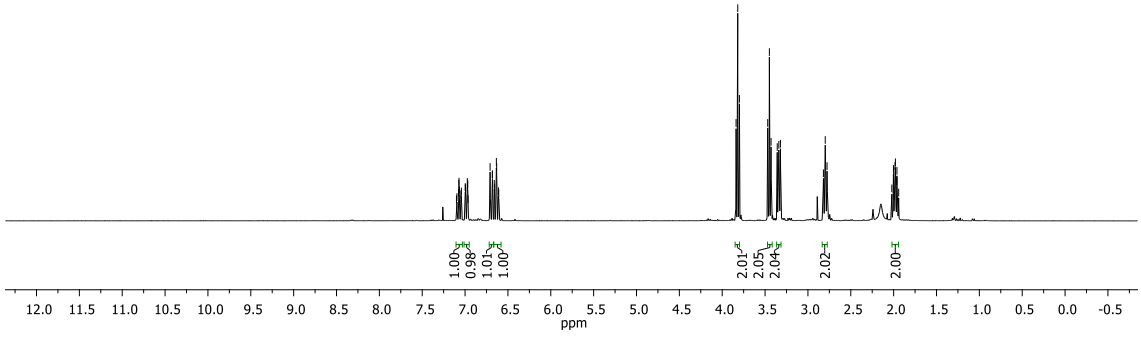

5,6-dihydro-4H-pyrrolo-[3,2,1-ij]-quinoline (7b)

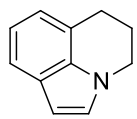

^{1}H NMR Spectrum
(300 MHz, $CDCl_3$)

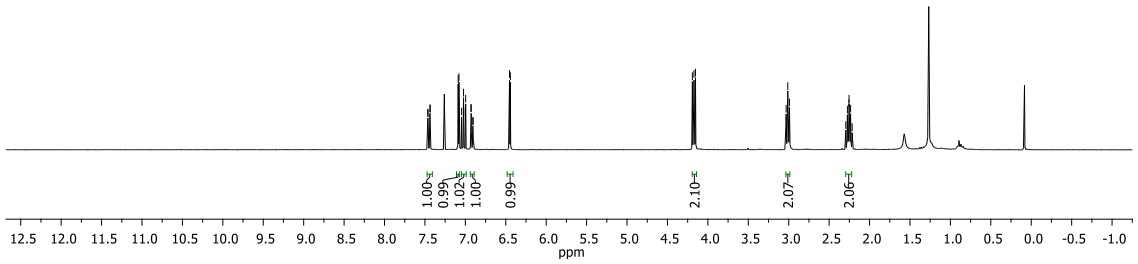

^{13}C NMR Spectrum
(75 MHz, $CDCl_3$)

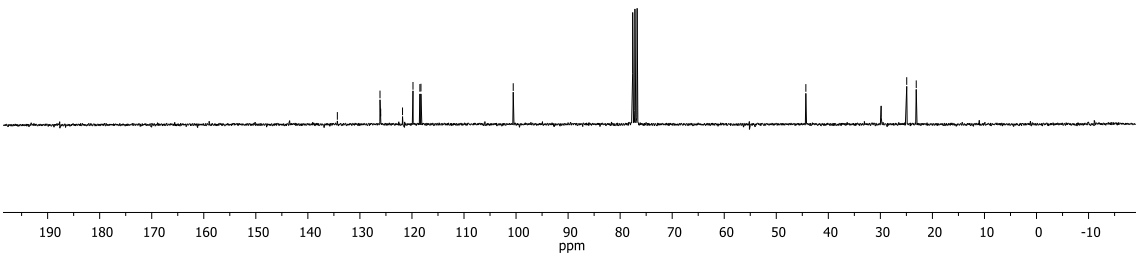

3,4-dihydro-6-methoxy-1(2H)-quinolinethanol (9a)

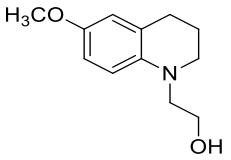

^{1}H NMR Spectrum
(300 MHz, $CDCl_3$)

^{13}C NMR Spectrum
(75 MHz, $CDCl_3$)

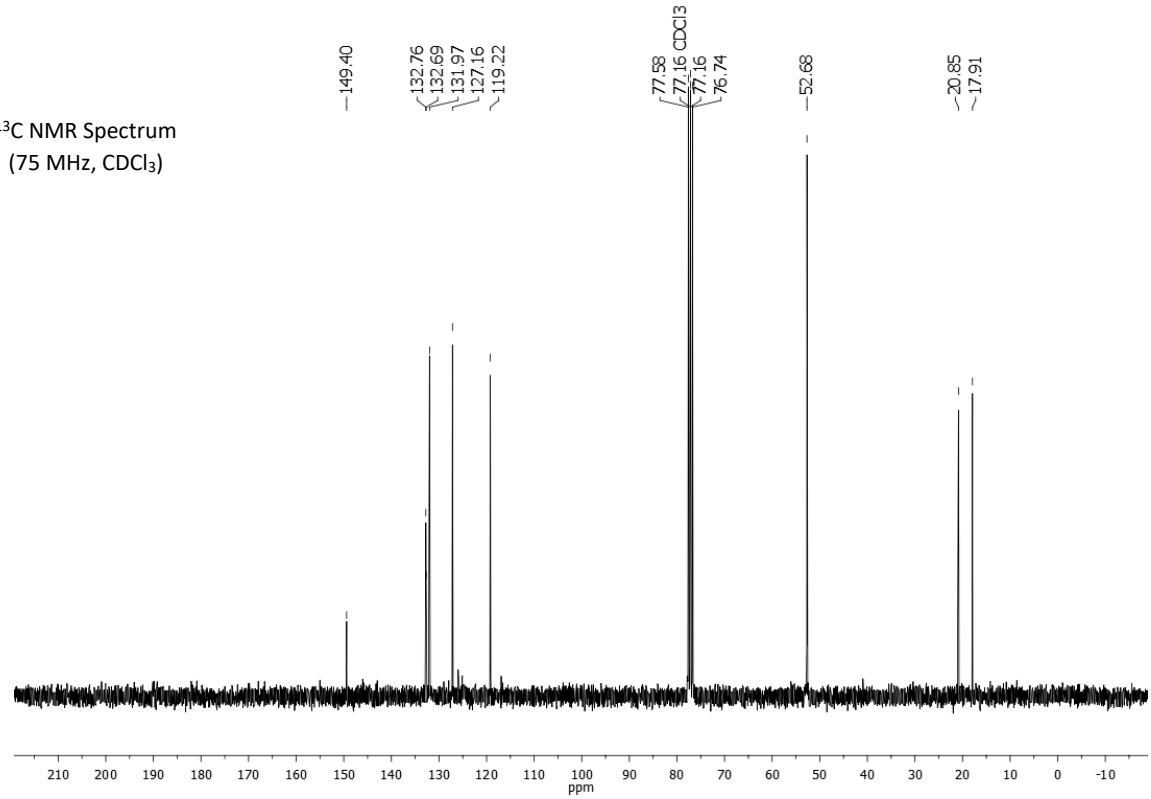

COSY Spectrum
($CDCl_3$)

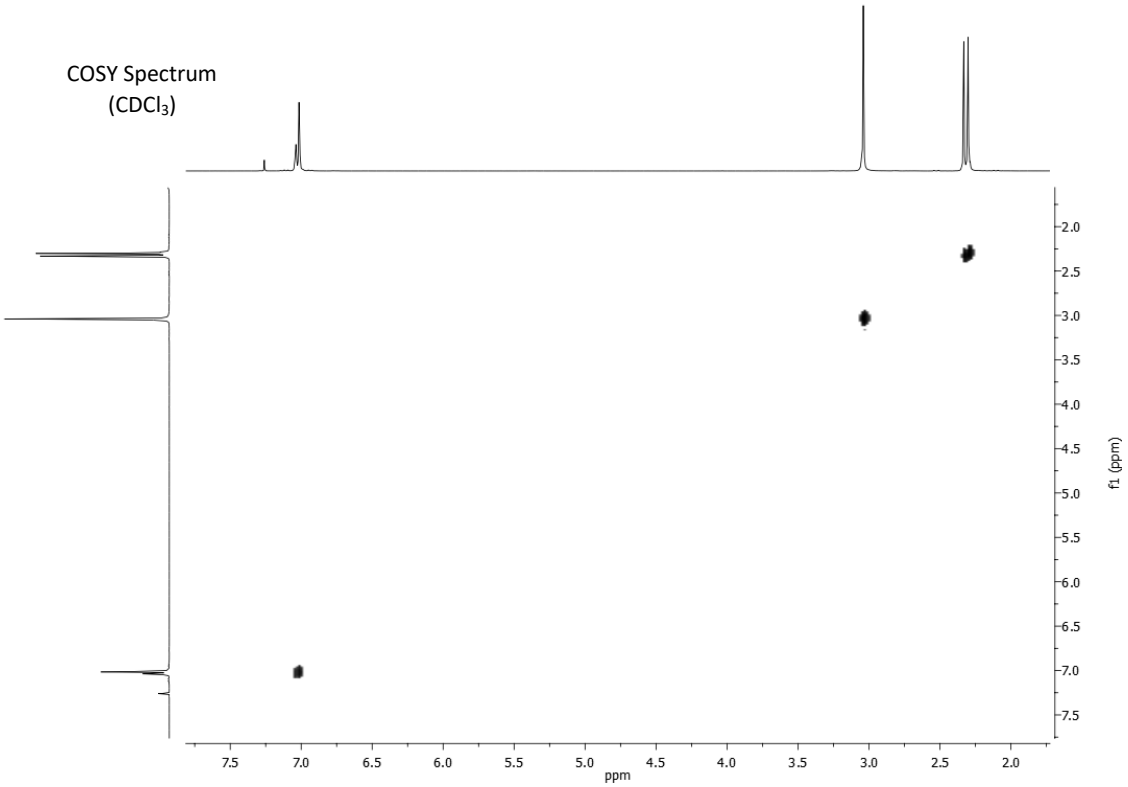

ed-HSQC Spectrum
($CDCl_3$)

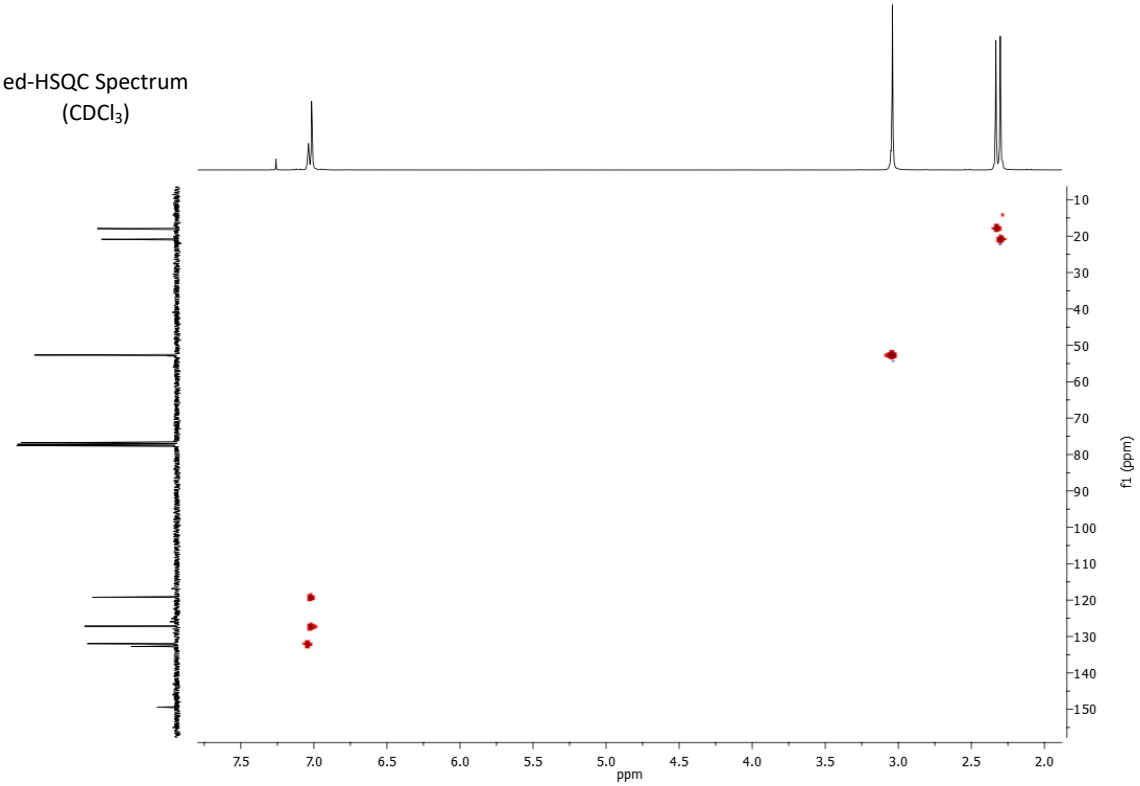

5,6-dihydro-8-methoxy-4H-pyrrolo[3,2,1-ij]quinoline (9b)

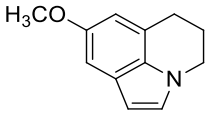

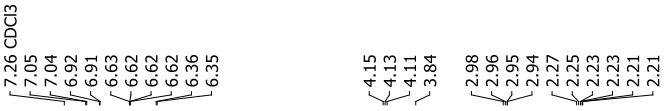

^{1}H NMR Spectrum
(300 MHz, $CDCl_3$)

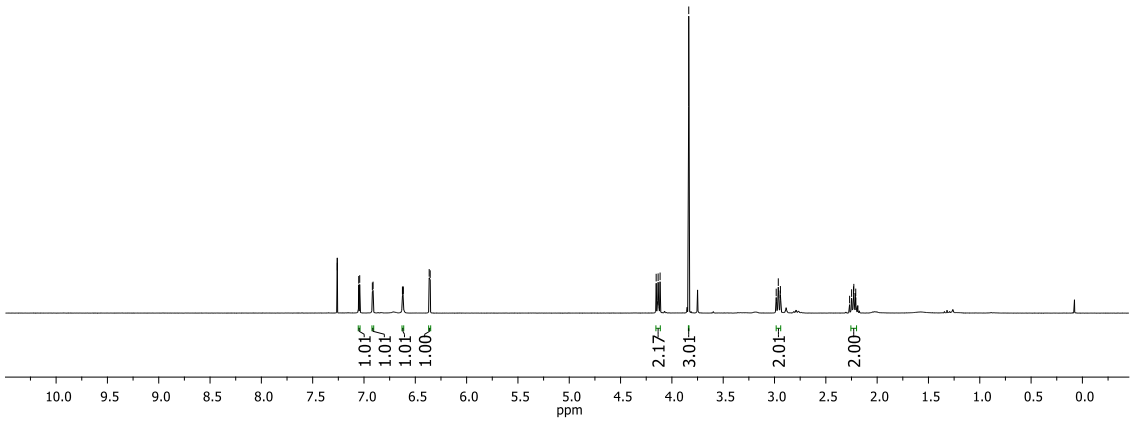

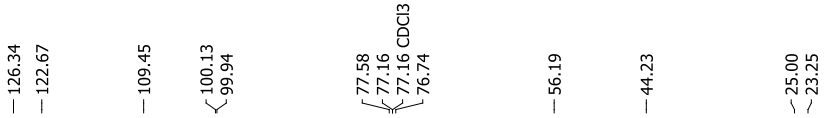

^{13}C NMR Spectrum
(75 MHz, $CDCl_3$)

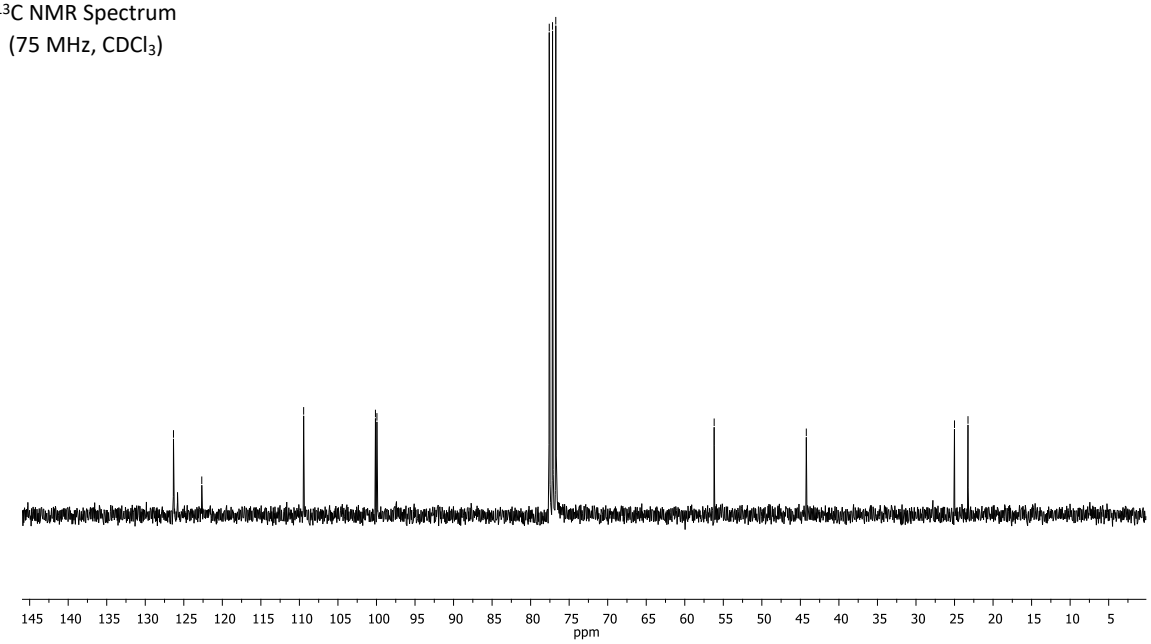

COSY Spectrum
($CDCl_3$)

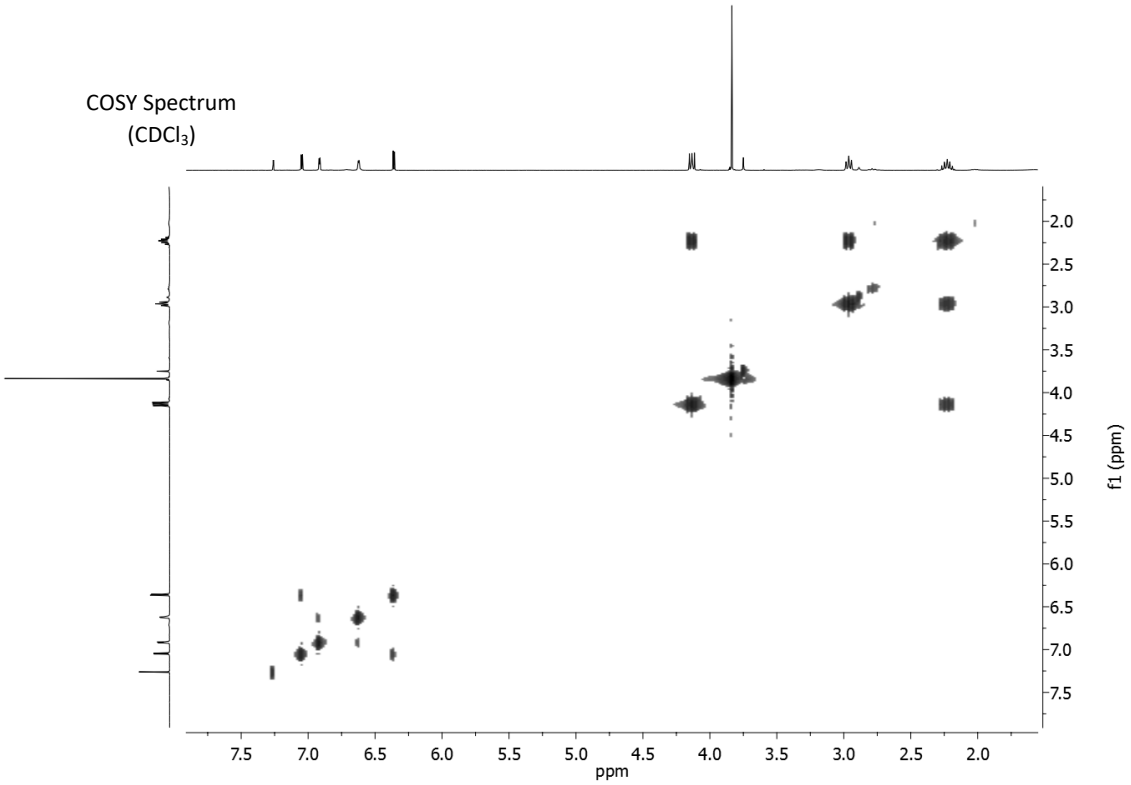

ed-HSQC Spectrum
($CDCl_3$)

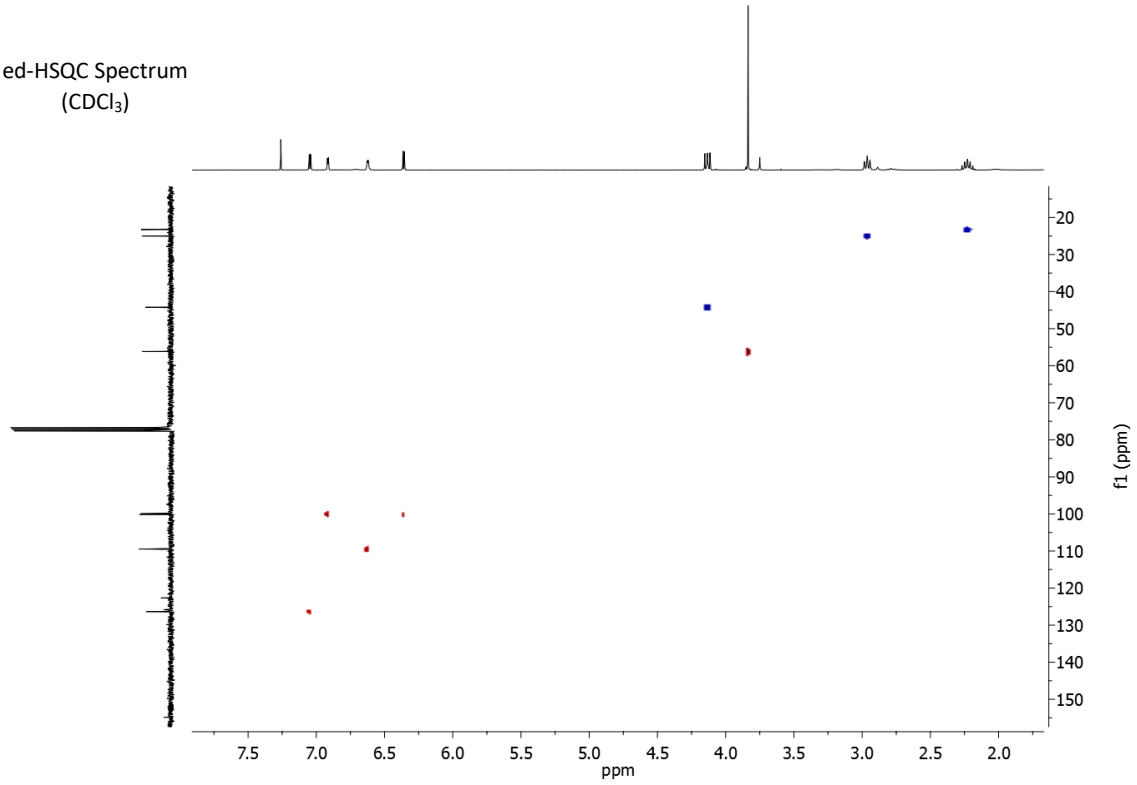

1H-benzimidazole-2-methanol (10)

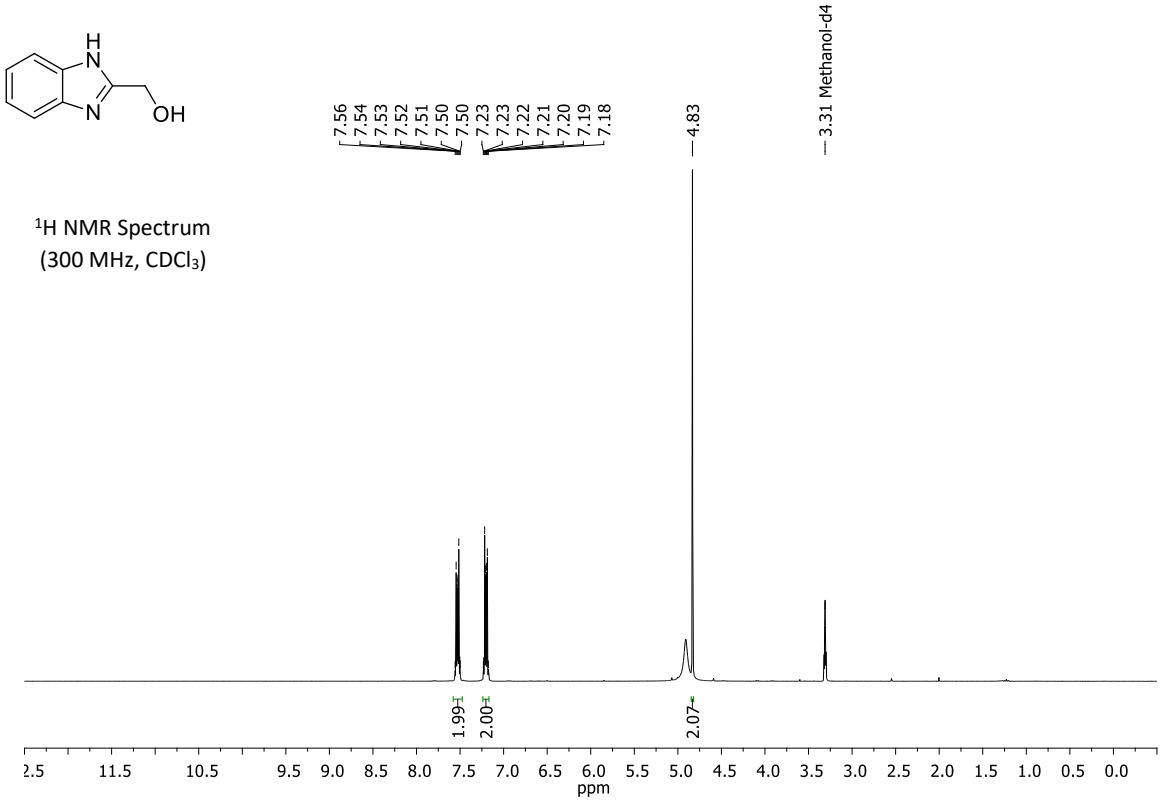

^{1}H NMR Spectrum
(300 MHz, $CDCl_3$)

2,3-dihydro-1H-indole-1-ethanol (14a) and 2-Indol-1-yl-ethanol (14b)

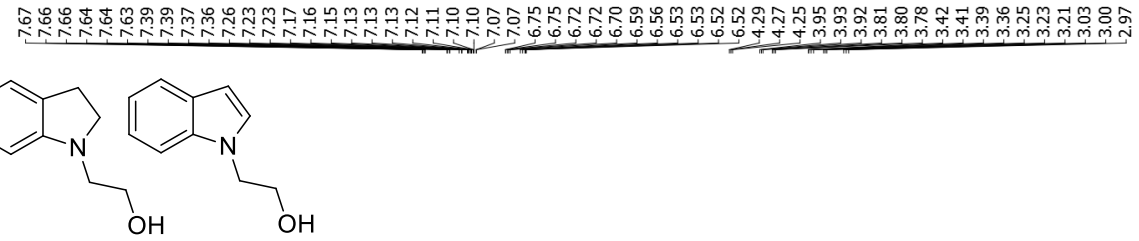

^{1}H NMR Spectrum
(300 MHz, $CDCl_3$)

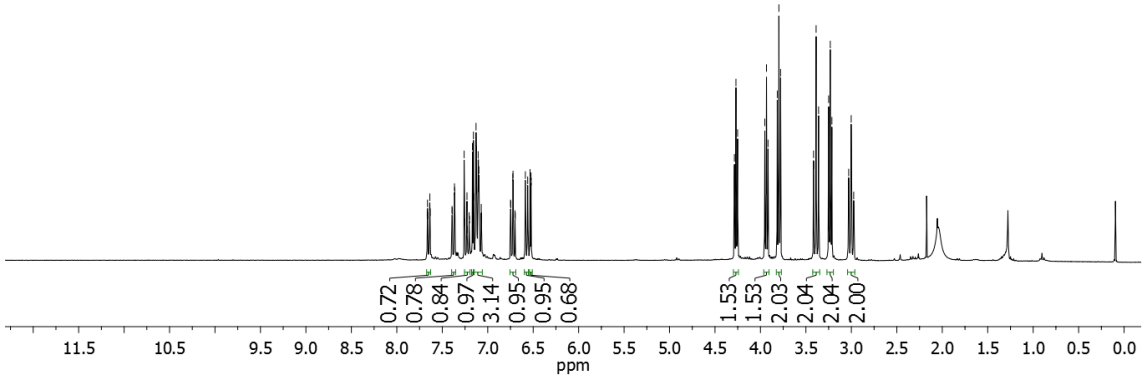

^{13}C NMR Spectrum
(75 MHz, $CDCl_3$)

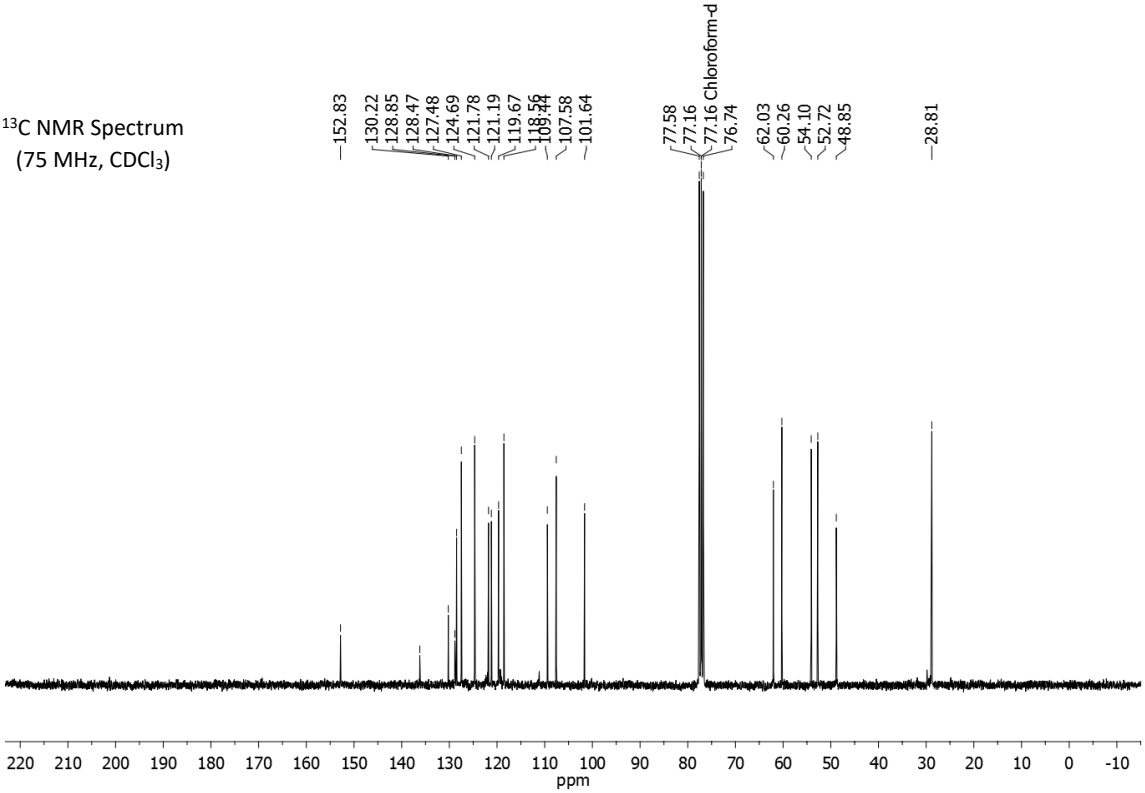

COSY Spectrum
($CDCl_3$)

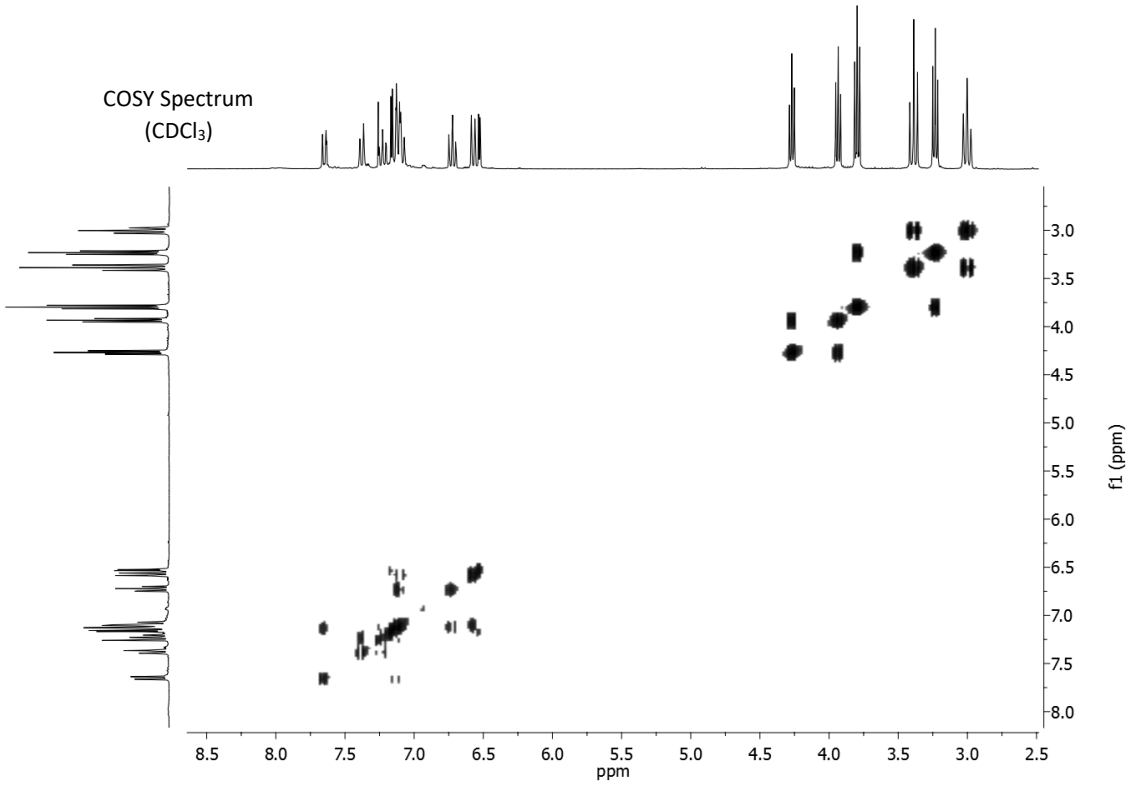

ed-HSQC Spectrum
($CDCl_3$)

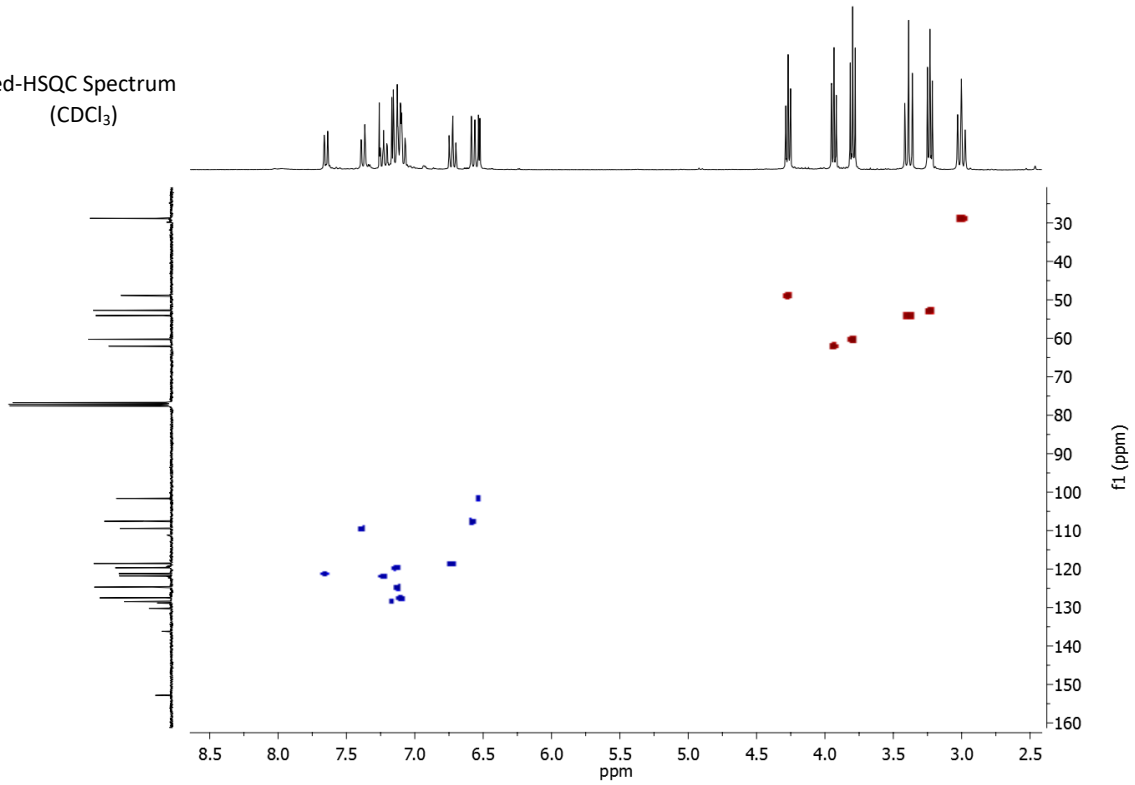

2-(5-methoxyindolin-1-yl)ethanol (15a)

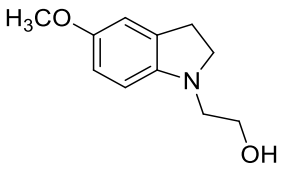

^{1}H NMR Spectrum
(300 MHz, $CDCl_3$)

^{13}C NMR Spectrum
(75 MHz, $CDCl_3$)

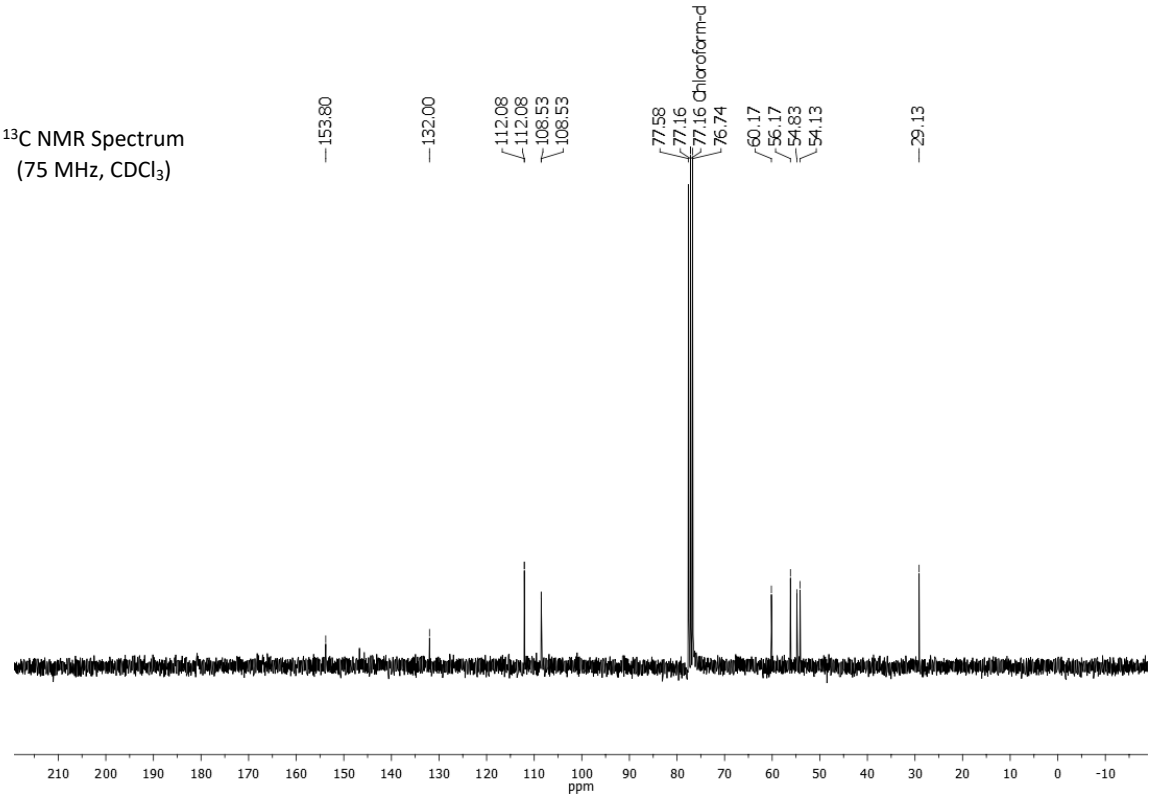

COSY Spectrum
($CDCl_3$)

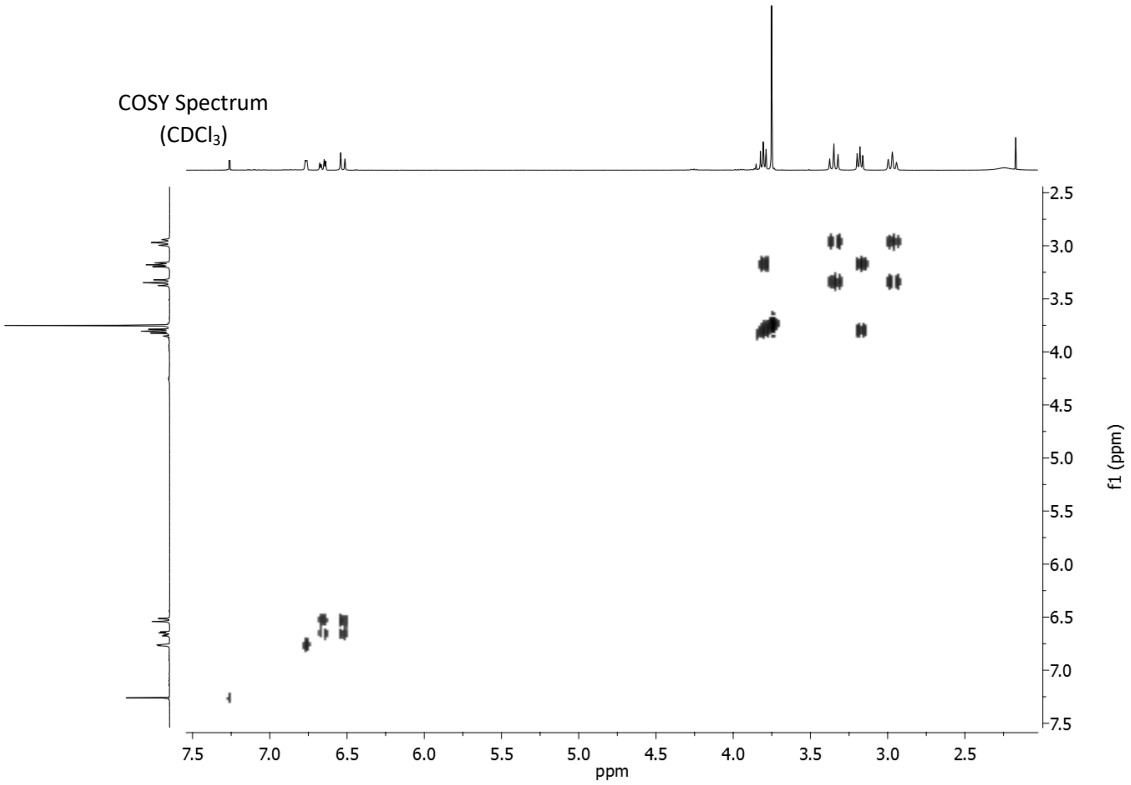

ed-HSQC Spectrum
($CDCl_3$)

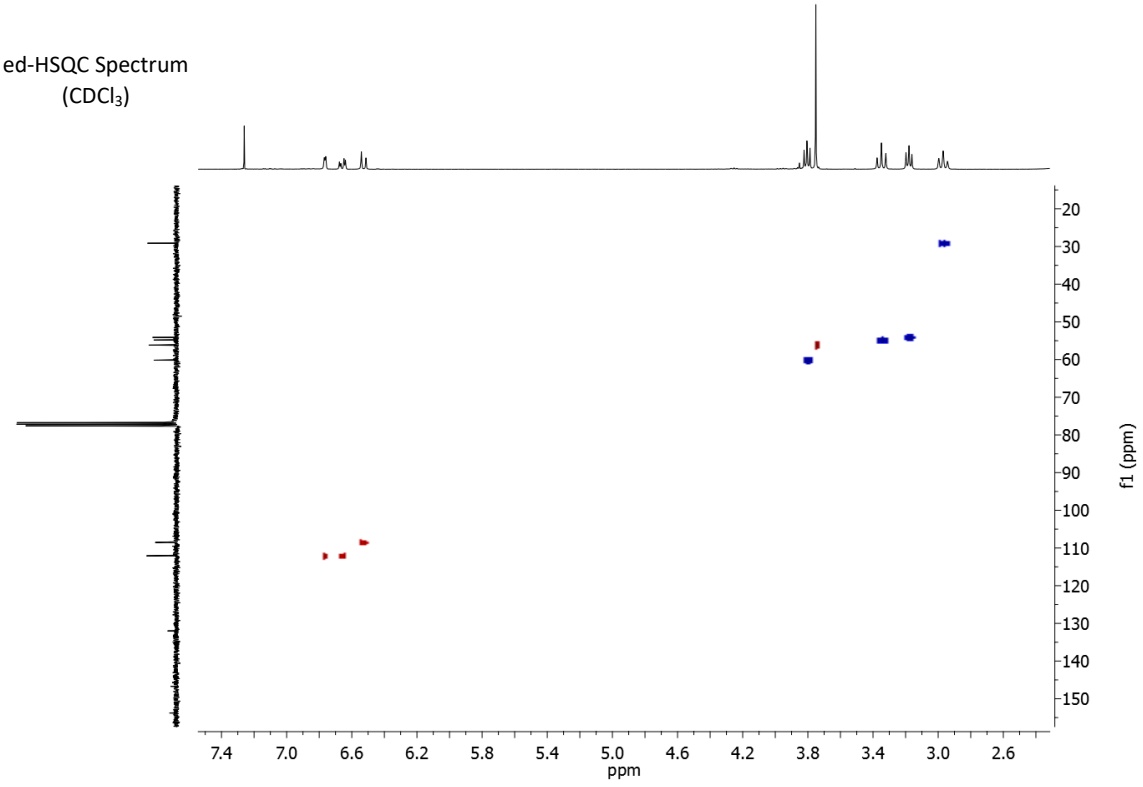

2-(5-methoxy-1H-indol-1-yl)ethanol (15b)

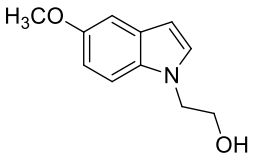

^{1}H NMR Spectrum
(300 MHz, $CDCl_3$)

^{13}C NMR Spectrum
(75 MHz, $CDCl_3$)

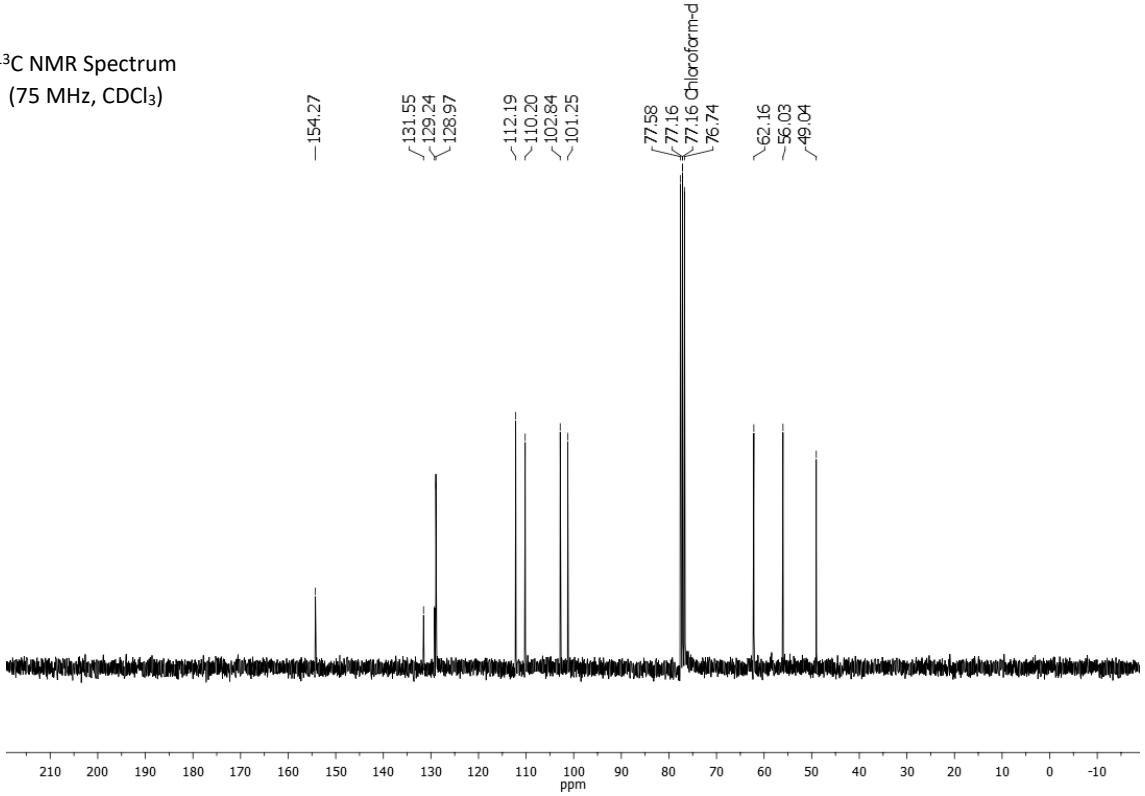

COSY Spectrum
($CDCl_3$)

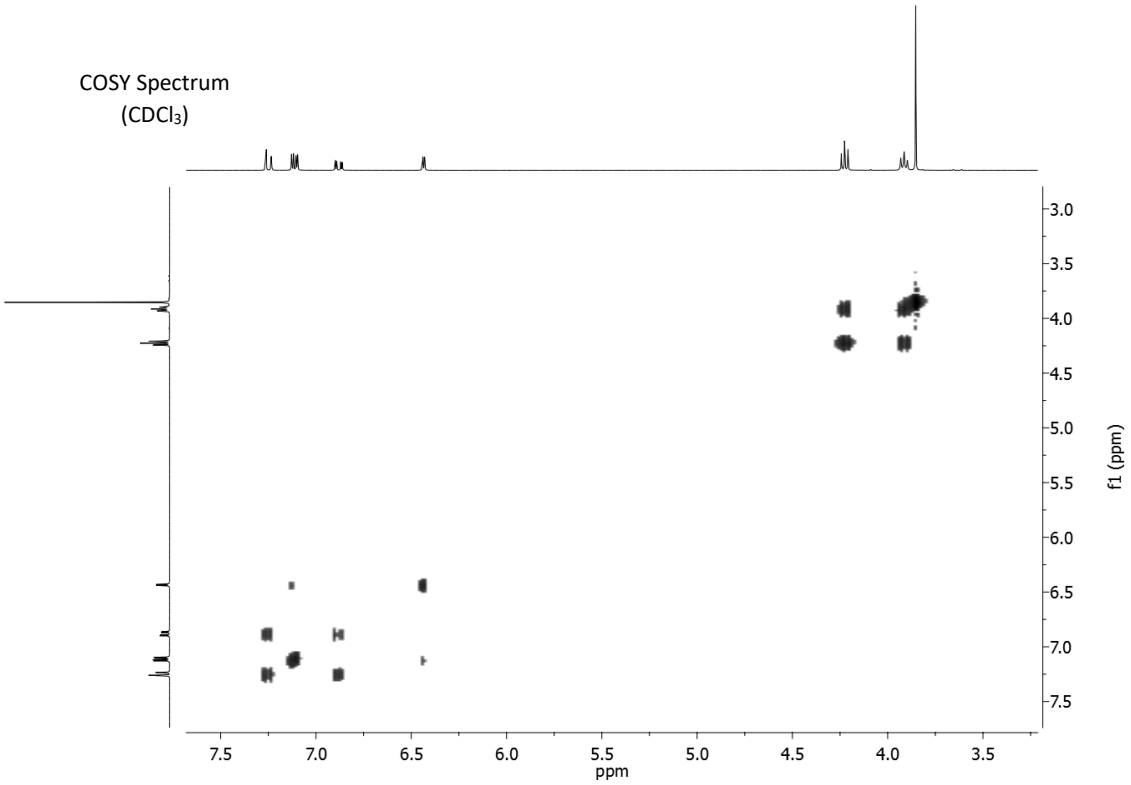

ed-HSQC Spectrum
($CDCl_3$)

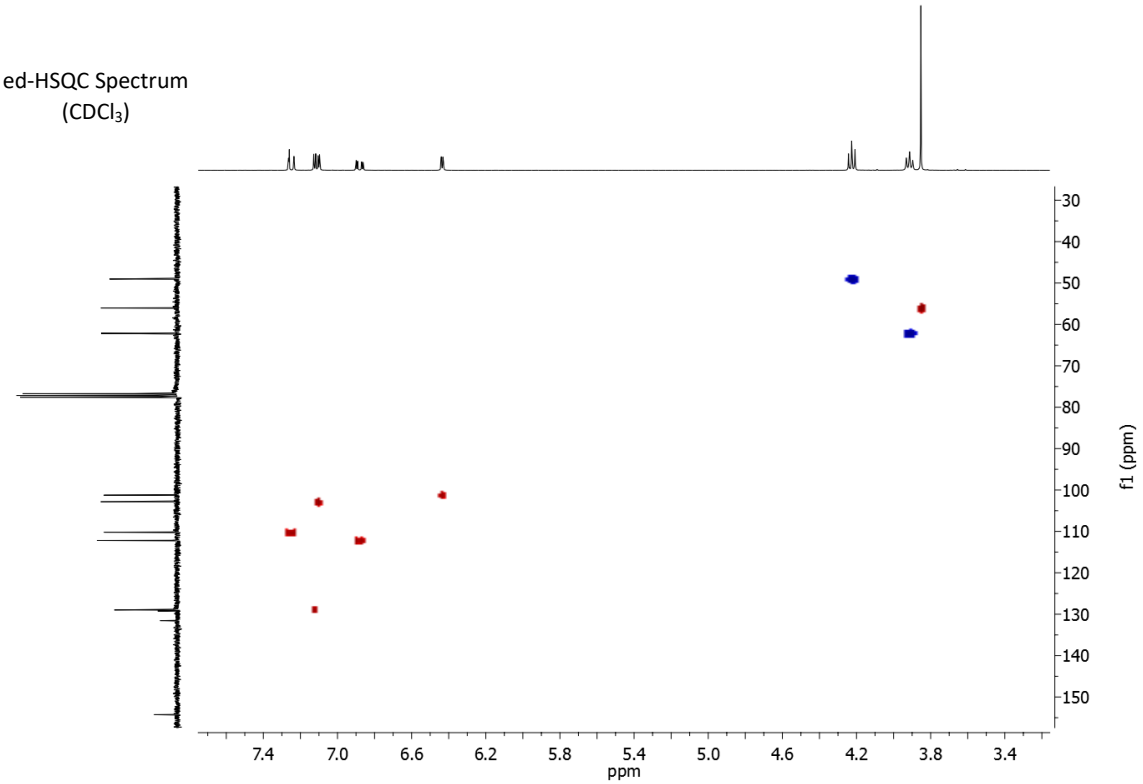

Capítulo 4

Patente Nacional 201600468

QUÍMICA VERDE PARA LA PRODUCCIÓN DE ß-AMINO ALCOHOLES

(19) OFICINA ESPAÑOLA DE PATENTES Y MARCAS

ESPAÑA

(11) Número de publicación: **2 644 751**

(21) Número de solicitud: 201600468

(51) Int. CI.:

C07C 213/08 (2006.01)
C07C 215/68 (2006.01)
B01J 23/44 (2006.01)

(12) SOLICITUD DE PATENTE A1

(22) Fecha de presentación:
31.05.2016

(43) Fecha de publicación de la solicitud:
30.11.2017

(71) Solicitantes:
UNIVERSITAT DE VALÈNCIA (100.0%)
Av. Blasco Ibáñez nº 13
46010 Valencia ES

(72) Inventor/es:
BALLESTEROS CAMPOS , Rafael ;
ABARCA GONZÁLEZ, Mª Belén;
BALLESTEROS GARRIDO , Rafael y
LLABRÉS CAMPANER , Pedro Juan

(54) Título: **Procedimiento de obtención de β-amino alcoholes**

Resumen

Procedimiento de obtención de β-amino alcoholes en el que, a partir de aminas y una mezcla diol/agua, se realizan las etapas de: añadir una mezcla catalítica a la amina de partida, a continuación, agregar la mezcla diol/agua; posteriormente, llevar a cabo la reacción a una temperatura de entre 130 y 200°C, durante 2-24 horas, filtrar el producto de reacción, a base de β-amino alcohol, mediante al menos una primera extracción con hexano y, seguidamente, al menos una segunda extracción con acetato de etilo, a fin de purificar el β-amino alcohol obtenido.

DESCRIPCIÓN

Procedimiento de obtención de β-amino alcoholes.

Objeto de la invención

La presente invención se refiere a un procedimiento de obtención de β-amino alcoholes.

La invención se incluye dentro del sector de la industria química-orgánica, específicamente, la que se encarga de la fabricación de compuestos biológicamente importantes como los aminoácidos o las morfolinas.

Antecedentes de la invención

La activación de alcoholes para alquilar aminas mediante procesos o reacciones de autotransferencia de hidrógeno, a los que también se les conoce como préstamo de hidrógeno o sistema de autoabastecimiento de hidrógenos activos, es una técnica ampliamente utilizada en la síntesis orgánica (*Esquema 1*) de productos de interés industrial. Muestras de ello son los trabajos de J. Williams *et al*,[1] Krische *et al*[2] y de M. Yus *et al*[3]. Una de las ventajas, entre otras, de estos procesos es que se evita el uso de haluros de alquilo más tóxicos. Dentro del tipo de alcoholes utilizados como material de partida para este tipo de reacciones, la mayor parte de los resultados se ha descrito con alcoholes fácilmente oxidables, por ejemplo, el alcohol bencílico y derivados. El uso de alcoholes alquílicos representa un mayor reto.

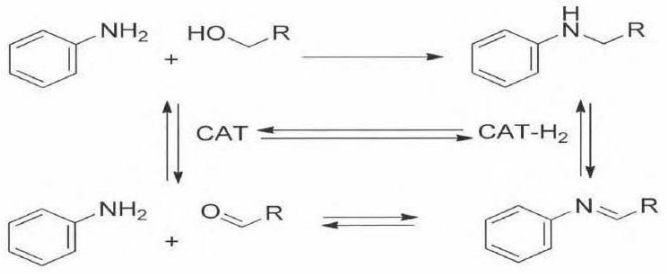

Esquema 1

Estos procesos o reacciones se efectúan mediante el empleo de catalizadores. En el estado de la técnica aparecen descritos catalizadores con un mayor potencial de deshidrogenación, siendo un ejemplo de ellos los que están descritos por Q. Yang *et* al.[4] Sin embargo, la mayor parte de los catalizadores, cuyo uso se ha publicado, son homogéneos, tales como los que describen Yang *et al*.[4] Estos catalizadores consisten en un complejo de un metal de transición con ligandos nitrogenados o con fosforo. Los catalizadores homogéneos, pese a que resultan muy eficaces, tienen una limitada aplicabilidad industrial debido a su coste (la mayoría son complejos de Os, Ru, Ir), su inestabilidad y la imposibilidad de reutilizarlos. Además, en muchas de estas reacciones de autotransferencia de hidrógeno se requiere la participación de co-reactivos como el tert-butóxido de metales alcalinos y disolventes orgánicos.

Debido al interés de este tipo de reacciones (*Esquema 1*), también se han utilizado diferentes sistemas catalizadores heterogéneos, pero fundamentalmente partiendo de alcoholes de tipo bencílico, por ejemplo, K. Shimizu *et al*.[5] Los sistemas heterogéneos se basan en metales de transición (oro, iridio, paladio, rutenio...) soportados sobre alúmina, titania o ferrita.

En general, el uso de dioles como material de partida, específicamente el etilenglicol, en este tipo de reacciones (*Esquema 1*) puede llevar a la obtención de β-amino alcoholes en un paso, pero representa un reto u obstáculo por dos razones. Por un lado, el etilenglicol es mucho más difícil de activar que los alcoholes bencílicos. Los productos de la reacción, el β-amino alcohol o el 2-hidroxietanal (*Esquema 2*), presentan un grupo alcohol que puede ser activado por el catalizador, con lo que podrían degradarse. Por otro lado, y siendo una desventaja técnica a tener en cuenta, usando catalizadores muy potentes, se puede también degradar el etilenglicol.

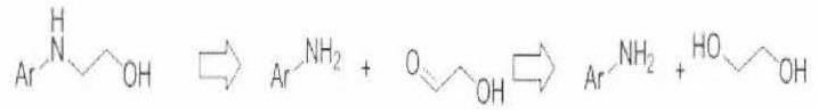

Esquema 2

Los β-amino alcoholes representan un producto de altísimo interés industrial dada su aplicabilidad en la síntesis de compuestos biológicamente relevantes como los aminoácidos o las morfolinas. Por ello, es necesario y tiene una especial relevancia el suministro de un proceso que permita la obtención de β-amino alcoholes de una manera lo menos costosa posible y de una forma lo más respetuosa posible con el medio ambiente.

Los β-amino alcoholes poseen potencial en la preparación de carbenos heterocíclicos, que son aquellos que se usan en muchas reacciones de catálisis. Un ejemplo de sus muchas aplicaciones se puede encontrar en el trabajo de T. J. Donohoe *et al*.[6] Sin embargo, en esta publicación no aparece ningún tipo de reacción que cumpla los criterios de la química verde, conocida en la técnica como la química ecológica, aquélla que respeta el medio ambiente, y, mucho menos, que utilice etilenglicol como material de partida en la preparación de β-amino alcoholes.

Se han encontrado dos referencias, como ejemplos de reacción de activación del etilenglicol, para la obtención de otro tipo de producto: una primera, la publicación de S. Michlik *et al*,[7] que, para sintetizar pirroles, utiliza un catalizador homogéneo (un complejo de iridio) que es muy caro, inestable y con pocas posibilidades de uso a escala industrial, y donde se genera el producto en un 32%; y una segunda, el documento de patente CN103539718, de China Petroleum & Ch. Sinopec Shanghai Research Institute, en donde suponen que el β-amino alcohol es un subproducto de una catálisis a 300ºC, cuyo objetivo es la síntesis de indol y empleo de un metal (Ag, Cu) como catalizador. Sin embargo, en esta última referencia no es aislado el β-amino alcohol.

Como alternativas de aplicación industrial, en el case del etilenglicol, se ha descrito la introducción de una etapa más con carbonato de dietilo para poder activarlo, según M.L Kantam *et al* (8) y A B. Shivarkar *et al*,[9] en donde se transforma el etilenglicol en 1,3-dioxola-2-ona. Sin embargo, este proceso reduce la eficiencia atómica y, además, está lejos de dar rendimientos aceptables.

Es importante tener en cuenta que, salvo los ejemplos arriba citados (Michlik y el documento de patente china), que utilizan etilenglicol, no se conoce ningún proceso real que obtenga β-amino alcoholes directamente del etilenglicol como material de partida sin modificación alguna, en un sistema catalítico heterogéneo.

Si bien existen muchas reacciones publicadas para activar cualquier tipo de alcohol por diferentes vías, todas ellas dan lugar a compuestos diferentes de los β-amino alcoholes. Un ejemplo es la publicación de A. Corma *et al*,[10] en donde se usa Pd/MgO para hacer reaccionar el etilenglicol con aminas; sin embargo, no se consigue obtener amino alcoholes, sino piperazinas u otros derivados, fruto de la polifuncionalización del etilenglicol. Además, un problema fundamental de dicha reacción reside en que el etilenglicol puede degradarse dando polímeros o mezclas de gases (CO/CO_2), en función del potencial del catalizador. A pesar de que existen muchas y muy variadas referencias sobre los procesos de auto-trasferencia de hidrógeno para dar aminas, en lo que concierne a los β-amino alcoholes solo existen los dos ejemplos citados anteriormente.

Por lo anterior, se hace necesario un procedimiento que sea capaz de monofuncionalizar el etilenglicol y en el que no se degrade el producto obtenido, en este caso, un β-amino alcohol.

Se han desarrollado protocolos para la generación de aminas por metodologías verdes, es decir, metodologías que respetan el medio ambiente. Por ejemplo, dos de las últimas publicaciones, que se citan a continuación, representan los primeros desarrollos de los autores en el campo de la autotransferencia de hidrógeno: "An efficient one pot transfer hydrogenation and *N*-alkylation of quinolines with alcohols mediated by Pd/C/Zn" de B. Abarca, R. Adam, R. Ballesteros, *Organic Biomolecular Chemistry*, **2012**, *10*, 1826-1833. DOI: 10.1039/C1OB05888F y "Triazolopyridines. Part 30.1. Hydrogen transfer reactions; pyridylcarbene formation". B. Abarca: R. Adam: S. Alom: R. Ballesteros: S. López-Molina. ARKIVOC, Vol. 2014, Issue 2, pp. 175-186.

Sin embargo, en ninguna de esas dos publicaciones se ha conseguido obtener β-amino alcoholes. Es cierto que el catalizador Pd/C es capaz de realizar procesos de hidrogenación-deshidrogenación; sin embargo, en el caso de esas dos publicaciones, los productos obtenidos han sido aminas terciarias o piridinas. En el caso particular de la primera de las dos publicaciones citadas antes se utiliza una combinación descrita como Pd/C/Zn. Sin embargo, ha de tenerse en cuenta que esa combinación no es un catalizador, ya que el Zn (metal en estado de oxidación 0) aporta electrones que se utilizan para reducir quinolinas (pasando a Zn^{2+}), sino que la misma es un reactivo (además, utilizado en un gran exceso) y no puede ser recuperado al final de la reacción, generando además problemas de escalado debido a la inestabilidad de los metales en estado de oxidación 0 a altas temperatura. En esa primera publicación se utiliza etilenglicol, pero el procedimiento de preparación no emplea, como materiales de partida, las aminas, sino las tetrahidroquinolinas, las cuales poseen propiedades distintas y dan como resultado un producto distinto a los β-amino alcoholes. Téngase en cuenta que, las tetrahidroquinolinas son compuestos que son mucho más difíciles de degradar y presentan una resistencia más elevada a generar sistemas polifuncionalizados. Por tanto, aunque las metodologías arriba citadas son relativamente innovadoras, teniendo en cuenta el gran número de catalizadores para la funcionalización de aminas, no permiten en ningún caso obtener β-amino alcoholes.

Así, no se ha encontrado en el estado de la técnica una publicación, enseñanza o documento de patente que consiga funcionalizar el etilenglicol para generar β-amino alcoholes, mediante el uso de sistemas catalíticos heterogéneos.

Debido a que, a día de hoy, la tendencia se dirige a la producción de catalizadores con mayor potencial, esta representa un problema a la hora de hacer reacciones con más de un centro activo, tal como, la formación de β-amino alcoholes a partir de etilenglicol. Esto es debido a que los catalizadores muy activos o de elevado potencial degradan los productos obtenidos, induciendo multi-funcionalizaciones, como es el caso, por ejemplo, de la publicación de Corma *et al*.[10]

La presente invención resuelve los problemas citados anteriormente y satisface la necesidad de un procedimiento para obtener β-amino alcoholes que es ecológico, se efectúa en un sistema catalítico heterogéneo y a un coste económico lo más bajo posible, y en el que no se degrada el producto obtenido.

Descripción de la invención

La presente invención suministra un procedimiento para obtener β-amino alcoholes que, a partir de una amina y una mezcla de diol/agua, se efectúa en un sistema catalítico heterogéneo y comprende las siguientes etapas:

- a la amina de partida, se añaden una mezcla catalítica sólida que comprende un metal soportado y un coactivante inorgánico sólido con carácter acido-base,

- a continuación, se agrega la mezcla diol/agua;

- posteriormente, se lleva a cabo la reacción, a una temperatura de entre 130 y 200ºC, durante 2 a 24 horas.

- se filtra el producto de reacción, a base de β-amino alcohol, a través de un filtro microporoso, mediante al menos una extracción con hexano y, seguidamente, al menos una segunda extracción con acetato de etilo, a fin de purificar el β-amino alcohol obtenido.

Por lo anterior, el presente proceso plantea un punto de inflexión en la concepción de catalizadores empleados en procesos de autotransferencia de hidrógeno. Por otra parte, es el único ejemplo de utilización de un sistema catalizador heterogéneo que es capaz de mono funcionalizar el etilenglicol para generar β-amino alcoholes y no degradar el producto formado (β-amino alcohol).

Mediante este procedimiento se trabaja con una mezcla catalítica que comprende un metal, soportado sobre un sustrato, y un coactivante sólido inorgánico, cuya función es catalítica también. Opcionalmente, este metal es seleccionado de entre los metales de los grupos IIIB a IIB del sistema periódico de elementos. También, opcionalmente, éste puede ser óxidos e hidróxidos de dichos metales de transición, y una aleación de Pt-Sn. Preferiblemente, el metal soportado es un metal seleccionado de entre los siguientes elementos: Pd, Au, Pt, Cu, Ag, Ru, óxidos e hidróxidos de éstos.

Opcionalmente, el metal está soportado sobre un sustrato sólido que es seleccionado de entre los siguientes elementos: TiO_2, Al_2O_3, SiO_2, Fe_3O_4, Fe_2O_3, MgO, Ga_2O, CeO_2, NiO, zeolitas, grafito, grafeno, óxido de grafeno, diamante, nanotubos de carbón, negro de carbón.

Esta mezcla catalítica, es decir, el metal soportado sobre un sustrato sólido y el coactivante inorgánico sólido, permite activar el diol presente en una mezcla diol/gua, generando así aldehídos e hidrógeno. En presencia de aminas aromáticas, se forman iminas, las cuales son hidrogenadas (con el mismo hidrógeno que se había generado en la primera parte) para

obtener una amina secundaria y una molécula de agua como subproducto. Este procedimiento permite obtener β-amino alcoholes, evitándose la poli funcionalización, dado que al pasar por vía imina, la reacción es más difícil para el producto. Además, al utilizar el diol, como disolvente, se evita la degradación del producto por el propio catalizador.

Opcionalmente, después de obtener los β-amino alcoholes se recupera la mezcla catalítica (metal soportado y coactivante inorgánico sólido con carácter ácido-base) a través de una operación de filtrado y lavado con hexano/acetato de etilo y, posteriormente, un secado entre 140 y 160ºC, durante 2 a 6 horas.

Opcionalmente, el coactivante sólido inorgánico con carácter ácido-base se selecciona de entre los siguientes óxidos: CaO, BaO, ZnO, CeO_2, Al_2O_3, MgO, TiO_2, SiO_2. Preferiblemente, se seleccionan el ZnO, el SiO_2 y el Al_2O_3. Estos coactivantes sólidos, al estar en su estado de oxidación más estable y dadas las condiciones de reacción, permanecen inalterados durante todo el proceso catalítico y actúan (pese a su cantidad) como catalizadores. Por eso, se les denota como coactivantes. Quedan excluidos todos aquellos sólidos que no puedan soportar dichas condiciones (metales en estados de oxidación bajos o en forma metálica). Como opción preferente de coactivante se selecciona el ZnO.

Opcionalmente, la mezcla catalítica que se añade a la amina comprende paladio soportado sobre carbono y ZnO (coactivante solido inorgánico).

Al utilizar esta mezcla catalítica (catalizador soportado y coactivante sólido inorgánico con carácter ácido-base), se obtienen β-amino alcoholes, dado que el coactivante ayuda al metal soportado a realizar la primera etapa, pero al tratarse de dos sólidos independientes, la reacción es mucho más suave y no se degradan los productos (β-amino alcoholes). Esta mezcla de dos sólidos es extremadamente rara en catálisis, dado que solamente uno de los compuestos empleados es sólido en prácticamente el 100% de los catalizadores. En la presente invención son dos sólidos. Esto conlleva lógicamente mayores tiempos de reacción, quedando en cualquier caso en valores aceptables (12-70 h).

Se ha descubierto que la reacción donde se utiliza un catalizador y participa un coactivante del etilenglicol, desempeñando una función catalítica, es decir, sin que se transforme a lo largo de la reacción, permite sorprendentemente obtener β-amino alcoholes. Y, además, este coactivante no es capaz de degradar estos productos.

Por tanto, los amino alcoholes son obtenidos y aislados mediante una mezcla catalítica en un sistema heterogéneo, contrariamente a lo que ocurre en prácticamente todas las reacciones con etilenglicol descritas hasta ahora en los antecedentes de la técnica.

Opcionalmente, el diol comprendido en la mezcla diol-agua puede ser uno del siguiente grupo formado por: 1,2-etanodiol (etilenglicol), 1,2-propanodiol, 2,3-butanodiol, 1-feniletano-1,2-diol, 1,3-propanol, 1,2-ciclohexanodiol, 1,3-butanodiol y el triol glicerol, así como derivados cíclicos que por transformación dan dioles, tales como, el óxido de estireno. Preferiblemente, se seleccionan el 1,2-etanodiol (etilenglicol), y el 1,2-propanodiol. Las mezclas comprenden diferentes proporciones, desde 1/100 (diol/agua) a 100/1, v/v. En ningún caso se utilizan otros disolventes y mucho menos halogenados.

Las aminas de difícil oxidación comprenden aminas que no puedan dar lugar a una imina vía des-hidrogenación de forma rápida. Opcionalmente, como material de partida de la presente invención, se seleccionan aminas aromáticas de fórmula H_2N-Ar, donde Ar (grupo arilo) puede ser fenilo, orto/meta/para metilfenil, orto/meta/para nitrofenil orto/meta/para fluorofenil,

orto/meta/para aminofenil, orto/meta/para trifluorometilfenil, orto/meta/para trifluorometoxifenil, 2,3; 3,4; 4,5; 2,4; 2,5-dimetilfenil, 3,4,5-trimetilfenil, antracil o naftil. Opcionalmente, se puede seleccionar la *t*-butilamina.

Según otra realización opcional, la amina es una amina heterocíclica. Por ejemplo, piridinas, tiofenos, tiazoles, triazoles, quinolinas. Opcionalmente, se selecciona la tetrahidroquinolina.

El procedimiento se caracteriza por ser una reacción catalítica en un sistema heterogéneo, es decir, que tanto el propio catalizador como el coactivante se pueden recuperar por filtración y ser reutilizados. Además, no se requiere de pre-activación del diol. Tanto los reactivos, como los disolventes no poseen átomos de halógenos y las temperaturas de trabajo son asequibles industrialmente. Además, los rendimientos son superiores a todos los publicados hasta la fecha para dicha reacción o las derivadas con dietil carbonato. Es importante remarcar que la mezcla a la que se refiere esta invención es la única capaz de activar dioles de forma controlada evitando polimerizaciones.

Ventajas del presente procedimiento respecto del estado de la técnica:

- Reducción de costes: el agua y el etilenglicol son económicamente aceptables; el presente procedimiento de obtención de β-amino alcoholes es el único protocolo heterogéneo que no requiere activación con carbonato de dietilo a altas temperaturas. No se utiliza ningún metal de transición en disolución, lo cual reduce significativamente el coste del proceso. La reacción no requiere de ligandos fosforados para funcionar, lo que también tiene una repercusión en el coste total del proceso. Ninguna molécula utilizada en este proceso requiere condiciones anhidras o en atmósfera inerte. Tanto los catalizadores como los reactivos, los disolventes y los productos son estables al aire y la humedad, y pueden ser guardados en contenedores normales. Es decir, no se requiere el uso de cámara de guantes para conservar los catalizadores, como es el caso de muchos complejos de metales de transición que se usan en catálisis homogénea. Por ello, se reduce mucho los costes indirectos de la aplicación de la metodología. Los productos utilizados son comerciales y se usan sin ninguna purificación extra. No es necesario un tratamiento previo de ninguno de los componentes de esta aplicación.

- Reducción de residuos: al ser un procedimiento caracterizado por ser una catálisis heterogénea, el catalizador puede ser retirado sin mucha dificultad; puede ser reactivado y reutilizado, minimizando así los residuos y maximizando su precio; por otro lado, la presente invención permite no degradar de manera excesiva el disolvente, al generar crudos de reacción limpios y muy pocos productos secundarios. Además, es posible una purificación de los productos mediante extracción selectiva, una primera, que se lleva las impurezas y una segunda, que se queda con el amino alcohol.

- Reducción de compuestos halogenados: no se utiliza ningún haloderivado (cancerígenos), ni como reactivo ni como disolvente en la extracción o purificación. El catalizador puede ser reactivado con acetato de etilo.

- Economía atómica: el diol actúa como disolvente y reactivo, siendo además activado sin necesidad de transformación química; además, la reacción solo genera como subproducto una molécula de agua.

- Temperaturas moderadas: la presente invención permite un procedimiento de uso en donde se trabaja en un intervalo de temperaturas de entre 130 y 200ºC, preferiblemente una temperatura de trabajo que ronda los 150ºC, pudiendo ser fácilmente aplicable a nivel industrial.

Ejemplos de realización

En un recipiente de teflón primeramente se mezclaron la amina de partida (1 mmol), un catalizador de paladio sobre carbono, Pd/C (7%), y ZnO (3 eq); y, en segundo lugar, se adicionaron 12 ml de una mezcla de etilenglicol/agua al 50% v/v, para formar una mezcla de reacción. La mezcla de reacción se introdujo en una autoclave, el cual se cerró y se introdujo en una estufa a 150ºC, durante 24 h. Se dejó enfriar hasta temperatura ambiente, durante aproximadamente 2 h.

La mezcla de reacción se sometió a filtración mediante un filtro microporoso de jeringa, de 0,45 µm y de material de politetrafluoroetileno, PTFE, (VWR International). A continuación, se extrajo con acetato de etilo, AcOEt, (3x30 ml). La fase orgánica se secó con Na_2S0_4, se filtró por gravedad y se evaporó el disolvente a vacío.

El producto de reacción, crudo, fue purificado en un cromatotrón, utilizando como eluyentes hexano y AcOEt, obteniendo aminoalcoholes puros.

- 2-*p*-tolilaminoetanol, partiendo de *p*-tolilamina y etilenglicol

^{1}H NMR (300 MHz, $CDCl_3$) δ: 7.01 (d. 2H, J = 8 Hz, ArH), 6.61 (d. 2H, J = 8 Hz, ArH), 3.80 (t, 2H, J = 5 Hz, CH2), 3.27 (1, 2H, J = 5Hz), 2.9 (br s, 2H, NH and OH), 2.26 (s, 3H, Me).

^{13}C NMR (75 MHz, $CDCl_3$) δ: 146.0(1C, C), 130.0(1C, C), 127.4(1C, CH), 113.7(1C, CH), 61.4(1C, CH_2), 46.7(1C, CH_2), 20.6(1 C, CH_3),

Rendimiento aislado: 84%

Rendimiento aislado escala 1 gramo, con extracción selectiva, dos extracciones con hexano seguidas de dos con acetato de etilo (estas dos últimas contienen el producto) 45%.

- 2-*o*-tolilaminoetanol, partiendo de *o*-tolilamina y etilenglicol

^{1}H NMR (300 MHz, $CDCl_3$) δ: 7.03 (m, 2H), 6.60 (m, 2H), 3.78 (t, J=5.1 Hz, 2H), 3.26 (t, J=5.1 Hz, 2H), 2.09 (s, 3H).

^{13}C NMR (75 MHz, $CDCl_3$) δ: 145.9 (1C, C), 130.2 (1C, C), 127.1 (1C, CH), 122.6 (1C, CH), 117.6 (1 C, CH), 110.2 (1C, CH), 61.1 (1C, CH_2), 46.1 (1C, CH_2), 17.7 (1 C, CH_3).

HRMS [M+H$^+$]: 152.0994

Rendimiento aislado: 28%

- 2-*m*-tolilaminoetanol, partiendo de *m*-tolilamina y etilenglicol

^{1}H NMR (300 M Hz, $COCl_3$) δ: 7.00 (dd, J=11.0; 5.1 Hz, 1 H). 6.44 (m, 3H). 3.71 (t, J=5.2 50 Hz, 2H), 3.19 (t. J=5.2 Hz, 2H), 2.82 (s, 1H), 2.20 (s, 3H).

^{13}C NMR (75 MHz, $CDCl_3$) δ: 148.44 (1C, C), 139.54 (1C, C), 129.59 (1C, CH), 119.41 (1C, CH), 114.54 (1C, CH), 110.90 (1C, CH), 61.71 (1C, CH_2), 46.66 (1C, CH_2), 22.00 (1C, CH_3).

Rendimiento aislado: 39%

- 2-((2,3-dimetilfenil)amino)etanol, partiendo de 2,3-dimetilanilina y etilenglicol

^{1}H NMR (300 MHz, $CDCl_3$) δ: 7.04 (t. J = 7.8 Hz, 1 H), 6.64 (d, J = 7.5 Hz, 1 H), 6.56 (d, J = 8.1 Hz, 1H), 3.87 (t, J = 5.2, 2H), 3.34 (t, J = 5.2, 2H), 2.30 (s, 3H), 2.09 (s, 3H).

^{13}C NMR (75 MHz, $CDCl_3$) δ: 146.06 (1C, C), 136.87 (1C, C), 126.29 (1C, CH), 121.15 (1C, C), 120.03 (1C, CH), 108.55 (1C, CH), 61.37 (1C, CH_2), 46.48 (1C, CH_2), 20.81 (1C, CH_3), 12.65 (1C, CH_3).

HRMS [M+H$^+$]: 166.1219

Rendimiento aislado: 35%

- 2-((2,4-dimetilfenil)amino)etanol, partiendo de 2,4-dimetilanilina y etilenglicol

^{1}H NMR (300 MHz, $CDCl_3$) δ 6.94 (d, J = 8.1 Hz, 1H), 6.91 (s, 1H), 6.58 (d, J = 8.0 Hz, 1H), 3.86 (t, J = 5.2, 2H), 3.33 (t, J = 5.2, 2H), 2.24 (s, 3H), 2.15 (s, 3H).

^{13}C NMR (75 MHz, $CDCl_3$) δ 143.77 (1C, C), 131.27 (1C, CH), 127.47 (1C, CH), 126.97 25 (1C, C), 122.99 (1C, C), 110.61 (1C, CH), 61.37 (1C, CH_2), 46.53 (1C, CH_2), 20.46 (1C, CH_3), 17.58 (1C, CH_3).

HRMS [M+H$^+$]: 166.1217

Rendimiento aislado: 23%

- 2-((3,5-dimetilfenil)amino)etanol, partiendo de 3,5-dimetilanilina y etilenglicol

^{1}H NMR (300 M Hz, $CDCl_3$) δ: 6.43 (s, 1H), 6.31 (s, 2H), 3.80 (t. J=5.2 Hz, 2H), 3.28 (t, 35 J=5.2 Hz, 2H), 2.27 (s, 6H).

^{13}C NMR (300 MHz, $CDCl_3$) δ: 148.28 (1C, C), 139.06 (2C, C), 120.08 (1C, CH), 111.37 (2C, CH), 61.35 (1C, CH_2), 46.31 (1C, CH_2), 21.56 (2C, CH_3).

HRMS [M+H$^+$]: 166.1219

Rendimiento aislado: 30%

- 2-((3,4-dimetilfenil)amino)etanol, partiendo de 3,4-dimetilanilina y etilenglicol

^{1}H NMR (300 MHz, $CDCl_3$) δ: 6.96 (d, J=8.0 Hz, 1H), 6.50 (d, J=2.4 Hz, 1H), 6.44 (dd, J=8.0; 2.5, 1H), 3.81 (t. J=5.4 Hz, 2H), 3.28 (t, J=5.3 Hz, 2H), 2.72 (s, 1H), 2.21 (s, 3H), 2.17 (s, 3H).

^{13}C NMR (300 MHz, $CDCl_3$) δ: 146.33 (1C, C), 137.52 (1C, C), 130.45 (1C, CH), 126.22 (1C, C), 115.40 (1C, CH), 110.96 (1C, CH), 61.43 (1C, CH_2), 46.69 (1C, CH_2), 20.14 (1C, CH_3), 18.80 (1C, CH_3).

HRMS [M+H$^+$]: 166.1225

Rendimiento aislado: 30%

- 2-((2,5-dimetilfenil)amino)etanol, partiendo de 2,5-dimetilanilina y etilenglicol

^{1}H NMR (300 MHz, CDCl3) δ: 6.96 (d. J=7.4 Hz, 1 H), 6.53 (d, J=7.5 Hz, 1 H), 6.49 (s, 1H), 3.87 (t, J=5.3 Hz, 2H), 3.35 (t, J=5.3 Hz, 2H), 2.31 (s, 3H), 2.14 (s, 3H).

^{13}C NMR (300 MHz, CDCl3) δ: 146.24 (1C, C), 137.15 (1C, C), 130.50 (1C, CH), 120.04 10 (1C, C), 118.59 (1C, CH), 111.51 (1C, CH), 61.68 (1C, CH2), 46.48 (1C, CH2), 20.93 (1C, CH3), 17.45 (1C, CH3).

HRMS [M+H^{+}]: 166.1220

Rendimiento aislado: 30%

- 2-(naftalen-2-ilamino)etanol, partiendo de 2-amino naftaleno y etilenglicol

^{1}H NMR (300 MHz, CDCl3) δ: 7.68 (dd, J=8.1; 0.6 Hz, 1H), 7.64 (d, J=8.6 Hz, 1C), 7.62 20 (dd, J=8.1; 0.6 Hz, 1H), 7.37 (ddd, J=8.2; 6.8; 1.3 Hz, 1C). 7.22 (ddd, J=8.1; 6.9; 1.2 Hz, 1C), 6.94 (dd, J=8.7; 2.4 Hz. 1C), 6.90 (d, J=2.3 Hz, 1C), 3.91 (t, J=5.2 Hz, 2H), 3.42 (d, J=5.2 Hz, 2H), 3.00 (s, 1H).

^{13}C NMR (300 MHz, CDCl3) δ: 145.5 (1C, C), 135.16 (1C, C), 129.22 (1C, CH), 128.05 25 (1C, C), 127.79 (1C, CH), 126.56 (1C, CH), 126.17 (1C, CH), 122.53 (1C, CH), 118.38 (1C, CH), 105.64 (1C, CH), 61.20 (1C, CH2), 46.57 (1C, CH2).

HRMS [M+H^{+}]: 188.1058

Rendimiento aislado: 19%

- 2-((3-fluorofenil)amino)etanol, partiendo de 3-fluoroanilina y etilenglicol

^{1}H NMR (300 MHz, $CDCl_3$) δ: 7.03 (td, J=8.1; 6.7 Hz, 1C), 6.34 (m, 2H), 6.26 (dt, J=11.5; 35 2.3 Hz, 1C), 3.76 (t, J=5.2 Hz, 2H), 3.21 (t, J=5.2 Hz, 2H).

^{13}C NMR (300 MHz, $CDCl_3$) δ: 162.48 (1C, C), 149.78 (1C, C), 130.40 (1C, CH), 109.07 (1C, CH), 104.39 (1C, CH), 99.96 (1C, CH), 61.07 (1C, CH_2), 45.94 (1C, CH_2).

HRMS [M+H^{+}]: 156.0807

Rendimiento aislado: 32%

- 2-((2-fluorofenil)amino)etanol, partiendo de 2-fluoroanilina y etilenglicol

^{1}H NMR (300 MHz, $CDCl_3$) δ: 7.00 (m, 2H), 6.76 (td, J=8.4; 1.5 Hz, 1H), 6.66 (m, 1H), 3.86 (t, J=5.2 Hz, 2H), 3.35 (t, J=5.2 Hz, 2H).

^{13}C NMR (300 MHz, $CDCl_3$) δ: X (1C, C), X (1C, C), 124.76 (1C, CH), 117.58 (1C, CH), 50 114.88 (1C, CH), 112.74 (1C, CH), 61.38 (1C, CH_2), 46.04 (1H, CH_2).

HRMS [M+H^{+}]: 156.0811

Rendimiento aislado: 23%

- 2-((2-(trifluorometil)fenil)amino)etanol, partiendo de 2-trifluormetilanilina y etilenglicol

^{1}H NMR (300 MHz, $CDCl_3$) δ: 7.81 (ddd, J=8.0; 1.6; 0.5 Hz. 1H), 7.21 (m, 1H), 6.58 (m, 5 2H), 4.34 (t, J=4.6 Hz, 2H), 3.87 (t, J=4.6 Hz, 2H).

^{13}C NMR (300 MHz, $CDCl_3$) δ: 168.78 (1C, C), 150.97 (1C, C), 134.79 (1C, CH), 131.63 (1C, CH), 117.19 (1C, CH), 116.76 (1C, CH), 66.50 (1C, CH_2), 61.96 (1C, CH_2).

Rendimiento aislado: 41%

- 2-((2-(trifluorometoxi)fenil)amino)etanol, partiendo de 2-metoxianilina y etilenglicol

^{1}H NMR (300 MHz, $CDCl_3$) δ: 7.07 (m, 2H), 6.70 (dd, J=8.5; 1.5 Hz, 1H), 6.62 (m, 1H), 15 3.78 (t, J=5.2 Hz, 2H), 3.28 (t, J=5.2 Hz, 2H).

^{13}C NMR (300 MHz, $CDCl_3$) δ: 140.88 (1C, C), 134.89 (1C, C), 128.08 (1C, CH), 121.39 (1C, CH), 117.40 (1C, CH), 112.75 (1C, CH), 61.49 (1C, CH_2), 46.05 (1C, CH_2).

Rendimiento aislado: 8%

- 2-((3,4,5-(trimetoxi)fenil)amino)etanol, partiendo de 3,4,5-trimetoxianilina y etilenglicol

^{1}H NMR (400 MHz, $CDCl_3$) δ: 5.89 (s, 2 H), 3.83 (t. J=5.3 Hz, 2 H), 3.81 (s, 6 H), 3.76 (s, 25 3H). 3.27 (t. J=5.3 Hz, 2H).

^{13}C NMR (100 MHz, $CDCl_3$) δ: 153.9 (1C, C), 144, (1C, C) 9, 92.6 (1C, CH), 90.8 (1C, CH), 61.3, (1C, CH_3), 61.1, (1C, CH_3) 55.9, (1C, CH_2) 46.6(1C, CH_2).

HRMS [M+H^+]: 228.1230

Rendimiento aislado: 16%

Referencias bibliográficas

1. "Borrowing Hydrogen in the Activation of Alcohols". Advanced Synthesis Catalysis, Volume 349, Issue 10, pp. 1555-1575. Jul. 2, 2007.

2. "Catalytic carbonyl addition through transfer hydrogenation: a departure from preformed organometallic reagents". ACIEE (Angewandte Chemical International Edition in English), Vol. 48(1). 34-46 (Online ISSN: 1521-3773). 2009.

3. "Hydrogen Autotransfer in the N-Alkylation of Amines and Related Compounds using Alcohols and Amines as Electrophiles". Chemicals Review, 110 (3), pp 1611-1641. 2010.

4. "Substitution of alcohols by N-nucleophiles via transition metal-catalyzed dehydrogenation". Chemical Society Review, 44, pp. 2305-2329. 2015.

5. "Heterogeneous catalysis for the direct synthesis of chemicals by borrowing hydrogen methodology". Catalysis Science & Technology, 5, 1412-1427. 2015.

6. "Recent Developments in Methodology for the Direct Oxyamination of Olefins". Chemistry A European Journal. Vol. 17, Issue 1, pp. 58-76. Jan. 3, 2011.

7. "A sustainable catalytic pyrrole synthesis". Nature Chemistry,140-144. Jan. 20, 2013.

8. "An Efficient Synthesis of Organic Carbonates using Nanocrystalline Magnesium Oxide". Advanced Synthesis & Catalysis, Vol. 349, Issue 10, pp 1671 -1675, 2007.

9. "Tandem Synthesis of β-Amino Alcohols from Aniline, Dialkyl Carbonate, and Ethylene Glycol". Industrial & Engineering Chemistry Research, 47(8), pp 2484-2494. 2008.

10. "A Bifunctional Pd/MgO Solid Catalyst for the One-Pot Selective N-Monoalkylation of Amines with Alcohols". Chemistry A European Journal, Vol. 16, Issue 1, pp. 254-260, 2010.

REIVINDICACIONES

1. Procedimiento de obtención de β-amino alcoholes que, a partir de una amina y una mezcla de diol/agua, se **caracteriza** por efectuarse en un sistema catalítico heterogéneo y comprender las siguientes etapas:

- se añade una mezcla catalítica sólida que comprende un metal soportado y un coactivante inorgánico sólido con carácter ácido-base, a la amina de partida,

- a continuación, se agrega la mezcla diol/agua,

- posteriormente, se lleva a cabo la reacción a una temperatura de entre 130 y 200ºC, durante 2-24 horas.

- se filtra el producto de reacción, a base de β-amino alcohol, a través de un filtro microporoso, mediante al menos una primera extracción con hexano y, seguidamente, al menos una segunda extracción con acetato de etilo para purificar el β-amino alcohol obtenido.

2. Procedimiento según la reivindicación 1, **caracterizado** por que la amina es del tipo H_2N-Ar, siendo Ar uno de los siguientes elementos: fenilo, orto/meta/para metilfenil, orto/meta/para nitrofenil orto/meta/para fluorofenil, orto/meta/para aminofenil, orto/meta/para trifluorometilfenil, orto/meta/para trifluorometoxifenil, 2,3; 3,4; 4,5; 2,4; 2,5-dimetilfenil, 3,4,5-trimetilfenil, antracil o naftil.

3. Procedimiento según la reivindicación 1, **caracterizado** por que la amina es una amina heterocíclica.

4. Procedimiento según la reivindicación 1, **caracterizado** por que después de la obtención de los β-amino alcoholes, se recupera la mezcla catalítica a través de un filtrado y lavado con hexano/acetato de etilo y, posteriormente, un secado entre 140 y 160ºC, durante 2 a 6 horas.

5. Procedimiento según la reivindicación 1, **caracterizado** por que el diol de la mezcla diol/agua se selecciona de entre los siguientes elementos: 1,2-etanodiol (etilenglicol), 1,2propanodiol, 2,3-butanodiol, 1-feniletano-1,2-diol, 1,3-propanol, 1,2-cicloexanodiol, 1,3butanodiol, di-etilen-glicol, tri-etilen-glicol, tetr-etilen-glicol y el triol glicerol, y derivados cíclicos de los mismos.

6. Procedimiento según la reivindicación 1, **caracterizado** por que el coactivante solido inorgánico con carácter ácido-base se selecciona de entre los siguientes elementos: CaO, BaO, ZnO, CeO_2, AI_2O_3, MgO, TiO_2, SiO_2.

7. Procedimiento según la reivindicación 1, **caracterizado** por que el metal soportado es un metal seleccionado de entre los siguientes elementos: metales de transición de los grupos IIIB a IIB del sistema periódico de elementos, óxidos e hidróxidos de estos y una aleación de Pt-Sn.

8. Procedimiento según la reivindicación 7, **caracterizado** por que el metal soportado es un metal seleccionado de entre los siguientes elementos: Pd, Au, Pt, Cu, Ag, Ru, óxidos e hidróxidos de éstos.

9. Procedimiento según la reivindicación 1, **caracterizado** por que el metal es soportado sobre un sustrato sólido que es seleccionado de entre los siguientes elementos: TiO_2, Al_2O_3, SiO_2, Fe_3O_4, Fe_2O_3, MgO, Ga_2O, CeO_2, NiO, zeolitas, grafito, grafeno, óxido de grafeno, diamante, nanotubos de carbón, negro de carbón.

10. Procedimiento según la reivindicación 1, **caracterizado** por que la mezcla catalítica comprende paladio soportado sobre carbono y ZnO.

OFICINA ESPAÑOLA
DE PATENTES Y MARCAS

ESPAÑA

(21) N.º solicitud: 201600468

(22) Fecha de presentación de la solicitud: 31.05.2016

(32) Fecha de prioridad:

INFORME SOBRE EL ESTADO DE LA TECNICA

(51) Int. Cl.:	Ver Hoja Adicional

DOCUMENTOS RELEVANTES

Categoría	(56) Documentos citados	Reivindicaciones afectadas
A	B Anandkumar et al, Industrial Engineering Chemistry Research 2008, vol 47, nº 8, pp 2484-2494. "Tándem synthesis of B-aminoalcohols from aniline, dialkyl carbonate and ethylenglycol", todo el documento	1-10
A	B Abarca et al, Organic Biomolecular Chemistry 2012, vol 10, pp 1826-1833. "An efficient one pot transfer hydrogenation and N-alkylation of quinolines with alcohols mediated by Pd/C/Zn", resumen	1-10
A	CN 103539718 A (CHINA PETROLEUM CHEMICAL CORP Y SHANGHAI RESEARCH INSTITUTE OF PETROCHEMICAL TECHNOLOGY) 20/01/2014, resumen en inglés de la Base de Datos Espacenet	1

Categoría de los documentos citados
X: de particular relevancia
Y: de particular relevancia combinado con otro/s de la misma categoría
A: refleja el estado de la técnica
O: referido a divulgación no escrita
P: publicado entre la fecha de prioridad y la de presentación de la solicitud
E: documento anterior, pero publicado después de la fecha de presentación de la solicitud

El presente informe ha sido realizado
☒ para todas las reivindicaciones ☐ para las reivindicaciones nº:

Fecha de realización del informe	Examinador	Página
16.12.2016	M.Fernández Fernández	1/4

CLASIFICACIÓN OBJETO DE LA SOLICITUD

C07C213/08 (2006.01)
C07C215/68 (2006.01)
B01J23/44 (2006.01)

Documentación mínima buscada (sistema de clasificación seguido de los símbolos de clasificación)

C07C, B01J

Bases de datos electrónicas consultadas durante la búsqueda (nombre de la base de datos y, si es posible, términos de búsqueda utilizados)

INVENES, EPODOC, WPI, ESPACENET, CAS

OPINIÓN ESCRITA

Nº de solicitud: 201600468

Fecha de Realización de la Opinión Escrita: 16.12.2016

Declaración

Novedad (Art. 6.1 LP 11/1986)	Reivindicaciones Reivindicaciones	1-10	**SI** **NO**
Actividad inventiva (Art. 8.1 LP11/1986)	Reivindicaciones Reivindicaciones	1-10	**SI** **NO**

Se considera que la solicitud cumple con el requisito de aplicación industrial. Este requisito fue evaluado durante la fase de examen formal y técnico de la solicitud (Artículo 31.2 Ley 11/1986).

Base de la Opinión.-

La presente opinión se ha realizado sobre la base de la solicitud de patente tal y como se publica.

1. Documentos considerados.-

A continuación se relacionan los documentos pertenecientes al estado de la técnica tomados en consideración para la realización de esta opinión.

Documento	Número Publicación o Identificación	Fecha Publicación
D01	B Anandkumar et al, Industrial Engineering Chemistry Research 2008, vol 47, nº 8, pp 2484-2494. "Tándem synthesis of B-aminoalcohols from aniline, dialkyl carbonate and ethylenglycol", todo el documento	2008
D02	B Abarca et al, Organic Biomolecular Chemistry 2012, vol 10, pp 1826-1833. "An efficient one pot transfer hydrogenation and N-alkylation of quinolines with alcohols mediated by Pd/C/Zn", resumen	2012

2. Declaración motivada según los artículos 29.6 y 29.7 del Reglamento de ejecución de la Ley 11/1986, de 20 de marzo, de Patentes sobre la novedad y la actividad inventiva; citas y explicaciones en apoyo de esta declaración

La solicitud se refiere, reivindicaciones 1-10, a un procedimiento de obtención de B-aminoalcoholes a partir de una amina, preferentemente una amina aromática, y un diol, de preferencia etilenglicol, caracterizado porque se utiliza como catalizador Pd sobre C y ZnO.

El documento D1 se considera el más próximo del estado de la técnica, divulga un procedimiento de síntesis de B-aminoalcoholes a partir de anilinas, etilenglicol y dialquilcarbonato en presencia de una zeolita Na-Y, se utiliza dialquilcarbonato para producir un carbonato de etileno que reacciona posteriormente con la anilina para obtener N-feniletanolamina.

El documento D2 divulga un procedimiento de N-alquilación de quinolinas con alcoholes simples en el que se utiliza como catalizador Pd/C/Zn.

El procedimiento de la solicitud no se ha encontrado descrito con anterioridad, por lo que tiene novedad, además es inventivo ya que un técnico en la materia no puede deducir de manera evidente que las condiciones de reacción de la solicitud, en particular el catalizador heterogéneo, conduzcan a buenos resultados en la obtención de B-aminoalcoholes sin necesidad de intermediarios.

En conclusión, se considera que las reivindicaciones 1-10 de la solicitud cumplen las condiciones de novedad y actividad inventiva según los Art. 6.1 y 8.1 de la Ley de Patentes 11/1986.

Capítulo 5

Tetrahedron Letters, 2017, 58, 4880-4882

Tetrahedron Letters 58 (2017) 4880–4882

Contents lists available at ScienceDirect

Tetrahedron Letters

journal homepage: www.elsevier.com/locate/tetlet

Heterogeneous borrowing hydrogen reactions with Pd/C and ZnO: Diol scope

Pedro J. Llabres-Campaner, Patricia Woodbridge-Ortega, Rafael Ballesteros-Garrido *, Rafael Ballesteros, Belén Abarca

Departament de Química Orgànica, Universitat de València, Av. Vicent Andrés Estellés s/n, 46100 Burjassot, Valencia, Spain

ABSTRACT

A borrowing hydrogen reaction with different diols was employed for the preparation of complex beta- gamma- or epsilon- amino alcohols from p-toluidine and tetrahydroquinoline with the aim of better understanding the applicability of the Pd/C ZnO heterogeneous catalyst.

Introduction

Borrowing hydrogen (BH) reactions,[1] also known as hydrogen auto-transfer (HA) reactions[2] between amines and alcohols represent a unique opportunity to create molecular complexity from readily accessible reagents while being in coherence with green chemistry principals.[3] Among the different methodologies proposed, Pd, Ru, Mn, Ir and Co complexes have shown significant relevance under homogeneous conditions.[1b,4,5] Additionally, heterogeneous catalysts have been developed for this purpose.[6] Diols represent challenging compounds in BH reactions, ethylene glycol for example has recently been employed, however, double reactions are common.[4,7] In the course of our studies we have reported a catalyst combination (Pd/C 7 mol%, ZnO 3 equiv.)[8a] which is able to mono activate ethylene glycol to create β-amino alcohols. Herein, we present an extrapolation of this methodology to more complex alcohols in order to understand the limitations of this system.

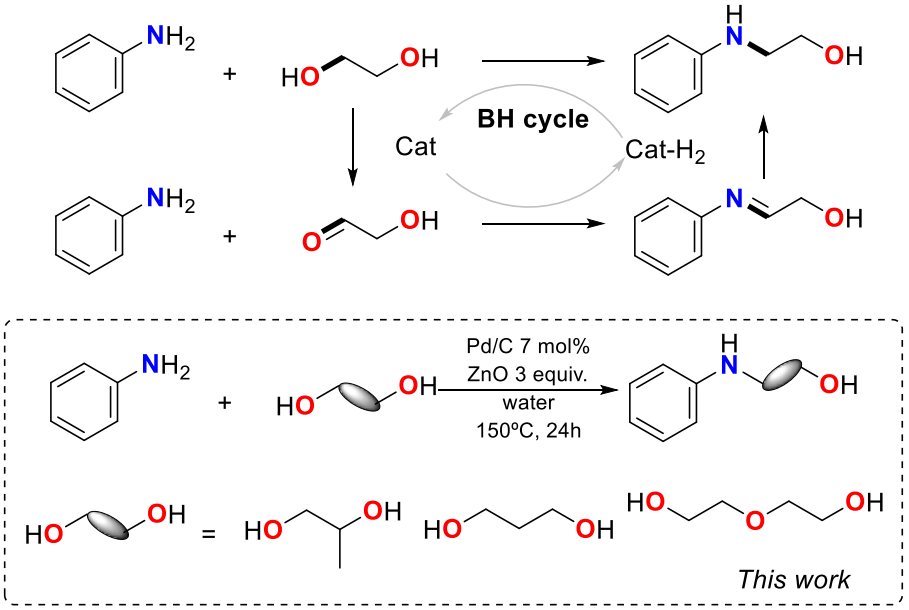

Scheme 1. BH/HA reactions with different diols

Results and Discussion

p-Toluidine 1a and tetrahydroquinoline 1b were selected as reagents using the same conditions that were employed for ethylene glycol **2**.[8a] Indeed, in our previous studies these compounds behaved differently under identical conditions. *p*-Toluidine **1a** gave amino alcohols **3a** in excellent yields, and tetrahydroquinoline **1b** afforded a mixture of amino alcohol **3b** and indole **4** (*Scheme 2*).[8] At this point is important to note, that β-amino alcohols are BH/HA products, however, indoles do not require the final hydrogenation step. This is known as an Acceptor-less Dehydrogenate Condensation (ADC)[9] pathway which has been proposed as a powerful strategy for the preparation of heterocycles and has been exclusively observed with **1b**.

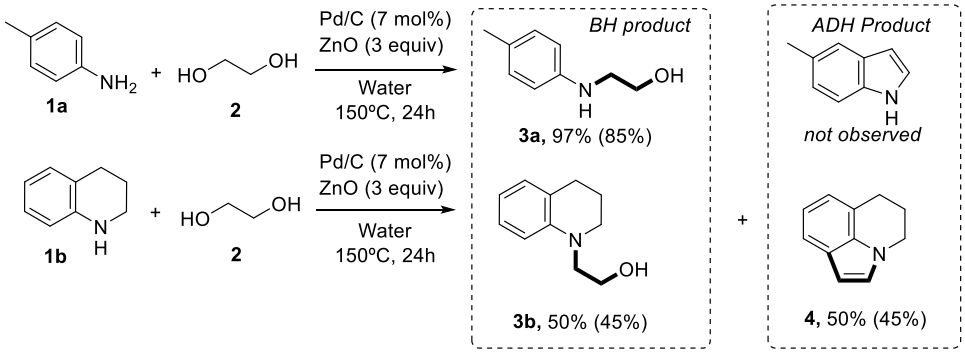

Scheme 2. Chemical behavior of *p*-toluidine **1a** and tetrahydroquinoline **1b** with ethylene glycol. Isolated yields are given in brackets.

Propane 1,2-diol **5** was first selected due to its unsymmetrical structure (*Scheme 3*). When this diol was submitted to the reaction with *p*-toluidine **1a**, amino alcohol **6a** was formed in 95% yield (NMR); however, isolation from the remaining diol was difficult and resulted in only a 45% isolated yield. When tetrahydroquinoline **1b** was submitted to these conditions the corresponding amino alcohol **6b** was obtained in 30% yield (NMR), in the presence of a mixture of indoles **7** (85:15) which were obtained via an ADC process as previously reported.

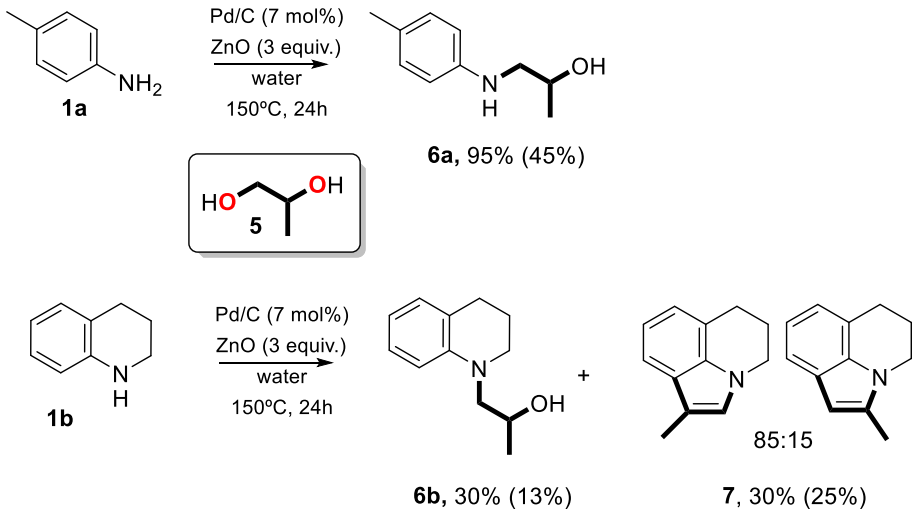

Scheme 3. Chemical behavior of **1a** and **1b** with propane 1,2-diol **5**. Isolated yields are given in brackets.

Although these results clearly remark the selectivity of the process to α-substituted-β-amino alcohols such as compounds **6a** and **6b**, it is important to note that the oxidation of asymmetrical diol **5** have been proposed to be affordable in both, primary and secondary alcohols,[10] yielding either to aldehyde **8a** or ketone **8b** (*Figure 1*), and that a tautomeric equilibrium is present in this system through compound **8c**.[11] However, the more stable iminium intermediate (less steric hindrance) may be associated with the aldehyde alcohol **6a**. The lower yield for tetrahydroquinoline **1b** may also be related to steric hindrance. Being a cyclic amine **1b** the iminium intermediate (*Figure 1, center*) may possess steric hindrance due to the absence of free rotation. Both BH products (**6a** and **6b**) clearly indicate that the reaction of aldehyde **8a** is preferred. The corresponding ADC products **7** observed with tetrahydroquinoline 1b also indicate this feature although a minimal 15% of the other isomer was present: this adds evidence for an equilibrium process.

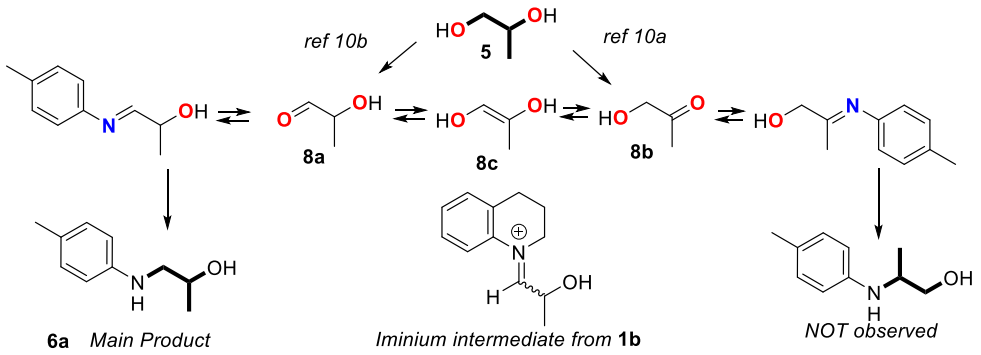

Figure 1. Imine equilibrium during the formation of alcohol **6a**.

When symmetrical propane diol **9** was submitted to the reaction conditions a mixture of products was also obtained (*Scheme 4*). For compound **1a**, 90% conversion was observed, however the corresponding BH product λ-amino acid **10a** was only obtained in 10% isolated yield. A major component of this reaction was the corresponding propyl amine **11a**. Dehydroxilation of these compounds is rare,[12] however Bruneau and co-workers previously observed this feature under homogeneous BH conditions, presumably involving elimination and hydrogenation reactions.[13] Additionally, quinoline **12** was isolated in 15% yield, presumably via a Skraup-like mechanism.[14]

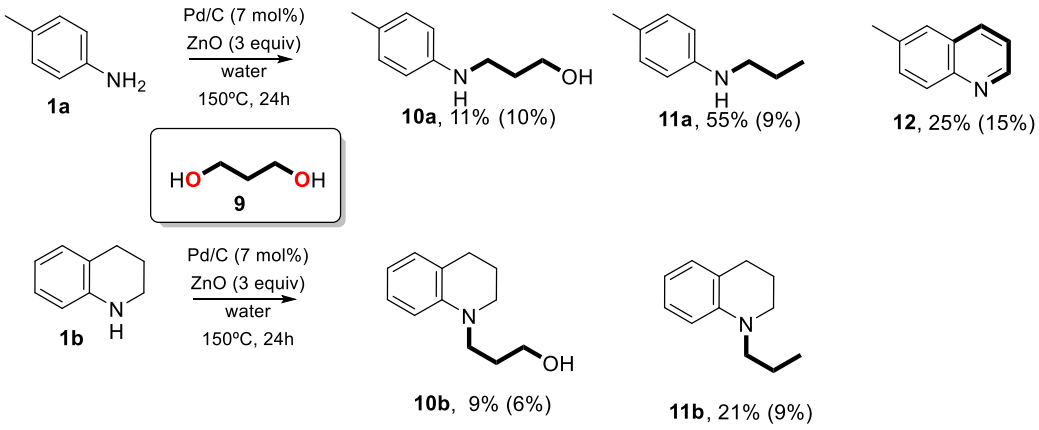

Scheme 4. Chemical behavior of *p*-toluidine and tetrahydroquinoline with propane 1,3-diol.

Comparing these results with tetrahydroquinoline **1b**, similar behavior was observed, however the conversion was decreased. Compounds **10b** and **11b** were obtained in poor yields. Under these conditions quinolines were not observed since secondary amines such as tetrahydroquinoline cannot afford these kinds of products.

Finally, diol **13** was employed with the aim of exploring more complex systems. Diol **13** contains central ether that in principle should avoid any tautomeric pathways, thus, only ε-amino alcohols should be expected. Indeed *p*-toluidine **1a** afforded compound **14a** in good yield (*Scheme 5*), however isolation from the remaining diols proved difficult (38% isolated yield). Nevertheless, this methodology did not require desymmetrization of diol **13**. Similar results were obtained with **1b**, albeit in lower yield; in this case no side-products were observed.

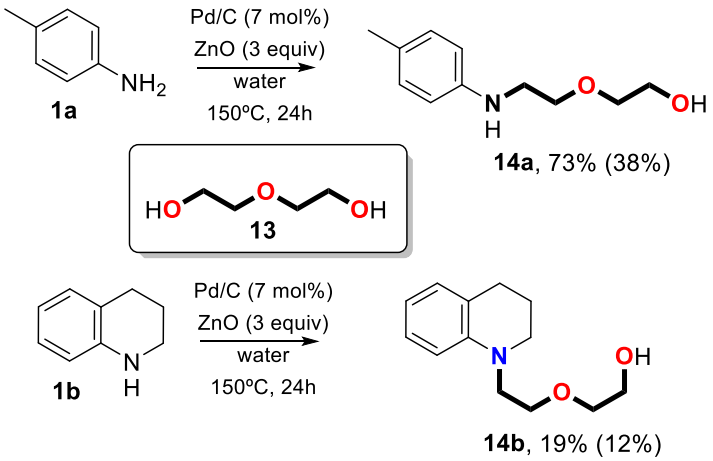

Scheme 5. Chemical behavior of *p*-toluidine **1a** and tetrahydroquinoline **1b** with diethylene glycol **12**.

Conclusions

The combination of Pd/C and ZnO has been proven to be an adequate heterogeneous catalyst for the single-alcohol activation of different diols, with particularly interesting results obtained using propane-1,2-diol **5** and diethylene glycol **13**. In all cases the corresponding amino alcohols could be obtained, thus this methodology represents a different approach for the preparation of these compounds. No derivatization of the diols was required, and all reactions were performed in water:diol mixtures. The use of 1,3-propanodiol **9** afforded dehydroxylated compounds **11a** and **11b** and quinoline **12** via a Skraup-like mechanism.

Associated Content

Supporting Information

Experimental procedure, compound characterization and ^{1}H- and ^{13}C-NMR spectra of new compounds (PDF).

Author Information

Corresponding Author:
*E-mail: rafael.ballesteros-garrido@uv.es
Notes
The authors declare no competing financial interest.

Acknowledgements

R. B-G is much indebted to the Postdoctoral fellow 2013 of the “Ministerio de Economía y Competitividad” (Spain, FPDI-2013-17464). This work was financially supported by the “Ministerio de Ciencia e Innovación” (Spain) (Project CONSOLIDER-INGENIO SUPRAMED CSD 2010-00065 and from University of Valencia (Spain) (UV-INV-AE 15-332846)). Acknowledgments to the “Central Services for Experimental Research” (SCSIE) of University of Valencia and NANBIOSIS platform.

References

1) a) A.J.A. Watson, J.M.J. Williams, *Science*, **2010**, *329*, 635. b) M.H.S.A. Hamid, P.A. Slatford, J.M.J. Williams, *Adv. Synth. Catal.*, **2007**, *349*, 1555.

2) G. Guillena, D.J. Ramon, M. Yus, *Chem. Rev.*, **2010**, *110*, 1611.

3) a) C.J. Li, B.M. Trost, *PNAS*, **2008**, *105*, 13197. b) B.M. Trost, *Angew. Chem. Int. Ed.*, **1995**, *34*, 259.

4) a) S. Michlik, R. Kempe, *Nat. Chem.*, **2013**, *5*, 140. b) N. Andrushko, V. Andrushko, P. Roose, K. Moonen, A. Börner, *ChemCatChem*, **2010**, *2*, 640. c) M.H.M.S. Hamid, C.L. Allen, G.W. Lamb, A.C. Maxwell, H.C. Maytum, A.J.A. Watson, J.M.J. Williams, *J. Am. Chem. Soc.*, **2009**, *131*, 1766. d) S. Bähn, A. Tillack, S. Imm, K. Mevius, D. Michalik, D. Hollmann, L. Neubert, M. Beller, *ChemSuSChem*, **2009**, *2*, 551.

5) a) J. Muzart, *Eur. J. Org. Chem.*, **2015**, 5693. b) L.C. Yang, Y.N. Wang, Y. Zhang, Y. Zhao, *ACS Catal.*, **2017**, *7*, 93. c) A. Putra Eka, Y. Oe, T. Ohta, *Eur. J. Org. Chem.*, **2013**, 6146.

6) K.I. Shimizu, *Catal. Sci. Technol.*, **2015**, *5*, 1412.

7) a) M. Selva, A. Perosa, M. Fabris, *Green Chem.*, **2008**, *10*, 1068. b) A.B. Shivarkar, S.P. Gupte, R.V. Chaudhari, *SYNLETT*, **2006**, *9*, 1374. c) N. Andrushko, V. Andrushko, P. Roose, K. Moonen, A. Börner, *ChemCatChem*, **2010**, *2*, 640.

8) a) P.J. Llabres-Campaner, R. Ballesteros-Garrido, R. Ballesteros, B. Abarca, Tetrahedron, **2017**, 73, 5552. b) R. Adam, R. Ballesteros, B. Abarca, *Org. Biomol. Chem.*, **2012**, *10*, 1826.

9) For a review on ADC see: a) C. Gunanathan, D. Milstein, *Science*, **2013**, *341*, 1229712. b) T. Hille, T. Irrgang, R. Kempe, Angew. Chem. Int. Ed., **2017**, 56, 371. c) F. Kallmeier, B. Dudziec, T. Irrgang, R. Kempe, *Angew. Chem. Int. Ed.*, **2017**, *56*, 7261. d) D. Forberg, J. Obenauf, M. Friedrich, S.M. Hühne, W. Mader, W. Motz, R. Kempe, *Catal. Sci. Technol.*, **2014**, *4*, 4188.

10) a) R.M. Painter, D.M. Pearson, R.M. Waymouth, *Angew. Chem. Int. Ed.*, **2010**, *49*, 9456. b) Z. Han, L. Rong, J. Wu, L. Zhang, Z. Wang, K. Ding, *Angew. Chem. Int. Ed.*, **2012**, *51*, 1304.

11) L.M. Azofra, M.M. Quesada-Moreno, I. Alkorta, J.R. Avilés-Moreno, J. Elguero, J.J. López-González, *ChemPhysChem*, **2015**, *16*, 2226.

12) S.D. Lacroix, A. Pennycook, S. Liu, T.T. Eisenhart, A.C. Marr, *Catal. Sci. Technol.*, **2012**, *2*, 288.

13) A. Labed, F. Jiang, I. Labed, A. Lator, M. Peters, M. Achard, A. Kabouche, Z. Kabouche, G.V.M. Sharma, C. Bruneau, *ChemCatChem*, **2015**, *7*, 1090.

14) R.H. Manske, *Chem. Rev.*, **1942**, *30*, 113.

15) Z. Wu, L. Zhou, W.D. Jiang, Z. Li, X. Zhou, *Eur. J. Org. Chem.*, **2010**, 4971.

16) A. Sharif, P. Lichtor, S. Buchwald, *J. Am. Chem. Soc.*, **2007**, *129*, 3490.

17) B. Bhayana, B. Fors, S. Buchwald, *Organic Lett.*, **2009**, *11*, 3954.

18) C. Mathis, B. Gist, C. Frederickson, K. Midkiff, C. Marvin, *Tetrahedron Lett.*, **2013**, *54*, 2101.

SUPPORTING INFORMATION

Heterogeneous Borrowing Hydrogen Reaction with Pd/C and ZnO: Diol Scope

Pedro J. Llabres-Campaner, Patricia Woodbridge-Ortega, Rafael Ballesteros-Garrido, Rafael Ballesteros and Belén Abarca*

Departament de Química Orgànica, Universitat de València, Av. Vicent Andrés Estellés s/n, 46100 Burjassot, Valencia, Spain.
rafael.ballesteros-garrido@uv.es

Table of contents

S1. Experimental Methods

General procedure: amine (1 mmol, **1a** or **1b**), Pd/C (0.07 mmol), ZnO (3 mmol), distilled water (6 mL) and diol (6 mL) were added to a 20 mL Teflon flask. The flask was then sealed into a steel autoclave and placed in a preheated oven at 150 ºC for 24 h. The reaction mixture was cooled to room temperature, distilled water (25 mL) was added and the crude material was filtered through a 0.2µm Teflon filter. The reaction mixture was extracted with ethyl acetate (3x15mL) and the organic layers were combined, dried with Na_2SO_4, filtered and concentrated to afford the crude reaction mixture which was checked by NMR to evaluate the overall yield. The crude reaction mixture was purified by chromatotron (1 mm, silica, from hexane to hexane/AcOEt 1:3) affording pure compounds.

S2. Compound characterization

1-[(4-Methylphenyl)amino]-2-propanol (**6a**)[15] Isolated yield: 68 mg (45%). Oil. ^{1}H NMR (300 MHz, $CDCl_3$) δ: 7.00 (d, J= 8.6 Hz, 2H), 6.59 (d, J= 8.5 Hz, 2H), 4.01 (m, 1H), 3.21 (dd, J= 12.9; 3.3 Hz, 1H), 2.97 (dd, J= 12.9; 8.6 Hz, 1H), 2.25 (s, 3H), 1.26 (d, J= 6.2 Hz, 3H). ^{13}C NMR (300 MHz, $CDCl_3$) δ: 146.02 (1C, C), 129.87 (2C, CH), 127.31 (1C, C), 113.62 (2C, CH), 66.46 (1C, CH), 52.26 (1C, CH_2), 20.88 (1C, CH_3), 20.47 (1C, CH_3).

1-(3,4-Dihydroquinolin-1(2H)-yl)propan-2-ol (**6b**) Isolated yield: 25 mg (13%). Oil. ^{1}H NMR (300 MHz, $CDCl_3$) δ: 7.09-7.00 (m, 1H), 6.99-6.95 (m, 1H), 6.69 (d, J= 8.3 Hz, 1H), 6.63 (td, J= 7.3; 1.1 Hz, 1H), 4.19-4.07 (m, 1H), 3.40-3.25 (m, 2H), 3.20 (s, 1H), 3.18 (d, J= 2.8 Hz, 1H), 2.79 (t, J= 6.4 Hz, 2H), 2.02-1.91 (m, 2H), 1.24 (d, J= 6.2 Hz, 3H). ^{13}C NMR (300 MHz, $CDCl_3$) δ: 146.31 (1C, C), 129.53 (1C, CH), 127.22 (1C, CH), 123.19 (1C, C), 116.98 (1C, CH), 112.12 (1C, CH), 65.60 (1C, CH), 60.84 (1C, CH_2), 51.11 (1C, CH_2), 28.16 (1C, CH_2), 22.32 (1C, CH_2), 20.29 (1C, CH_3). HRMS for $C_{12}H_{17}NO$ [M+H$^+$]: calculated: 191.1310; found: 191.1382. IR (ATR): 3381, 2927, 2842, 1601, 1573, 1504, 1456, 1373, 1346, 1329, 1302, 1241, 1212, 1194, 1131, 1095, 1058, 1011, 938, 872, 831, 800, 743, 718.

1-Methyl-5,6-dihydro-4*H*-pyrrolo[3,2,1-*ij*]quinoline (**7**) & *2-methyl-5,6-dihydro-4H-pyrrolo[3,2,1-ij]quinoline* (**7'**) Isolated yield: 43 mg (25%). Oil. ^{1}H NMR (300 MHz, $CDCl_3$) δ: 7.43 (dd, J= 7.9; 0.8 Hz, 1H), 7.38 (dd, J= 7.9; 0.8 Hz, 1H'), 7.09-6.84 (m, 3H'), 7.05 (m, 1H), 6.94 (dd, J= 7.0; 0.9 Hz, 1H), 6.88 (d, J= 1.0 Hz, 1H), 4.12 (m, 2H), 4.05 (m, 2H'), 3.00 (m, 2H), 2.79 (m, 2H'), 2.44 (d, J= 0.9 Hz, 3H'), 2.38 (d, J= 1.0 Hz, 3H), 2.26 (m. 2H), 2.05-1.95 (m, 2H'). ^{13}C NMR (300 MHz, $CDCl_3$) δ: 134.60 (1C, C), 129.31 (1C, C), 127.20 (1C, C), 126.15 (1C, C), 123.76 (1C, CH), 121.58 (1C', CH), 119.41 (1C, CH), 118.36 (1C, CH), 116.54 (1C, CH), 110.21 (1C', CH), 43.93 (1C, CH_2), 24.97 (1C, CH_2), 23.08 (1C, CH_2), 9.69 (1C, CH_3). HRMS for $C_{12}H_{13}N$ [M+H$^+$]: calculated: 172.1121; found: 172.1117. IR (ATR): 3051, 2926, 2857, 1610, 1541, 1495, 1475, 1454, 1396, 1368, 1339, 1249, 1195, 1162, 1070, 1033, 1019, 841, 773, 743, 602.

3-(p-Tolylamino)propan-1-ol (**10a**)[16] Isolated yield: 17 mg (10%). Oil. ^{1}H NMR (300 MHz, $CDCl_3$) δ: 7.00 (d, J= 8.3 Hz, 2H), 6.62 (m, 2H), 3.82 (t, J= 5.8 Hz, 2H), 3.28 (t, J= 6.4 Hz, 1H), 2.24 (s, 3H), 1.89 (m, 2H). ^{13}C NMR (300 MHz, $CDCl_3$) δ: 148.35 (1C, C), 130.17 (2C, CH), 127.11 (1C, C), 114.13 (2C, CH), 62.28 (1C, CH_2), 43.20 (1C, CH_2), 32.21 (1C, CH_2), 20.80 (1C, CH_3).

4-Methyl-N-propyl-benzenamine (**11a**)[15] Isolated yield: 14 mg (9%). Oil. ^{1}H NMR (300 MHz, $CDCl_3$) δ: 6.99 (d, J= 8.0 Hz, 2H), 6.55 (m, 2H), 3.07 (t, J= 7.1 Hz, 2H), 2.25 (s, 3H), 1.63 (m, 2H), 0.99 (t, J= 7.4 Hz, 3H). ^{13}C NMR (300 MHz, $CDCl_3$) δ: 129.86 (2C, CH), 128.98 (1C, C), 126.81 (1C, C), 113.35 (2C, CH), 46.58 (1C, CH_2), 22.80 (1C, CH_2), 20.52 (1C, CH_3), 11.77 (1C, CH_3).

6-Methylquinoline (**12**)[17] Isolated yield: 15%. Oil. ^{1}H NMR (300 MHz, $CDCl_3$) δ: 8.85 (dd, J= 4.3; 1.7 Hz, 1H), 8.09 (d, J= 8.4 Hz, 1H), 8.02 (d, J= 8.5 Hz, 1H), 7.59 (d, J= 0.8 Hz, 1H), 7.56 (dd, J= 8.6; 2.0 Hz, 1H), 7.37 (dd, J= 8.3; 4.3 Hz, 1H), 2.54 (s, 3H). ^{13}C NMR (300 MHz, $CDCl_3$) δ: 149.68 (1C, CH), 146.96 (1C, C), 136.54 (1C, C), 135.52 (1C, CH), 131.94 (1C, CH), 129.13 (1C, CH), 128.44 (1C, C), 126.78 (1C, CH), 121.25 (1C, CH), 21.77 (1C, CH^3).

3-[(1,2,3,4-Tetrahydro-1-naphtalenyl)amino]-1-propanol (**10b**)[18] Isolated yield: traces. Oil. ^{1}H NMR (300 MHz, $CDCl_3$) δ: 7.07 (m, 1H), 6.95 (d, J= 6.9 Hz, 1H), 6.68 (m, 1H), 6.60 (t, J= 6.9 Hz, 1H), 3.75 (t, J= 5.9 Hz, 2H), 3.38 (d, J= 6.9 Hz, 2H), 3.31 (t, J= 5.9 Hz, 2H), 2.75 (t, J= 6.4 Hz, 2H), 1.97 (m, 2H), 1.88 (m, 2H). ^{13}C NMR (300 MHz, $CDCl_3$) δ: 145.15 (1C, C), 129.47 (1C, CH), 127.25 (1C, CH), 123.05 (1C, C), 116.68 (1C, CH), 111.60 (1C, CH), 61.12 (1C, CH2), 49.63 (1C, CH_2), 29.36 (1C, CH_2), 28.11 (1C, CH_2), 22.00 (1C, CH_2).

1,2,3,4-Tetrahydro-N-propyl-1-naphtalenamine (**11b**)[7] Isolated yield: 28 mg (16%). Oil. ^{1}H NMR (300 MHz, $CDCl_3$) δ: 7.04 (m, 1H), 6.94 (m, 1H), 6.55 (m, 2H), 3.29 (m, 2H), 3.20 (m, 2H), 2.76 (t, J= 6.3 Hz, 2H), 1.96 (m, 2H), 1.63 (m, 2H), 0.95 (t, J= 7.4 Hz, 3H). ^{13}C NMR (300 MHz, $CDCl_3$) δ: 145.33 (1C, C), 129.24 (1C, CH), 127.16 (1C, CH), 122.24 (1C, CH), 115.29 (1C, CH), 110.59 (1C, CH), 53.42 (1C, CH_2), 49.65 (1C, CH_2), 28.36 (1C, CH_2), 22.38 (1C, CH_2), 19.59 (1C, CH_2), 11.71 (1C, CH_3). IR (ATR): 2926, 2854, 1600, 1505, 1456, 1376, 1345, 1329, 1304, 1242, 1195, 1104, 1073, 1059, 800, 771, 741, 716, 604.

2-[2-[(4-Methylphenyl)amino]ethoxy]-ethanol (**14a**) Isolated yield: 64 mg (38%). Oil. ^{1}H NMR (300 MHz, $CDCl_3$) δ: 7.00 (d, J= 8.4 Hz, 2H), 6.58 (d, J= 8.4 Hz, 2H), 3.75 (t, J= 4.5 Hz, 2H), 3.71 (t, J= 5.2 Hz, 2H), 3.59 (t, J= 4.5 Hz, 2H), 3.30 (t, J= 5.2 Hz, 2H). ^{13}C NMR (300 MHz, $CDCl_3$) δ: 145.89 (1C, C), 129.83 (2C, CH), 127.17 (1C, C), 113.58 (2C, CH), 72.30 (1C, CH2), 69.78 (1C, CH_2), 61.80 (1C, CH_2), 44.21 (1C, CH_2), 20.47 (1C, CH_3). HRMS for $C_{11}H_{17}NO_2$ [M+H^+]: calculated: 196.1332; found: 196.1137. IR (ATR): 3360, 2916, 2863, 1616, 1518, 1456, 1351, 1318, 1303, 1251, 1182, 1120, 1060, 927, 885, 805, 753, 604.

2-[2-(3,4-Dihydro-6-methyl-1(2H)-quinolinyl)ethoxy]-ethanol (**14b**) Isolated yield: 26 mg (12%). Oil. ^{1}H NMR (300 MHz, $CDCl_3$) δ: 7.04 (td, J= 8.2; 1.7 Hz, 1H), 6.94 (dd, J= 7.3; 1.4 Hz, 1H), 6.64-6.54 (m, 2H), 3.75-3.66 (m, 4H), 3.60-3.55 (m, 2H), 3.52-3.46 (m, 2H), 3.38-3.32 (m, 2H), 2.76 (t, J= 6.3 Hz, 2H), 1.99-1.90 (m, 2H). ^{13}C NMR (300 MHz, $CDCl_3$) δ: 145.33 (1C, C), 129.44 (1C, CH), 127.20 (1C, CH), 122.54 (1C, C), 116.01 (1C, CH), 110.76 (1C, CH), 72.46 (1C, CH_2), 68.53 (1C, CH_2), 62.03 (1C, CH_2), 51.44 (1C, CH_2), 50.50 (1C, CH_2), 28.27 (1C, CH_2), 22.35 (1C, CH_2). HRMS for $C_{13}H_{19}NO_2$ [M+H^+]: calculated: 222.1489; found: 222.1488. IR (ATR): 2925, 2857, 1601, 1505, 1456, 1345, 1330, 1303, 1195, 1120, 1057, 1006, 743.

S3. NMR spectra

^{1}HNMR, ^{13}CNMR, H-COSY and edited HSQC of new compounds are shown.

1-(3,4-dihydroquinolin-1(2H)-yl)propan-2-ol (6b)

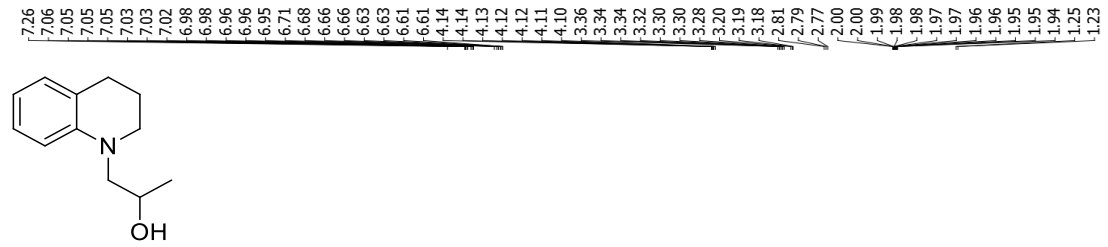

^{1}H NMR Spectrum
(300 MHz, $CDCl_3$)

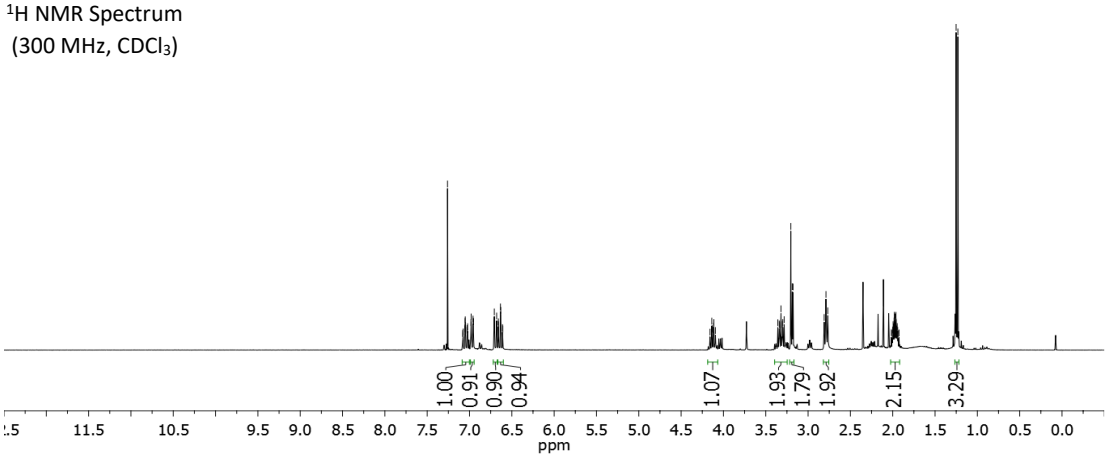

^{13}C NMR Spectrum
(75 MHz, $CDCl_3$)

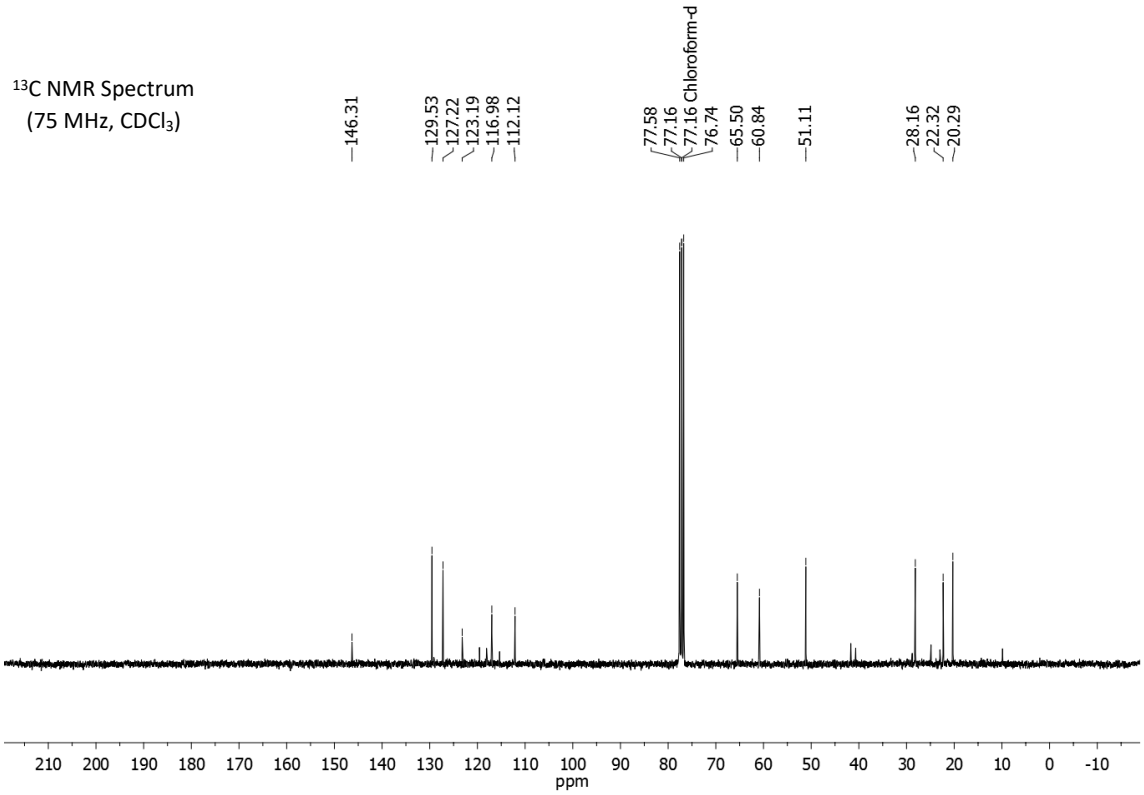

COSY Spectrum
($CDCl_3$)

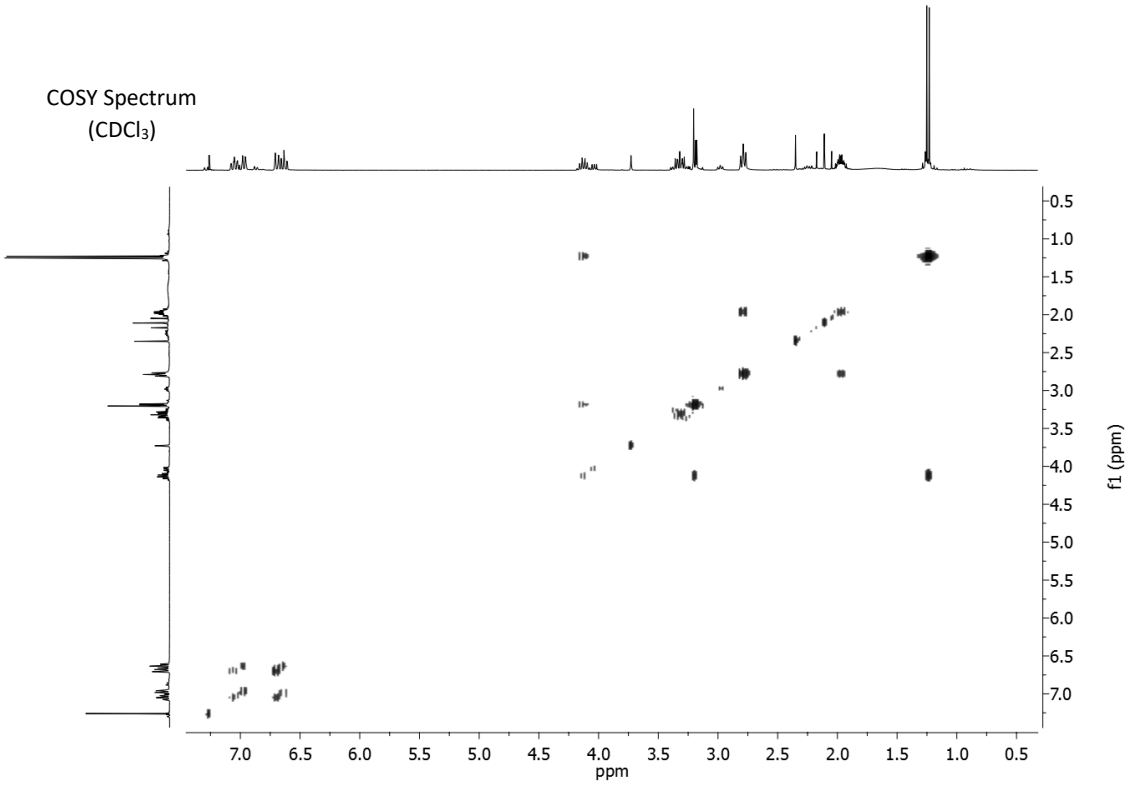

ed-HSQC Spectrum
($CDCl_3$)

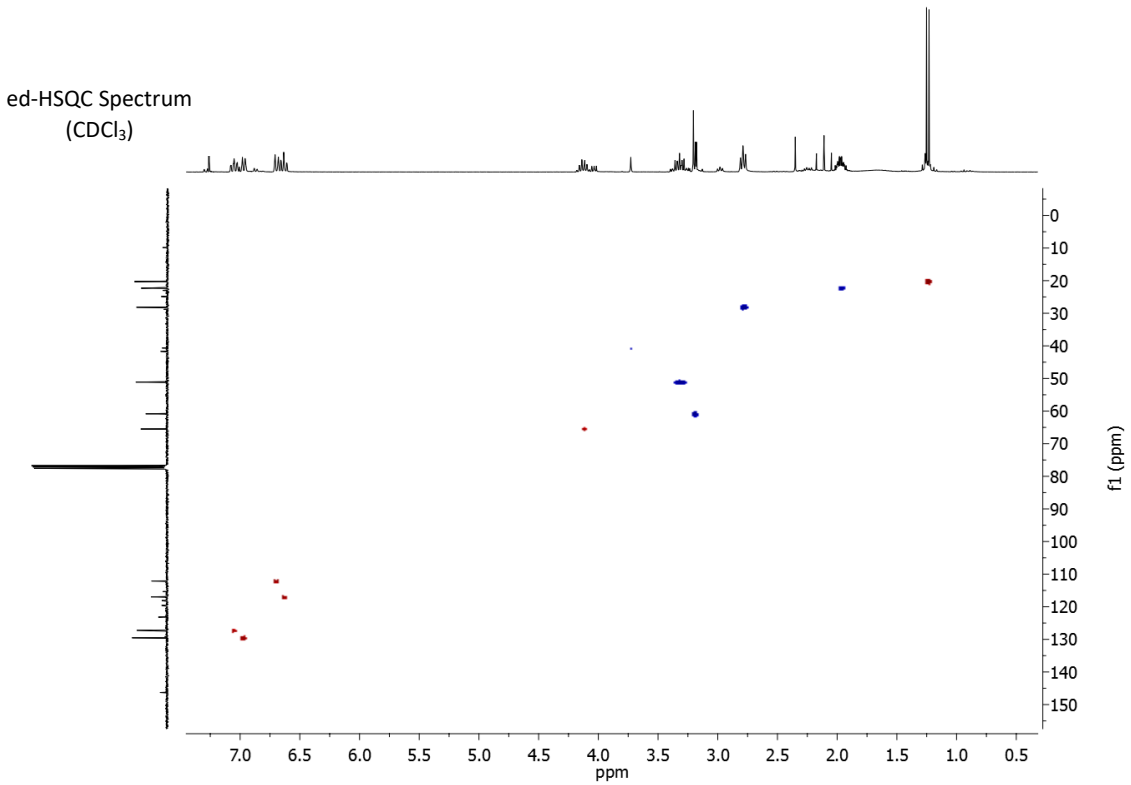

1-methyl-5,6-dihydro-4H-pyrrolo[3,2,1-ij]quinoline (7)
2-methyl-5,6-dihydro-4H-pyrrolo[3,2,1-ij]quinoline (7')

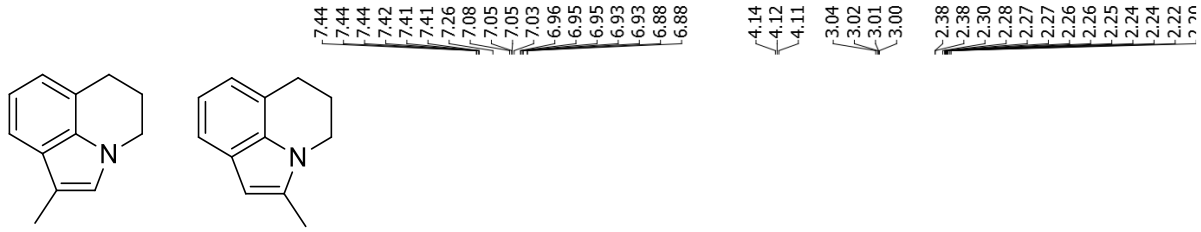

^{1}H NMR Spectrum
(300 MHz, $CDCl_3$)

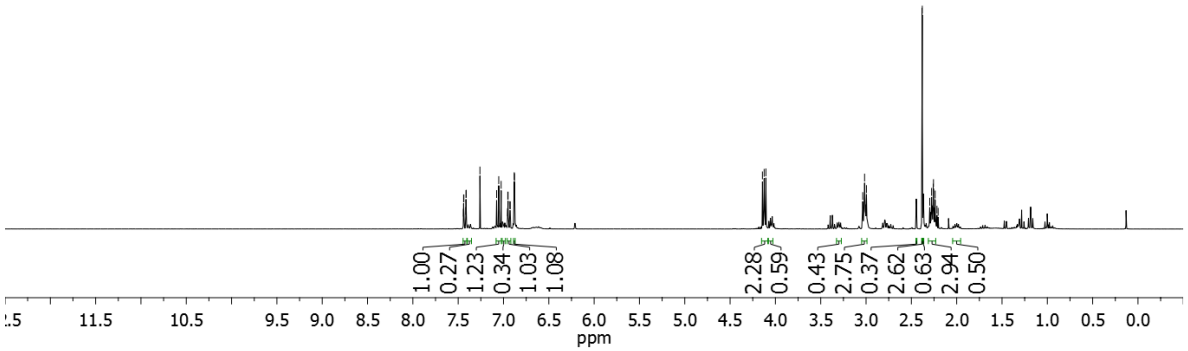

^{13}C NMR Spectrum
(75 MHz, $CDCl_3$)

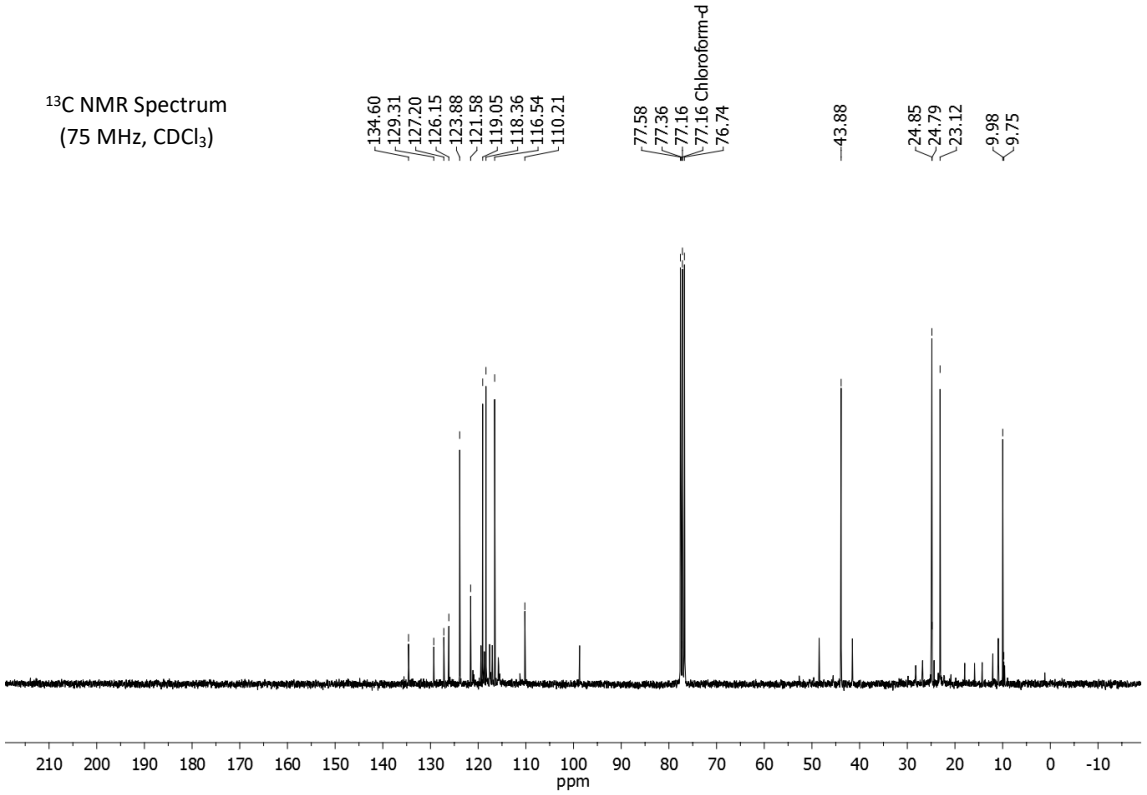

COSY Spectrum
($CDCl_3$)

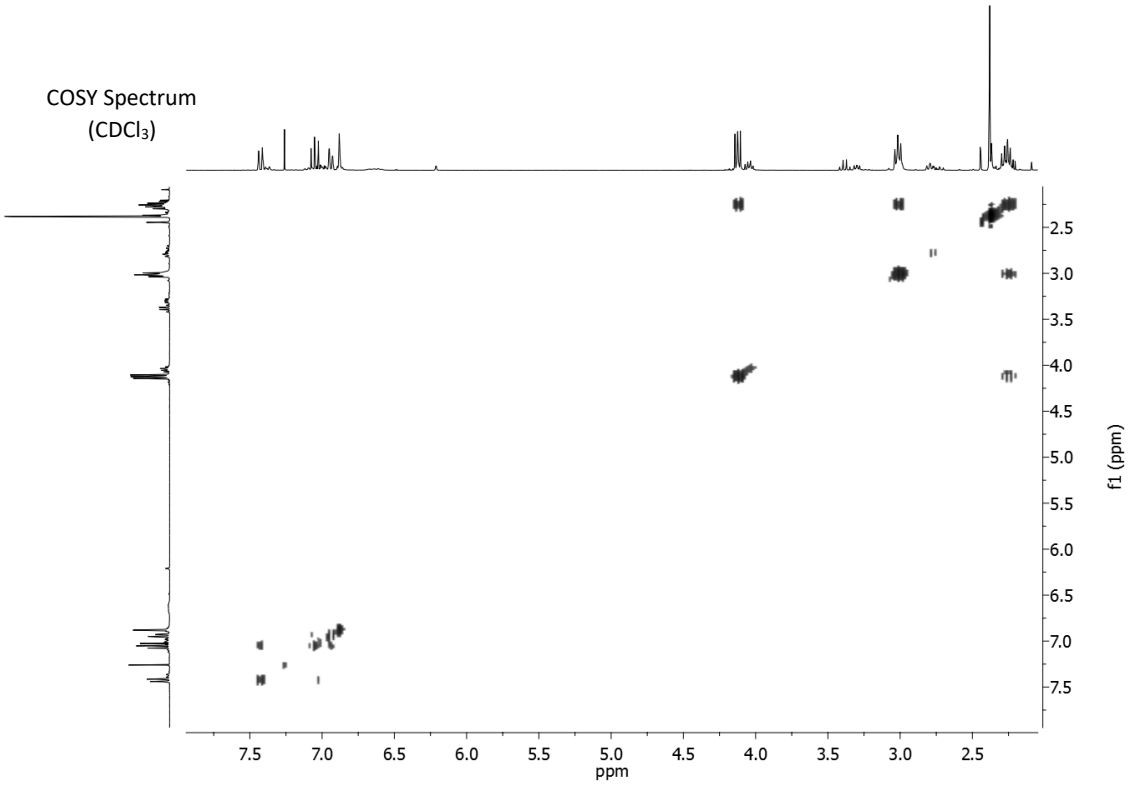

ed-HSQC Spectrum
($CDCl_3$)

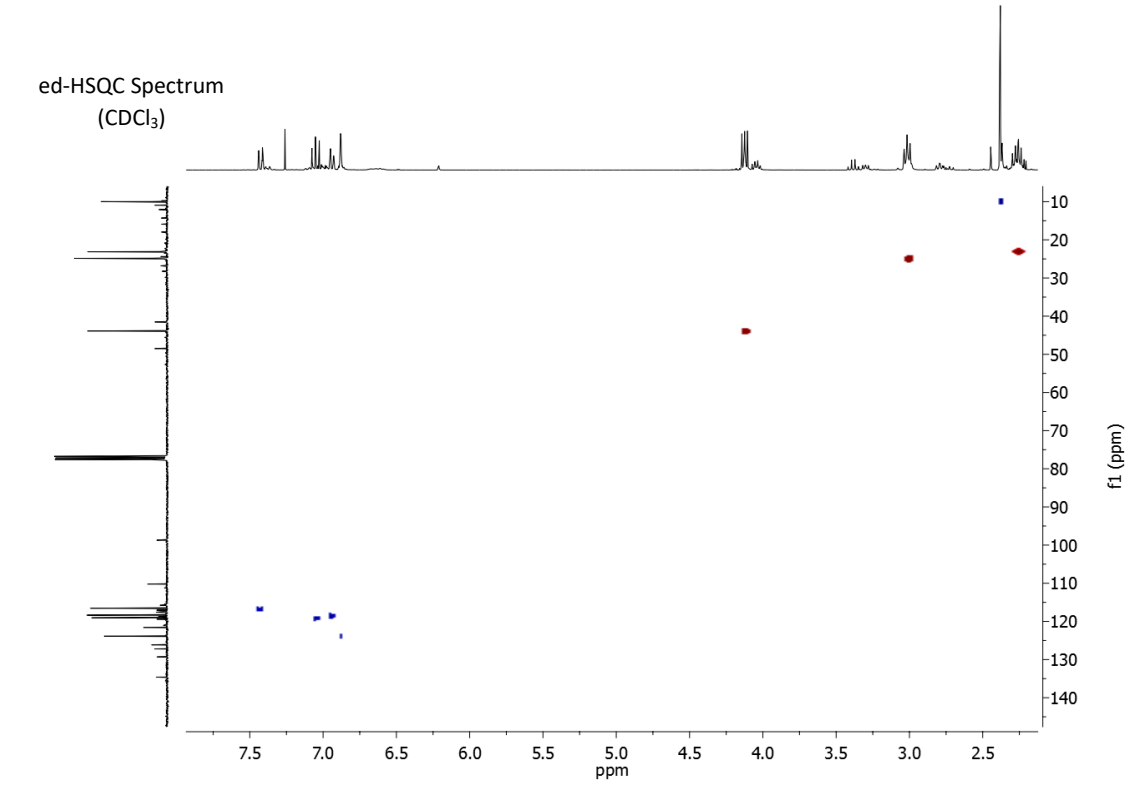

2-[2-[(4-methylphenyl)amino]ethoxy]-ethanol (14a)

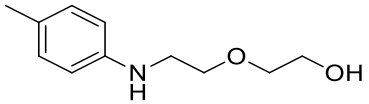

^{1}H NMR Spectrum
(300 MHz, $CDCl_3$)

^{13}C NMR Spectrum
(75 MHz, $CDCl_3$)

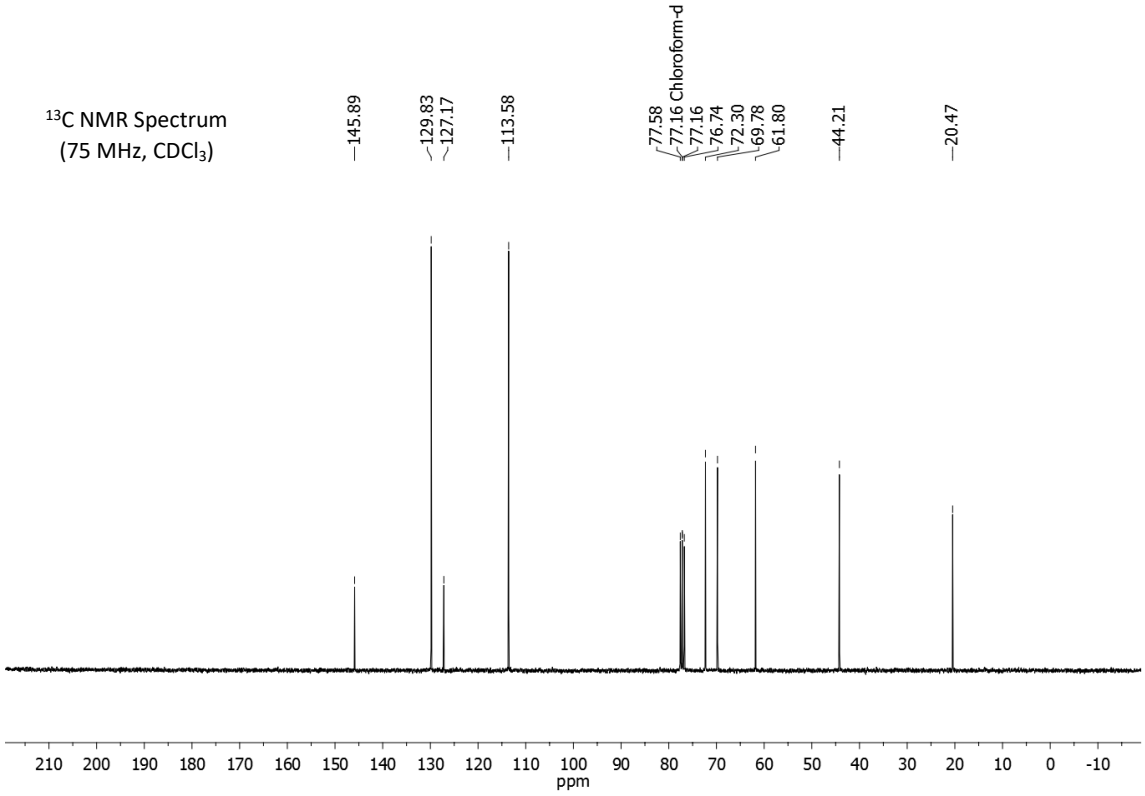

COSY Spectrum
($CDCl_3$)

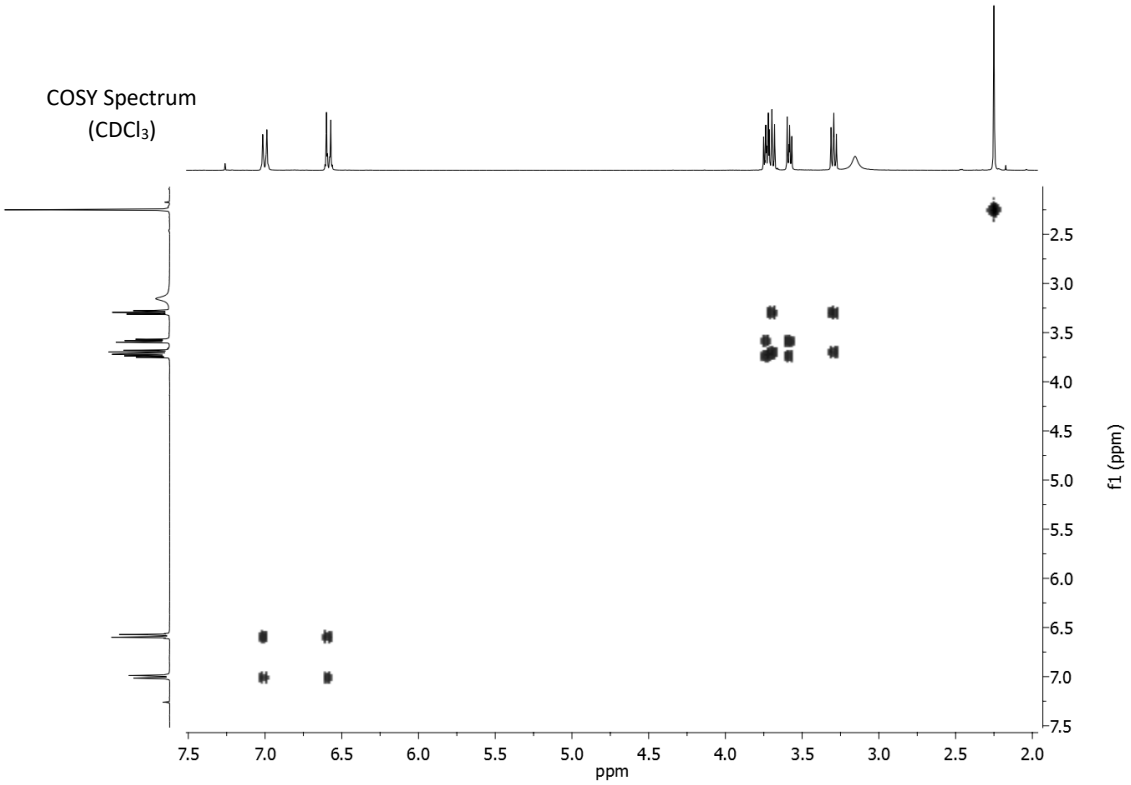

ed-HSQC Spectrum
($CDCl_3$)

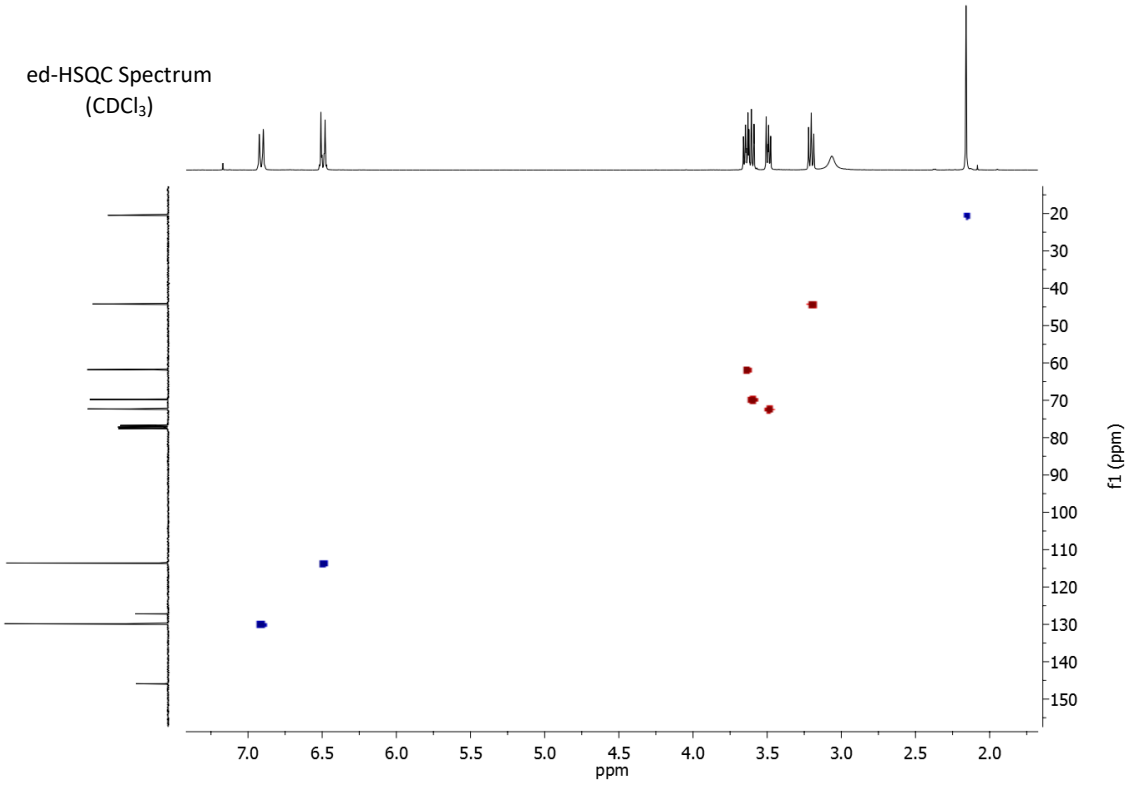

2-[2-(3,4-dihydro-6-methyl-1(2H)-quinolinyl)ethoxy]-ethanol (14b)

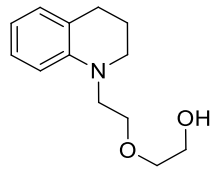

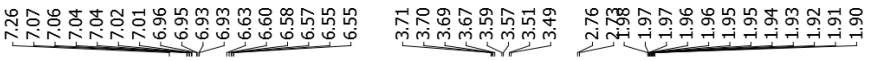

^{1}H NMR Spectrum
(300 MHz, $CDCl_3$)

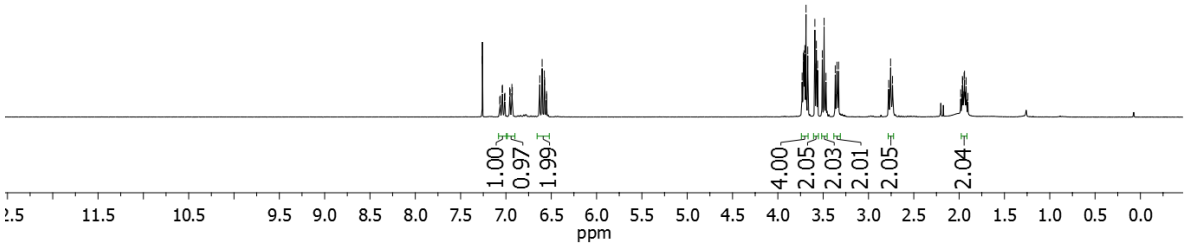

^{13}C NMR Spectrum
(75 MHz, $CDCl_3$)

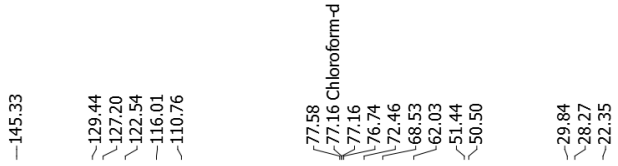

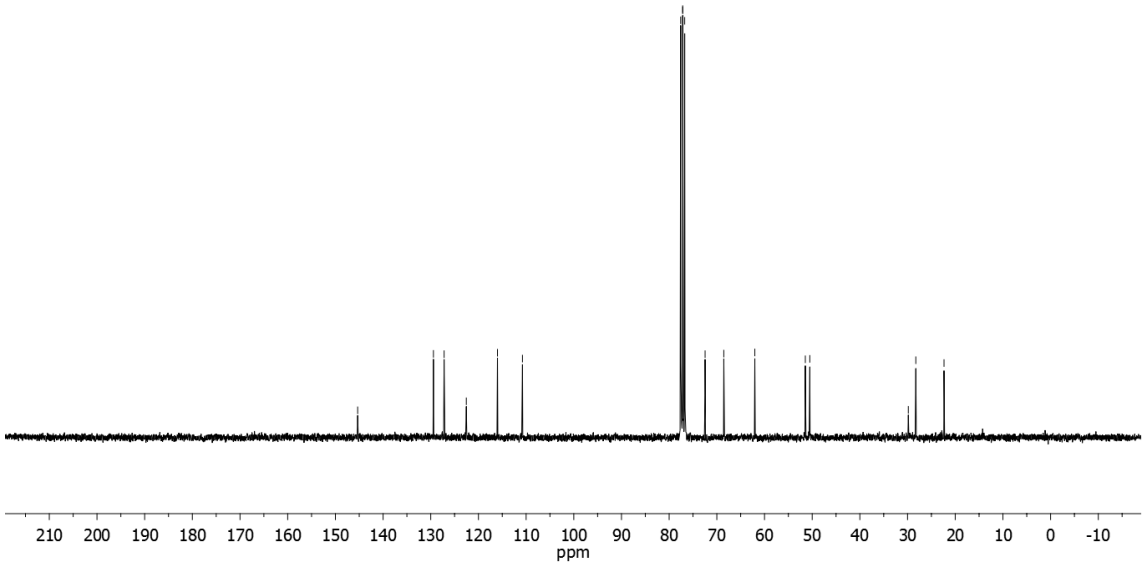

COSY Spectrum
($CDCl_3$)

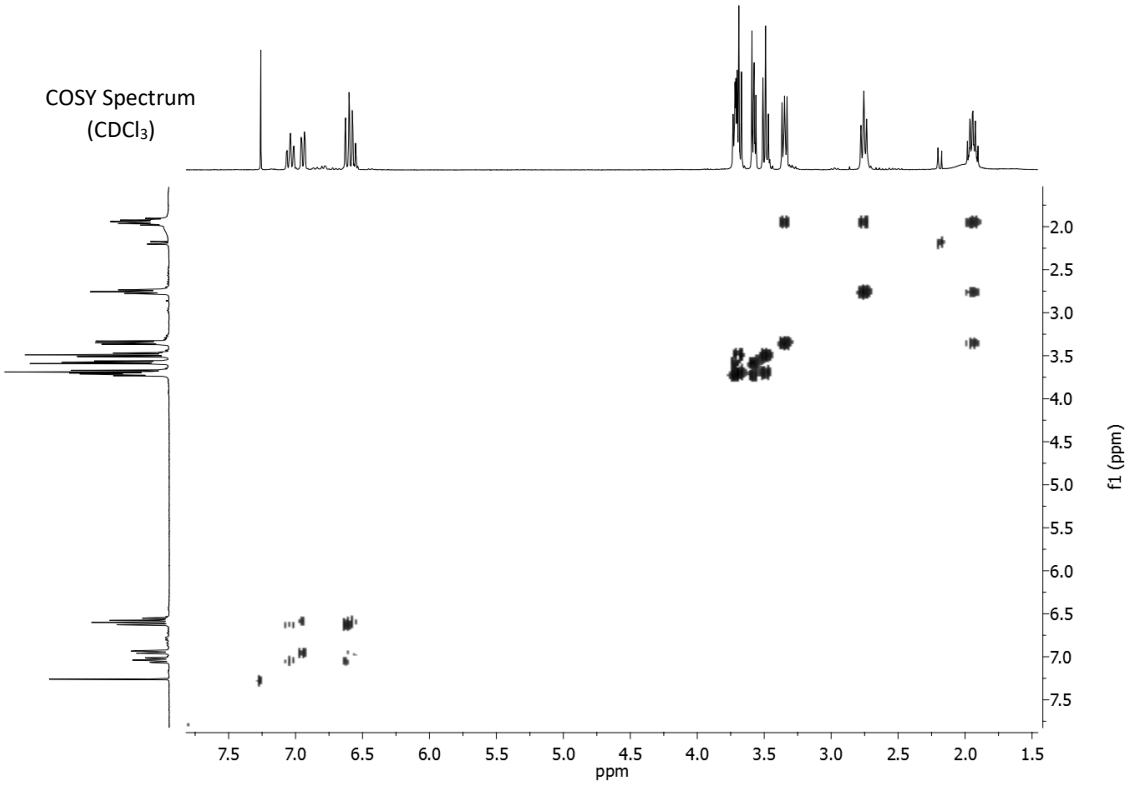

ed-HSQC Spectrum
($CDCl_3$)

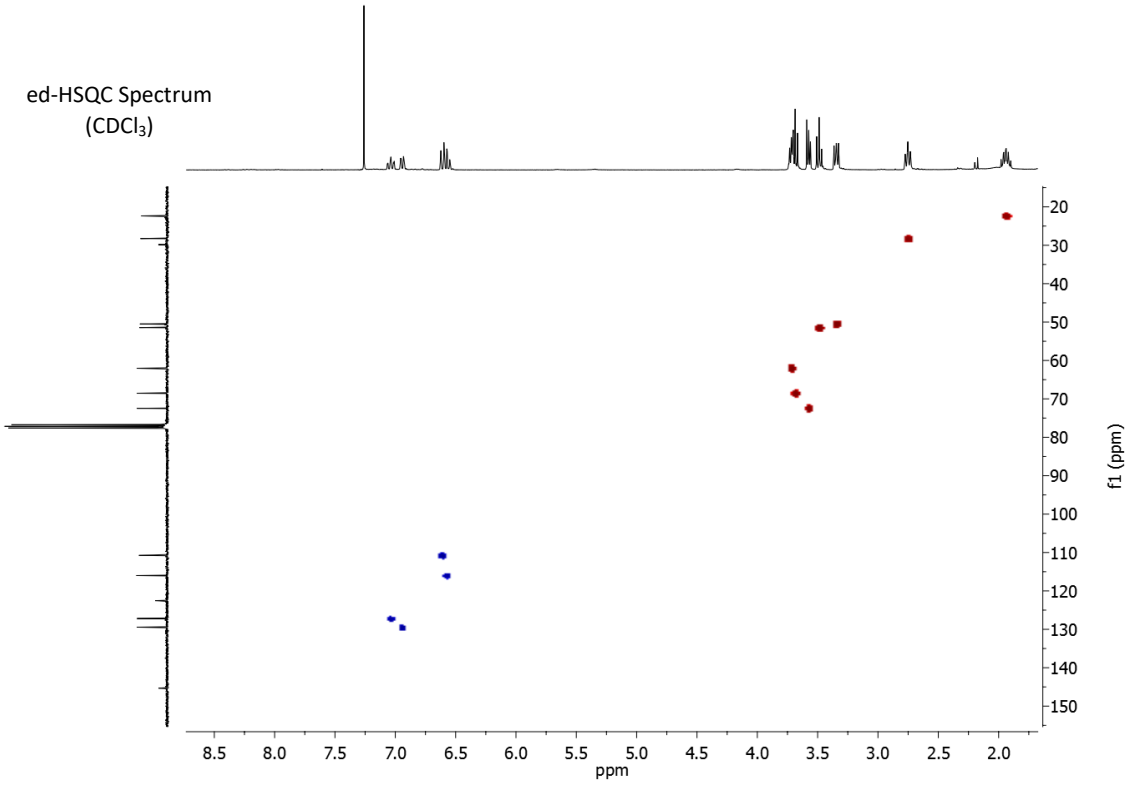

Capítulo 6

Journal of Organic Chemistry, 2018, 83, 521-526

JOC The Journal of Organic Chemistry Cite This: J. Org. Chem. 2018, 83, 521−526

Note

pubs.acs.org/joc

Straight Access to Indoles from Anilines and Ethylene Glycol by Heterogeneous Acceptorless Dehydrogenative Condensation

Pedro Juan Llabres-Campaner, Rafael Ballesteros-Garrido,* Rafael Ballesteros, and Belén Abarca

Departamento de Química Orgánica, Facultad de Farmacia Universidad de Valencia, Vicent Andres Estelles s/n 46100 Burjassot, Spain

Supporting Information

ABSTRACT

The development of original strategies for the preparation of indole derivatives is a major goal in drug design due to the importance of this heterocycle. Herein, we report the first straight access to indoles from anilines and ethylene glycol by heterogeneous catalysis, based on an acceptorless dehy-drogenative condensation, under noninert conditions. In order to achieve high selectivity, a combina-tion of Pt/Al_2O_3 and ZnO have been found to be able to slowly dehydrogenate ethylene glycol generating, after condensation with the amine and tautomeric equilibrium, the corresponding pyrrole-ring unsubstituted indoles.

Indole scaffold is present in a large number of important compounds in pharmaceutical chemistry.[1a] Thus, significant strategies have been reported for the synthesis of this heterocycle.[1b-d] For example, Fischer,[2a] Reissert,[2b] Grandberg,[2c] or Bischler[2d] original methodologies allowed the preparation of in-doles bearing different substituents on the pyrrole ring. However, for the synthesis of pyrrole-ring un-substituted indoles, just a few examples are reported. Leimgruber-Batcho[3a-c] strategy developed by Corey[3d] or Madelung[4a] modification developed by Saegusa[4b] are some examples where C2-C3 unsubstituted indoles are prepared. A straight and simple approach to this heterocycle free from hydrazine or halo carbonyl derivatives still represents a challenge. Ethylene glycol and aniline (*Figure 1*) appear to be the most ideal reagents for generate pyrrole-ring unsubstituted indoles.[5] It has been reported that at high temperatures (350 ºC) these two reagents can yield to indole in gas phase.[6a-b]

Interestingly, some authors have reported that diols and anilines can be converted into indoles with homogeneous Ir/Ru catalyst.[6c-e] In the course of our studies we discovered that a combination of a classical hydrogenating catalyst Pd/C and large excess of metallic Zn or ZnO were able to activate ethylene glycol.[7] It is important to note the high stability of ethylene glycol and the possibility of double functionalization limits the efficiency of the transformation.[8] If a mono dehydrogenation of ethylene glycol can be performed, in presence of anilines and avoiding Borrowing Hydrogen (BH) path,[9] indoles should be obtained, through a tautomerism followed by conventional acylation/elimination reaction (*Figure 1*).

Under BH conditions few examples are known with ethylene glycol and anilines.[8a,10] However, Kempe has recently reported on the use of Acceptorless Borrowing Hydrogen (BH) reaction[11a-c] (called Acceptorless Dehydrogenative Condensation or ADC[11d]) for the preparation of pyridines and pyrroles.

Herein we report a heterogeneous acceptorless dehydrogenative condensation for the preparation of indoles from neat ethylene glycol and anilines. This methodology allows the preparation of pyrrole-ring unsubstituted indoles with high efficiency.

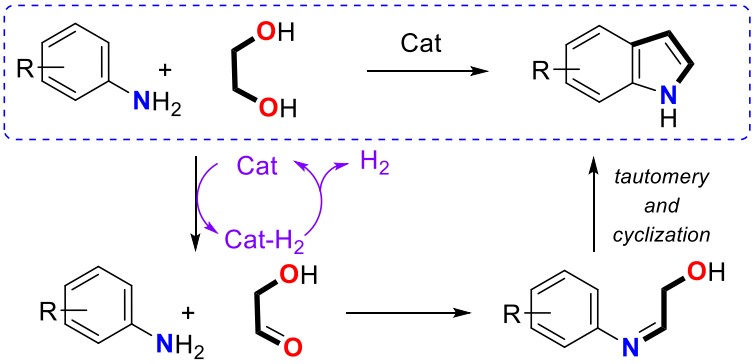

Figure 1. Indole synthesis through ADC/tautomeric approach.

The catalyst screening was performed with the common catalysts employed for hydrogenation, under heterogeneous conditions, which is indeed required for a BH reaction (Pt/Al_2O_3, Ru/Al_2O_3 and Pd/C) using *p*-toluidine as aniline. Initial tests with the previous catalyst afforded negative results (*Table 1*).

Table 1. Catalyst screening.

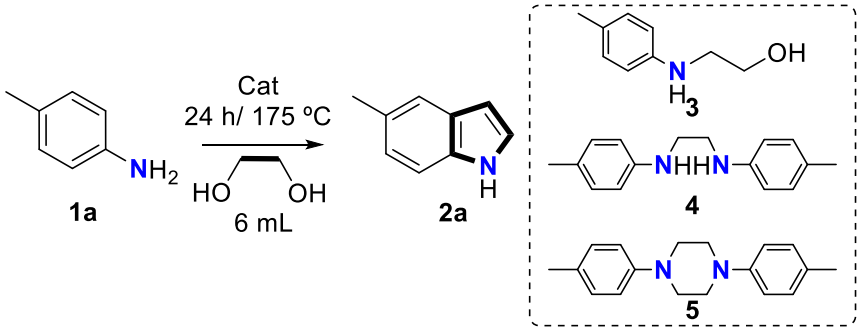

Catalyst	Co-catalyst	Concentration	Conversion	Yield (2a)
Pd/C (7%)	ZnO (18%)	0.2 M	90%	66%
Pt/Al_2O_3 (7%)	ZnO (18%)	0.2 M	76%	49%
Ru/Al_2O_3 (7%)	ZnO (18%)	0.2 M	69%	11%
Pt/Al_2O_3 (3.5%)	ZnO (9%)	0.4 M	91%	65%
Pt/Al_2O_3 (1.7%)	**ZnO (4.5%)**	**0.66 M**	**92%**	**75%**
Pd/C (1.7%)	ZnO (4.5%)	0.66 M	95%	20%
Pt/Al_2O_3 (1.2%)	ZnO (3%)	1 M	73%	60%

ZnO was introduced as co-catalyst to activate the diol. In our previous studies Zn[7a] and ZnO[7c] were successfully employed to activate ethylene glycol. ZnO is known to activate alcohols[12] and (as nanoparticle) has been reported as a catalyst for organic reactions.[12] When the catalyst was combined with ZnO, conversion increased, ZnO-Pt/Al_2O_3 combination revealed as the most powerful catalyst. 0.6 M concentration of amine in ethylene glycol (4 mmol of **1a** in 6 mL) was found ideal for high conversion and yield. With different conditions side products appeared (See S1 for detailed scope). Amino alcohol **3** and dimers **4** and **5** were the major side products, being able to be rationalized by a BH path (vide infra).

Watanabe reported on dimers formation **4** and **5** with anilines and ethylene glycol under $RuCl_3$ catalysis.[6e] However, their presence could only be detected when the reaction was carried out with Pd/C. For elevated conversions and yields 24h were required. When the temperature was reduced to 150ºC conversion decreased. All reactions were carried out in presence of air and moisture, no specific conditions were required.

In *Table 2*, the scope with different anilines is presented. In all cases, the presence of electron-donating groups induced the formation of the indole. Reaction with compound **1b** afforded

dimethylated indole **2b** in 81% isolated yield. Dimethoxy and trimethoxy derivatives **2c** and **2d** were isolated in high yields (84% and 88%, entries 3 and 4). Surprisingly, reaction with aniline **1e** afforded moderate yield (43% isolated yield for indole **2e**). This result pointed out this methodology requires the presence of donor substituents in the aromatic ring. Benzodioxol and benzodioxane anilines **1f** and **1g** afforded indoles **2f** and **2g** in excellent yields (**2g** was obtained in the presence of an isomer mixture of 75:25). Naphthylamine **1h** afforded the corresponding indole **2h** in 90% isolated yield. Although deactivated anilines like nitro or cyano derivatives did not afford any conversion, with fluorinated aniline **1i** bisindoles **6** (due to the symmetry of compound **6** *Z* or *E* configuration cannot be determined) were obtained in moderate yield (36% yield), this result pointed out that reaction mechanism involved different features (vide infra).

Table 2. Scope of the methodology using different anilines. Isolated yields are shown.

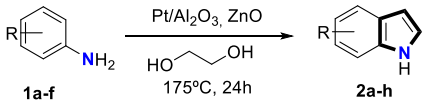

Entry	Aniline (**1a-f**)	Product	Yield
1	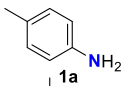 **1a**	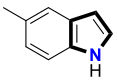	**2a** 70%
2	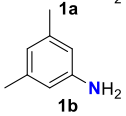 **1b**	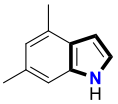	**2b** 81%
3	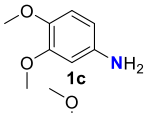 **1c**	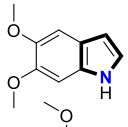	**2c** 84%
4	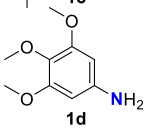 **1d**	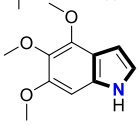	**2d** 88%
5	 **1e**	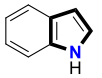	**2e** 43%
6	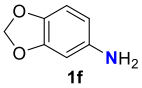 **1f**	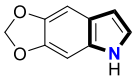	**2f** 86%
7	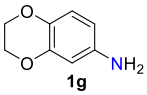 **1g**	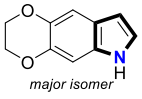 *major isomer*	**2g** 80%
8	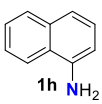 **1h**	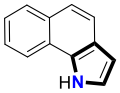	**2h** 90%
9	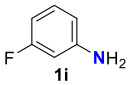 **1i**	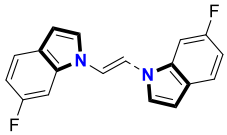	**6** 36%
10	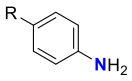	R = NO_2, CN no conversion	

In *Figure 2*, rational mechanism is presented. In first step, ethylene glycol is transformed into the corresponding mono-aldehyde[13] 7 by means of Pt/ Al_2O_3in presence of ZnO as activating agent (conversion dramatically decreased when smaller amount of ZnO are employed, *Table S1*). Nevertheless, 7 has never been isolated under these conditions.[14] It has been reported that a competitive oxidative pathway[15] with O_2 could be also responsible for the obtention of aldehydes from alcohols. However, when the reaction was performed in absence of O_2 (all solvents and reagents were degassed with argon) similar results were obtained. The presence of molecular hydrogen was also confirmed by GC (by taking a sample of the internal gas of the flask after the reaction, see SI) being this another evidence of the ADC path. The relatively long reaction time (24h) and also the absence of 7 may indicate that this first step is the rate limiting one. This hypothesis can be supported by the fact that this step must be mediated by both catalysts, while all the subsequent steps do not require catalyst necessarily. Then, the amine generates the corresponding imine. Under normal BH/HA conditions, this imine would be re-hydrogenated to afford compound 3 (*Figure 3, grey path*). However, employing ethylene glycol, a tautomeric equilibrium of this imine in combination with Pt/ Al_2O_3 limited re-hydrogenation capacity, yields to a different compound undergoing indole formation. Madsen, Williams, and Bruneau have reported on a similar tautomeric feature with amino alcohols under BH reactions in homogeneous phase.[6c,8a,16] The use of ZnO nanoparticles as a catalyst has recently been reported.[12f-g] In our case, the small particle size and the solubility[17] of this oxide may be responsible of an easier co-participation between ZnO and Pt/Al_2O_3 in the first step of the catalytic cycle. The formation of just 3, 4 or 5 as side products clearly indicates that the C-N bond formation is the first step; as no side products derived from an initial cyclization (formation of C-C bond and then formation of the C-N bond) have ever been observed.

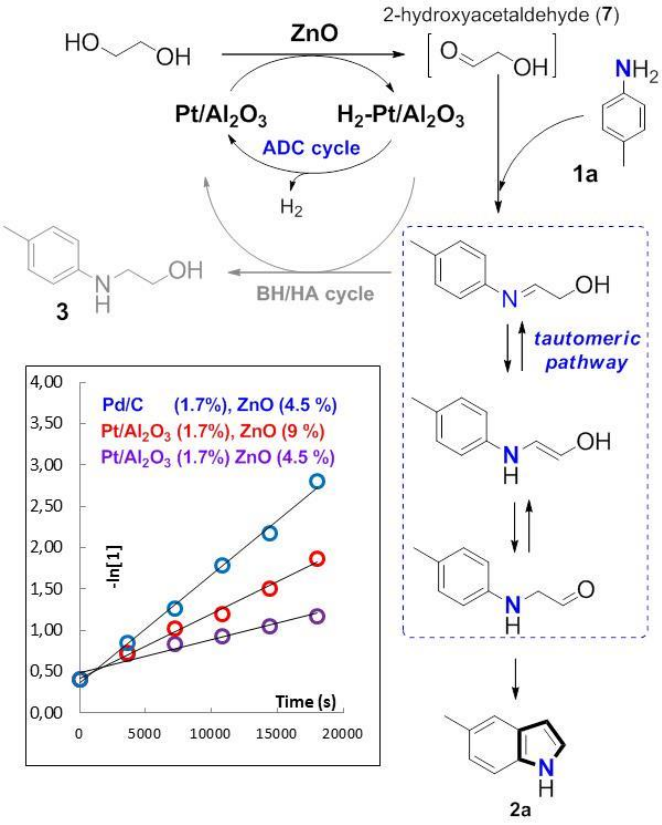

Figure 2. Rational mechanism and kinetic study (inset).

By evaluating the rate of aniline conversion with three different catalysts, we could determine how slow kinetics helps in the formation of indole 2a. This rate (*Figure 2, inset*) for Pd/C was higher than for Pt/ Al_2O_3. With Pd/C the selectivity towards 3, 4 and 5 also increased. Indeed, the faster the dehydrogenation of ethylene glycol, the faster the obtention of side products derived from the BH cycle (3, 4 and 5).[6e] When double quantity of ZnO with Pt/Al_2O_3 was employed the rate also increased, but the selectivity was similar to the standard conditions. The kinetic study also indicated that between the two Pt/Al_2O_3 conditions (more or less ZnO) no significant differences were found in terms selectivity and conversion at long times. However, as noted, with Pd/C kinetics and selectivity were completely different. Under our conditions and without the possibility of re-hydrogenation (due to the Pd/C), the formation of dimers may be explained through accumulation of imine in the reaction (see SI for more details). Competitive experiment between aniline 1d and 1i (*Scheme 1, top*) clearly indicated that electron rich one reacts faster as no trace of 6 was observed. When ethylene glycol was replaced by 1,2-propanediol (8) small conversion with 1d was obtained at 175 ºC. By increasing reaction time (48h), indole 9 was obtained as unique compound. Although compound 8 oxidation may afford two possible products (10 and 10'') that are under tautomeric equilibrium (*Scheme 1, bottom*), the imine formation is faster with aldehydes and the methyl substituent is only present at position *3* in compound 9.[18]

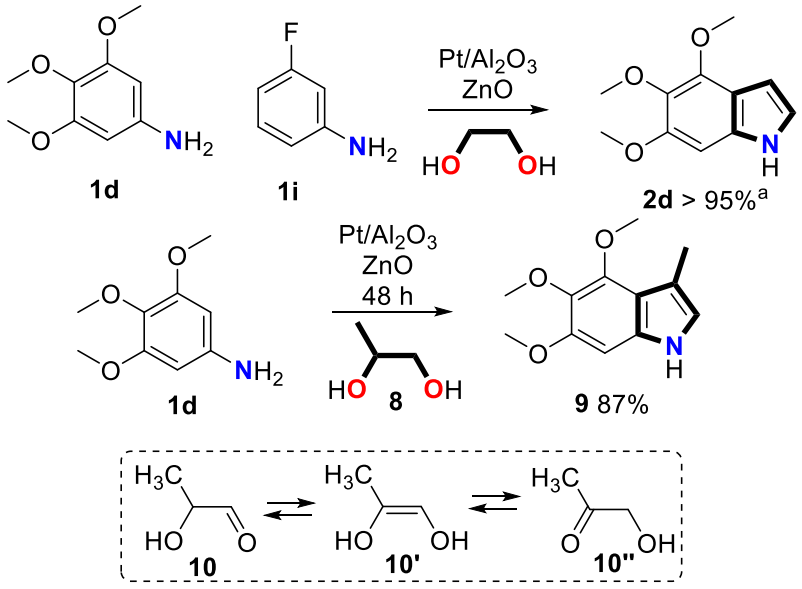

Scheme 1. Competitive experience and 1,2-propanediol (**8**) test.

The indole formation was also explored with different *N*-substituted anilines (11, 13 and 15) and m-phenylenediamine (16) (*Scheme 2*). *N*-methylated aniline 11 afforded indole 12 in good yield. When tetrahydroquinolines 13a and 13b were employed, the corresponding indoles were obtained in moderated (14a, 50% isolated yield) to excellent yields (14b, 89% isolated yield). However, when indoline 15 was submitted to the reaction conditions, no indole was formed.[19-20] With *m*-phenylenediamine (16), excellent yield (87%) was obtained for the bis-indole 17.

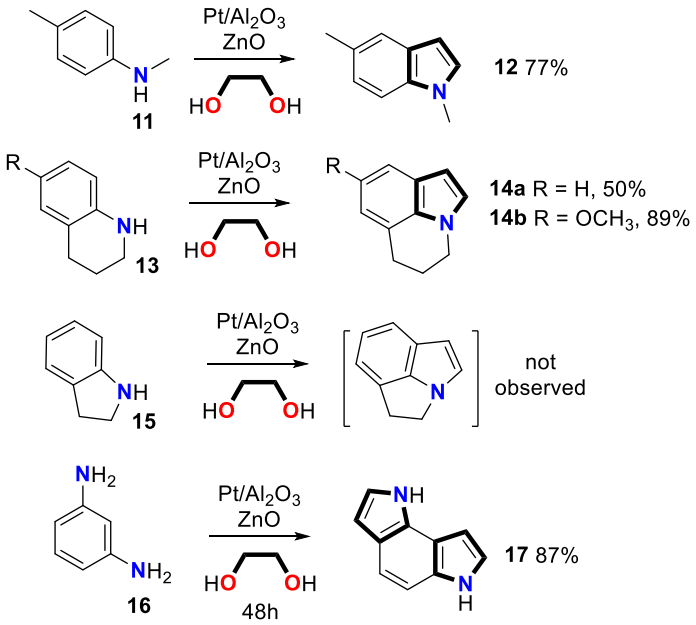

Scheme 2. *N*-substituted indoles and bis-indole **17**.

As it has been outlined before, our methodology allows the transformation of ethylene glycol into the corresponding monoaldehyde 7. In the literature bis-indoles are present in many natural products i.e. Streptindole (18) or Arinsodoline (19) (*Scheme 3, top*).[21] Retrosynthetic analysis suggests that with our methodology, and employing indole 2e as reagent, alcohol 20 may be accessible. As proof of the presence of 7, we attempted the standard reaction starting from 2e. Only a 5% of compound 20 was obtained, however, by increasing temperature and catalyst loading we were able to achieve 23% yield of 20, which can be transformed into 18 and 19 by esterification.[22] Despite the low yield, it is important to highlight that we have been able to access natural products Streptindole's and Arindosoline's precursor 20 in two steps from simple building blocks like aniline and ethylene glycol.

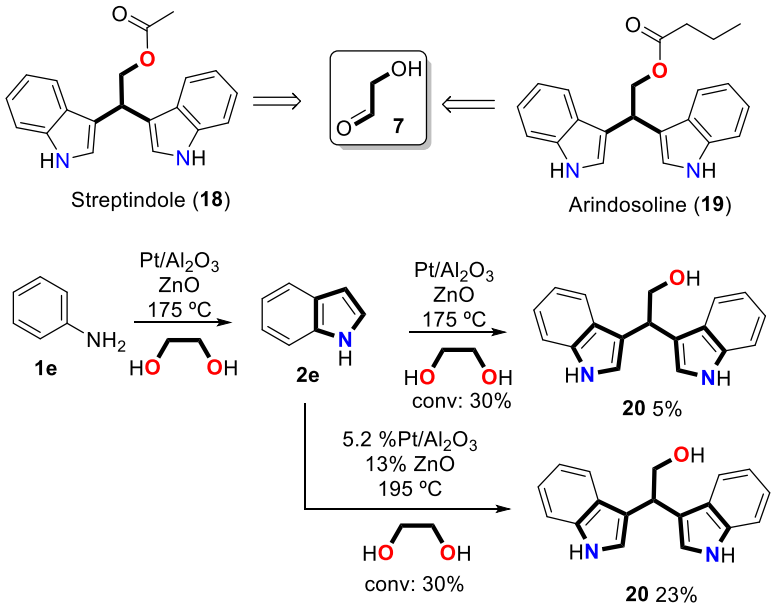

Scheme 3. 2-hydroxyacetaldehyde (**7**) as precursor of natural products, yields are given for isolated compound.

In conclusion, herein we present a new access towards pyrrole-ring unsubstituted indoles based on a heterogeneous ADC reaction between anilines and ethylene glycol. The combination of Pt/Al_2O_3 and ZnO has been found to be able to slowly transform glycol into the corresponding 2-hydroxyacetaldehyde (7) by means of dehydrogenation. In addition, we have been able to capture this intermediate into a natural product precursor (20). Tautomeric equilibrium of the imine intermediate has revealed crucial for the indole formation. This reaction is possible due to mono-activation of ethylene glycol that takes place thanks to the combination of Pt/Al_2O_3 and ZnO. This is an original heterogeneous approach towards pyrrole-ring unsubstituted indoles by an atom efficient protocol. The complementarity between air and moisture stability and economical catalysts (Pt/Al_2O_3 and ZnO) represents a different and efficient approach towards indoles.

EXPERIMENTAL SECTION

Materials and Measurements. Starting materials, if commercially available, were purchased and used as such. ^{1}H and (^{1}H decoupled) ^{13}C nuclear magnetic resonance (NMR) spectra were recorded at 300 and 75 MHz. Chemical shifts are reported in δ units, parts per million (ppm), and were measured relative to the signals for residual chloroform. Coupling constants (J) are given in Hz. COSY and HSQC experiments were performed for new compounds. IR spectra were recorded using FT-IR ATR. HRMS were recorded using TOF electrospray ionization (ESI-positive). The solvents used were of spectroscopic or equivalent grade. Water was twice distilled and passed through a Millipore apparatus. All reaction mixtures were filtered through a 0.45 µm PTFE 25 mm syringe filter.

General Procedure. Aniline (4 mmol) (indole, THQ or indoline), 1.7% of Pt/Al2O3 (273 mg), 4.5% of ZnO nanoparticles (250 mg) (<100 nm particle size (DLS), < 0 nm average particle size (APS), 20 wt % in H2O), and 6 mL of ethylene glycol were mixed manually inside a 50 mL quick-thread glass reaction tube. The tube was sealed with an Easy-On PTFE cap and put into a Carousel 12 Plus reaction station at 175 °C for 24 h. The reaction mixture was cooled to room temperature, and it needed to be opened carefully to depressurize the tube. After that, 30 mL of ethyl acetate was added, and the crude was filtered through a 0.45 µm PTFE filter. The reaction mixture was extracted with distilled water (3 × 20 mL), and the organic layer was dried with Na2SO4, filtered, and concentrated to afford the reaction crude that was checked by 1H NMR. The crude reaction product was purified by column chromatography using Merck 60 (0.040−0.063 mm) silica gel and a mixture of hexane(5):ethyl acetate (1) as eluent.

5-Methylindole (2a)[23]: 360 mg, 70% yield, powder, mp 59 – 60 ºC. ^{1}H NMR (300 MHz, $CDCl_3$) δ: 7.44 (m, 2H), 7.26 (d, J= 8.5 Hz, 1H), 7.12 (d, J= 3.0 Hz, 1H), 6.44 (d, J= 3.0 Hz, 1H), 2.39 (s, 3H). ^{13}C NMR (75 MHz, $CDCl_3$) δ: 148.0 (1C, C), 138.6 (1C, C), 134.0 (1C, C), 130.2 (1C, CH), 121.2 (2C, CH), 119.4 (1C, CH), 94.8 (1C, CH), 20.9 (1C, CH_3).

4,6-Dimethylindole (2b)[24]: 463 mg, 81% yield, oil. ^{1}H NMR (300 MHz, $CDCl_3$) δ: 8.01 (bs, 1H), 7.13 (m, 1H), 7.04 (s, 1H), 6.78 (s, 1H), 6.52 (ddd, J= 3.1; 2.1; 0.9 Hz, 1H), 2.54 (s, 3H), 2.44 (s, 3H). ^{13}C NMR (75 MHz, $CDCl_3$) δ: 136.1 (1C, C), 132.0 (1C, C), 129.9 (1C, C), 125.7 (1C, C), 122.9 (1C, CH), 122.0 (1C, CH), 108.6(1C, CH), 101.1 (1C, CH), 21.8 (1C, CH_3), 18.8 (1C, CH_3).

5,6-Dimethoxyindole (2c)[25]: 725 mg, 84% yield, powder. mp 150 - 151 ºC. ^{1}H NMR (300 MHz, $CDCl_3$) δ: 8.06 (bs, 1H), 7.10 (s, 1H), 7.08 (dd, J= 3.1; 2.4 Hz, 1H), 6.89 (s, 1H), 6.45 (ddd, J= 3.0; 2.1; 0.9 Hz, 1H), 3.92 (s, 3H), 3.90 (s, 3H). ^{13}C NMR (75 MHz, $CDCl_3$) δ: 147.2 (1C, C), 145.3 (1C, C), 130.3 (1C, C), 122.8(1C, CH), 120.7 (1C, C), 102.4 (2C, CH), 94.6 (1C, CH), 56.4 (1C, CH_3), 56.3 (1C, CH_3).

4,5,6-Trimethoxyindole (*2d*): 842 mg, 88% yield, oil. ^{1}H NMR (300 MHz, $CDCl_3$) δ: 8.07 (bs, 1H), 7.04 (dd, J= 3.3; 2.4 Hz, 1H), 6.65 (d, J=0.8 Hz, 1H), 6.65 (ddd, J= 3.2; 2.2; 0.9 Hz, 1H), 4.11 (s, 3H), 3.88 (s, 6H). ^{13}C NMR (75 MHz, $CDCl_3$) δ: 151.3 (2C, C), 146.1 (1C, C), 132.9 (1C, C), 122.3(1C, CH), 115.1 (1C, C), 100.5 (1C, CH), 89.6 (1C, CH), 61.7 (1C, CH_3), 60.8 (1C, CH_3), 56.4 (1C, CH_3). HRMS (ESI-TOF) m/z: [M+H$^+$] Calctd for $C_{11}H_{14}NO_3$ 208.0968; Found: 208.0957. IR (ATR): 3381, 2927, 2842, 1601, 1456, 1346, 1329, 1302, 1241, 1194, 1095, 1011, 938, 831.

1H-Indole (2e)[26]: 201 mg, 43% yield, mp 53 – 54 ºC. ^{1}H NMR (300 MHz, $CDCl_3$) δ: 7.68 (ddt, J= 7.8; 1.6; 0.8 Hz, 1H), 7.41 (ddd, J= 8.1; 1.9; 1.0 Hz, 1H), 7.25-7.19 (m, 2H), 7.17-7.11 (m, 1H), 6.59-6.56 (m, 1H). ^{13}C NMR (75 MHz, $CDCl_3$) δ: 135.9 (1C, C), 128.0 (1C, C), 124.2 (1C, CH), 122.1 (1C, CH), 120.9 (1C, CH), 119.8 (1C, CH), 111.1 (1C, CH), 102.8 (1C, CH).

5H-[1,3]Dioxolo[4,5-f]indole (2f)[27]: 644 mg 86% yield, oil. ^{1}H NMR (300 MHz, $CDCl_3$) δ: 8.01 (bs, 1H), 7.07 (dd, J= 3.1; 2.5 Hz, 1H), 7.02 (s, 1H), 6.84 (s, 1H), 6.44 (ddd, J= 3.1; 2.1; 0.9 Hz, 1H), 5.93 (s, 2H). ^{13}C NMR (75 MHz, $CDCl_3$) δ: 145.0 (1C, C), 143.1 (1C, C), 130.7 (1C, C), 122.9 (1C, CH), 121.8 (1C, C), 102.9 (1C, CH), 100.7 (1C, CH_2), 99.2 (1C, CH), 92.0 (1C, CH).

3,6-Dihydro-2H-[1,4]dioxino[2,3-f]indole (2g) (75%) & *2,3-dihydro-7H-[1,4]dioxino[2,3-e]indole* (2g') (25%)[28]: 560 mg, 80% yield, oil. ^{1}H NMR (300 MHz, $CDCl_3$) δ: 8.02 (bs, 1H'), 7.87 (bs, 1H), 7.12 (m, 1H'), 7.10-7.07 (m, 1H and 1H'), 6.88 (m, 1H and 1H'), 6.78 (d, J= 8.7 Hz, 1H'), 6.55 (ddd, J= 3.0; 2.2; 0.9 Hz, 1H'), 6.39 (ddd, J= 3.1; 2.0; 0.9 Hz, 1H), 4.39 (m, 2H'), 4.33-4.23 (m, 2H' and 4H). ^{13}C NMR (75 MHz, $CDCl_3$) δ: 124.0, 106.9, 102.1, 98.3, 65.05, 64.7, 64.4.

1H-Benz[g]indole (2h)[29]: 603 mg, 90% yield, powder. mp 168 - 169 ºC. ^{1}H NMR (300 MHz, $CDCl_3$) δ: 8.85 (bs, 1H), 7.97 (t, J= 8.4 Hz, 2H), 7.75 (d, J= 8.7 Hz, 1H), 7.53 (m, 2H), 7.45 (ddd, J= 8.1; 7.0; 1.3 Hz, 1H), 7.26 (t, J= 2.8 Hz, 1H), 6.71 (dd, J= 3.0; 2.1 Hz, 1H). ^{13}C NMR (75 MHz, $CDCl_3$). δ: 130.5 (2C, C), 129.0 (1C, CH), 125.6 (1C, CH), 124.0 (1C, CH), 123.9(1C, C), 122.4 (1C, CH), 121.9(1C, C), 120.9 (1C, CH), 120.8 (1C, CH), 119.5 (1C, CH), 104.4 (1C, CH).

2-((4-Methylphenyl)amino)ethanol (3)[30]: traces, oil. ^{1}H NMR (300 MHz, $CDCl_3$) δ: 7.01 (d, J=8.6 Hz, 2H), 6.60 (d, J=8.5 Hz, 2H), 3.82 (t, J= 5.2 Hz, 2H), 3.28 (t, J= 5.2 Hz, 2H), 2.85 (bs, 1H), 2.25 (s, 3H). ^{13}C NMR (75 MHz, $CDCl_3$) δ: 145.8(1C, C), 129.9 (2C, CH), 127.5 (1C, C), 113.7 (2C, CH), 61.4 (1C, CH_2), 46.8 (1C, CH_2), 20.5 (1C, CH_3).

N,N'-Bis(4-methylphenyl)-1,2-ethanediamine (4)[7c]: traces, oil. ^{1}H NMR (300 MHz, $CDCl_3$) δ: 7.01 (d, J= 8.0 Hz, 4H), 6.64 (d, J= 8.4 Hz, 4H), 3.39 (s, 4H), 2.25 (s, 6H). ^{13}C NMR (75 MHz, $CDCl_3$) δ:

145.1 (2C, C), 130.0 (4C, CH), 128.0 (2C, C), 114.0 (4C, CH), 44.2 (2C, CH_2), 20.5 (2C, CH_3). HRMS (ESI-TOF) m/z: [M+H$^+$] Calcd for $C_{16}H_{21}N_2$ 241.1699; Found 241.1688. IR (ATR): 2918, 2858, 1616, 1517, 1464, 1317, 1296, 1256, 1182, 1127, 806.

1,4-Bis(4-methylphenyl)-piperazine (5)[7c]: traces, oil. ^{1}H NMR (300 MHz, $CDCl_3$) δ: 7.11 (d, J= 8.6 Hz, 4H), 6.91 (d, J= 8.5 Hz, 4H), 3.30 (s, 8H), 2.29 (s, 6H). ^{13}C NMR (75 MHz, $CDCl_3$) δ: 149.3 (2C, C), 129.8 (6C, C and CH), 116.9 (4C, CH), 50.2 (4C, CH_2), 20.6 (2C, CH_3). HRMS (ESI-TOF) m/z: [M+H$^+$] Calctd for $C_{18}H_{23}N_2$ 267.1856; Found: 267.1844. IR (ATR): 2953, 2919, 2855, 2820, 2360, 2343, 1743, 1615, 1515, 1489, 1384, 1293, 1229, 1180, 1041, 823, 771.

(Z,E)-1,2-Bis(6-fluoro-1H-indol-1-yl)ethene (6): 423 mg, 36% yield, oil. ^{1}H NMR (300 MHz, Acetone-d6) δ: 7.54 (m, 4H), 7.46 (d, J= 3.2 Hz, 2H), 7.44 (m, 2H), 6.99 (m, 2H), 6.68 (d, J= 3.1 Hz, 2H). ^{13}C NMR (75 MHz, Acetone-*d*6) δ: 164.5 (2C, d, J= 244.0 Hz, C), 132.4 (4C, C), 122.3 (2C, CH), 115.3 (2C, CH), 111.6 (2C, d, J= 21.4 Hz, CH), 106.6 (2C, d, J= 25.7, CH), 97.4 (2C, CH). HRMS (ESI-TOF) m/z: [M+H$^+$] Calctd for $C_{18}H_{14}F_2N_2$ 295.1041; Found: 295.1040. IR (ATR): 3377, 3003, 2926, 1732, 1603, 1567, 1483, 1409, 1272, 1185, 1121, 750.

4,5,6-Trimethoxy-3-methyl-1H-indole (9): 751 mg, 87% yield, oil. ^{1}H NMR (300 MHz, $CDCl_3$) δ: 7.77 (bs, 1H), 6.56 (d, J= 0.6 Hz, 1H), 6.24 (dt, J= 2.0; 0.9 Hz, 1H), 4.07 (s, 3H), 3.87 (s, 3H), 3.86 (s, 3H), 2.39 (d, J= 1.0 Hz, 3H). ^{13}C NMR (75 MHz, $CDCl_3$) δ: 150.3 (1C, C), 145.3 (1C, C), 136.7 (1C, C), 133.1 (1C, C), 133.1 (1C, C), 115.9 (1C, C), 98.0 (1C, CH), 89.5 (1C, CH), 61.6 (1C, CH_3), 60.7 (1C, CH_3), 56.5 (1C, CH_3), 13.7 (1C, CH_3). HRMS (ESI-TOF) m/z: [M+H$^+$] Calcd for $C_{12}H_{16}NO_3$ 222.1125; Found 222.1127. IR (ATR): 1626, 1495, 1466, 1441, 1325, 1202, 1134, 1037, 752, 707.

1,5-Dimethyl-1H-indole (12)[31]: 446 mg, 77% yield, oil. ^{1}H NMR (300 MHz, $CDCl_3$) δ: 7.47 (dt, J= 1.6; 0.8 Hz, 1H), 7.27 (d, J= 8.3 Hz, 1H), 7.11 (dd, J= 8.3; 1.6 Hz, 1H), 7.05 (d, 3.1 Hz, 1H), 6.45 (dd, J= 3.1; 0.8 Hz, 1H), 3.80 (s, 3H), 2.52 (s, 3H). ^{13}C NMR (75 MHz, $CDCl_3$) δ: 135.3 (1C, C), 128.9 (1C, CH), 128.8 (1C, C), 128.5 (1C, C), 123.2 (1C, CH), 120.6 (1C, CH), 109.0 (1C, CH), 100.4 (1C, CH), 32.9 (1C, CH_3), 21.5 (1C, CH_3).

5,6-Dihydro-4H-pyrrolo-[3,2,1-ij]-quinoline (14a)[32]: 315 mg, 50% yield, oil. ^{1}H NMR (300 MHz, $CDCl_3$) δ: 7.37 (dd, J= 7.9; 0.8 Hz, 1H), 7.00 (d, J= 3.0 Hz, 1H), 6.94 (dd, J= 7.9; 7.1 Hz, 1H), 6.84 (dd, J= 7.1; 0.9 Hz, 1H), 6.37 (d, J= 3.0 Hz, 1H), 4.09 (t, J= 5.7 Hz, 2H), 2.93 (t, J= 6.1 Hz, 2H), 2.17 (m, 2H). ^{13}C NMR (75 MHz, $CDCl_3$) δ: 134.3 (1C, CH), 126.1(1C, CH), 126.0 (1C, C), 122.0 (1C, C), 119.8 (1C, CH), 118.7 (1C, CH), 118.3(1C, CH), 100.5 (1C, CH), 44.3 (1C, CH_2), 24.9 (1C, CH_2), 23.1 (1C, CH_2).

8-Methoxy-5,6-dihydro-4H-pyrrolo[3,2,1-ij]quinoline (14b): 663 mg, 89% yield, oil. ^{1}H NMR (300 MHz, $CDCl_3$)δ: 7.05 (d, J= 2.9 Hz, 1H), 6.91 (d, J= 2.2 Hz, 1H), 6.62 (dd, J= 1.5; 0.6 Hz, 1H), 6.36 (d, J= 2.9 Hz, 1H), 4.13 (t, J= 5.7 Hz, 2H), 3.84 (s, 3H), 2.96 (dd, J= 8.9; 3.4 Hz, 2H), 2.28-2.17 (m, 2H). ^{13}C NMR (75 MHz, $CDCl_3$) δ: 154.84 (1C, C), 126.34 (1C, CH), 125.8 (1C, C), 122.7(2C, C), 109.4 (1C, CH), 100.1 (1C, CH), 99.9 (1C, CH), 56.2 (1C, CH_3), 44.2 (1C, CH_2), 25.0 (1C, CH_2), 23.2

(1C, CH_2). HRMS (ESI-TOF) m/z: [M+H$^+$] Calcd for $C_{12}H_{14}NO$: 188.1070; Found 188.1066. IR (ATR): 2938, 1618, 1601, 1495, 1436, 1342, 1261, 1218, 1047, 830,716.

1,6-Dihydropyrrolo[2,3-e]indole (17)[33]: 542 mg, 87% yield, oil. ^{1}H NMR (300 MHz, MeOD) δ: 7.35 (d, J= 8.6 Hz, 1H), 7.17 (m, 2H), 7.11 (d, J= 3.1 Hz, 1H), 6.71 (dd, J= 3.1; 0.8 Hz, 1H), 6.53 (d, J= 3.1 Hz, 1H). ^{13}C NMR (75 MHz, MeOD) δ: 134.2 (1C, C), 130.2 (1C, C), 122.4 (1C, CH), 121.36 (1C, C), 121.1 (1C, CH), 115.6 (1C, CH), 114.8 (1C, C), 106.0 (1C, CH), 103.2 (1C, CH), 98.7 (1C, CH).

2,2-Di(1H-indol-3-yl)ethan-1-ol (20)[21d] 220 mg, 23% yield, oil. ^{1}H NMR (300 MHz, $CDCl_3$) δ: 8.03 (bs, 1H), 7.61 (d, J= 8.0 Hz, 2H), 7.38 (dt, J= 8.2; 0.9 Hz, 2H), 7.19 (ddd, J= 8.2; 7.1; 1.2 Hz, 2H), 7.11 (dd, J= 2.3; 0.6 Hz, 2H), 7.07 (ddd, J= 8.0; 7.0; 1.0 Hz, 2H), 4.80 (t, J= 6.2 Hz, 1H), 4.31 (d, J= 6.2 Hz, 2H). ^{13}C NMR (125 MHz, $CDCl_3$) δ: 136.7 (2C, C), 127.1 (2C, C), 122.7 (2C, CH), 122.3 (2C, CH), 119.61 (2C, CH), 119,6 (2C, CH), 116.4 (2C, CH), 111.35 (2C, CH), 66.0 (1C, CH_2), 37.3 (1C, CH).

ASSOCIATED CONTENT

Supporting Information

The Supporting Information is available free of charge on the ACS Publications website at DOI: 10.1021/acs.joc.7b02722.

Complete screening of conditions, complete mechanistic analysis, and spectroscopic characterization (PDF)

AUTHOR INFORMATION

Corresponding Author

*E-mail: rafael.ballesteros-garrido@uv.es.

ORCID

Rafael Ballesteros-Garrido: 0000-0002-8364-114X

Notes

The authors declare no competing financial interest.

ACKNOWLEDGMENTS

R.B.-G. is indebted to the Postdoctoral Fellow 2013 program of the Ministerio de Economía y Competitividad (Spain, FPDI-2013-17464). We are especially grateful to “Central Service for Experimental Research” (SCSIE) of University of Valencia and the NANBIOSIS platform. This work was financially from University of Valencia (Spain) (UV-INV-AE 15-332846). Prof. H. Garcia and Dr. J. Albero (ITQ, UPV) are acknowledged for their help with the GC molecular hydrogen determination. We gratefully acknowledge the suggestions and advice from the reviewers and the Editor to improve the quality of this contribution.

REFERENCES

1) a) G.W. Gribble in *Indole Ring Synthesis: From Natural Products to Drug Discovery*, Chichester, UK, John Wiley & Sons, Inc., **2016**. b) M. Inman, C.J. Moody, *Chem. Sci.*, **2013**, *4*, 29. c) D.F. Taber, P.K. Tirunahari, *Tetrahedron*, **2011**, *67*, 7195. d) G.R. Humphrey, J.T. Kuethe, *Chem. Rev.*, **2006**, *106*, 2875. e*)* R.J. *Sundberg* in *The Chemistry of Indoles. Organic Chemistry, a Series of Monographs, Vol. 18.* Academic Press, New York–London, **1970**.

2) a) E. Fischer, F. Jourdan, *Ber. Dtsch. Chem. Ges.*, **1883**, *16*, 2241. b) A. Reissert, *Ber. Dtsch. Chem. Ges.*, **1897**, *30*, 1030. c) I. Grandberg, T.I. Zuyanova, N.I. Afonina, T.A. Ivanova, *Dokl. Akad. Nauk SSSR*, **1967**, *176*, 583. d) A. Bischler, *Ber. Dtsch. Chem. Ges.*, **1892**, *25*, 2860.

3) a) R.D. Clark, D.B. Repke, *Heterocycles*, **1984**, *22*, 195. b) A. Batcho, W. Leimgruber, *Org. Synth.*, **1985**, *63*, 214. c) A.D. Batcho, W. Leimgruber, *Org. Synth. Coll.,* **1990**, *7*, 34. d) F. He, Y. Bo, J.D. Altom, E.J. Corey, *J. Am. Chem. Soc.*, **1999**, *121*, 6771.

4) a) W. Madelung, *Ber.*, **1912**, *45*, 1128. b) Y. Ito, K. Kobayashi, T. Saegusa, *J. Am. Chem. Soc.*, **1977**, *99*, 3532.

5) Unsubstituted indoles are referred to indoles without substituents at N, C2 and C3 atoms, some examples are reported see ref 3d and 4b.

6) a) M. Campanati, S. Franceschini, O. Piccolo, A. Vaccari, *J. Catal.*, **2005***, 232,* 1. b) J. Xing, X. Jia, *Adv. Mat. Res.*, **2011**, *295-297*, 668. c) M. Tursky, L.L.R. Lorentz-Petersen, L.B. Olsen, R. Madsen, *Org. Biomol. Chem*., **2010**, *8*, 5576. This methodology has also been explored by d) M. Zhang, F. Xie, X.T. Wang, F. Yan, T. Wang, M. Chen, Y. Ding, *RSC Adv*., **2013**, *3*, 6022. e) Y. Tsuji, T. Keun, Y. Watanabe, *J. Org. Chem.*, **1987**, *52*, 1673. The indole formationcan be improved adding $SnCl_2$ see: C.S. Cho, M.J. Lee, S.C. Shim, M.C. Kim, *Bull. Korean Chem. Soc.,* **1999**, *20*, 119. f) H. Lee, C. Yi, *Organometallics,* **2016***, 35,* 1973. Epoxides have also been employed, i.e. see: M. Peña-Lopez, H. Neumann, M. Beller, *Chem. Eur. J.*, **2014**, *20*, 1818.

7) a) R. Adam, R. Ballesteros, B. Abarca, *Org. Biomol. Chem.*, **2012**, *10*, 1826. b) For a review on Pd-Catalyzed Hydrogen-Transfer Reactions see: J. Muzart*, Eur. J. Org. Chem.,* **2015**, 5693. c) P.J. Llabres-Campaner, R. Ballesteros-Garrido, R. Ballesteros, B. Abarca, *Tetrahedron*, **2017**, *73*, 5552.

8) a) M.S. Haniti, A. Hamid, C.L. Allen, G.W. Lamb, A.C. Maxwell, H.C. Maytum, A.J.A. Watson, J.M.J. Williams, *J. Am. Chem. Soc.*, **2009**, *131*, 1766. b) M. Selva, A. Perosa, M. Fabris, *Green Chem.*, **2008**, *10*, 1068. c) A.B. Shivarkar, S.P. Gupte, R.V. Chaudhari, *SYNLETT*, **2006**, 1374. d) S. Bähn, A. Tillack, S. Imm, K. Mevius, D. Michalik, D. Hollmann, L. Neubert, M. Beller, *ChemSusChem,* **2009**, *2*, 551. e) N. Andrushko, V. Andrushko, P. Roose, K. Moonen, A. Börner, *ChemCatChem*, **2010**, *2*, 640.

9) Borrowing Hydrogen (BH) reactions are also named as Hydrogen Autotransfer (HA) reactions: a) A.J.A. Watson, J.M.J. Williams, *Science*, **2010**, *329*, 635. b) M.H.S.A. Hamid, P.A. Slatford, J.M.J. Williams, *Adv. Synth. Catal.*, **2007**, *349*, 1555. c) G. Guillena, D.J. Ramon, M. Yus, *Chem. Rev.*, **2010**, *110*, 1611.

10) S. Michlik, R. Kempe, *Nat. Chem.*, **2013**, *5*, 140.

11) a) T. Hille, T. Irrgang, R. Kempe, *Angew. Chem. Int. Ed.*, **2017**, *56*, 371. b) F. Kallmeier, B. Dudziec, T. Irrgang, R. Kempe, *Angew. Chem. Int. Ed.*, **2017**, *56*, 7261. c) D. Forberg, J. Obenauf, M. Friedrich, S.M. Hühne, W. Mader, W. Motz, R. Kempe, *Catal. Sci. Technol.*, **2014**, *4*, 4188. d) For a review on ADC see e) C. Gunanathan, D. Milstein, *Science*, **2013**, *341*, 1229712.

12) a) S.J.J. Kolboe, *Catal.*, **1972**, *27*, 379. b) H.D. Müller, F. Steinbach, *Nature*, **1970**, *225*, 728. c) J.M. Vohs, M.A. Barteau, *Surf. Sci.*, **1989**, *221*, 590. d) M.I. Nokkosmäski, E.T. Kuoppala, E.A. Leppämäki, A.O.I. Krausse, *J. Anal. Appl. Pyrolysis*, **2000,** *55*, 119. e) T. Nakajima, K. Tanabe, T. Yamaguchi, I. Matsuzaki, S. Mishima, *Appl. Catal.*, **1989**, *52*, 237. f) M. Hosseini-Sarvari, Z. Razmi, *Appl. Surf. Sci.*, **2015**, *324*, 265–

274. g) A. Hassanpour, R.H. Khanmiri, J. Abolhasani, *Synthetic Commun.*, **2015**, *45*, 727. h) L. Dinparast, H. Valizadech, *Monatsh. Chem.*, **2015**, *146*, 313.

13) 2-Hydroxyacetaldehyde (**7**) is a particular molecule also known as glycolaldehyde. It has been proposed as a fundamental motive in the origin of live and has a complex tautomeric equilibrium. See: D. Ritson, J.D. Sutherland, *Nat. Chem.*, **2012**, *4*, 895–899. Tautomery: L.M. Azofra, M.M. Quesada-Moreno, I. Alkorta, J.R. Avilés-Moreno, J. Elguero, J.J. López-González, ChemPhysChem, **2015**, *16*, 2226. It can be obtained from cellulose with H_2WO_4, see: G. Liang, A. Wang, L. Li, G. Xu, N. Yan, T. Zhang, *Angew. Chem. Int. Ed.*, **2017**, *56*, 3050.

14) a) L. Xin, Z. Zhang, J. Qi, D. Chadderdon, W. Li, *Appl. Catal. B-Environ*., **2012**, *125*, 85. b) B.N. Zope, D.D. Hibbitts, M. Neurock, R.J. Davis*, Science,* **2010**, *330*, 74. c) Y. Kwon, S.C.S. Lai, P. Rodriguez, M.T.M. Koper, *J. Am. Chem. Soc.*, **2011**, *133*, 6914. d) Y.H. Ke, X.X. Qin, C.L. Liu, R.Z. Yang, W.S. Dong, *Catal. Sci. Technol.*, **2014**, *4*, 3141. e) S.A. Kholodar, C.L. Allen, A.M. Gulick, A.S. Murkin, *J. Am. Chem. Soc.*, **2015**, *137*, 2748.

15) H. Liu, H.R. Tan, E.S. Tok, S. Jaenicke, G.K. Chuah, *ChemCatChem*, **2016**, *8*, 968.

16) A. Labed, F. Jiang, I. Labed, A. Lator, M. Peters, M. Achard, A. Kabouche, Z. Kabouche, G.V.M. Sharma, C. Bruneau, *ChemCatChem.*, **2015**, *7*, 1090.

17) ZnO has been reported to be soluble in hot ethylene glycol: J. Wang, Y. Chen, W. Shen, Z. Zhu, Y. Xu, Y. Fang, *Catal Commun.*, **2017**, *89*, 52.

18) For this compound either C1 or C2 oxidation have been proposed although ketone formation is favoured: a) R.M. Painter, D.M. Pearson, R.M. Waymouth, *Angew. Chem. Int. Ed.*, **2010**, *49*, 9456. b) Z. Han, L. Rong, J. Wu, L. Zhang, Z. Wang, K. Ding, *Angew. Chem. Int. Ed.*, **2012**, *51*, 13041.

19) a) X. Jiang, W. Tang, D. Xue, J. Xo, C. Wang, ACS *Catal.*, **2017**, *7*, 1831. b) K.H. He, F.F. Tan, C.Z. Zhou, G.J. Zhou, X.L. Yang, Y. Li, *Angew. Chem. Int. Ed.*, **2017**, *56*, 3080.

20) a) M. Yagoubi, A.C.F. Cruz, P.L. Nichols, R.L. Elliott, M.C. Willis, *Angew. Chem. Int. Ed.*, **2010**, *49*, 7958. b) A.B. Smith III, L. Kürti, A.H. Davulcu, Y.H. Cho, K. Ohmoto, *J. Org. Chem.*, **2007**, *72*, 4611. c) A.B. Smith, III, L. Kúrti, A.H. Davulcu, *Org. Lett.*, **2006**, *8*, 2167.

21) T. Osawa, M. Namiki, *Tetrahedron Lett.*, **1983**, *24*, 4719. b) E. Fahy, B.C.M. Potts, D.J. Faulkner, K.J. Smith, *Nat. Prod.*, **1991**, *54*, 564. c) R. Bell, S. Carmeli, N. Sar, *J. Nat. Prod.,* **1994**, *57*, 1587. d) G. Bifulco, I. Bruno, R. Riccio, J. Lavayre, G. Bourdy, *J. Nat. Prod.,* **2000**, *63*, 596.

22) For efficient synthesis of these natural products see: a) J. Xiang, J. Wang, M. Wang, X. Meng, A. Wu, *Org. Biomol. Chem*., **2015**, *13*, 4240. b) T. Abe, S.I. Nakamura, R. Yanada, T. Choshi, S. Hibino, M. Ishikura, *Org. Lett.*, **2013**, *15*, 3622. c) G. Bartoli, M. Bosco, G. Foglia, A. Giuliani, E. Marcantoni, L. Sambri, *Synthesis,* **2004**, 895.

23) P. Thansandote, D. Hulcoop, M. Langer, M. Lautens, *J. Org. Chem*., **2009**, *74*, 1673.

24) O. Onajole, M. Pieroni, S. Tipparaju, S. Lun, J. Stec, G. Chen, H. Gunosewoyo, H. Guo, N. Ammerman W. Bishai, A. Kozikowski, *J. Med. Chem*., **2013**, *56*, 4093.

25) I. Choi, H. Chung, J.W. Par, Y.K. Chung, *Org. Lett.*, **2016**, *18*, 5508.

26) K.R. Randles, R.C. Storr, *Tetrahedron Lett.*, **1987**, 45, 5555.

27) I. Taydakov, T. Dutova, E. Sidorenko, S. Krasnoelsky, Chem. *Heterocycl. Commun*., **2011**, *47*, 521.

28) D. Zembower, Y. Xie, A. Koohang, M. Kuffel, M. Ames, Y. Zhou, R. Mishra, A. Mar, M. Flavin, Z. Xu, *Anticancer Agents Med. Chem*., **2012**, *12*, 1117.

29) H. Aramoto, Y. Obora, Y. Ishii, *J. Org. Chem*., **2009**, *74*, 628.

30) A. Shafir, P. Lichtor, S. Buchwald, *J. Am. Chem. Soc.*, **2007**, *129*, 3490.

31) D. Solé, F. Pérez-Janer, E. Zulaica, J.F. Guastavino, I. Fernández, *ACS Catal.*, **2016**, *6*, 1691.

32) Z. Shi, C. Zhang, S. Li, D. Pan, S. Ding, Y. Cui, N. Jiao, *Angew. Chem. Int. Ed.*, **2009**, *48*, 4572.

33) S.A. Samsoniya, *Heterocycl. Commun.*, **2010**, 99.

Supporting Information

Straight Access to Indoles from Anilines by Heterogeneous Acceptorless Dehydrogenative Condensation

Pedro Juan Llabres-Campaner[a], Rafael Ballesteros-Garrido*[a,b], Rafael Ballesteros[a] and Belén Abarca[a]

[a] Pedro Juan Llabres-Campaner, Dr. Rafael Ballesteros-Garrido, Pr. Rafael Ballesteros and Pr. Belén Abarca
Departmento de Química Orgánica, Facultad de Farmacia
Universidad de Valencia, Vicent Andres Estelles s/n 46100 Burjassot
E-mail: rafael.ballesteros-garrido@uv.es
[b] Dr. Rafael Ballesteros-Garrido Department
ICMOL Universidad de Valencia
Calle Catedrático José Beltrán Martínez, 2, 46980 Paterna Spain

Contents

S1. Complete screening of conditions

In the attempt of finding the conditions in which the selectivity towards indole **2a** were the highest, changes in concentration of *p*-toluidine **1a**, temperature and time, amount of ethylene glycol, kind and percentage of transition metal catalyst and kind and percentage of ZnO were carried out (*Table S1*). First reactions at 150ºC (*entries 1-7*) allowed to determine that Pt/Al_2O_3 induced the best selectivity towards **2a** in comparison with Ru/Al_2O_3 and Pd/C, that the presence of ZnO was needed, and that the use of a suspension of nanoparticles of ZnO in water instead of regular ZnO afforded better results. Increase of temperature to 175 ºC increased the conversion of **1a**, obtaining again the best results with Pt/Al_2O_3 and nanoparticles of ZnO (*entries 8-10*). Increase of the concentration of **1a** by reducing the amount of ethylene glycol or increasing of the amount of **1a** (*entries 12-19*) improved even more the conversion and selectivity of the reaction, affording the best results with 0.66 M of **1a** and 6 mL of ethylene glycol (*entry 19*). Finally, changes in the duration of the reaction and concentration of **1a** (*entries 20-22*) did not afforded better results.

Table S1. Screening conditions for the preparation of indole **2a**

Entry	[1a] (M)	T (ºC)	t (h)	EG (mL)	Catalyst	ZnO	Conversion[a] (%)	Selectivity (%) by ^{1}H-NMR		
								2a	3	4&5
1	0.08	150	24	12	Pt/Al_2O_3 7%	ZnO 18%	76	64	17	-
2	0.08	150	24	12	Ru/Al_2O_3 7%	ZnO 18%	69	16	55	-
3	0.08	150	24	12	Pd/C 7%	ZnO 18%	90	66	0	traces
4	0.08	150	24	12	Pt/Al_2O_3 7%	-	40	95	0	-
5	0.08	150	24	12	Ru/Al_2O_3 7%	-	5	90	10	-
6	0.08	150	24	12	Pd/C 7%	ZnO nano 18%	75	54	36	traces
7	0.08	150	24	12	Pt/Al_2O_3 7%	ZnO nano 18%	72	70	21	-
8	0.08	175	24	12	Pt/Al_2O_3 7%	ZnO 18%	90	71	0	-
9	0.08	175	24	12	Pd/C 7%	ZnO nano 18%	78	60	10	traces
10	0.08	175	24	12	Pt/Al_2O_3 7%	ZnO nano 18%	86	76	0	-
11	0.16	175	24	6	Pt/Al_2O_3 7%	ZnO 18%	81	55	0	-
12	0.33	175	24	6	Pt/Al_2O_3 3,5%	ZnO 9%	95	80	0	-
13	0.33	175	24	6	Pd/C 3,5%	ZnO 9%	82	47	0	traces
14	0.33	175	24	6	Pt/Al_2O_3 3,5%	ZnO nano 9%	90	80	0	-
15	0.33	175	24	6	Pt/Al_2O_3 3,5%	-	51	48	0	-
16	0.66	175	24	6	Pt/Al_2O_3 1,75%	ZnO 4,5%	88	76	7	-
17	**0.66**	**175**	**24**	**6**	**Pt/Al_2O_3 1,75%**	**ZnO nano 4,5%**	**92**	**82**	**2**	**-**
18	1.66	175	24	6	Pt/Al_2O_3 0,7%	ZnO 1,8%	70	75	15	-
19	0.66	175	24	3	Pt/Al_2O_3 3,5%	ZnO 9%	80	56	0	-
20	0.33	175	48	6	Pt/Al_2O_3 3,5%	ZnO 9%	95	60	0	-
21	1	175	24	6	Pt/Al_2O_3 1,15%	ZnO nano 3%	73	83	11	-
22	1	175	12	6	Pt/Al_2O_3 1,15%	ZnO nano 3%	63	73	21	-

[a] Conversion based on *p*-toluidine **1a** in ^{1}H-NMR.

S2. Kinetic studies

Kinetic studies regarding the proposed mechanism of the reaction were carried out. Different reactions with *p*-toluidine **1a** at the standard conditions at different times (1-24h) were analyzed to evaluate the yield of all the found products (**2**-**5**) at each time, based on the ^{1}H-NMR spectra. As it can be seen in *Figure S1*, the amount of **1a** was decreasing while all the other products were generating. β-amino alcohol **3** increased its amount in the first 8h, after that its concentration was constant until 20h. Side products **4** and **5** reached their maximum yield in the first 5 hours of reaction, where the concentration of aniline **1a** was highest, however, after that, these products were not generated any more.

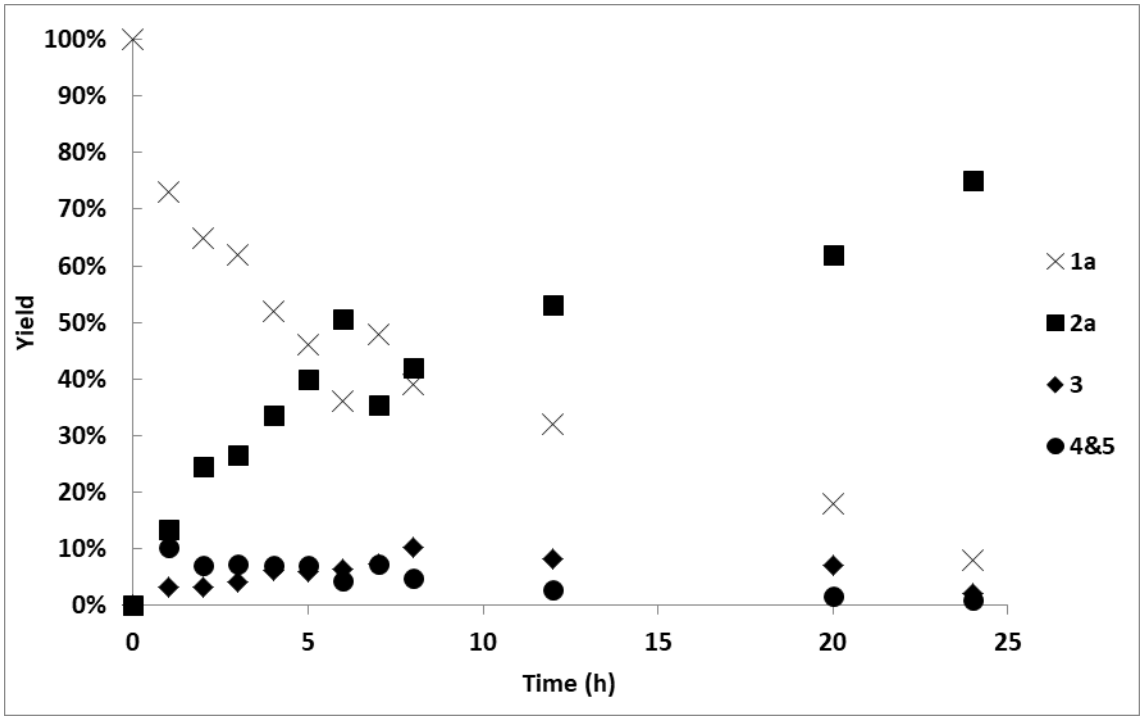

Figure S1. Representation of the yield of products in the reaction at different times measured by ^{1}H-NMR.

S3. Proposed rational mechanism for the formation of compound 6

In the proposed rational mechanism in *Figure 2*, a tautomeric pathway between imine and aldehyde is needed to achieve indoles. In the case of employing 3-fluoroaniline (**1i**), once the imine is formed and tautomerize to the aldehyde, the deactivation induced by fluorine obstructs the ring formation to indole (it does not happen in the case of employing p-toluidine **1a**). Moreover, heterogeneous catalyst Pt/Al_2O_3 does not favor re-hydrogenation of imine to complete the BH cycle, and obtention of β-amino alcohol is very slow. Thus, this aldehyde that cannot turn neither into indole or into β-amino alcohol can react with remaining 3-fluoroaniline **1i**, obtaining dimer **7**. As re-hydrogenation of this dimer is, again, not favored, the formation of bis-indole **6** may be possible after overreaction of **7** (*Scheme S1*).

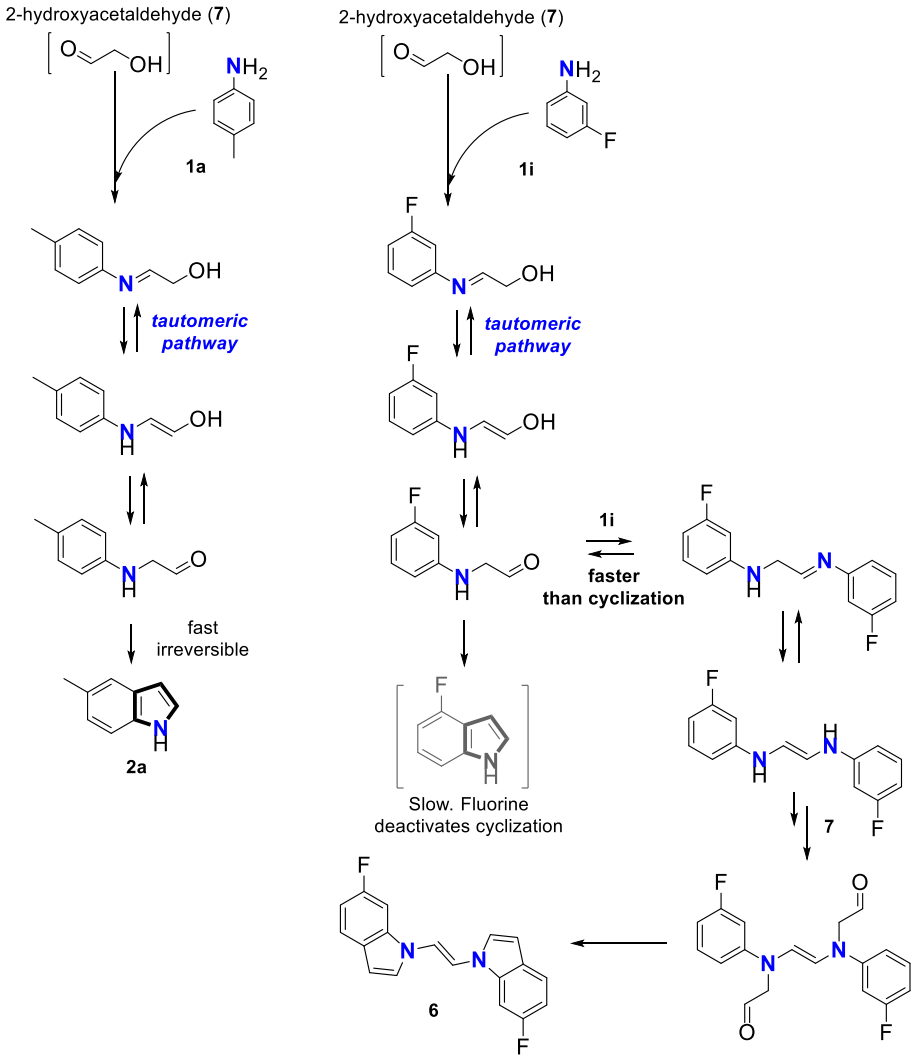

Scheme S1. Rational mechanism of the formation of compound **6**.

S4. NMR spectra of synthesized products

5-methylindole (2a)

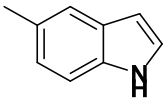

^{1}H NMR Spectrum
(300 MHz, $CDCl_3$)

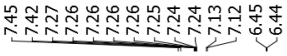

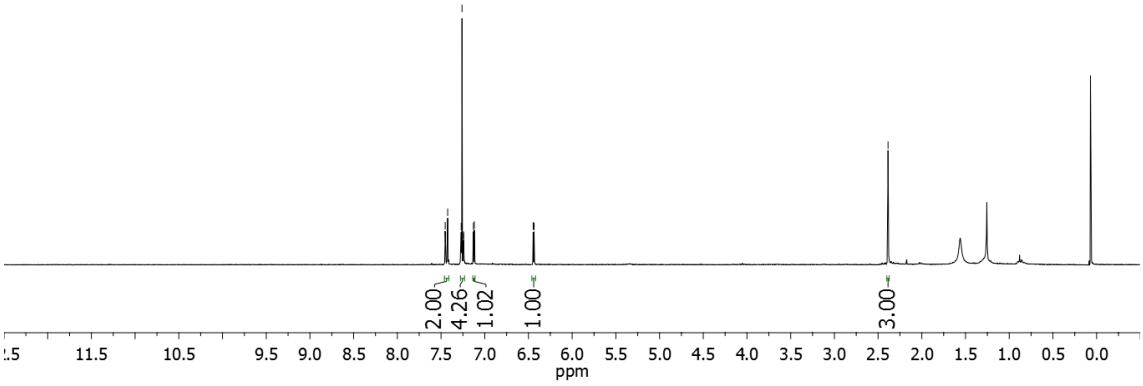

^{13}C NMR Spectrum
(75 MHz, $CDCl_3$)

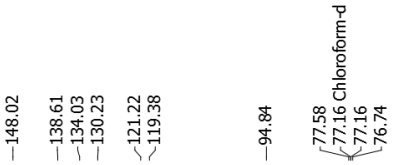

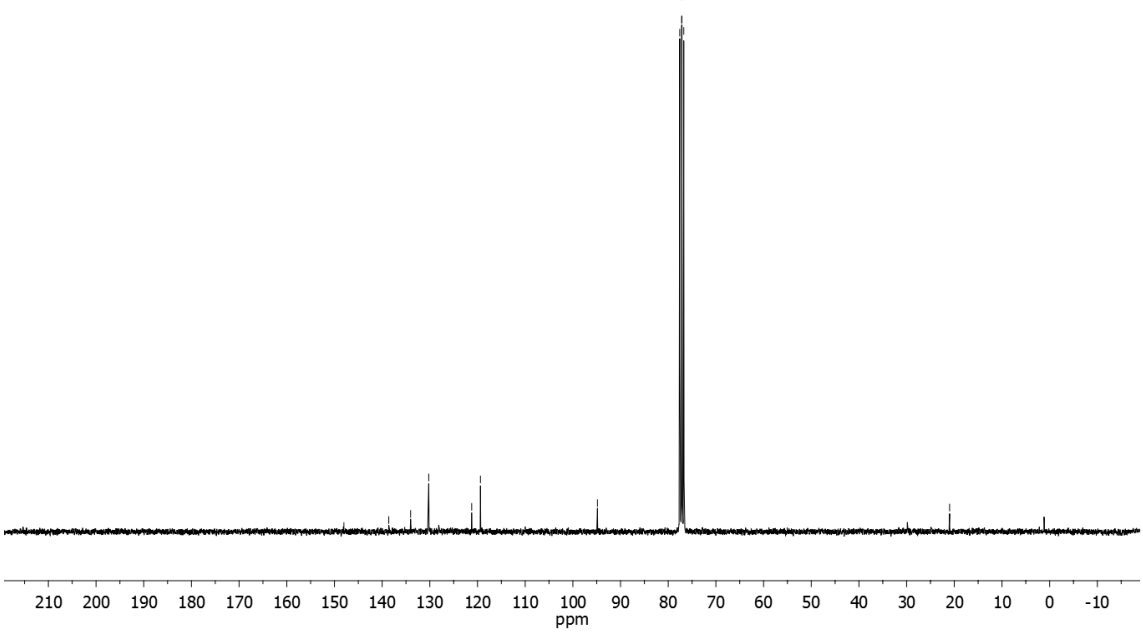

4,6-dimethylindole (2b)

^{1}H NMR Spectrum
(300 MHz, $CDCl_3$)

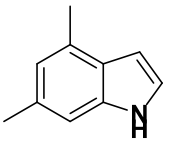

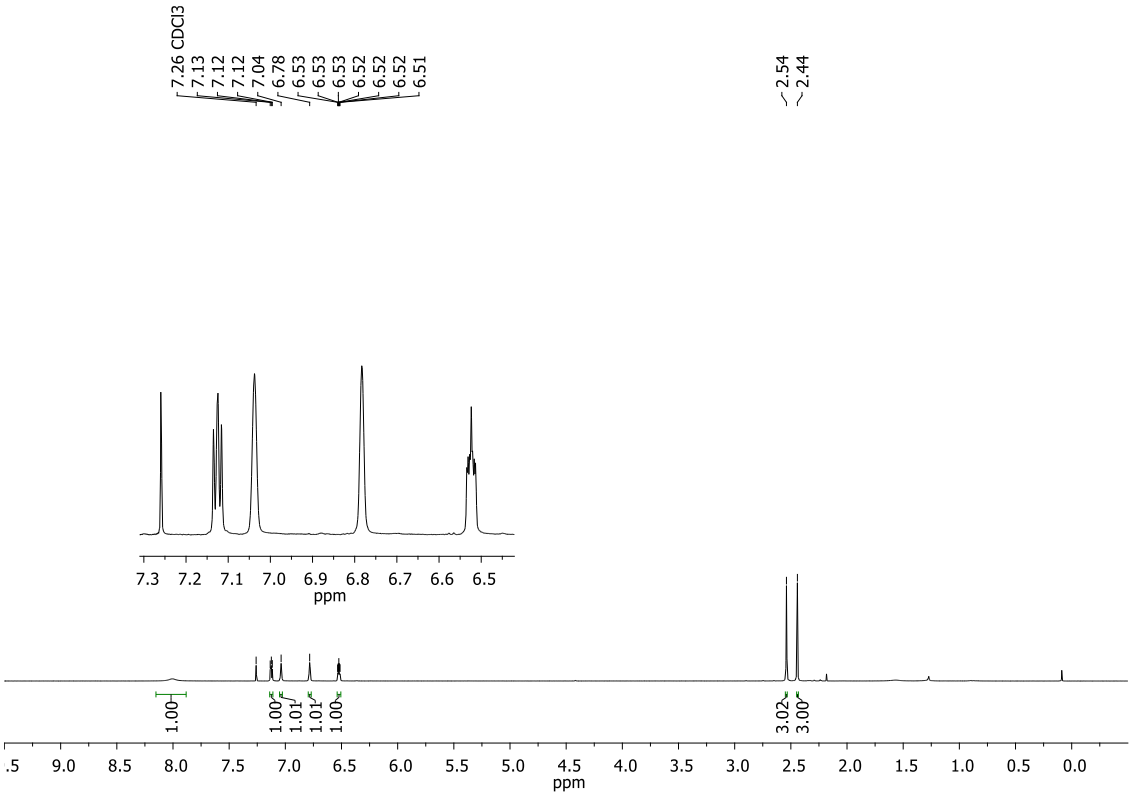

^{13}C NMR Spectrum
(75 MHz, $CDCl_3$)

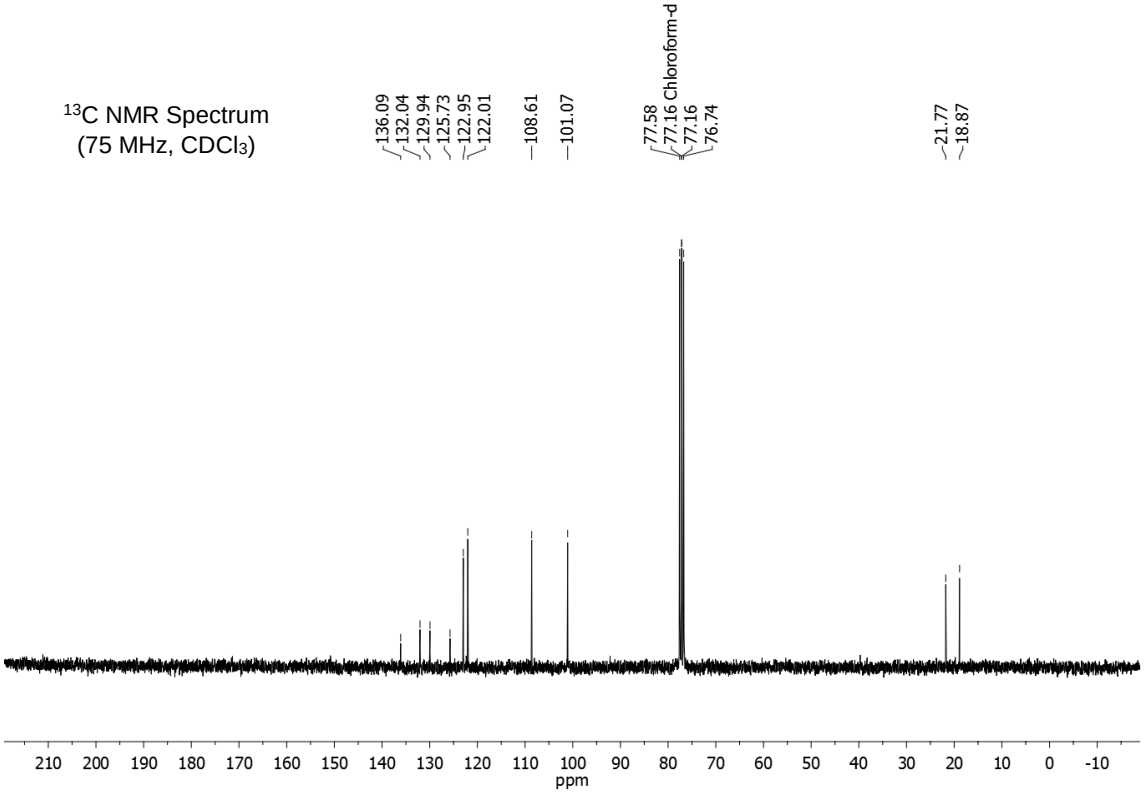

5.6-dimethoxyindole (2c)

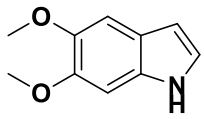

^{1}H NMR Spectrum
(300 MHz, $CDCl_3$)

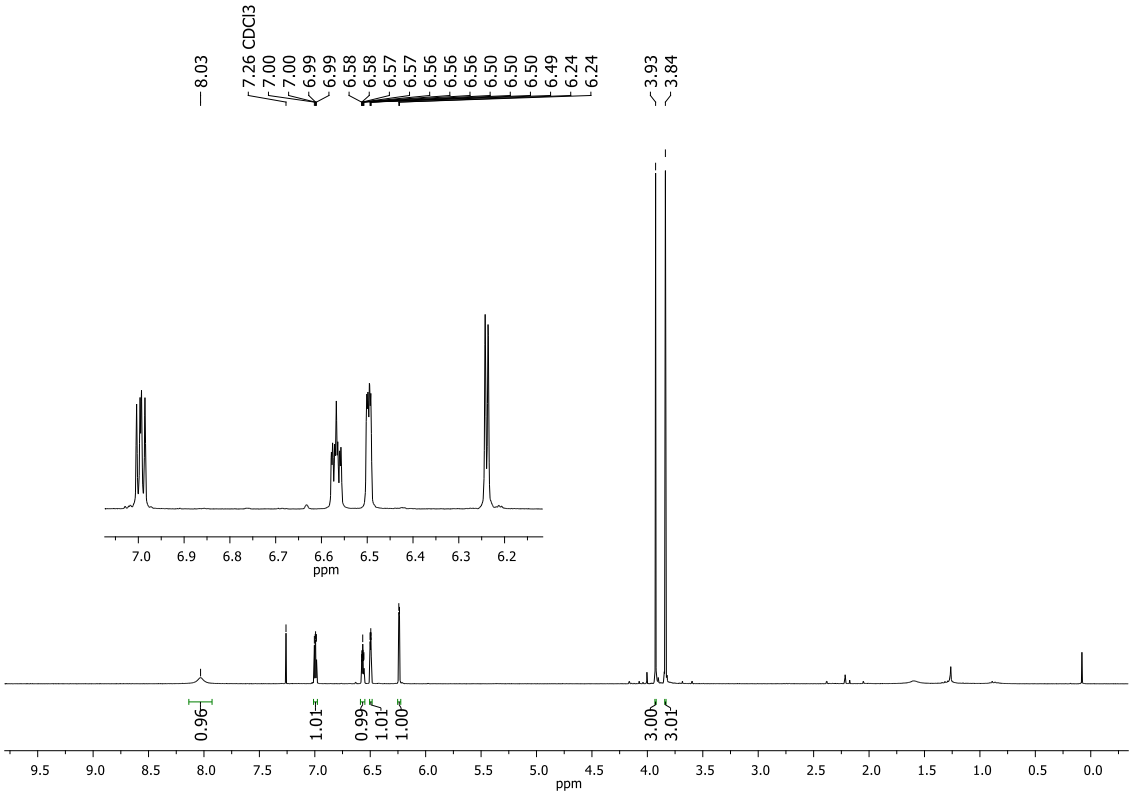

^{13}C NMR Spectrum
(75 MHz, $CDCl_3$)

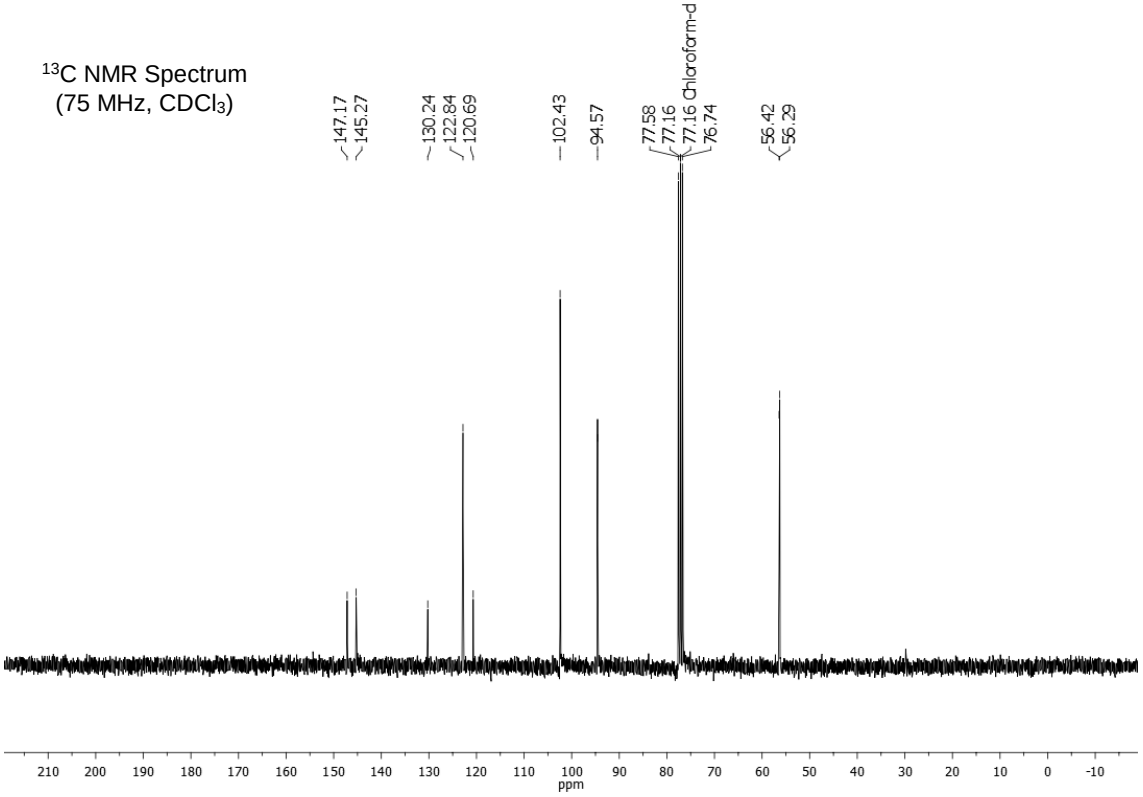

4,5,6-trimethoxyindole (2d)

^{1}H NMR Spectrum
(300 MHz, $CDCl_3$)

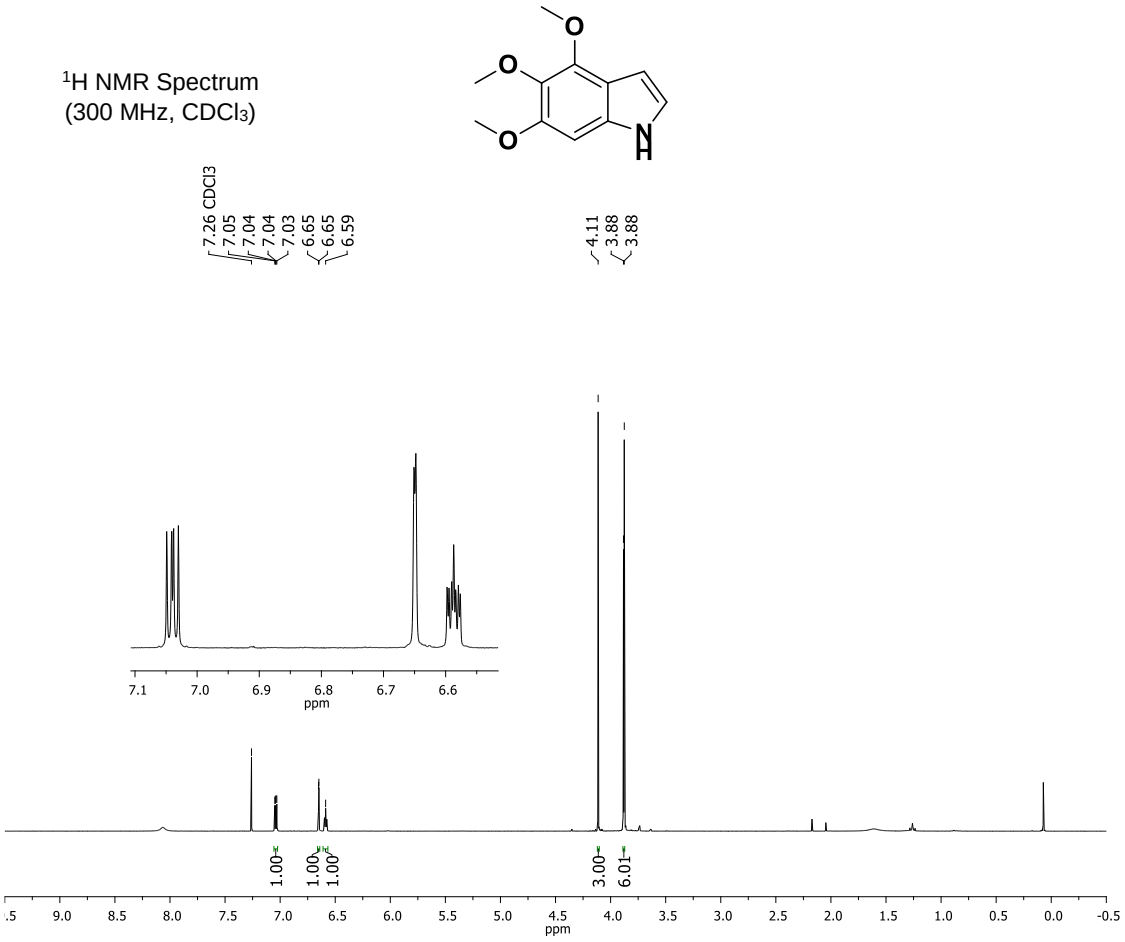

^{13}C NMR Spectrum
(75 MHz, $CDCl_3$)

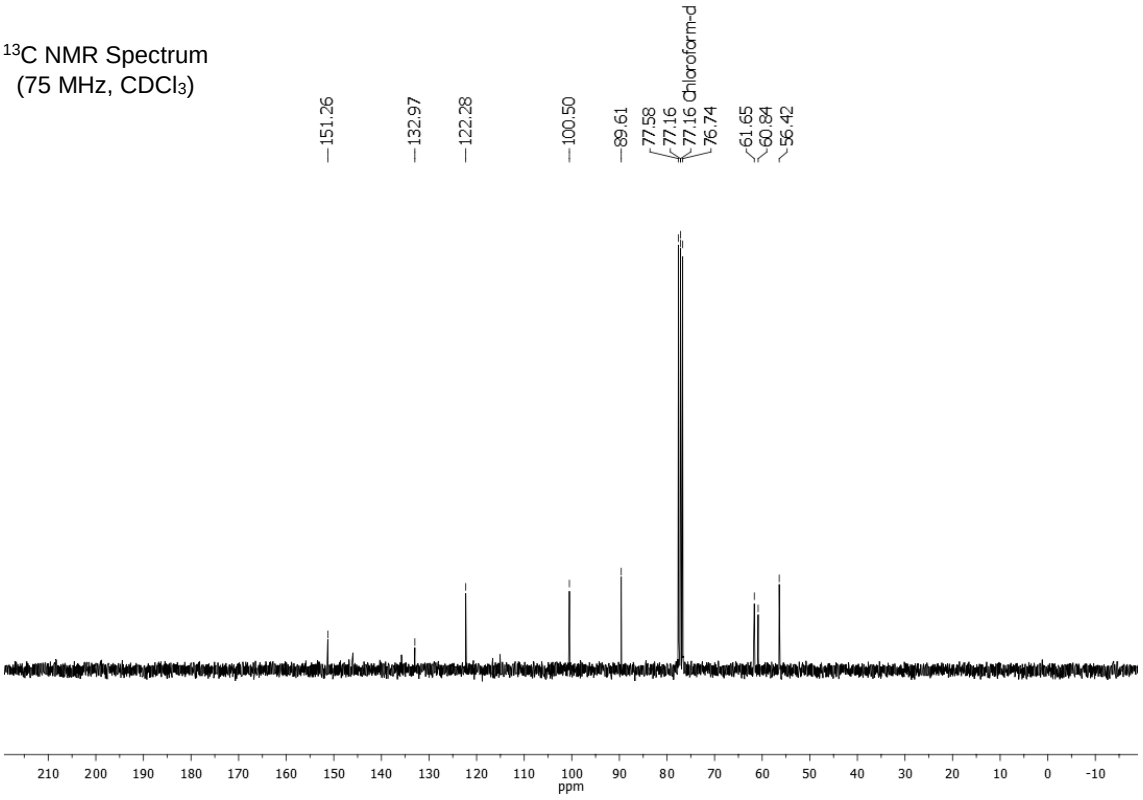

COSY Spectrum
($CDCl_3$)

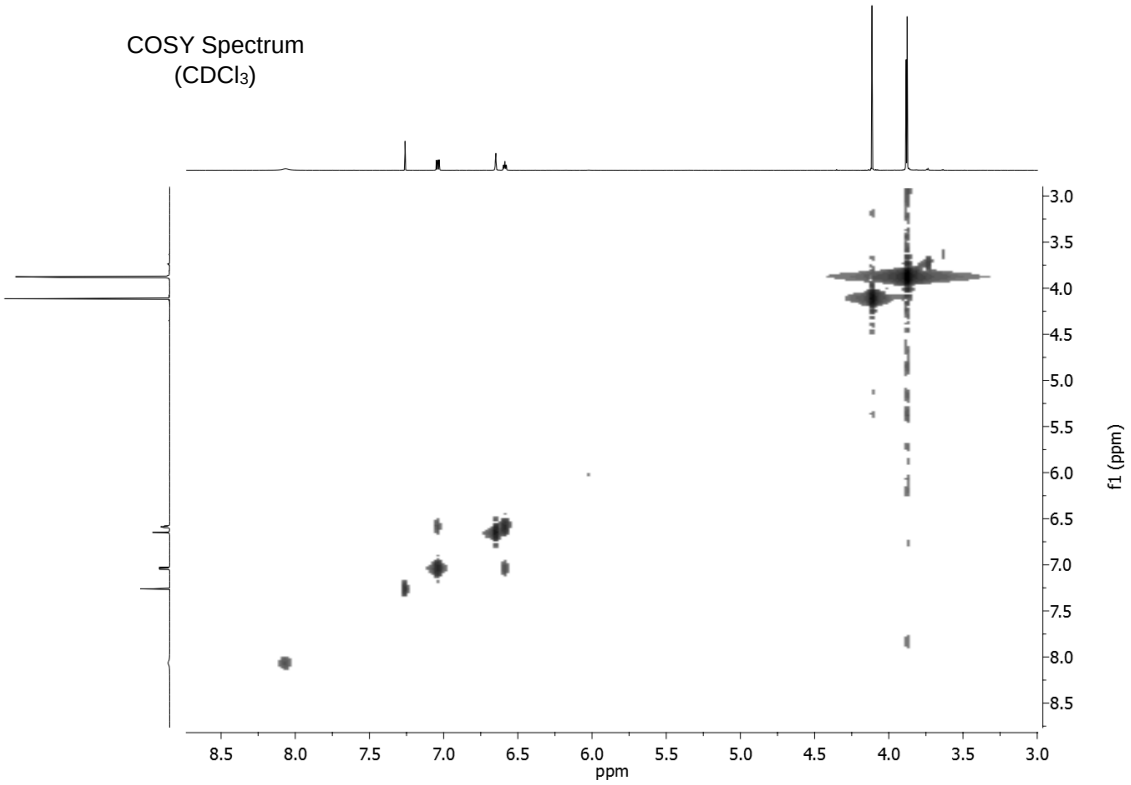

ed-HSQC Spectrum
($CDCl_3$)

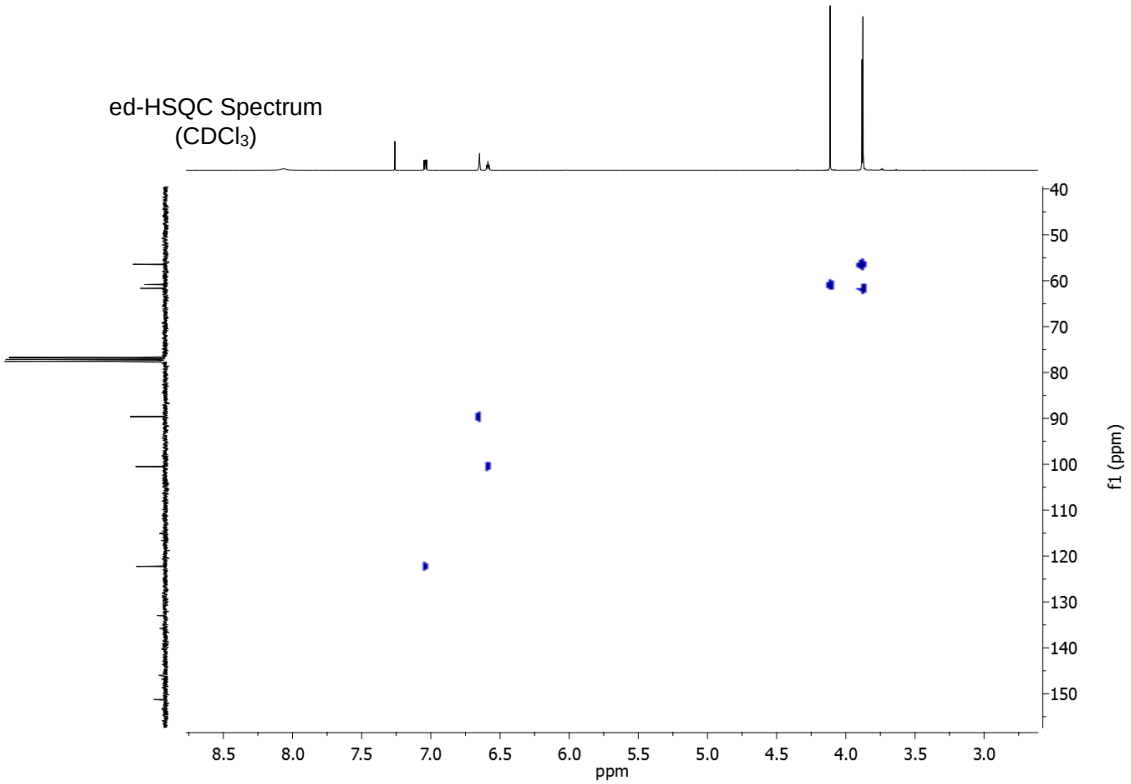

1*H*-Indole (2e)

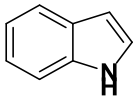

^{1}H NMR Spectrum
(300 MHz, $CDCl_3$)

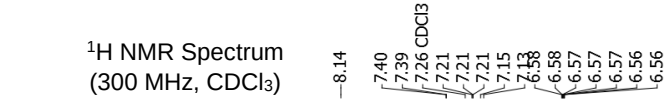

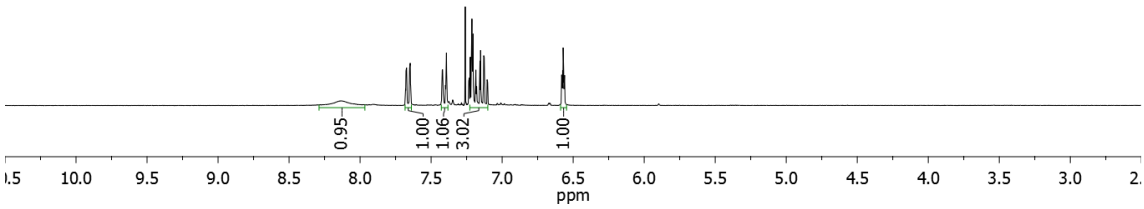

^{13}C NMR Spectrum
(75 MHz, $CDCl_3$)

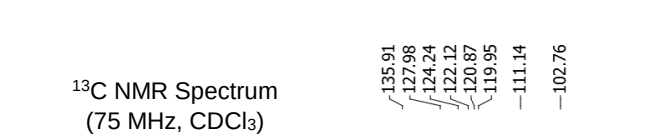

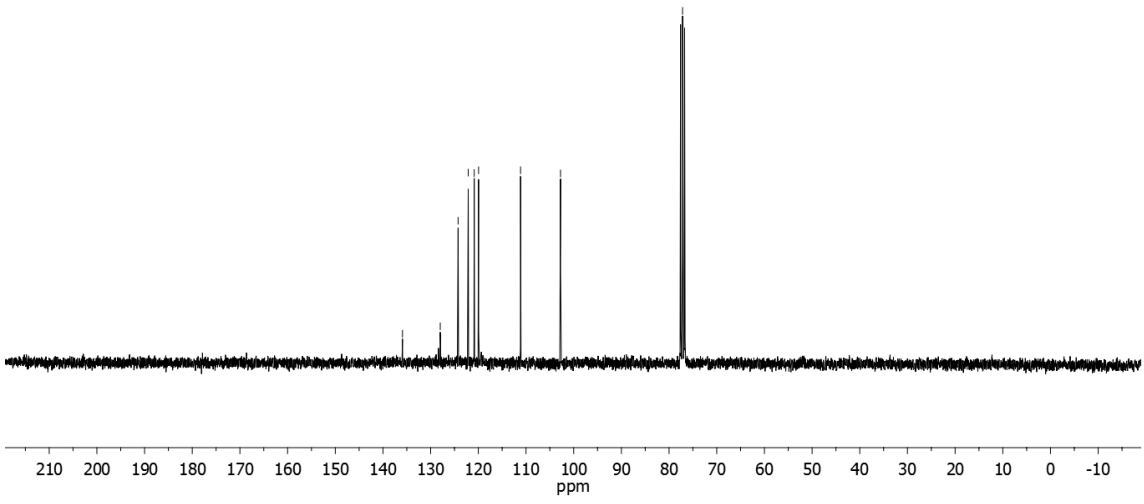

5*H*-[1,3]dioxolo[4,5-f]indole (2f)

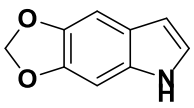

^{1}H NMR Spectrum
(300 MHz, $CDCl_3$)

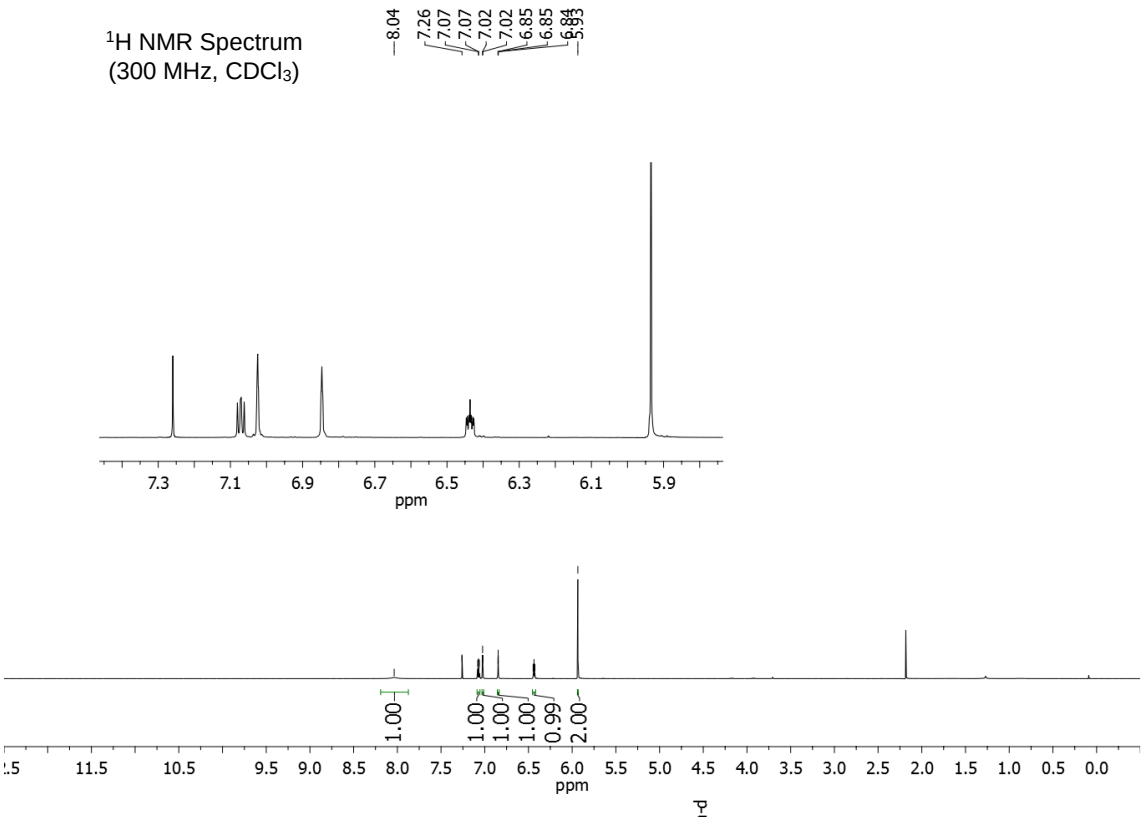

^{13}C NMR Spectrum
(75 MHz, $CDCl_3$)

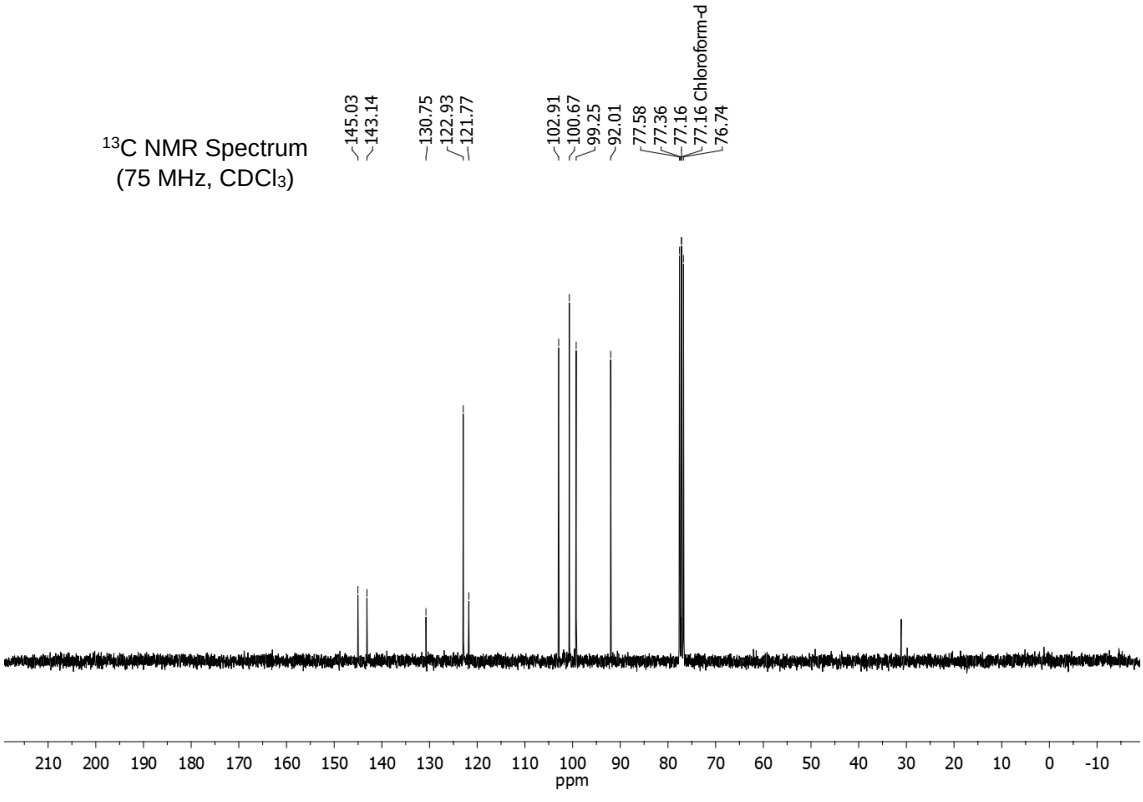

3,6-dihydro-2H-[1,4]dioxino[2,3-f]indole (2g) & 2,3-dihydro-7H-[1,4]dioxino[2,3-e] indole (2g')

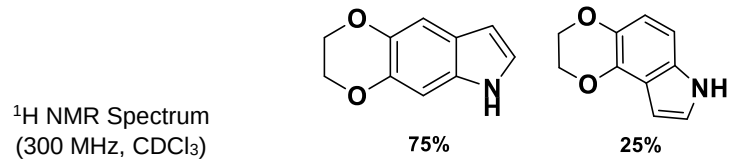

^{1}H NMR Spectrum
(300 MHz, $CDCl_3$)

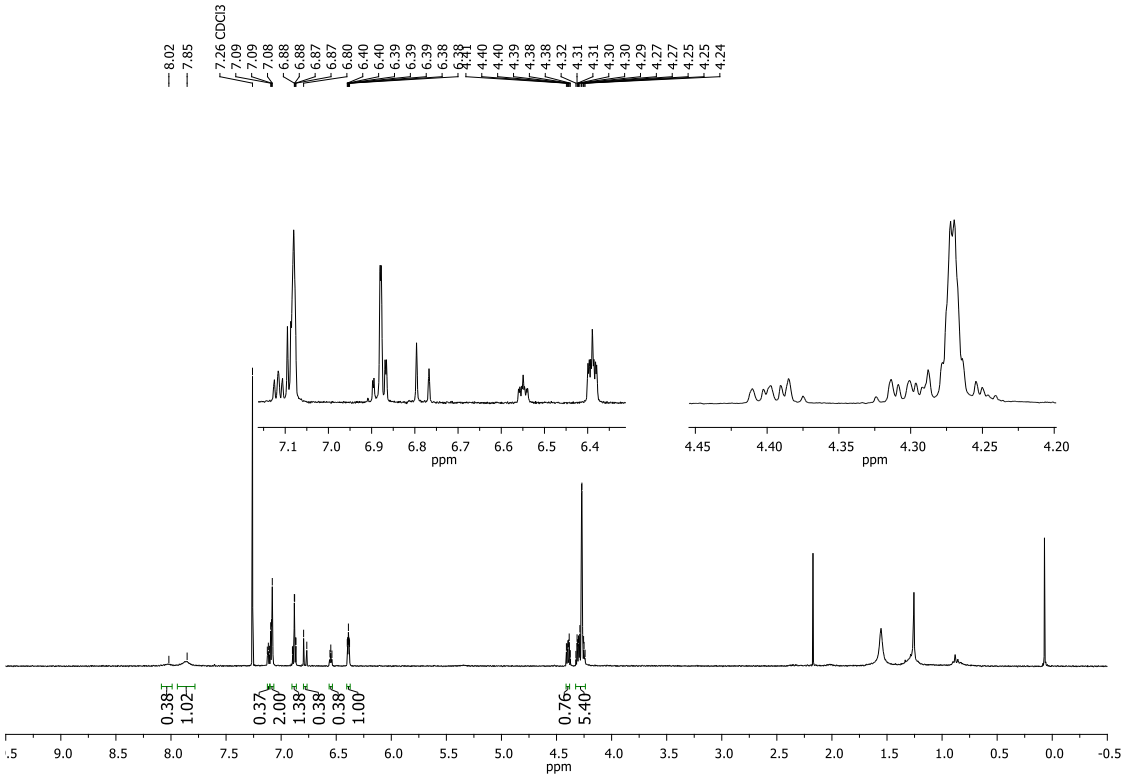

^{13}C NMR Spectrum
(75 MHz, $CDCl_3$)

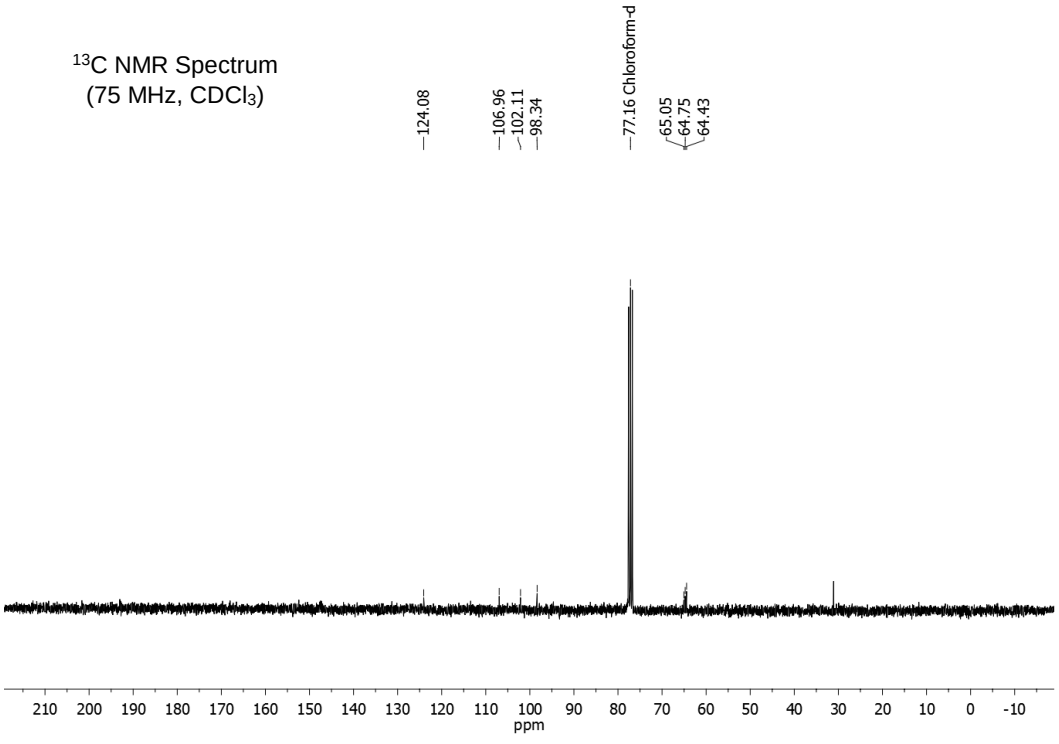

1*H*-benz[g]indole (2h)

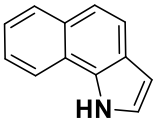

^{1}H NMR Spectrum
(300 MHz, $CDCl_3$)

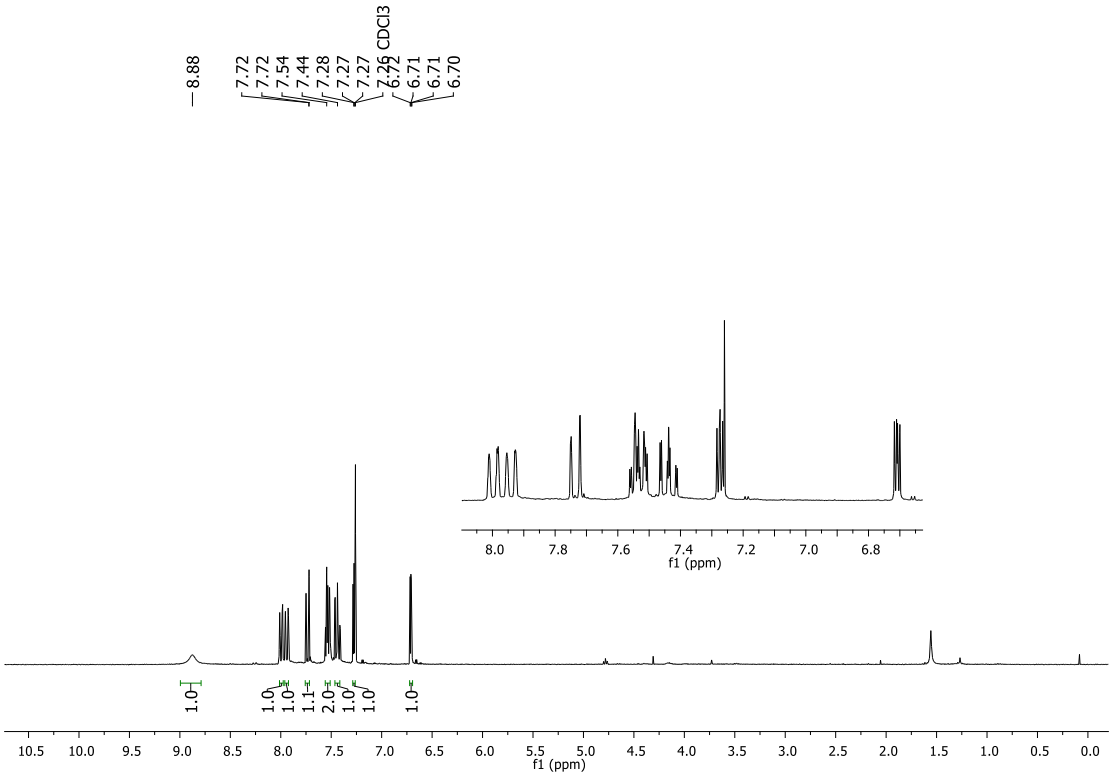

^{13}C NMR Spectrum
(75 MHz, $CDCl_3$)

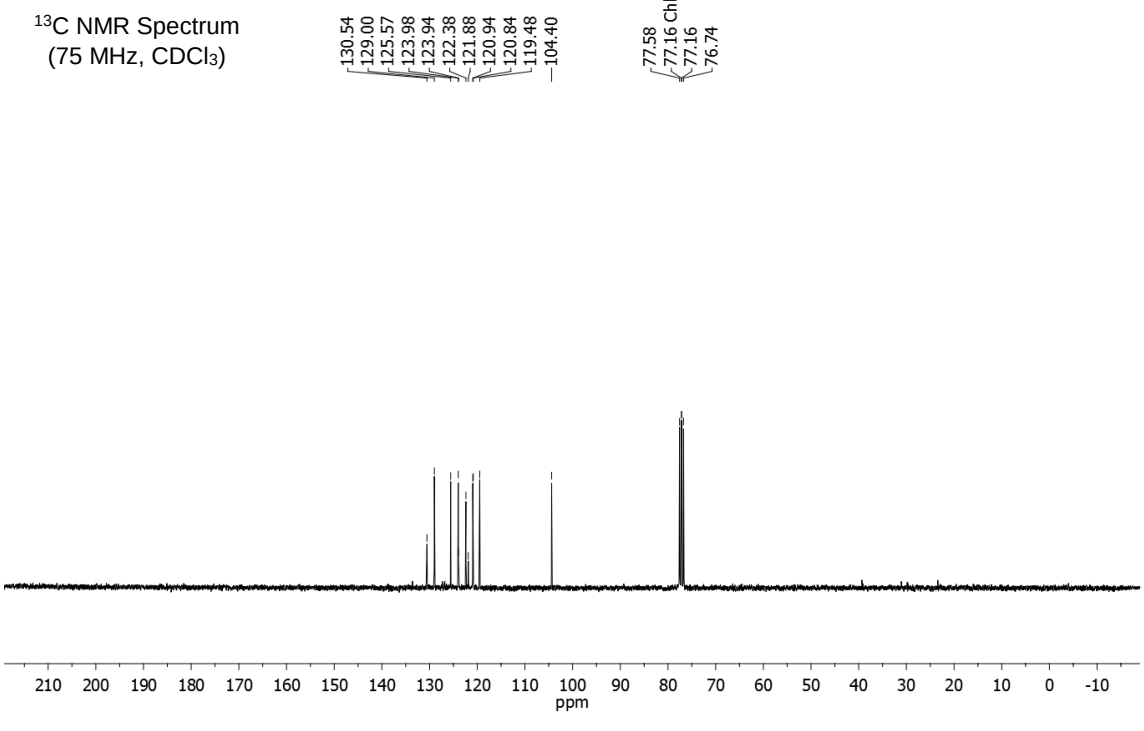

2-((4-methylphenyl)amino)ethanol (3)

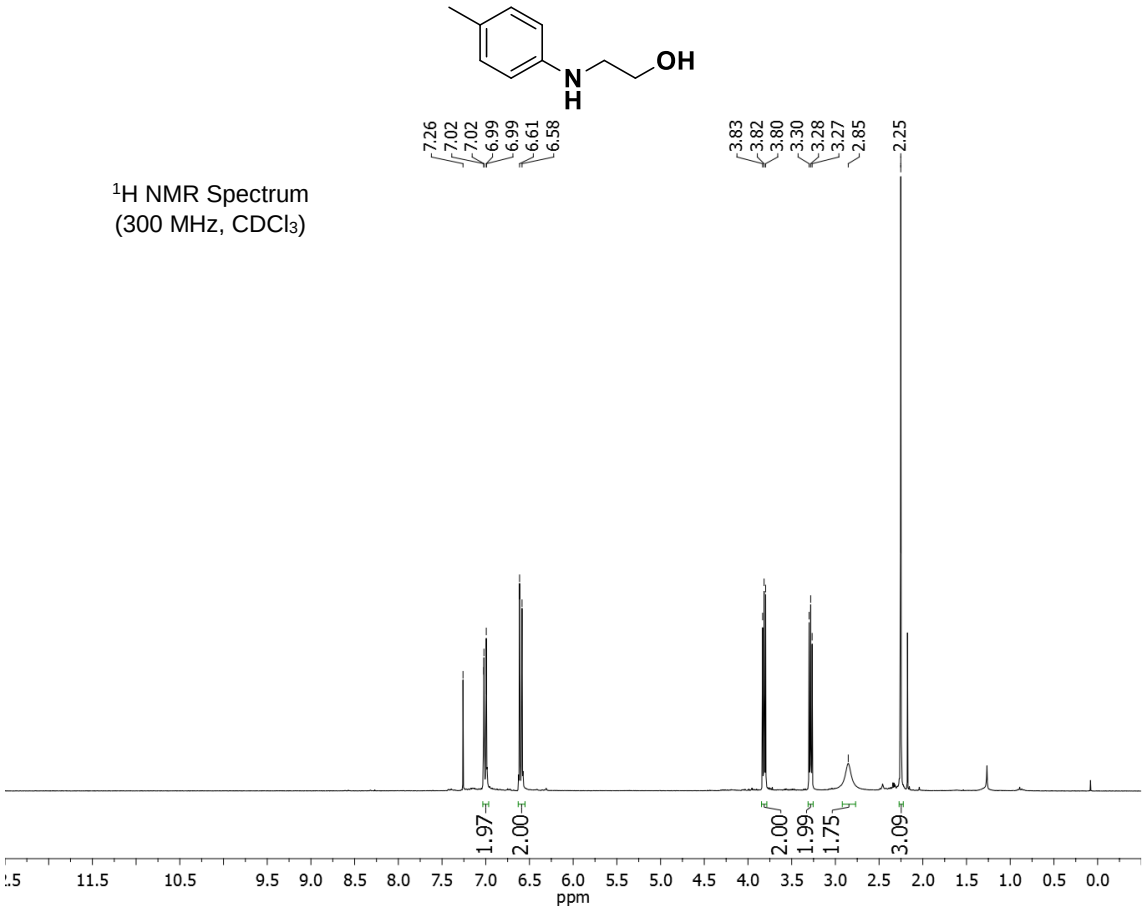

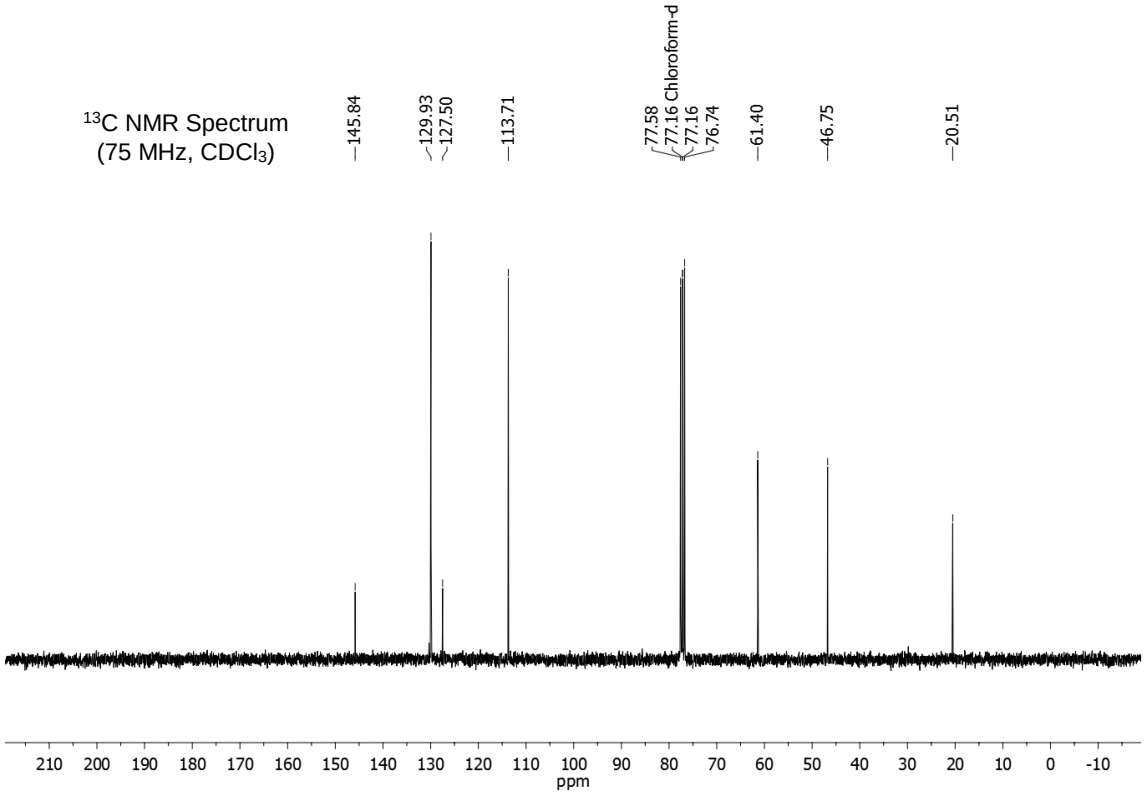

N,N'-bis(4-methylphenyl)-1,2-ethanediamine (4)

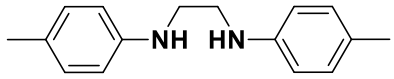

^{1}H NMR Spectrum
(300 MHz, $CDCl_3$)

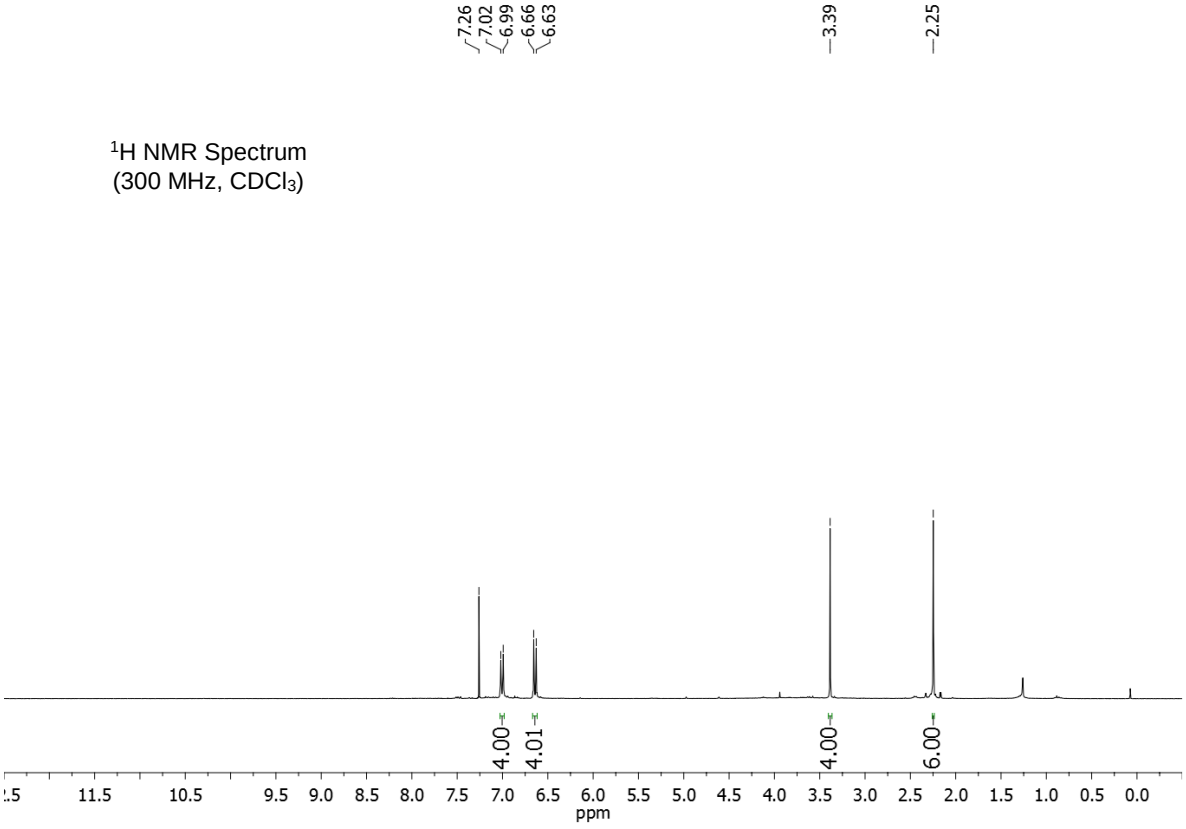

^{13}C NMR Spectrum
(75 MHz, $CDCl_3$)

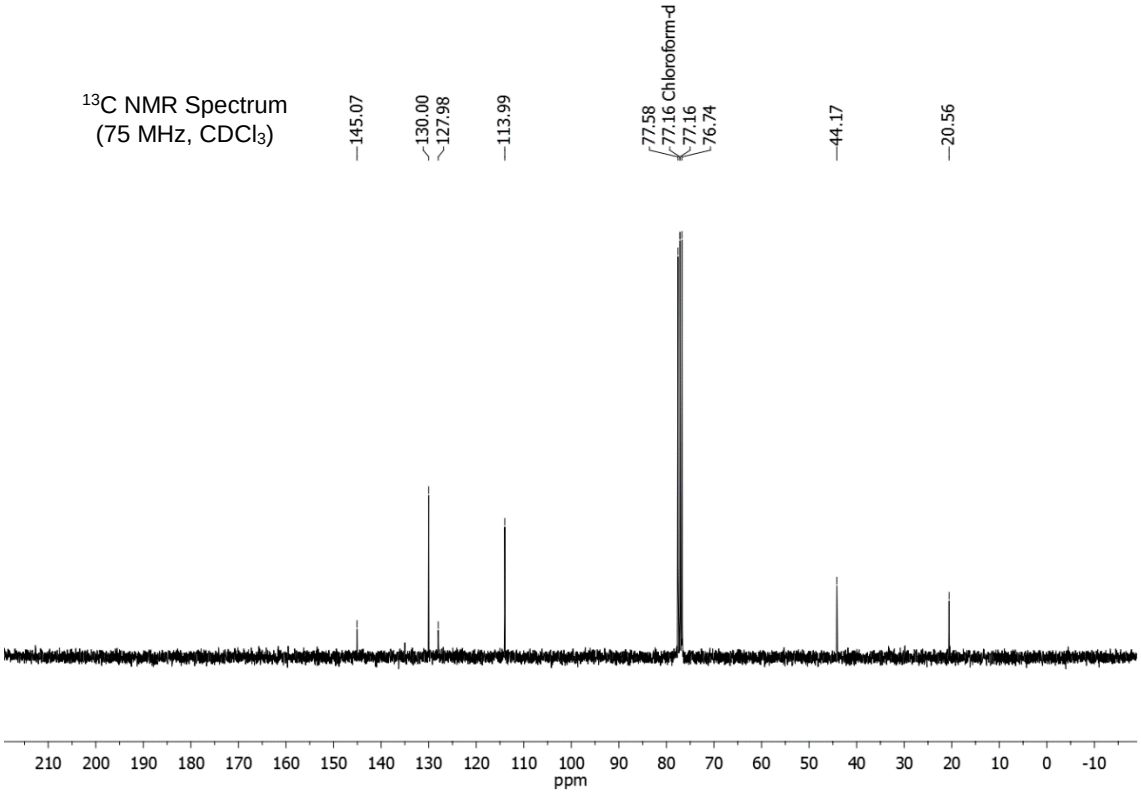

COSY Spectrum
($CDCl_3$)

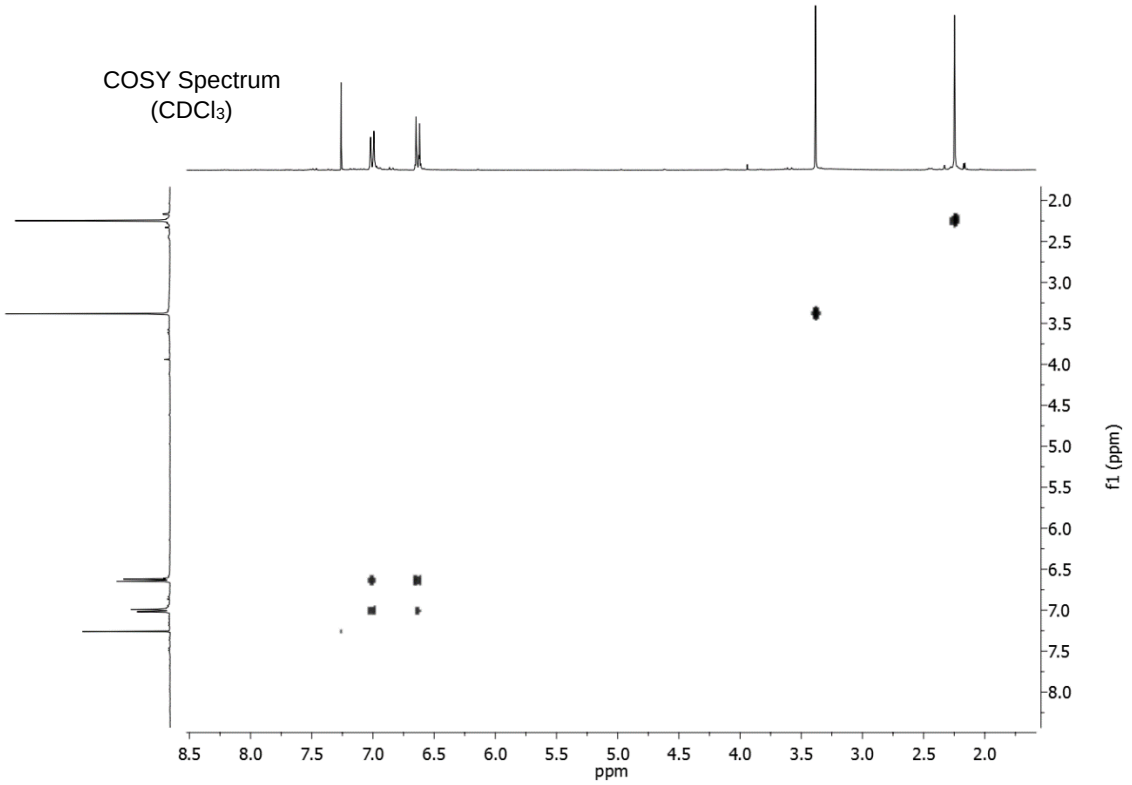

ed-HSQC Spectrum
($CDCl_3$)

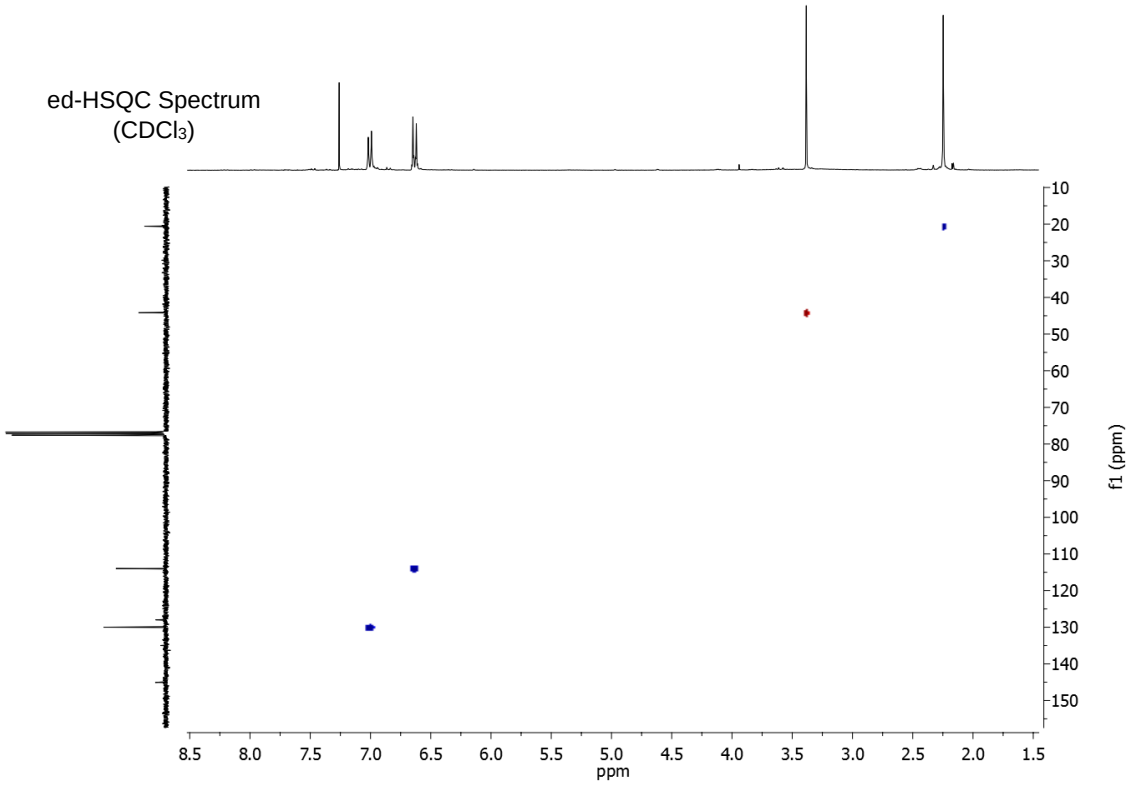

1,4-bis(4-methylphenyl)-piperazine (5)

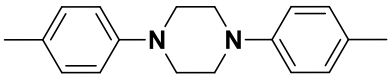

^{1}H NMR Spectrum
(300 MHz, $CDCl_3$)

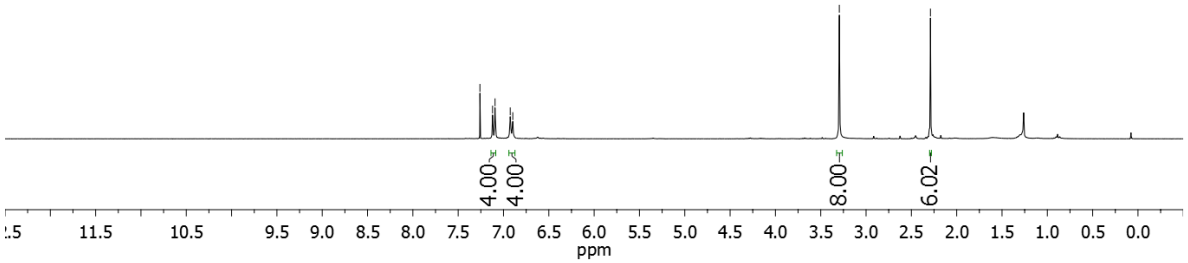

^{13}C NMR Spectrum
(75 MHz, $CDCl_3$)

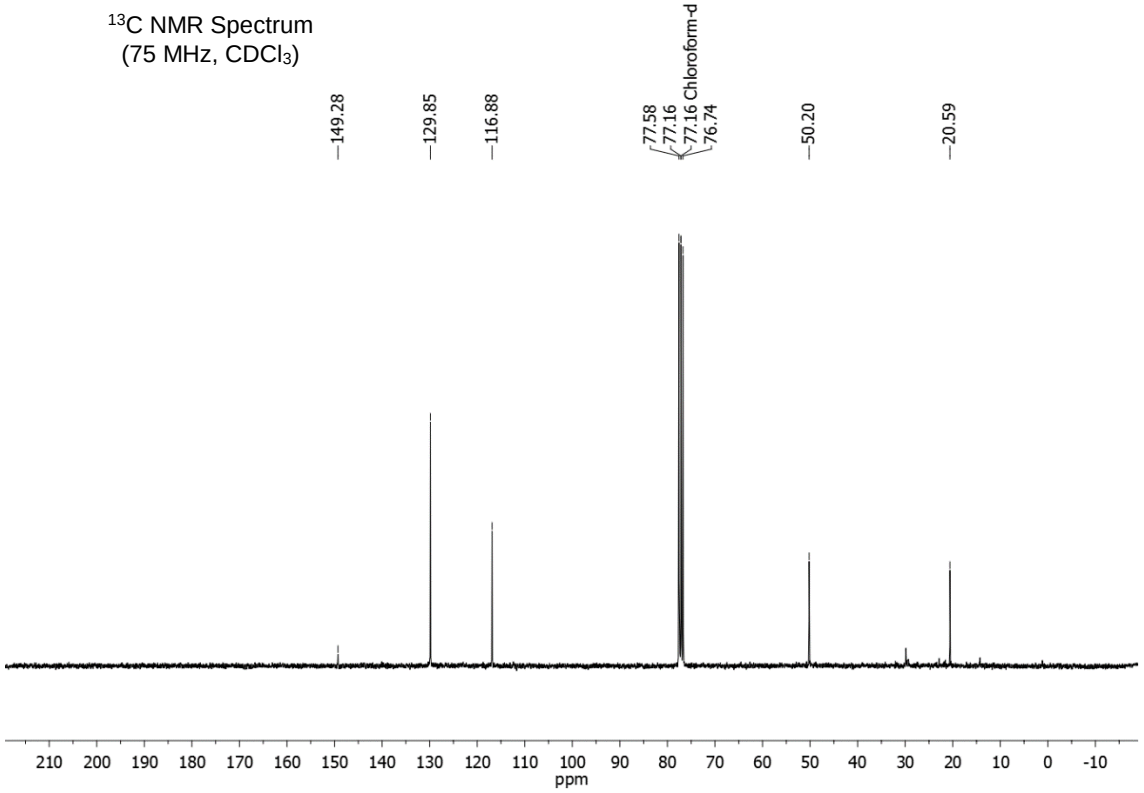

COSY Spectrum ($CDCl_3$)

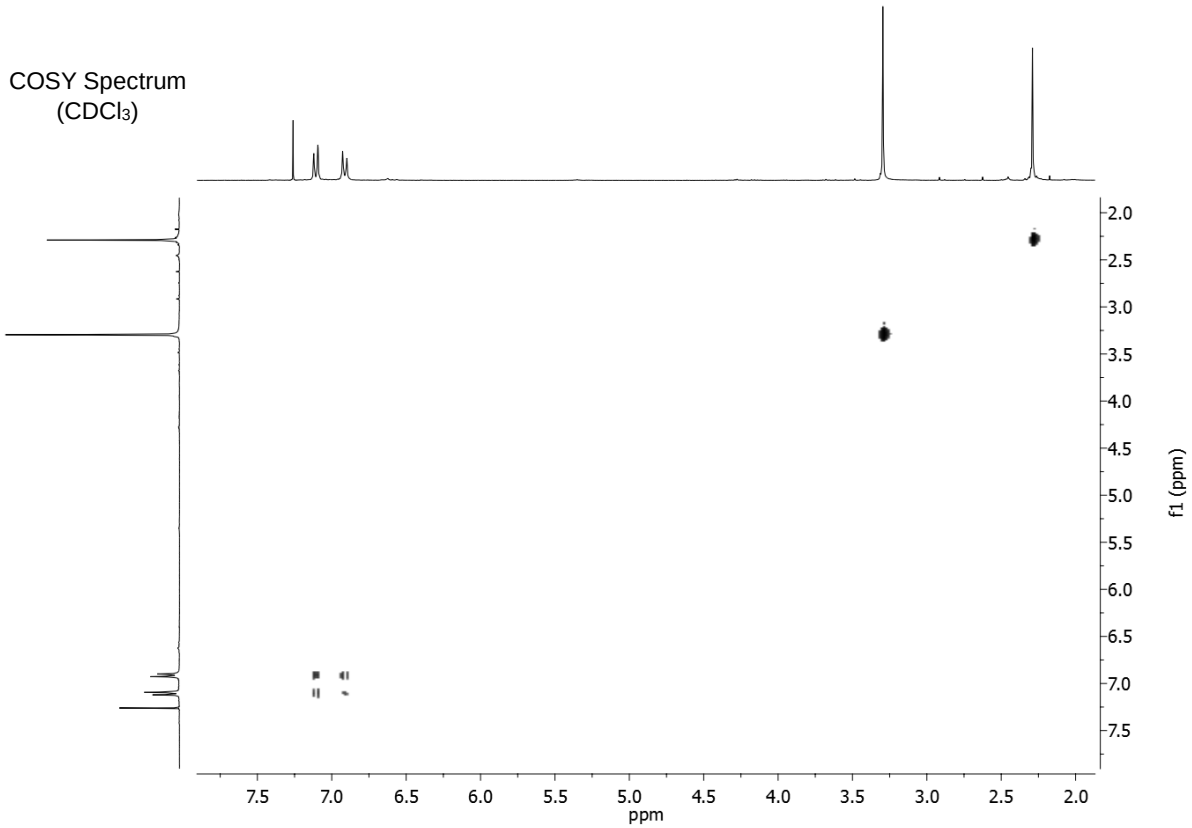

ed-HSQC Spectrum ($CDCl_3$)

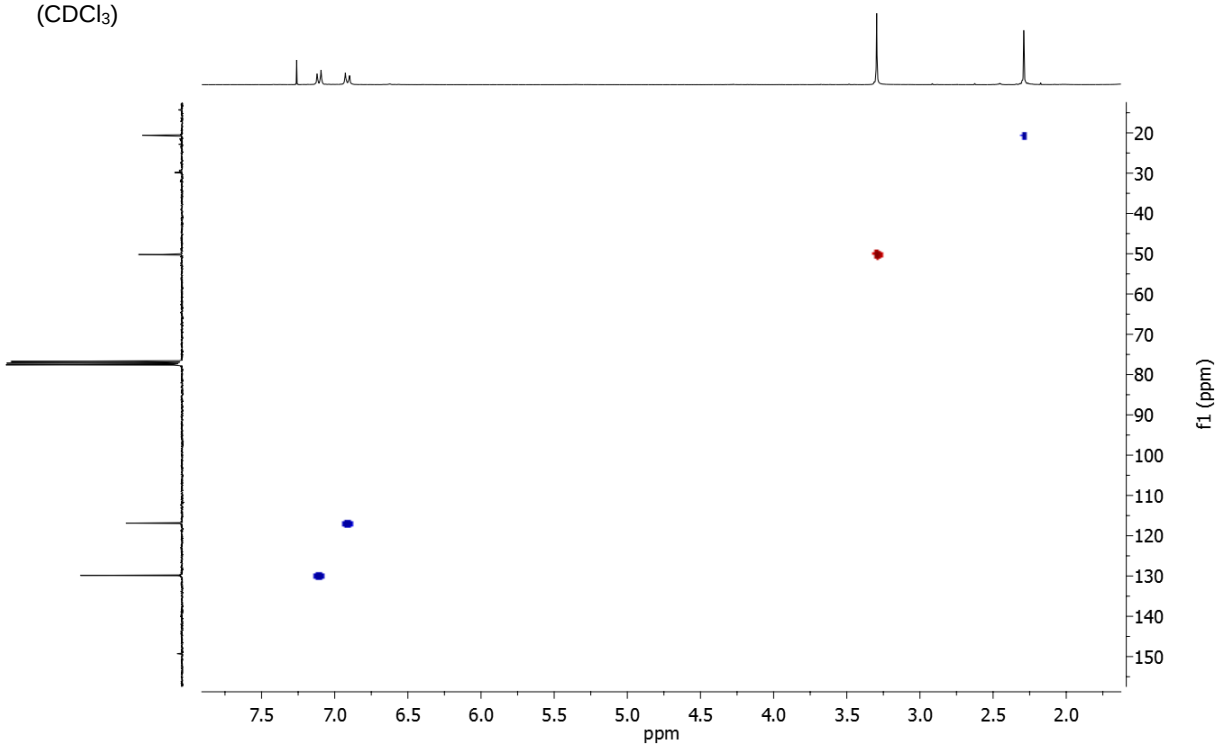

(*Z*, *E*)-1,2-bis(6-fluoro-1*H*-indol-1-yl)ethene (6)

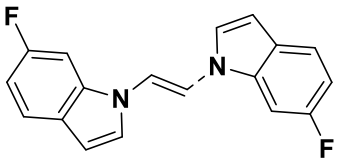

^{1}H NMR Spectrum
(300 MHz, Acetone-d6)

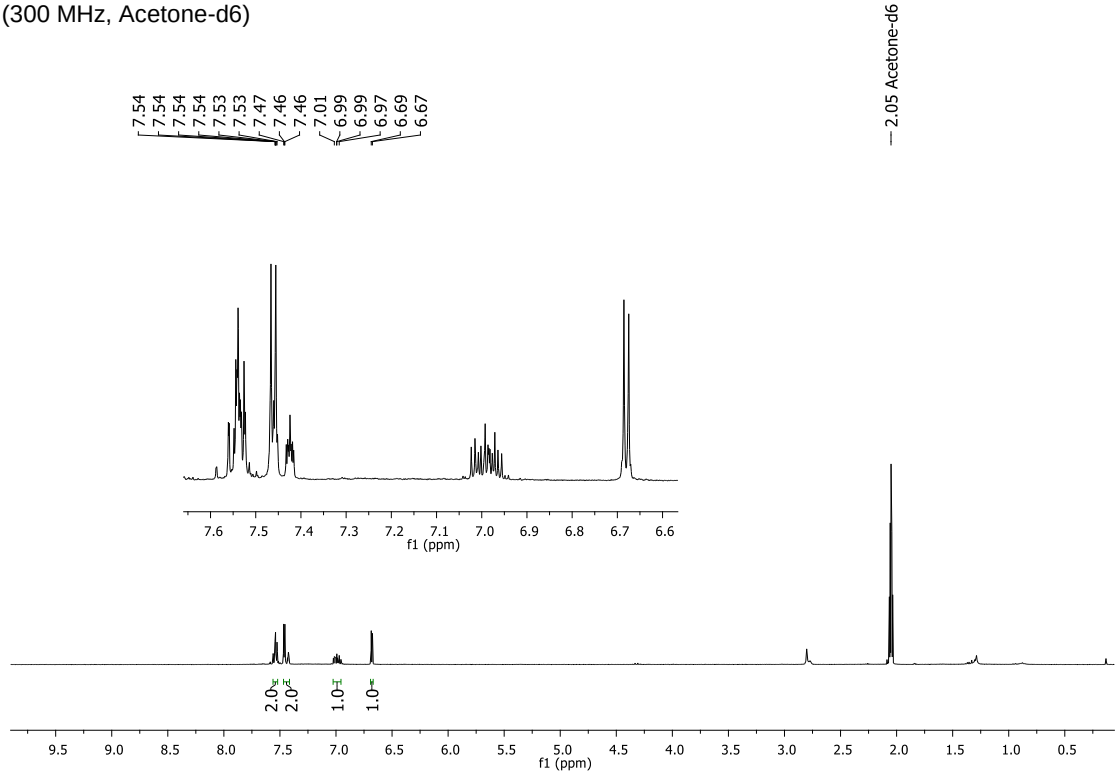

^{13}C NMR Spectrum
(75 MHz, Acetone-d6)

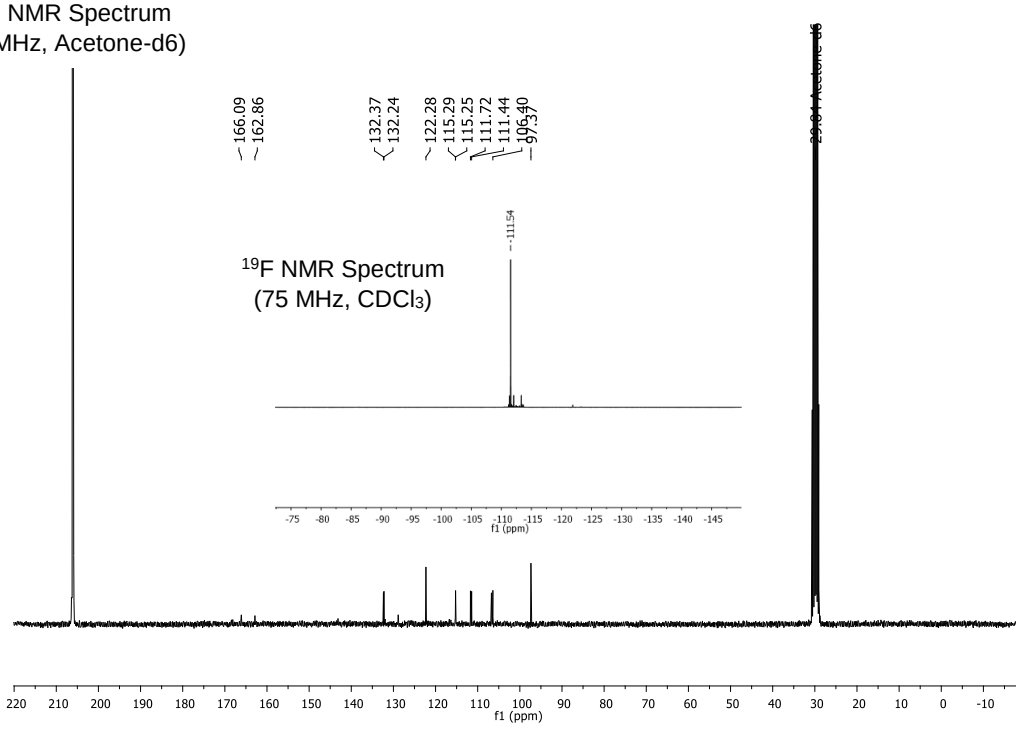

^{19}F NMR Spectrum
(75 MHz, $CDCl_3$)

4,5,6-trimethoxy-3-methyl-1H-indole (9)

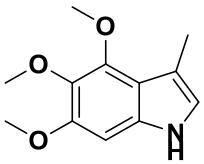

^{1}H NMR Spectrum
(300 MHz, $CDCl_3$)

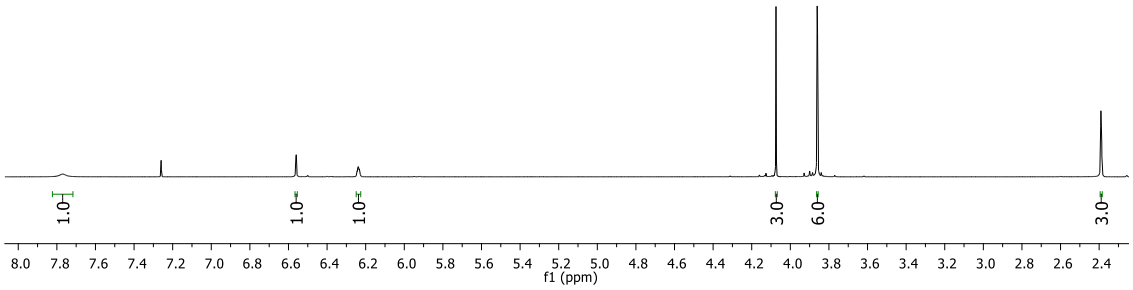

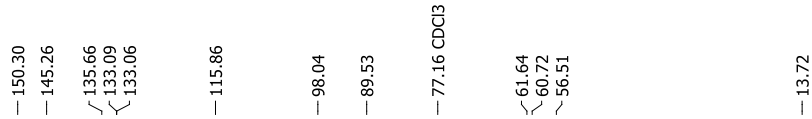

^{13}C NMR Spectrum
(75 MHz, $CDCl_3$)

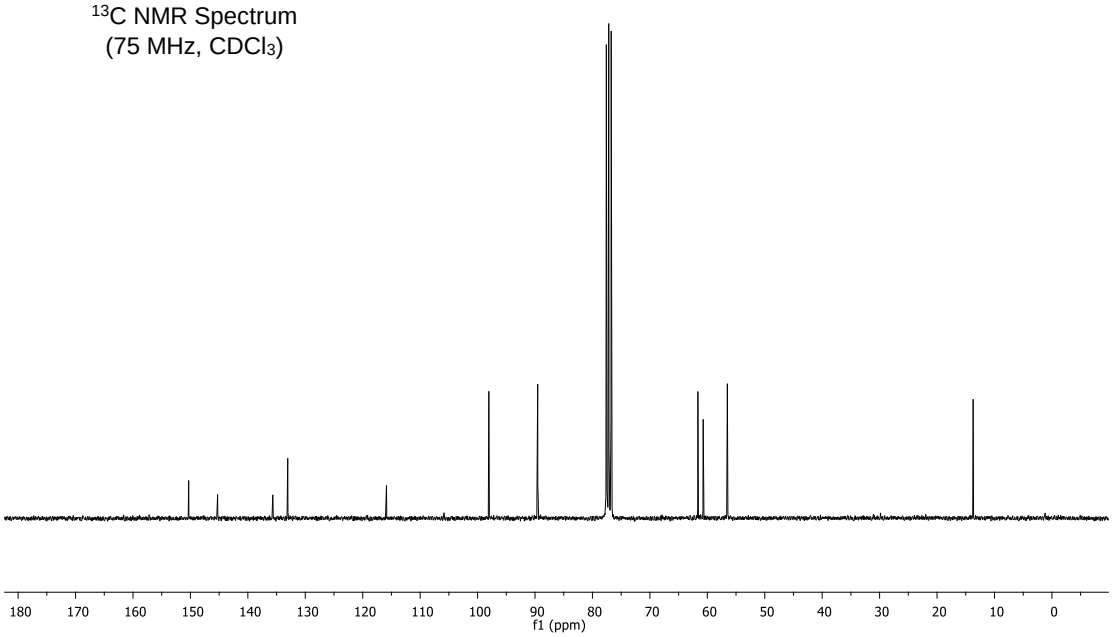

COSY Spectrum
($CDCl_3$)

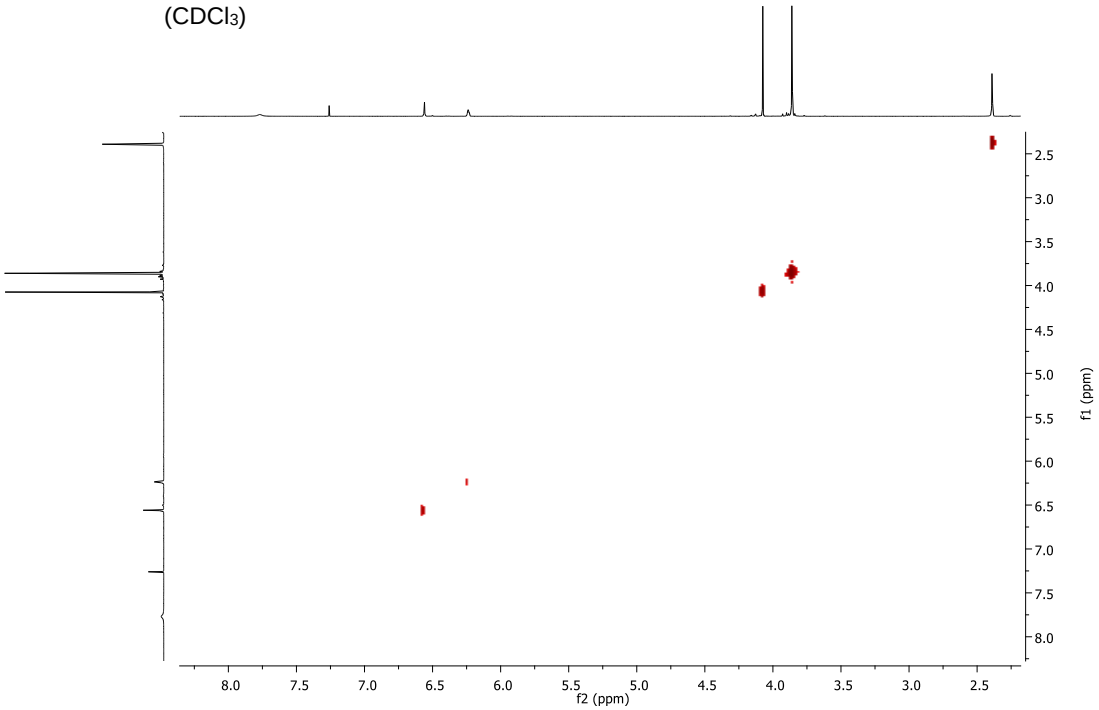

ed-HSQC Spectrum
($CDCl_3$)

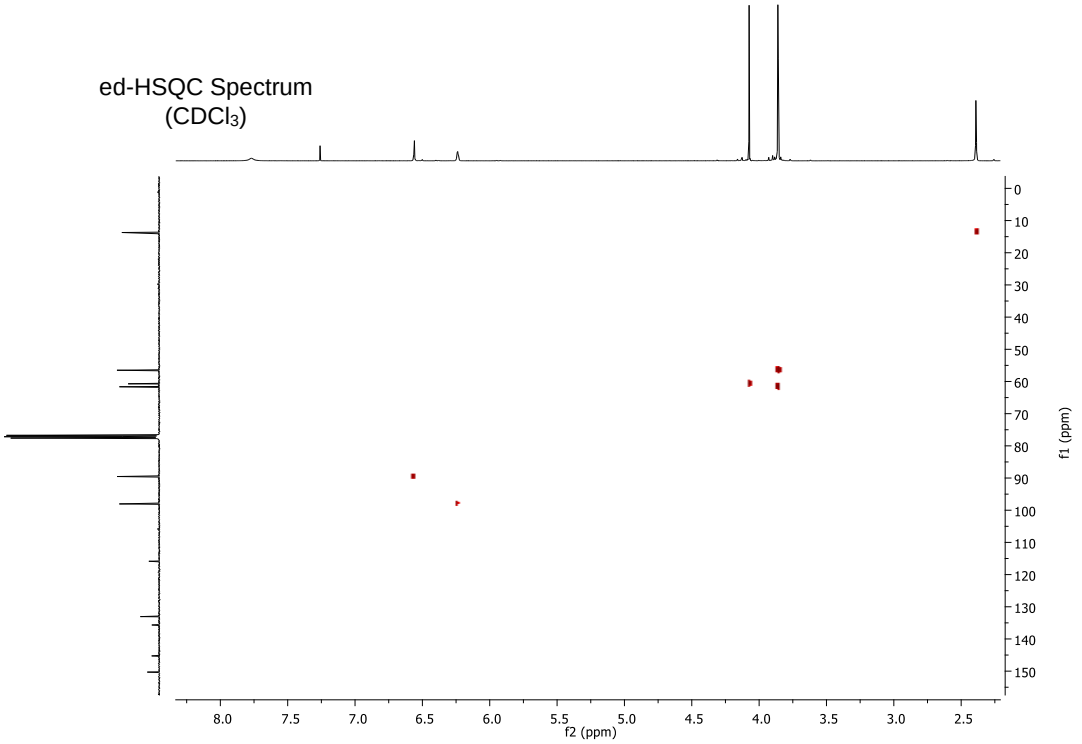

1,5-dimethyl-1H-indole (12)

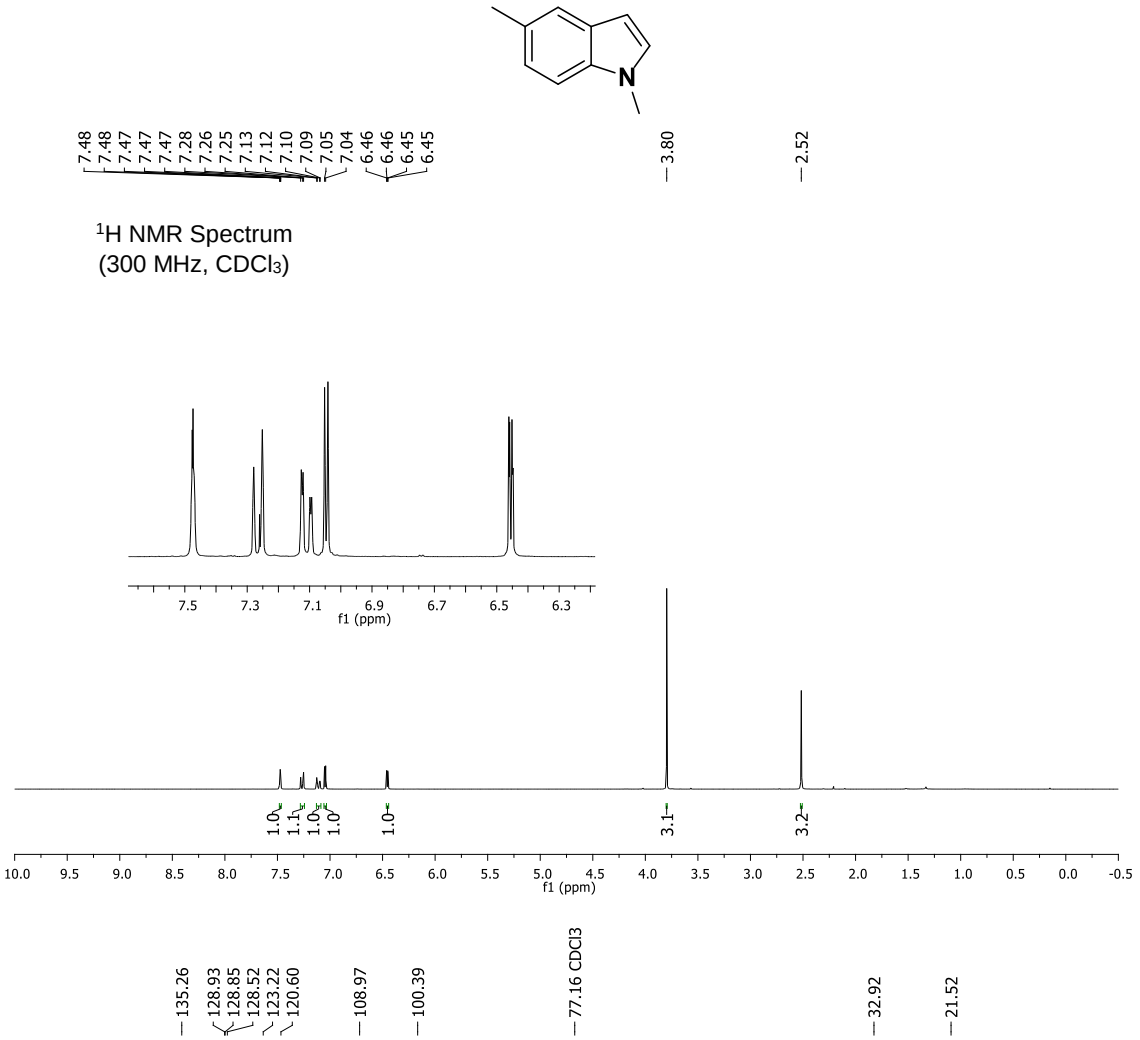

^{1}H NMR Spectrum
(300 MHz, $CDCl_3$)

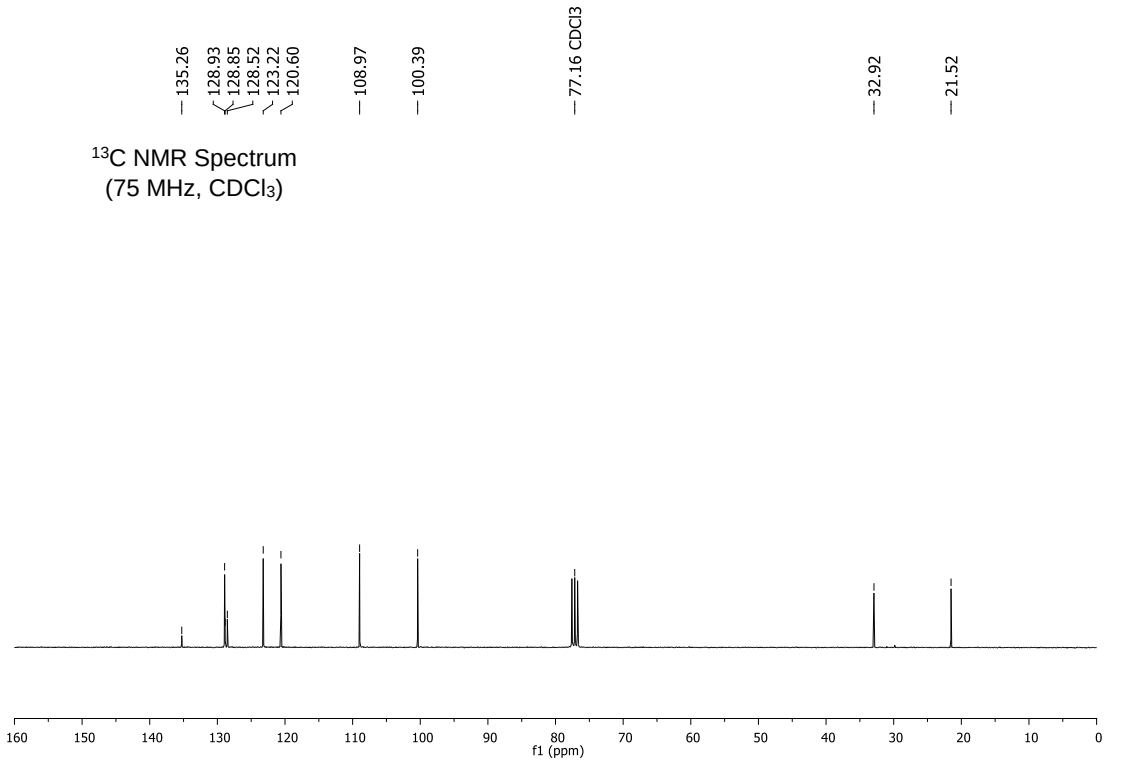

^{13}C NMR Spectrum
(75 MHz, $CDCl_3$)

5,6-dihydro-4H-pyrrolo-[3,2,1-ij]-quinoline(14a)

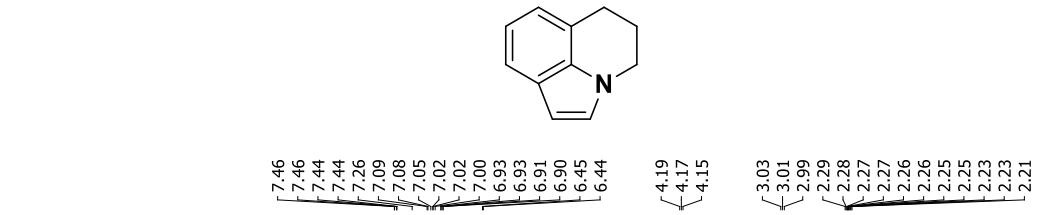

^{1}H NMR Spectrum
(300 MHz, $CDCl_3$)

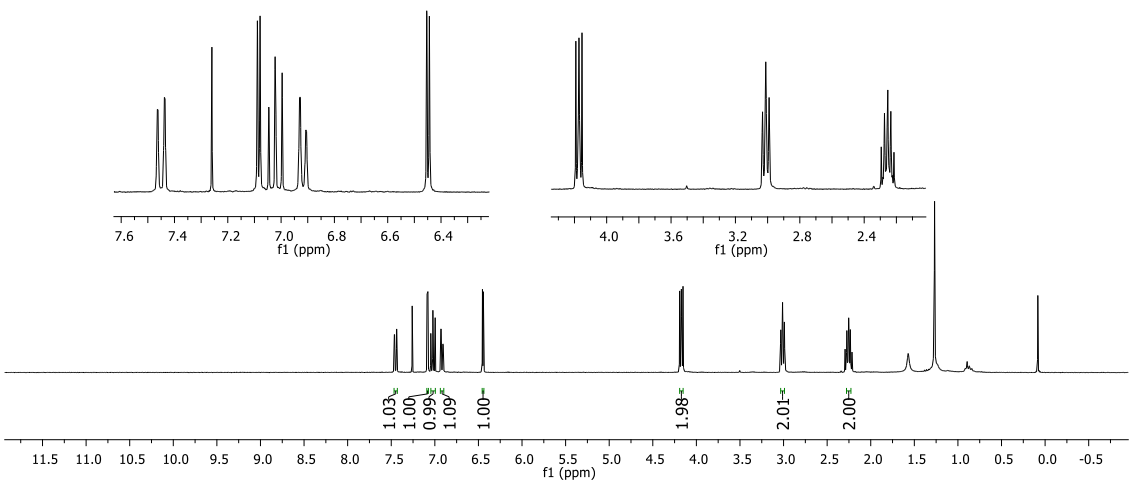

^{13}C NMR Spectrum
(75 MHz, $CDCl_3$)

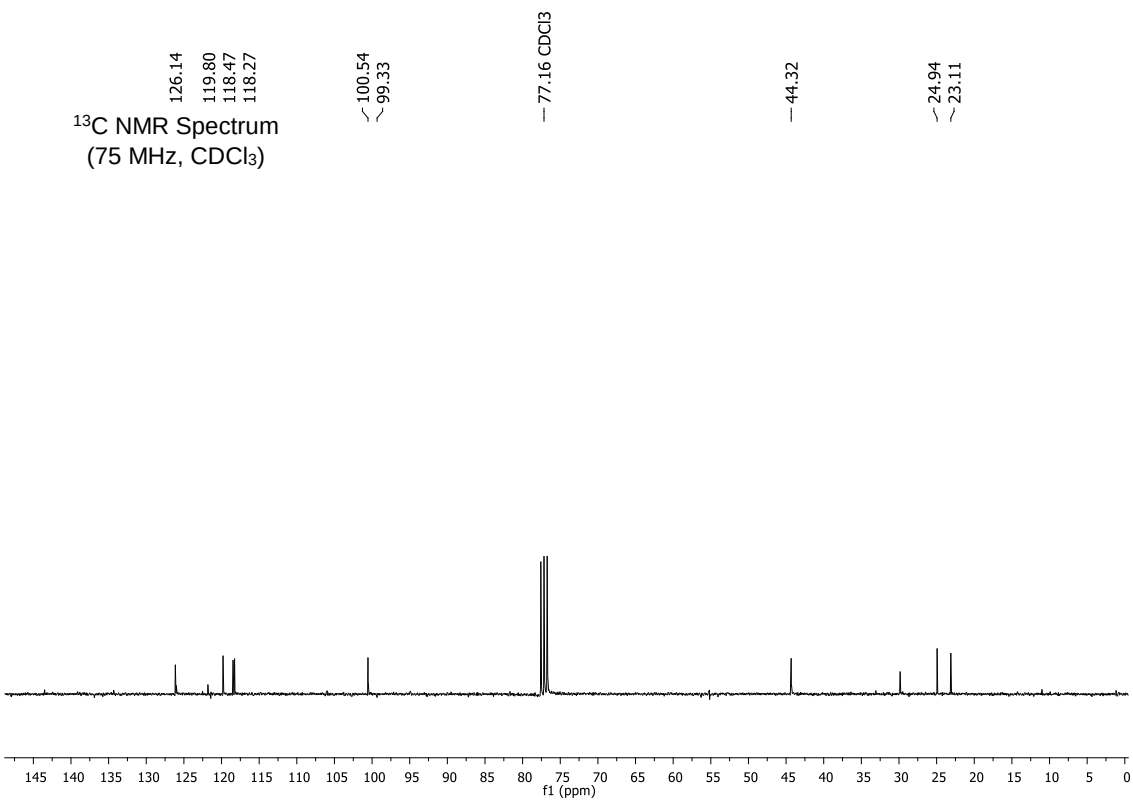

8-methoxy-5,6-dihydro-4*H*-pyrrolo[3,2,1-*ij*]quinoline (14b)

^{1}H NMR Spectrum
(300 MHz, $CDCl_3$)

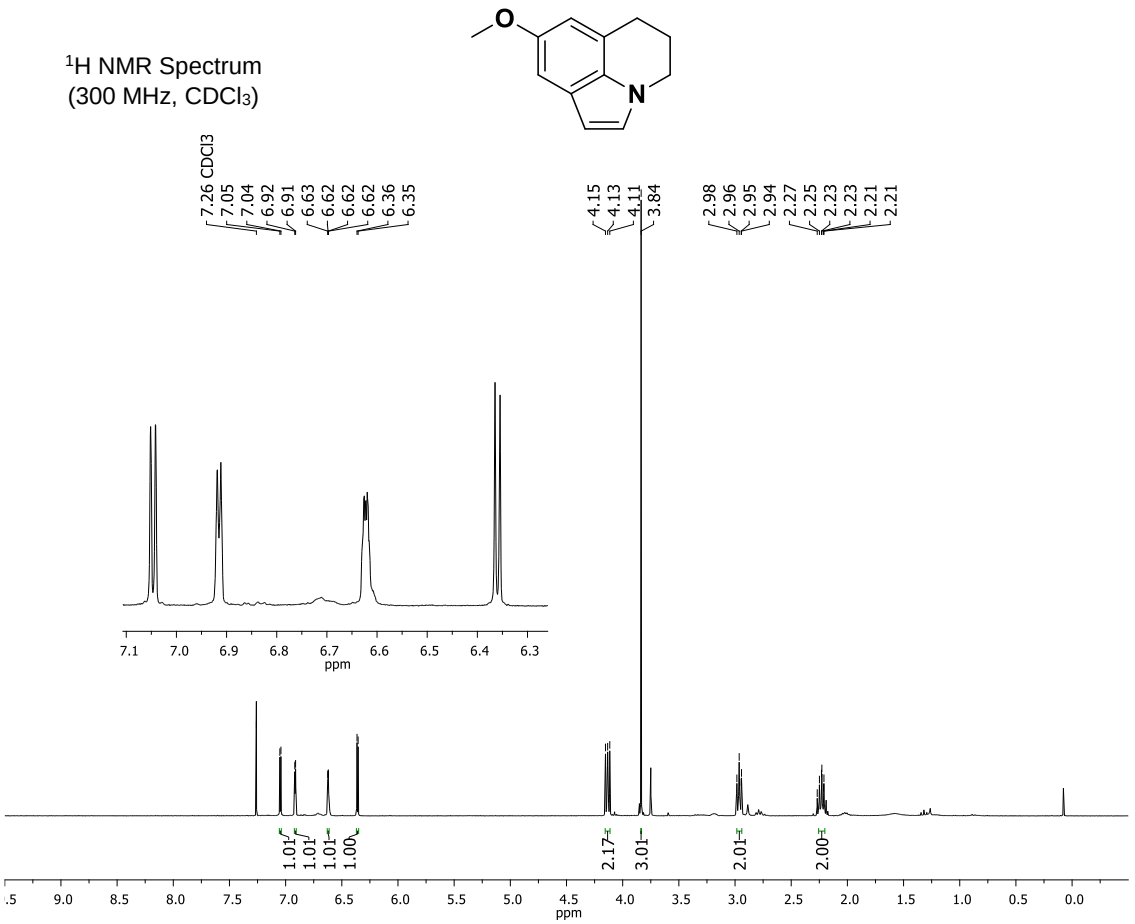

^{13}C NMR Spectrum
(75 MHz, $CDCl_3$)

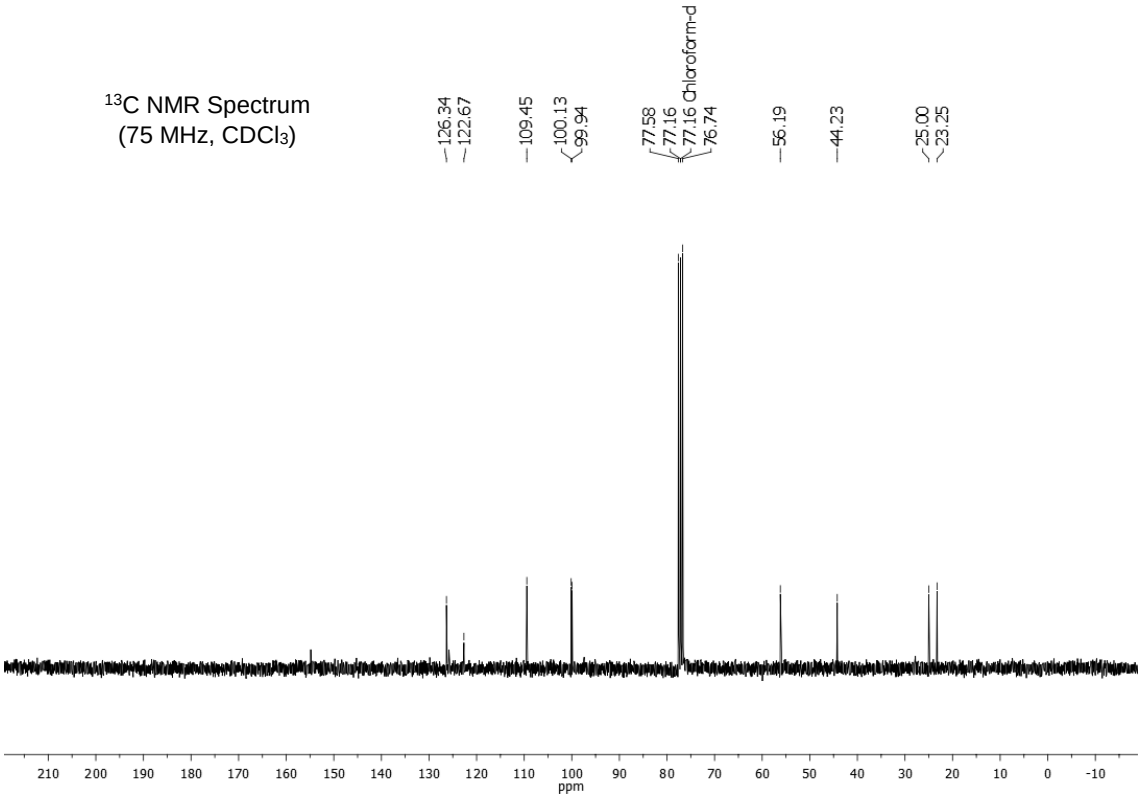

COSY Spectrum
($CDCl_3$)

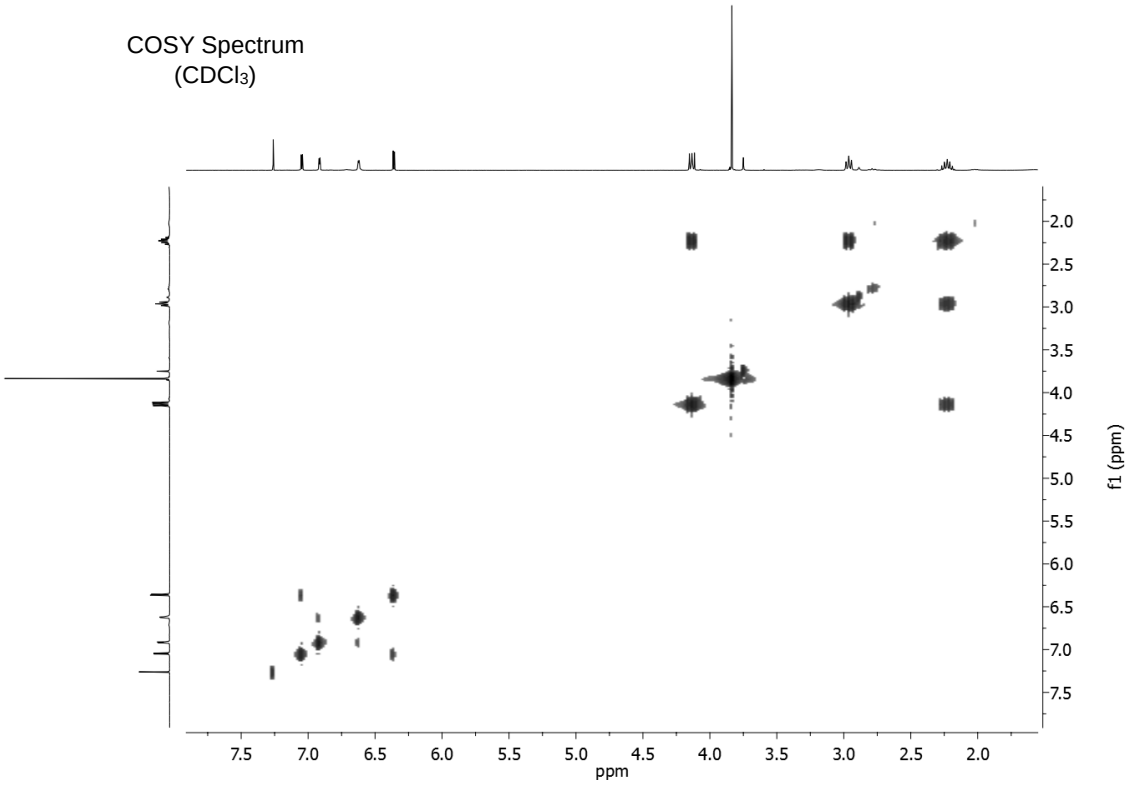

ed-HSQC Spectrum
($CDCl_3$)

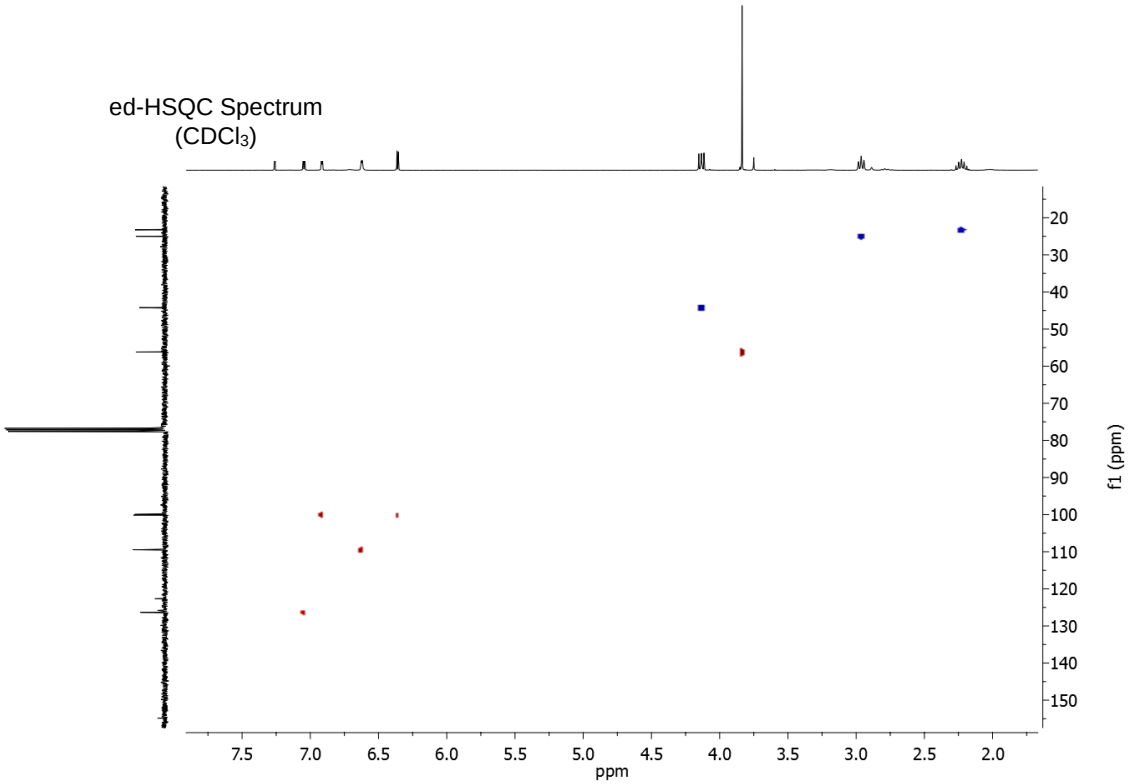

1,6-dihydropyrrolo[2,3-*e*]indole (17)

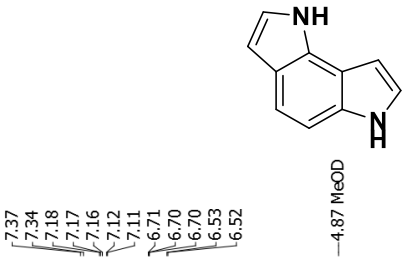

^{1}H NMR Spectrum
(300 MHz, MeOD)

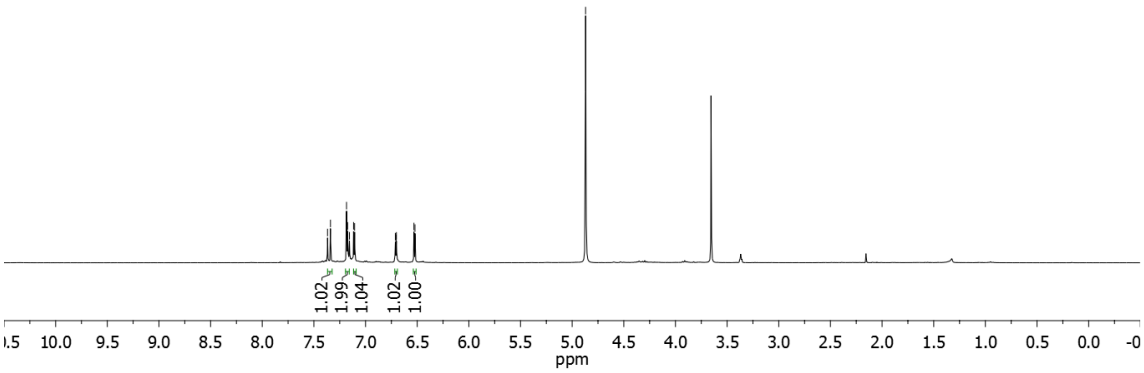

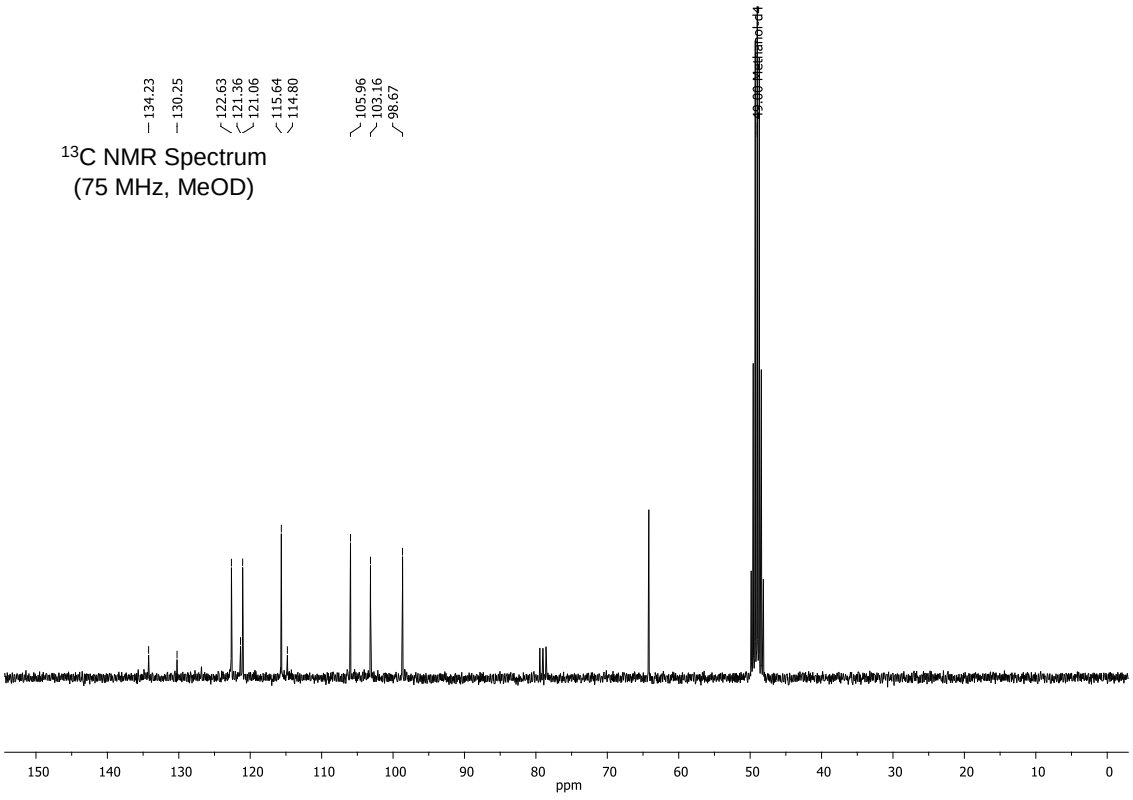

^{13}C NMR Spectrum
(75 MHz, MeOD)

2,2-di(1H-indol-3-yl)ethan-1-ol (20)

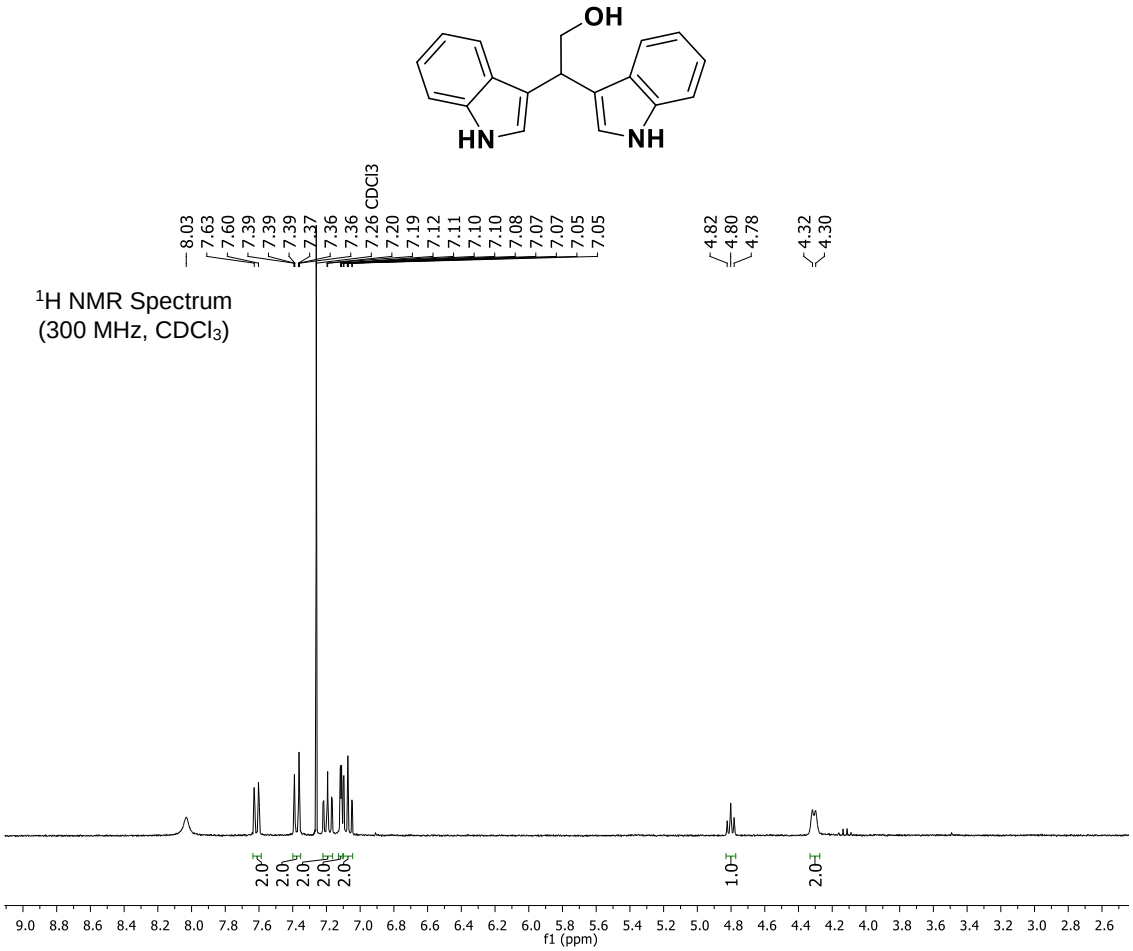

^{1}H NMR Spectrum
(300 MHz, $CDCl_3$)

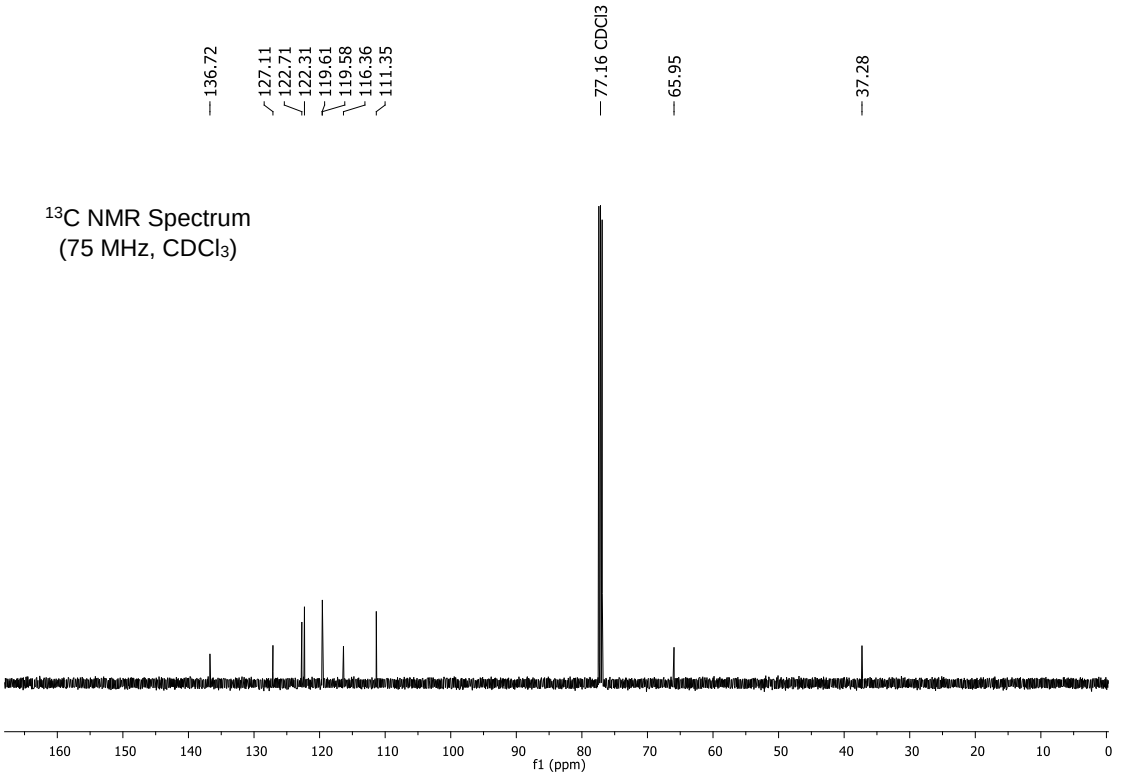

^{13}C NMR Spectrum
(75 MHz, $CDCl_3$)

COSY Spectrum
($CDCl_3$)

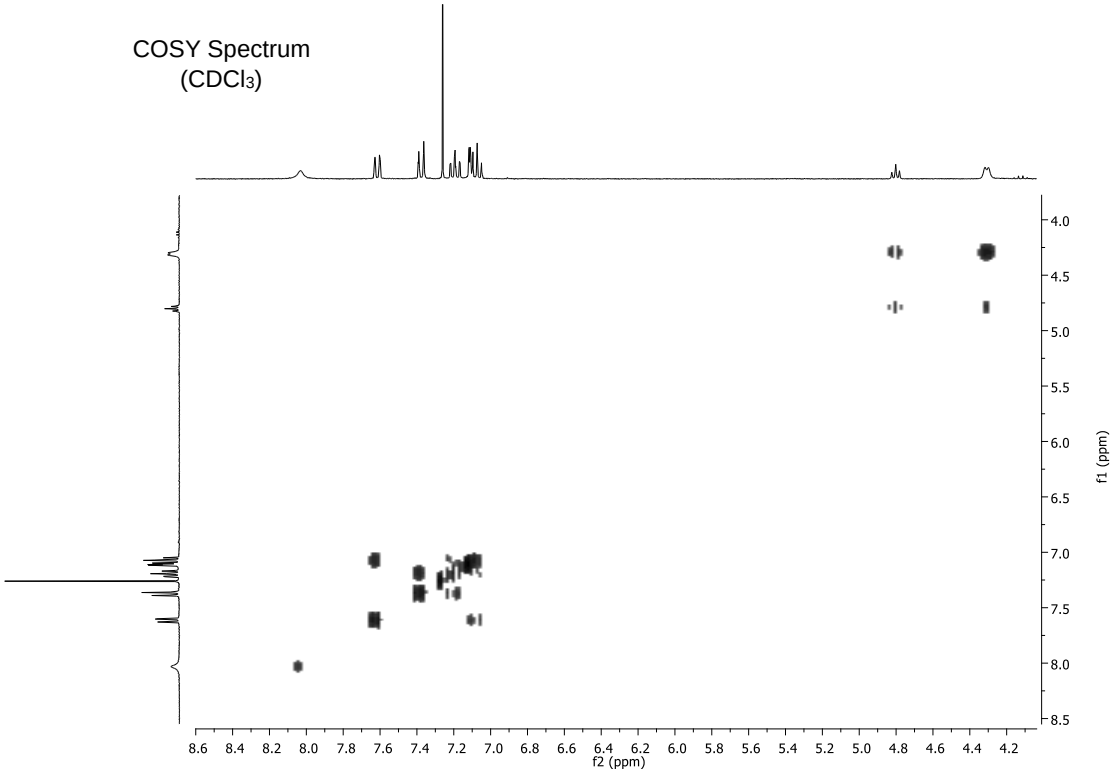

ed-HSQC Spectrum
($CDCl_3$)

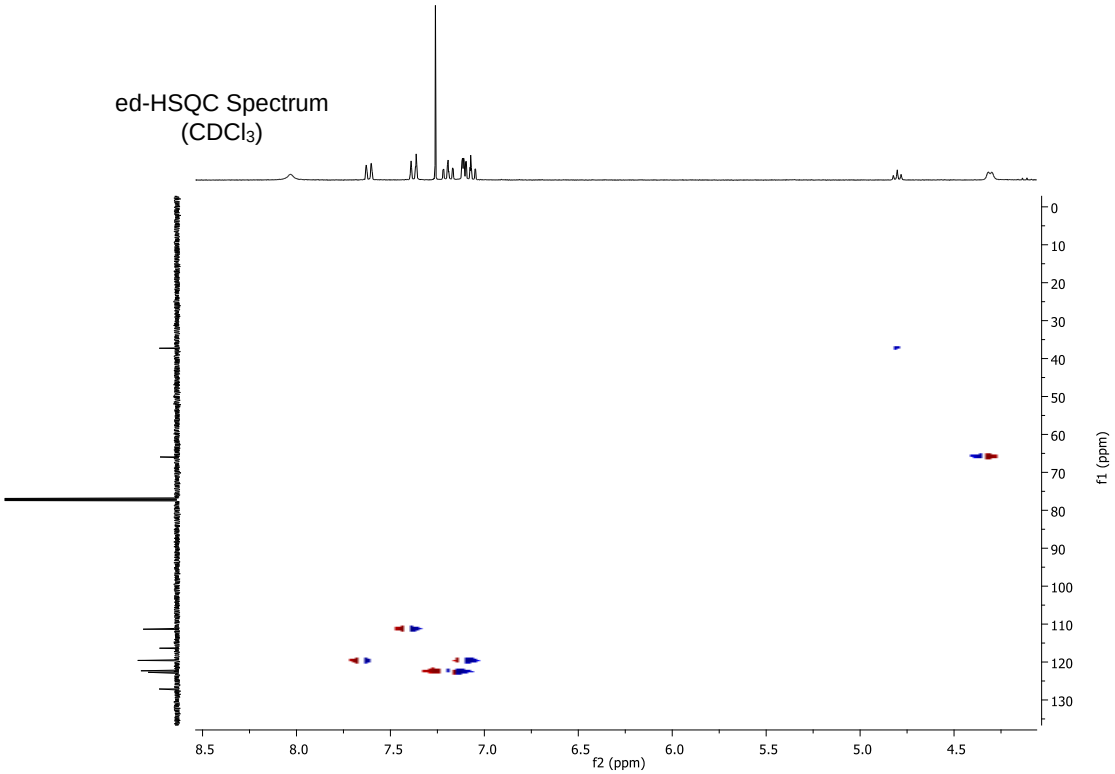

S5. Hydrogen detection

Hydrogen was detected by taking a sample of the reaction atmosphere (inside the flask) after 24h at the reaction conditions. It was measured with a GC 7890A Agilent Technologies having a MolSieve 5A column, TC detector and Ar as carrier gas.

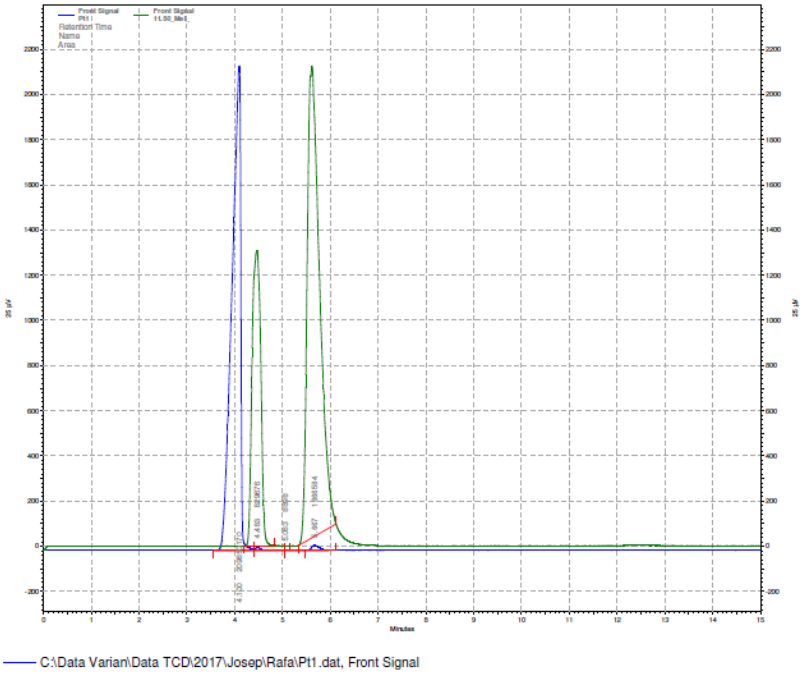

Figure S2. Blue chromatogram corresponds to the reaction, pick at 4.1 min is H2. Green chromatogram corresponds to a different sample containing O2 (4.483 min) and N2 (5.66 min)

Area % Report

Data File: C:\Data Varian\Data TCD\2017\Josep\Rafa\Pt1.dat
Method: C:\Methods TCD\Diego_50g.met
Acquired: 24/10/2017 10:06:33
Printed: 24/10/2017 10:28:36

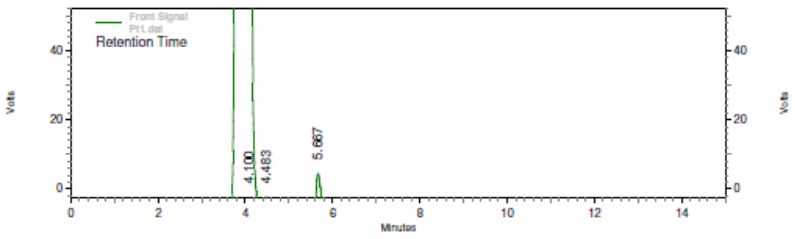

Front Signal Results

Name	Retention Time	Area	Area Percent	Height %
	4.100	209850170	98.727	98.31
	4.483	829676	0.390	0.69
	5.063	8898	0.004	0.01
	5.667	1866584	0.878	1.00
Totals		212555328	100.000	100.00

PARTE II: SÍNTESIS DE NUEVOS DIQUATS BASADOS EN [1,2,3]TRIAZOLO [1,5-*a*]PIRIDINAS Y [1,2,3]TRIAZOLO[1,5-*a*]QUINOLINAS Y SU INTERACCIÓN CON ADN

Capítulo 7

Introducción y objetivos

Introducción

En nuestro grupo de investigación se lleva trabajando desde hace muchos años con la estructura básica de la [1,2,3]triazolo[1,5-*a*]piridina.[32] Recientemente, se prepararon monosales y disales de triazolopiridinio con interesantes propiedades terapéuticas para el tratamiento de tripanosomiasis como la *Leishmania* y la enfermedad de *Chagas*. La alquilación de estas moléculas en la posición *2* se llevaba a cabo mediante el uso de haloalcanos (*Esquema II.1*). Siendo las sales resultantes solubles en agua, estables y activas *in vitro* sobre cepas de *Leishmania*.[60]

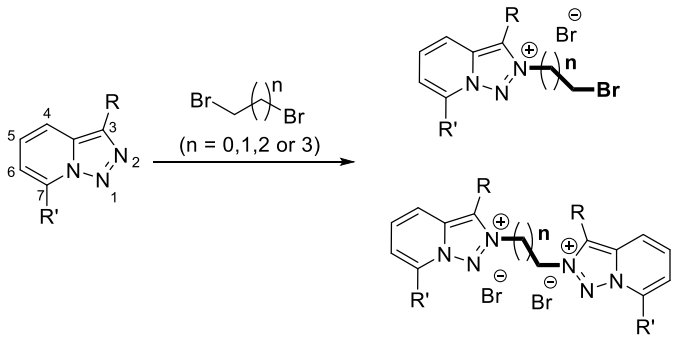

Esquema II.1. Alquilación de derivados de triazolopiridinas con bromoalcanos para obtener monosales y disales activas frente a Leishmania.

Los estudios mencionados nos aproximaron a la estructura de los dicationes conocidos como diquats. El diquat (**1**) es una molécula con estructura de dicatión de bipiridina cuaternaria obtenida normalmente por reacción de la 2,2'-bipiridina y el 1,2-dibromoetano, en forma de sal bromada (bromuro de 6,7-dihidropiridil[1,2-*a*:2',1'-*c*]pirazina-8,8'-diium) (*Esquema II.2*).

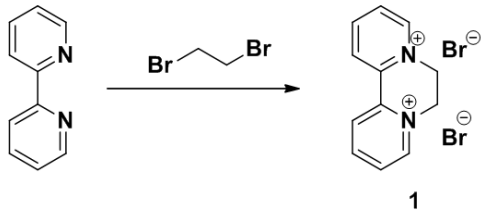

1

Esquema II.2. Síntesis genérica del diquat (**1**).

Esta molécula fue reportada por primera vez en 1958 por R.L. Jones y colaboradores,[61] como un potente herbicida, debido a su capacidad de producir estrés oxidativo en las células por la generación de Especies Reactivas de Oxígeno (Reactive Oxygen Species, ROS) (*Esquema II.3*).

[60] A. Martín-Montes, R. Ballesteros-Garrido, R. Martín-Escolano, C. Marın, R. Guitiérrez-Sánchez, B. Abarca, R. Ballesteros, M. Sanchez-Moreno, *RSC Adv.*, **2017**,*7*, 15715.
[61] R.L. Jones, R.C. Brian, R.F. Homer, J.A. Stubbs, *Nature*, **1958**, *181*, 446.

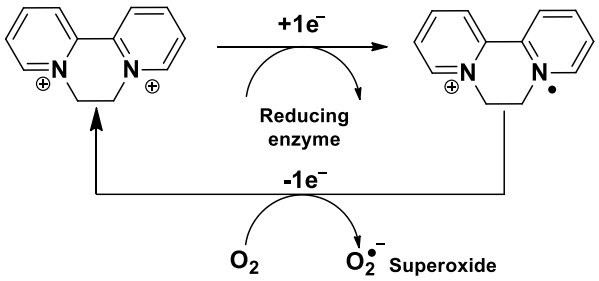

Esquema II.3. Mecanismo de acción del Diquat (**1**) como productor de ROS.

Además, el diquat ha demostrado tener papeles importantes como complejo de transferencia de carga o como modulador supramolecular.[62] Moléculas derivadas del diquat pueden poseer quiralidad axial, resultando en dos posibles configuraciones enantioméricas, *P* y *M*, interconvertibles entre sí por una baja barrera energética de unas 17-18 kcal·mol^{-1} (*Figura II.1*), tal y como estudiaron J. Lacour y colaboradores en 2002 y 2010.[63] En estos trabajos, buscaron la resolución de la mezcla racémica utilizando los aniones quirales hexacoordinados BINPHAT y TRISPHAT, obteniendo un exceso enantiomérico de más del 96% en muchos casos.

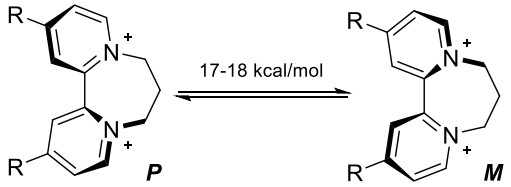

Figura II.1. Conformaciones *P* y *M* de un derivado de la molécula de diquat.

La resolución de las mezclas racémicas *P* y *M* del diquat y sus derivados también ha sido abordada recientemente por Teply y colaboradores[64]. En ese trabajo, sintetizan derivados de diquat con barreras energéticas de racemización lo suficientemente elevadas (≈230 kJ/mol^{-1} a 180ºC) como para obtener un exceso enantiomérico superior al 98% utilizando el anión quiral triflato como contranión (*Esquema II.4*). Con este método, consiguen además los primeros marcadores/colorantes derivados de un diquat no racémico, los cuales a modo de "proof of concept" utilizan para separar mezclas racémicas de conocidos analitos quirales como BINOL phosphate, Chlocyphos, Warfarin o Carprofen.

[62] T.C. Stancliffe, A. Pirie, *FEBS Lett.*, **1971**, *17*, 297.
[63] a) C. Pasquini, V. Desvergnes-Breuil, J.J. Jodry, A. Dalla Cort, J. Lacour, *Tetrahedron Lett.,* **2002**, *43*, 423. b) J. Vachon, G. Bernandinelli, J. Lacour, *Chem. Eur. J.*, **2010**, *16*, 2797.
[64] H.R. Talele, D. Koval, L. Severa, P.E. Reyes-Gutiérrez, I. Cisarová, P. Sázelová, D. Saman, L. Bednárová, V. Kasicka, F. Teply, *Chem. Eur. J.*, **2018**, *24 (30)*, 7601-7604.

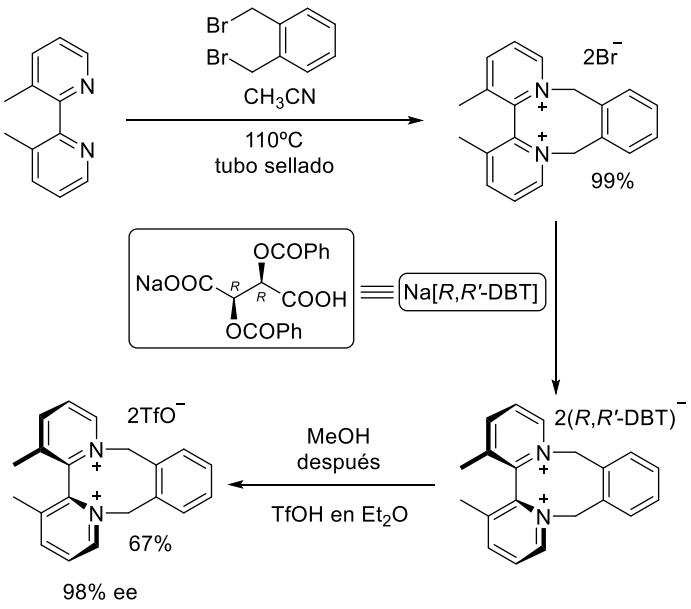

Esquema II.4. Síntesis y resolución de un derivado de diquat con elevada barrera energética de racemización mediante intercambio aniónico descrito por Teply *et al* en 2018.

En la bibliografía se pueden encontrar también otros derivados sin simetría *C2*, como los di-piridino di-hidrohelicenos descritos por Zysman-Colman y colaboradores en 2015[65] (*Figura II.2*).

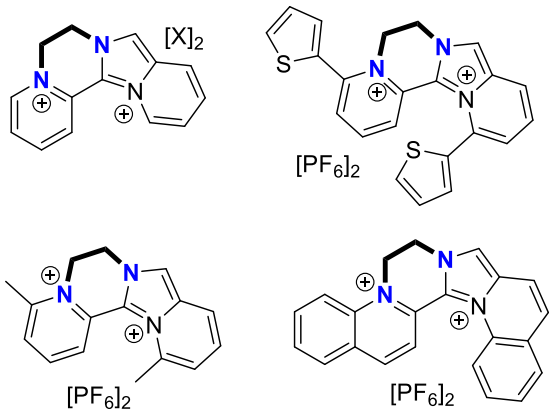

Figura II.2. Moléculas derivadas del diquat descritas por Zysman-Colman *et al* en 2015.

En cuanto a sus propiedades, el diquat es conocido por interaccionar fuertemente con ADN debido a su estructura aromática y su carga di-catiónica. Zhuang y colaboradores[66] reportaron en 2012 que el modo mayoritario de interacción del diquat con la doble hélice del ADN era mediante interacciones puramente electrostáticas, sin que ocurriera intercalación. Sin embargo, se puede pensar que la incorporación de los sustituyentes aromáticos apropiados puede llevar a formas de unión intercalantes.

Algo parecido propusieron Gunnlaugsson y colaboradores[67] en 2012 cuando anclaron a la molécula de diquat unos residuos fuertemente intercalantes (*Figura II.3*).

[65] A. Santoro, R.M. Lord, J.J. Loughrey, P.C. McGowan, M.A. Halcrow, A.F. Henwood, C. Thomson, E. Zysman-Colman, *Chem. Eur. J.*, **2015**, *21*, 7035.
[66] Q. Zhang, C. Wang, W. Liu, X. Zhang, S. Zhuang, *Environ. Chem. Lett.*, **2012**, *10*, 35.
[67] G.J. Ryan, R.B.P. Elmes, S.J. Quinn, T. Gunnlaugsson, *Supramol. Chem.*, **2012**, *24*, 175.

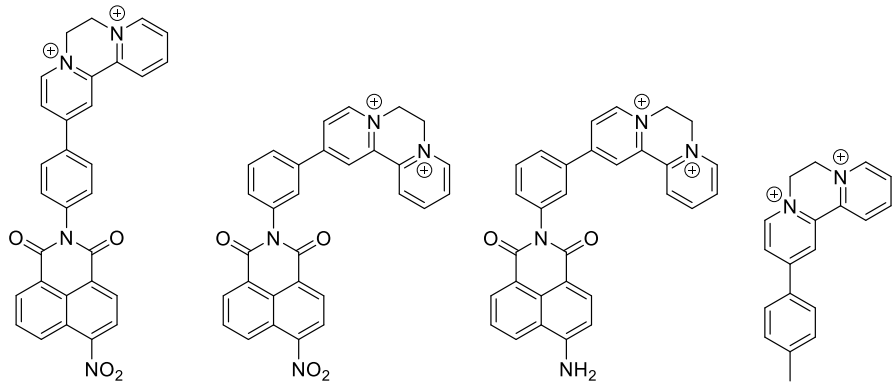

Figura II.3. Moléculas derivadas del diquats descritas por Gunnlaugsson en 2012.

Sin embargo, la intercalación directa de la zona dicatiónica todavía no ha sido explorada. Una interesante manera de alcanzar interacciones intercalantes más fuertes podría ser reemplazar los anillos de piridina por residuos aromáticos condensados.

En este punto, y teniendo en cuenta que en nuestro grupo hay una larga experiencia en el estudio de [1,2,3]triazolo[1,5-*a*]piridinas (**TP**) y derivados,[32] consideramos esas estructuras como 'building blocks' para la preparación de nuevos derivados de diquat. Una de ellas, 3-(2'-piridil)-[1,2,3]triazolo[1,5-*a*]piridina (**PTP**),[33] tiene la misma disposición de los átomos de nitrógeno que la 2,2'-bipiridina, lo cual debería permitir la ciclación con dihaloalcanos. Por otra parte, el anillo de triazolopiridina es un sistema electron-rico que puede ser fácilmente expandido por la adición de un anillo aromático extra formando 3-(2'-piridil)-[1,2,3]triazolo[1,5-*a*]quinolina (**PTQ**)[34] (*Figura II.4*).

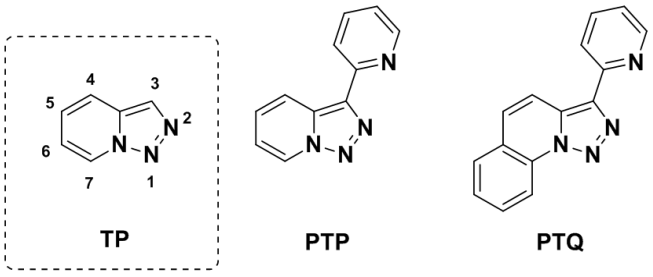

Figura II.4. Estructura general de la [1,2,3]triazolo[1,5-*a*]piridinas (**TP**), 3-(2'-piridil)-[1,2,3]triazolo[1,5-*a*]piridina (**PTP**) y 3-(2'-piridil)-[1,2,3]triazolo[1,5-*a*]quinolina (**PTQ**).

La síntesis de análogos de diquat basados en estructuras de **PTP** y **PTQ** representa un reto, además de una oportunidad, para obtener nuevas moléculas con estructura de diquat, con simetría *C1*, que pueden mostrar helicidad (*Figura II.5*).

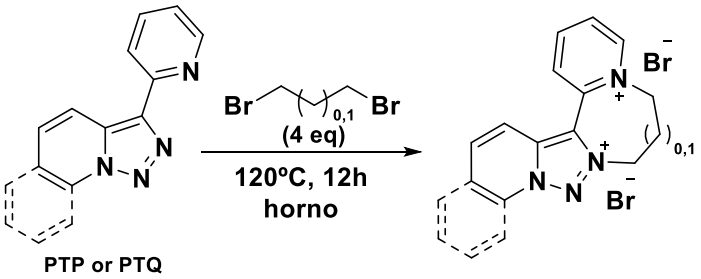

Figura II.5. Propuesta de obtención de derivados de diquat a partir de **PTP** y **PTQ** mediante alquilación con 1,2-dibromoetano y 1,3-dibromopropano.

Además, estas moléculas deberían presentar también un elevado coeficiente de absorción molar y una intensa emisión fluorescente, facilitando el estudio de su interacción con ADN por técnicas espectroscópicas. Aquí, se presenta la primera síntesis de análogos de diquat basados en **PTP** y **PTQ**, su caracterización estructural, propiedades espectroscópicas, comportamiento redox y el estudio de su capacidad de interaccionar con ADN.

Objetivos

Los objetivos de esta segunda parte fueron:

1. Síntesis de nuevas estructuras tipo diquat basadas en [1,2,3]triazolo[1,5-*a*]piridina (**PTP**) y [1,2,3]triazolo[1,5-*a*]quinolina (**PTQ**).
2. Estudio de sus propiedades estructurales, quiralidad axial, ópticas y electrónicas.
3. Estudio de su interacción con ADN.

Capítulo 8

Chemistry A European Journal, 2017, 23, 12825-12832

ChemPubSoc Europe
DOI: 10.1002/chem.201701618
CHEMISTRY A European Journal Full Paper

Conformation Analysis

Synthesis, Optical Properties, and DNA Interaction of New Diquats Based on Triazolopyridines and Triazoloquinolines

Pedro J. Llabres-Campaner,[a] Lluís Guijarro,[b] Claudia Giarratano,[a] Rafael Ballesteros-Garrido,*[a, b] Ramón J. Zaragozá,[c] M. José Aurell,[c] Enrique García-España,[b] Rafael Ballesteros,[a] and Belén Abarca[a]

ABSTRACT

Novel diquat derivatives based on [1,2,3]triazolo[1,5-*a*]pyridine and [1,2,3]triazolo[1,5-*a*]quinoline have been synthesized in excellent yields. In order to evaluate the effect of the alkyl bridge length ethane and propane dibromo alkanes were used. Theoretical calculations predict a very small energetic barrier between the two possible enantiomers P (Ra) and M (Sa), making them very difficult to resolve. At difference with the original diquat cation, thermal denaturation studies of ct-DNA. UV-Visible and fluorescence titrations with ct-DNA evidence the intercalation of the quinoline derivative in DNA.

Introduction

Diquat (**1**) is a quaternary bipyridinium cation generally obtained by reaction of 2,2'-bipyridine and 1,2-dibromoethane as its bromide salt (6,7-dihydrodipyrido[1,2-*a*:2',1'-*c*]pyrazine-8,8'-diium bromide) (*Scheme 1*).[1] **1** was first reported in 1958 by R. L. Jones *et al,* as a powerful herbicide agent.[2] The herbicide activity is directly related to its capacity to produce oxidative stress in cells[3,4] by generating Reactive Oxygen Species (ROS).[5] In addition, **1** has shown relevance as an ion-pair charge-transfer complex[6] and as a supramolecular modulator.[7] Similar structures have been reported in the literature employing different alkylating agents or even more complex dinitrogenated compounds.[8-11] A number of related dicationic derivatives obtained by using different alkylating agents have also been reported. Diquat derivatives possess axial chirality, affording two enantiomeric *P* (R_a) and *M* (S_a) configurations. The dihedral angle between the two pyridine rings depends on the length of the alkyl bridge.[12] Other derivatives without C2 symmetry can also be found, for example the dipyridiniumdihydrohelicenes described by Zysman-Colman in 2015, which show helical structure.[8]

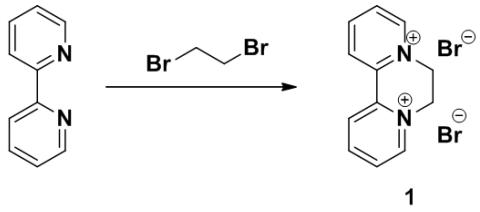

Scheme 1. General synthesis of diquat.

Diquat is known to interact with DNA due to its aromatic structure and dicationic charge. While diquat was reported to interact with DNA only through electrostatic interactions,[13] the incorporation of appropriate aromatic substituents can lead to intercalative binding modes.[14] An interesting way to achieve stronger intercalative interactions might be to replace the bypiridine rings by condensed aromatic moieties. Since our group has a large background in the study of [1,2,3]triazolo[1,5-*a*]pyridines (**TP**, *Figure 1*) and their derivatives, we considered that those structures might be good building blocks for preparing new diquat derivatives. [15] As a matter of fact, one of them, 3-(2'-pyridil)-[1,2,3]triazolo[1,5-*a*]pyridine (**PTP**),[16] has the same nitrogen atom disposition than 2,2'-bypiridine which should permit cyclization with dialkyl halides. On the other hand, the triazolopyridine ring is an electron rich system that can be easily expanded by the addition of an extra aromatic ring forming [1,2,3]triazolo[1,5-*a*]quinoline (**PTQ**).[17]

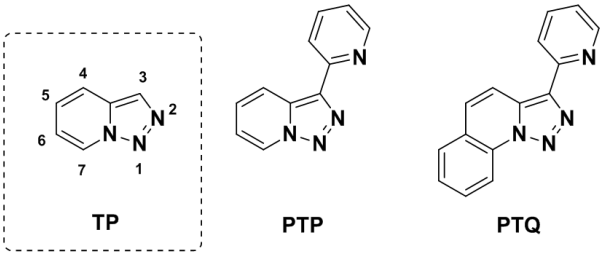

Figure 1. General structure of [1,2,3]triazolo[1,5-*a*]pyridine (TP), 3-(2'-pyridil)-[1,2,3]triazolo[1,5-*a*]pyridine (PTP) and 3-(2'-pyridil)-[1,2,3]triazolo[1,5-*a*]quinoline (PTQ).

Therefore, the synthesis of diquat analogues based on [1,2,3]triazolo[1,5-*a*]pyridine (TP) and [1,2,3]triazolo[1,5-*a*]quinoline represents a challenge, and also an opportunity to obtain new diquat-like molecules of C1 symmetry that can display helicity. Moreover these molecules should present high molar absorptivity and intense fluorescence emission facilitating the study of their interaction with DNA by direct spectroscopic techniques.[18] Herein, we present the first synthesis of diquat analogues based on PTP and PTQ, their structural characterization, spectroscopic properties, redox behavior and the study of their capacity to interact with DNA.

Results and Discussion

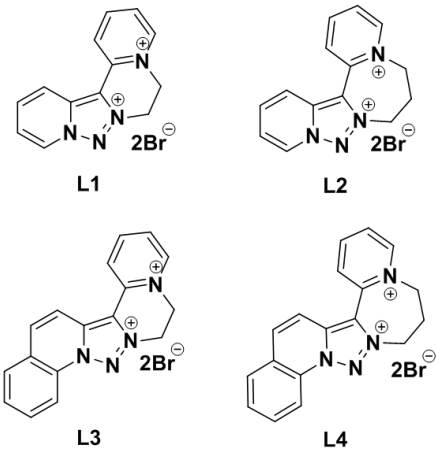

Figure 2. Target diquats **L1-L4.**

L1-**L4** (*Figure 2*) were synthesized by mixing 3-(2-pyridil)-[1,2,3]triazolo[1,5-*a*]pyridine (**PTP**)[16] or 3-(2-pyridil)-[1,2,3]triazolo[1,5-*a*]quinoline (**PTQ**)[17] with 1,2-dibromoethane or 1,3-dibromopropane heating at 120 ºC for 12 h (Scheme 2). Water soluble yellow powders were obtained in all cases. The presence of bromine ion was verified by Elementary and ICP analysis (See SI).

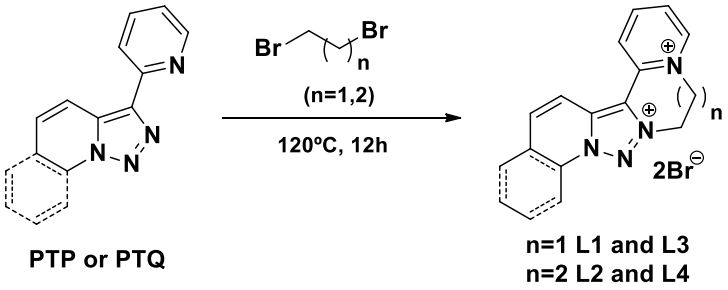

Scheme 2. Synthetic procedure of compounds **L1**-**L4**.

The ^{1}H-NMR spectra of **L1**-**L4** in D_2O (*Figure 3*) showed, as expected, dramatic changes in the aromatic signals compared to the parent compounds **PTP** and **PTQ** (see SI). In spite that all ^{1}H signals could be assigned by means of 2D-NMR and NOE-Diff experiments (See SI), it was hard to identify any trend in the aromatic domain because of the complexity of the signals. However, the signals corresponding to the ethylene and propylene bridges (*Figure 3, right*)

showed significant differences independently of the aromatic core. **L1** and **L3** presented an AA'BB' system in the 5.4-5.8 ppm range, while **L2** and **L4** showed two shielded triplets (around 5.1 ppm for the N-CH_2 hydrogen atoms) and a quintuplet around 3.2 ppm (middle CH_2 hydrogen atoms). NOE-Diff experiments allowed the differentiation of these signals (See SI); the hydrogen atoms of the methylene group close to the triazole ring being more shielded than those close to the pyridine ring. The presence of an AA'BB' spin system in L1 and L3 indicates that these four hydrogen atoms are not equivalent, even considering the P-M equilibrium. However, the triplet signals found in the compounds with the propane bridge (L2 and L4) suggest that these hydrogens may have different conformations without changing necessarily the configuration of the axial chirality (*P* or *M*). As a consequence of this equilibrium the signals appear as triplets even if the hydrogen atoms are not equivalent. NMR analysis of L1 and L2 carried out at different temperatures (25 ºC-80 ºC) (see SI) did not show any significant change with temperature. Only a better resolution in the aromatic region was observed at 80ºC without any evidence of decomposition or partial deuteration of the acidic positions at long times.

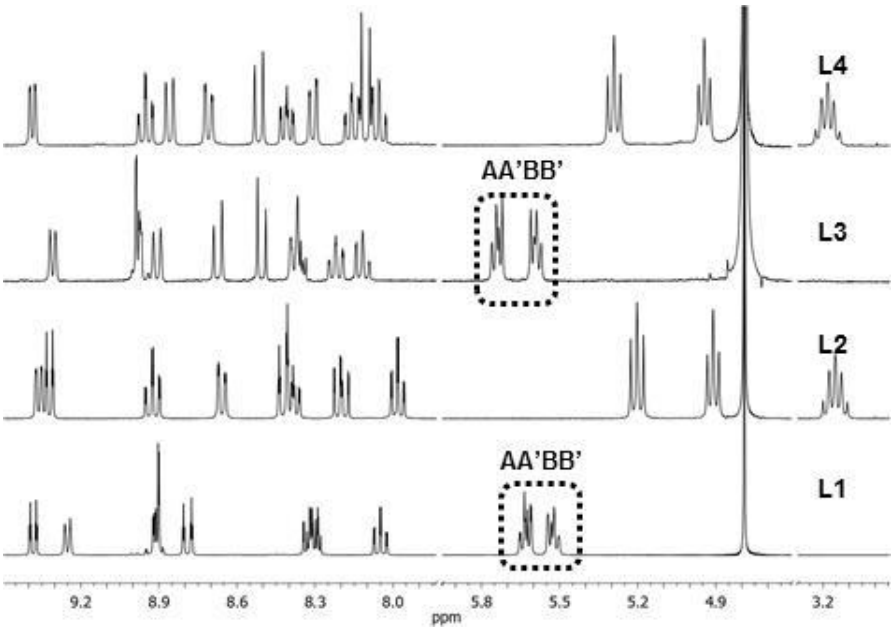

Figure 3. ^{1}H-NMR spectra of compounds **L1**-**L4**.

In order to clarify the observed differences in NMR, DFT conformational analysis (see computational methods and SI) of **L1** and **L2** were carried out. The calculations show that **L1** possesses two enantiomeric conformers (*P* and *M*, atropoisomers), which are interconvertible through only one transition state (TS). The small energetic barrier between both enantiomers (6.0 kcal/mol), allows for a very quick transformation between them at room temperature (*Figure 4*). Although **L2** presents also two enantiomeric conformers (*P* and *M*), interestingly, the interconversion between them is more complex due to the different possible conformers that can occur in this seven-membered ring. The conversion proceeds, in this case, through three different TS, generating two more energetic but stable conformers (*L2-b* and *L2-c*, *Figure 5*). As observed, in this situation the corresponding *N*-CH2 hydrogen atoms appear in the ^{1}H-

NMR spectrum as triplets. The maximum TS value of 9.2 kcal/mol allows for a very quick transformation at room temperature.

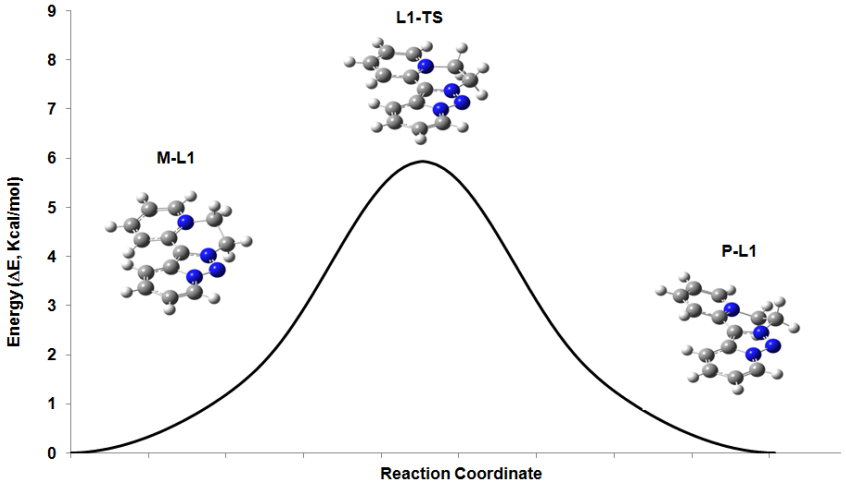

Figure 4. Energy profile (IRC, *ΔE*) corresponding to the conversion of ***M*-L1** into ***P*-L1** in vacuum.

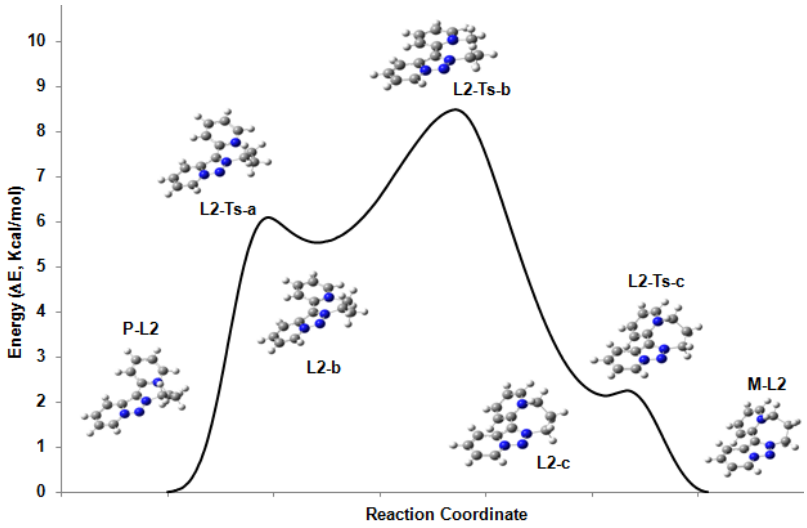

Figure 5. Energy profile (IRC, *ΔE*) corresponding to the conversion of ***P*-L2** into ***M*-L2** in vacuum.

Molecular orbital calculations can be used to estimate ^{13}C-NMR chemical shifts. Ab initio and DFT calculations of NMR shielding at very accurate levels of approximation are available in literature.[19-22] The GIAO (Gauge Including Atomic Orbital) method, implemented in the Gaussian package, is now widely used for these purposes. Good quality shielding results depend on the quality of the basis sets selected. Excellent results are obtained using B3LYP as DFT method and 6-311++G** as basis set. In the case of **L1**, the results are practically the same than the experimental spectrum in agreement with the only stable conformer found (*Figure 6, up*). In the case of **L2**, we found three stable conformers (**P/M-L2**, **L2-b** and **L2-c**), being conformer **P/M-L2** the most stable. Conformers **L2-b** and **L2-c** have energy values of 5.9 kcal/mol and 2.4 kcal/mol above the previous conformer, respectively. Conformers **L2-b** and

L2-c show large discrepancies between the calculated and the experimental carbon signals (see SI), including carbons *C6* and *C8* which are most sensitive to conformational changes. However, the calculated values of the more stable conformer (**P/M-L2**) fit quite accurately the experimental data (*Figure 6, down*). Only carbon *C7* shows a major discrepancy with the experimental data (+4.55 ppm), possibly due to its high mobility. This indicates that conformer **P/M-L2** has the largest contribution to the compound **L2** according to calculations.

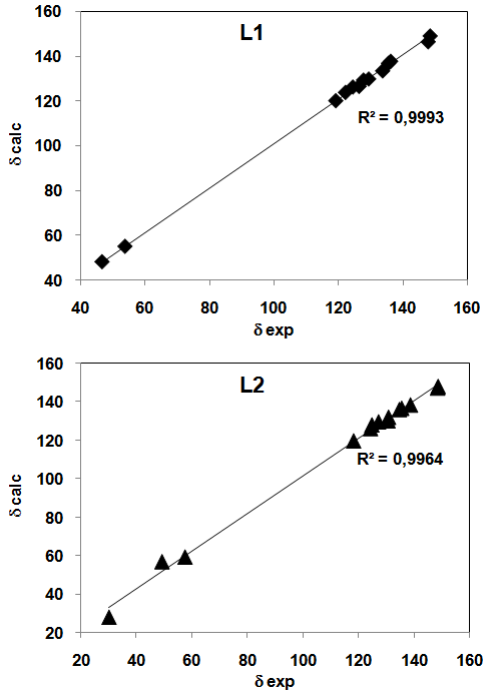

Figure 6. Correlation between theoretical and experimental ^{13}C-NMR signals for **L1** and **L2**.

UV-Vis spectra, steady-state fluorescence emission spectra and quantum yield calculations were recorded for all compounds in water solution (phosphate buffer). In *Table 1* spectral features of compounds **L1-L4** are presented.

Table 1. Photophysical and electrochemical data for **L1-L4**

Compound	L1	L2	L3	L4
λ_{max} [nm]	340	327	343	325
ε_{max} [10^3 M^{-1} cm^{-1}]	8.8	7.5	13,6	11,3
λ_{em} [nm]	430	438	472	474
Φ_{PL} (%)	7.8	4.1	21.5	21.0
$E^1_{1/2}$ [V]	-0.31	-0.35	-0.48	-0.33
ΔE_p [V]	0.57	0.67	0.21	0.70

$E^2_{1/2}$ [V]	-0.63	-	-0.75	-0.61
ΔE_p [V]	0.08	-	0.08	0.62
K_{SV} [10^3 M^{-1}][a]	-	-	4,25	3,38

[a] Stern-Volmer values calculated for the interaction with ct-DNA.

Surprisingly, independently from the aromatic core, large changes in the absorption spectra are observed depending on the size of the non-aromatic cycles. **L1** and **L3** have similar absorption bands centered at 340 nm, while **L2** and **L4**, with seven-membered cycles, have bands around 325 nm. These results outline the more efficient conjugation induced by the higher planarity of the six-membered cycle (smaller dihedral angle) (*Figure 7*).

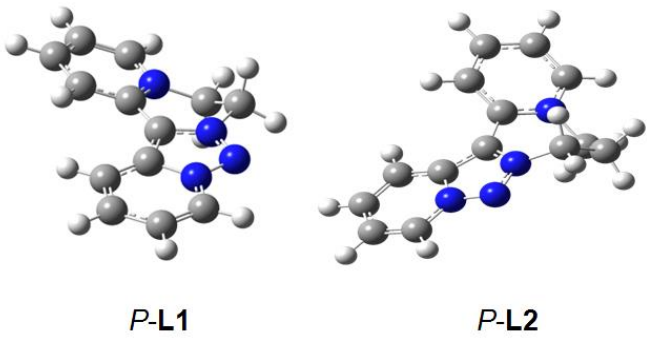

Figure 7. Theoretical conformation of P-L1 and P-L2.

The emission spectra of **L1**-**L4** are also reported in *Table 1* and showed in *Figure 8*. **L1** and **L2** display similar emission bands at 430 nm and 438 nm, respectively, with a Stokes shift ranging from 90 nm to 111 nm. Quantum yield are more different; 7.8% for **L1** and 4.1% for **L2**. All these values are in agreement with those of **PTP** that possess the same core structure, and in the case of quantum yields, with the induced planarity of **L1**. The increase of conjugation in **L3** and **L4** causes a bathochromic shift to 472 nm and 475 nm, respectively, with a Stokes shift of 129 nm for **L3** and of 139 nm for **L4**. It is well known that compounds derived from **PTQ** exhibit high quantum yields,[23] the observed values for **L3** and **L4** were close to 21% (*Table 1*).

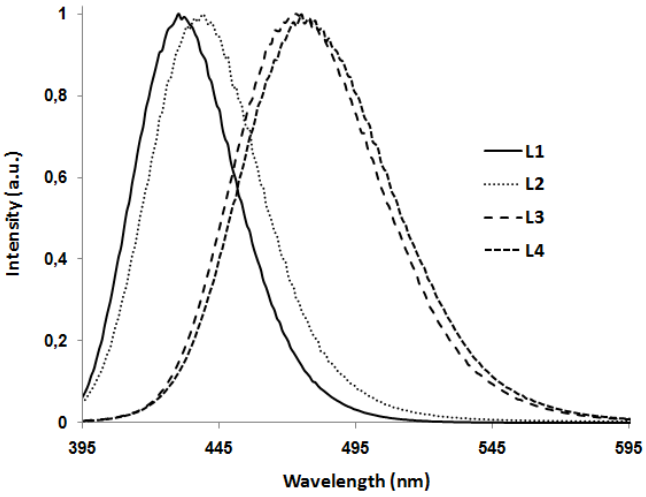

Figure 8. Emission spectra of **L1**-**L4**.

The electrochemical properties of **L1**-**L4** were studied by cyclic voltammetry (*Table 1*). All ligands underwent two reversible, one-electron reductions. First, the radical cation species was formed by addition of one electron, being this process more difficult for **L3** (lower reduction potential). Since the pyridine ring is electron deficient, the first reduction should occur at this ring. For **L3**, the high electron density of the triazole ring combined with the greater planarity of the molecule makes pyridine less electron deficient, shifting the reduction potential to more negative values in comparison with the other derivatives. The values of potential for the second reduction agree with the previous rationalization. This trend is not observed when comparing the original diquat (**1**) and its analogue with a propylene bridge (3-diquat).[24] In this case a shift of 0.20 V is observed upon increasing the chain length owing to the reduced conjugation yielded by the increase of the dihedral angle. These similarities agree with HRMS results, all compounds **L1**-**L4** showed a molecular ion at mass m/z corresponding to a radical cation instead of the expected signal at m/2z. This behavior has also been found for **1** in the literature.[25]

Finally, we studied the interaction of these new diquats with DNA. As we have noted before, triazolopyridines have significant potential for interacting with DNA.[26] However, cationic triazolopyridines had rarely been studied. As these compounds combine important features for DNA interaction (planarity, aromaticity, cationic nature…) we considered interesting to explore how the structural differences between them could induce changes in their interaction with DNA. It is well known that upon heating the double stranded DNA helix dissociates into two single stranded chains at well-defined temperature (Tm value).[27] Non-covalent binding of small molecules to ds-polynucleotides usually has certain effect on the thermal stability of double helix thus giving different Tm values. Therefore, the difference between the Tm values of free- and complexed polynucleotides (ΔTm value) is an important factor in the characterization of small molecule/ds-polynucleotide interactions. Thermal melting studies were performed using calf tymus DNA (ct-DNA) as DNA model, at different [L]/[ct-DNA] concentration ratios (r).

Table 2. Variation on the melting temperature (ΔT_m)[a] measured as a difference between the free ct-DNA (58.2 ± 1 ºC from experimental data~$5x10^{-5}$M) and the ligand-bound ct-DNA at different concentration ratios.[b]

	r[b]		
Ligand	**0.1**	**0.2**	**0.5**
L1	1.6	5.3	9.2
L2	2.6	5.4	8.3
L3	13.2	18.6	26.4
L4	13.1	18.2	24.9

[a] ΔT_m values in ºC. Errors are estimated to be ±1ºC. [b] r=[**L**]/[ct-DNA].

As shown by the results in *Table 2*, an increase of the melting temperature was observed in all cases. ΔTm values were much higher for pyridyltriazoloquinoline derivatives (**L3** and **L4**) at any *r* studied. The relatively small changes induced by **L1** and **L2** suggest an electroestatic interaction. Inclusion of an extra aromatic ring seems to provide to the pyridyltriazoloquinoline derivatives an additional intercalative binding mode that induces stabilization of the double helix. However, this point cannot be proven only by these experiments since this method does not provide unambiguous evidence to distinguish intercalation from other binding modes. Nevertheless, melting temperature experiments allowed us to clearly identify differences in DNA binding induced by the two types of aromatic core.

As it has been extensively reported,[28] binding of molecules to the DNA double helix is usually accompanied by significant changes in the absorbance spectra of the bound molecule. UV-Vis titrations can provide additional information to determine whether an interaction is taking place or not, and also of what kind of interaction occurs (electrostatic or intercalative).

The absorption spectra of **L1**-**L4** upon addition of increasing amounts of ct-DNA (0 to 10 eq.) were recorded. In all cases, an increase in absorption was observed between 200 and 300 nm due to the intrinsic DNA absorbance in this region. However, the absorption in the 300-400 nm region, where ct-DNA does not absorb, remained unaltered for **L1** and **L2**, while, for **L3** and **L4** a decrease of the absorbance and a change in the shape of the UV-Vis bands was observed (see SI). *Figure 9* shows, as an example, an UV-Visible titration of **L4** with ct-DNA. A decrease of the absorbance of **L3** and **L4** is an evidence of conformational changes in the molecule, possibly induced by a strong interaction with ct-DNA by intercalation. These results support those obtained by the thermal denaturation studies.

Therefore, the presence of an extra aromatic moiety seems to favor the intercalation of the quinoline derivatives **L3** and **L4** within the ct-DNA base-pairs.

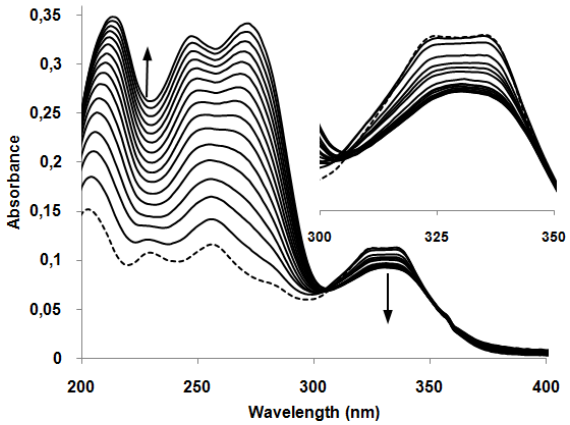

Figure 9. Changes in the UV-Visible absorption spectrum of **L4** 10µM in 1mM phosphate buffer, upon addition of ct-DNA (1-10 eq) in 1mM phosphate buffer.

These systems were also studied by steady-state fluorescence spectroscopy. Since ct-DNA does not absorb at λ > 300 nm, the strong fluorescence emission of **L1**-**L4** in the 400-600 nm region, λ_{exc}= 327-343 nm (see Table 1), was used to perform direct fluorometric titrations. All titrations induced quenching of the fluorescent emission but, interestingly, the pyridyltriazolopyridine and pyridyltriazoloquinoline derivatives had a different behavior. While **L1** and **L2** suffered quenching of their emission without any shifting of the wavelength, **L3** and **L4** bore a hypsochromic shift (*Figure 10*), a well known phenomena for intercalative compounds.[13,14,17] *Figure 11* shows the fluorescence changes experimented by **L4** during titration with ct-DNA. Only for **L3** and **L4** it was possible to apply a Stern-Volmer, the value of the constant being higher for **L3** (4.25 10^3 M^{-1}) than for **L4** (3.38 10^3 M^{-1}), which can be attributed to the planarity of **L3** (*Table 1*).

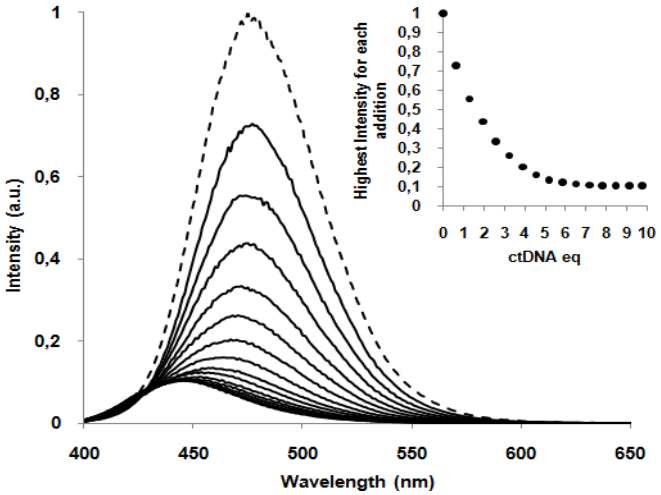

Figure 10. Changes in the emission spectrum of **L4** 10µM in 1mM phosphate buffer, upon addition of ct-DNA (1-10 eq) in 1mM phosphate buffer.

Conclusions

Synthesis of novel diquat derivatives based on **PTP** and **PTQ** have been carried out with yields up to 90%. These are able to adopt helical conformations in two different enantiomers (*P* or

M), which are interconvertible with a very low energetic barrier, according to the theoretical studies. The values of the reduction potential of these molecules are in concordance with those registered for the original diquat cation. **L3** presents a lower reduction potential due to the conjugation of the rings that make pyridine ring less electron deficient. The compounds are also able to interact with DNA electrostatically or by intercalation. Thermal denaturation studies, UV-Visible and fluorescence titrations with ct-DNA were performed, showing, on the one hand, electrostatic interaction for the **PTP** derivatives (**L1** and **L2**), and on the other hand, not only an electrostatic binding mode but also intercalation for the **PTQ** derivatives (**L3** and **L4**). Herein, we have reported how the behavior of diquats can be modulated by controlling the ring size and the number of aromatic rings leading to molecules that interact exclusively by electrostatic forces or through a combination of electrostatic and intercalative binding modes.

Experimental section

*Synthesis of 6,7-dihydropyrido[1,2-a-]pyrido[1`,2`:3,4][1,2,3]triazolo [5,1-c]pyrazine-5,8-diium bromide (**L1**):* 3-(2-pyridil)-[1,2,3]triazolo[1,5-*a*]pyridine[15] (100 mg, 0.51 mmol) was dissolved in 1,2-dibromoethane (1 mL, 11.6 mmol) and was put into an oven at 120 ºC for 15 h observing a precipitate. After that, it was allowed to cool down and it was washed with hot ethyl acetate. After three washes followed by decantation a yellow powder was obtained. Isolated yield: 95%. M.p.= 311 - 312 °C. ^{1}H NMR (300 MHz, D_2O): $\delta =$ 9.38 (dt, J = 7.1, 1.0Hz, 1H), 9.27 – 9.23 (m, 1H), 8.95 – 8.88 (m, 2H), 8.79 (dt, J = 9.2, 1.1Hz, 1H), 8.35 – 8.27 (m, 2H), 8.05 (td, J = 7.2, 1.2Hz, 1H), 5.66 – 5.59 (m, 2H), 5.52 (dd, J = 7.7, 4.6Hz, 2H). ^{13}C NMR (75 MHz, D_2O): $\delta =$ 148.9 (CH), 147.8 (CH), 136.2 (C), 135.5 (CH), 133.7(C), 129.4 (CH), 127.8 (CH), 126.4 (CH), 124.5 (CH), 122.2 (C), 119.2 (CH), 54.0 (CH_2), 46.9 (CH_2). HRMS for $C_{17}H_{14}N_4^{2+}$: found m/z 224.1027 (calculated for $[L1]^{\bullet+}$ 224.1051); found m/z 223.0976 (calculated for $[L1\text{-}H]^{\bullet+}$ 223.0937). Elementary analysis for $C_{13}H_{12}N_4Br_2{\cdot}2H_2O$ Calcd. C 37.17, H 3.84, N 13.34; found C 37.00, H 3.68, N 12.96 IR (νmax, cm-1) = 3410, 3350, 3040, 2980, 1650, 1630, 1580, 1540, 1510, 1450,1350, 1280, 1210, 1150,1070, 850, 783, 730, 695, 657, 602.

*Synthesis of 7,8-dihydro-6H-pyrido[1,2-a]pyrido[1',2':3,4][1,2,3] triazolo[5,1-c][1,4]diazepine-5,9-diium bromide (**L2**):* 3-(2-pyridil)-[1,2,3]triazolo[1,5-*a*]pyridine[15] (100 mg, 0.51 mmol) was dissolved in 1,3-dibromopropane (1 mL, 9.8 mmol) and was put into an oven at 120 ºC for 15 h. After that, it was allowed to cool down and it was washed with hot ethyl acetate. After three washes followed by decantation a yellow powder was obtained. Isolated yield: 90%. M.p.= 244 – 245 °C. ^{1}H NMR (300 MHz, D_2O):$\delta =$ 9.36 (dd, J = 6.1, 0.9Hz, 1H), 9.32 (dt, J = 7.1, 1.0Hz, 1H), 8.92 (td, J = 8.0, 1.4Hz, 1H), 8.66 (dd, J = 8.0, 1.2Hz, 1H), 8.42 (dt, J = 9.2, 1.1Hz, 1H), 8.40 – 8.35 (m, 1H), 8.20 (ddd, J = 9.2, 7.2, 0.9Hz, 1H), 7.98 (td, J = 7.1, 1.2Hz, 1H), 5.24 – 5.16 (m, 2H), 4.91 (t, J = 6.6Hz, 2H), 3.20 – 3.10 (m, 2H). ^{13}C NMR (75 MHz, D_2O): $\delta =$ 148.7 (CH), 148.5 (CH), 138.7 (C), 135.53 (C), 134.7 (CH), 130.8 (CH), 130.6 (CH), 127.2 (CH), 124.8 (C), 124.3 (CH), 118.2 (CH), 57.4 (CH_2), 49.1 (CH_2), 30.0 (CH_2). HRMS for $C_{14}H_{14}N_4^{2+}$: found m/z 238.1171 (calculated for $[L2]^{\bullet+}$ 238.1207); found m/z 237.1128 (calculated for $[L2\text{-}H]^{\bullet+}$ 237.1129). Elementary analysis for $C_{14}H_{14}N_4Br_2{\cdot}H2O$ Calcd. C 40.41, H 3.88, N 13.46; found C 40.08, H 3.99, N 13.08. IR (νmax, cm-1) = 3470, 3410, 3090, 3040, 2970, 1650, 1620, 1580, 1430, 1390, 1330, 1290, 1240, 1190, 1080, 998, 947, 894, 857, 779, 766, 743, 703, 661.

*Synthesis of 6,7-dihydropyrido[2'',1'':3',4']pyrazino[1',2':3,4] [1,2,3]triazolo[1,5-a]quinoline-5,8-diium bromide (**L3**):* 3-(2-pyridil)-[1,2,3]triazolo[1,5-*a*]quinoline[15] (100 mg, 0.4 mmol) was dissolved in 1,2-dibromoethane (1 mL, 11.6 mmol) and was put into an oven at 120 ºC for 15 h. After that, it was allowed to cool down and it was washed with hot ethyl acetate. After three washes followed by decantation a yellow powder was obtained. Isolated yield: 92%. M.p. = 298 – 299 ºC. ^{1}H NMR (300 MHz, D_2O): δ = 9.31 (d, J = 6.1Hz, 1H), 8.98 (dd, J = 4.4, 1.1Hz, 1H), 8.92 (t, J = 6.9Hz, 1H), 8.67 (d, J = 9.6Hz, 1H), 8.51 (d, J = 9.6Hz, 1H), 8.41 – 8.33 (m, 1H), 8.21 (dd, J = 11.5, 4.3Hz, 1H), 8.12 (t, J = 7.2Hz, 1H), 5.74 (dd, J = 7.5, 4.5Hz, 1H), 5.59 (dd, J = 7.4, 4.7Hz, 1H). ^{13}C NMR (75 MHz, D_2O): δ= 148.8 (CH), 147.8 (CH), 137.3 (CH), 136.6 (C), 133.8 (CH), 133.2 (C), 131.9 (CH), 130.6 (CH), 130.5 (C), 126.7 (CH), 126.4 (2C), 117.0 (CH), 112.8 (CH), 54.2 (CH_2), 47.0 (CH_2). HRMS for $C_{17}H_{14}N_4^{2+}$: found m/z 274.1190 (calculated for $[L3]^{\bullet+}$ 274.1207); found m/z 273.1135 (calculated for $[L3\text{-}H]^{\bullet+}$ 273.1129). Elementary analysis for $C_{17}H_{14}N_4Br_2$·H2O Calcd. C 45.16, H 3.54, N 12.39; found C 44.99, H 3.54, N 12.70. IR (νmax, cm-1) = 3428, 3007, 1626, 1474, 1293, 1224, 1168, 838, 780, 726, 707, 688, 672.

*Synthesis of 7,8-dihydro-6H-pyrido[2'',1'':3',4'][1,4]diazepino [1',2':3,4][1,2,3]triazolo[1,5-a]quinoline-5,9-diium bromide (**L4**):* 3-(2-pyridil)-[1,2,3]triazolo[1,5-*a*]quinoline[15] (100 mg, 0.4 mmol) was dissolved in 1,3-dibromopropane (1 mL, 9.8 mmol) and was put into an oven at 120 ºC for 15 h. After that, it was allowed to cool down and it was washed with hot ethyl acetate. After three washes followed by decantation a yellow powder was obtained. Isolated yield: 93%. M.p.= 239 – 240 ºC. ^{1}H NMR (300 MHz, D_2O): δ= 9.35 (dd, J = 6.1, 1.1Hz, 1H), 8.91 (td, J = 8.0, 1.3Hz, 1H), 8.82 (d, J = 8.5Hz, 1H), 8.67 (dd, J = 8.0, 1.2Hz, 1H), 8.48 (d, J = 9.5Hz, 1H), 8.37 (ddd, J = 7.7, 6.1, 1.4Hz, 1H), 8.27 (dd, J = 8.0, 1.2Hz, 1H), 8.16 – 7.97 (m, 1H), 5.25 (t, J = 7.3Hz, 1H), 4.91 (t, J = 6.5Hz, 1H), 3.20 – 3.08 (m, 1H). ^{13}CNMR (75 MHz, D_2O): δ= 148.9 (CH), 147.9 (CH), 138.7 (C), 136.3 (CH), 134.5 (C), 133.4 (CH), 131.7 (CH), 131.0 (CH), 130.7 (CH), 130.4 (CH), 130.01 (C), 126.03 (C), 125.68 (C), 116.7 (CH), 112.0 (CH), 57.4 (CH_2) 49.4 (CH_2), 29.9 (CH_2).HRMS for $C_{18}H_{16}N_4^{2+}$: found m/z 288.1324 (calculated for $[L4]^{\bullet+}$ 288.1364); found m/z 287.1289 (calculated for $[L4\text{-}H]^{\bullet+}$ 287.1286). Elementary analysis for $C_{18}H_{16}N_4Br_2$ Calcd. C 48.24, H 3.60, N 12.50; found C 48.11, H 3.58, N 12.81. IR (νmax, cm-1) = 3426, 3008, 1626, 1474, 1440, 1283, 1225, 1166, 1071, 837, 820, 781, 726, 687.

Computational methods

All calculations were carried out with the Gaussian 09 suite of programs.[29] Density functional theory[30] calculations (DFT) have been carried out using the B3LYP[31] exchange-correlation functionals, together with the standard 6-31G** basis set.[32] The stationary points were characterised by frequency computations in order to verify that TSs have one and only one imaginary frequency. The intrinsic reaction coordinate (IRC),[33] in vacuum, were traced in order to check the energy profiles connecting each TS to the two associated minima using the second order González–Schlegel integration method.[34] The inclusion of solvent effects has been considered by using a relatively simple self-consistent reaction field (SCRF) method[35] based on the polarizable continuum model (PCM) of Tomasi's group.[36] Geometries have been fully optimized with PCM. The used solvent was water (solvent used in NMR spectroscopy).

NMR calculations of absolute shielding using gauge including atomic orbital method (GIAO) were carried out using 6-311++G** as basis set.

UV-Vis and Spectrofluorometric measurements. ct-DNA was purchased from commercial sources as sodium salt and used without further purification. All stock solutions were prepared in 1 mM phosphate buffer (pH=7.4). The polynucleotide concentration was determined by absorption spectroscopy, using the molar extinction coefficient of 6600 M−1·cm^{-1} at 260 nm. Titration experiments were carried out at room temperature by adding increasing amounts of polynucleotide from 6.5x10^{-5} M stock solution to a 1x10^{-5} M ligand solution. UV-Vis absorption spectra were recorded on a spectroscopy system using quartz cells with a 1 cm path length. The absorbance of aqueous solutions of L are proportional to its concentration up to 100 µM, hence no significant intermolecular aggregation of the compound, which would be expected to give rise to hypsochromic shift, occurred in the concentration range needed for the following spectroscopic studies. The emission spectra were recorded with a spectrofluorometer in the 360-650 nm range with excitation wavelength required for each compound. All studies were performed at 25ºC.

Melting point experiments. Thermal melting curves were measured on a UV-Vis spectrometer equipped with a Peltier temperature controller system. Changes on the absorption at 260 nm at different temperatures were followed for 5x10^{-5}M solutions (pH 7.4, 1 mM phosphate buffer) of the polynucleotide in the presence or absence of the ligand/complex. The Tm values were taken from the maximum of the first derivative. ΔTm values were calculated subtracting Tm for the free nucleic acid (58.2 ± 1 ºC from experimental data) from Tm for the complex. Every ΔTm value reported here was the average of at least two measurements, with an estimated error in ΔTm of ±1 ºC.

Electrochemical Measurements. Cyclic voltammetric experiments were performed on TRIS 50mM and NaCl 0.15 mol·dm^{-3} aqueous solutions at pH 7.4 using 10-3 M receptor concentration. Electrochemical experiments were performed with BAS CV 50W and Metrohm PGSTAT 101 Autolab in a conventional three-compartment cell with glassy-carbon working electrode. Prior to each voltammetric run, the electrode was polished with an aqueous suspension of alumina on a soft surface, rinsed with water and dried. An Ag/AgCl (3 M NaCl) reference electrode and platinum wire auxiliary electrode completed the three-electrode configuration. The cyclic voltammograms were recorded at scan rates of 50–500 mV s-1.

Acknowledgments

R. B-G is much indebted to the Posdoctoral fellow 2013 of the Ministerio de Economía y Competitividad (Spain, FPDI-2013-17464). This work was financially supported by Ministerio de Ciencia e Innovación (Spain) (Projects CONSOLIDER-INGENIO SUPRAMED CSD 2010-00065, CTQ2016-78499-C6-1-R), Unidad de Excelencia María de Maeztu MDM-15-0538) and Generalitat Valenciana (PROMETEO II 2015-002) and University of Valencia (UV-INV-AE 15-332846). We also acknowledge Mass Spectrometry, Atomic Absorption and NMR service from the Central Services for Experimental Research (SCSIE) of University of Valencia and NANBIOSIS platform.

Keywords: diquat • [1,2,3]triazolo[1,5-*a*]pyridine• [1,2,3]triazolo[1,5-*a*]quinoline • DNA interaction

References

1) K. Kunert, A.D. Dodge in *Target Sides of Herbicidal Action*, Eds: R.C. Kirkwood, CRC press, Boca Raton, Florida (USA), **1989**, pp. 45.

2) R. L. Jones, R.C. Brian, R.F. Homer, J.A. Stubbs, *Nature*, **1958**, *181*, 446.

3) T.C. Stancliffe, A. Pirie, *FEBS Lett*, **1971**, *17*, 297.

4) J.Y. Hong, M. Lebofsky, A. Farhood, H. Jaeschke, *Am. J. Physiol. Gastrointest. Liver Physiol.*, **2009**, *296*, 572.

5) G.M. Jones, J.A. Vale, *Clin. Toxicol.*, **2000**, *38*, 123.

6) B. Coe, R. Curati, C. Fitzgerald, *Synthesis*, **2006**, *1*, 146.

7) B.L. Allwood, F.H. Kohnke, A.M.Z. Slawin, J.F. Stoddart, D.J. Williams, *J. Chem. Soc.*, **1985**, 311.

8) A. Santoro, R.M. Lord, J.J. Loughrey, P.C. McGowan, M.A. Halcrow, A.F. Henwood, C. Thomson, E. Zysman-Colman, *Chem. Eur. J.*, **2015**, *21*, 7035.

9) a) M. Krompieca, I. Grudzkaa, M. Filapeka, Ł. Skorkaa, S. Krompieca, M. Łapkowskib, M. Kaniad, W. Danikiewiczd, *Electrochim. Acta*, **2011**, *56*, 8108-8114. b) Y. Mori, K. Isozaki K. Maeda, *J. Chem. Soc., Perkin Trans. 2*, **1997**, 1969.

10) Y. Xiao, L. Chu, Y. Sanakis, P. Liu, *J. Am. Chem. Soc.*, **2009**, *131*, 9931.

11) C. Pasquini, V. Desvergnes-Breuil, J. Jodry, A.D. Cort, J. Lacour, *Tetrahedron Lett.*,**2002**, *43*, 423.

12) a) J. Vachon, G. Bernardinelli, J. Lacour, *Chem. Eur. J.*, **2010**, *16*, 2797. b) J. E. Derry, T.A. Hamor, *Nature*, **1969**, *221*, 464. c) C. Campa, J. Camps, J. Font, P. De March, *J. Org. Chem.*, **1987**, *52*, 521. d) R. P. Thummel, F. Lefoulon, R. Mahadevan, *J. Org. Chem.*, **1985**, *50*, 3824.

13) Q. Zhang, C. Wang, W. Liu, X. Zhang, S. Zhuang, *Environ. Chem. Lett.*, **2012**, *10*, 35.

14) G.J. Ryan, R.B.P. Elmes, S.J. Quinn, T. Gunnlaugsson, *Supramol. Chem.*, **2012**, *24(3)*, 175.

15) B. Abarca, R. Ballesteros-Garrido in *Topics in Heterocyclic Chemistry. Chemistry of 1,2,3-triazoles*. Springer, Heildelberg, **2015**.

16) a) P.L. Battaglia, M. Carcelli, F. Ferraro, L. Mavilla, C. Pilizzi, G. J. Pilizzi, *Chem. Soc. Dalton Trans.*, **1994**, 2651. b) B. Abarca, R. Ballesteros, M. Elmasnaouy, *Tetrahedron*, **1998**, *54*, 15287.

17) R. Ballesteros-Garrido, F. Blanco, R. Ballesteros, F. R. Leroux, B. Abarca, F. Colobert, I. Alkorta, J. Elguero, *Eur. J. Org. Chem.*, **2009**, *33*, 5765.

18) M. Hosseini, F. Khaki, M. Dadmehr, M.R. Ganjali, *J. Fluoresc.*, **2016**, *26*, 1123.

19) M. Barfield, P. Fagerness, *J. Am. Chem. Soc.*, **1997**, *119*, 8699.

20) J. Jaroszewska-Manaj, D. Maciejewska, I. Wawer, *Magn. Reson. Chem.*, **2000**, *38*, 482.

21) D.J. Giesen, N. Zumbulyadis, *Phys. Chem. Chem. Phys.*, **2002**, *4*, 5498.

22) S.N. Azizi, C. Esmaili, *Word Appl. Sci. J.*, **2009**, *7*, 559.

23) R. Ballesteros-Garrido, E. Delgado-Pinar, B-. Abarca, R. Ballesteros, F.R. Leroux, F. Colobert, R.J. Zaragozá, E. García-España, *Tetrahedron*, **2012**, *68*, 3701.

24) C.M. Elliot, R.A. Freitag, D. Blaney, *J. Am. Chem. Soc.*, **1985**, *107*, 4647.

25) Y.C. Tsao, Y.C. Lai, H.C. Liu, R.H. Liu, D.L. Lin, *J. Analytical Toxicology*, **2016**, 1.

26) R. Adam, P. Bilbao-Ramos, B. Abarca, R. Ballesteros, M.E. González-Rosende, M.A. Dea-Ayuela, F. Estevan, G. Alzuet-Piña, *Org. Biomol. Chem.*, **2015**, *13*, 4903.

27) J.L. Mergny, L. Lacroix, *Oligonucleotides*, **2003**, *13*, 515.

28) a) C.V. Kumar, E.H. Asuncion, *J. Am. Chem. Soc.*, **1993**, *115*, 8547. b) M. Cusumano, M.L. Di Pietro, A. Giannetto, P.A. Vainiglia, *J. Inorg. Biochem.*, **2005**, *99*, 560. c) M. Inclań, M.T. Albelda, J.C. Frías, S. Blasco, B. Verdejo, C. Serena, C. Salat-Canela, M. L. Díaz, A. García-España, E. García-España, *J. Am. Chem. Soc.*, **2012**, *134*, 9644.

29) M.J. Frisch, *et al*., Gaussian 09, Revision A.02, Gaussian, Inc., Wallingford, CT, **2009**.

30) a) R.G. Parr, W. Yang, *Density Functional Theory of Atoms and Molecules*; Oxford University Press: New York, **1989**. b) T. Ziegler, *Chem. Rev.*, **1991**, *91*, 651.

31) a) A.D. Becke, *J. Chem. Phys.*, **1993**, *98*, 5648. b) C. Lee, W. Yang, R.G. Parr, *Phys. Rev. B*, **1988**, *37*, 785.

32) W.J. Hehre, L. Radom, P.V.R. Schleyer, J.A. Pople, *Ab initio Molecular Orbital Theory*, Wiley: New York, **1986**.

33) K. Fukui, *J. Phys. Chem.*, **1970**, *74*, 4161.

34) a) C. González, H.B. Schlegel, *J. Phys. Chem.*, **1990**, *94*, 5523. b) C. González, H.B. Schlegel, *J. Chem. Phys.*, **1991**, *95*, 5853.

35) a) J. Tomasi, M. Persico, *Chem. Rev.*, **1994**, *94*, 2027. b) B.Y. Simkin, I. Sheikhet. *Quantum Chemical and Statistical Theory of Solutions-A Computational Approach*, Ellis Horwood: London, **1995**.

36) a) E. Cances, B. Mennunci, J. Tomasi, *J. Chem. Phys.*, **1997**, *107*, 3032. b) M. Cossi, V. Barone, R. Cammi, J. Tomasi, *Chem. Phys. Lett.*, **1996**, *255*, 32. c) V. Barone, M. Cossi, J. Tomasi, *J. Comp. Chem.*, **1998**, *19*, 404.

Supporting Information

Synthesis, optical properties and DNA interaction of novel Diquats based on Triazolopyridines and Triazoloquinolines

Pedro J. Llabres-Campaner,[a] Lluís Guijarro,[b] Claudia Giarratano,[a] Rafael Ballesteros-Garrido*,[a,b] Ramón J. Zaragozá,[c] M. José Aurell,[c] Enrique García-España,[b] Rafael Ballesteros[a] and Belén Abarca[a]

[a] P.J. Llabres-Campaner, C. Giarratano, Dr. R. Ballesteros-Garrido, Prof. R. Ballesteros and Prof. B. Abarca
Department of Organic Chemistry, Faculty of Pharmacy
University of Valencia
Av. Vicent Andrés Estellés, s/n. 46100, Burjassot (Valencia), Spain
E-mail: *rafael.ballesteros-garrido@uv.es*

[b] Dr. R. Ballesteros-Garrido, L. Guijarro and Dr. E. García-España
Instituto de Ciencia Molecular (ICMOL)
University of Valencia
C/ Catedrático José Beltrán, 2, 46980, Paterna (Valencia), Spain

[c] Prof. Ramón J. Zaragozá and Prof. M. José Aurell
Department of Organic Chemistry, Faculty of Chemistry
University of Valencia
Av. Vicent Andrés Estellés, s/n. 46100, Burjassot (Valencia), Spain

Supporting information for this article is given via a link at the end of the document.

Contents

S1. Materials and methods

Starting materials, if commercially available, were purchased and used as such. The solvents used were of spectroscopic or equivalent grade. When known compounds had to be prepared by literature procedures, pertinent references are given. Melting points or ranges (m.p.) given were determined on a Büchi B-545 heated stage. ^{1}H and (^{1}H decoupled) ^{13}C nuclear magnetic resonance (NMR) spectra were recorded at 300 and 75 MHz. Chemical shifts are reported in δ units, parts per million (ppm), and were measured relative to the signals for residual deuterated water or deuterated methanol. Coupling constants (J) are given in Hz. Coupling patterns are abbreviated as, for example, s (singlet), d (doublet), t (triplet), q (quartet), td (triplet of doublets), m (multiplet), app. s (apparent singlet) and br. (broad). COSY and DEPT/ed-HSQC experiments were performed for all compounds. IR spectra were recorded using FT-IR ATR. HRMS were recorded using TOF electro-spray ionization (ESI-positive). UV-Visible spectra were measured on an Agilent 8453 spectrometer equipped with a Peltier temperature controller system (±0.1 °C). The emission spectra were recorded with a PTI MO-5020 spectrofluorimeter in the 300–700 nm range. Elemental analyses were performed using CE Instruments CHNS1100 Elemental Analyzer. The ICP analyses were performed using an Inductively Coupled Plasma Spectrometer with an Agilent 7900 Mass Detector. ct-DNA was purchased from commercial sources as sodium salt and used without further purification. Stock solutions of ct-DNA were prepared by dissolving 1-2 mg of the sodium salt in 200 µL of phosphate buffer (pH=7.4), stock solution was maintained at 4 ºC overnight and stored at -10 ºC. The polynucleotide concentration was determined by absorption spectroscopy, for that, aliquots of 1 µl from the stock solution were added to a 1 ml cuvete, after each addition absorption spectra was recorded, and the concentration was calculated by using the given molar extinction coefficient at 260 nm (6600 M−1cm−1), ct-DNA stock solution concentration was given as an average of at least 5 measurements. All stock ligand solutions were prepared in phosphate buffer at 1 mM. Thermal melting experiments were performed at room temperature by using an Agilent Cary 100 UV-Visible system equipped with a temperature controller system. Electrochemical experiments were performed with BAS CV 50W and Metrohm PGSTAT 101 Autolab in a conventional three-compartment cell with glassy-carbon working electrode. Prior to each voltammetric run, the electrode was polished with an aqueous suspension of alumina on a soft surface, rinsed with water and dried. An Ag/AgCl (3 M NaCl) reference electrode and platinum wire auxiliary electrode completed the three-electrode configuration. The cyclic voltammograms were recorded at scan rates of 50 – 500 mV s-1.

S2. NMR analysis

S2.1. NMR spectra

^{1}H-NMR of protonated and deprotonated **PTP** and **PTQ**, and ^{1}H-NMR, ^{13}C-NMR, H-COSY and DEPT/ed-HSQC of **L1**-**L4** are shown.

3-(2-pyridil)-[1,2,3]triazolo[1,5-*a*]pyridine (PTP)

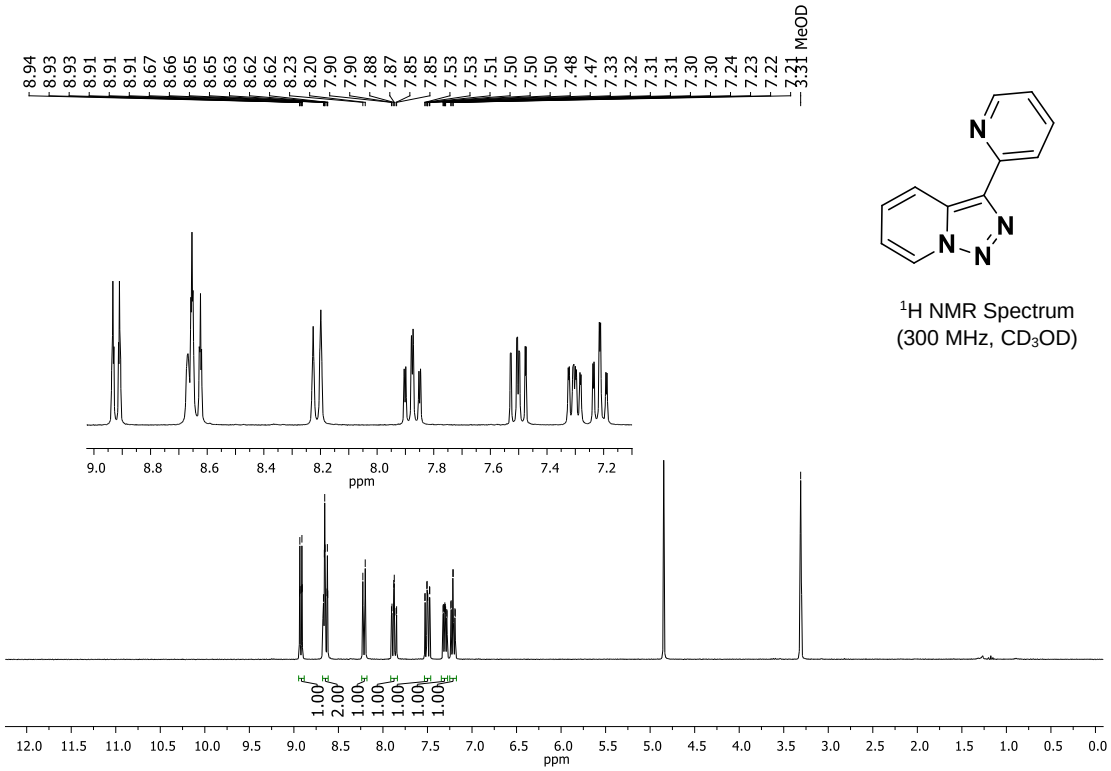

^{1}H NMR Spectrum
(300 MHz, CD_3OD)

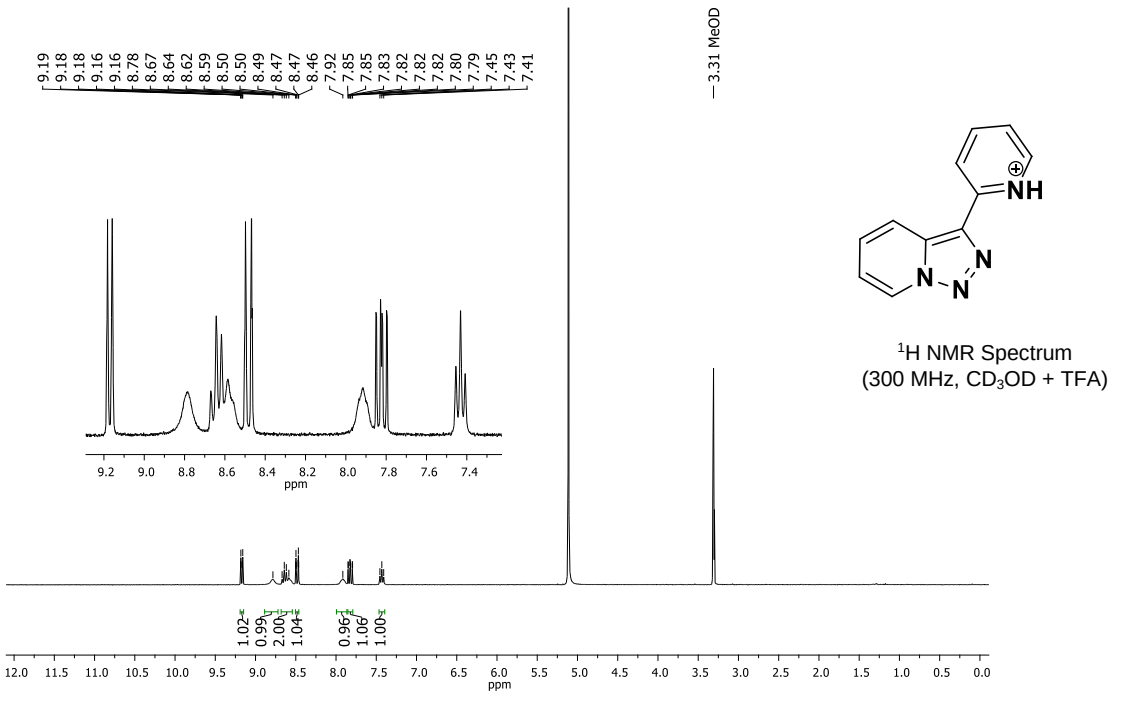

^{1}H NMR Spectrum
(300 MHz, CD_3OD + TFA)

3-(2-pyridil)-[1,2,3]triazolo[1,5-*a*]quinoline (PTQ)

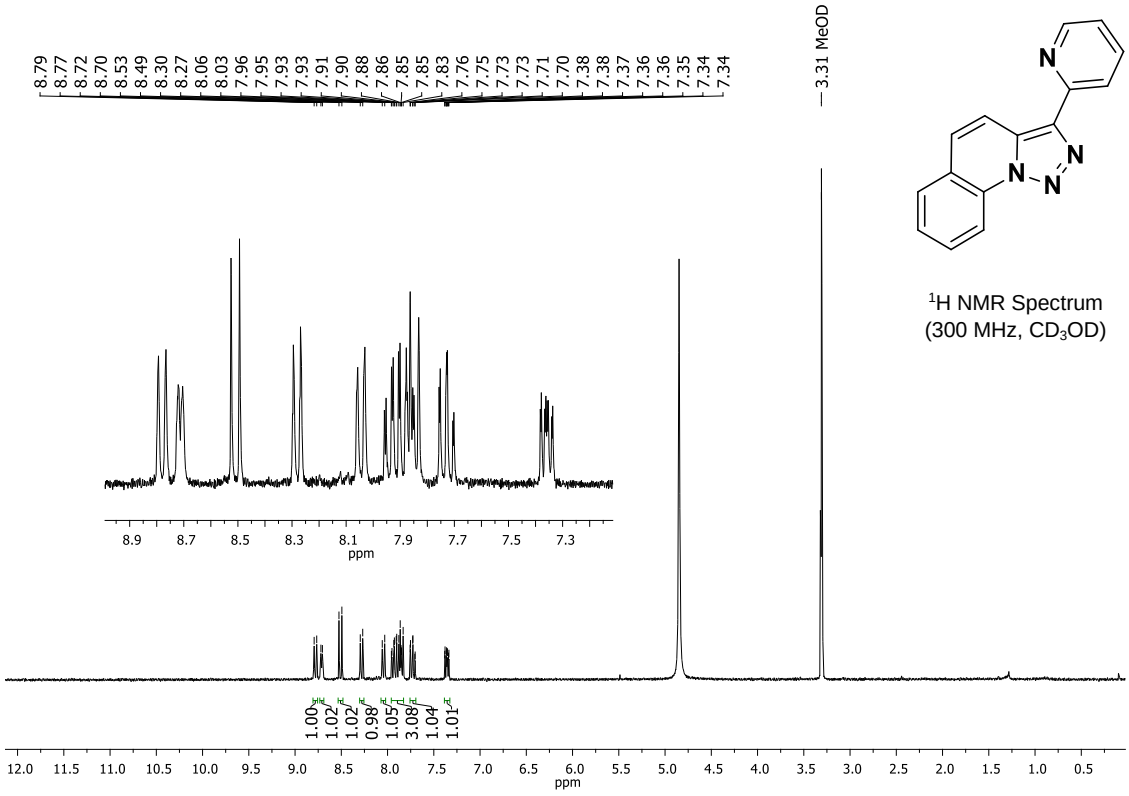

^{1}H NMR Spectrum
(300 MHz, CD_3OD)

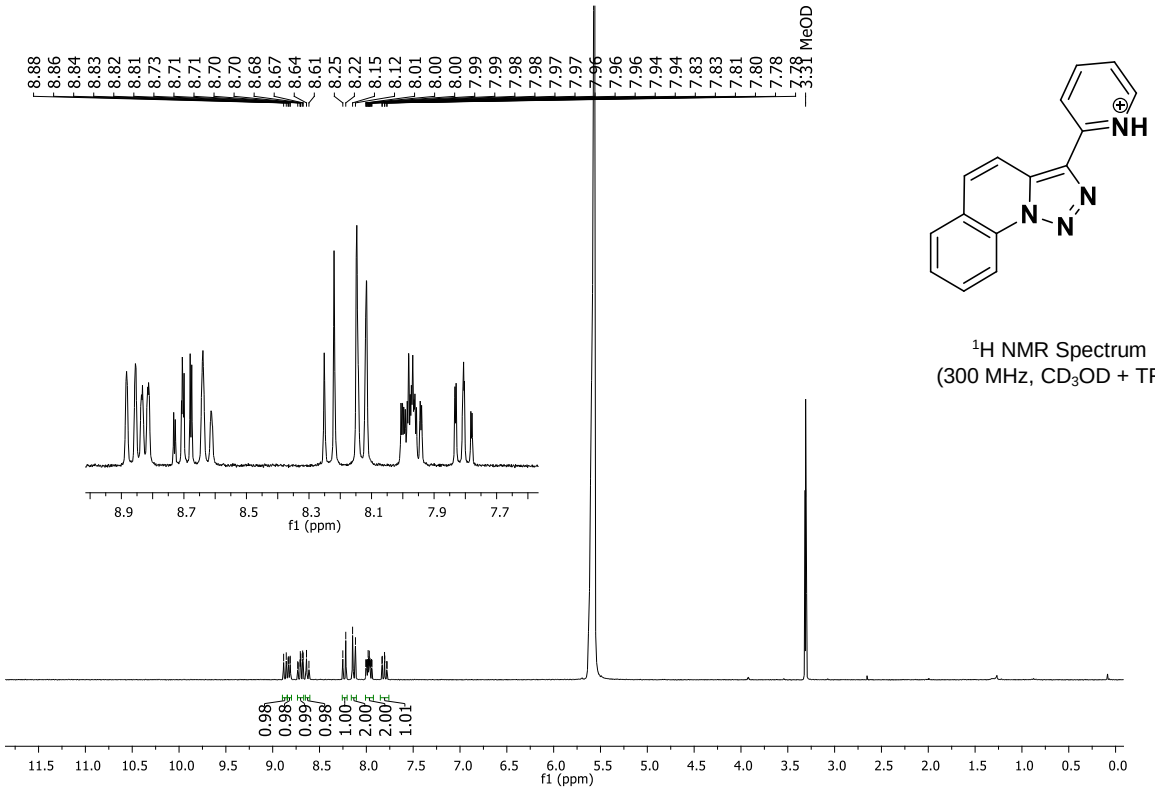

^{1}H NMR Spectrum
(300 MHz, CD_3OD + TFA)

6,7-dihydropyrido[1,2-*a*]pyrido[1`,2`:3,4][1,2,3]triazolo[5,1-*c*]pyrazine-5,8-diium bromide (L1)

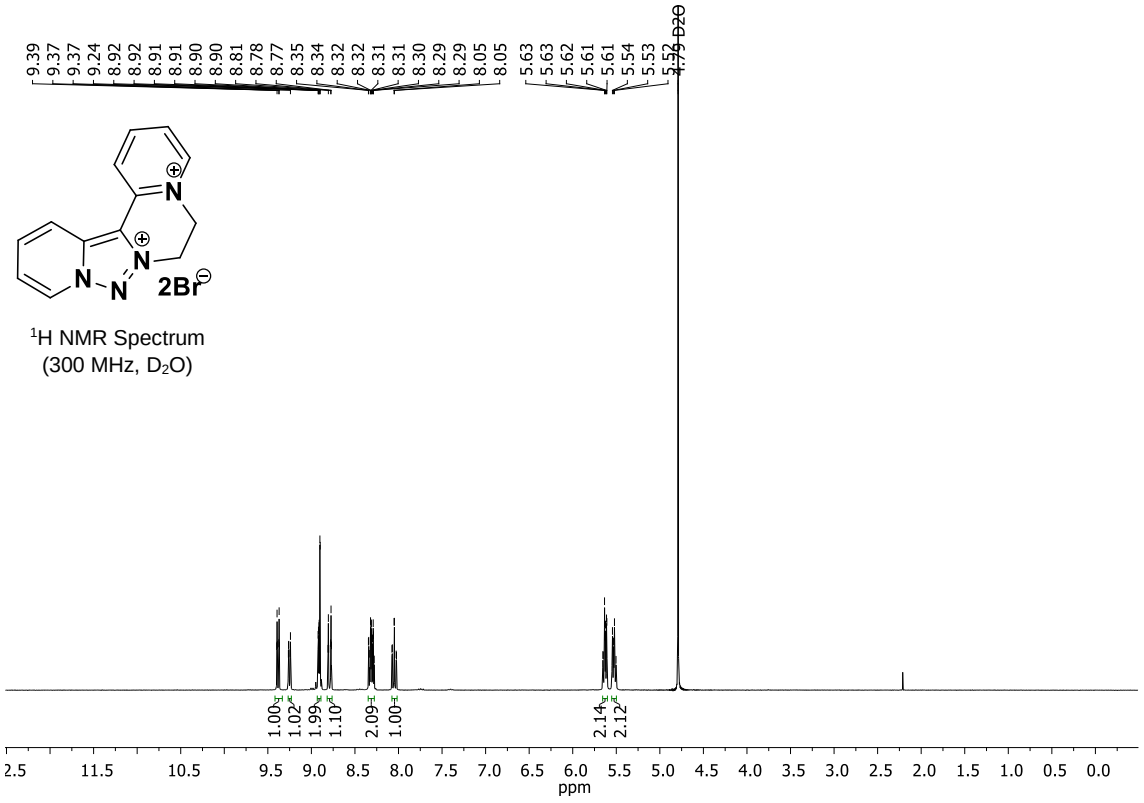

^{1}H NMR Spectrum
(300 MHz, D_2O)

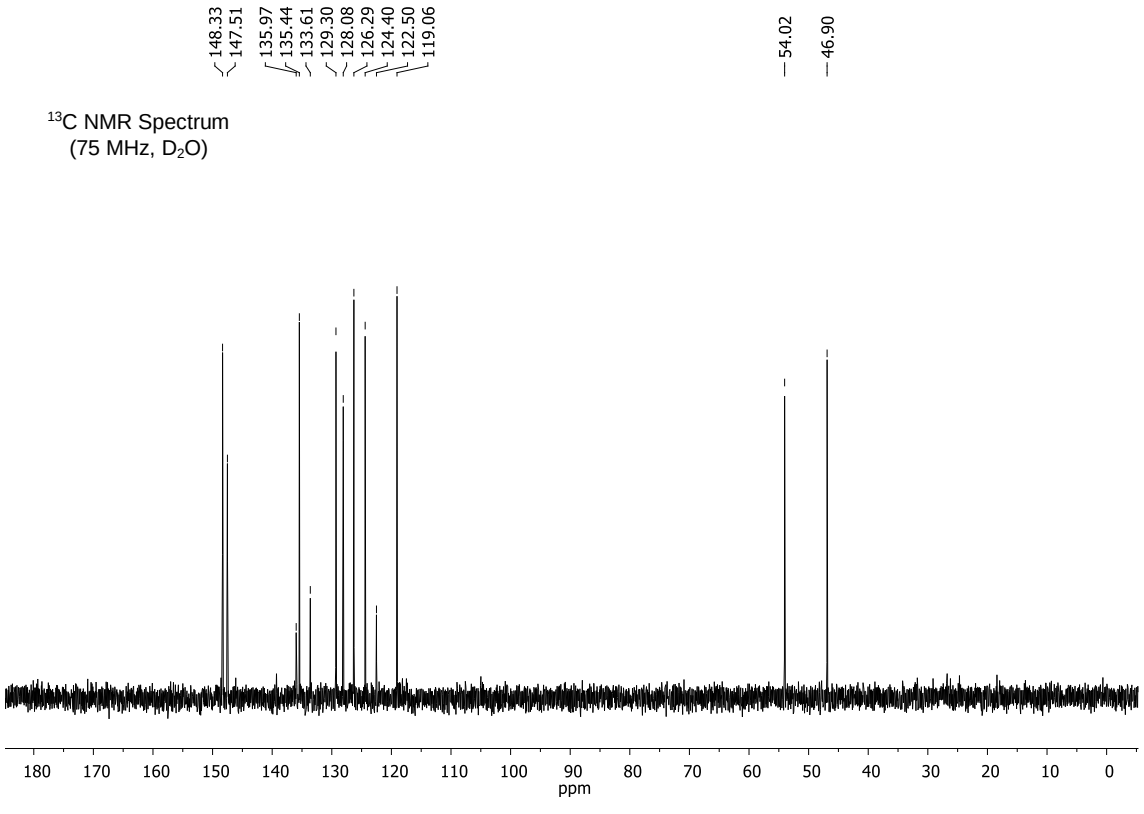

^{13}C NMR Spectrum
(75 MHz, D_2O)

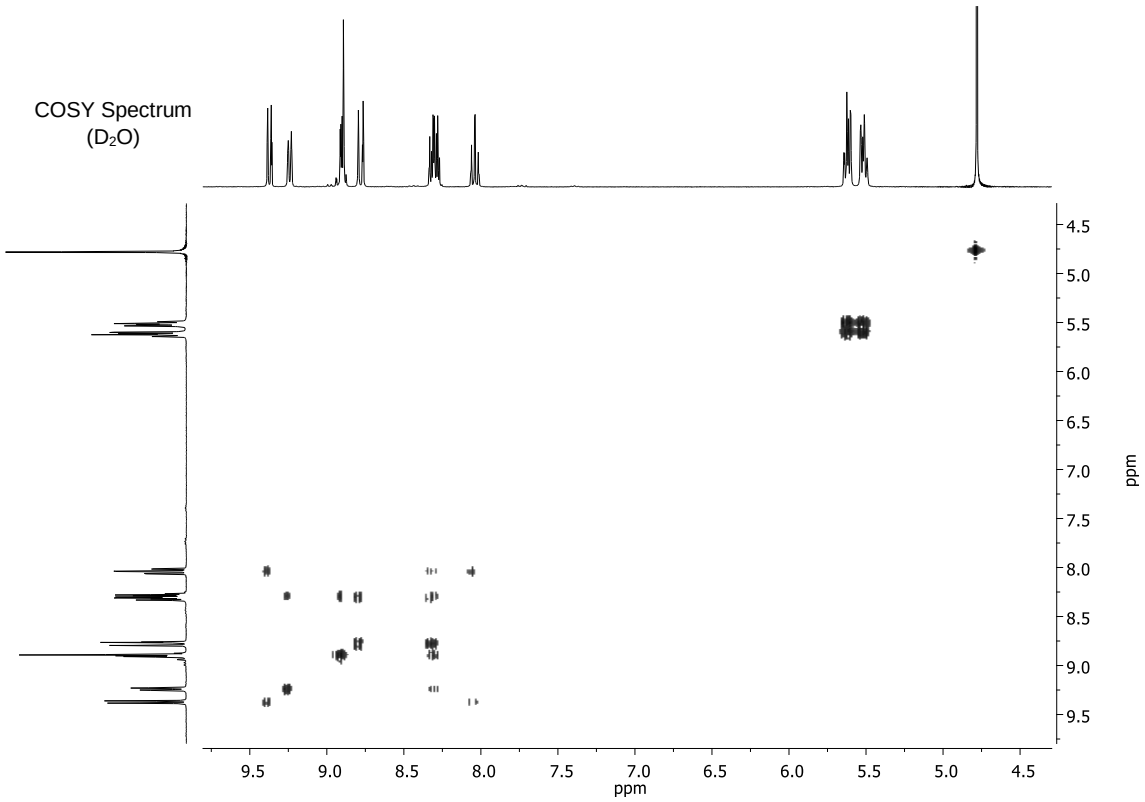
COSY Spectrum
(D2O)
4.5
5.0
5.5
6.0
6.5
7.0
7.5
8.0
8.5
9.0
9.5
ppm
9.5 9.0 8.5 8.0 7.5 7.0 6.5 6.0 5.5 5.0 4.5
ppm

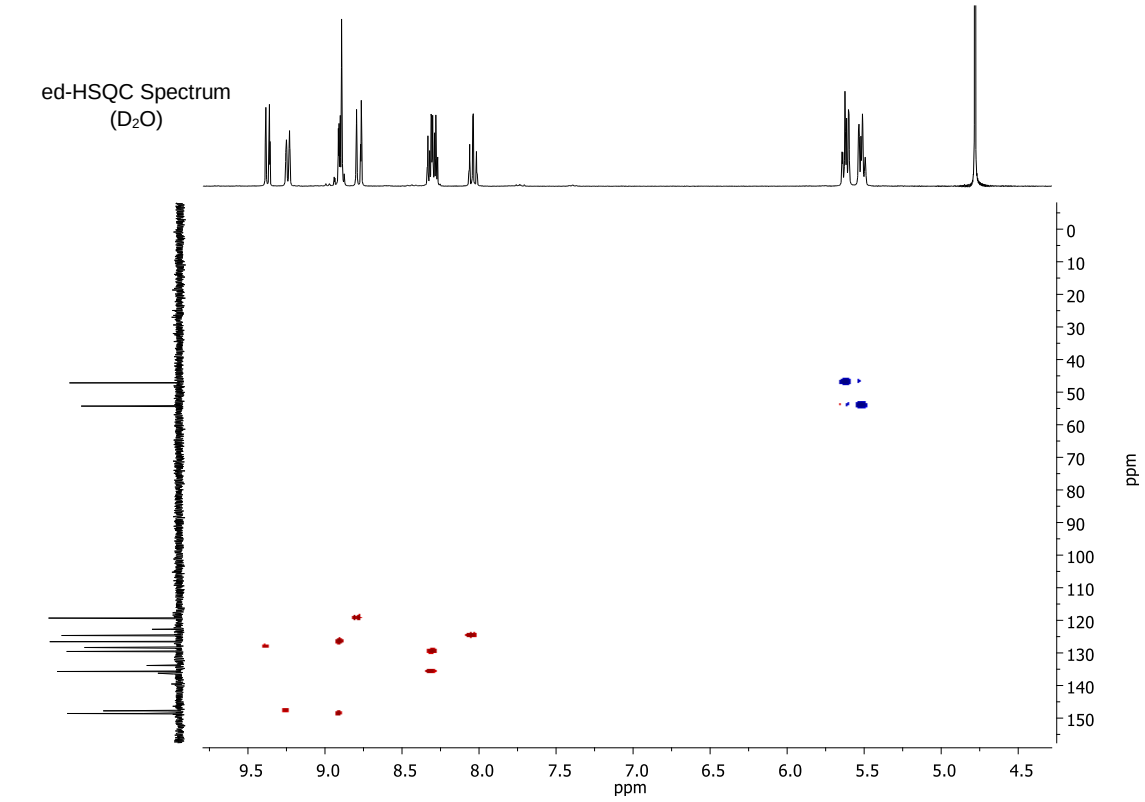
ed-HSQC Spectrum
(D2O)
0
10
20
30
40
50
60
70
80
90
100
110
120
130
140
150
ppm
9.5 9.0 8.5 8.0 7.5 7.0 6.5 6.0 5.5 5.0 4.5
ppm

7,8-dihydro-6H-pyrido[1,2-*a*]pyrido[1',2':3,4][1,2,3]triazolo[5,1-*c*][1,4]diazepine-5,9-diium bromide (L2)

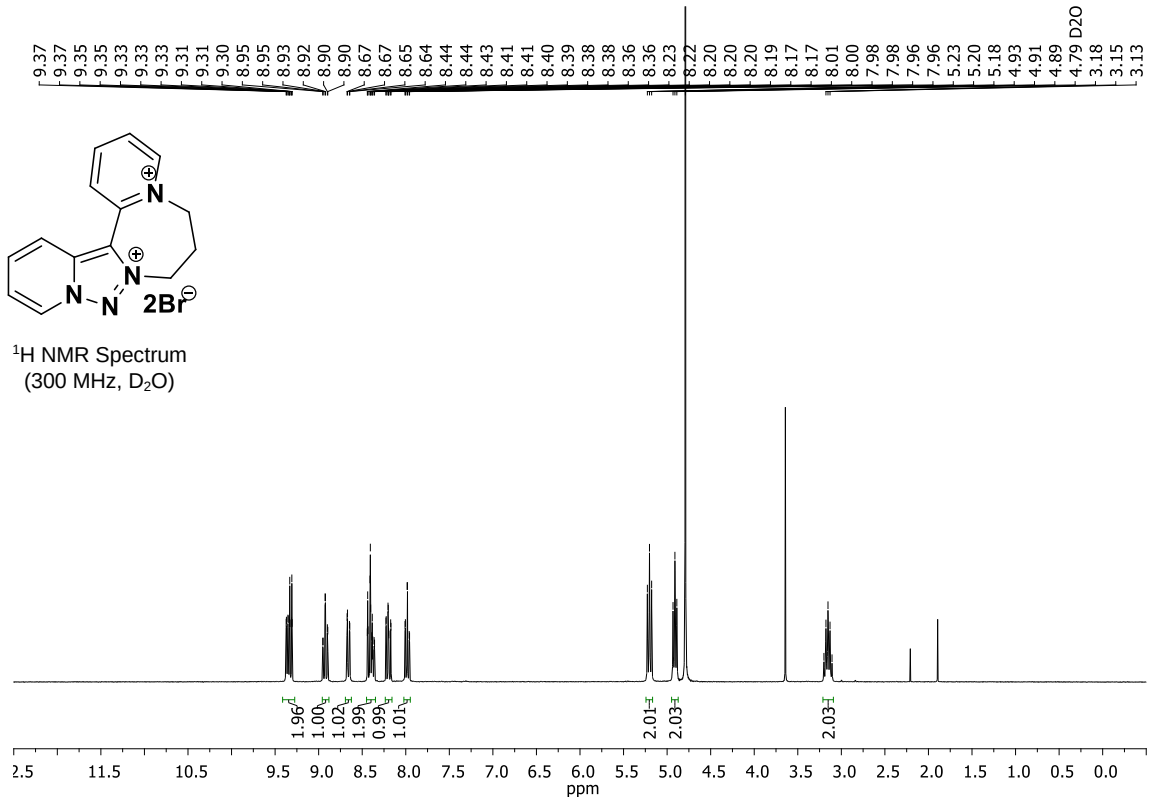

^{1}H NMR Spectrum
(300 MHz, D_2O)

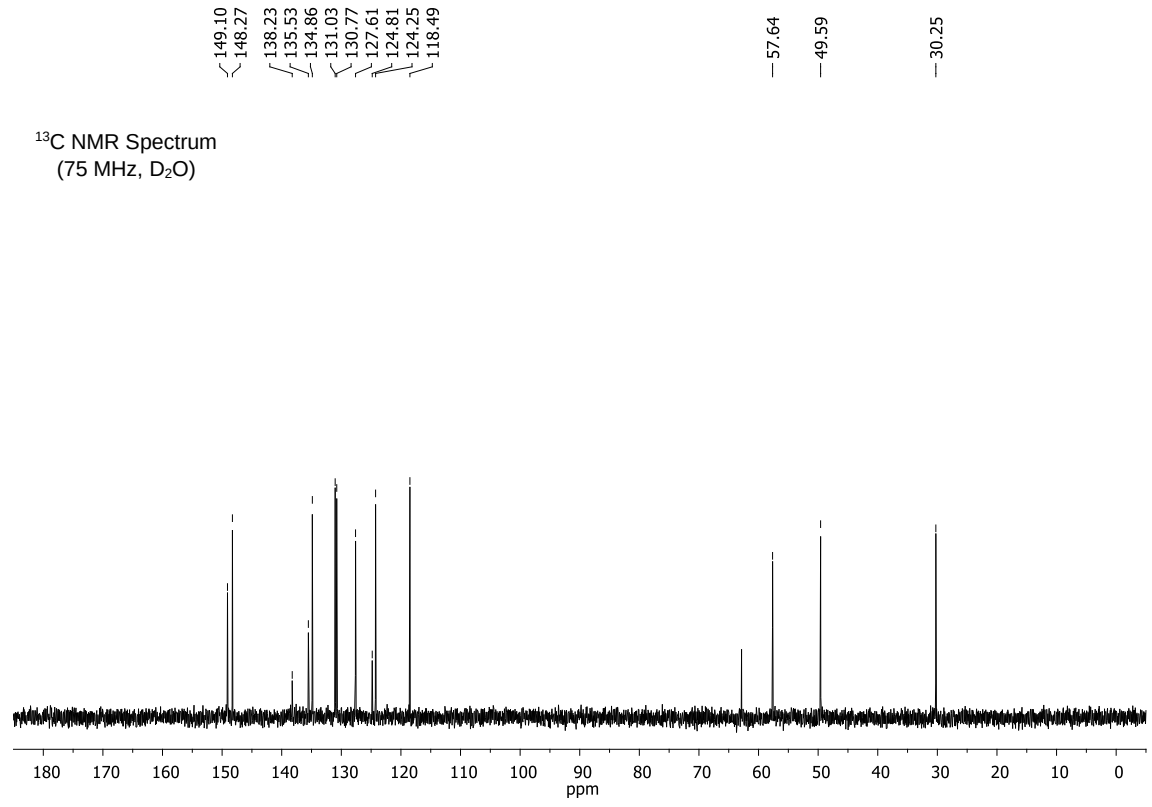

^{13}C NMR Spectrum
(75 MHz, D_2O)

COSY Spectrum
(D_2O)

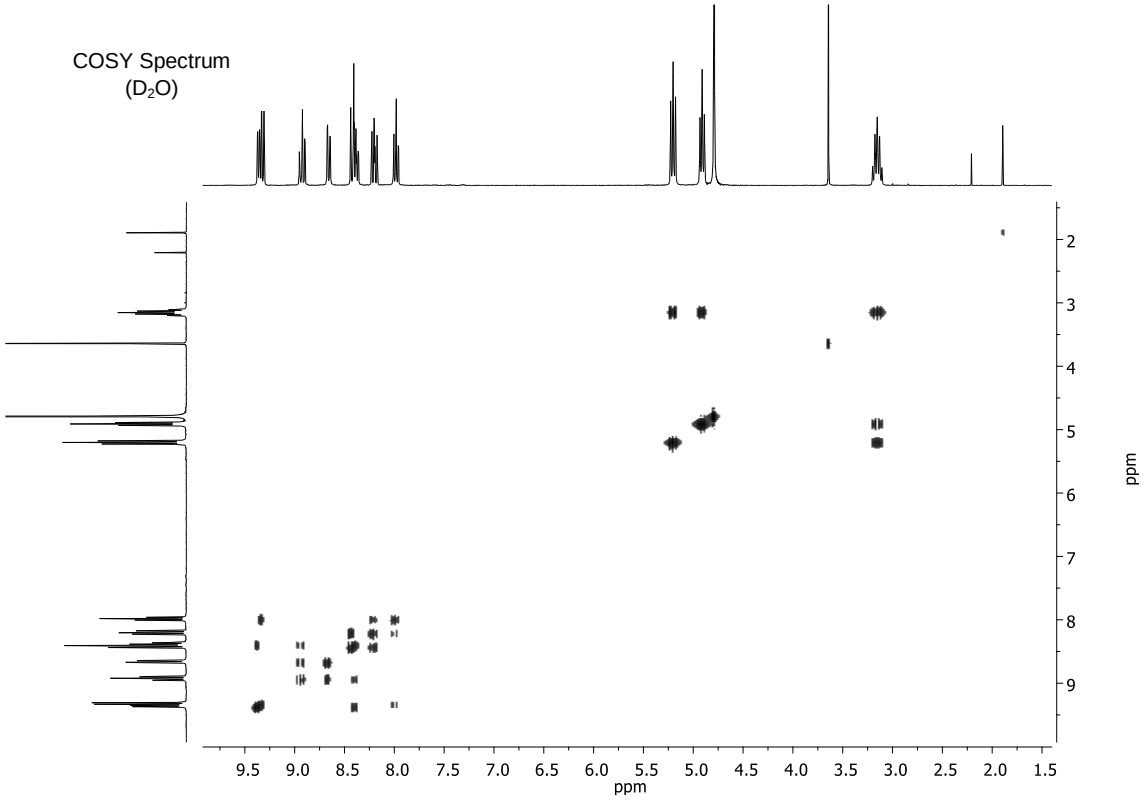

ed-HSQC Spectrum
(D_2O)

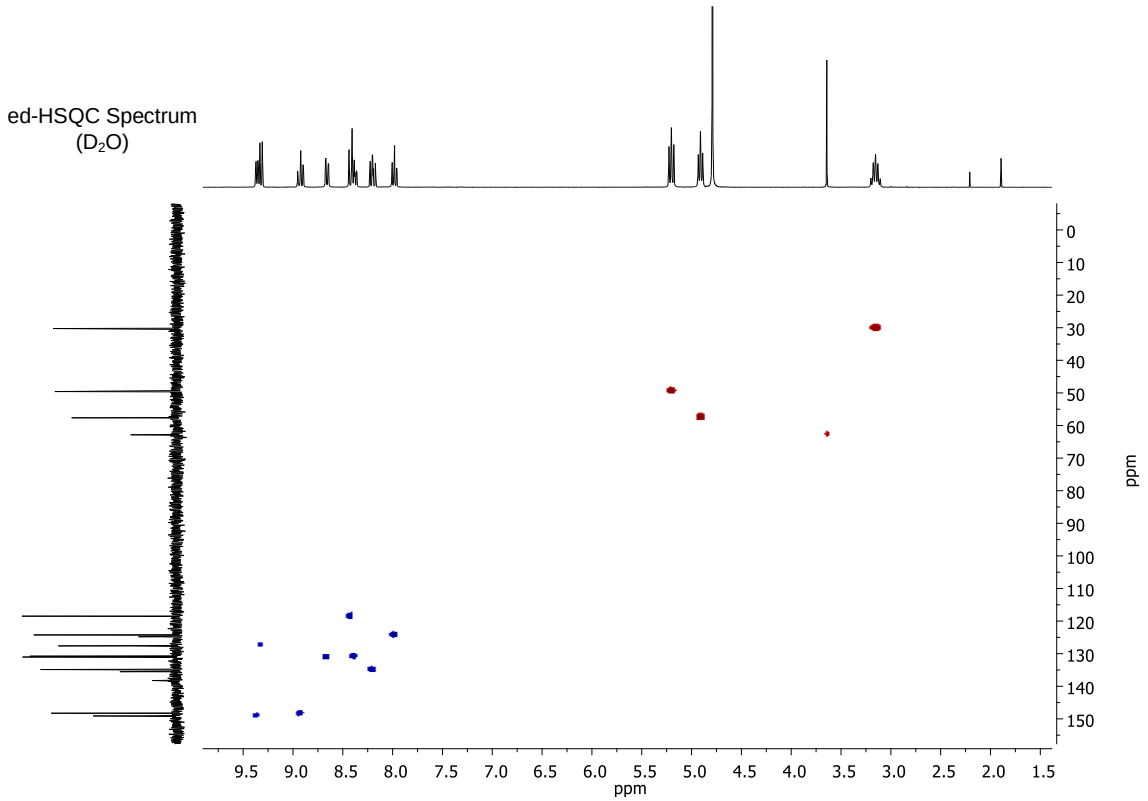

6,7-dihydropyrido[2'',1'':3',4']pyrazino[1',2':3,4][1,2,3]triazolo[1,5-*a*]quinoline-5,8-diium bromide (L3)

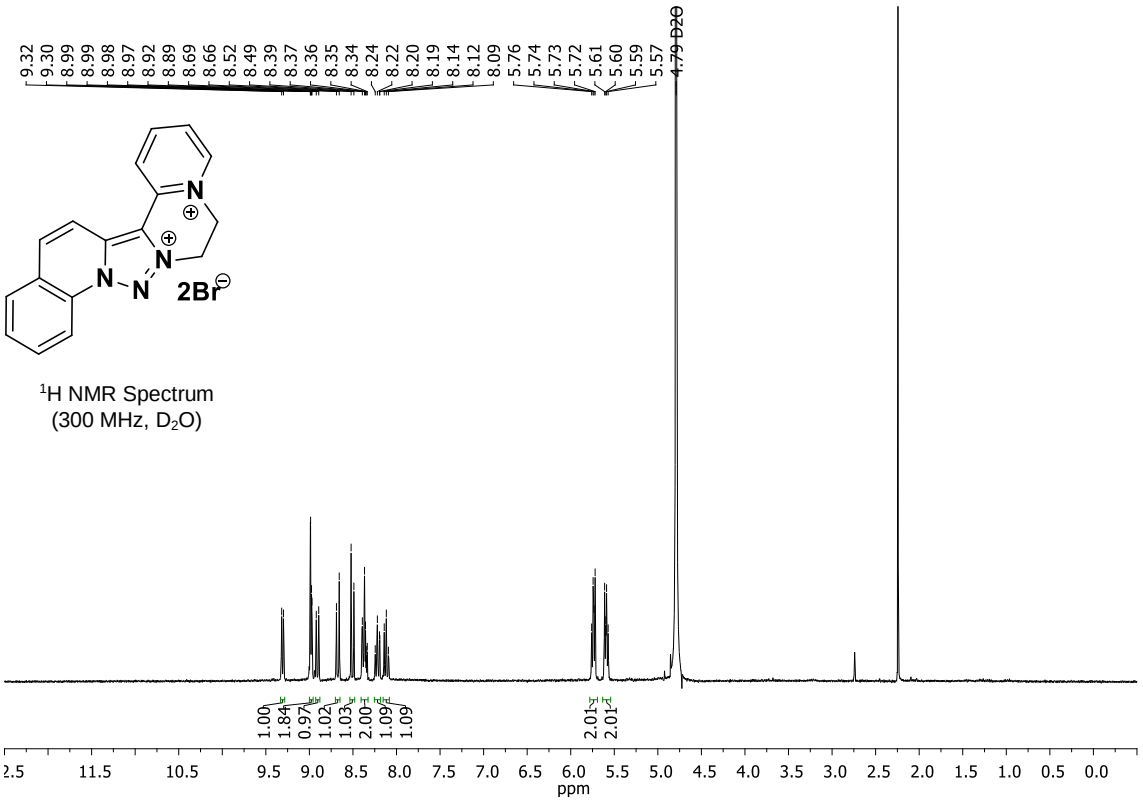

^{1}H NMR Spectrum
(300 MHz, D_2O)

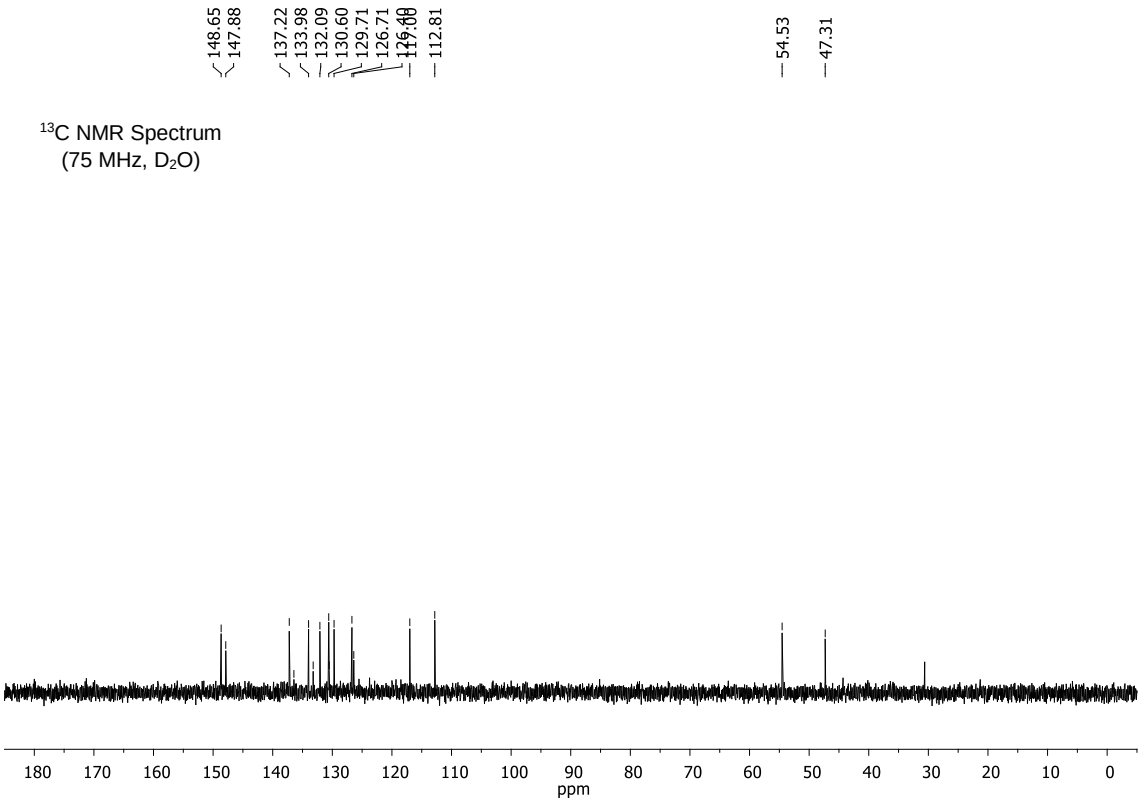

^{13}C NMR Spectrum
(75 MHz, D_2O)

DEPT Spectrum
(75 MHz, D_2O)

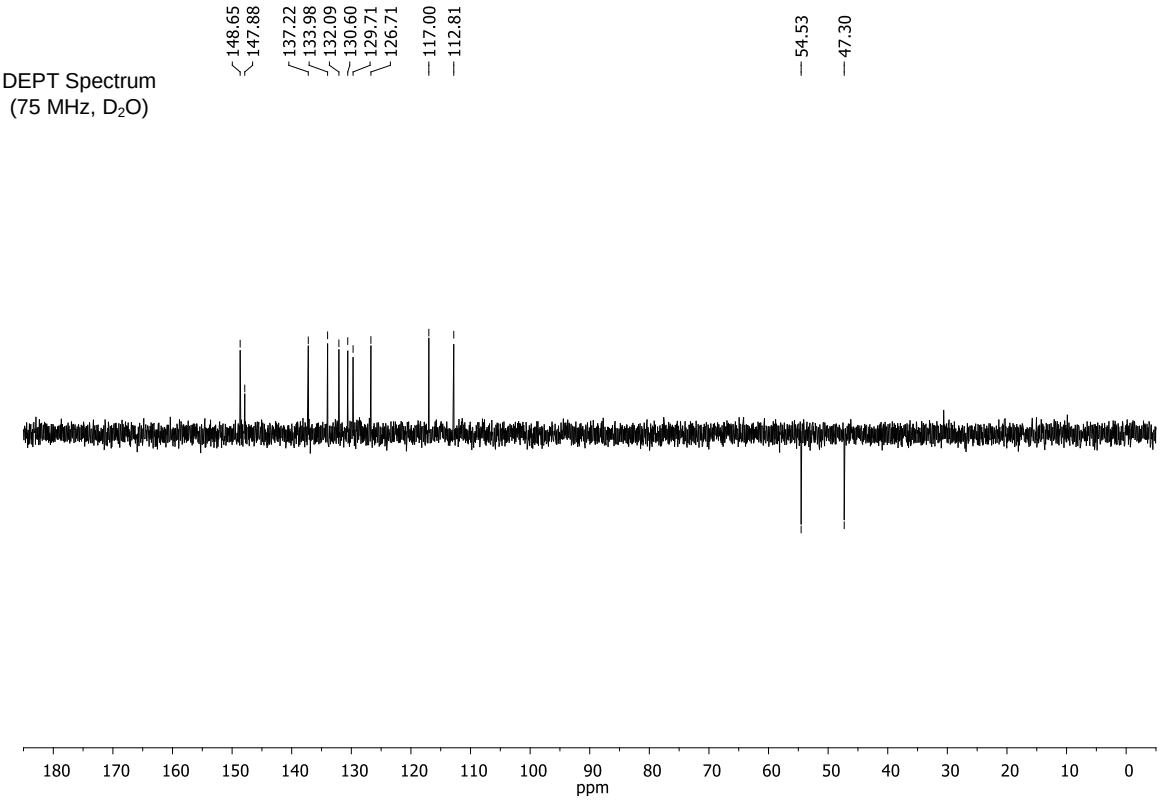

COSY Spectrum
(D_2O)

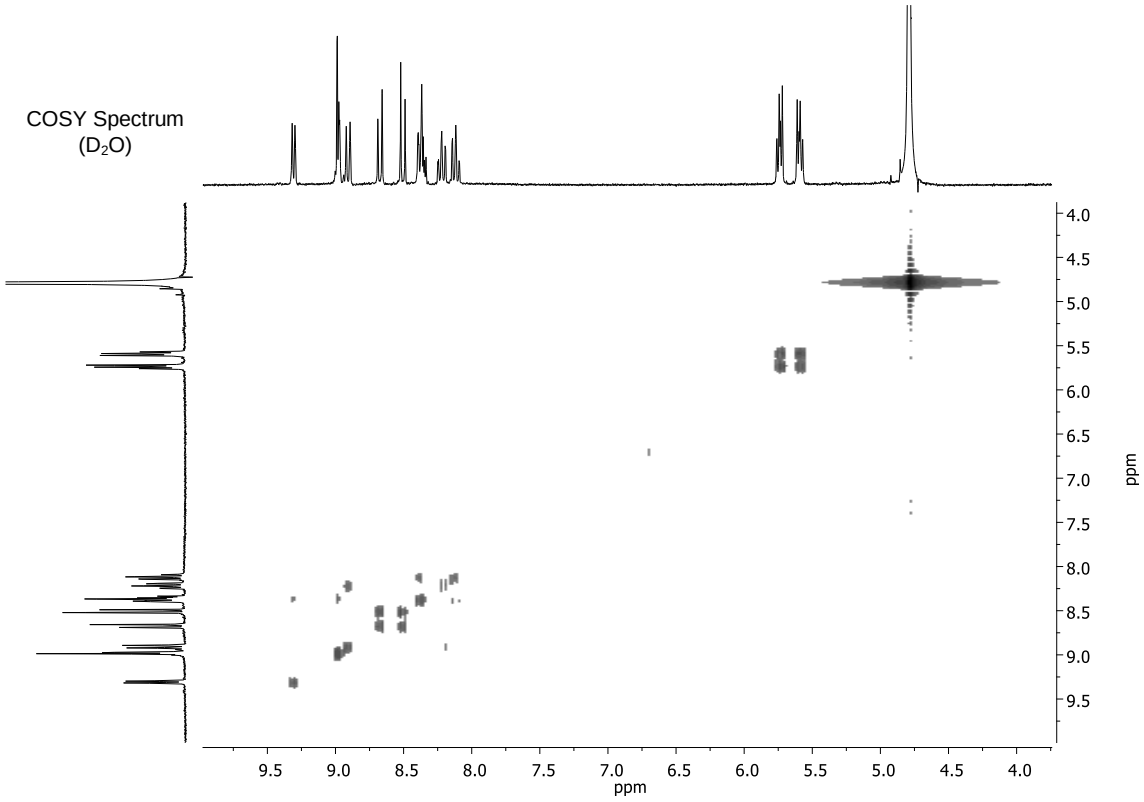

7,8-dihydro-6H-pyrido[2'',1'':3',4'][1,4]diazepino[1',2':3,4][1,2,3]triazolo[1,5-*a*]quinoline-5,9-diium bromide (L4)

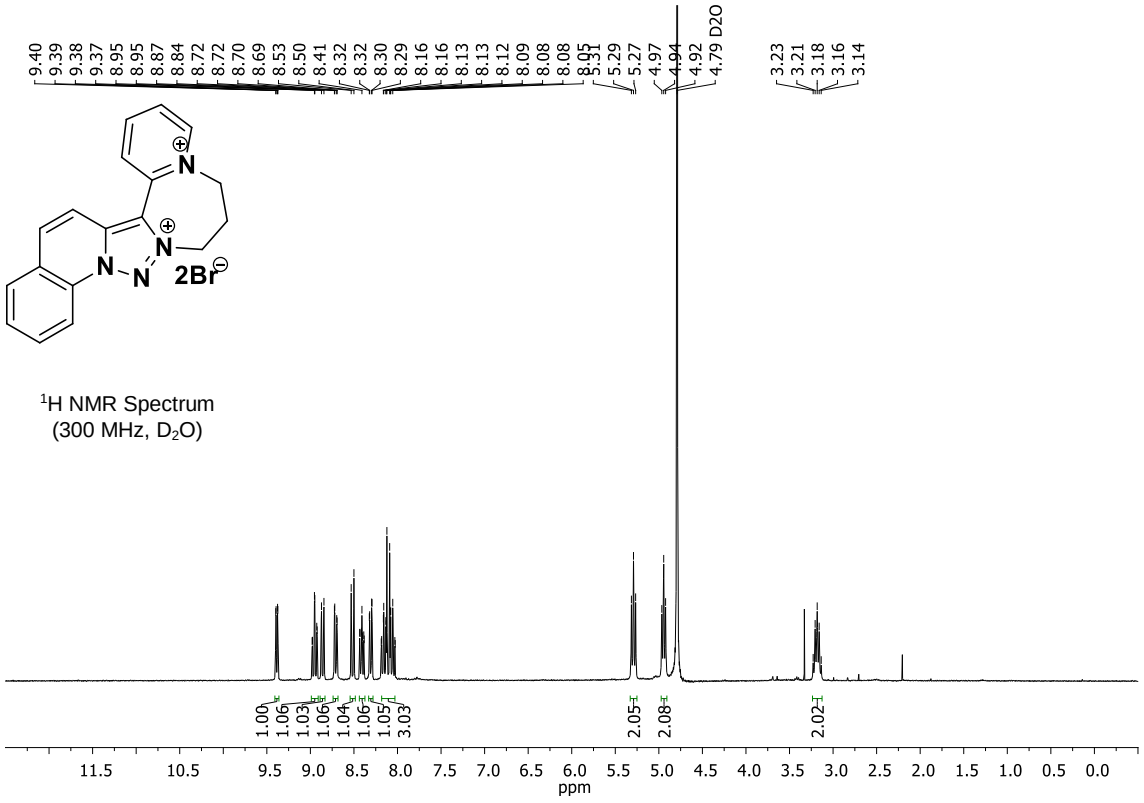

^{1}H NMR Spectrum
(300 MHz, D_2O)

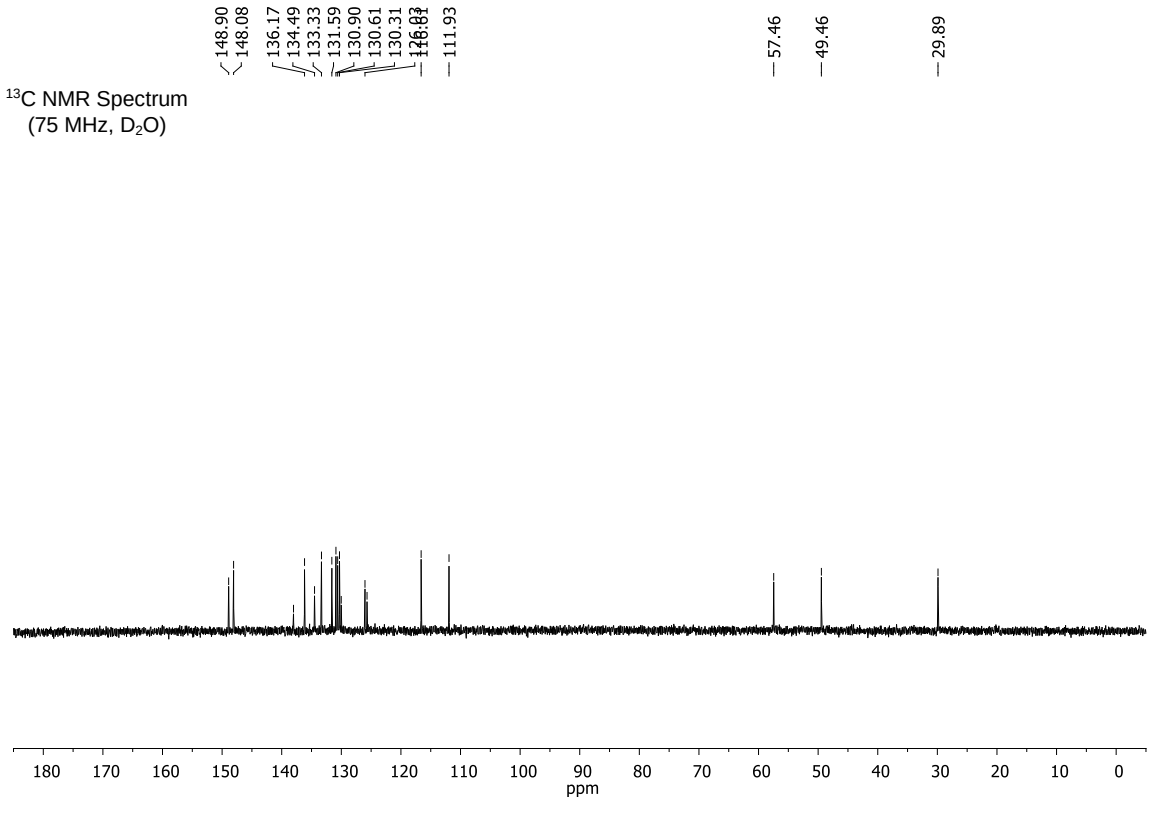

^{13}C NMR Spectrum
(75 MHz, D_2O)

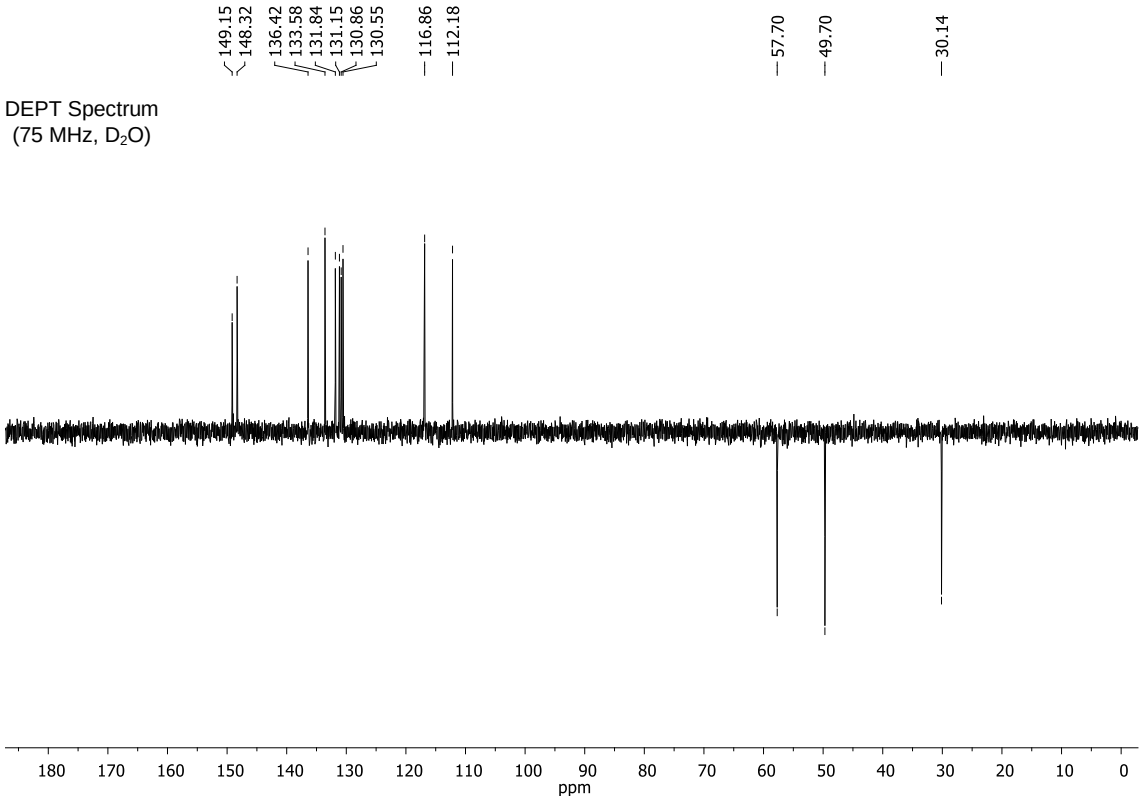
149.15
148.32
136.42
133.58
131.84
131.15
130.86
130.55
116.86
112.18
57.70
49.70
30.14
DEPT Spectrum
(75 MHz, D2O)
180 170 160 150 140 130 120 110 100 90 80 70 60 50 40 30 20 10 0
ppm

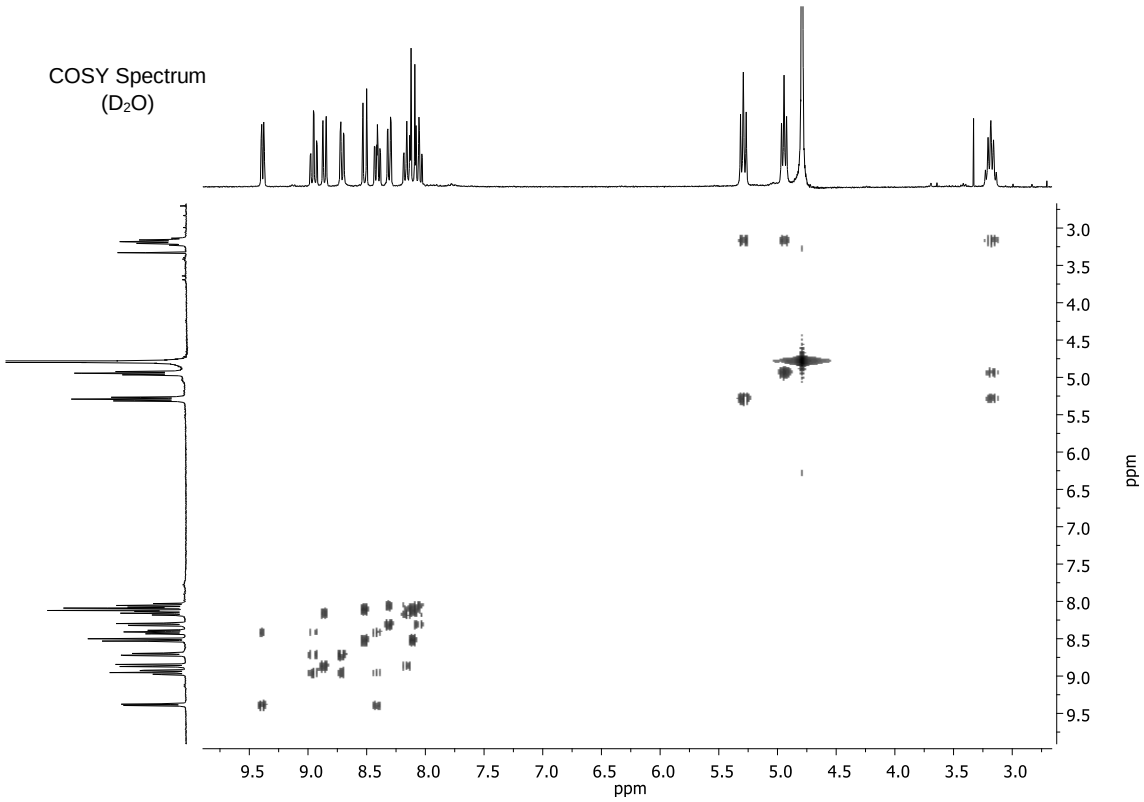
COSY Spectrum
(D2O)
3.0 3.5 4.0 4.5 5.0 5.5 6.0 6.5 7.0 7.5 8.0 8.5 9.0 9.5
ppm
9.5 9.0 8.5 8.0 7.5 7.0 6.5 6.0 5.5 5.0 4.5 4.0 3.5 3.0
ppm

S2.2. Signal assignation using NOE-Diff

Application of the Nuclear Overhauser Effect (NOE) to our molecules allowed us to determine which aliphatic signal corresponded to each CH_2 protons of the bridges. The main difference when NOE effect was applied to both signals was the excitation of the *H4* (pyridine ring) when signals at 5.53 ppm in **L1** and 4.91 ppm in **L2** were irradiated, being indicative that those signals are hydrogen *H6* in both cases.

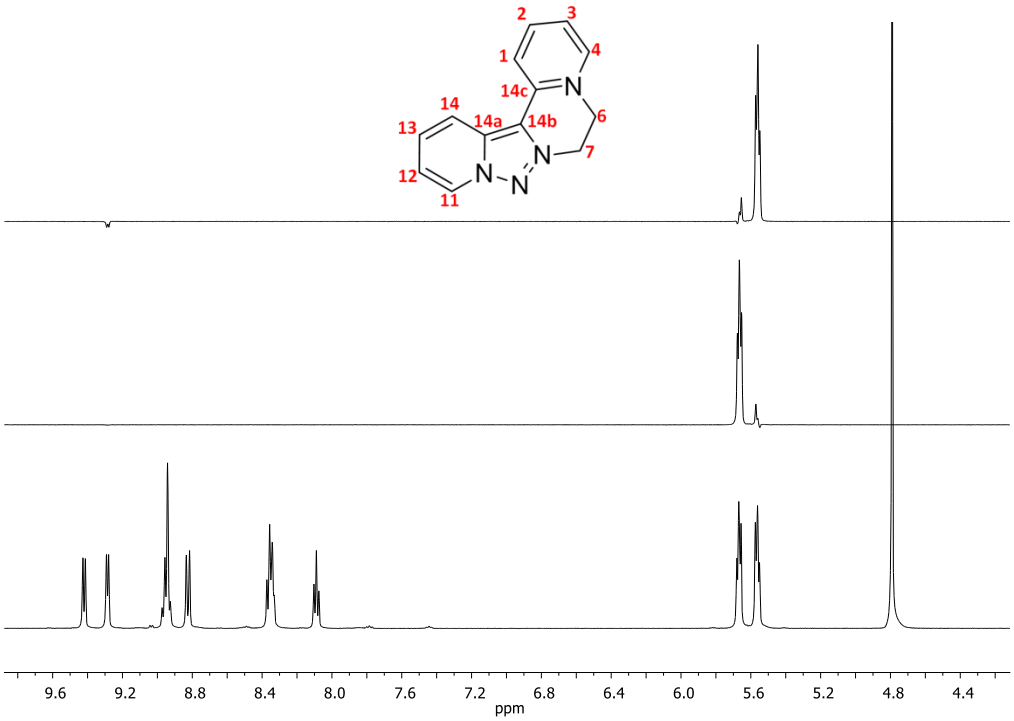

Figure S1. NOE-Diff spectrum of **L1** in D_2O.

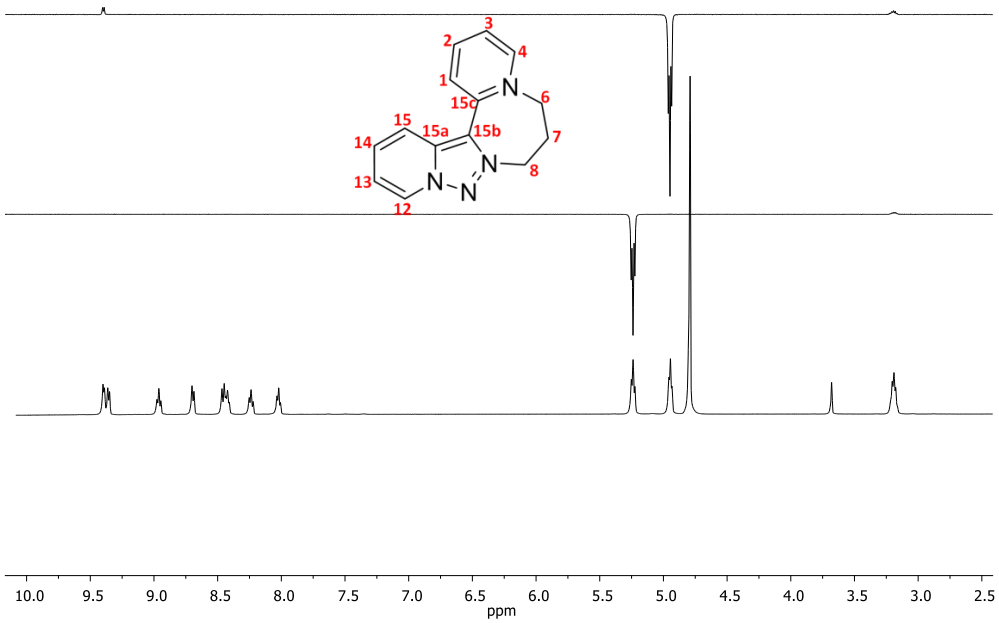

Figure S2. NOE-Diff spectrum of **L2** in D_2O.

S2.3. ^{1}H-NMR spectra with increasing temperature

^{1}H-NMR spectra of **L1** and **L2** were carried out at temperatures between 25ºC and 80ºC in order to identify relevant conformational changes. However, it was not possible to identify changes with significant evidences. Only changes in signals resolution in the aromatic region were detected, as long as displacements of all signals to low field. There was also no evidence of decomposition and/or partial deuteration of the acidic positions at high temperatures.

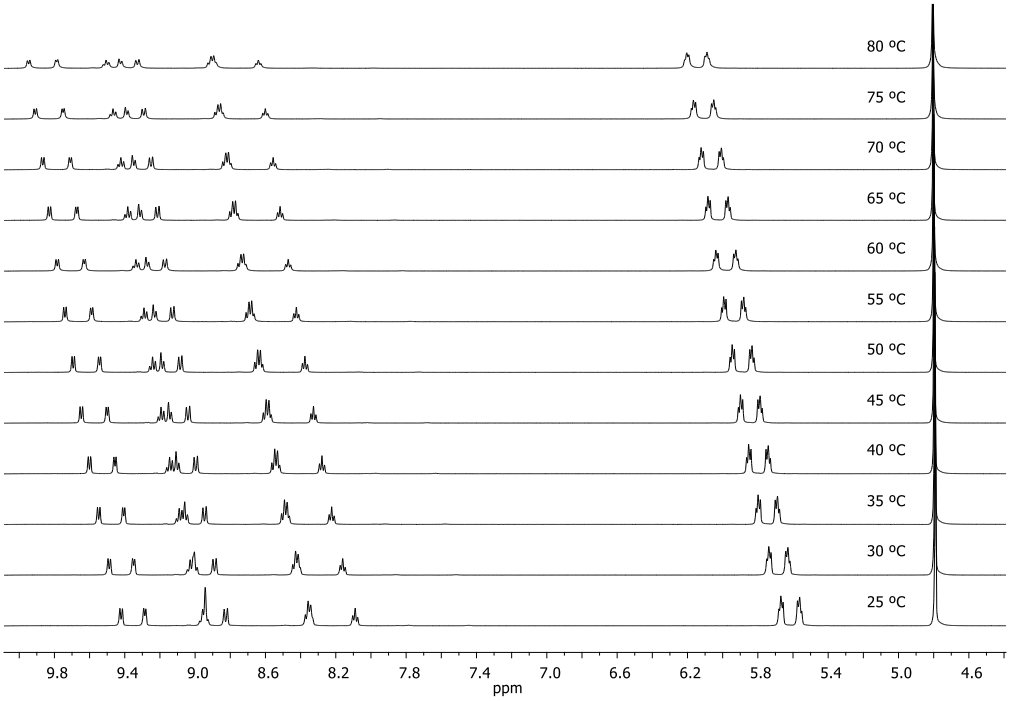

Figure S3. ^{1}H-NMR spectra of **L1** in D_2O with increasing values of temperature (25ºC-80ºC).

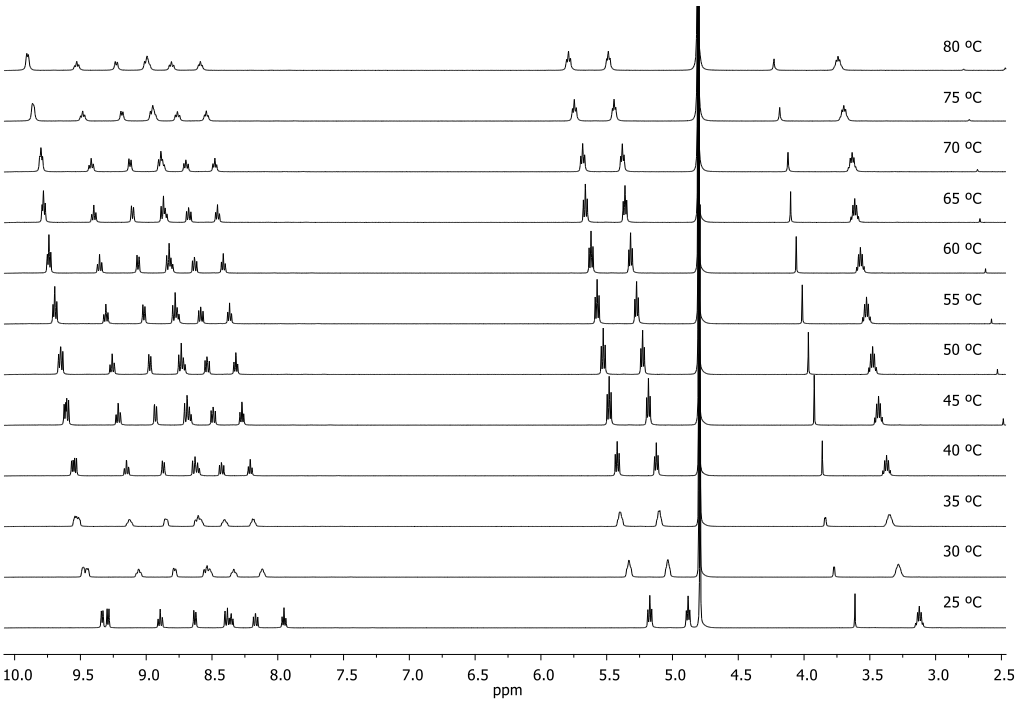

Figure S4. ^{1}H-NMR spectra of **L2** in D_2O with increasing values of temperature (25ºC-80ºC).

S3. UV-Visible titrations

Changes in the absorption spectrum of **L1**-**L4** upon addition of ct-DNA (1-10 eq) in are shown. As it can be seen, absorption of **L1** and **L2** remained unaltered between 300 nm and 400 nm (where ct-DNA does not absorb), while in the case of **L3** and **L4** a decrease of the absorbance at this range at the time that the UV-Visible profile changed.

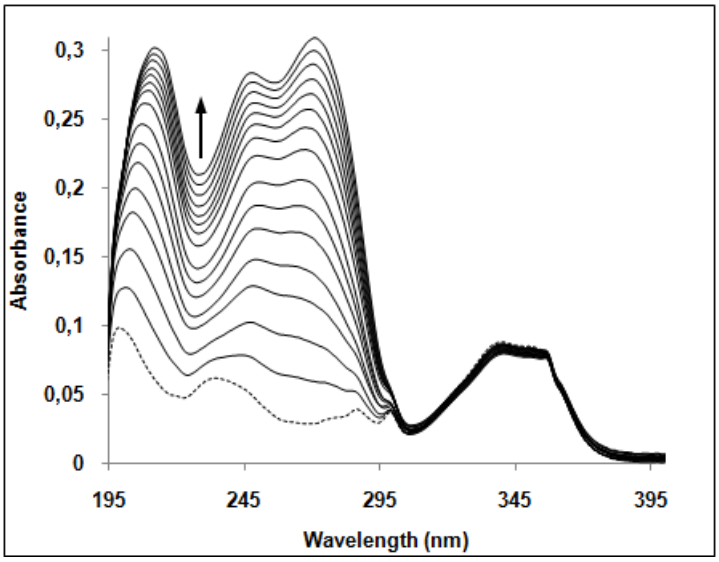

Figure S5. Changes in the absorption spectrum of **L1** 10 µM in 1 mM phosphate buffer, upon addition of ct-DNA (1-10 eq) in 1 mM phosphate buffer.

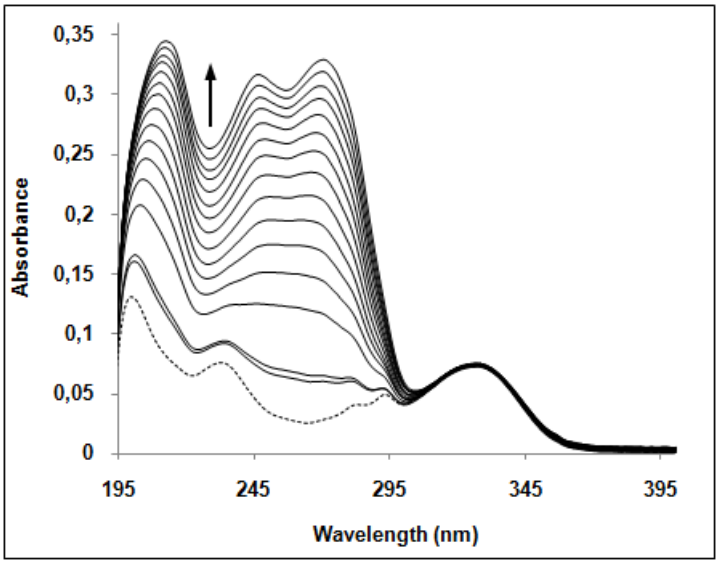

Figure S6. Changes in the absorption spectrum of **L2** 10 µM in 1 mM phosphate buffer, upon addition of ct-DNA (1-10 eq) in 1 mM phosphate buffer.

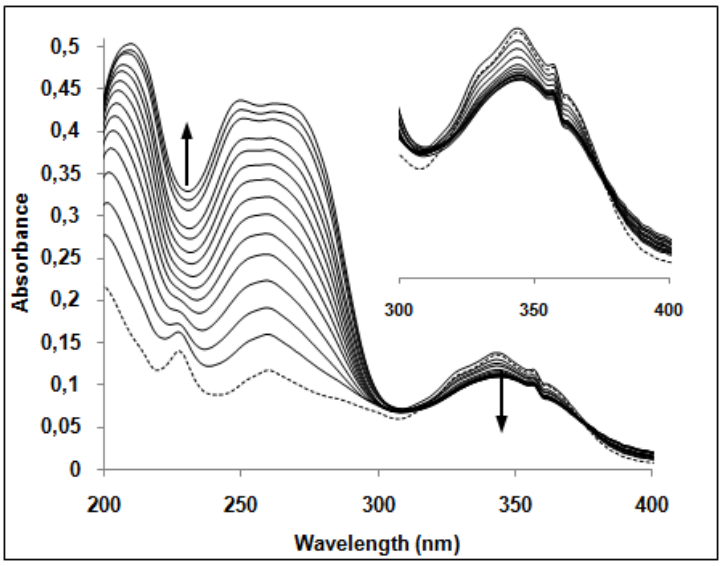

Figure S7. Changes in the absorption spectrum of **L3** 10 µM in 1 mM phosphate buffer, upon addition of ct-DNA (1-10 eq) in 1 mM phosphate buffer.

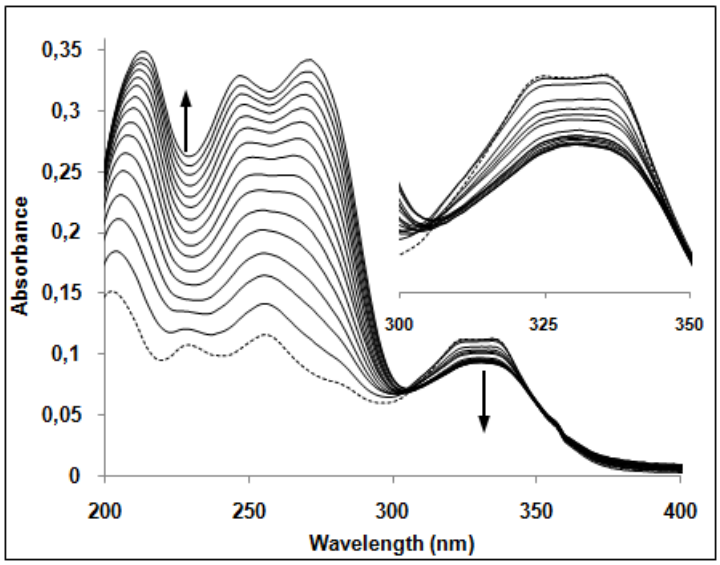

Figure S8. Changes in the absorption spectrum of **L4** 10 µM in 1 mM phosphate buffer, upon addition of ct-DNA (1-10 eq) in 1 mM phosphate buffer.

S4. Fluorescence titrations

Changes in the emission spectrum of **L1**-**L4** upon addition of ct-DNA (1-10 eq) in are shown. As it can be seen, while **L1** and **L2** suffered quenching of their emission without shifting of the wavelength, **L3** and **L4** suffered quenching and also hypsochromic shift.

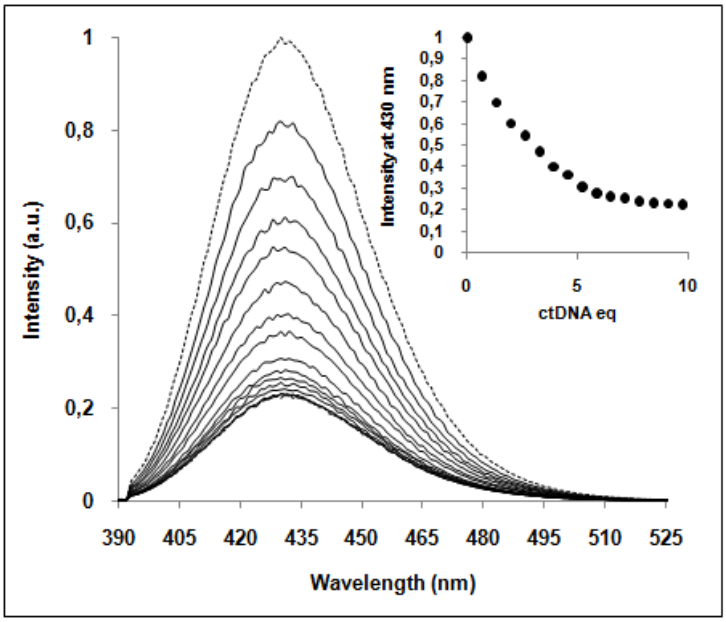

Figure S9. Changes in the emission spectrum of **L1** 10 µM in 1 mM phosphate buffer, upon addition of ct-DNA (1-10 eq) in 1 mM phosphate buffer.

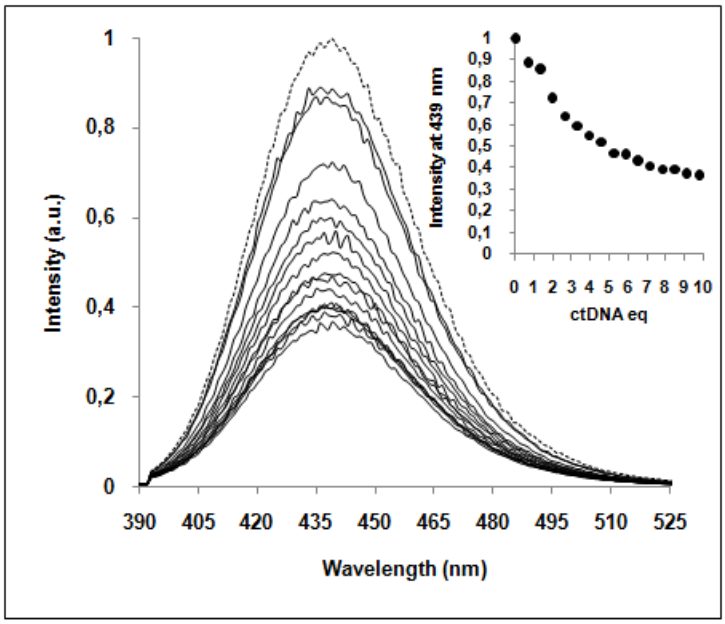

Figure S10. Changes in the emission spectrum of **L2** 10 µM in 1 mM phosphate buffer, upon addition of ct-DNA (1-10 eq) in 1 mM phosphate buffer.

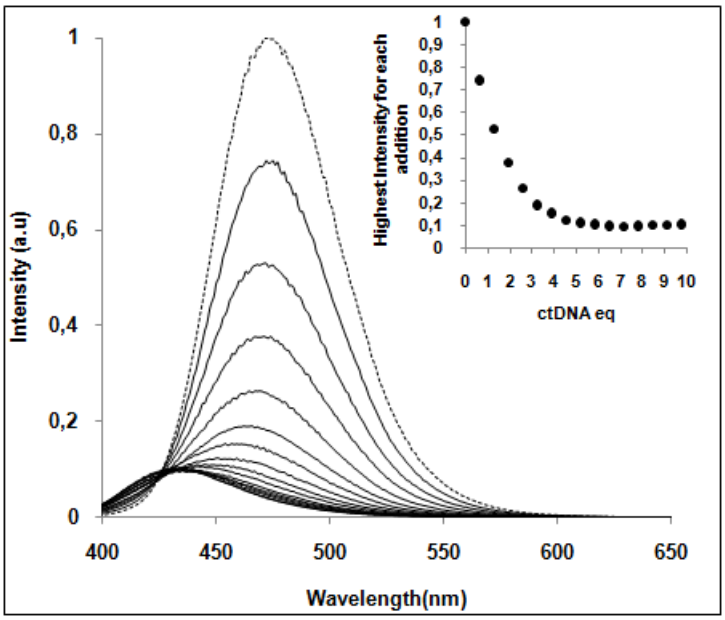

Figure S11. Changes in the emission spectrum of **L3** 10 µM in 1 mM phosphate buffer, upon addition of ct-DNA (1-10 eq) in 1 mM phosphate buffer.

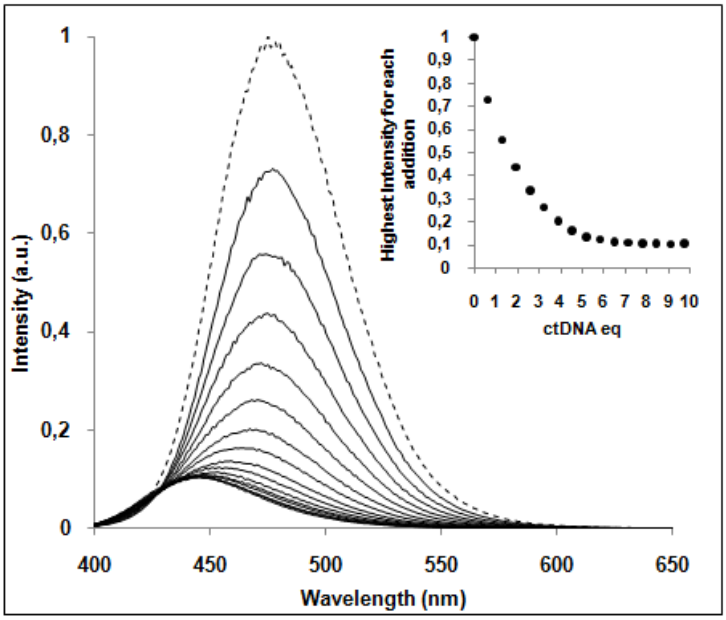

Figure S12. Changes in the emission spectrum of **L4** 10 µM in 1 mM phosphate buffer, upon addition of ct-DNA (1-10 eq) in 1 mM phosphate buffer.

S5. Cyclic Voltammograms

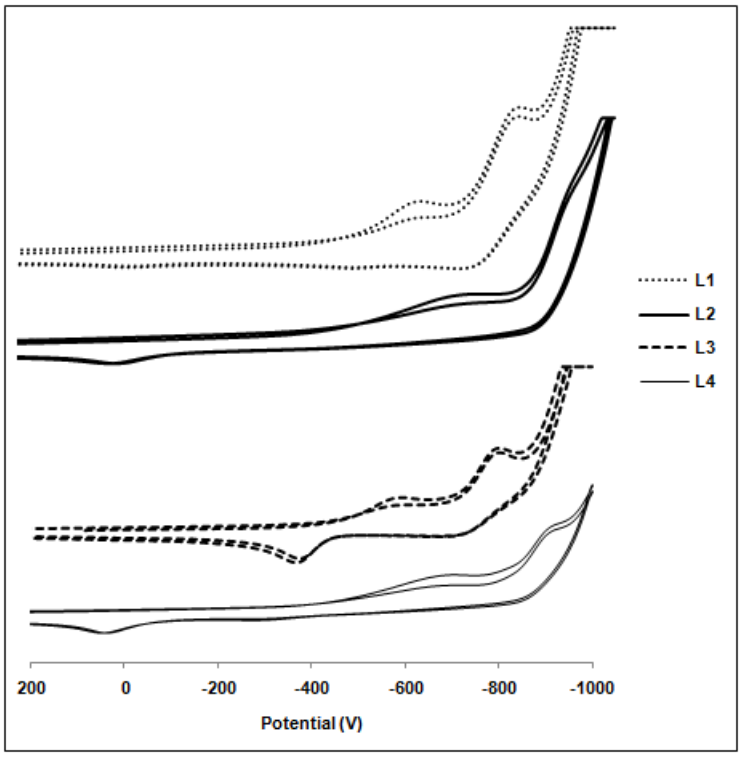

Figure S13. Cyclic Voltammograms of compounds **L1**-**L4**.

S6. IR spectra

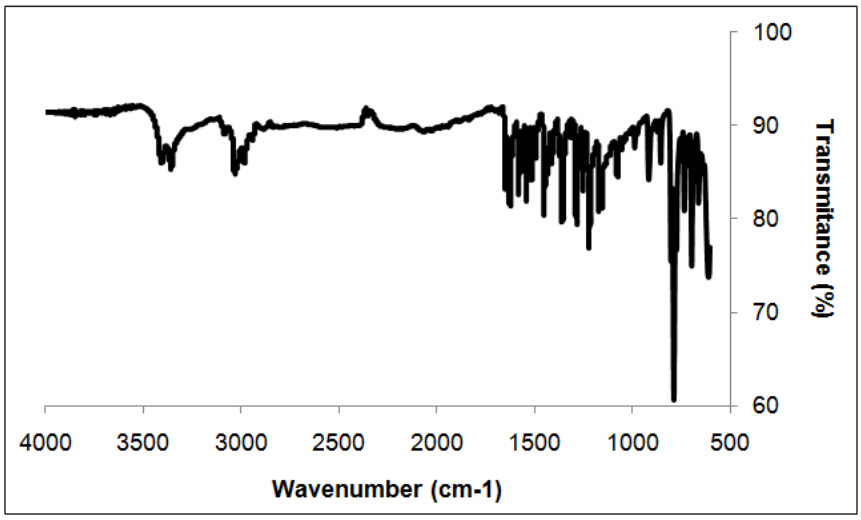

Figure S14. IR spectra of **L1**.

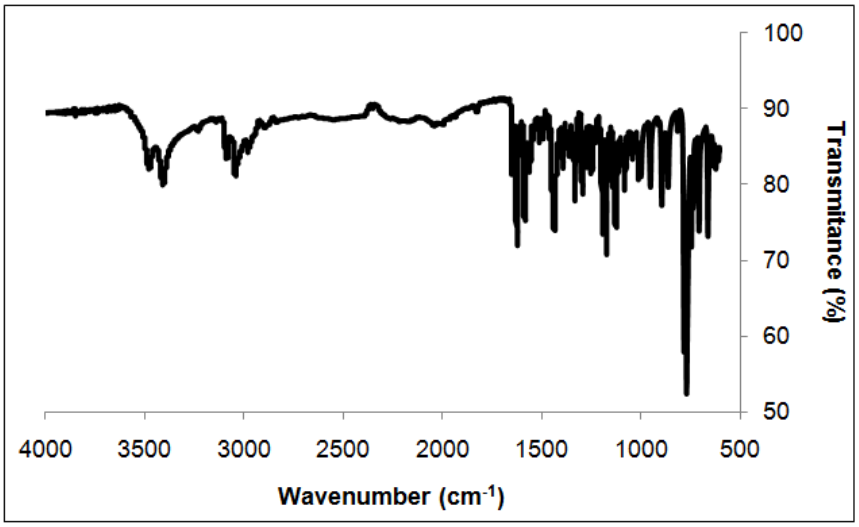

Figure S15. IR spectra of **L2**.

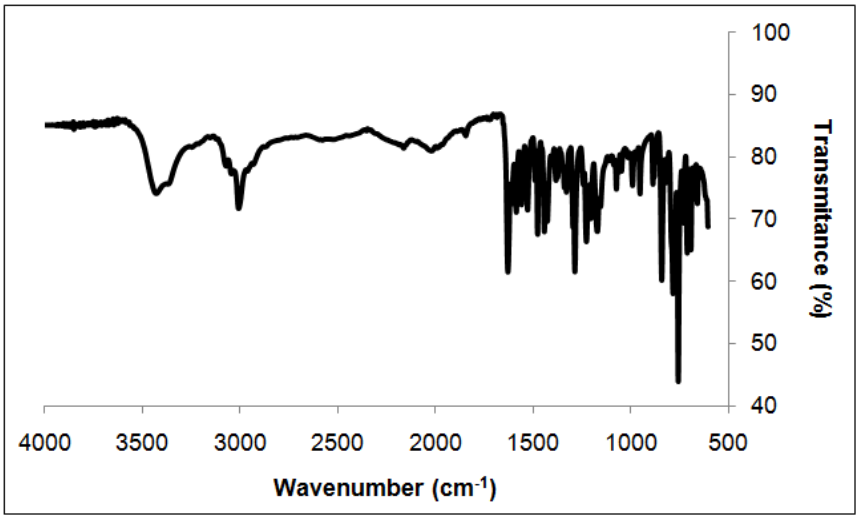

Figure S16. IR spectra of **L3**.

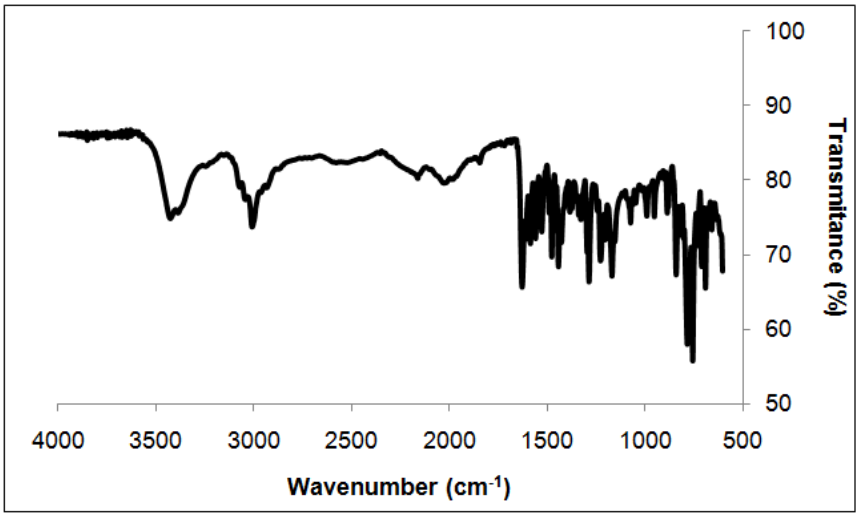

Figure S17. IR spectra of **L4**.

S7. ICP/MS analyses

ICP/MS analyses were performed in order to add an extra evidence of bromide presence as counter ion. For this experience, water solutions were prepared for each sample. Normally, samples are previously digested in nitric acid at 220ºC to eliminate any organic matter that could generate interference. However, this process also oxidizes bromide generating bromine that escapes at this temperature. For our samples, digestion was avoided and the sample was directly submitted to the analysis, even if deviations could be expected derived from the diquat **L1**-**L4**.

Results are presented in *Table S1* accompanied from the expected values obtained from elementary analysis. The obtained values fit with the presence of two bromine atoms per molecule.

Table S1. ICP/MS analyses of **L1**-**L4** determining the amount of bromide anion (mg/g) per molecule.

	Br (mg/g)	
	Experimental	**Calculated**
L1	355,2 ± 1,5	375,7
L2	377,0 ± 2,0	382,1
L3	319,1 ± 1,1	351,4
L4	315,3 ± 1,8	354,6

S8. DNA thermal denaturation curves

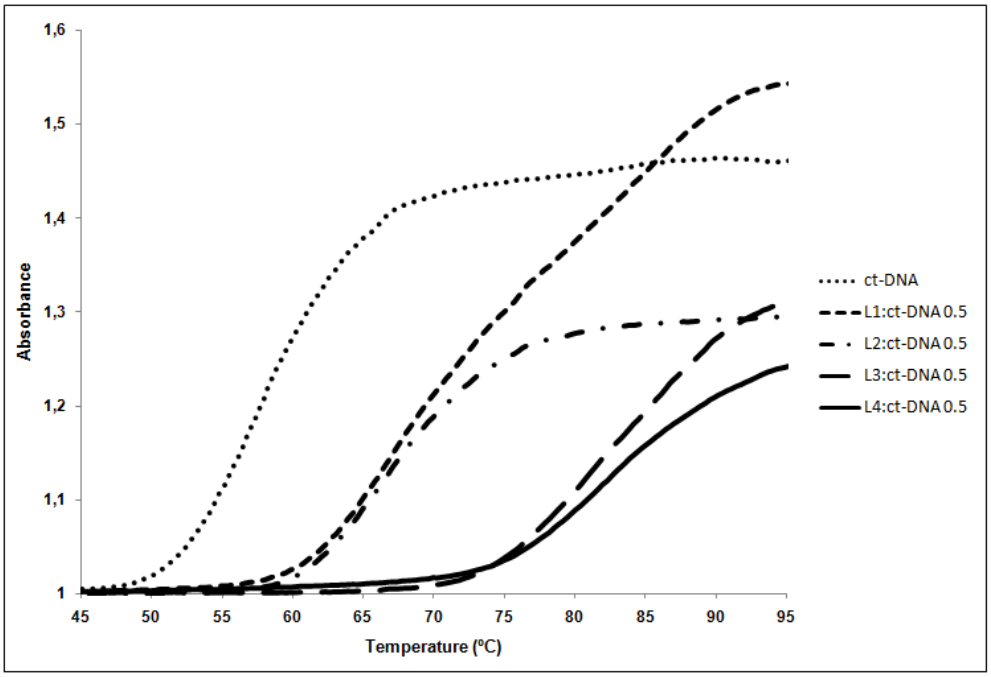

Figure S18. DNA thermal denaturation curves of free ct-DNA and **L1**-**L4**:ct-DNA at 0.5 range.

S9. Theoretical Calculations

3-D representations

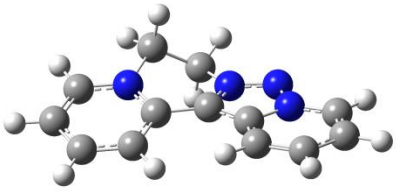

***M*-L1**

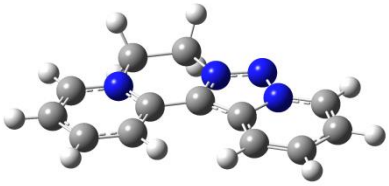

L1-TS

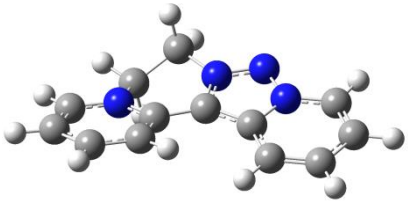

***P*-L1**

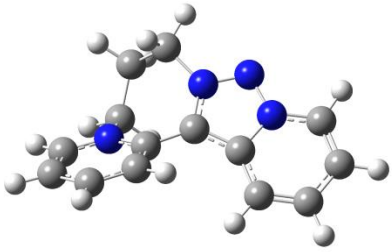

***P*-L2**

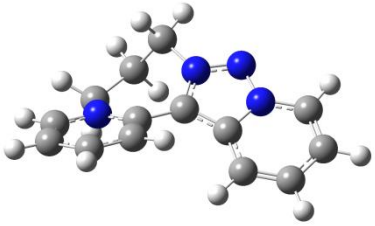

L2-Ts-a

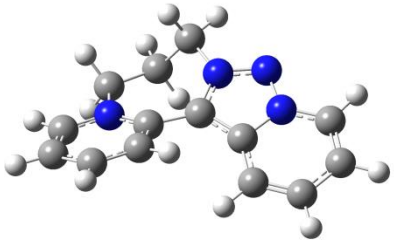

L2-b

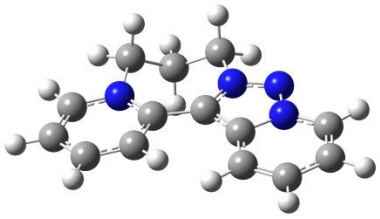

L2-Ts-b

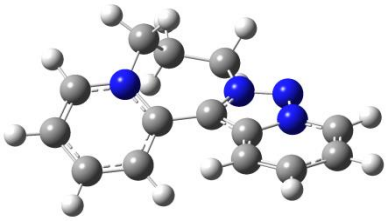

L2-c

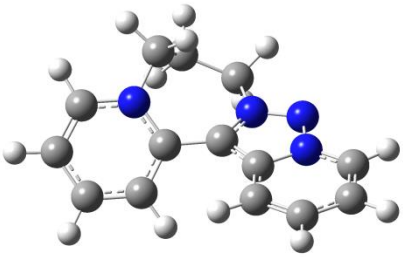

L2-Ts-c

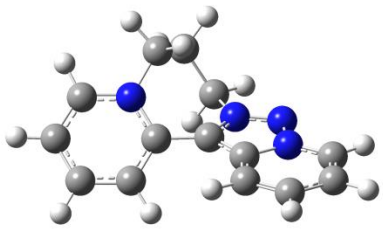

***M*-L2**

^{13}C-NMR chemical shift simulation

Molecular orbital calculations can be used to good estimates ^{13}C-NMR chemical shifts. Ab initio and DFT calculation of NMR shielding at very accurate levels of approximation are available in literature.[1-4] The GIAO (Gauge Including Atomic Orbital) method, implemented in the Gaussian package, is now widely used for these purposes. Good quality shielding results depend on the quality of the basis sets selected. Excellent results are obtained using B3LYP as DFT method and 6-311++G** as basis set.[3] The NMR calculations yield absolute shielding constants (σ) while experimental data is typically given as relative shielding constants (δ) to the tetramethylsilane (TMS).

Equation (1) is used to convert computed absolute shieldings (σ_{calc}), to computed relative shieldings (δ_{calc}), which can be used to compare to the experimentally measured relative shieldings (δ_{exp}).

$$\delta_{calc} = I + S\,\sigma_{calc} \qquad (1)$$

The variable *I* represent the shielding of the TMS, and ideally *S* is -1 for ^{13}C shifts. The best results are achieved when *I* and *S* are empirically determined by regressing σ_{calc} against δ_{exp} over a diverse set of organic compounds. *I*is the resulting intercept of the regression equation and *S* is the slope. We have used for *I* and *S* the values of 175.0 and -0.961, respectively.[3]

Table S2 and *Table S3* shows the values of computed relative shielding (δ_{calc}), experimentally assigned relative shielding (δ_{exp}) and differences (Dif.), in water, between the calculated and experimental value for compounds **L1** and **L2**, respectively. It should be noted that these calculations are referred to the static molecule as represented in Figure x, while experimental NMR spectra are averages affected by dynamic processes such as conformational equilibrium.

Table S2. ^{13}C-NMR δ shift (ppm) experimental (δ_{exp}) data for **L1** and calculated (δ_{calc}; B3LYP/6-311++G**) and difference (Dif.=δ_{exp}-δ_{calc}), in water, for conformer **L1**.

	L1	**L1**	
	δ_{exp}	δ_{calc}	Dif.
C1	126,5	126,5	0.0
C2	148,6	149,0	-0,4
C3	129,6	129,8	-0,2
C4	147,8	146,4	+1,4
C6	54,3	55,1	-0,8
C7	47,2	48,2	-1,0
C11	128,3	129,3	-1,0
C12	124,7	126,2	-1,5
C13	135,7	137,7	-2,0
C14	119,3	120,1	-0,8
C14a	133,8	133,4	+0,4
C14b	122,8	123,8	-1,0
C14c	136,2	136,8	-0,6

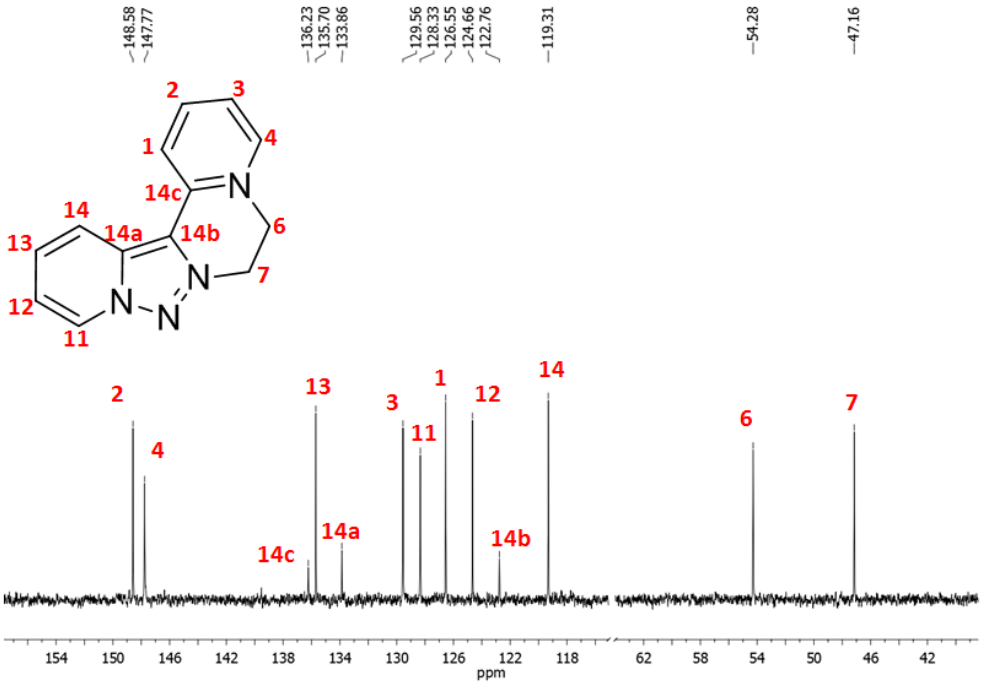

Table S3. ^{13}C-NMR δ shift (ppm) experimental (δ_{exp}) data for **L2** and calculated (δ_{calc}; B3LYP/6-311++G**) and difference (Dif.=δ_{exp}-δ_{calc}), in water, for conformers ***P*/*M*-L2**, **L2-b** and **L2-c**.

	L2	***PIM*-L2**		**L2-b**		**L2-c**	
	δ_{exp}	δ_{calc}	Dif.	δ_{calc}	Dif.	δ_{calc}	Dif.
C1	131,0	131,8	-0,8	132,3	-1,3	132,1	-1,1
C2	149,1	148,6	+0,5	147,4	+1,7	148,1	+1,0
C3	130,8	130,9	-0,1	129,6	+1,2	130,3	0,5
C4	148,3	148,2	+0,1	149,0	-0,7	147,3	+1,0
C6	57,6	59,0	-1,4	65,5	-7,9	59,4	-1,8
C7	30,2	34,8	-4,6	29,2	+1,0	28,1	+2,1
C8	49,6	51,1	-1,5	54,3	-4,7	57,0	-7,4
C12	127,6	128,4	-0,8	128,6	-1,0	128,1	-0,5
C13	124,2	125,7	-1,5	125,8	-1,6	126,2	-2,0
C14	134,9	136,7	-1,8	137,2	-2,3	136,8	-1,9
C15	119,5	119,1	+0,4	119,8	-0,3	119,8	-0,3
C15a	135,5	135,0	+0,5	136,8	-1,3	136,1	-0,6
C15b	124,8	125,6	-0,8	125,2	-0,4	126,7	-1,9
C15c	138,2	140,2	-2,0	139,4	-1,2	138,5	-0,3

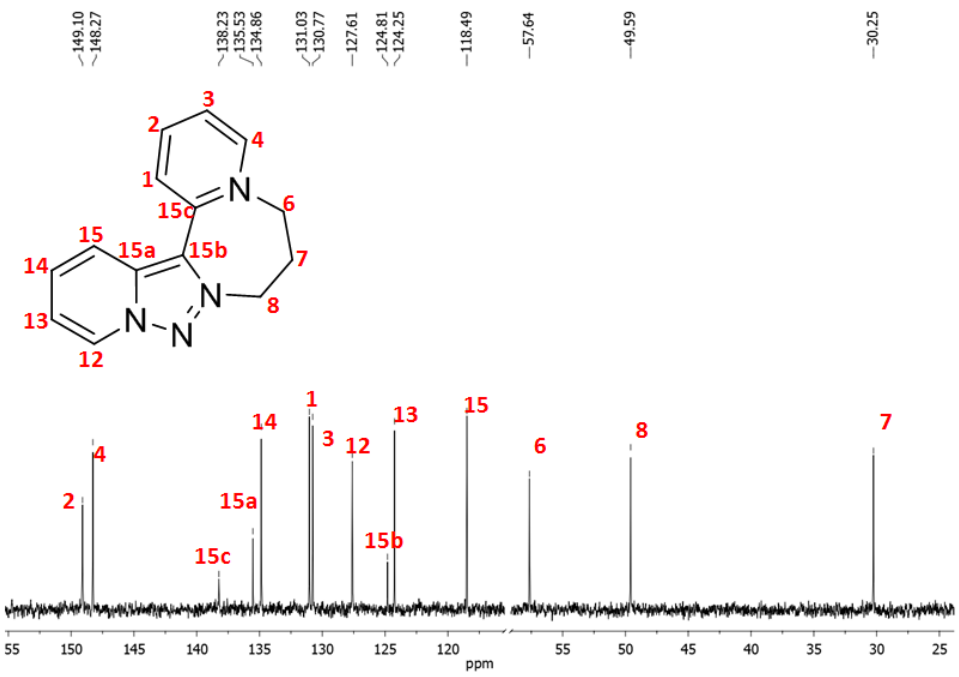

References

1) M. Barfield, P. Fagerness, *J. Am. Chem. Soc.*, **1997**, *119*, 8699.

2) J. Jaroszewska-Manaj, D. Maciejewska, I. Wawer, *Magn. Reson. Chem.*, **2000**, *38*, 482.

3) D.J. Giesen, N. Zumbulyadis, *Phys. Chem. Chem. Phys.*, **2002**, *4*, 5498.

4) S.N. Azizi, C. Esmaili, *Word Appl. Sci. J.*, **2009**, *7*, 559.

PARTE III: PREPARACIÓN DE METAL ORGANIC FRAMEWORK$_S$ (MOF$_S$) Y ESTUDIO DE SUS APLICACIONES

Capítulo 9

Introducción y objetivos

Introducción

La química de los materiales está siendo hoy en día muy investigada. El descubrimiento de nuevos materiales con propiedades que permitan su aplicación directa en beneficio de la vida de las personas es sin duda uno de los mayores retos de la ciencia.

Un campo muy estudiado es sin duda el de los MOF. Los MOF (Metal-Organic Frameworks o Redes Metalo-Orgánicas) son estructuras tridimensionales formadas por un clúster metálico rodeado de moléculas espaciadoras orgánicas. Metales como Zn, Zr, Fe o Cu pueden asociarse con moléculas orgánicas para formar estas redes tridimensionales, de diversas geometrías según el entorno del metal, y de tamaño de poro variable.

Los MOF pueden ser aprovechados en campos tan dispares como la catálisis, la cromatografía, el atrapamiento de gases, el encapsulamiento de fármacos…

En nuestro grupo de investigación se detectó una falta de investigación en el entendimiento de las propiedades macroscópicas de los MOF asociadas a su estructura atómica y molecular. Pocas investigaciones han ido encaminadas a entender, por ejemplo, de qué depende el crecimiento de los cristales, y cómo éste puede ser modulado y controlado. La mayoría de los MOF son obtenidos en forma de polvos cristalinos de tamaño micrométrico, con pocos casos reportados de cristales obtenidos a escala milimétrica, lo que facilitaría su manejo y permitiría el estudio de monocristales.

Así, inicialmente se abordó la obtención de cristales de MOF de tamaños cercanos al milímetro de arista y el estudio de la influencia del espaciador en este tamaño. Se utilizó como referencia el MOF-5, un MOF creado a partir de un clúster metálico de Zn(II) y usando como espaciador ácido tereftálico. El resultado son cristales de geometría cúbica (*Figura III.1*).

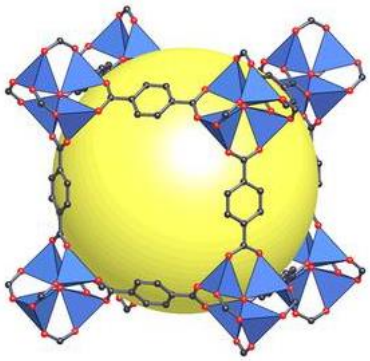

Figura III.1. Estructura del MOF-5. Clúster de Zn(II) y espaciadores de ácido tereftálico.

La síntesis ordinaria de este MOF da como resultado un polvo cristalino de color blanco, con cristales de geometría cúbica de tamaño microscópico. Sin embargo, se detectó que una pequeña modificación en el espaciador, añadiendo al anillo aromático del ácido tereftálico un grupo amino (ácido 2-aminotereftálico), y aplicando las condiciones de síntesis adecuadas, daba como resultado cristales de tamaño que rondaba el milímetro de arista. Este MOF es conocido como IRMOF-3 (*Figura III.2*).

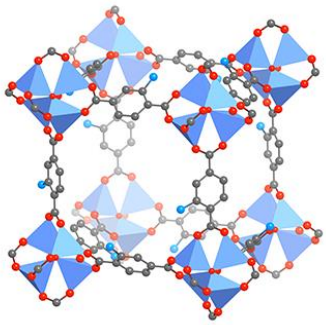

Figura III.2. Estructura del IRMOF-3. Clúster de Zn(II) y espaciadores de ácido 2-aminotereftálico.

El estudio de la dependencia del tamaño del cristal con el porcentaje de ácido 2-aminotereftálico en la estructura, y la relación entre el porcentaje de ácido añadido a la síntesis y el finalmente incluido en la estructura final fueron también objeto de estudio.

Utilizando los conocimientos para obtener monocristales de gran tamaño, se pretendió estudiar el comportamiento de una molécula con propiedades espectroscópicas conocidas, dentro del entorno de un MOF. Sin embargo, la mayoría de MOF contienen espaciadores orgánicos aromáticos (debido a su rigidez), lo que le confiere un color específico al cristal. Sería imposible estudiar así las propiedades espectroscópicas de una molécula en su interior.

Por tanto, se propuso crear un nuevo MOF transparente, utilizando un espaciador que aportara igualmente rigidez, pero sin el componente de absorción de luz. Para ello se seleccionó el ácido biciclo[2.2.2]octano-1,4-dicarboxílico como espaciador, obteniendo el primer MOF transparente (TMOF).

Como molécula a estudiar, se eligió el pireno, una molécula orgánica de conocido patrón espectroscópico y de tamaño adecuado para el tamaño de poro.

Objetivos

Los objetivos de esta tercera parte de la tesis fueron:

1. Síntesis de cristales de MOF a escala milimétrica, manejables de manera individual, así como el estudio de las condiciones de síntesis que favorecen diferentes tamaños de cristal.
2. Síntesis de cristales de MOF transparentes, con el objetivo de introducir dentro una molécula y evaluar sus propiedades espectroscópicas en el interior de los poros.

Capítulo 10

Dalton Transactions, 2017, 46, 7397-7402

Dalton Transactions

COMMUNICATION

View Article Online
View Journal | View Issue

Cite this: *Dalton Trans.*, 2017, **46**, 7397

Received 9th March 2017,
Accepted 10th May 2017

DOI: 10.1039/c7dt00855d

rsc.li/dalton

Bicyclo[2.2.2]octane-1,4-dicarboxylic acid: towards transparent metal–organic frameworks†

P. J. Llabres-Campaner,[a] J. Pitarch-Jarque,[b] R. Ballesteros-Garrido, *[a,b] B. Abarca,[a] R. Ballesteros [a] and E. García-España [b]

Abstract

The preparation of transparent porous materials can offer a different acces towards the study of molecules under solid confined space. Metal Organic Frameworks represents an unique oportunity due to their tunnable pore size, however, aromatic linkers present strong absortion and reduce the transparency. Herein, we report the first example of MOF with biciclic organic dicarboxilic linkers and its use as solid solvent.

Introduction

Metal Organic Frameworks (MOFs)[1] represent a large variety of materials with significant applications in many fields[1] like gas storage,[2] catalysis,[3] sensors[4] and medicine.[5] These materials present tuneable pore size thanks to the variety of metallic clusters and organic linkers that can be employed in their preparation.[1e,6] Depending on their characteristics, MOFs can accommodate inside their pores species of different sizes ranging from small molecules to large proteins.[7] Owing to the small pore size that some MOFs have, the inclusion may occur in occasions even without any intermolecular interaction between the guest species. In addition, diffusion of molecules inside MOFs has found significant application in the field of medicine.[5,9] The preparation of MOFs requires the use of rigid organic ligands that very often contain aromatic units or spacers.[1,7] Among the commonly reported spacers, terephthalic acid (**1**) (*Figure 1*) is one of the most employed. Aromatic ligands moieties like 1 provide significant absorption in the UV spectrum, being transparent in their solid state only from 350 nm to 800 nm (*Figure 1, bottom*). However, the preparation of MOFs with an extended transparency in the UV domain (below 320 nm) may find significant applications in materials science. To achieve this goal, it is necessary to select carefully ligands and metals with the least possible absorbance in the UV-Vis region.

MOFs with a higher range of transparency (or a reduced absorption) can, on the other hand, offer a new way to study confined guest molecules. To achieve the preparation of MOFs with minimum absorption in the full UV-Vis range, Zn(II) based MOFs are particularly adequate because Zn(II), being a *d10* metal ion, has no absorption in the visible region. In this respect, Yagui *et al*, have reported a large variety of Zn(II) based MOFs with important properties.[1e] One of the most common MOFs is MOF-5,[10] which is composed by terephthalic acid (**1**) and Zn_4O clusters arranged in a cubic network composed by **1** on the edges and the metal cluster on the vertices. After careful bibliographic examination of reported dicarboxylic ligands, we found that the bicyclic compound **2** meets both rigidity and absence of aromaticity, being therefore suitable for the preparation of transparent metal-organic frameworks (TMOFs) (*Figure 1*).[11] The [2.2.2] bicyclic moiety of **2** provides rigidity and a conformation similar to that observed with classic terephthalic acid (**1**). The reduction of the absorption properties is induced by the absence of aromatic rings. As shown in *Figure 1*, **2** is more transparent than **1** in the UV, particularly below 350 nm.

In spite that other nitrogenated bicyclic compounds had been already employed as ligands for the preparation of MOFs (i.e. DABCO (**3**) in pillar-layer MOFs),[12] as far as we know, **2** had, surprisingly, never been used.

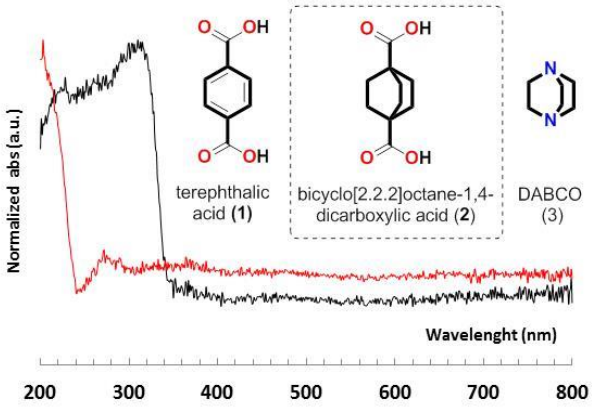

Fig. 1. Compounds **1**, **2** and **3**. Diffused reflectance spectra of **1** (blue) and **2** (red) recorded of powder samples from 200 nm to 800 nm (normalized values).

Results and discussion

For the preparation of the transparent material several tests were performed following the most successful methodologies reported for MOF-5.[10,13] $Zn(NO_3)_2 \cdot 6H_2O$ was employed as metal source and dimethyl formamide (DMF), diethyl formamide (DEF) or dibutyl formamide (DBF) as solvent in a range of temperatures from 80ºC to 115ºC. The concentration and stoichiometry employed was the one reported by Stoddart *et al*[13] The most significant results were obtained using DMF as solvent at low temperatures (80ºC or 95ºC, 72h). Indeed, reproducible transparent needles (TMOF) were formed as unique material under these conditions. Similar results were obtained when using DEF at 80ºC (*Figure 2*). Moreover, by changing the temperature, three other crops of crystals suitable for X-ray diffraction (**TMOF2**, **TMOF3** and **TMOF4**) could be also obtained. However, these crystals were always minoritary and appeared in the presence of amorphous solids or TMOF crystals (See ESI for a complete description of conditions).

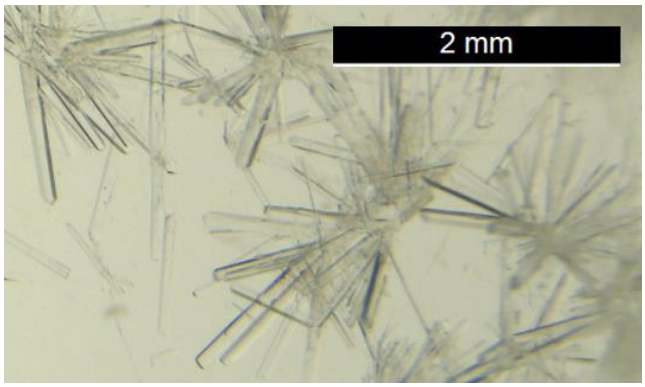

Fig. 2. Microscope picture of needles of TMOF obtained at 80ºC in DMF, 72 h.

When using DMF as a solvent and temperatures ranging from 80ºC to 95ºC, only TMOF needles were formed with good yield (ca. 45% yield). Single-crystal X-ray diffraction reveals that this material (TMOF) crystallizes in the monoclinic space group P2/n. There is one independent Zn(II) in the asymmetric unit that is coordinated by four carboxylate oxygen atoms from distinct ligands (**2**) in a distorted tetrahedral coordination geometry (*Figure 3b and ESI*). Interestingly, the Zn atom is bridged by the carboxylate groups from **2** forming an infinite anionic chain along the c axis. The intra chain Zn···Zn distance is 3.451(1) Å. Finally, a non-interpenetrated three-dimensional (3D) architecture is created by repeating these joints. The crystal structure exhibits an almost cubic three-dimensional framework with wide open channels with an aperture of approximately 4.5 × 4.1 $Å^2$ (excluding van der Waals radii)[14] running along the crystallographic *a* axis (*Figures 3a and 3c*). The channels are occupied by the structurally disordered DMF solvent molecules.[15]

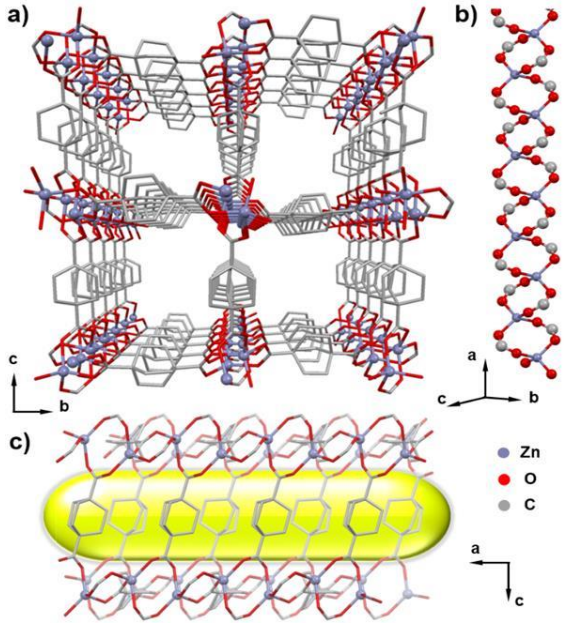

Fig. 3. a) TMOF view along *a* axis, b) detail of the O-Zn-O chain, c) illustrative pore dimension into the channels. Hydrogen atoms and internal DMF have been omitted for clarity.

The second structure, **TMOF2**, was obtained using DEF as a solvent at 95ºC. **TMOF2** crystallize in the trigonal space group P3121. In this case, Zn(II) forms a distorted Zn_4O cluster involving six carboxylate groups and a DEF molecule (*Figure 4*). As result of the coordination of the DEF molecule, three Zn(II) have a tetrahedral coordination and one Zn(II) atom (Zn2) is penta-coordinated forming an extra bond with an oxygen atom of a DEF molecule (*Figure 4b and ESI*). The carboxylate group that is bridging both Zn(II) atoms has two possible coordination positions and the DEF molecule is coordinated to both Zn(II) atoms with 50% occupancy. The carboxylate carbon atoms in the $Zn_4O((CO_2)_6)$DEF-type cluster serve as the points-of-extension that define the vertexes of a trigonal prismatic secondary building unit that forms a non-interpenetrated MOF. The crystal structure exhibits a 3-D framework with wide open channels of approximately[14] 13.2 × 6.1 $Å^2$ running along the crystallographic *a* and *b* axis, and also along the bisection of both axis [110] (*Figure 4b and ESI*). The channels have the same topology in the three directions and in their interior there are disordered DEF molecules that cannot be properly modelled.

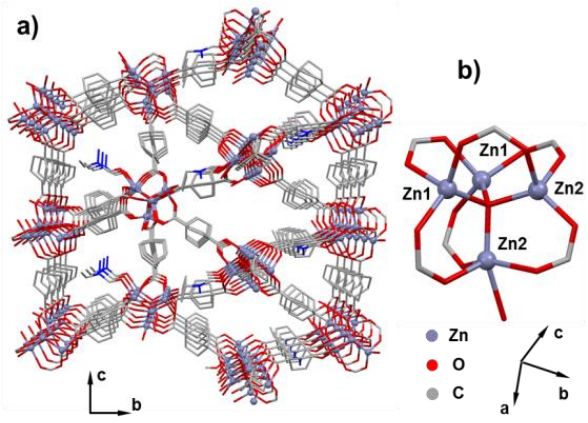

Fig. 4. TMOF2. a) view along *a* axis, b) detail of the Zn_4O cluster. Hydrogen atoms and internal DEF have been omitted for clarity.

The other structures, **TMOF3** and **TMOF4**, were obtained in poor yield at higher temperatures (and also accompanied by an amorphous solid). **TMOF3** and **TMOF4** might have evolved from **TMOF** owing to their structural similarities. **TMOF3** and **TMOF4** are non-interpenetrated MOFs that crystallize in the monoclinic space groups P2/c and I2/a, respectively. In both cases, the asymmetric unit is composed by Zn(**2**)$_2$ building units. These units consist of a Zn(II) coordinated by four oxygen atoms from distinct carboxylate ligands with a distorted tetrahedral coordination geometry. The Zn(II) cations are bridged by two carboxylate groups. Similarly to **TMOF**, these infinite anionic chains grow along a unique direction, the *c* axis in the case of **TMOF3** and the *a* axis in the case of **TMOF4** (*Figures 5b and 5d*). **TMOF3** exhibits an almost cubical three-dimensional framework with wide open channels filled with DMF solvent molecules; the aperture of each channel being of approximately 4.5 × 4.4 Å^2 (*Figures 5a and 5c*).

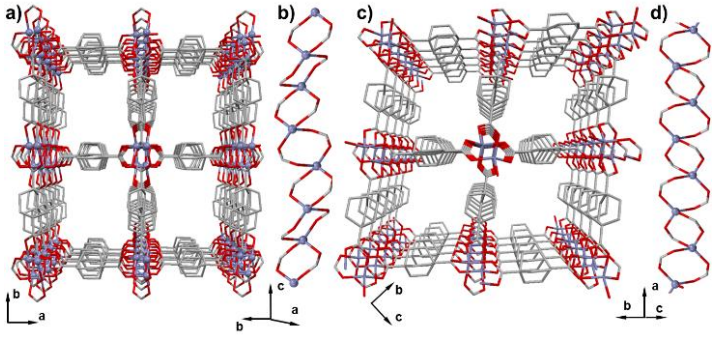

Fig. 5. TMOF3 a) view along *c* axis, b) detail of the O-Zn-O chain, TMOF4 c) view along *a* axis, d) detail of the O-Zn-O chain.

In order to validate our hypothesis concerning the potential of **TMOF** as a transparent porous host, we studied the effects of introducing pyrene inside the pores because of its spectroscopic properties. Pyrene has well-defined absorption bands in the 300-350 nm range and a characteristic fluorescence emission. To carry out this experiment, crystals of **TMOF** were immersed in a pyrene solution in DMF at 45ºC for 24 h and then they were washed with DMF. The PXRD diffraction of the corresponding materials is presented in *Figure 6*.

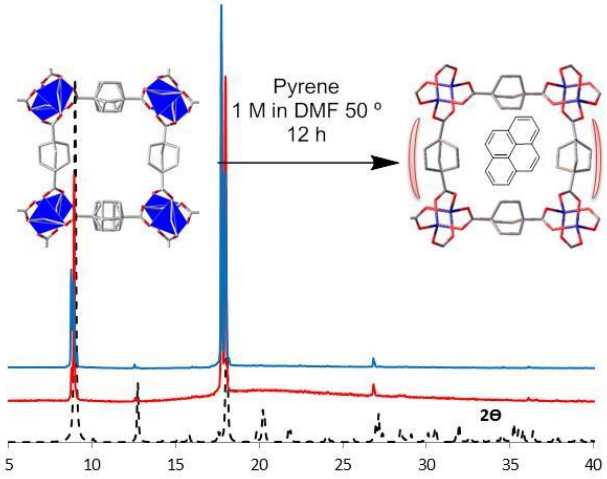

Fig 6. PXRD pattern of **TMOF** (blue), **Pyrene@TMOF** (red) and calculated from **TMOF** (dashed black).

As it can be observed, the diffraction pattern remains unchanged and agrees well with the model calculated from CIF. Nevertheless, a **Pyrene@TMOF** single crystal was also submitted to

X-ray diffraction and a similar structure (compared with **TMOF**) was observed. Although the pyrene molecules could not be located, a significant expansion of the channels appeared (*Figure 6, right*), indicating that something bulky was allocated inside the pores.[16] In order to study these materials with more detail by spectroscopic techniques complete removal of DMF was required. This was achieved by heating at 120 ºC under vacuum.[17] After activation, TMOF and **Pyrene@TMOF** afforded similar PXRD patterns (**Figure 7 inset**). Elementary analysis was performed, and the values obtained did not allow a quantitative determination of the amount of pyrene. This clearly indicated relative low loading values. By treatment with a base (KOH/EtOH and sonication) the material was degraded, and the remaining solution was analysed by UV. The results showed that pyrene concentration was around 0.003 % in weight. Considering the role of **TMOF** as solvent (for pyrene), we calculated the molal (m) concentration of pyrene inside **TMOF**. Molal concentrations were used since the weight of the **TMOF** needles can be measured with much more accuracy than their corresponding volume. The value was close to 10^{-3} m. Although this may seem small, it is indeed a high value in UV-Vis or fluorescence techniques (normal values for fluorescence are 10^{-5} M). As a reference, in water, at constant temperature, molar and molar values can be considered equal. Then, with the materials free from DMF, the spectra could be recorded with minimum interference.[17] Diffuse reflectance measurements of pyrene, **TMOF** and **Pyrene@TMOF** are presented in *Figure 7*. As expected, **TMOF** is transparent above 300 nm. Indeed, there is a band at 200 nm that can be associated to COOH and another one at 275 that can be attributed to the ZnO chains. **Pyrene@TMOF** (*red spectrum, Figure 7*) presents the same bands, but in addition, well-defined bands appear in the 300-350 nm range.

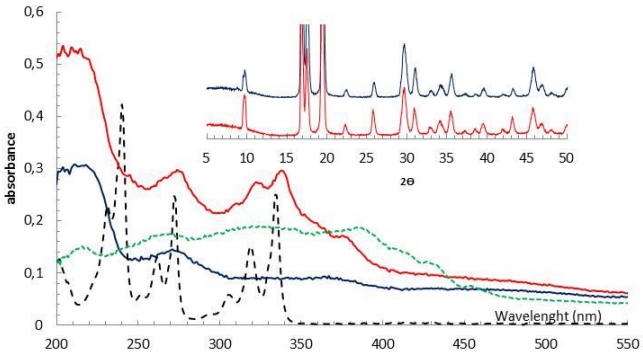

Fig. 7. Diffuse reflectance experiments for activated **TMOF** (blue), activated **Pyrene@TMOF** (red), pyrene (solid state green) and a solution of Pyrene (dashed black, 10^{-4} M in ethanol, recorded on a liquid phase UV/Vis spectrometer) Inset: PXRD pattern of activated **TMOF** (blue) and **Pyrene@TMOF** (red).

This result was in agreement with the presence of pyrene but also outlined the idea of **TMOF** acting as a solvent. When diffuse reflectance of single crystals of pyrene (*Figure 7, green*) was carried out a broad shape-less band appeared in the 200-450 nm range. However, in ethanol solution (*Figure 7, dashed black*) the bands in the 300-350 nm range were again observed. This constitutes a strong indication that pyrene behaves as in solution, notwithstanding it is inside a solid. The fluorescence emission spectrum of **TMOF** shows just a weak band centred at 390 nm. **Pyrene@TMOF** presents a strong emission at 395 nm followed by a more intense one centred at 480 nm (*Figure 8*). As shown in *Figure 8*, the fluorescence emission spectra of pyrene in the solid state or in an ethanol solution are different. The emission of the pyrene located inside the cavity gathers features of both spectra, the one recorded in the solid state and the one recorded in ethanol. Solid state fluorescence quantum yield measurements clearly confirmed the presence of pyrene, indeed **TMOF** ΦF was 6.1 % (λ=340 nm) and **Pyrene@TMOF** was ΦF: 13.5 % (λ=340 nm).[18]

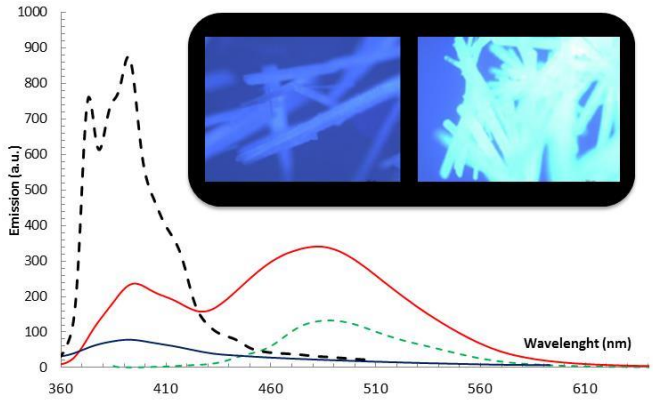

Fig. 8. Solid state fluorescence: Top left: **TMOF**. Top right: **Pyrene@TMOF**. Bottom: solid state fluorescence spectra for **TMOF** (blue) **Pyrene@TMOF** (red) and Pyrene (dashed green). Emission of 10^{-5} M (EtOH) also included as reference (dashed black).

In the literature there are a few examples were pyrene inside porous materials can behave in this way, presenting these two bands. For example, a similar pattern was reported for pyrene included in a NaY zeolite.[19] Furthermore, highly concentrated pyrene solutions behave also in this way.[20] A possible explanation might be that both monomer (385 nm) and excimer (485 nm) coexist inside the **TMOF** structure. On the other hand, a pyrene excimer has been found inside pairs of β-cyclodextrines with an internal diameter of 7.8 Å.21 This value is similar to the diameter of **TMOF**. The network deformations detected in the X-ray studies may be a consequence of this excimer formation.

Conclusions

Herein we have reported for the first time a MOF performed with a bicyclic organic linker (**2**) allowing the preparation of **TMOF** with high reproducibility and good yield. In addition, we have shown three complementary structures that can be obtained by increasing the temperature. The transparency conferred by the bicyclic ligand (**2**) results in an extremely transparent MOF. This has been employed as a proof of concept to study a solid solution of **Pyrene@TMOF** by spectroscopic techniques. The presence of pyrene induces a small structure deformation, but it provides a significant fluorescence emission. As a consequence, pyrene can behave as in solution at a high level of concentration. All of this has been performed with macroscopic size (1-2 mm) crystals. This work presents one of the most transparent MOF ever reported; further studies are ongoing with the aim of understanding the dynamics of pyrene inside **TMOF**.

Acknowledgements

R. B-G is much indebted to the Posdoctoral fellow 2013 of the Ministerio de Economía y Competitividad (Spain, FPDI-2013-17464). This work was financially supported by the Ministerio de Ciencia e Innovación (Spain) (Projects CONSOLIDER-INGENIO SUPRAMED CSD 2010-00065, CTQ2016-78499-C6-1-R), Unidad de Excelencia María de Maeztu MDM-15-0538) and Generalitat Valenciana (PROMETEO II 2015-002) and from University of Valencia (Spain) (UV-INV-AE 15-332846). We are especially grateful to Dr. Moliner and Dr. Molins from Mintota (UV) for the diffuse reflectance equipment and the "Central Service for Experimental Research" (SCSIE) of University of Valencia.

Notes and references

Preparation of TMOF: Freshly distilled DMF, DEF or DBF DBF (20 mL) was added to an Erlenmeyer flask containing Bicyclo[2.2.2]octane-1,4-dicarboxylic acid (0.8 mmol, 158.4 mg) and $Zn(NO_3)_2 \cdot 6H_2O$ (2.2 mmol, 658 mg). The mixture was stirred for 10 min or until the solid dissolved. Portions (2 mL each) were removed by syringe and injected through a 25 mm syringe filter (0.45 PTFE membrane) into ten 5 mL scintillation vials, which were then sealed with polypropylene-lined screw caps. The vials were placed in a plate and heated in an oven for 72 h at 80, 95 or 116 ºC. The vials were removed and cooled to room temperature for 2 h, upon which **TMOF** crystals were washed three times with fresh DMF after crystals were washed two times with methylene chloride. If activation was required, vials were placed again into the oven at 120ºC for 12 h under vacuum. Reproducible and quantitative experiences were observed for **TMOF** 55±10 yield.

Pyrene@TMOF1: 15 mg of activated **TMOF** were immersed into a DMF solution (2 ml) of Pyrene (25 mg) at 60ºC for 12h. Then, the corresponding liquid phase was removed, and the material was cleaned 3 times with DMF (4 mL) to remove the excess of outsider pyrene. Materials were dried and activated over vacuum at 120ºC and 12h. The same experience was performed with freshly prepare non-activated **TMOF** affording similar result in order to compare non-activated sample.

References

1) a) M. Eddaoudi, D.B. Moler, H.L. Li, B. L. Chen, T. M. Reineke, M. O'Keeffe, O. M. Yaghi, *Acc. Chem. Res.*, **2001**, *34*, 319. b) G. Ferey, *Chem. Soc. Rev.*, **2008**, *37*, 191. c) S. Kitagawa, R. Kitaura, S. Noro, *Angew. Chem. Int. Ed.*, **2004**, *43*, 2334. d) O.M. Yaghi, M. O'Keeffe, N.W. Ockwig, H.K. Chae, M. Eddaoudi, J. Kim, *Nature*, **2003**, *423*, 705. e) M. O'Keeffe, O. M. Yaghi, *Chem. Rev.*, **2012**, *112*, 675.

2) a) K. Sumida, D.L. Rogow, J.A. Mason, T.M. McDonald, E.D. Bloch, Z.R. Herm, T.H. Bae, J.R. Long, *Chem. Rev.*, **2012**, *112*, 724. b) M. Paik Suh, H.J. Park, T.K. Prasad, D.W. Lim, *Chem. Rev.*, **2012**, *112*, 782. c) Y. He, W. Zhou, G. Qian, B. Chen, *Chem. Soc. Rev.*, **2014**, *43*, 5657.

3) a) J.Y. Lee, O.K. Farha, J. Roberts, K.A. Scheidt, S.B.T. Nguyen, J.T. Hupp, *Chem. Soc. Rev.*, **2009**, *38*, 1450. b) A. Dhakshinamoorthy, H. Garcia, *Chem. Soc. Rev.*, **2014**, *43*, 5750.

4) a) L.E. Kreno, K. Leong, O.K. Farha, M. Allendorf, R.P. Van Duyne, J T. Hupp, *Chem. Rev.*, **2012**, *112*, 1105. b) Z. Hu, B.J. Deibert, J. Li, *Chem. Soc. Rev.*, **2014**, *43*, 5815.

5) a) P. Horcajada, R. Gref, T. Baati, P.K. Allan, G. Maurin, P. Couvreur, G. Férey, R.E. Morris, C. Serre, *Chem. Rev.*, **2012**, *112*, 1232. b) S. Keskin, S. Kızılel, *Ind. Eng. Chem. Res.*, **2011**, *50*, 1799.

6) M. Eddaoudi, J. Kim, N. Rosi, D. Vodak, J. Wachter, M. O'Keeffe, O.M. Yaghi, *Science*, **2002**, *295*, 469.

7) a) H.K. Chae, D.Y. Siberio-Pérez, J. Kim, Y. Go, M. Eddaoudi, A.J. Matzger, M. O'Keeffe, O.M. Yaghi, *Nature*, **2004**, *427*, 523. b) M. Müller, A. Devaux, C.H. Yang, L. De Cola, R.A. Fischer, *Photochem. Photobiol. Sci.*, **2010**, *9*, 846. c) M.J. Dong, M. Zhao, S. Ou, C. Zou and C.D. Wu, *Angew. Chem. Int. Ed.*, **2014**, *53*, 1575. d) J. Yu, Y. Cui, C. Wu, Y. Yang, Z. Wang, M. O'Keeffe, B. Chen, Q. Guodong, *Angew. Chem. Int. Ed.*, **2012**, *51*, 10542. e) J. Yu, Y. Cui, H. Xu, Y. Yang, Z. Wang, B. Chen, G. Qian, *Nat. Commun.*, **2013**, *4*, 2719. f) H. Deng, S. Grunder, K.E. Cordova, C. Valente, H. Furukawa, M. Hmadeh, F. Gándara, A.C. Whalley, Z. Liu, S. Asahina, H. Kazumori, M. O'Keeffe, O. Terasaki, J. F. Stoddart, O.M. Yaghi, *Science*, **2012**, *336*, 1018.

8) R. Ballesteros-Garrido, A.P. da Costa, P. Atienzar, M. Alvaro, C. Baleizão, H. García, *RSC Adv.*, **2016**, *6*, 35191.

9) P. Horcajada, T. Chalati, C. Serre, B. Gillet, C. Sebrie, T. Baati, J.F. Euban, D. Heurtaux, P. Clayette, C. Kreuz, J.S Chang, Y.K. Hwang, V. Marsaud, P.N. Bories, L. Cynober, S. Gil, G. Férey, P. Couvreur, R. Gref, *Nat. Materials*, **2010**, *9*, 172.

10) H. Li, M. Eddaoudi, M. O'Keeffe, O.M. Yaghi, *Nature*, **1999**, *402*, 276.

11) Efficient synthesis of ligand **2** can be found in: N. Le Marquer, M.Y. Laurent, A. Martel, *Synthesis* **2015**, *47*, 2185.

12) Many contribution concerning Pilar-Layer MOF are reporting using DABCO (**3**) as pillar unit i.e. a) O. Shekhah, K. Hirai, H. Wang, H. Uehara, M. Kondo, S. Diring, D. Zacher, R.A. Fischer, O. Sakata, S. Kitagawa, S. Furukawa and C. Wöll, *Dalton Trans.*, **2011**, *40*, 4954. b) D. Braga, L. Maini, P.P. Mazzeo, B. Ventura, *Chem. Eur. J.*, **2010**, *16*, 1553. c) I.M. Hauptvogel, R. Biedermann, N. Klein, I. Senkovska, A. Cadiau, D. Wallacher, R. Feyerherm, S. Kaskellnorg, *Chem. Eur. J.*, **2011**, *50*, 8367. d) H. Hahm, K. Yoo, H. Ha, M. Kim, *Inorg. Chem.*, **2016**, *55*, 7576.

13) S. Han, Y. Wei, C. Valente, I. Lagzi, J.J. Gassensmith, A. Coskun, J.F. Stoddart, B.A. Grzybowski, *J. Am. Chem. Soc.*, **2010**, *132*, 16358.

14) A van der Waals radius of C (1.70 Å) was used in determination of distance parameters. See: A. Bondi, *J. Phys. Chem.*, **1964**, *68*, 441.

15) The particular 3D structure of TMOF can be associated to a ROD. a) N.L. Rosi, J. Kim, M. Eddaoudi, B. Chen, M. O'Keeffe, O.M. Yaghi, *J. Am. Chem. Soc.*, **2005**, *127*, 1504. b) M. O'Keeffe, A. Andersson, *Acta Cryst.*, **1977**, *33*, 914.

16) Although pyrene could not be located, nanoporosity is indeed a new strategy for the small molecule X-ray diffraction see: Y. Inokuma, S. Yoshioka, J. Ariyoshi, T. Arai, Y. Hitora, K. Takada, S. Matsunaga, K. Rissanen, M. Fujita, *Nature*, **2013**, *495*, 461.

17) In order to avoid interferences in elementary analysis, UV/Vis and fluorescence caused by the presence of DMF activation was performed, this induced, as indicated in Figure 7 a modification of the XRPD pattern, similar in TMOF and Pyrene@TMOF, however macroscopical aspect remained the same (needles, see ESI).

18) Reported quantum yield for Pyrene in solid state is 67%. See: R. Katoh, K. Suzuki, A. Furube, M. Kotani, K. Tokumaru, *J. Phys. Chem. C*, **2009**, *113*, 2961. However, when absorbed to surfaces significant modifications of these values can be observed. See: S.A. Ruetten, J.K. Thomas, *J. Phys. Chem. B*, **1998**, *102*, 598.

19) a) K.A.W.Y. Cheng, N.P. Schepp, F.L. Cozens, *Photochm. Photobiol.*, **2006**, *82*, 132. b) X. Liu, K.K. Lu, J.K. Thomas, *J. Phys. Chem.*, **1989**, *93*, 4120.

20) J.B. Birksand, L.G. Christophorous, *Spectrochimica Acta*, **963**, *19*, 401.

21) M. Hara, S. Tojo, K. Kawai, T. Majima, *Phys. Chem. Chem. Phys.*, **2004**, *6* , 3215.

Supporting Information

Bicyclo[2.2.2]octane-1,4-dicarboxylic acid: Towards Transparent Metal Organic Frameworks.

P. J. Llabres-Campaner[a], J. Pitarch-Jarque[b], R. Ballesteros-Garrido*[a], B. Abarca[a], R. Ballesteros[a] and E. García-España[b].

[a]Departament de Química Orgànica, Universitat de València, Av. Vicent Andrés Estellés s/n, 46100 Burjassot, Valencia, Spain

[b]Instituto de Ciencia Molecular ICMOL, C/ Catedrático José Beltrán 2, 46980 Paterna, Valencia, Spain

E-mail: rafael.ballesteros-garrido@uv.es

Contents

S1. General Conditions

Starting materials, if commercially available, were purchased and used as such. *N,N*-dimethylformamide (DMF), *N,N*-diethylformamide (DEF) and *N,N*-dibuthylformamide (DBF) were distilled before using. All reagent solutions were filtered through a 0.45 µm PTFE 25mm Syringe Filter. IR spectra were recorded using FT-IR ATR. Microscopic images were taken using Stereoscopic Microscope LEICA M165 FC and Fluorescence Optical Microscope LEICA DM IRBE. DRX powder spectra were performed on a BRUKER AXS D5005 powder diffractometer (Cu radiation, 40 kV, 30 mA, 0.05 steps, 6 s). Single-crystal X-ray diffraction (SXRD) data were collected on a Xcalibur diffractometer (Agilent Technologies, Sapphire 3 CCD detector) using a single wavelength X-ray source with MoKα radiation, λ = 0.71073 Å and also in a Bruker-Nonius Kappa CCD using a single wavelength X-ray source with MoKα radiation, λ = 0.71073 Å, and the data reduction was performed with Denzo software.[1] Diffuse Reflectance spectra were performed using an Agilent Technologies CARI60 UV-VIS Spectrometer and a Harrick Video-Barrelino Diffuse Reflection Probe. Elemental analyses were performed in a CE Instruments EA 1110 CHNS.

S2. Detailed Synthesis Conditions

Different conditions were applied in order to see differences in the final **TMOF** structure.

TMOF was obtained using DMF as solvent, at 80ºC or 95ºC and also using DEF at 80ºC. Using DEF at higher temperatures, DBF or DMF at 116ºC gave mixtures of amorphous **TMOF2**, **TMOF3** and **TMOF4**.

The overall yield was around 55±10%.

Table S1. TMOF synthesis conditions

[2]	$[Zn(NO_3)_2 \cdot 6H_2O]$	Solvent	Time	Temperature	Obtained MOF
40 mM	100 mM	DMF	72h	80 ºC	**TMOF**
40 mM	100 mM	DMF	72h	95 ºC	
40 mM	100 mM	DMF	72h	116 ºC	**TMOF3, TMOF4**
40 mM	100 mM	DEF	72h	80 ºC	**TMOF**
40 mM	100 mM	DEF	72h	95 ºC	**TMOF2**
40 mM	100 mM	DEF	72h	116 ºC	**TMOF3 TMOF4**
40 mM	100 mM	DBF	72h	80 ºC	
40 mM	100 mM	DBF	72h	95 ºC	

S3. Single Crystal X-ray Diffraction Analyses

Single-crystal X-ray diffraction (SXRD) data for **TMOF, TMOF2**, **TMOF3** and **TMOF4** were collected on a Xcalibur diffractometer (Agilent Technologies, Sapphire 3 CCD detector) using a single wavelength X-ray source with MoKα radiation, λ = 0.71073 Å. **Pyrene@TMOF** crystals data was collected in a Bruker-Nonius Kappa CCD using a single wavelength X-ray source with MoKα radiation, λ = 0.71073 Å, and the data reduction was performed with Denzo software.

The selected single crystals were mounted using Paratone-N hydrocarbon oil[2] on the top of a loop fixed on a goniometer head and immediately transferred to the diffractometer. Pre-

experiment, data collection, analytical absorption correction, and data reduction were performed with the Oxford program suite CrysAlisPro.[3] Empirical absorption correction was applied using spherical harmonics, implemented in SCALE3 ABSPACK scaling algorithm.

The data collection was performed at 120(1)K in all cases.

The crystal structures were solved with SHELXT[4], using direct methods and were refined by full-matrix least-squares methods on F^2 with SHELXL2014. All programs used during the crystal structure determination process are included in the OLEX2 software.[5]
The program PLATON[6] was used to check the results of the X-ray analyses. The electron densities corresponding to the disordered guest molecules of **TMOF2** and **Pyrene@TMOF1** were flattened using 'SQUEEZE'[7] option of PLATON.

The crystallographic details of both the MOFs are summarized in *Table S2*. CCDC 1532005-1532009 contains the supplementary crystallographic data for this paper. These data can be obtained free of charge from The Cambridge Crystallographic Data Centre via www.ccdc.cam.ac.uk/data_request/cif.

Table S2. Crystal data and structure refinement for **TMOF, TMOF2, TMOF3, TMOF4** and **Pyrene@TMOF**.

	TMOF	**TMOF2**	**TMOF3**	**TMOF4**	**Pyrene@TMOF**
Empirical formula	$C_{44.34}H_{51.66}N_{2.34}O_{17.66}Zn_4$	$C_{17}H_{18}NO_7Zn_2$	$C_{11}H_{12}N_{0.33}O_{5.33}Zn$	$C_{10}H_{12}O_{4.75}Zn$	$C_{10}H_{12}O_4Zn$
Formula weight	1161.37	479.06	299.55	273.57	261.59
Temperature/K	120.0(1)	120.0(1)	120.0(1)	120.0(1)	120.0(1)
Crystal system	monoclinic	trigonal	monoclinic	monoclinic	monoclinic
Space group	P2/n	$P3_121$	P2/c	I2/a	C2/c
a/Å	6.1341(4)	12.7557(5)	10.2596(5)	6.1355(4)	6.1210(2)
b/Å	19.5931(11)	12.7557(5)	10.3121(3)	13.0213(7)	19.5910(9)
c/Å	19.6981(13)	30.6370(8)	11.9721(6)	14.8255(7)	19.6970(7)
α/°	90	90	90	90	90
β/°	90.564(6)	90	107.106(5)	91.798(5)	90.675(2)
γ/°	90	120	90	90	90
Volume/Å³	2367.3(3)	4317.1(3)	1210.6(1)	1183.86(12)	2361.83(16)
Z	2	6	4	4	8
ρ_{calc}g/cm³	1.629	1.106	1.644	1.535	1.471
μ/mm⁻¹	2.078	1.692	2.040	2.074	2.070
F(000)	1191.0	1458.0	612.0	560.0	1072
2Θ range	6.23 to 50	6.38 to 50	5.73 to 52.98	7.34 to 52	4.14 to 50
Radiation				0.71073	
Refl. collected	8422	12519	5962	2838	3904
Independent refl.	4129	5069	2491	1166	2078
R_{int}	0.0698	0.0543	0.0494	0.0391	0.044
restraints/param	49/400	177/314	88/237	6/110	37/199
GOF	1.065	1.020	1.148	1.069	1.102
R_1, wR_2[I>=2σ (I)]	0.0999, 0.2664	0.0557, 0.1463	0.0773, 0.2046	0.0385, 0.0925	0.0707, 0.2119
R_1, wR_2[all data]	0.1222, 0.2865	0.0668, 0.1548	0.0832, 0.2087	0.0432, 0.0975	0.0801, 0.2302

TMOF

A colourless, block crystal (0.38 x 0.14 x 0.14 mm) of $[Zn_2(C_{10}H_{12}O_4)_2]\cdot(DMF)_{1.667}$, was measured at 120(1) K using MoKα radiation, λ = 0.71073 Å.
The structure was solved by direct methods with SHELXT and was refined with SHELXL in the monoclinic space group *P*2/*n* with *Z* = 2.

The crystal structure exhibits a three-dimensional framework with wide open channels of approximately 4.4 × 4.1 Å running along the crystallographic *a* axis. Most of the structure is disordered over two sets of positions since it lies about several symmetry elements, inversion centres, two-fold axes and mirror planes.

Some soft SHELXL restraints (DELU, ISOR) had to be used to correct the geometry of the disordered parts and the thermal parameters of the corresponding atoms. Hydrogen positions were calculated after each cycle of refinement using a riding model, with C-H = 0.97 Å and Uiso(H) = 1.2Ueq(C). The presence of solvent molecules could easily be seen by the residual peaks located in the open channels. There are two different DMF molecules. One of them has occupancy of 0.5 and the other one has occupancy of 0.33. These solvent molecules are located on a C2 axis and they have two different orientations.

One of the 1,4-bicyclo[2.2.2]octane-1,4-dicarboxylic acid units is disordered with two different positions for the carbon atoms of the cycle due to a rotation around its central axis and has been modelled with an occupancy of 0.5 for each carbon atom.

The final refinement was conducted with the reflection data within a 0.80 Å resolution limit, a total of 8422 reflections of which 4129 were independent and 3008 were greater than 2σ(*I*). Final full matrix least-squares refinement on *F*2 converged to *R*1 = 0.0999 and *wR*2 = 0.2865 (*I*>2σ(*I*)) with GOF = 1.065. Crystallographic data and additional details of data collection and refinement are summarized in Table S2. Drawings with atomic labels are represented in *Figure S1*.

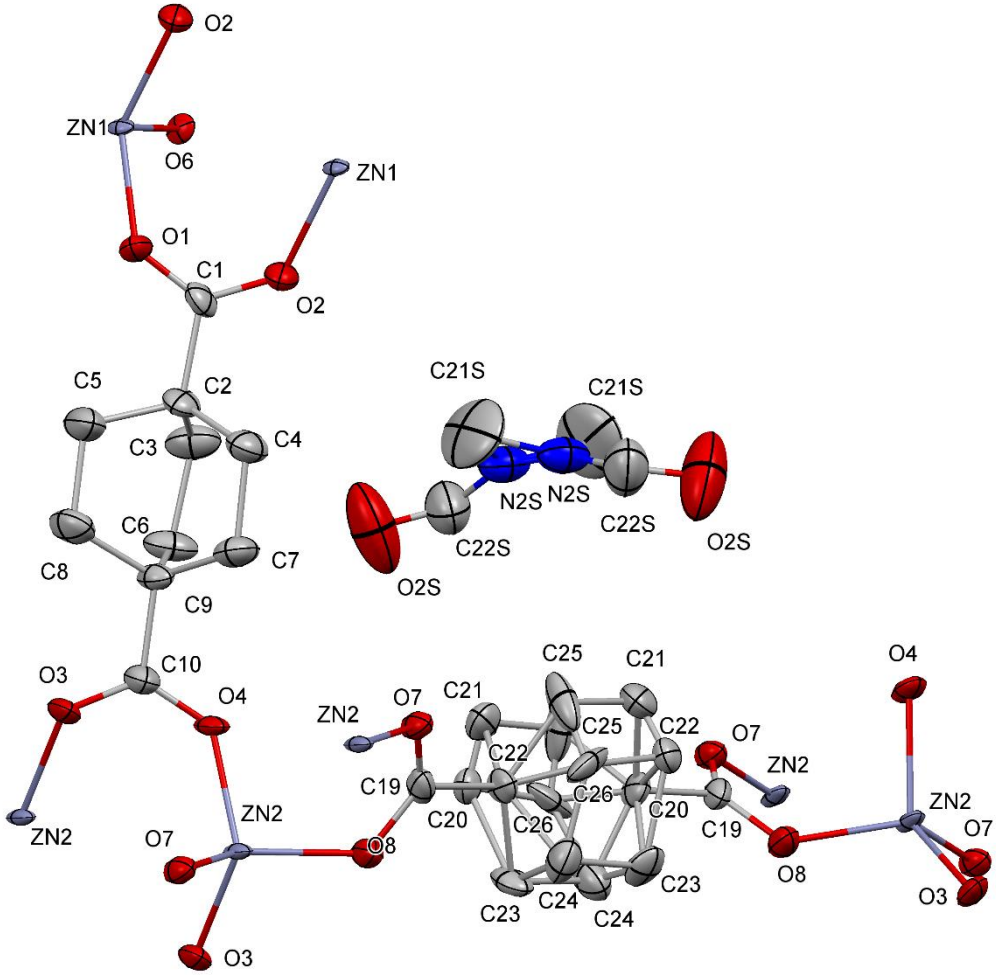

Figure S1. The building block including the asymmetric unit present in crystalline **TMOF** with all non–hydrogen atoms represented by thermal ellipsoids drawn at the 50% probability level. All hydrogen atoms were omitted for clarity.

TMOF2

A colourless, hexagonal crystal (0.73 x 049 x 0.44 mm) of $[Zn_2O(C_{10}H_{12}O_4)\ (C_{10}H_{12}O_4)_{0.5}(DEF)_{0.5}]\ (DEF)_{0.4}$ was measured at 120(1) K using MoKα radiation, λ = 0.71073 Å.

The structure was solved by direct methods with SHELXT and was refined with the SHELXL software package (*S3*), crystallized in the trigonal*P3121* space group with *Z* = 6.

The crystal structure exhibits a three-dimensional framework with wide open channels of approximately 13.2×6.1 $Å^8$ running along the crystallographic *a* and *b* axis, and also along the bisection of both axes. Most of the structure is disordered over two sets of positions since it lies about several symmetry elements.

One of the 1,4-bicyclo[2.2.2]octane-1,4-dicarboxylic acid units is disordered with two different positions. These units also have to different positions for the carbon atoms of the cycles due to a rotation around its central axis. They have been modelled with occupancy of 0.5 and 0.25 for each carbon atom. The oxygen atoms (O3 and O4) of the carboxylate group have occupancy of 0.5.

One of the Zinc atoms (Zn2) is coordinated with a disordered DMF molecule with occupancy of 0.5

Some soft *SHELXL* restraints (*DELU*, *ISOR*, *SIMU*) had to be used to correct the geometry of the disordered parts and the thermal parameters of the corresponding atoms. Hydrogen positions were calculated after each cycle of refinement using a riding model, with C-H = 0.93 Å and *U*iso(H) = 1.2*U*eq(C) for aromatic H atoms, and with C-H = 0.97 Å and *U*iso(H) = 1.2*U*eq(C) for methyl H atoms.

The presence of solvent molecules in the channels could easily be seen by the residual peaks located in the open channels. Unfortunately, they were disordered so badly that it could not be modelled even with restraints and there were too many A alerts in the Checkcif (without solvent molecules: *R*1 = 0.115 for 2492 reflections of $I > 2\sigma(I)$ and *wR*2 = 0.360 for all data). Consequently, SQUEEZE (from PLATON) was used to calculate the void space, the electron count and to get a new *HKL* file (With SQUEEZE: *R*1 = 0.0557 for 2492 reflections of $I > 2\sigma(I)$ and *wR*2 = 0.1548 for all data). According to the SQUEEZE results and the different experimental evidences (see manuscript), a total number of 0.7 *N*,*N*-diethylformamide (DEF) solvent molecules (39 electrons) was considered per unit cell. The volume fraction was calculated to 1683.1 $Å^3$ which corresponds to 39% of the unit cell volume, and to 39 electrons per unit cell allocated to solvent molecules (0.4 molecules of DEF).

Crystallographic data and additional details of data collection and refinement are summarized in *Table S2*. Drawings with atomic labels are represented in *Figure S2*.

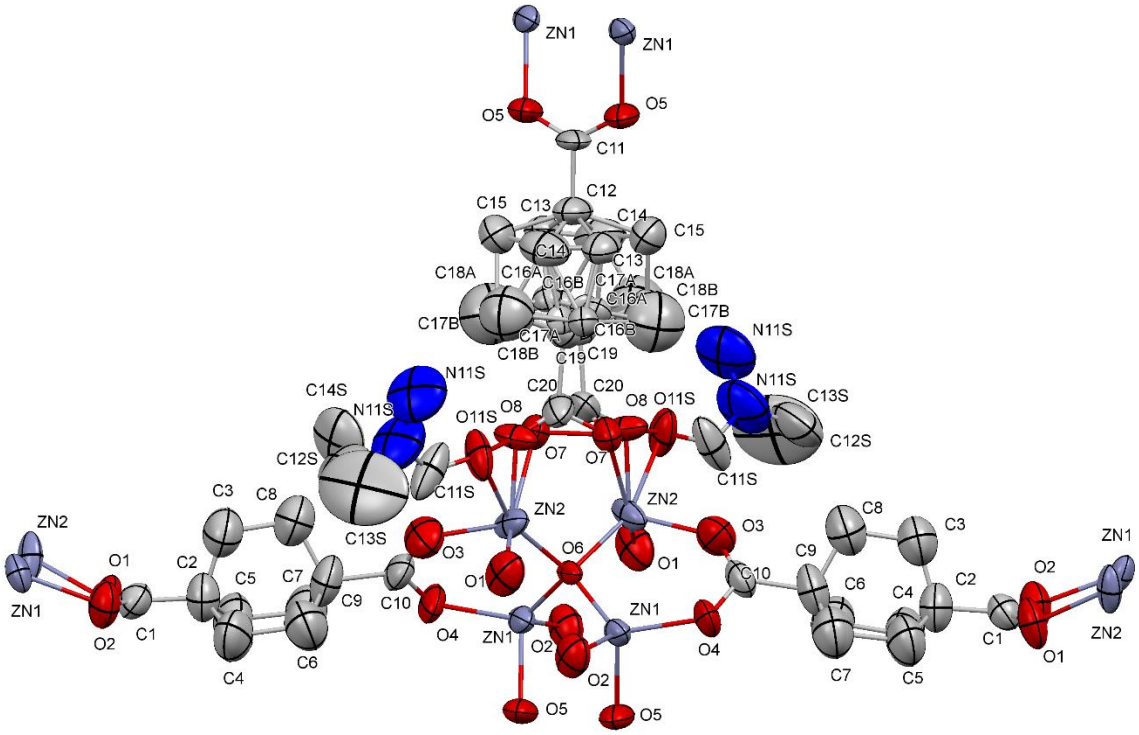

Figure S2. The building block including the asymmetric unit present in crystalline **TMOF2** with all non–hydrogen atoms represented by thermal ellipsoids drawn at the 50% probability level. All hydrogen atoms were omitted for clarity

TMOF3

A colourless, laminar crystal (0.4 × 0.23 × 0.15mm) of $[Zn(C_{10}H_{12}O_5)]\cdot(DMF)_{0.33}$, was measured at 120(1) K using MoKα radiation, λ = 0.71073 Å.

The structure was solved by direct methods with SHELXT and was refined with the SHELXL software package (*S3*), in the monoclinic space group *P*2/*c* with *Z* = 4.

The crystal structure exhibits a three-dimensional framework with wide open channels of approximately 4.5 × 4.4 Å running along the crystallographic *c* axis. Most of the structure is disordered over two sets of positions since it lies about several symmetry elements, inversion centers, two-fold axes and mirror planes.

Some soft SHELXL restraints (DELU, ISOR) had to be used to correct the geometry of the disordered parts and the thermal parameters of the corresponding atoms. All hydrogen positions were calculated after each cycle of refinement using a riding model, with C-H = 0.97 Å and Uiso(H) = 1.2Ueq(C). The presence of solvent molecules could easily be seen by the residual peaks located in the open channels. There is a disordered DMF solvent molecule placed in the middle of the channels with occupancy of 0.33. These solvent molecules located on a glide plane and it has two different orientations.

The 1,4-bicyclo[2.2.2]octane-1,4-dicarboxylic acid units are disordered with two different positions for the carbon atoms of the cycles due to a rotation around its central axis. They have been modelled with occupancy of 0.5 for each carbon atom. Also the oxygen atoms (O3 and O4) of a carboxylate group have two possible locations.

The final refinement was conducted with the reflection data within a θ_{max} = 26.5° resolution limit, a total of 5962 reflections of which 2491 were independent and 2224 were greater than 2σ(*I*). Final full matrix least-squares refinement on F^2 converged to *R*1 = 0.0773 and *wR*2 = 0.2087 with GOF = 1.148. Crystallographic data and additional details of data collection and refinement are summarized in *Table S2*. Drawings with atomic labels are represented in *Figure S3.*

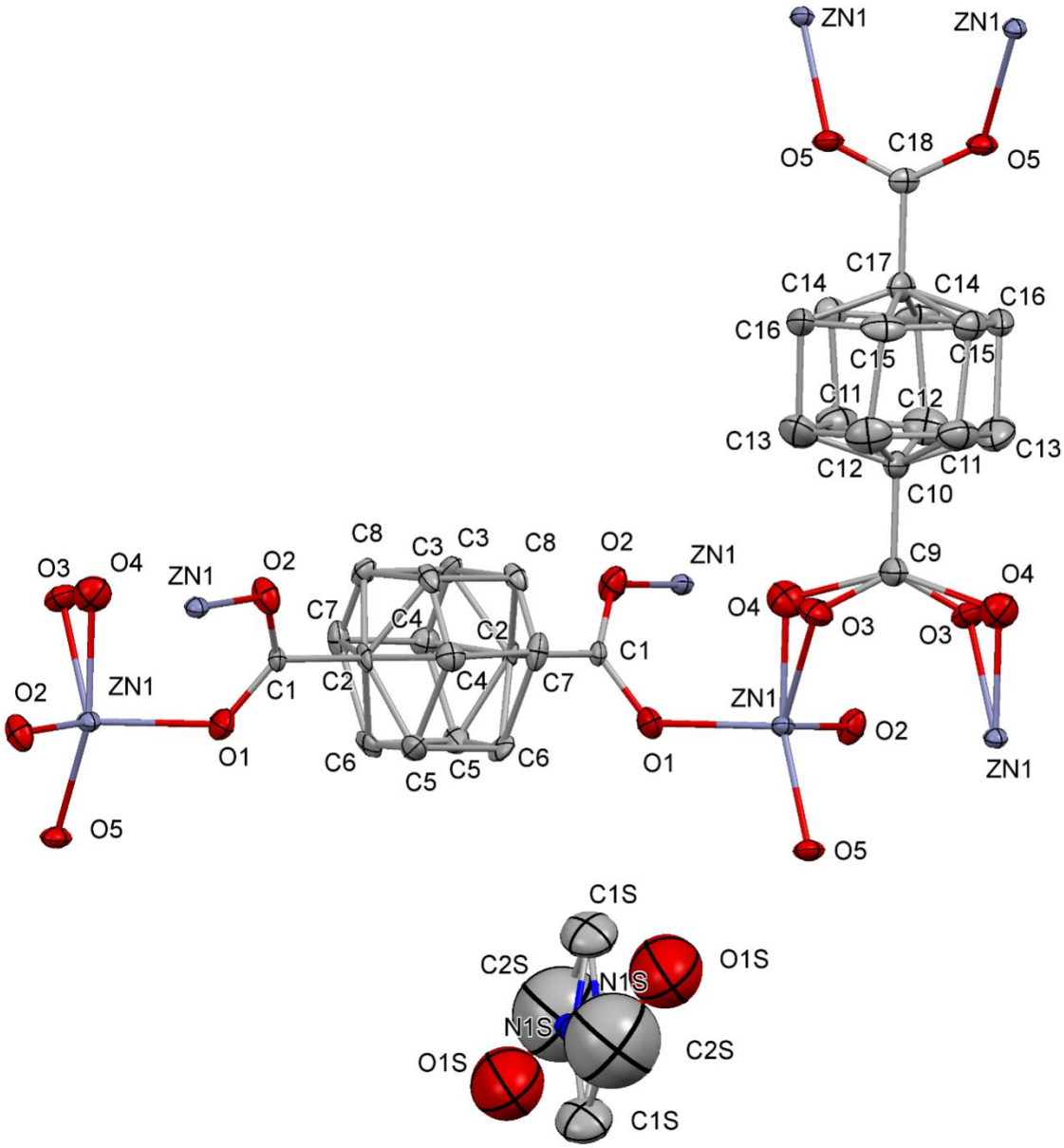

Figure S3. The building block including the asymmetric unit present in crystalline **TMOF3** with all non–hydrogen atoms represented by thermal ellipsoids drawn at the 50% probability level. All hydrogen atoms were omitted for clarity.

TMOF4

A colourless, laminar crystal (0.29 × 0.13 × 0.09mm) of $[Zn(C_{10}H_{12}O_4)]\cdot(H_2O)_{0.65}$, was measured at 120(1) K using MoKα radiation, λ = 0.71073 Å.

The structure was solved by direct methods with SHELXT and was refined with the SHELXL software package (*S3*), in the monoclinic space group *I*2/*a* with *Z* = 4.

The crystal structure exhibits a three-dimensional framework with wide open channels of approximately 3.7 × 3.7 Å running along the crystallographic *a* axis.

All hydrogen positions were calculated after each cycle of refinement using a riding model, with C-H = 0.97 Å and Uiso(H) = 1.2Ueq(C). The presence of solvent molecules could easily be seen by the residual peaks located in the open channels. There are two water molecules placed in the middle of the channels with occupancy of 0.125 and 0.25. The hydrogen atoms of the water molecules have not been located.

The 1,4-bicyclo[2.2.2]octane-1,4-dicarboxylic acid is disordered with two different positions for the carbon atoms of the cycle due to a rotation around its central axis. They have been modelled with occupancy of 0.5 for each carbon atom.

The final refinement was conducted with the reflection data within a θ_{max} = 26.0° resolution limit, a total of 2838 reflections of which 1166 were independent and 1055 were greater than 2σ(*I*). Final full matrix least-squares refinement on F^2 converged to *R*1 = 0.0384 and *wR*2 = 0.0981 with GOF = 1.073. Crystallographic data and additional details of data collection and refinement are summarized in *Table S2*. Drawings with atomic labels are represented in *Figure S4*.

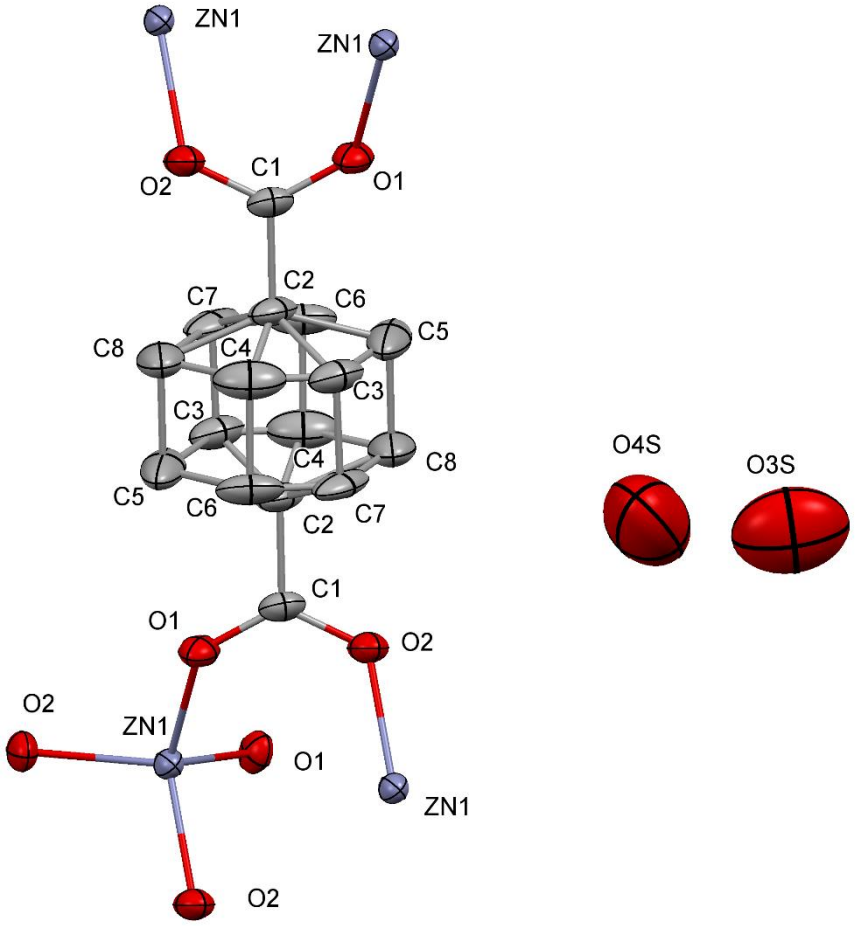

Figure S4. The building block including the asymmetric unit present in crystalline **TMOF4** with all non–hydrogen atoms represented by thermal ellipsoids drawn at the 50% probability level. All hydrogen atoms were omitted for clarity.

Pyrene@TMOF

A colorless, block crystal (0.4 × 0.2 × 0.2mm) of $[C_{10}H_{12}O_4Zn)]$(Solvent), was measured at 120(1) K using MoKα radiation, λ = 0.71073 Å.

The structure was solved by direct methods with SHELXT and was refined with the SHELXL software package (*S3*), in the monoclinic space group *C*2/*c* with *Z* = 8.

The crystal structure exhibits a three-dimensional framework with wide open channels of approximately 4.6 × 4.1Å running along the crystallographic *a* axis. Most of the structure is disordered over two sets of positions since it lies about several symmetry elements, inversion centers, two-fold axes and mirror planes.

Some soft SHELXL restraints (DELU, ISOR) had to be used to correct the geometry of the disordered parts and the thermal parameters of the corresponding atoms. All hydrogen positions were calculated after each cycle of refinement using a riding model, with C-H = 0.97 Å and Uiso(H) = 1.2Ueq(C). The presence of host molecules in the open channels could not be due to the great disorder of the electronic density points. This could indicate the presence of disordered DMF molecules and pyrene molecules. Consequently, SQUEEZE (from PLATON) was used to calculate the void space, the electron count and to get a new *HKL* file. According to the SQUEEZE the total volume of the voids per unit cell is 436 $Å^3$ (18%) and the total number of electrons placed in the voids is 354 electrons.

The two different 1,4-bicyclo[2.2.2]octane-1,4-dicarboxylic acid units are disordered with two different positions for the carbon atoms of the bicycles due to a rotation around its central axis in one of them or because the bicyclic atoms had two different possible positions. They have been modelled with occupancy of 0.5 for each carbon atom.

The final refinement was conducted with the reflection data within a θ_{max} = 25° resolution limit, a total of 3904reflections of which 2078 were independent and 1837 were greater than 2σ(*I*). Final full matrix least-squares refinement on F^2 converged to *R*1 = 0.0707 and *wR*2 = 0.2302 with GOF = 1.188. Crystallographic data and additional details of data collection and refinement are summarized in *Table S2*. Drawings with atomic labels are represented in *Figure S5*.

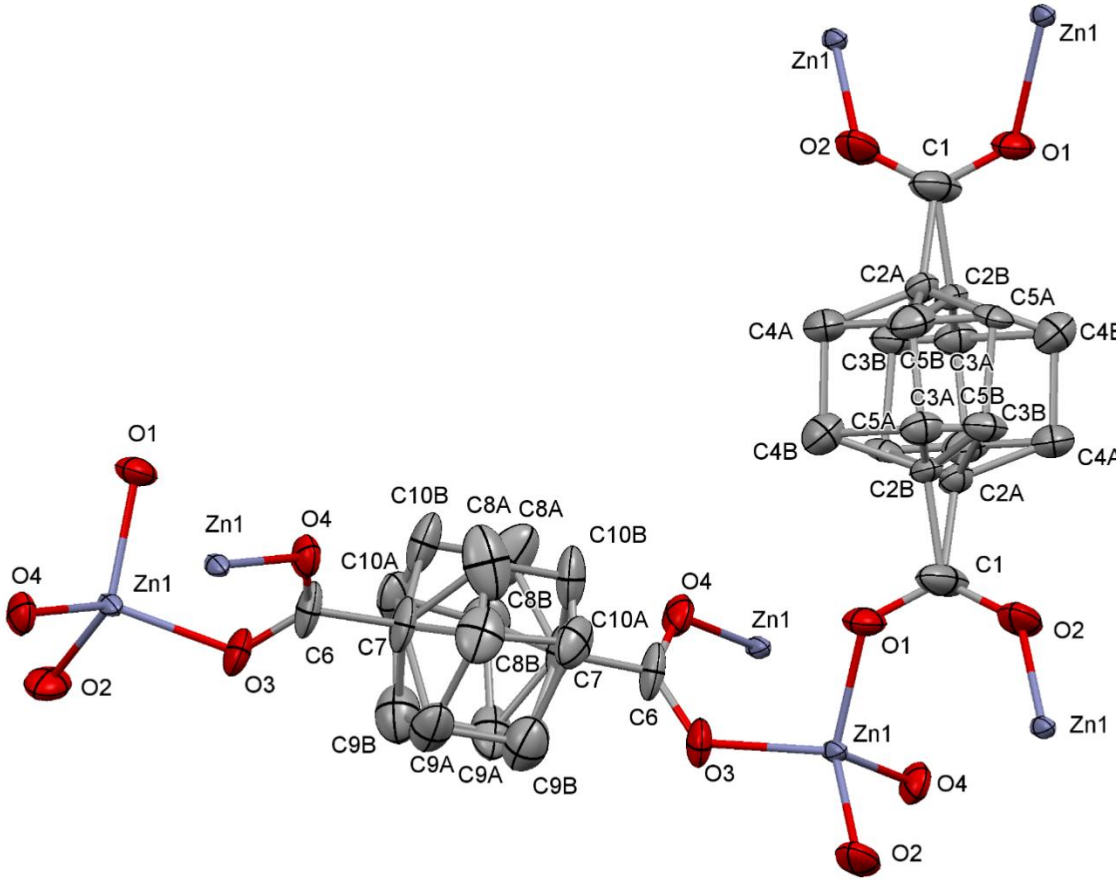

Figure S5. The building block including the asymmetric unit present in crystalline **Pyrene@TMOF** with all non–hydrogen atoms represented by thermal ellipsoids drawn at the 50% probability level. All hydrogen atoms were omitted for clarity.

S4. Infrared Spectra

Infrared spectra of byciclo[2.2.2]octane-1,4-dicarboxylic acid (**2**), **TMOF**, pyrene and **Pyrene@TMOF** are shown.

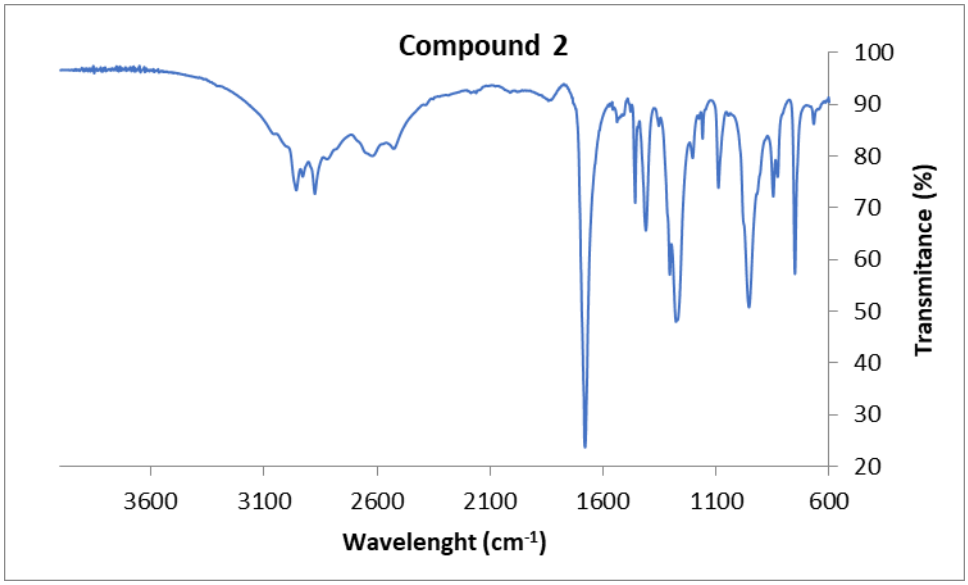

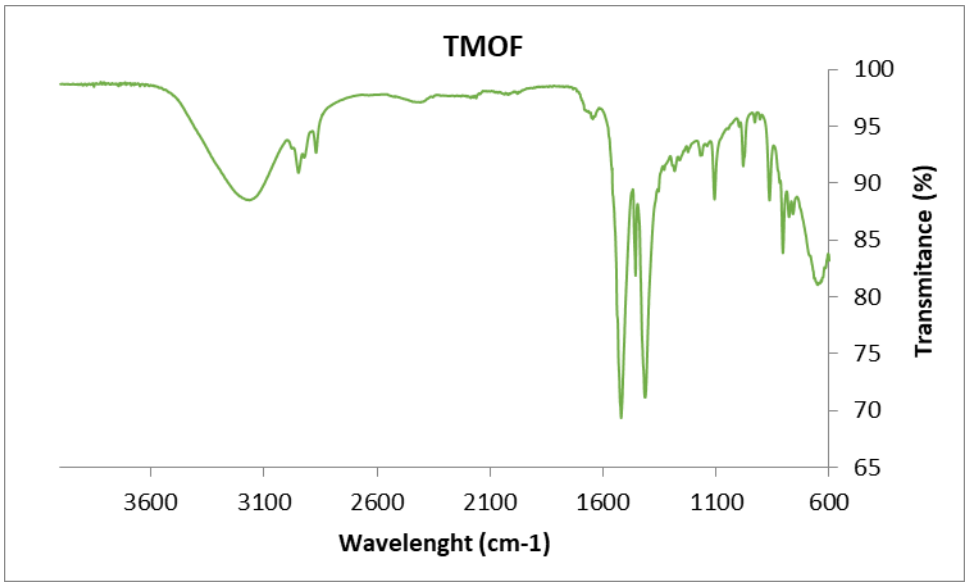

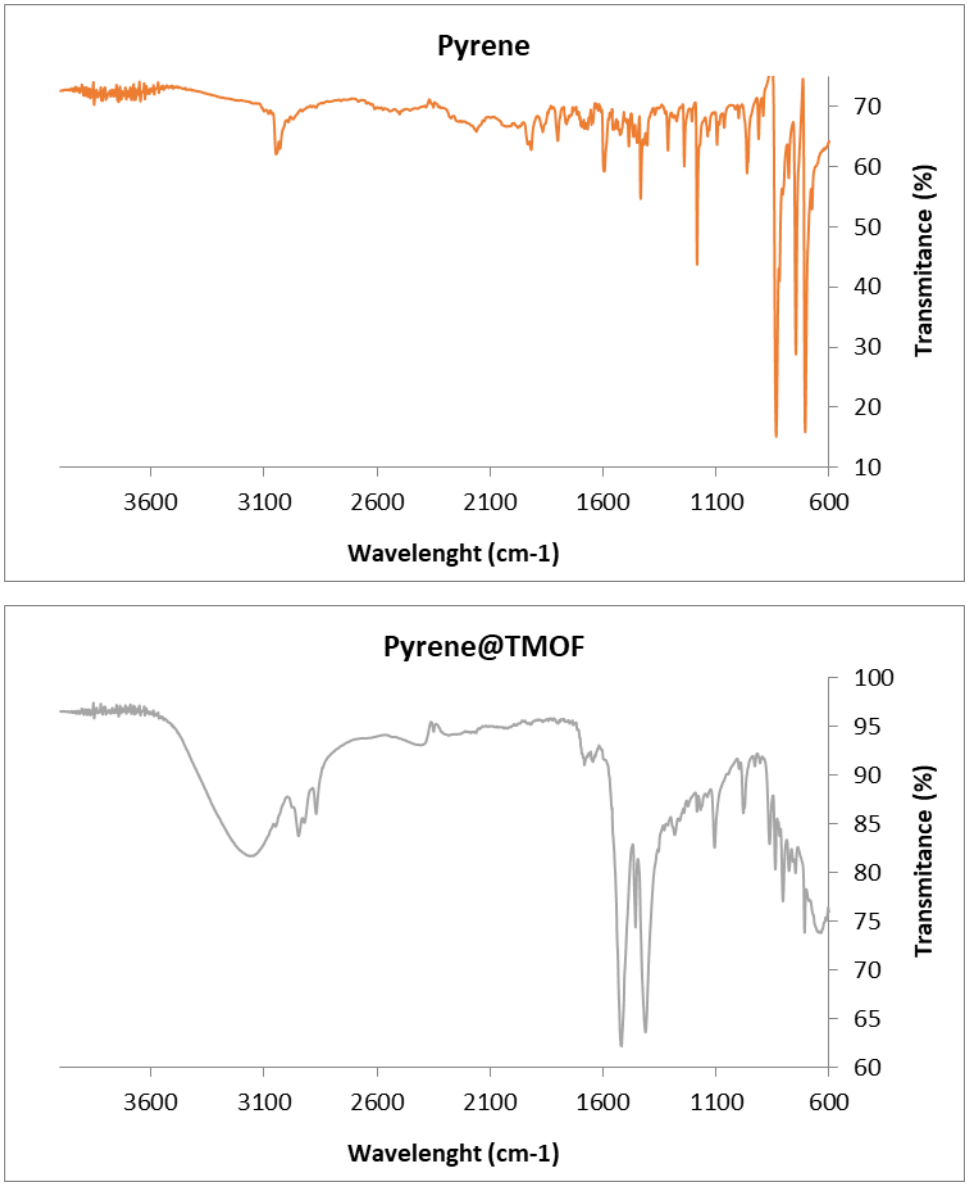

Figure S6. Infrared spectrum of byciclo[2.2.2]octane-1,4-dicarboxylic acid (**2**), **TMOF**, pyrene **and Pyrene@TMOF**.

S5. Microscope Images

Microscopic images (*Figure S7 a-d*) and Fluorescence Microscopic images (*Figure S7 e-h*) of **TMOF** and **Pyrene@TMOF** are shown. Presence of pyrene inside the structure of **TMOF** was confirmed by comparison of fluorescence emission of **TMOF** (e-f) and fluorescence emission of **Pyrene@TMOF** (g-h), showing an increase of this emission.

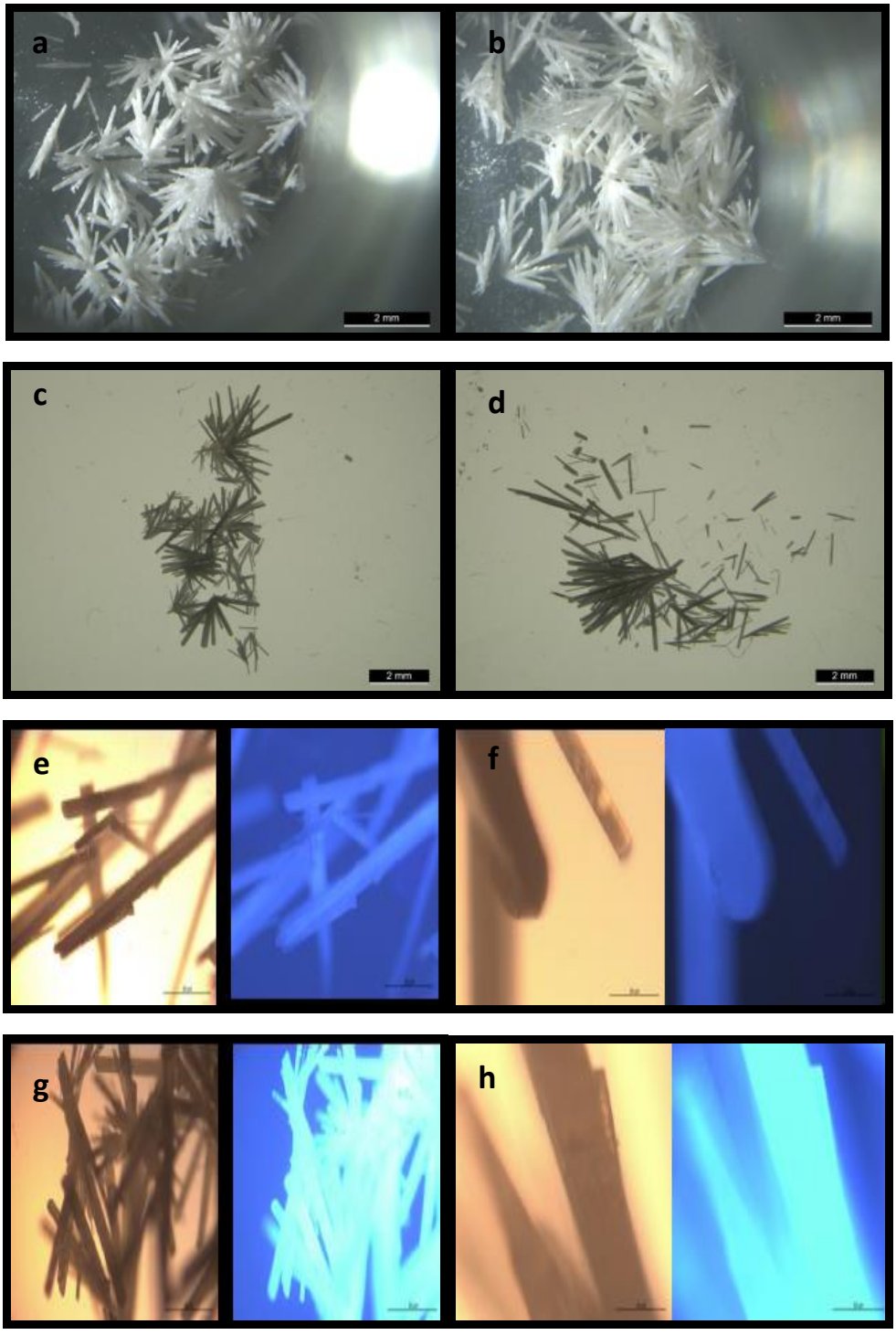

Figure S7. Microscopic images of activated (a-b) and non-activated (c-d) needles of **TMOF** taken by Stereoscopic Microscope. Microscopic images of **TMOF** (e-f) and **Pyrene@TMOF** (g-h) taken with Fluorescence Optical Microscope with and without wavelenght filter.

S6. Elemental Analysis

In order to figure out if pyrene molecules were introduced into the cavities of TMOF, elemental analysis of both **TMOF** and **Pyrene@TMOF** were carried out. This experiment did not report any conclusion because concentration of pyrene into TMOF resulted about 10^{-3} m, being difficult to observe changes in elemental analysis.

Table S3. Elemental analysis

Sample	Nitrogen	Carbon	Hydrogen
Pyrene@TMOF	0.16%	40.13%	4.67%
	0.21%	40.26%	4.13%
TMOF	0.14%	40.32%	5.00%
	0.15%	40.38%	4.85%

1) Z. Otwinowski and W. Minor, *Methods Enzymol.*, **1997**, *276*, 307.

2) H. Hope, *Acta Cryst.*, **1988**, B44, 22.

3) Agilent (**2014**). *CrysAlis PRO*. Agilent Technologies Ltd, Yarnton, Oxfordshire, England.

4) G.M. Sheldrick, *Acta Cryst.*, **2015**, *A71*, 3.

5) O.V. Dolomanov, L.J. Bourhis, R.J. Gildea, J.A.K. Howard, H. Puschmann, J. Appl. Cryst., **2009**, *42*, 339.

6) A.L. Spek, *Acta Cryst.*, **2009**, *65*, 148.

7) A.L. Spek, *Acta Cryst.*, **2015**, 71, 9

8) A van der Waals radius of C (1.70 Å) was used in determination of distance parameters. (A. Bondi, *J. Phys. Chem.,* **1964**, *68*, 441).

Capítulo 11

Dalton Transactions submitted (MOF-5/IRMOF-3)

[Paper under submission]

Empirical modeling material composition and size in MOF-5/IRMOF-3 mixtures

Pedro J. Llabrés-Campaner,[a] Ramón José Zaragozá,[a] Maria Jose Aurell,[a] Rafael Ballesteros,[a] Belén Abarca,[a] Enrique Garcia-España,[b] Guillermo Rodrigo,[c] and Rafael Ballesteros-Garrido[a,b,c,*]

[a.] *Departament de Química Orgànica, Universitat de València, Av. Vicent Andrés Estellés s/n, 46100 Burjassot, Spain.*
[b.] *Instituto de Ciencia Molecular (ICMOL), Universitat de València, c/ Cat. José Beltrán 2, 46980 Paterna, Spain.*
[c.] *Instituto de Biología Integrativa de Sistemas (I2SysBio), Universitat de València – CSIC, c/ Cat. Agustín Escardino 9, 46980 Paterna, Spain.*
[*] *Send correspondence to rafael.ballesteros-garrido@uv.es*

Abstract

Systematic analyses on the composition and size of metal-organic frameworks built with Zn_4O and terephthalic/amino-terephthalic acid mixtures, together with a kinetic assay, highlight how these ligands behave differently, which reveals the complexity of crystal growth in these frameworks and the ability to tune it on purpose.

Metal-organic frameworks (MOFs)[1] are porous crystalline materials with unique properties for gas storage,[2] separation,[3] or catalysis.[4] In addition, its porosity has been also exploited to develop molecular gates,[5] encapsulate relevant biomolecules,[6] or even perform chromatographic separations.[7] The most common technique to obtain these structures consists in solvothermal crystal growth. MOF size is usually in the scale of micrometers; notwithstanding, some materials have been reported to grow up to the macroscopic scale (millimeters).[7,8] This fact establishes a new difference between MOFs and further synthetic porous materials of wide use, such as zeolites or MCM-41[9]. Certainly, the ability to create macroscopic nanostructured materials is an important challenge that may boost novel applications.

However, the construction of such three-dimensional networks is an extremely complex process that depends on several parameters. The synthesis of **MOF-5** [$Zn_4O(BDC)_3$], also known as **IRMOF-1**, is prepared with 1,4-benzene dicarboxilyc acid (BDC)[10] —in the following ligand **1**— and usually performs with dimethyl formamide (DMF). This yields microcrystals (*Fig. 1a*), i.e., materials in the scale of micrometers. By contrast, the use of diethyl formamide (DEF), also acceptable in this case, leads to millimetric cubes.[7,11] In addition to the medium, small chemical modifications of the ligand impact on the final size too. Previous work revealed the viability of obtaining **MOF-5**-like structures with up to 8 different ligands.[11] Interestingly, the use of 2-amino terephthalic acid —in the following ligand **2**— together with Zn_4O leads to crystals in the scale of millimetres with DMF (*Fig. 1b*), known as **IRMOF-3**.[11] Therefore, the ratio between the sizes of **IRMOF-3** and **MOF-5** appears to be larger than one order of magnitude with DMF.

Because **MOF-5** and **IRMOF-3** represent a pair of nanostructured materials with almost equal composition and geometry, herein we explored the possibility of creating heterogeneous materials by employing mixtures of ligand **1** and **2**. Mixed-ligand MOFs have already been created and studied,[11c,12] but the final composition and functionality of the material may result unpredictable. Through an experimental approach of systematic mixing, we wondered whether the resulting crystals span over a broad range in terms of size (functionality), trying to infer afterwards a simple, but predictive empirical model (*Fig. 1c*).

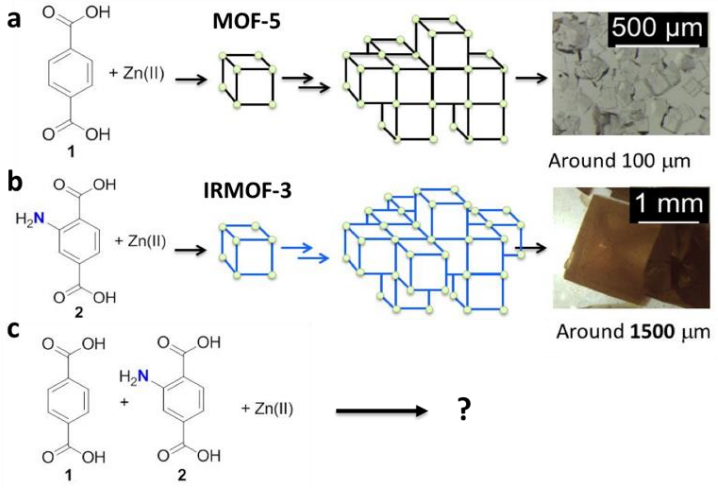

Figure 1. Reaction schematics for material preparation, highlighting the macroscopic differences between a) **MOF-5** and b) **IRMOF-3**. c) Question addressed in this work.

To shed light on how differently the two MOFs grow, we first performed a kinetic study. Despite their relevance to gain chemical insight, these studies are scarce in the field.[13] **MOF-5** crystals started to be observable at 12-14 hours; however, it took more time (24-48 hours) for **IRMOF-3** crystals (*Fig. 2 inset*). More precisely, we measured with time the remaining amount of Zn(II) in solution during material formation (*Fig. 2*). Our data were roughly described with an

exponential decay model (Eq. 1). In the case of **MOF-5**, we fitted $k = 0.122 \pm 0.044$, while in the case of **IRMOF-3**, $k = 0.094 \pm 0.046$ (k denotes the kinetic constant, in h^{-1}). Although the difference between both kinetics appears to be statistically non-significant, the faster assembly of Zn(II)–ligand **1** is supported by the higher Zn(II) consumption at 16 hours for **MOF-5** and the visual observation of these crystals already at that time. Arguably, **MOF-5** crystals are expected to be smaller than **IRMOF-3** crystals because, at least in part, many more macroscopic nucleation seeds appear, yielding a larger amount of **MOF-5** crystals, as observed.

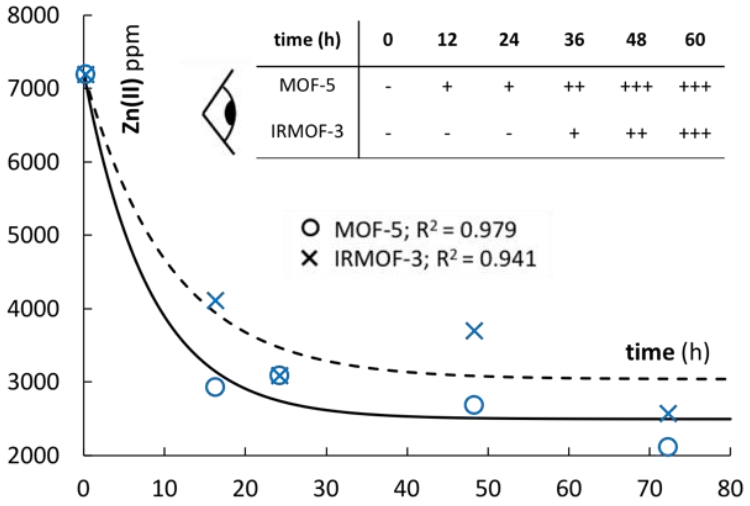

time (h)	0	12	24	36	48	60
MOF-5	-	+	+	++	+++	+++
IRMOF-3	-	-	-	+	++	+++

Figure 2. Visual observation of crystal appearance (inset: + indicates qualitative observation, - no crystals) and time-dependent Zn(II) amount in solution during MOF growth. Solid and dashed lines fit data. See ESI S5 for exact ICP values and errors.

To investigate the formation of mixed-ligand MOFs, we prepared under the same conditions a series of samples with different concentrations of ligand **1** and **2** (*Table 1*), maintaining constant the total ligand amount (in DMF, see ESI). Crystalline structure was verified for all engineered materials by PXRD (*Fig. 3a*) after activation. The same pattern was observed in all cases, but with variations in intensity. Careful examination of PXRD indicated that interpenetration was present in samples containing more than 50% of ligand **2** (see Fig. S16 in ESI). However, a sample with 20% presented distinctive relative heights of the peaks at 6.8º and 13.8º for an interpenetrated MOF.[14] The quality of **IRMOF-3** PXRD was low; a large-scale synthesis (10 fold) gave acceptable PXRD with reduced noise (Fig. S17). Moreover, we observed that the activation process broke the large crystals. To extract direct information, we decided to perform direct PXRD of MOFs immersed in DMF (after three rounds of solvent exchange). In Fig. 3c, PXRDs of **MOF-5** (activated), **MOF-5** calculated from ciff file,[10] and DMF-immersed **MOF-5** are presented. As it was seen, the former pattern is the simplest. This experience was repeated for all samples and again similar spectra were obtained, confirming the constant structure. Only pure **IRMOF-3** presented extra bands at 17º and 25º. Those differences might be induced by a specific phase growth, as already reported for other MOFs with large size (Fig. S18).[15]

Table 1 reports the ligand distribution employed in each of the 11 samples, together with the yield obtained. Each condition was repeated 10 times. We observed similar yields in all samples (around 50%). Of note, we found a distinctive ligand distribution within the crystals, which did not correspond to the distribution of the reagent mixture. Indeed, following a plot comparing the initial and within-crystal concentration of ligand **2** (as a ratio, denoted by x_0 and x, respectively), we observed a clear deviation from linearity (*Fig. 3b*). To model this behavior,

we introduced the incomplete beta function[16] (β; Eq. 2). Thus, we have x = β (x_0|a,b), where *a* and *b* are two control parameters. We fitted *a* = 0.487 and *b* = 0.479 by nonlinear regression, obtaining a curve that described well our data (*Fig. 3b*). This model resulted statistically significant with respect to the null model x = x_0 (Snedecor's F-test, *P* < 10-3). Under different growth conditions, this trend may change, as derived from previous data[11c] (i.e., without inflexion point). In this case, the β function, which is very plastic, is still valid to capture the behavior with other parameter values (see ESI).

Table 1. Reagent concentrations for crystal growth, yield of the process, ligand ratio, and resulting size (each condition was repeated 10 times).

[Zn^{2+}] (μM)	[**1**] (μM)	[**2**] (μM)	Yield[a] (%)	[**2**] / ([**1**]+[**2**]) (%)		Size[c] (mm)
				Initial	Within[b]	
100	78.3	0	55	0	0	0.101
100	70.5	7.8	53	10	23.1	0.129
100	62.6	15.7	57	20	33.3	0.243
100	54.8	23.5	62	30	37.5	0.383
100	47.0	31.3	56	40	41.2	1.151
100	39.2	39.2	54	50	47.4	1.118
100	31.3	47.0	53	60	50	1.116
100	23.5	54.8	51	70	61.5	1.165
100	15.7	62.6	51	80	72.2	1.380
100	7.8	70.5	48	90	83.3	1.376
100	0	78.3	47	100	100	1.534

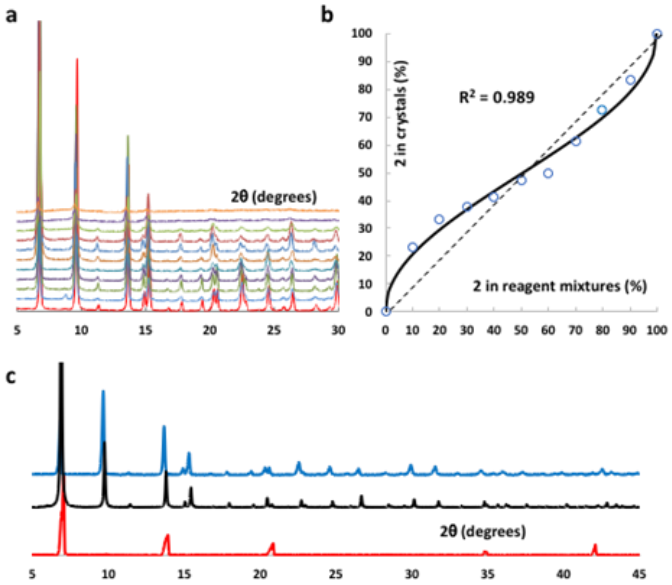

Figure 3. a) PXRD patterns of all materials. b) Within-crystal vs. initial concentration of ligand **2** (as a ratio, open circles). Solid line fits data, while dashed line is the linear trend. c) PXRD of activated **MOF-5** (blue), calculated from **MOF-5** ciff (black), and DMF-immersed **MOF-5** (red).

At this point, it is important to note that MOFs grow distinctively.[11,13] In first place, different metal-organic aggregates are created to form nanostructures[13b] and, in second place, these nanostructures combine each other, in addition to layered growth,[13a] to end with macroscopic crystals. According to our data, ligand **2** was in excess within the crystals regarding the reaction

stoichiometry when ligand **1** dominates the reagent mixture. However, ligand **2** was in defect within the crystals when this ligand dominates the mixture. Arguably, a difference in crystal emergence (metal-ligand assembly kinetics), together with ligand exchange processes[12a], may underlie this behavior. By means of a rough theoretical model and calculations (Fig. S4), both processes revealed similar energies (1 Kcal/mol difference, see ESI), which indicates that both can take place at the same time. This is in coherence with the observed results.

Subsequently, all 11 samples were examined by optical microscopy to obtain images of the resulting materials, finding that size changes with the ligand ratio (see ESI). We measured the edge sizes of the different crystalline cubes (values summarized in *Table 1*). In our hands and in agreement with previous observations, **MOF-5** grew to form transparent cubes of 0.1 mm edge (only ligand **1**). **IRMOF-3** grew, by contrast, to form yellowish cubes of 1.1-1.8 mm edge (only ligand **2**). With ligand mixtures, we found intermediate sizes of the resulting cubes. The whole experience was reproduced twice to verify this trend; similar results in crystal size were obtained. Crystal edge size (*y*) was plotted against ligand ratio (*x*), revealing a logistic trend in the logarithmic scale (Eq. 3), as this property spans over one order of magnitude (*Fig. 4a*). Indeed, this was statistically significant (Snedecor's F-test, $P < 10\text{-}3$) with respect to a null linear model, $y = y_{min} + (y_{max} - y_{min})x$. In our case, we fitted by least squares $x_{50} = 36.7\%$ and $n = 33.3$ over average values, with $y_{min} = 0.111$ mm and $y_{max} = 1.286$ mm. Parameter x_{50} describes the transition between crystals of small size and crystals of large size. In materials in which ligand **2** satisfies $x < x_{50}$, edge size was smaller than 0.3 mm, and the resulting cubes were totally transparent. In addition, when $x >> x_{50}$ (i.e., ligand **2** from 61.5 to 100%), we observed transparent yellowish cubes with edge size larger than 1 mm. However, in the transition range (i.e., from 37.5 to 50%, when x is around x_{50}), heterogeneous crystals in terms of transparency were observed systematically, and the variability in size was higher. We hypothesized that the existence of clusters, as previously reported for similar systems,[11c] might explain this. Furthermore, similar to modulators employed to enhance crystal size by slowing the reaction rate,[17] ligand **2** may act as such through *N* coordination to the metal cluster. For illustrative purposes, *Fig. 4b* shows representative images of materials with larger size.

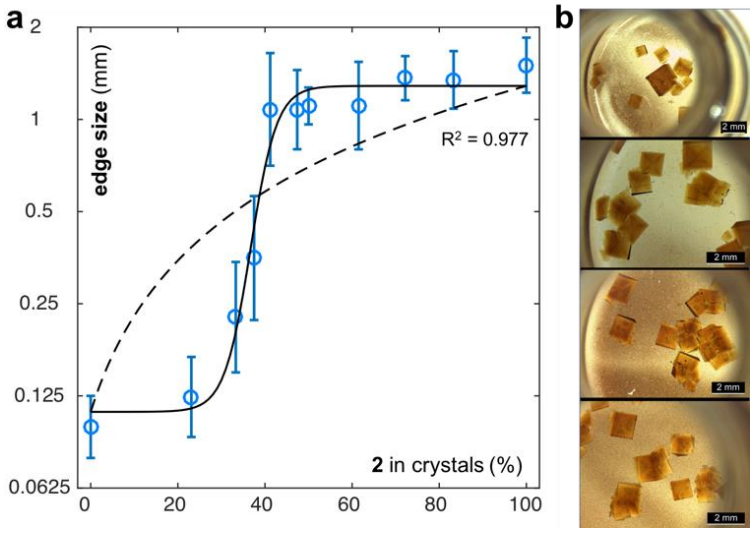

Figure 5. a) Crystal edge size (log2 scale) vs. within-crystal concentration of ligand **2** (as a ratio). Solid line fits data, while dashed line is the linear trend. Error bars indicate size dispersion of each sample. b) Representative images of materials containing 61.5% (top), 72.2%, 83.3%, and 100% (bottom) of ligand **2**. Scale bar of 2 mm.

In conclusion, the studies carried out in this work (with **MOF-5/IRMOF-3**) clearly indicate that material size is a functional property that can vary with ligand ratio. Moreover, the resulting distribution of size can be well explained with a logistic model. As a consequence, this empirical model could be used as a computational tool to guide the chemical reaction design to obtain materials of a given size. We envision that these materials, especially those bigger, might be exploited as nanostructured containers to be loaded with specific compounds (e.g., pharmacological drugs) affording long-time release. In addition, material composition can also vary in a non-linear way. In this case, this can be modeled with an incomplete beta function. Notably, both empirical models only require two independent parameters that need to be adjusted, which stresses the applicability of these models. Here, we reported a novel within-crystal ligand distribution, compared to previous results, followed by changes in the reaction conditions (e.g., from DEF to DMF, less temperature). The incomplete beta function can be parameterized to describe multiple scenarios, including these two. We also anticipate its relevance to describe reactivities between molecules in other scenarios involving pairs of related molecules that work together (e.g., co-polymerization[18a] or processes involving enantiomers[18b)]. All in all, as different mathematical models start to emerge to describe MOFs,[19] our ability to engineer these materials on purpose increases.

Notes and references

Material preparation

Reagents were mixed and dissolved in 2 mL of freshly distilled DMF into a glass flask with Teflon cap at 80 ºC for 72 h. 11 mixture conditions were assayed. Each experiment was repeated 10 times (all 110 vials were prepared simultaneously to ensure equal conditions). After 3x washing with DMF and 3x washing with $CHCl_3$, MOFs were activated under vacuum at 120 ºC for 50 h.

Analytical techniques

Yield calculated from activated MOFs (pooling 5 of the 10 samples). Material composition calculated by ^{1}H-NMR. Digestion of evacuated and activated MOFs performed by sonicating 6 mg of sample in 1 mL NaOD/D_2O/DMSO-d^6 (pooling 3 of the 10 samples). Zn(II) in solution measured by ICP for one sample. Material size calculated through representative images acquired with a Leica microscope.

Mathematical modeling

To model the incorporation of Zn(II) into the material (z) with time (t), we followed an exponential decay model, which reads

$$z = z_{min} + (z_{max} - z_{min})e^{-kt} \quad (1)$$

where *k* is the observed kinetic constant, and z_{min}/z_{max} the minimal/maximal concentration of metal. In addition, to model the concentration of one ligand (x) in mixed-ligand materials, we used the incomplete beta function, given by

$$\beta(x|a,b) = \frac{\int_0^x p^{a-1}(1-p)^{b-1}dp}{\int_0^1 p^{a-1}(1-p)^{b-1}dp} \quad (2)$$

where *a* and *b* are two parameters that determine the shape of the function. Finally, to quantitatively describe material size (*y*), we made use of a logistic function, given by

$$\log_2 y = \log_2 y_{min} + \frac{\log_2 (y_{max} / y_{min})}{1+\exp(-n(x-x_{50}))} \quad (3)$$

where x_{50} represents the concentration of input molecule (ligand **2**) at which the system reaches half of its upper bound, n is a parameter that encapsulates the non-linearity of the system, and ymin/ymax the lower/upper bound of the property measured.

Acknowledgements

This work was supported by the Ministerio de Economía y Competitividad (CTQ2016-78499-C6-1-R), Unidad de Excelencia María de Maeztu (MDM-15-0538) and Generalitat Valenciana (PROMETEO II 2015-002).

References

1) (a) M. Eddaoudi, D.B. Moler, H.L. Li, B.L. Chen, T.M. Reineke, M. O'Keeffe, and O.M. Yaghi, *Acc. Chem. Res*., **2001**, *34*, 319–330. (b) G. Ferey, *Chem. Soc. Rev.,* **2008**, *37*, 191–214. (c) S. Kitagawa, R. Kitaura, and S. Noro, *Angew. Chem. Int. Ed.,* **2004**, *43*, 2334–2375. (d) O.M. Yaghi, M. O'Keeffe, N.W. Ockwig, H.K. Chae, M. Eddaoudi, and J. Kim, *Nature,* **2003**, *423*, 705–714. (e) M. O'Keeffe and O.M. Yaghi, *Chem. Rev.,* **2012**, *112*, 675–702.
2) (a) K. Sumida, D.L. Rogow, J.A. Mason, T.M. McDonald, E.D. Bloch, Z.R. Herm, T-H. Bae, and J.R. Long*, Chem. Rev.,* **2012**, *112*, 724–781. (b) M.P. Suh, H.J. Park, T.K. Prasad, and D-W. Lim, *Chem. Rev.,* **2012**, *112*, 782–835. (c) Y. He, W. Zhou, G. Qian, and B. Chen, *Chem. Soc. Rev.,* **2014**, *43*, 5657–5678.
3) (a) Z. Kang, L. Fana, and D. Sun, *J. Mater. Chem. A,* **2017**, *5*, 10073–10091. (b) Z. Xhao, X. Ma, A. Kasik, Z. Li, and Y.S. Lin, *Ind. Eng. Chem. Res.*, **2013**, *52*, 1102–1108.
4) (a) J.Y. Lee, O.K. Farha, J. Roberts, K.A. Scheidt, S.B.T. Nguyen, and J.T. Hupp, *Chem. Soc. Rev*., **2009**, *38*, 1450–1459. (b) A. Dhakshinamoorthy and H. Garcia*, Chem. Soc. Rev.,* **2014**, *43*, 5750–5765.
5) (a) B. Tam and O. Yazaydin, *J. Mater. Chem. A*, **2017**, *5*, 8690–8696. (b) S-M. Hyun, J.H. Lee, G.Y. Jung, Y.K. Kim, T.K. Kim, S. Jeoung, S.K. Kwak, D. Moon, and H.R. Moon, *Inorg. Chem.*, **2016**, *55*, 1920–1925.
6) (a) H.K. Chae, D.Y. Siberio-Pérez, J. Kim, Y. Go, M. Eddaoudi, A.J. Matzger, M. O'Keeffe, and O.M. Yaghi, *Nature*, **2004**, *427*, 523–527. (b) M.J. Dong, M. Zhao, S. Ou, C. Zou, and C.D. Wu, *Angew. Chem. Int. Ed.,* **2014**, *53*, 1575–1579. (c) J. Yu, Y. Cui, C. Wu, Y. Yang, Z. Wang, M. O'Keeffe, B. Chen, and Q. Guodong, *Angew. Chem. Int. Ed.*, **2012**, *51*, 10542–10545. (d) H. Deng, S. Grunder, K.E. Cordova, C. Valente, H. Furukawa, M. Hmadeh, F. Gándara, A.C. Whalley, Z. Liu, S. Asahina, H. Kazumori, M. O'Keeffe, O. Terasaki, J.F. Stoddart, and O.M. Yaghi, *Science,* **2012**, *336*, 1018–1023.
7) S. Han, Y. Wei, C. Valente, I. Lagzi, J.J. Gassensmith, A. Coskun, J.F. Stoddart, and B.A. Grzybowski, *J. Am. Chem. Soc.,* **2010**, *132*, 16358–16361.
8) (a) R.A. Smaldone, R.S. Forgan, H. Furukawa, J.J. Gassensmith, A.M.Z. Slawin, O.M. Yaghi, and J.F. Stoddart, *Angew. Chem. Int. Ed.*, **2010**, *49*, 8630–8634. (b) L. Li, F. Sun, J. Jia, T. Borjigina, and G. Zhu, *CrystEngComm*, **2013**, *15*, 4094–4098. (c) C.A. Trickett, K.J. Gagnon, S. Lee, F. Gándara, H.B. Bürgi, and O.M. Yaghi*, Angew. Chem. Int. Ed.,* **2015**, *54*, 11162–11167. (d) D. Rankine, A. Avellaneda, M.R. Hill, C.J. Doonan, and C.J. Sumby, *Chem. Commun.,* **2012**, *48*, 10328–10330. (e) S. Furukawa, K. Hirai, K. Nakagawa, Y. Takashima, R. Matsuda, T. Tsuruoka, M. Kondo, R. Haruki, D. Tanaka, H. Sakamoto, S. Shimomura, O. Sakata, and S. Kitagawa, *Angew. Chem. Int. Ed.,* **2009**, *121*, 1798–1802. (f) K. Koh, A.G. Wong-Foy, and A.J. Matzger, *Chem. Commun*., **2009**, *41*, 6162–6164. (g) S. Furukawa, K. Hirai, Y. Takashima, K. Nakagawa, M. Kondo, T. Tsuruoka, O. Sakata, and S. Kitagawa, *Chem. Commun.,* **2009**, *34*, 5097–5099.
9) (a) A. Corma, *Chem. Rev*., **1997**, *97*, 2373–2420. (b) A. Corma, *J. Catal.*, **2003**, *216*, 298–312. (c) M. Kruk, M. Jaroniec, and A. Sayari, *J. Phys. Chem. B*, **1997**, *101*, 583–589.
10) H. Li, M. Eddaoudi, M. O'Keeffe, and O.M. Yaghi, *Nature,* **1999**, *402*, 276–279.
11) (a) M. Eddaoudi, J. Kim, N. Rosi, D. Vodak, J. Wachter, M. O'Keeffe, and O.M. Yaghi, *Science,* **2002**, *295*, 469–472. (b) H. Deng, C.J. Doonan, H. Furukawa, R.B. Ferreira, J. Towne, C.B. Knobler, B. Wang, and O.M. Yaghi, *Science*, **2010**, *327*, 846–850. (c) X. Kong, H. Deng, F. Yan, J. Kim, J.A. Swisher, B. Smit, O.M. Yaghi, and J.A. Reimer, *Science*, **2013**, *341*, 882–885.

12) (a) A.F. Gross, E. Sherman, S.L. Mahoney, and J.J. Vajo, *J. Phys. Chem. A*, **2013**, *117*, 3771–3776. (b) M. Du, X.J. Jiang, and X.J. Zhao, *Inorg. Chem.*, **2007**, *46*, 3984–3995. (c) Z. Yin, Y.L. Zhou, M.H. Zeng, and M. Kurmoo, *Dalton Transact.*, **2015**, *44*, 5258–5275.

13) (a) P. Cubillas, K. Etherington, M.W. Anderson, and M.P. Attfie, *CrystEngComm,* **2014**, *16*, 9834–9841. (b) C. Zheng, H. F. Greer, C.Y. Chianga, and W. Zhou, *CrystEngComm,* **2014**, *16*, 1064–1070. (c) J.P. Patterson, P. Abellan, M.S. Denny Jr., C. Park, N.D. Browning, S.M. Cohen, J.E. Evans, and N.C. Gianneschi, *J. Am. Chem. Soc.,* **2015**, *137*, 7322−7328.

14) B. Chen, X. Wang, Q. Zhang, X. Xi, J. Cai, H. Qi, S. Shi, J. Wang, D. Yuana, M. Fang *J. Mater. Chem.,* **2010**, *20*, 3758-3767

15) A.K. Gupta and S. Nadarajah, Handbook of beta distribution and its applications. CRC press, **2004**.

16) (a) S. Rostamniaa, H. Xin, Appl. *Organometal. Chem*. **2014**, *28*, 359–363. (b) J-M. Yang, Q. Liu, Y-S. Kang, W-Y. Sun, *Dalton Trans.,* **2014**, *43*, 16707-16712. (c)L. Li, F. Sun, J. Jia, T. Borjigina, G. Zhu, *CrystEngComm,* **2013**, *15*, 4094-4098.

17) (a) R.J. Marshall, C.L. Hobday, C.F. Murphie, S.L. Griffin, C.A. Morrison, S.A. Moggach, and R.S. Forgan, *J. Mater. Chem. A***, 2016**, *4*, 6955–6963. (b) B. Van de Voorde, I. Stassen, B. Bueken, F. Vermoortele, D. De Vos, R. Ameloot, J.C. Tan, and T.D. Bennett, *J. Mater. Chem. A,* **2015**, *3*, 1737–1742. (c) Z. Hu and D. Zhao, *Dalton Transact.*, **2015**, *44*, 19018–19040. (d) O.V. Gutov, S. Molina, E.C. Escudero-Adán, and A. Shafir, *Chem. Eur. J.,* **2016**, *22*, 13582–13587. (e) C.V. McGuire and R.S. Forgan, *Chem. Commun.,* **2015**, *51*, 5199–5217.

18) (a) K.R. Sharma, *J. Encapsul. Adsor. Sci*., **2013**, *3*, 77–92. (b) C.T. Yeung, K.H. Yim, H.Y. Wong, R. Pal, W.S. Lo, S.C. Yan, M.Y-M. Wong, D. Yufit, D.E. Smiles, L.J. McCormick, S.J. Teat, D.K. Shuh, W.T. Wong, and G.L. Law, *Nat. Commun*., **2017**, *8*, 1128.

19) (a) T. Titze, A. Lauerer, L. Heinke, C. Chmelik, N.E. Zimmermann, F.J. Keil, D.M. Ruthven, and J. Kärger, *Angew. Chem. Int. Ed.*, **2015**, *54*, 14580–14583. (b) S. Han, T.M. Hermans, P.E. Fuller, Y. Wei, and B.A. Grzybowski, *Angew. Chem. Ind Ed.*, **2012**, *124*, 2716–2720. (c) R. Sabouni, H. Kazemian, and S. Rohani, *Environ. Sci. Technol*., **2013**, *47*, 9372–9380. (d) F-X. Coudert and A.H. Fuchs, *Coord. Chem. Rev.*, **2016**, *307*, 211–236.

Supporting Information

Empirical Modeling material composition and size in MOF-5/IRMOF-3 mixtures

Pedro J. Llabrés-Campaner[a], Ramón José Zaragozá,[a] Maria Jose Aurell,[a] Rafael Ballesteros,[a] Belén Abarca,[a] Enrique Garcia-España,[b] Guillermo Rodrigo,[c] and Rafael Ballesteros-Garrido[a,b,c]

[d.] *Departament de Química Orgànica, Universitat de València, Av. Vicent Andrés Estellés s/n, 46100 Burjassot, Spain.*
[e.] *Instituto de Ciencia Molecular (ICMOL), Universitat de València, c/ Cat. José Beltrán 2, 46980 Paterna, Spain.*
[f.] *Instituto de Biología Integrativa de Sistemas (I2SysBio), Universitat de València – CSIC, c/ Cat. Agustín Escardino 9, 46980 Paterna, Spain.*
[*] *Send correspondence to rafael.ballesteros-garrido@uv.es*

Contents

S1. General conditions

Starting materials, if commercially available, were purchased and used as such. *N,N*-dimethylformamide (DMF), was distilled before using. All reagent solutions were filtered through a 0.45 μm PTFE 25mm Syringe Filter. IR spectra were recorded using FT-IR ATR. Microscopic images were taken using Stereoscopic Microscope LEICA M165 FC. DRX powder spectra were performed on a BRUKER AXS D5005 powder diffractometer (Cu radiation, 40 kV, 30 mA, 0.05 steps, 6 s). ^{1}H magnetic resonance (NMR) spectra were recorded at 300 MHz. Chemical shifts are reported in δ units, parts per million (ppm), and were measured relative to the signals for residual deuterated dimethyl sulfoxide. All calculations were carried out with the Gaussian 09 suite of programs.[1] Initially, density functional theory[2] calculations (DFT) have carried out using the B3LYP[3] exchange-correlation functionals, together with the standard 6-31G** basis set, in gas phase.[4] Subsequently, since the reactions are carried out in polar solvents, the inclusion of solvent effects have been considered by using a relatively simple self-consistent reaction field (SCRF) method,[5] based on the polarizable continuum model (PCM) of Tomasi's group.[6] Geometries have been fully optimized with PCM. As solvent we have used *N*,*N*-dimethylformamide.

S2. Detailed synthesis conditions

All the MOF synthesis were performed at 80°C during 72h at atmospheric pressure. Mother solutions of **1**, **2** and **$Zn(NO_3)_2{\cdot}6H_2O$** were prepared. **1**, **2** and **$Zn(NO_3)_2{\cdot}6H_2O$** were dissolved in the total amount of DMF needed for a 2 mL/vial. The proportion L:Zn was always constant at 78,3:100 μmol

Table S1. Conditions for all the MOF crystals synthesis.

Vial	Percentage (%)		Amount (μmol)			Volume of DMF solution (mL)		
	1	**2**	**1**	**2**	**Zn^{2+}**	**1**	**2**	**Zn^{2+}**
1	100	0	78,3	0	100	1	0	1
2	90	10	70,5	7,8	100	0,9	0,1	1
3	80	20	62,7	15,7	100	0,8	0,2	1
4	70	30	54,8	23,5	100	0,7	0,3	1
5	60	40	47,0	31,3	100	0,6	0,4	1
6	50	50	39,2	39,2	100	0,5	0,5	1
7	40	60	31,3	47,0	100	0,4	0,6	1
8	30	70	23,5	54,8	100	0,3	0,7	1
9	20	80	15,7	62,7	100	0,2	0,8	1
10	10	90	7,8	70,5	100	0,1	0,9	1
11	0	100	0	78,3	100	0	1	1
TOTAL			430,8	430,8	1100	5,5	5,5	11
10 replays			4308	4308	11000	55	55	110

Stock solutions of **1** and **2** (861.6 μmol) in freshly distilled DMF (11 mL) and 2200 μmol of **$Zn(NO_3)_2 \cdot 6H_2O$** in 22 mL of freshly distilled DMF were prepared. Then, then volume established in each vial was taken, containing the exactly amount required for each one keeping global volume at 2 mL.

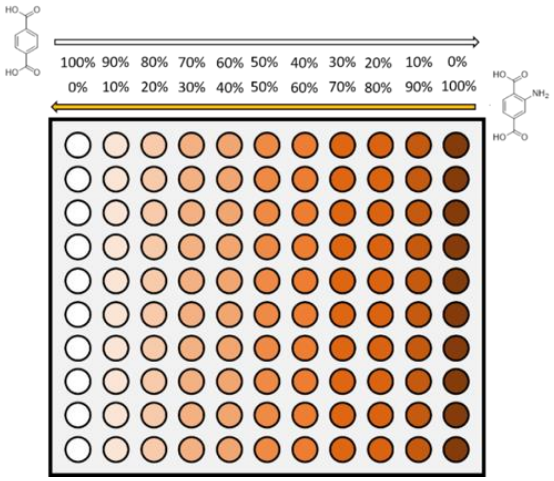

Figure S1. Representation of the followed methodology to synthesize all the MOF crystals.

S3. ^{1}H-NMR of digested MOFs

8 mg of dried MOF was digested and dissolved with sonication in 1 mL dilute NaOD solution (prepared from 100 μL of 40% NaOD/D_2O solution (Aldrich) and 10 mL of DMSO-*d6*). The digestion solution was used directly for ^{1}H-NMR.

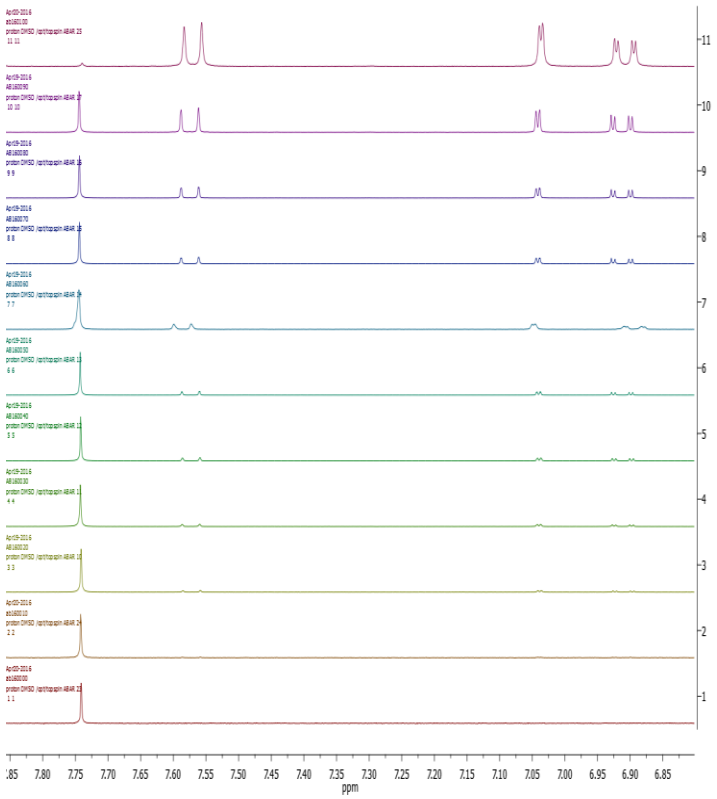

Figure S2. ^{1}H-NMR spectra of dissolved crystals of each series.

S4. IR spectra of MOF crystals

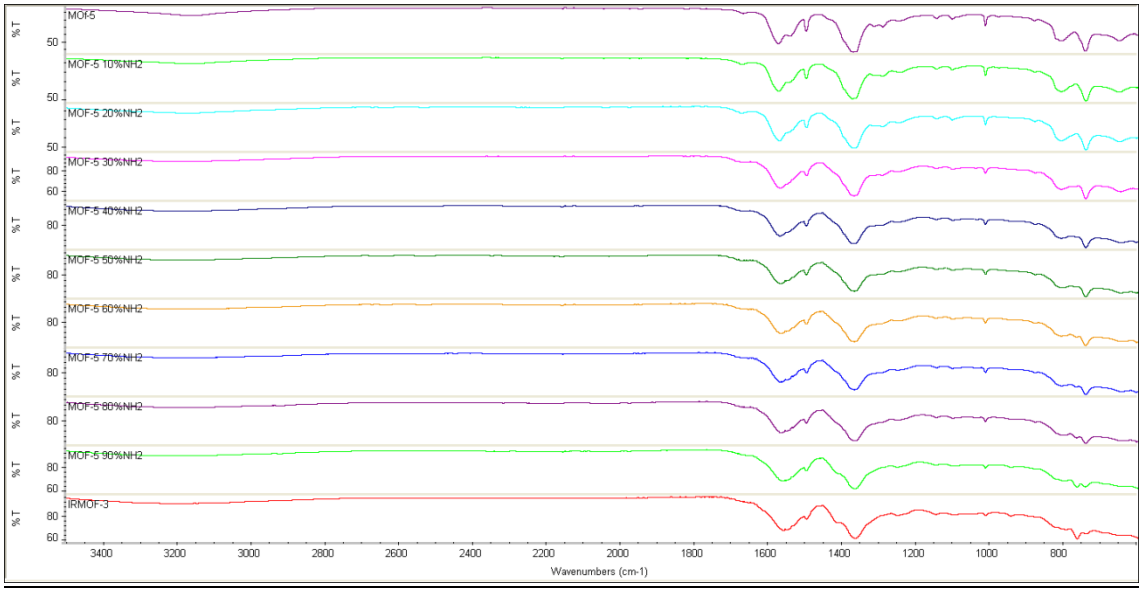

Figure S3. IR spectra of all MOF crystals

S5. Experimental growth kinetics

Independent vials containing 100% of **1** and **2**, respectively, were put into the oven at 80ºC by 0, 16, 24, 36, 48, 60 and 72 hours. After these times, the remaining DMF was filtered and added to 1 mL of HCl (1 M). The corresponding solution was analysed by ICP.

	Zn (mg/L)		Zn (mg/L)
IRMOF3-16h	4140 ± 34	**MOF5-16h**	2957 ± 54
IRMOF3-24h	3125 ± 122	**MOF5-24h**	3113 ± 81
IRMOF3-48h	3727 ± 57	**MOF5-48h**	2715 ± 27
IRMOF3-72h	2600 ± 52	**MOF5-72h**	2140 ± 5

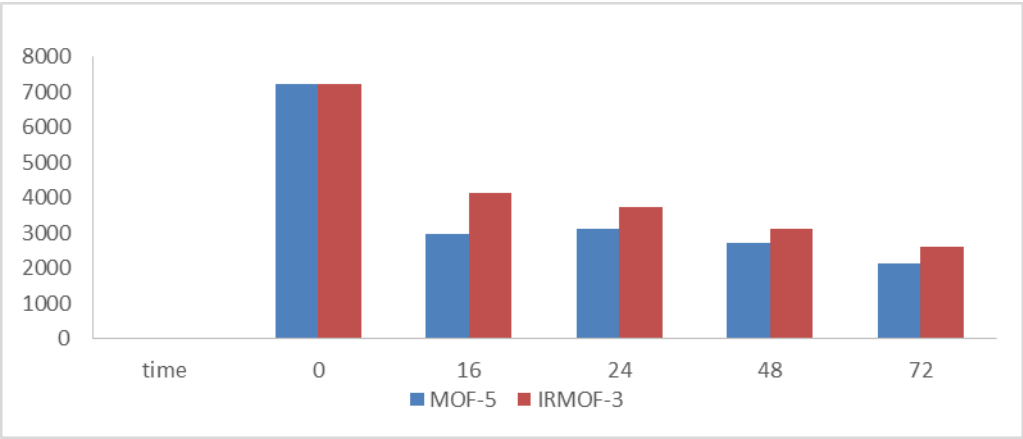

Figure S4. ICP (ppm) results for Zn(II) concentration.

S6. Microscopic images of MOF crystals

Highlighted images of MOF crystals (percentage of **2** is indicated).

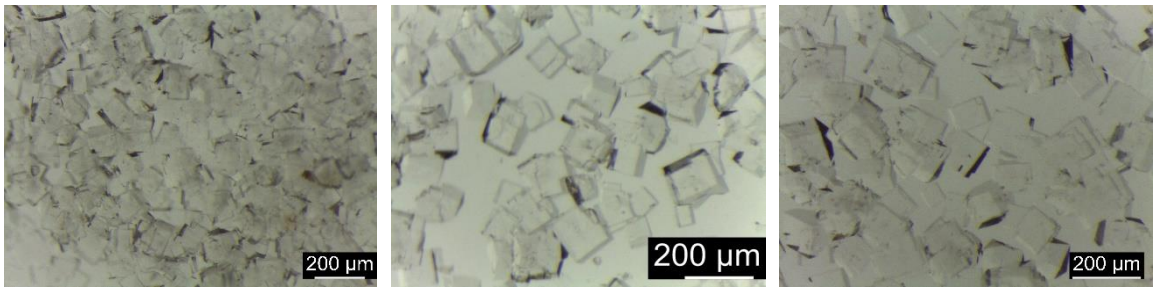

Figure S5: 0% (MOF-5)

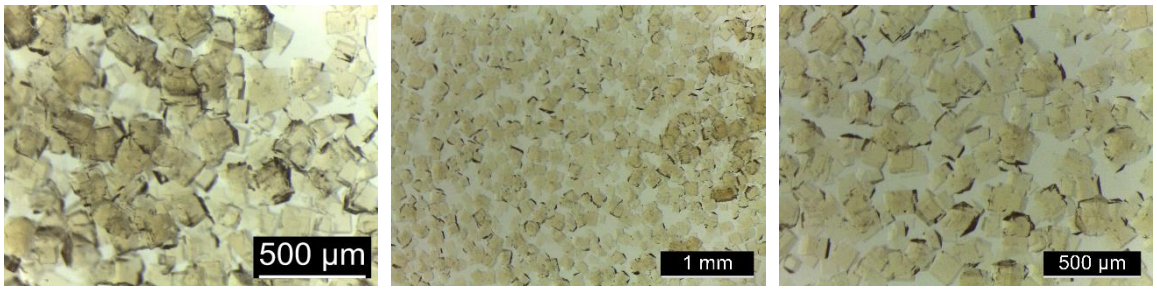

Figure S6: 10%

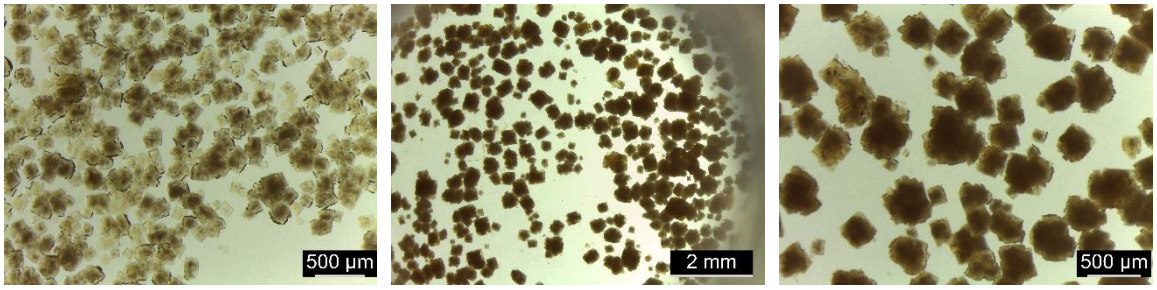

Figure S7: 20%

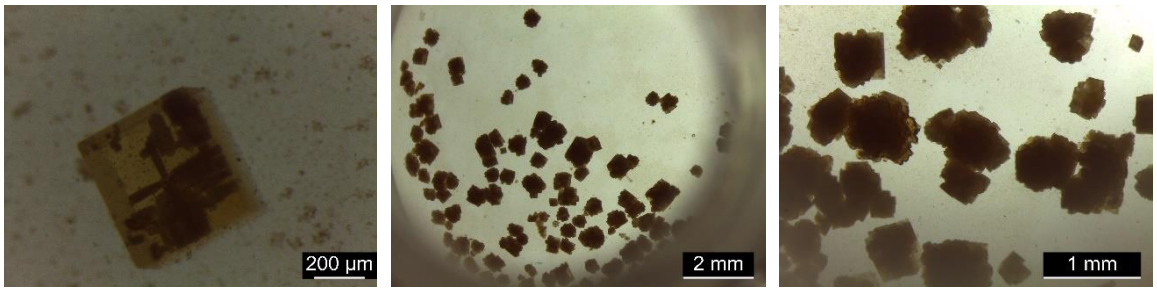

Figure S8: 30%

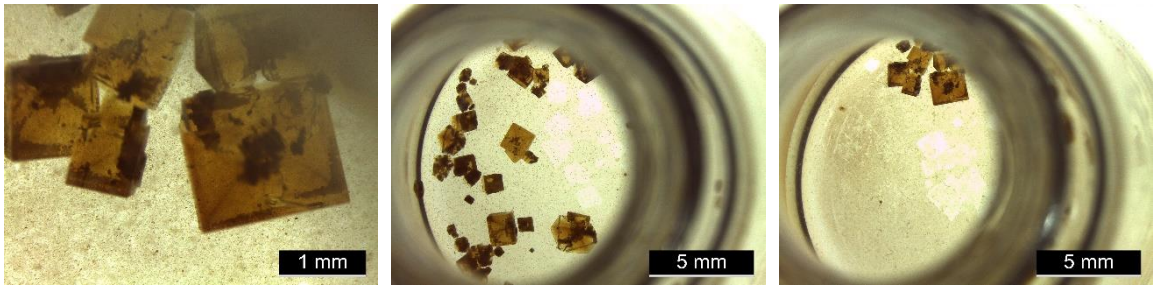

Figure S9: 40%

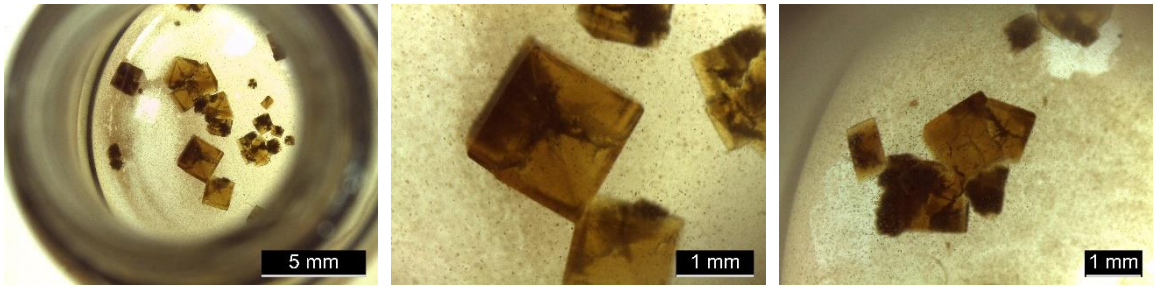

Figure S10: 50%

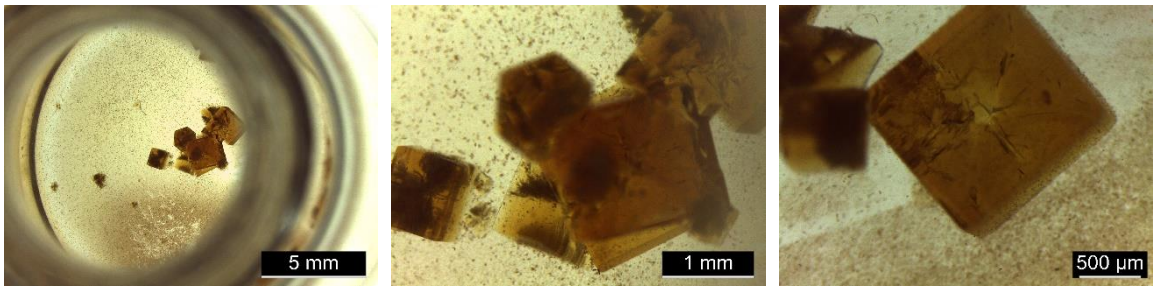

Figure S11: 60%

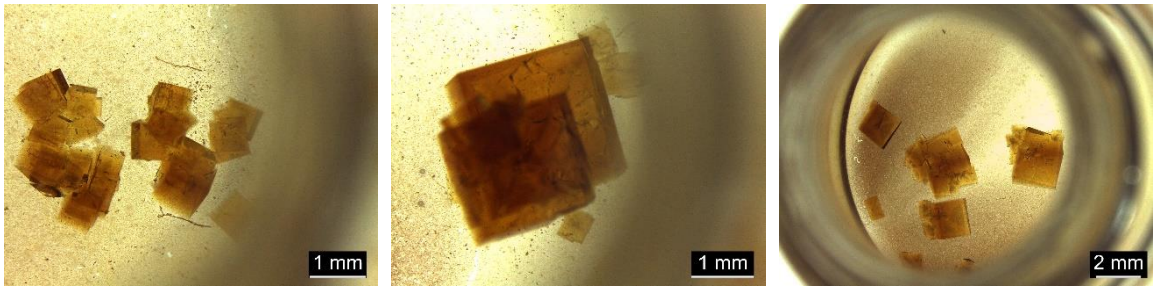

Figure S12: 70%

Figure S13: 80%

Figure S14: 90%

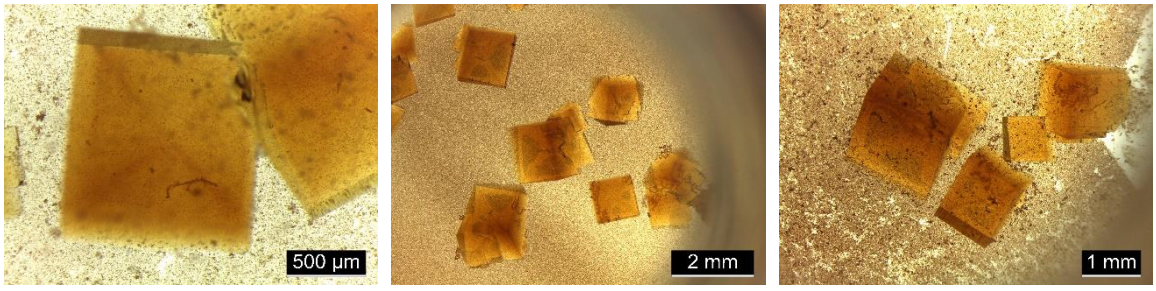

Figure S15: 100% (IRMOF-3)

S8. PXRD

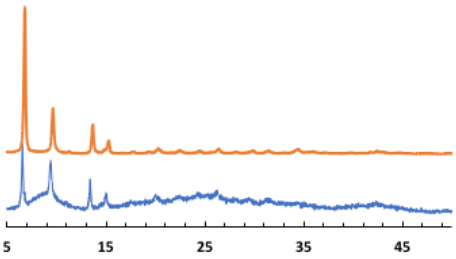

Figure S16. PXRD of IRMOF-3 Obtained under reported condtions (big crystlas, blue line) and 10 fold synthesis (orange).

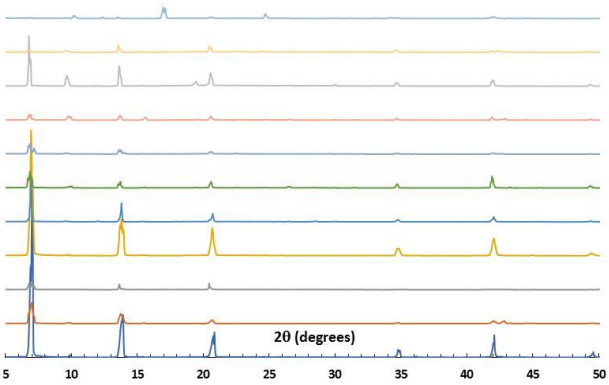

Figure S17. PXRD of DMF immersed crystals from **IRMOF-3** (top) to **MOF-5** (bottom).

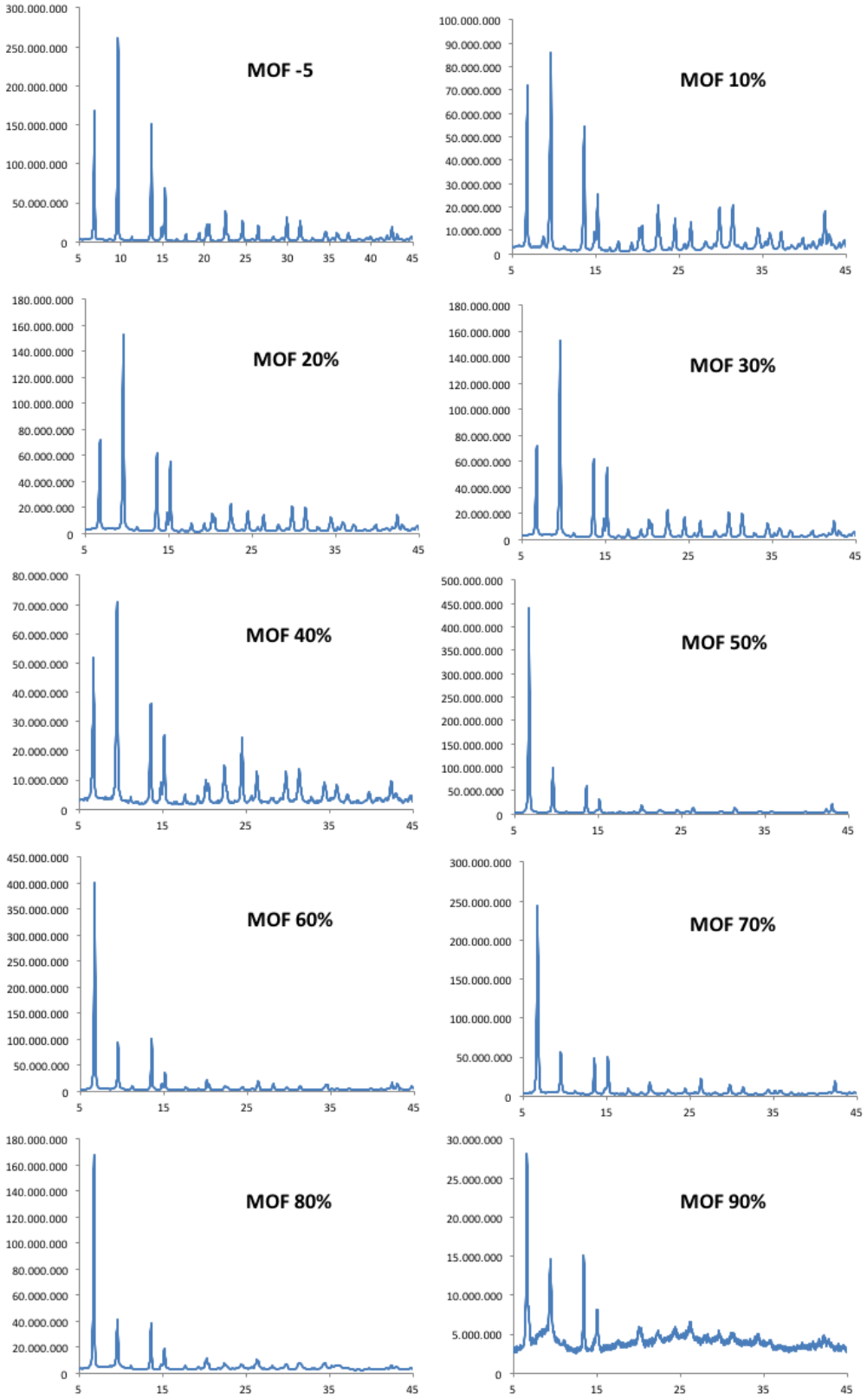

Figure S18. PXRD from **MOF-5** until MOF 90% of ligand **2** sample.

S8. Theoretical calculations of structures

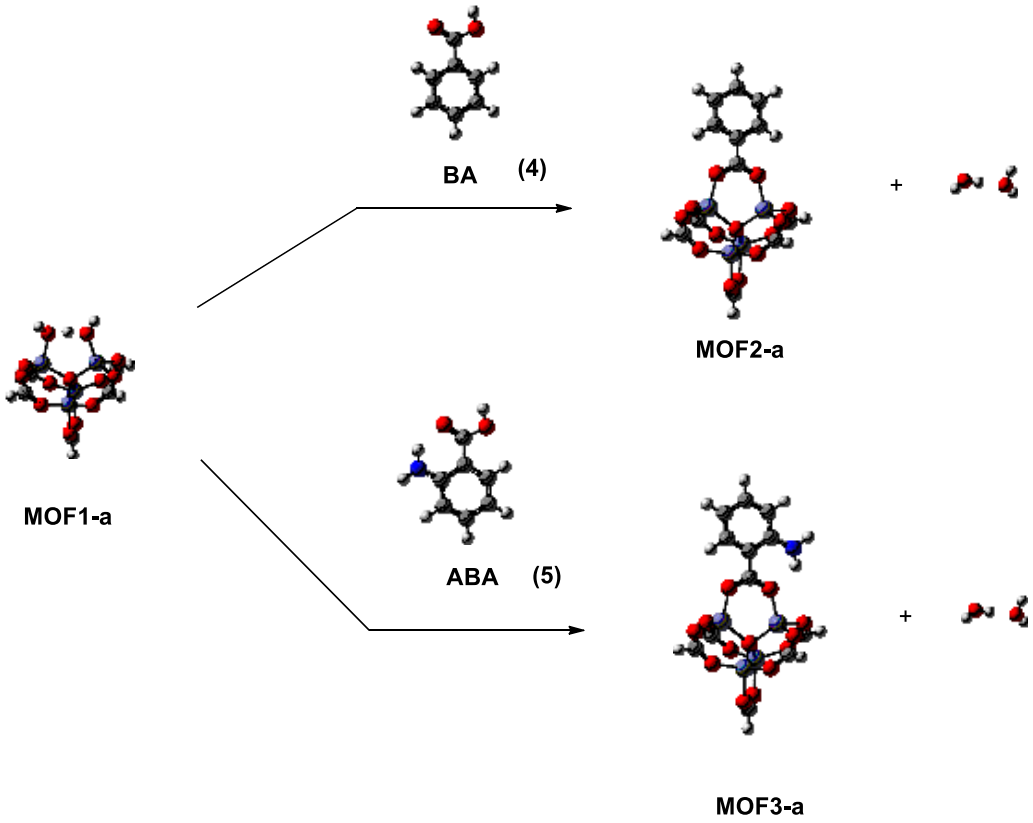

Scheme S1: Transformation of MOF1-a in MOF2-a or MOF3-a.

Table S2. B3LYP/6-31G** total energies (*E*, au) and relative energies (Δ*E*, kcal/mol) of species involved in the transformation of **MOF1-a** in **MOF2-a / MOF3-a** and in the transformation of **MOF1-b** in **MOF2-b / MOF3-**b.

	gas-phase		N,N-dimethylformamide	
	E(a.u.)	ΔE(kcal/mol)	E(a.u.)	ΔE(kcal/mol)
BA (**4**)	-420,835432		-420,842222	
ABA (**5**)	-476,201325	0,00[a]	-476,209131	
ABA-2	-476,196342	3,13[a]		
ABA-3	-476,188532	8,03[a]		
2H2O	-152,851505		-152,863528	
MOF1-a	-8290,344699		-8290,383602	
MOF1-a+BA	-8711,180131		-8711,225823	
MOF2-a	-8558,331757		-8558,369128	
MOF2-a+2H2O	-8711,183262		-8711,232656	

(MOF2-a+2H2O)-(MOF1-a+BA)		-2,0		-4,3
MOF1-a+ABA	-8766,546025		-8766,592732	
MOF3-a	-8613,695076		-8613,734186	
MOF3-a+2H2O	-8766,546581		-8766,597714	
(MOF3-a+2H2O)-(MOF1-a+ABA)		-0,3		-3,1
MOF1-b	-9445,709492		-9445,747381	
MOF1-b+BA	-9866,544924		-9866,589603	
MOF2-b	-9713,696853		-9713,733000	
MOF2-b+2H2O	-9866,548358		-9866,596528	
(MOF2-b+2H2O)-(MOF1-b+BA)		-2,2		-4,3
MOF1-b+ABA	-9921,910817		-9921,956511	
MOF3-b	-9769,059927		-9769,097940	
MOF3-b+2H2O	-9921,911433		-9921,961468	
(MOF3-b+2H2O)-(MOF1-b+ABA)		-0,4		-3,1

[a] Three conformations have been calculated for o-aminobenzoic acid. The most stable is indicated as ABA.

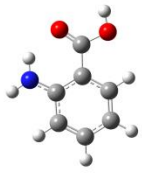	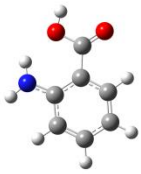	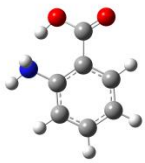
ABA (5)	ABA-2	ABA-3

Figure S19. Three conformations of the o-aminobenzoic acid.

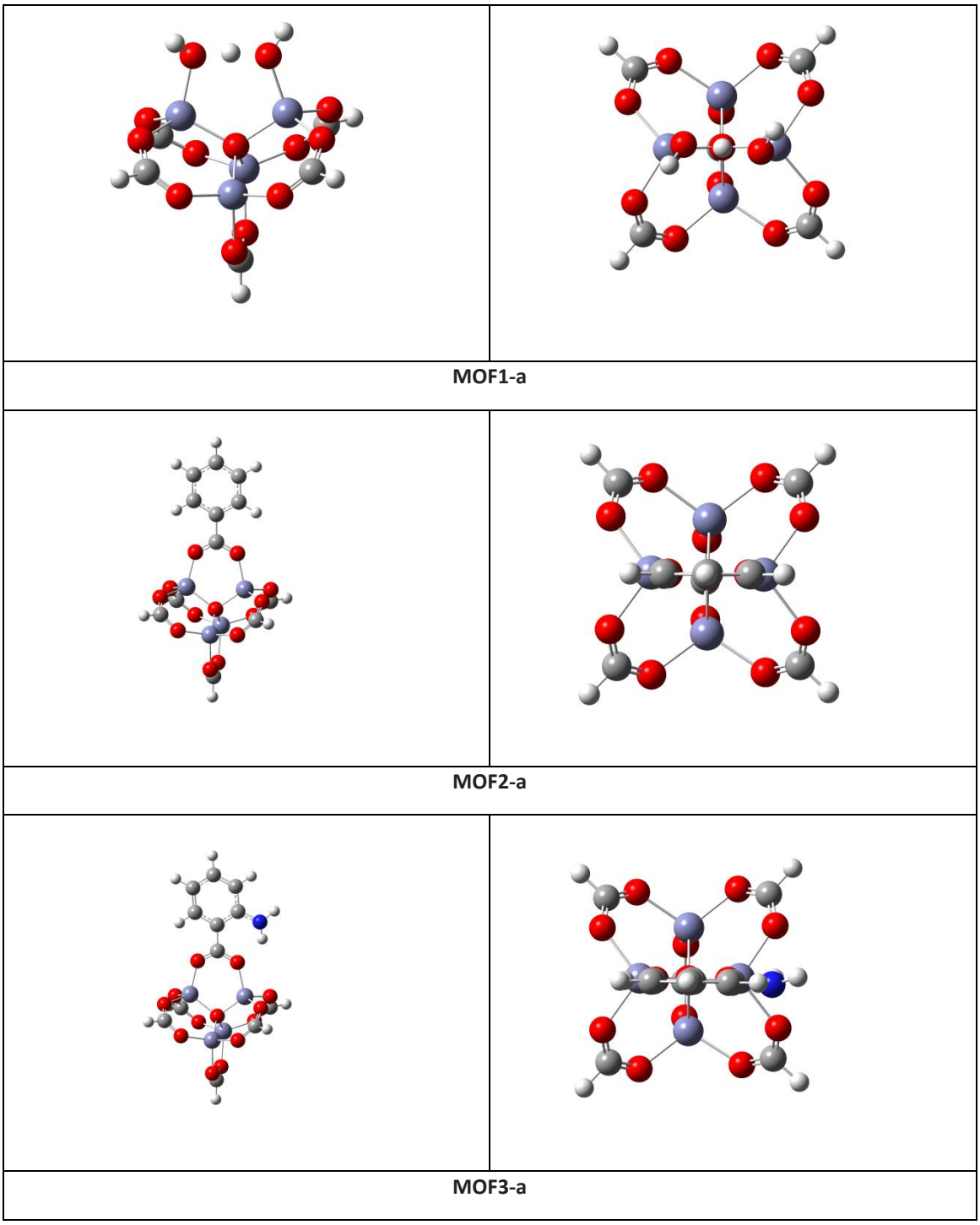

Figure S20. Different views of **MOF1-a, MOF2-a** and **MOF3-a**.

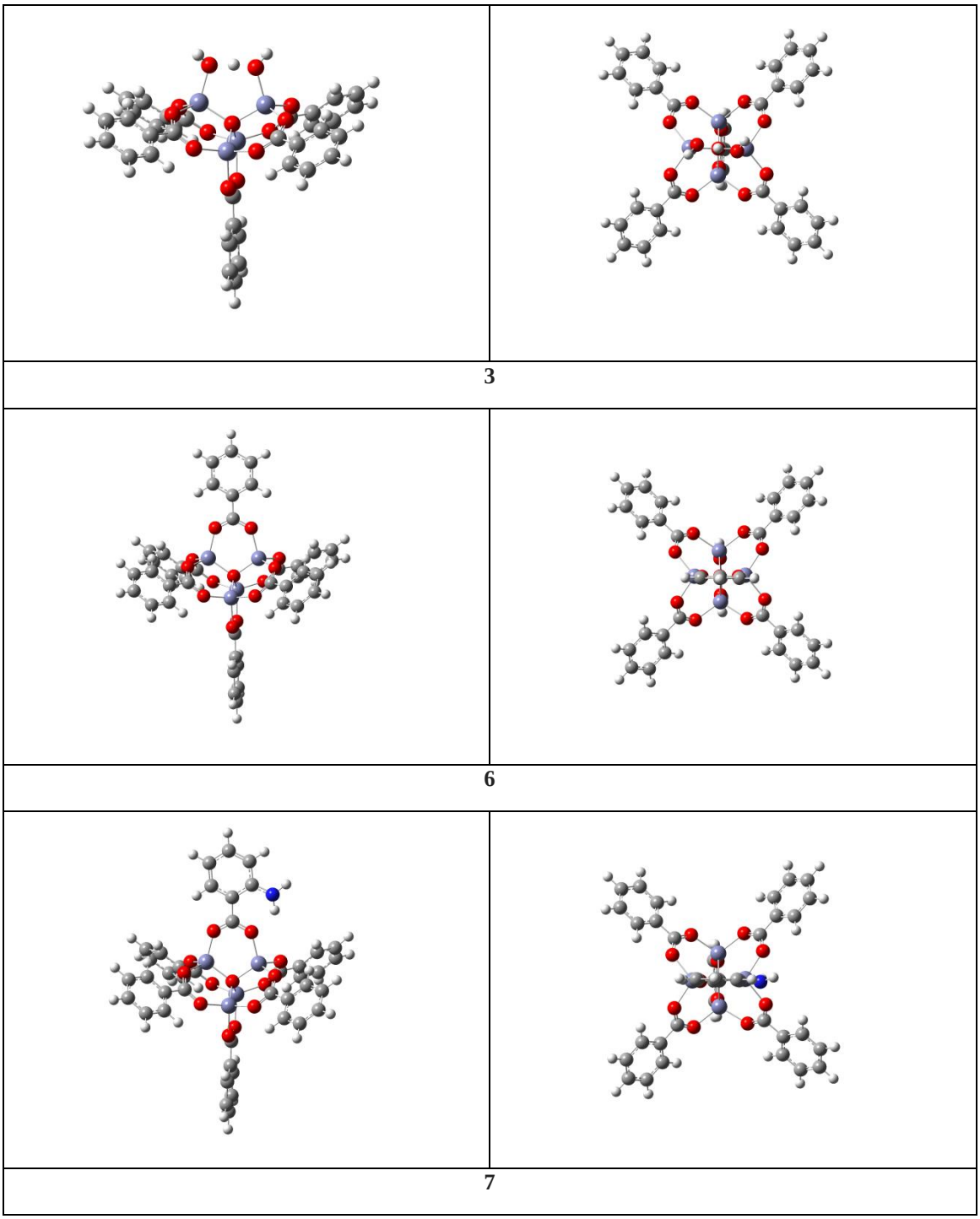

Figure S21. Different views of **3**, **6** and **7.**

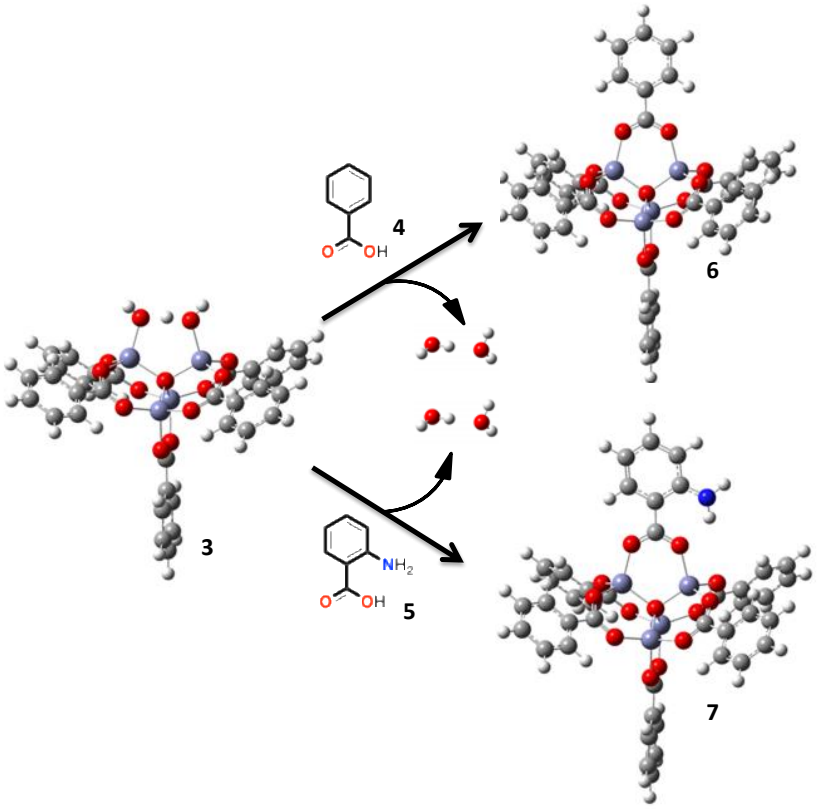

Figure S22. Model reagent **3**, composed by five benzoic acid unities and the Zn(II) oxo-cluster (Zn_4O) bearing H_2O and OH^- at the free position, is reacted with benzoic acid (**4**) or 2-amino benzoic acid (**5**) giving **6** and **7** as model products

S9. Logistic model

$$Y = Y_{min} + \frac{Y_{max} - Y_{min}}{1 + e^{-n(x-B)}}$$

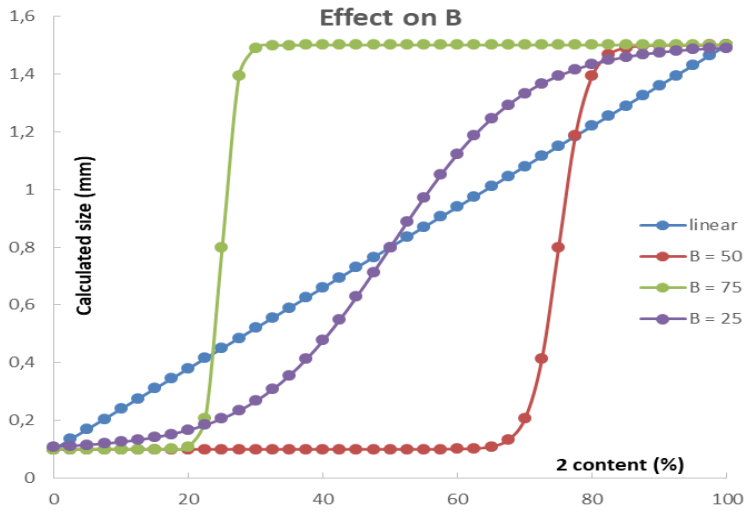

Figure S23. Effect of B on the logistic model.

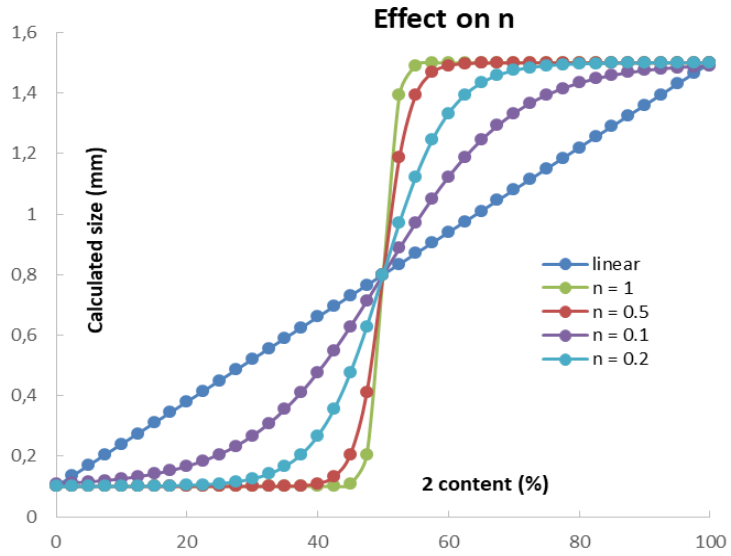

Figure S24: Effect of n on the logistic model.

S10. Beta incomplete function

$$\beta(x|a,b) = \frac{\int_0^x p^{a-1}(1-p)^{b-1}dp}{\int_0^1 p^{a-1}(1-p)^{b-1}dp}$$

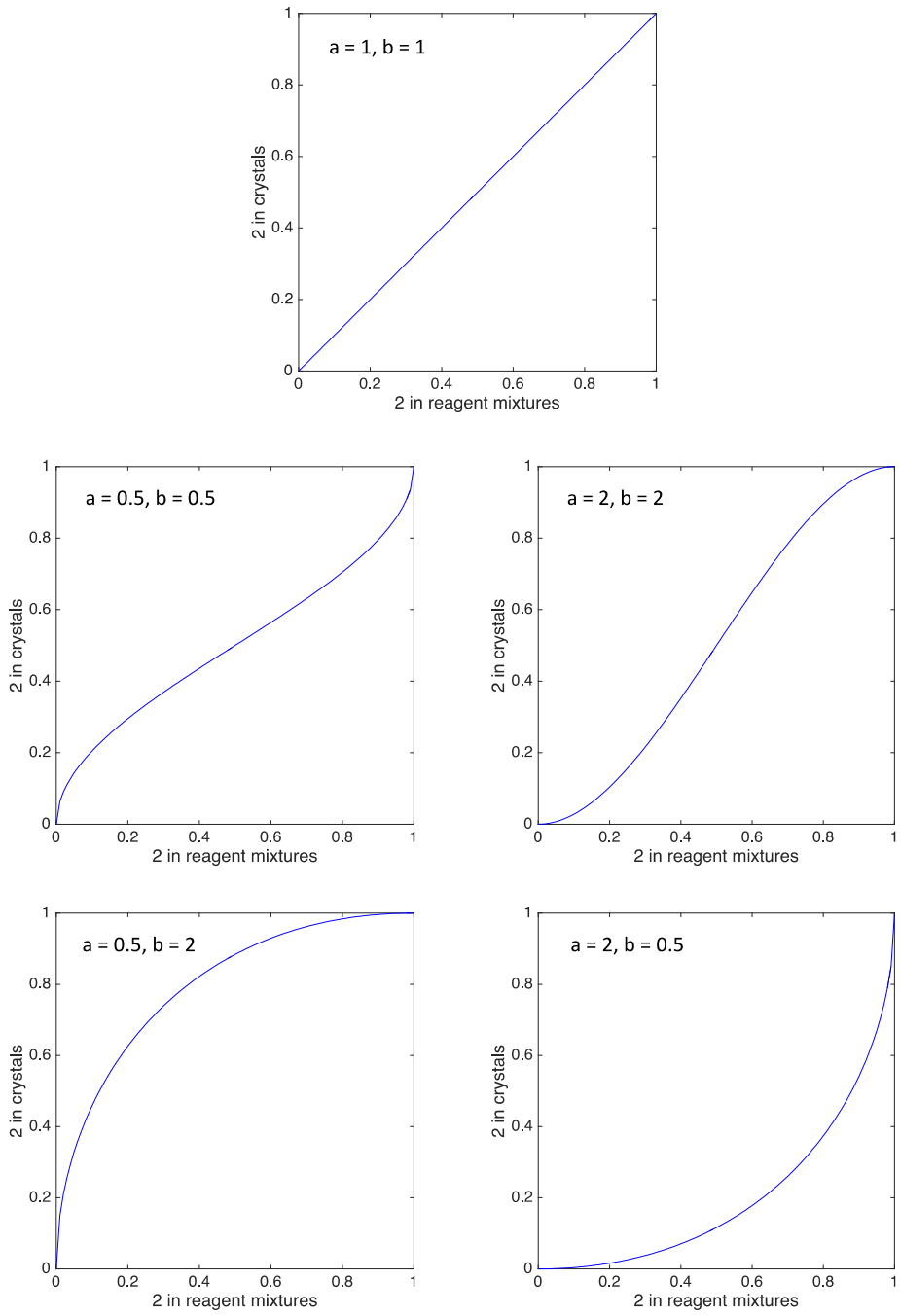

Figure S25. Shape of Beta incomplete function according to different a/b parameter values.

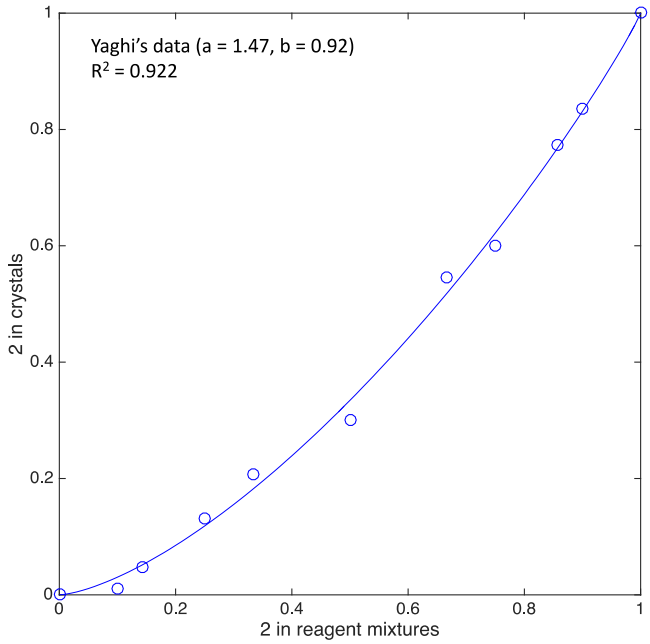

Figure S26. Fitting of Beta incomplete function to data obtained from Yaghi's results (MOF-5/IRMOF-3 mixtures obtained in diethylformamide at 100 ºC and 48 h.[7]

References

1) M.J. Frisch, et al., Gaussian 09, Revision A.02, Gaussian, Inc., Wallingford, CT, 2009.

2) (a) R.G. Parr, W. Yang, Density Functional Theory of Atoms and Molecules, Oxford University Press, New York, **1989**. (b) T. Ziegler, *Chem. Rev.*, **1991**, *91*, 651-667.

3) (a) A.D. Becke, *J. Chem. Phys.*, **1993**, *98*, 5648-5652. (b) C. Lee, W. Yang, R.G. Parr, *Phys. Rev. B*, **1988**, *37*, 785-789.

4) W.J. Hehre, L. Radom, P. von R. Schleyer, J.A. Pople, Ab initio Molecular Orbital Theory, Wiley, New York, **1986**.

5) (a) J. Tomasi, M. Persico, *Chem. Rev.*, **1994**, *94*, 2027-2094. (b) B.Y. Simkin, I. Sheikhet, Quantum Chemical and Statistical Theory of Solutions-A Computational Approach, Ellis Horwood, London, **1995**.

6) (a) E. Cances, B. Mennunci, J. Tomasi, *J. Chem. Phys.*, **1997**, *107*, 3032-3041. (b) M. Cossi, V. Barone, R. Cammi, J. Tomasi, Chem. Phys. Lett. **1996**, 255, 327-335. (c) V. Barone, M. Cossi, J. Tomasi, *J. Comp. Chem.*, **1998**, *19*, 404-417.

7) H. Deng, C.J. Doonan, H. Furukawa, R.B. Ferreira, J. Towne, C.B. Knobler, B. Wang, O.M. Yaghi, *Science*, **2010**.

CONCLUSIONES GENERALES

PARTE I

- ✓ En el primer trabajo de la parte I, se probó la combinación Pd/C-ZnO como un catalizador heterogéneo adecuado para la mono-activación de etilenglicol en presencia de aminas aromáticas en un ciclo de Autotransferencia o Préstamo de Hidrógeno, en una mezcla etilenglicol/agua. Se preparó así una amplia familia de β-amino alcoholes por medio de un nuevo protocolo.

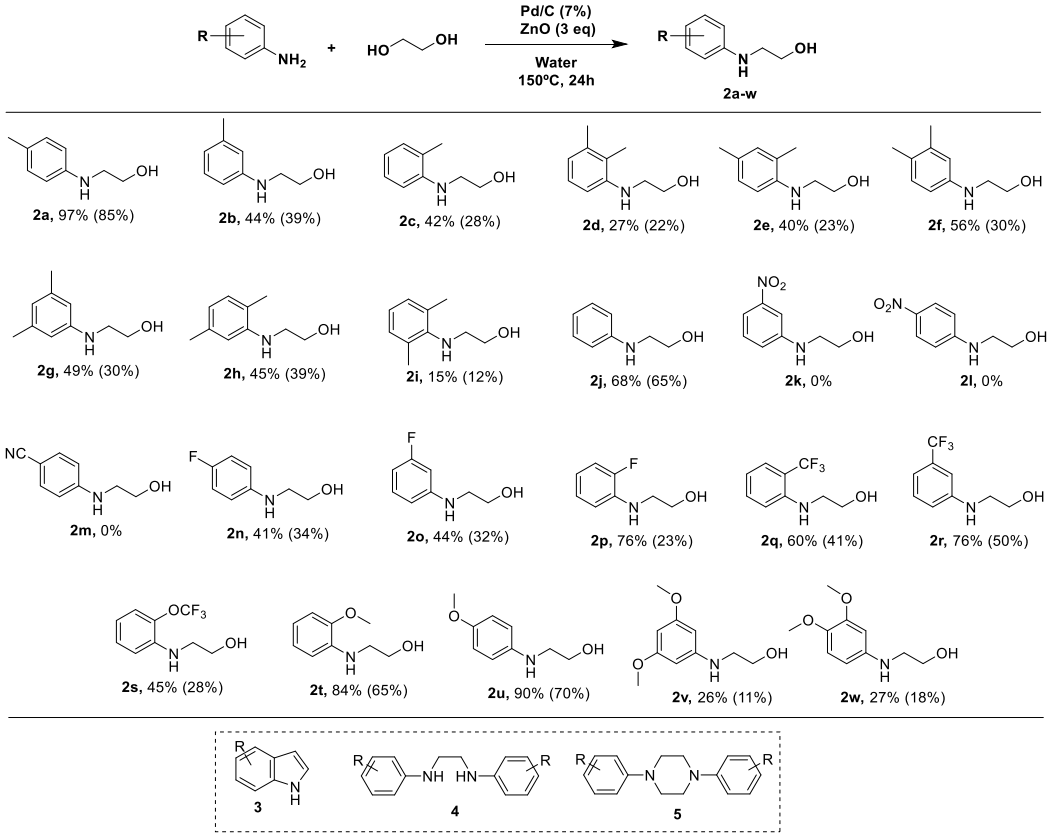

Familia de β-amino alcoholes **2a-w** obtenida tras la optimización del proceso catalítico.
Estructura de productos secundarios **3-5**

La presente metodología demostró ser muy interesante y útil dado que es estable al aire y a la humedad (no requiere atmósfera inerte). Además, se probó que la combinación Pd/C-ZnO es capaz de hidrogenar indoles a indolinas, induciendo reacciones AH/BH tándem de manera heterogénea. Esta es la única aproximación heterogénea a β-amino alcoholes con gran eficiencia atómica y sin derivatización previa del etilenglicol.

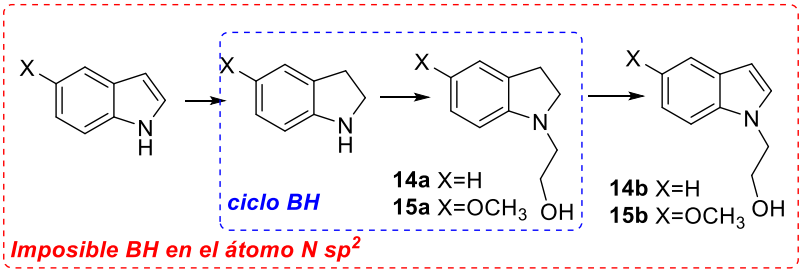

Reactivo de partida	Conversion	Selectividad combinada
Indol (**11**) (X=H)	72%	65% (**14a**+**14b**)
Indolina (**12**) (X=H)	>95%	75% (**14a**+**14b**)
5-Metoxi indol (**13**) ($X=OCH_3$)	52%	>95%(**15a**+**15b**)

Hidrogenación de indoles a indolinas y posterior reacción de éstas con alcoholes para obtener los derivados de β-amino alcohol (reacción tándem).

La complementariedad entre procesos de AH/BH, un catalizador barato como el Pd/C y un agente activante de alcoholes como el ZnO representan una aproximación diferente a la obtención de amino alcoholes (*Tetrahedron* **2017**, *73*, 5552).

✓ Este proceso metodológico fue patentado dado que cumplía todos los requisitos para ello.

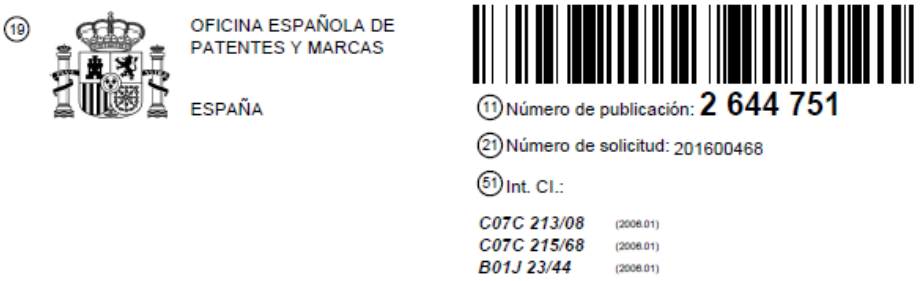
(19) OFICINA ESPAÑOLA DE PATENTES Y MARCAS

ESPAÑA

(11) Número de publicación: **2 644 751**

(21) Número de solicitud: 201600468

(51) Int. CI.:

C07C 213/08 (2006.01)
C07C 215/68 (2006.01)
B01J 23/44 (2006.01)

(12) SOLICITUD DE PATENTE A1

(22) Fecha de presentación:
31.05.2016

(43) Fecha de publicación de la solicitud:
30.11.2017

(71) Solicitantes:
UNIVERSITAT DE VALÈNCIA (100.0%)
Av. Blasco Ibáñez nº 13
46010 Valencia ES

(72) Inventor/es:
BALLESTEROS CAMPOS , Rafael ;
ABARCA GONZÁLEZ, Mª Belén;
BALLESTEROS GARRIDO , Rafael y
LLABRÉS CAMPANER , Pedro Juan

(54) Título: Procedimiento de obtención de β-amino alcoholes

Patente Nacional derivada del proceso catalítico llevado a cabo en nuestro laboratorio

✓ En el segundo trabajo de la parte I (*Tetrahedron Lett.* **2017**, *58*, 4880) se combinó de nuevo Pd/C con ZnO para, en una catálisis heterogénea, mono activar distintos dioles más complejos que el etilenglicol y hacerlos reaccionar con anilinas, evaluando así el alcance del sistema catalítico.

Se obtuvieron resultados interesantes con dioles como el 1,2-propanodiol o el dietilen glicol, obteniéndose en estos y más casos el correspondiente amino alcohol.

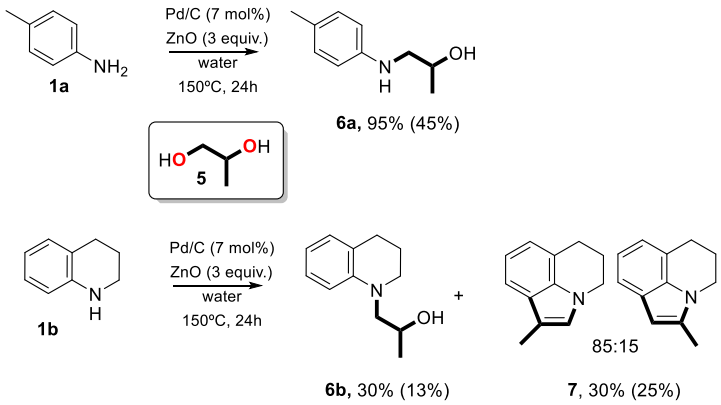

Reacción de anilina (**1a**) y 1,2,3,4-tetrahidroquinolina (**1b**) con 1,2-propanodiol (**5**), bajo las condiciones de reacción de nuestra metodología.

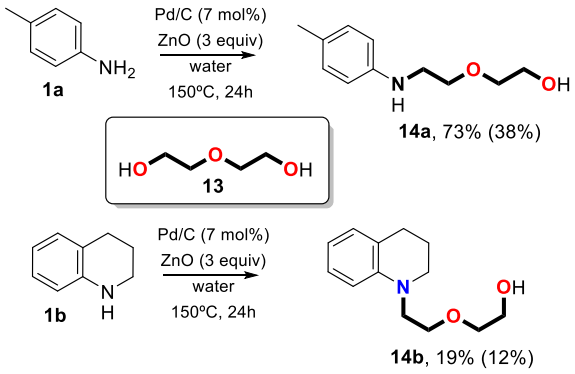

Reacción de anilina (**1a**) y 1,2,3,4-tetrahidroquinolina (**1b**) con dietilen glicol (**13**), bajo las condiciones de reacción de nuestra metodología

El uso de 1,3-propanodiol dio como resultado los compuestos des-hidroxilados **11a** y **11b** y la quinolina **12** mediante un mecanismo tipo Skraup.

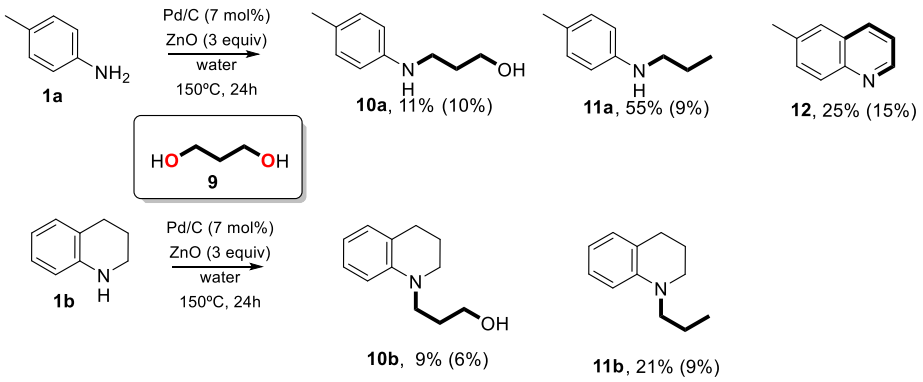

Reacción de anilina (**1a**) y 1,2,3,4-tetrahidroquinolina (**1b**) con 1,3-propanodiol (**9**), bajo las condiciones de reacción de nuestra metodología

✓ Finalmente, en el tercer trabajo de la parte I (*J. Org. Chem.* **2018**, *83*, 521) se presentó un acceso diferente a la obtención de indoles no sustituidos en el anillo pirrólico, mediante una reacción de 'Condensación Deshidrogenativa sin Aceptores Heterogéneos' entre anilinas y etilenglicol.

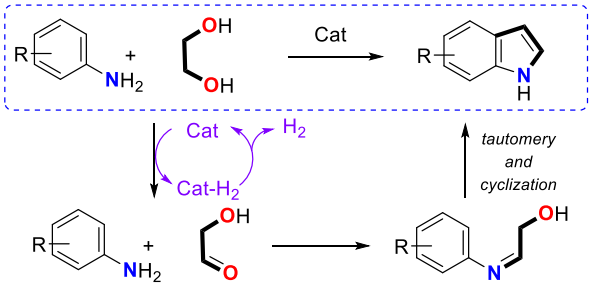

Reacción de 'Condensación Deshidrogenativa sin Aceptores Heterogéneos' de anilinas y etilenglicol para la obtención directa de indoles.

Esta vez, la combinación de Pt/Al_2O_3 y ZnO fue la utilizada para transformar el glicol en 2-hidroxiacetaldehído de manera lenta. El equilibrio tautomérico del intermedio imínico fue clave para la formación final del indol, mediante reacción intramolecular.

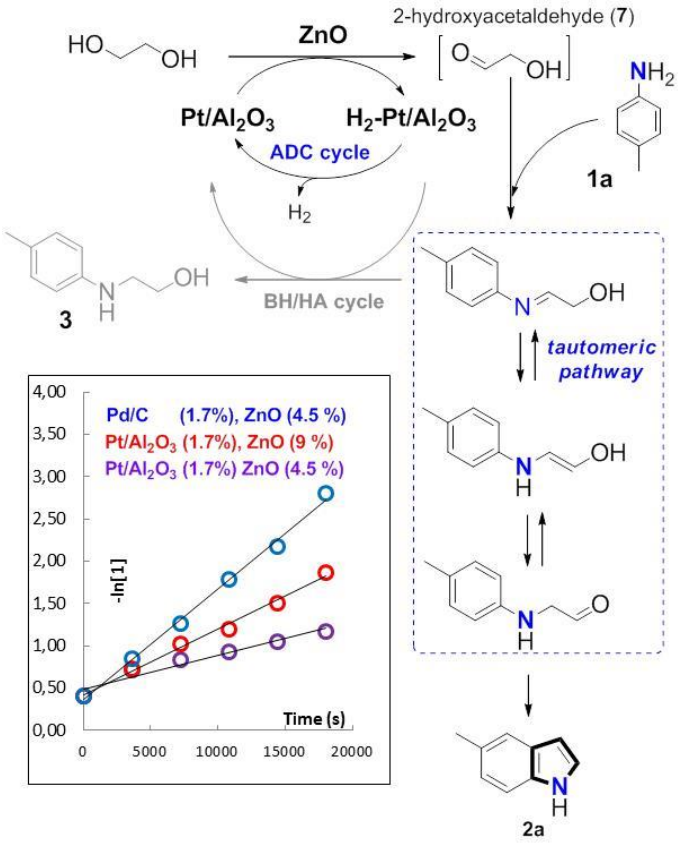

Mecanismo detallado de la reacción de 'Condensación Deshidrogenativa sin Aceptores Heterogéneos'. Resalta la tautomería del intermedio imínico y al final ciclación intramolecular.

De esta manera, se obtuvo un mecanismo de reacción original y eficiente para la obtención de indoles a partir de anilinas y etilenglicol.

PARTE II

- ✓ En la parte II se consiguió satisfactoriamente sintetizar nuevas estructuras tipo diquat basadas en [1,2,3]triazolo[1,5-*a*]piridina (**PTP**) y [1,2,3]triazolo[1,5-*a*]quinolina (**PTQ**), con buenos rendimientos (alrededor de 90%) y con un procedimiento sencillo (*Chem. Eur. J.* **2017**, *23*, 12825).

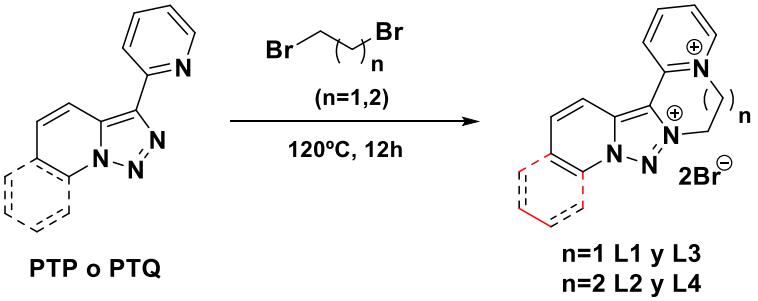

Esquema general de la obtención de derivados de diquat (**L1** – **L4**) a partir de **PTP** y **PTQ**.

Se determinó que estas estructuras son capaces de adoptar conformaciones helicoidales, obteniéndose dos enantiómeros diferentes (*P* o *M*), los cuales son interconvertibles con

una barrera energética moderadamente baja, de acuerdo con los estudios teóricos llevados a cabo.

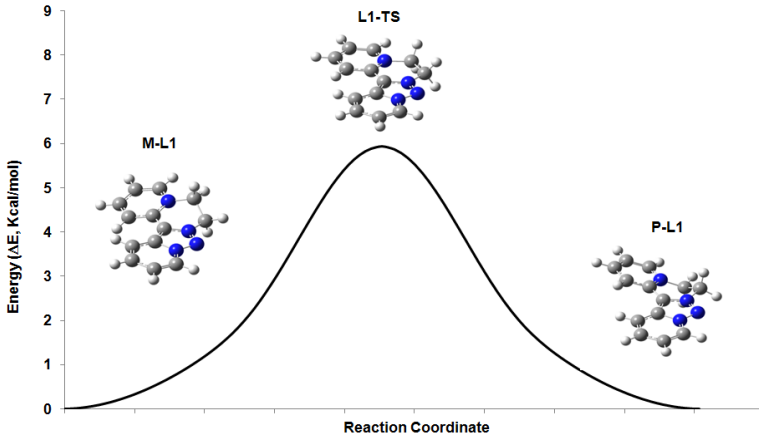

Perfil energético correspondiente a la conversión de ***M*-L1** into ***P*-L1**.

Los valores del potencial de reducción de estas moléculas se encuentran en concordancia con las registradas para el diquat original. El compuesto **L3** presentó un potencial de reducción menor debido a la conjugación existente entre los anillos, haciendo al anillo de piridina menos electro-deficiente.

Los compuestos fueron capaces de interaccionar con ADN de forma electrostática o por intercalación. Los estudios de desnaturalización térmica llevados a cabo, así como las valoraciones por UV-Visible y fluorescencia con ct-DNA mostraron que, por una parte, los derivados de **PTP** (**L1** y **L2**) interaccionaban de manera mayoritariamente electrostática, mientras que los derivados de **PTQ** (**L3** y **L4**), además de hacerlo de manera electrostática, añadían una interacción por intercalación.

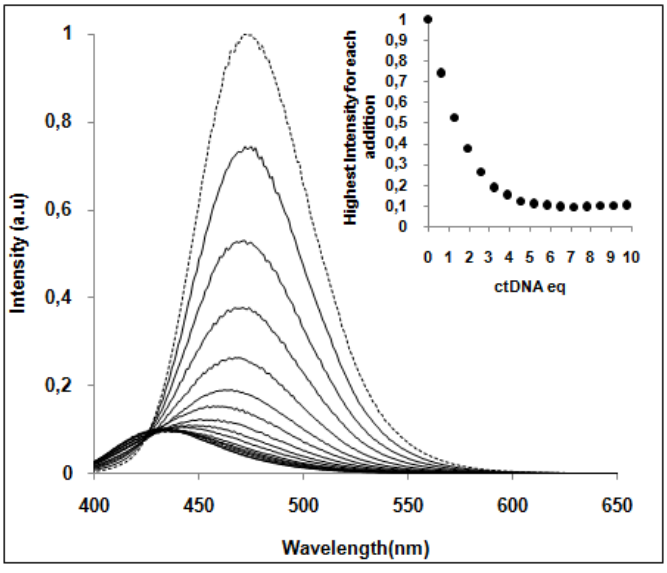

Cambios en la en el espectro de emission de **L3** 10 µM en un tampón fosfato 1 mM, tras adición de ct-DNA (1-10 eq) en un tampón fosfato 1mM.

De este modo, en esta parte de la tesis se ha reportado como el comportamiento de las estructuras tipo diquat puede ser modulado mediante el control del tamaño y/o el número

de los anillos, haciendo que estas moléculas puedan interaccionar con ADN electrostáticamente o añadiendo también la intercalación.

PARTE III

- ✓ En el primer trabajo de la parte III (*Dalton Trans*. 2017, *46,* 7397) se consiguió reportar por primera vez un *Metal Organic Framework* (MOF) construido con un espaciador orgánic~~o~~ bicíclico, permitiendo la preparación del **TMOF** con alta reproducibilidad y buenos rendimientos. Además, se detectaron tres posibles estructuras de este MOF, obtenidas solamente por una modulación de la temperatura de síntesis.

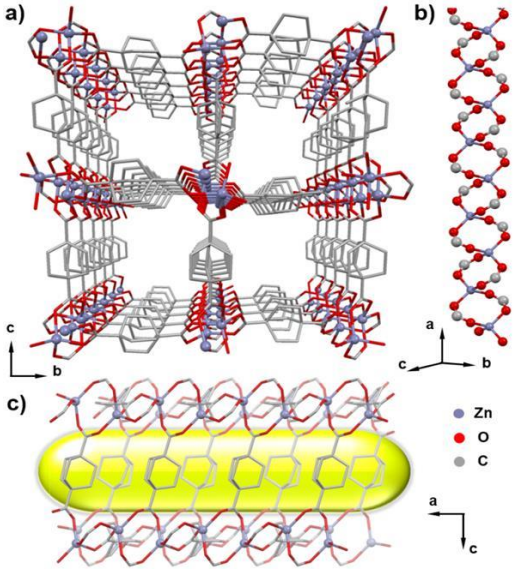

Estructura tridimensional del **TMOF**.

La transparencia conferida por el ligando bicíclico resultó así en un MOF completamente transparente a la luz. Esta característica fue utilizada para el estudio como disolvente sólido del MOF introduciendo pireno al entramado. La presencia de pireno en la estructura condujo a una ligera deformación de la estructura, pero añadió una fuerte emisión fluorescente. Como consecuencia, el pireno se comportó como si estuviera en disolución a concentraciones elevadas. Estos estudios se realizaron con cristales de MOF de tamaño macroscópico (1-2 mm).

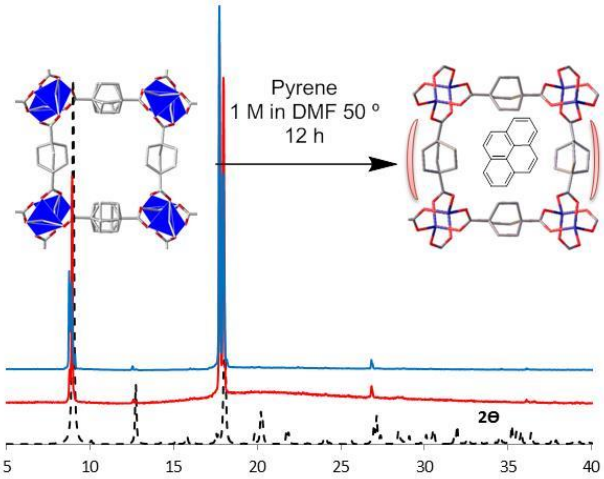

Inserción del pireno en la estructura del **TMOF**. Patrón de Difracción de Rayos X de Polvo del **TMOF** (azul), **Pyrene@TMOF** (rojo) y el calculado para el **TMOF** (negro discontínuo)

En este primer estudio de la parte III, se presentó pues uno de los MOF más transparentes reportados en la bibliografía y su uso como disolvente sólido.

✓ En el segundo trabajo de la parte III se consiguió, mediante el uso de **MOF-5** e **IRMOF-3** y la mezcla de sus ligandos espaciadores, establecer que el tamaño de los cristales de MOF depende, entre otros factores, del ratio de espaciador presente en la estructura. La distribución de tamaños de cristal en función del porcentaje de uno y otro ligando pudo ser explicada con un modelo logístico. Como consecuencia, este modelo empírico podría ser utilizado como herramienta computacional para guiar el diseño de reacciones de obtención de MOF de un determinado tamaño concreto. Además, la composición del material cuando se parte de una mezcla de ligandos puede variar de una forma no lineal, la cual puede ser modelada con una función beta incompleta.

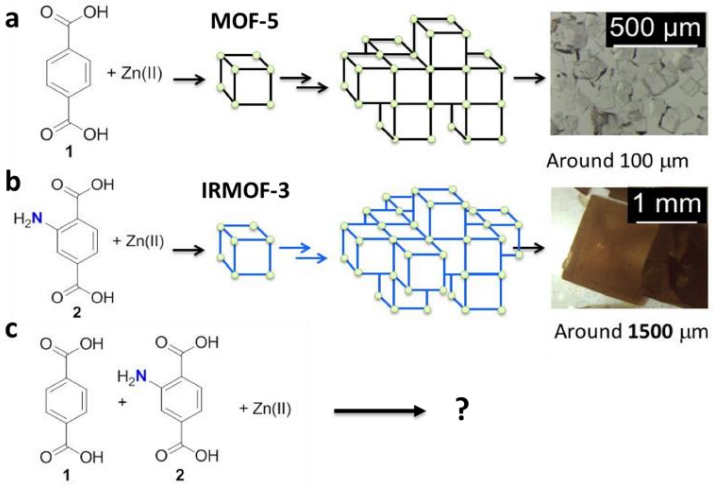

Diferencias macroscópicas entre el a) **MOF-5** y el b) **IRMOF-3**. c) Objetivo de este trabajo.

Así, se reportaron nuevos cristales de distribución de ligando y tamaño variables, además de una optimización de las condiciones de reacción de estos (uso de DMF, menor temperatura…).